

BIOIMPEDANCE
& BIOELECTRICITY
BASICS

SECOND EDITION



SVERRE GRIMNES
ØRJAN G. MARTINSEN



BIOIMPEDANCE AND BIOELECTRICITY BASICS

This page intentionally left blank

BIOIMPEDANCE AND BIOELECTRICITY BASICS

Second Edition

Sverre Grimnes

and

Ørjan Grøttem Martinsen

Department of Physics, University of Oslo and Department of Biomedical
and Clinical Engineering, Rikshospitalet HF, Oslo



AMSTERDAM • BOSTON • HEIDELBERG • LONDON • NEW YORK • OXFORD
PARIS • SAN DIEGO • SAN FRANCISCO • SYDNEY • TOKYO

Butterworth-Heinemann is an imprint of Elsevier



Academic Press is an imprint of Elsevier
Linacre House, Jordan Hill, Oxford OX2 8DP, UK
84 Theobald's Road, London WC1X 8RR, UK
525 B Street, Suite 1900, San Diego, CA 92101-4495, USA
30 Corporate Drive, Suite 400, Burlington, MA 01803, USA

First edition 2000
Second edition 2008

Copyright © 2008 Elsevier Ltd. All rights reserved

No part of this publication may be reproduced, stored in a retrieval system or transmitted in any form or by any means electronic, mechanical, photocopying, recording or otherwise without the prior written permission of the publisher

Permissions may be sought directly from Elsevier's Science & Technology Rights Department in Oxford, UK: phone (+44) (0) 1865 843830; fax (+44) (0) 1865 853333; email: permissions@elsevier.com. Alternatively you can submit your request online by visiting the Elsevier web site at <http://elsevier.com/locate/permissions>, and selecting *Obtaining permission to use Elsevier material*

Notice

No responsibility is assumed by the publisher for any injury and/or damage to persons or property as a matter of products liability, negligence or otherwise, or from any use or operation of any methods, products, instructions or ideas contained in the material herein. Because of rapid advances in the medical sciences, in particular, independent verification of diagnoses and drug dosages should be made

British Library Cataloguing in Publication Data

A catalogue record for this book is available from the British Library

Library of Congress Cataloging-in-Publication Data

A catalog record for this book is available from the Library of Congress

ISBN: 978-0-12-374004-5

For information on all Academic Press publications
visit our web site at books.elsevier.com

Printed and bound in Great Britain

08 09 10 10 9 8 7 6 5 4 3 2 1

Working together to grow
libraries in developing countries

www.elsevier.com | www.bookaid.org | www.sabre.org

ELSEVIER

BOOK AID
International

Sabre Foundation

CONTENTS

PREFACE ix

1 INTRODUCTION 1

2 ELECTROLYTICS 7

- 2.1 Ionic and Electronic DC Conduction 7
- 2.2 The Basic Electrolytic Experiment 12
- 2.3 Bulk Electrolytic DC Conductance 15
- 2.4 Interphase Phenomena 26
- 2.5 Electrode and AC Phenomena 41
- Problems 55

3 DIELECTRICS 57

- 3.1 Polarization in a Uniform Dielectric 58
- 3.2 The Basic Capacitor Experiment 64
- 3.3 Complex Permittivity and Immittivity 65
- 3.4 AC Polarization and Relaxation in a Uniform Dielectric 70

- 3.5 Interfacial Polarization 79
- 3.6 The Basic Membrane Experiment 85
- 3.7 The Basic Suspension Experiment 87
- 3.8 Dispersion and Dielectric Spectroscopy 89
- Problems 91

4 PASSIVE TISSUE ELECTRICAL PROPERTIES 93

- 4.1 Basic Biomaterials 93
- 4.2 Tissue and Organs 102
- 4.3 Special Electrical Properties 124
- Problems 137

5 EXCITABLE TISSUE AND BIOELECTRIC SIGNALS 139

- 5.1 Cell Polarization 140
- 5.2 Action Potential 143
- 5.3 The Neuron 147
- 5.4 Axon Transmission 151
- 5.5 Receptors 157
- Problems 159

6 GEOMETRICAL ANALYSIS 161

- 6.1 Volume Conductors 162
- 6.2 Two-electrode Systems 163
- 6.3 Sphere Sources, Ideal 3D Models 165
- 6.4 Line Sources, Ideal 2D Models 177
- 6.5 Signal Transfer in Tissue Volumes 180
- 6.6 Three- and Four-electrode Impedance Systems 191
- 6.7 Finite Element Method (FEM) 196
- 6.8 Tomography (EIT) 198
- 6.9 Duality of Dielectrics and Conductors 203
- Problems 204

7 INSTRUMENTATION AND MEASUREMENT 205

- 7.1 General Network Theory, the Black Box 206
- 7.2 Signals and Measurement 213
- 7.3 Bridges, Impedance Analyzers, Lock-in Amplifiers 236
- 7.4 Electrodes: Design and Properties 253
- Problems 281

8 DATA AND MODELS 283

- 8.1 Models, Descriptive and Explanatory 284
- 8.2 Equations and Equivalent Circuits 286
- 8.3 Data Calculation and Presentation 321
- 8.4 Data Analysis 322
- Problems 331

9 CLINICAL APPLICATIONS 333

- 9.1 Electrocardiography 335
- 9.2 Impedance Plethysmography 347
- 9.3 Impedance Cardiography 353
- 9.4 Tissue Characterization in Neurology 355
- 9.5 EEG, ENG/ERG/EOG 355
- 9.6 Electrogastrography 356
- 9.7 EMG and Neurography 357
- 9.8 Electrical Impedance Myography 357
- 9.9 Electrotherapy 358
- 9.10 Body Composition Analysis 363
- 9.11 Implanted Active Thoracic Devices 367
- 9.12 Defibrillation and Electroshock 372
- 9.13 Electrosurgery 374
- 9.14 Cell Suspensions 378
- 9.15 Skin Instrumentation 388
- 9.16 Non-medical Applications 397
- 9.17 Electrical Safety 398

10 HISTORY OF BIOIMPEDANCE AND BIOELECTRICITY 411

11 APPENDIX 419

- 11.1 Vectors and Scalars, Complex Numbers 419
- 11.2 Equivalent Circuit Equations 424
- 11.3 Global Symbols 430
- 11.4 Physical Dimensions 432

REFERENCES 435

- Recommended Books and Review Articles 435

INDEX 461

This page intentionally left blank

PREFACE

The second edition of our book “Bioimpedance and Bioelectricity Basics” (BBB) gave us the chance of increasing the emphasis on bioelectricity and the signals generated by living tissue itself. This has resulted in a new chapter (Excitable tissue electrical properties) and in general a better equilibrium between bioimpedance and bioelectricity. We have extended the chapter on models with statistical approaches such as multivariate analysis for the interpretation of measurement results. We have kept the balance from the first edition between both a mathematical and verbal description, and we have put increased emphasis on the illustrations. We have added exercises and problems for the students and for readers wanting increased penetration into a topic.

Although this book has been written primarily for graduate and post-graduate students in biomedical engineering and biophysics, we hope it will be useful also for other researchers coming in touch with our area, for example, from biotechnology in general, electrophysiology, odontology, pharmacy and plant biology. Some devoted medical doctors in the field of neurology, cardiology, dermatology, clinical chemistry and microbiology have not been forgotten. We have on certain subjects reverted to an almost “Adam and Eve” approach. In addition, the number of illustrations was high in the first edition and has been increased in the new edition. We have not renounced on mathematical equations, but usually tried to include an often extended discussion on their implications. To keep the book within the “basic” framework, we have imposed certain boundaries: we have excluded magnetism, which is already well covered by Malmivuo and Plonsey (1995). We have excluded a broader treatment of EIT, which is now well covered by Holder (2005). We have limited the book to sine wave and step function variables, omitting a more general treatment by the theory of Laplace transforms. And we have limited the number of application examples.

BBB first edition did grow out of a certain frustration of having used unnecessarily much time ourselves learning some of the theory and practice of bioimpedance, and out of a certain hope that a new book could pave an easier and more efficient way for people seeking basic knowledge about our discipline. Bioimpedance and bioelectricity must perhaps be considered as rather specialized fields, but obviously based on an extract from scientific basic disciplines. All these disciplines cannot be taught in their full extensions, but with this book it should be possible to gather many of them into *one single subject and one course*. For the newcomer it is also an advantage to be presented a unified set of terminology and symbols, to avoid the start with the silent terminology of the paradigms of each area, bewildering traditions illustrated for instance by the different use of the term “polarization” and such symbols as m and α .

Our background in the fields of biomedical engineering, physics and instrumentation is of course discernible. All the same we have found it necessary to cover a much broader range of topics. Our emphasis is on systems with galvanic contact with tissue, not so much on the interaction between tissue and airborne electromagnetic fields and waves. A large part has been dedicated to model thinking. The importance of the *geometry* of the measuring system cannot be overemphasized. We hope that the balance between the descriptive and quantitative/theoretical text parts will be appreciated.

Our field offer many challenges. In order to understand the phenomena of interest, a certain basic knowledge of electrochemistry, electronic engineering, physics, physiology, mathematics and model thinking is needed. And that is what is to be found in the chapters of this book.

Tips to the Reader


A **bold** symbol is either a space vector or a complex number. A non-bold symbol is either a scalar, or a magnitude, or real part of a vector. In the literature, an intelligent guess often has to be made. A phase angle is denoted by φ , a loss angle by δ . In the literature the loss angle is often called a phase angle, which it of course also is.


Φ is used for a potential difference in space and V for a voltage difference in a circuit. Φ may designate not only the potential at a defined position, but also as a function of position in space, the potential *field* $\Phi(x,y,z)$.

Global symbols used all over the book are tabulated in Chapter 11, and are *not* explained locally in the text.

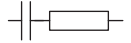
Impedance variables such as Z , R , X , ρ and C_s are preferably used when components are connected in series. *Admittance* variables such as Y , G , B , σ and C_p are preferably used when components are connected in parallel. *Immittance* is the combined term for both impedance and admittance. It is often used in order to force the reader to be sensitive to the choice: there is no such thing as an immittance equation.

Units are often written in square brackets, for example, [V] or [volt]

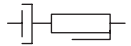
In figures: smooth border line symbolizes a bounded volume: 

In figures: zigzag border line symbolizes an infinite volume: 

Ideal capacitor and resistor components are drawn as usual:



Electrolytic components with frequency dependent values are drawn:



A Wessel diagram is the same as an Argand diagram: a diagram in the complex plane.

The International System of units [SI] is used in BBB. Notice that the choice of systems also influences the formulas. For instance, Coulomb's law differs by the factor $4\pi\epsilon_0$ between the old cgs system [$F = q_1q_2/\epsilon_r r^2$] based on centimeter and not meter, and the SI system [$F = q_1q_2/4\pi\epsilon_r\epsilon_0 r^2$]. Or in cgs: $\mathbf{D} = \epsilon_r\mathbf{E}$ and in SI: $\mathbf{D} = \epsilon\mathbf{E}$.

Be aware of the fact that in the literature $\log x$ may mean the common logarithm $\log_{10}x$ or (in particular in mathematics) the natural logarithm $\ln x$. In BBB $\log x$ means $\log_{10}x$.

ACKNOWLEDGMENTS

We are greatly indebted to the many colleagues and friends who have contributed to BBB in various ways. We are in particular indebted to the late Herman P. Schwan at the University of Pennsylvania for the long discussions, which had a significant influence on the first edition. In this second edition we would particularly like to mention Fernando Seoane, Mart Min, Rafael Davalos, Stig Ollmar, Antonio Piccoli, Irina S. Mudraya, Seward Rutkove, Donald P. Bernstein, Michael Bodo, Todd M. Zielinski, Uwe Pliquett, Jonathan Newell and Hermann Scharfetter. Last, but not least, we appreciate the great support from our two Ks: Kari and Kjersti.

Supporting material accompanying this book

A full Solutions Manual is available for downloading by teachers and lecturers who adopt or recommend this text for class use. For further details and access please visit <http://textbooks.elsevier.com/>

This page intentionally left blank

1 Introduction¹

Bioimpedance, bioelectricity and the electrical properties of tissue are much about the same things.

Bioimpedance deals with some passive electrical properties of tissue: the ability to oppose (*impede*) electric current flow. *Bioelectricity* deals with the ability of tissue to generate electricity, as for instance done by the heart (electrocardiography (ECG)). This electricity is *endogenic*, that is generated by the tissue itself. Bioelectricity is also about how tissue can be controlled by electricity. Such electricity together with the electricity used for measuring bioimpedance is *exogenic* (i.e. with externally applied electricity).

Bioimpedance and bioelectricity methods use electrodes with galvanic coupling to tissue. The instrumentation uses electronic circuitry and wires coupled to the electrodes. The charge carriers flowing in the copper wires are electrons. The charge carriers in living tissue are (with some exceptions) ions. An electrode proper is the site of charge carrier conversion from ions to electrons and vice versa. It is practical to divide problems into *circuit problems* and *field problems*. Circuit problems are about wires, capacitors, resistors, semiconductors, batteries, etc. The current flow is confined to the wires, and for example, a voltage difference [volt] is measured between two points in the circuitry. Field problems are related to volume conductors and quantities which are a function of position in that volume (e.g. the potential field $\Phi(xyz)$, also [volt]).

There is a duality in the electrical properties of tissue: tissue may be regarded as a volume *conductor* or a *dielectric*. In the frequency range <100 kHz most tissues are predominantly *electrolytic conductors*. Therefore we start the book with electrolytics (Chapter 2), covering also the electric double layer being so sensitive to surface properties. With high resolution techniques it is possible to extract important capacitive, that is *dielectric*, properties even at low frequencies (e.g. 10 Hz). At higher frequencies (e.g. 50 kHz), the dielectric properties of tissue (Chapter 3) may dominate. At the highest frequencies tissue properties become more and more equal to that of water, pure water has a characteristic relaxation frequency of approximately 18 GHz.

In tissue and the living cell there is an inseparable alliance between *electricity* and *chemistry*. Electrolytic theory and electrochemistry therefore form an important

¹Global symbols in BBB are not explained locally, but are found in Table 11.1. Tips to the reader are found in the Preface.

basis for our subject; it is not possible to understand what is going on in tissue during electric current flow without knowing some electrochemistry.

Bioimpedance and bioelectricity is about *biomaterials* in a broad sense: materials that are living, have lived or are potential building blocks for living tissue. The tissue of interest may be plant, fruit, egg, fish, animal or the human body. But it may also be dead biological material such as hair or nail; or excised material such as beef or a piece of stratum corneum. The basic building block is the living cell, and a prerequisite for its life is that it is surrounded by an electrolyte solution. Great caution must be imposed on the state of the biomaterial sample. A material may change completely from the living, wetted state with large contributions from interfacial counter-ion mechanisms, via a denaturation or death process to a more or less dead and dry sample, and further out to the extreme: to be measured in a vacuum chamber. It is important to remember this when for example, ionic versus electronic/semiconductive properties are discussed. Life is so diversified and the situation is complex: bacteria may for instance be in dry surroundings and encapsulated in a sleeping state, and it is difficult to give them a clear living status.

What is bioimpedance and -permittivity?

Impedance is the ratio between voltage and current. It applies to both direct current (DC) and alternating current (AC) cases. *Admittance* is the inverse of impedance, that is not *impede* but *admit* current flow. *Immittance* is the combined term for impedance and admittance, so a better and more generic term than bioimpedance is *bioimmittance*.

A dielectric is traditionally a dry insulator being able to store electrical energy. An electrostatic field can not penetrate a metal but can penetrate all through (Latin: dia) a dielectric. The most important *dielectric* quantity is *permittivity* ϵ . Permittivity is the ability to *permit* storage of electric energy. Under linear conditions and for the same tissue, unity cell admittance Y , unity cell impedance $Z = 1/Y$ and complex permittivity ϵ all contain the same information, but differently presented. All these quantities are based upon the equations of Maxwell (1873), Chapter 8 here in bioimpedance and bioelectricity basics (BBB). The Maxwell equations are based upon the velocity of light and that light is electromagnetic radiation. There is a direct link between the electrical permittivity of a material and its optical refractive index.

Note the difference between resistance, conductance, impedance, admittance, immittance – and resistivity, conductivity, impedivity, admittivity, immittivity, permittivity. The –ance parameters are dependent both on the electrical properties of the sample and the measuring system geometry. The –ivity parameters are material constants only dependent on the electrical properties of the sample and not its dimensions (Chapter 3).

Bioimmittance is frequency dependent. In dielectric or electrolytic models there is a choice between a step (*relaxational*) and sinusoidal (single frequency) waveform excitation. As long as linear conditions prevail, the information gathered is the same. At high voltage and current levels the system is non-linear, and models and parameters must be chosen with care. Results obtained with one variable can

not necessarily be recalculated to other forms. In such cases one single pulse may be the best waveform because it limits heat and sample destruction.

What is bioelectricity?

Bioelectricity is about the electrical phenomena of life processes, and is a parallel to the medical subject *electrophysiology*. One basic mechanism is the energy consuming cell membrane ion pumps polarising a cell, and the *action potential* generated if the cell is excited and ion channels open. The depolarisation process generates current flow also in the extracellular volume, which again results in measurable *biopotential* differences in the tissue. An important part of the subject is intracellular and extracellular single cell measurements with microelectrodes. Single neuron activity and signal transmission can be studied by recording potentials with multiple microelectrode arrays.

In addition to measure on endogenic sources, bioelectricity also comprises the use of active stimulating current carrying (CC) electrodes. Since bioelectricity is about life processes the experiments are per definition *in vivo* or *ex vivo*.

Electricity is used clinically for the treatment of patients, *electrotherapy*, Chapter 9. Low energy current pulses for nerve excitation are used for pain relief, also with implanted devices. Organ functions are activated with implanted pacemakers and external muscle stimulators. Small DC currents are used for speeding up the healing of non-union bone fractures. High energy methods are clearly operating in the non-linear region. It must not be ignored that most models extensively treated by textbooks are limited to linear cases. Many applications such as defibrillation or electroporation are clearly in the non-linear range; a sine wave excitation does not lead to a sine wave response.

Defibrillation is a life-saving procedure; electroporation is used for a very short opening of cells. Surgery and ablation are performed using high frequency currents, this is *electrosurgery*.

How are the quantities of bioimpedance and bioelectricity measured and controlled?

Bioelectricity experiments are performed *in vivo* or *ex vivo* with pick-up electrodes and stimulation electrodes. Electrotherapeutical methods use electricity controlled by current or voltage, charge, energy, waveform and time.

Bioimmittance is measured *in vivo* or *in vitro*. The tissue may be kept alive and perfused under *ex vivo* conditions. Bioimmittance can be measured with 2-, 3- or 4-electrode systems. With 4 electrodes one electrode pair is current carrying and the other pair picks up the corresponding potential difference somewhere else in the tissue. If the measured voltage is divided on the applied current, the *transfer impedance* is calculated. If no voltage is measured, the transfer impedance is zero. This is equivalent to the bioelectricity case where a signal from the source (e.g. the heart) is transferred to the skin surface electrodes. Zero transfer impedance does not mean that the tissue is very well conducting, only that no signal transfer occurs. With the bioimpedance 2-electrode system the transfer factor is eliminated because current application and

signal pick-up occur at the same site, then measured impedance more directly reflects tissue electrical properties.

Single cells are measured with microelectrodes and clamp and patch techniques, Chapters 5 and 7.

Exogenic current is usually applied with electrodes in galvanic contact with tissue. It is also possible to apply it by a magnetic field without making physical contact with the tissue. Biopotential is more difficult to measure without galvanic contact.

The *technology* of the instrumentation is often based upon lock-in technique because it has superior noise suppression properties, Chapter 7. The prerequisite is a reference signal, which is always accessible in immittance measurements.

Models

Science is very much about the use of models, in order to *describe* and therefore predict, and in order to *explain* and therefore understand. BBB emphasises model thinking, Chapter 8. The selected model often dictates the measuring method to be used. The interpretation of the results is very dependent on the angle of view and the model used. But models have their shortcomings. Important models for bioimpedance are empirical and can therefore only be described. Because tissue behaves predominantly electrolytic, a model's treatment of DC conductivity is for instance important. With high energy pulses or DC the principle of superposition often is not valid, and different contributions cannot simply be added. Many high energy applications such as defibrillation or electroporation are clearly in the non-linear range; a sine wave excitation does not lead to a sine wave response. Many researchers have been led astray by using a «wrong» model; for example, a series model for processes actually physically occurring in parallel. Another example is that a dispersion model presupposes that the measured volume is independent of frequency, and this not always the case in a measuring set-up. It is a part of a very general problem in bioimpedance: how to select or limit the measured volume.

The classical models for bioimpedance and bioelectricity are mathematical equations and equivalent circuit diagrams having the same electrical behavior as the tissue to be modeled. Another class are the statistical models determining the correspondence between bioelectrical measurements and physiological variables (e.g. tissue characterization).

What are the applications of bioimpedance and bioelectricity? (cf. Chapter 9)

Clinical applications

Many clinical applications are well established: Recording bioelectric signals from the heart (ECG) was introduced by Waller already in 1887 and brought into clinical use by Einthoven around 1905, and is still a most important examination in hospitals world-wide. Electrosurgery came in the same position from the 1930s. Recording bioelectric signals from the brain (electroencephalogram (EEG)) was introduced in the 1940s, pacemakers and defibrillators were taken into use in the

1960s. Lung plethysmography and respiration rate determination has been used in ECG monitors for several decades. Split electrodes with bioimpedance monitoring of electrode–tissue contact has been used for a long time in critical medical electrode applications.

In the last years new applications have emerged. Immittance based plethysmography is used to measure cardiac output both with transcutaneous electrodes and by pacemaker implants. Electrical impedance tomography (EIT) is used for lung imaging of newborns. Different kinds of skin diagnosis methods have been taken into use for skin cancer, dermatitis, skin moisture, sweat activity and hyperhidrosis. Pain relief is obtained with transcutaneous electrical nerve stimulation (TENS) or implanted devices. Organ ischemia and rejection processes can be monitored. The water balance can be determined together with the monitoring of dialysis treatment. In vivo applications of electroporation and drug therapy are exploited. Tissue ablation is performed with catheters or endoscopes with radio frequency (RF) current. Tissue characterisation can be done and needle position can be determined. Joint angles can be determined with skin electrodes.

Laboratory applications

Laboratory-on-a-chip systems use immittance and dielectric variables measured with microelectrodes. In flow sensors cell properties are measured with microelectrodes and cell characterisation and cell separation performed. Properties of protein molecules have for many years been determined by the established methods of electrophoresis. Electrophoresis is based upon the electric charge of cells and proteins and the driving force exerted by an electric field. All sorts of liquid suspensions with cells or bacteria can be measured with bioimmittance or permittivity. Cell adherence and cell micro-motion can be monitored with microelectrodes equipped with a thin surface coating.

On the borderline between medical and non-medical applications

Body composition and intra/extracellular fluid index can be determined for monitoring nutrition and physical training. Small portable loggers for heart rate and respiration rate during bicycling or treadmill exercise have found a large market as a part of the instrumentation for *sport medicine*.

Non-medical applications

Meat quality assessment is made with bioimpedance measurement. Fermentation can be followed in brewery industries. Plant properties can be determined in the living or dead state (wood quality).

Non-biological applications (outside scope of BBB)

Soil quality and humidity can be determined using immittance measurement. Geophysical properties related to oil drilling have been measured with impedance methods since the 1920s, Schlumberger (1920). Large iron bar electrodes and current levels of hundreds of ampere are used. Volcanic activity is monitored by impedance on Iceland.

Some basic problems

Electromagnetic hazards using bioimpedance and bioelectricity methods must be considered. How is the electric current spread from the electrodes in living tissue? Can we find the conductivity distribution in living tissue? What is the influence of body macro-membranes and anisotropy? For example, to what extent does an externally applied electric current follow blood vessels? Is it really a specific constant phase mechanism for the immittance in biological materials? Which are the different mechanisms of the α -dispersion? Which are the mechanisms of counterion relaxation, particularly at the cell membranes?

Who are working with bioimpedance and bioelectricity?

Industry, research institutes, interventional centers and universities are all doing basic research within our discipline. The goal of the industry is to develop competitive products. The goal of the institutes and universities is to develop new academic knowledge and publish it. Biomedical engineers, biophysicist, mathematicians, electrochemists and computer scientists are all involved in the development of new methods and new knowledge. On the bio side physiologists and biologists are important. Medical doctors are often clinically oriented and concerned with applications within their speciality: Anesthesia, Cardiology, Dermatology, Neurology, Physical medicine and Surgery.

2 Electrolytics

Chapter Contents

2.1. Ionic and Electronic DC Conduction

- 2.1.1. Ionization
- 2.1.2. Molecular Bonds

2.2. The Basic Electrolytic Experiment

2.3. Bulk Electrolytic DC Conductance

2.4. Interphase Phenomena

- 2.4.1. Faraday's Law
- 2.4.2. Migration and Diffusion
- 2.4.3. The Electric Double Layer, Perpendicular Fields
- 2.4.4. The Electric Double Layer, Lateral Fields
- 2.4.5. The Net Charge of a Particle
- 2.4.6. Electrokinesis

2.5. Electrode Dynamics and AC Phenomena

- 2.5.1. Electrode Equilibrium DC Potential, Zero External Current (cf. Section 7.4.4.)
- 2.5.2. The Monopolar Basic Experiment with DC Current Flow
- 2.5.3. DC/AC Equivalent Circuit for Electrode Processes
- 2.5.4. Non-linear Properties of Electrolytics

Problems

2.1. IONIC AND ELECTRONIC DC CONDUCTION

An *electrolyte* is a substance with ionic DC conductivity. Living tissue is electrically and macroscopically predominantly an electrolytic conductor. Both intracellular and extracellular liquids contain *ions free to migrate*. In pure electrolytes the charge carriers are ions, and there is no separate flow of electrons, they are all bound to their respective atoms. Tissue DC currents are therefore *ionic* currents, in contrast to the *electronic* current in metals. This is not contradictory to a possible local electronic conductance due to free electrons, for example, in the intracellular DNA molecules. New solid materials like organic polymers and glasses may

contain an appreciable amount of free ions with considerable mobility, so the materials of an electrolytic measuring cell are not limited to liquid media. Some of these solid media show a mixture of ionic and electronic conductivity.

Two *current carrying electrodes* in an electrolyte are the source and sink of electrons: from electrons of the metal, to ions or uncharged species of the electrolyte. *The electrode is the site of a charge carrier shift, a charge exchange between electrons and ions.*

In a metal the conductance electrons are free to move; they are like an electron gas not linked to particular metal atoms, but with a probability of being at a certain location at a certain time. The metal atoms can be considered bound but ionized, they have lost electrons. Electron transport in a metal involves no transport of metal ions and not even a transport of electrons all the way. When we supply an electron into a wire end, “another” electron is coming out of the other end. Current flow which seems to be so fast, is so only because it is not the same electron entering and leaving. Actually the migration velocity of *electrons* in a metal is *very slow*, of the order of 0.3 mm/s at rather high current densities. The migration velocity of *ions* in solution is also very slow. As studied by electrophoresis, the ion migration velocity is of the order of 10 mm/s.

The electronic conduction in the vacuum of a cathode ray tube (CRT) is very different. Friction is low and electron velocity is very high, of the order of thousands of meters per second (but with much fewer electrons engaged). When these fast electrons are stopped, there is a collision, for instance, with the phosphor plate that lights up in a CRT, or the anode of an X-ray tube, which emits X-rays.

Electric current flow in an ionic solution is a more complex event than in a metal. Electron current implies no transport of substance. Therefore an externally applied DC current can flow forever without changing the conductor. However, ion current implies a transport of substance. Therefore an externally applied DC current cannot flow forever without changing the conductor. At first changes will occur near the electrodes, but in a closed electrolytic cell with sufficiently long time the change will spread to the bulk of the electrolyte. Accordingly, *electrolytic long duration DC conductivity* is a difficult concept in a closed system.

The transfer of electric charge across the solution/electrode interphase is accompanied by an electrochemical reaction at each electrode (electrolysis). *We must keep the phenomena in the bulk of the solution separate from the phenomena at the electrodes.*

2.1.1. Ionization

Since the charge carriers of interest are ions, the *ionization* of atoms is of particular interest. The electrons of an atom are arranged in shells. The forces acting between atoms are of an electrostatic nature. In electrochemistry, the ionization of an atom is determined by the electron configuration of the *outermost* shell. If this shell is full, the atom has a noble gas configuration. This is a particularly stable form, implying that a large energy is necessary to remove, or add, an electron and thus ionize such an atom (see Table 2.1).

For hydrogen and helium the innermost K-shell is also the outermost shell. The K-shell is full with two electrons (the noble gas helium). The next L-shell is full with

TABLE 2.1 Electron Shell Configuration for the Lowest Atomic Number Atoms

	Protons in nucleus	Shell			Typical electrovalency	Ionization potential, (eV)	Atom radius (nm)	Positive ion radius (nm)	Negative ion radius (nm)
		K	L	M					
H	1	1	0	0	+1	13.6	0.037	0.00001?	0.154
He	2	2	0	0	Noble	24.6		N/A	N/A
Li	3	2	1	0	+1	5.4		0.068	N/A
Be	4	2	2	0	+2	9.3		0.044	N/A
B	5	2	3	0	+3	8.3		0.035	N/A
C	6	2	4	0	± 4	11.3	0.077	0.016	0.26
N	7	2	5	0	-3	14.5	0.070	0.025	0.17
O	8	2	6	0	-2	13.6	0.066	0.022	0.176
F	9	2	7	0	-1	17.4		N/A	0.133
Ne	10	2	8	0	Noble	21.6		N/A	N/A
Na	11	2	2	1	+1	5.1		0.097	N/A

Here, ionization potential is the *energy* necessary to remove the first electron from the valence (outermost) shell. Values for radii depend on how they are measured.

eight electrons (the noble gas neon). The chemical properties of an atom are determined by the electron configuration of the outermost shell. These electrons are called *valence* electrons, and their ionization potential (energy necessary to remove an electron) is for most atoms less than 20 eV. Chemical reactions and bonds are related to the valence electrons in the outermost shell, the electrons in the inner shells (affected by X-rays) and the nuclei (high-energy nuclear processes) are not affected. Ordinary chemical methods therefore involve energy levels <20 eV. The *electrovalency* z of an atom is the number of electrons available for transfer. The valency is thus $z = +1$ for Na and $z = -1$ for Cl (cf. Table 2.1). A valence electron is a rather broad concept comprising those electrons in the outer shell that may combine with other atoms and form molecules, whether it is by gaining, losing or *sharing* electrons.

The electrochemical properties are determined by the inclination of an atom to attain noble gas configuration of the outer electron shell. The atoms with few electrons in the outer shell (e.g. H, Li, Na) have a tendency to empty the shell, that is lose electrons and form positive ions. The atoms with a nearly filled shell (e.g. O, F) have a tendency to fill up the shell, that is gain electrons and form negative ions. “Tendency” here simply means that those configurations are lower energy level forms.

Electronegativity is the relative ability of an atom to gain electrons and become a negative ion. Clearly Na is not very electronegative, but F is highly electronegative. Pauling¹ worked out a scale of electronegativity (see Table 2.2).

¹Linus Pauling (1901–1994), American chemist. 1954 Nobel prize laureate in chemistry on the structure of proteins (and 1962 in peace). Important work also on chemical bonding and electronegativity, invented the paramagnetic oxygen analyzer.

TABLE 2.2 Pauling's Scale of Electronegativity for Some Selected Atoms

F	4.0	S	2.5
O	3.5	C	2.5
N	3.0	H	2.1
Cl	3.0	P	2.1
Br	2.8	Fe	1.8
I	2.5	Na	0.9

Electronegativity is not a purely quantitative term, but it is useful in the prediction of the strengths and polarities of ionic bonds between atoms, and thus possible electrochemical reactions. In electrochemistry the use of electrode equilibrium potential tables (Section 2.5.1) serve the same purpose. The atoms with small electronegativity (e.g. Na) are not inclined to gain an electron at all; it would move the ion away from noble gas configuration. Sodium's natural state is to lose an electron and be a positive ion. Fluorine is very electronegative with a Pauling scale value of 4, its L-shell is filled with just one extra electron. With a value of 2.5, carbon is in a middle position with the ability of both losing and gaining electrons. *Hydrogen* is in a special position; in principle it should be highly electronegative as one extra electron would bring it in noble gas configuration. But as we know it has a larger tendency to lose an electron and form a proton; accordingly its value is 2.1. Electronegative atoms are on the right-hand side of the periodic system in the three positions preceding a noble gas. A less electronegative atom more easily loses electrons, in accordance with small ionization energy (cf. Table 2.1). The ionization energy does not indicate the energy necessary for an atom to *gain* an electron and thus become a negative ion; this is defined by the *electron affinity*.

2.1.2. Molecular Bonds

Atoms far apart on the Pauling scale tend to form *ionic* molecular bonds; atoms near each other form *covalent* molecular bonds. The forces acting between atoms in a solid may be grouped into four different types of chemical bonds:

1. Ionic bonding
2. Covalent bonding
3. Metallic bonding
4. Van der Waals bonding

The *ionic* bonds are between unequal atoms. The ionization energy of, for example, a sodium atom is small (5.1 eV), so the sodium gives an electron to the highly electronegative chloride. The atoms are ionized, valence electrons are lost or gained, and the coulombic forces are mainly responsible for keeping the ions together in the solid. Since both electrons and ions are tightly bound at room

TABLE 2.3 Covalent Bond Lengths

Atom I	Atom II		Bond length (nm)
C	C	Diamond	0.154
C	C	Graphite	0.142
C	H		0.10
C	N		0.147
C	O		0.143
N	N	N ₂	0.11
H	H	H ₂	0.075
O	O	O ₂	0.12
H	O	H ₂ O	0.0965

temperature, solid ionic crystals in general exhibit no electrical conductivity, neither electronic nor ionic. There are lots of ions, but no mobility. In water the bonds are broken and the ions split (dissociation), causing ionic conductivity.

Covalent bonds are important in molecules formed by atoms of the same atomic number, for example N₂ in the air or carbon in diamond (Table 2.3). The atoms remain neutral, but they share valence electron *pairs*, one from each atom. The sharing of electron pairs always increases the apparent filling of the outermost shell. The number of electrons necessary to obtain noble gas configuration is the number of *unpaired* electrons. Each shared electron pair is a single *bond*. A carbon atom has four unpaired electrons and can share four electrons with other atoms and form four covalent bonds. Such covalent bonds can be extremely strong (diamond), and the electrons locally strongly bound. Therefore solid covalent crystals in general exhibit no electrical conductivity, neither electronic nor ionic. In biomaterials covalent bonds with carbon are very important, usually with no molecular ionic or electronic conductivity. However, the charges in such a molecule may be far apart and thus very large dipole moments and strong electric polarization may occur.

The sharing of electron pairs in carbon–carbon covalent bonds may be as a single bond or with double bonds. Single bonds have complete freedom of rotation, while double bonds are shorter and do not allow free rotation. The type of covalent bond is therefore important for electrical properties such as polarization and relaxation time.

In *metals* the bonds are of the valence type, but the valence electrons are highly mobile and do not belong to particular atoms. This causes the strong electronic conductivity of metals, and the atoms may be regarded as fixed positive ions.

An electron revolving around its nucleus may be considered as a rotating electrical dipole. Such a rotating dipole induces dipoles in neighboring atoms. *Van der Waals* forces are dipole–dipole attractive forces between such atoms. The forces are weak, and fall with the sixth power of the interatomic distance. Many organic molecules form aggregates (heterogeneous mass of parts or particles) held together by van der Waals forces.

2.2. THE BASIC ELECTROLYTIC EXPERIMENT

Set up

Now we will give the first and simple illustration of an electrolytic DC current flow system, an *electrolytic* cell.² It consists of a homogeneous electrolyte solution³ with two equal electrodes (Fig. 2.1). By homogeneous we here mean that the solution contains no boundaries or membranes, except the two electrodes and the isolating walls of the container. As electrolyte solution we choose the most important in the human body: aqueous NaCl solution, concentration 0.9% by weight. The Na^+ and Cl^- ions are charge carriers free to migrate in an electric field, thus contributing to DC conductivity.

A DC potential may develop at the electrode metal/solution interphase. The absolute potential of this interphase (half-cell electrode potential) cannot be measured, it must be considered unknown. But the potential difference between the *two* electrodes can be measured with an ordinary voltmeter connected to the two metal wires from the electrodes. If the metals were different, they could generate a potential difference of 1V or more. But here we presume that the *same* electrode material is used, and that the measured potential difference is small. We will discuss the case for three different electrode materials important in biological work: *platinum, silver coated with silver chloride and carbon*. To the extent that both electrodes are equal we have a symmetrical (bipolar) system, and the voltage–current dependence should not be polarity dependent.

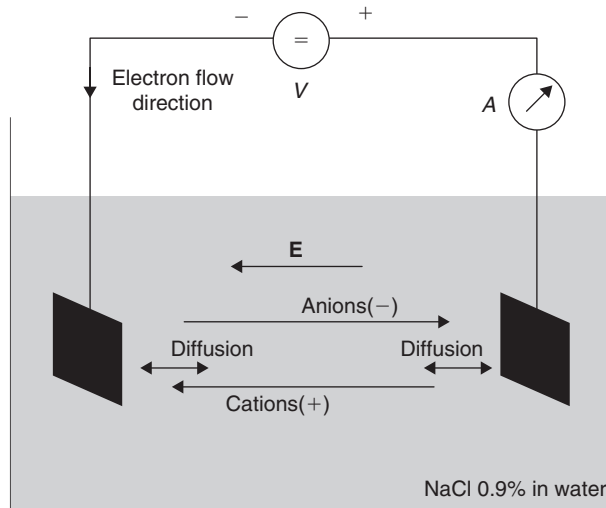


Figure 2.1 The basic electrolytic experiment, shown with material transport directions.

²An *electrolytic* cell is an electrochemical cell used with an externally applied electric current. A *galvanic* cell is an electrochemical cell from which energy is drawn.

³If NaCl is dissolved in water, then NaCl is the *solute* (and the electrolyte), and water is the *solvent*, together they are the *solution*.

We connect the DC supply to the electrode metal wires and adjust the voltage so that a suitable DC current flows. An electric field is accordingly set up in the solution between the electrodes. Positive ions (e.g. Na^+) migrate in the same direction as the E-field all the way up to the cathode; they are *cations*. Negative ions (e.g. Cl^-) migrate in the opposite direction in the same directions as the electrons in the wires; they are *anions*. Anode and cathode are defined from *current flow direction*, and not necessarily from the polarity of the external voltage source. In the bulk of the electrolyte, no change in composition or concentration occurs during the $\text{Na}^+ \text{Cl}^-$ migration: the same amount of ions enters and leaves a volume.

We must not forget a second possible transport mechanism different from migration: ionization of *neutral* species may take place at an electrode. These neutral species cannot be transported to the electrode by migration, as they are not charged. The transport is caused by diffusion, that is by the concentration gradient near the electrode.

Findings

Platinum Electrodes

We adjust our DC supply to about 0.5 V, but no DC current is flowing.

We must increase the voltage to about 2 V to get a DC current, but then the current rapidly increases with voltage. With DC current flowing, gas bubbles are seen on both the anode and cathode metal surfaces.

Carbon Electrodes

We must again increase the voltage to about 2 V to get a DC current flowing. Gas bubbles are seen on both electrodes, but on the anode an erosion process of the carbon surface seems to take place.

Silver–Silver Chloride Electrodes

Large DC current flows with the voltage supply adjusted to only a tenth of a volt. Initially no gas bubbles are seen on any of the electrodes. At the anode the color stays the same, but the cathode loses the silver chloride layer and a pure silver surface appears after some time.

Discussion

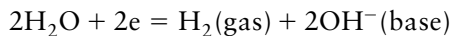
With platinum and carbon, an applied DC voltage does not necessarily lead to current flow. There must be energy barriers in the system, and a sufficiently high voltage must be applied to overcome this barrier. It is a non-linear system, not obeying Ohm's law. It can be shown that the bulk solution obeys Ohm's law, and therefore the energy barrier is not in the bulk, but near the electrodes. When the voltage is turned on, Na^+ ions migrate to the cathode and Cl^- ions migrate to the anode. But arrival at the electrodes does not lead to an exchange of electrons with the metal, a surface charge is built up opposing the external electric field, and the current stops. An electrode

is the interphase at which electronic and ionic conduction meets. Without DC current, there is no electron transfer, no chemical reaction and no faradaic current.

At the Cathode

With current flowing, anions and cations migrate to opposite directions. The simplest hypothesis dealing with a saline solution would be that Na^+ ions are discharged at the cathode, and Cl^- ions at the anode. It is not that simple, Na^+ ions are not discharged at the cathode. Sodium has a very small electronegativity, which means that it takes a large energy and a large negative voltage on the cathode to impose electrons on Na^+ ions. At much lower voltages two other processes start: reduction of dissolved neutral oxygen, and decomposition of water molecules. Both processes are linked with *non-charged species*, which are transported to the electron transfer sites by diffusion, not by migration. So in Fig. 2.1 there are two transport mechanisms: migration and diffusion. The reaction of non-charged species at the electrodes must not be overlooked, these species are charged or *ionized* (at least as one step) in the electrode reaction.

The concentration of dissolved oxygen is small, so the DC current from the oxygen reduction is not large. As long as our voltage supply is adjusted for a current lower than this current, the oxygen reduction current is sufficient. If a larger current is wanted, the voltage must be increased so that water is decomposed additionally. The water reaction at the cathode is:



Actually it is more complicated: the different versions of the hydrogen ion are active, for example the oxonium ion H_3O^+ .

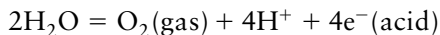
In conclusion, neutral metals and carbon do not have the ability to be reduced, so electrode material cannot be ionized at the cathode and enter the solution. Dissolved oxygen is reduced, at higher currents free hydrogen gas is also bubbled up and the solution near the cathode becomes basic. Na^+ need not be considered (but is necessary for the conductivity of the solution, so that the voltage drop in the solution is not too high). The positive silver ions of the silver chloride are neutralized, and little by little the AgCl layer is decomposed and pure silver appears on the surface. The color changes, but the color of AgCl is not so easy to define. AgCl is photosensitive, and in films exposed to light there are already grains of pure silver, which are gray or black of color.

At the Anode

The electrode reaction at the cathode was not due to the discharge of Na^+ . Is the current at the anode due to the discharge of Cl^- ions? Yes. Chloride is highly electronegative, but less energy is necessary for taking electrons from the chloride ions than from water molecules. Neutral Cl_2 gas is formed at the platinum anode. It does not react with platinum and leaves the area as gas bubbles. It *does* react with carbon and destroys the carbon surface. At the silver chloride surface it reacts with silver oxidized by the anode and forms more silver chloride. Ag^+ will not enter the

solution, if it does it will combine with Cl^- and form AgCl . In aqueous solution the solubility of AgCl is very low, only very small amounts will dissolve in the solvent, and it will soon precipitate.

OH^- ions may be discharged, but there are few of them and they do not contribute very much to the DC current. With large currents water may be decomposed, with oxygen leaving the area as gas bubbles according to:



If oxygen gas is developed, the solution turns acidic near the anode. The importance of this reaction depends on the current level and what current level the Cl^- concentration will take care of alone.

We may therefore conclude that silver chloride behaves rather differently from platinum and carbon. Silver undergoes an electrochemical reaction with one of the ions of the electrolyte (Cl^-), silver may be oxidized or silver ions reduced. The transfer of electrons oxidizing or reducing species at an electrode is called a *redox* process. *The results indicate that if we are to apply large DC currents to tissue, and we are to use noble metals as electrode material directly on the tissue, the passage of DC current is accompanied by the development of H_2 gas and a basic milieu at the cathode, and Cl_2 gas and perhaps oxygen and an acidic milieu at the anode.* However, in real tissue systems (not the model of Fig. 2.1), organic molecule redox systems will contribute to additional electrode reactions at low current levels.

What happens if we replace the DC voltage with a sinusoidal AC voltage? If the frequency is sufficiently high (e.g. 1 MHz), the migration processes in the bulk electrolyte will take place (back and forth), but no accumulation process or reactions will take place at the electrodes. If the frequency is very low (e.g. 0.1 Hz), the result will depend on the dimensions of the cell and the degree of reversibility of the reactions. If gas has time to bubble away, the process is certainly irreversible.

2.3. BULK ELECTROLYTIC DC CONDUCTANCE

According to the Arrhenius⁴ theory of *dissociation*, molecules of acids, bases and salts react with water molecules to form separate ions. Water *ionizes* the substances, and these ions give their solution the property of conducting electricity. Positive and negative ions free to migrate in the electric field contribute separately to the electric current flow, but because of different mobilities they do not carry equal portions of the current.

Environment of Ions

In aqueous solutions an ion is not alone. Two zones surround it: the ion attracts ions of opposite sign, and it attracts water molecules. A water molecule has a strong

⁴Svante August Arrhenius (1859–1927), Swedish physicist and chemist. 1903 Nobel prize laureate in chemistry on electrolytic dissociation theory.

electric dipole moment: even if its net charge is zero, water is a polar material. The process of solvent molecules forming a sheath around each electrolyte ion is generally called solvation. When the solvent is water, the process is called *hydration*. Hydration is strong because the water molecules have a large permanent dipole moment. The water molecular sheath stabilizes each ion and hinders ions of the opposite sign to approach so near to each other that they recombine: the substance stays dissociated and ionized. The hydration number is the average number of water molecules forming the sheath. Cations are usually less hydrated, and the hydration sheath less effectively covers large ions. Figure 2.2 shows the hydration process for a sodium ion in water. It is a statistical concept, so that *in average* there are more oriented water molecules (and other ions of opposite sign) near the Na^+ ion.

Hydration is the build-up of a sheath of *dipoles* around a central ion, owing to ion–*dipole* forces. According to Debye⁵–Hückel, the central ion is also surrounded by a slight excess of *ions* of the opposite charge sign, formed by ion–*ion* forces. They called this an *ionic atmosphere*. Both the hydration and the ionic atmosphere will increase the effective dimension and reduce the apparent charge of the center ion, and thus retard migration.

The ionic atmosphere is a statistical concept: within the *Debye length* from the central ion, there is an increased probability of finding an ion of opposite charge. A few Debye lengths (of the order of some tenths of nm) define a region of space charge where electroneutrality no longer holds. If the charge of an ion suddenly disappeared, it would take a time of the order of $1\ \mu\text{s}$ for the molecules to rearrange and the ionic atmosphere to disappear. This is an example of a *relaxation time*.

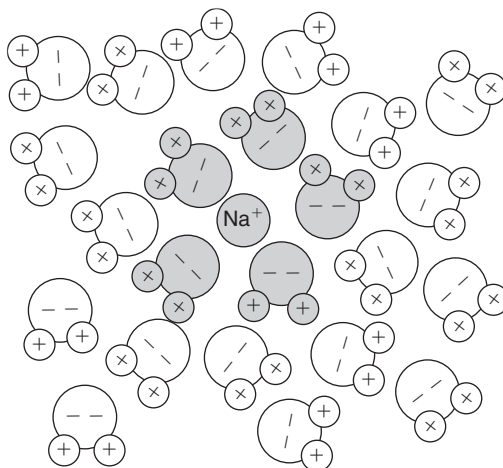


Figure 2.2 Na^+ ion hydrated by water molecules forming a hydration sheath around it.

⁵Peter Joseph Debye (1884–1966), Dutch/American physicist. 1936 Nobel prize laureate in chemistry on molecular structure and dipole moments.

Contributions to Ionic Conductivity

Kohlrausch⁶ showed that conductivity is composed of separate contributions from anions (−) and cations (+). The current density J (A/m^2) of a single anion–cation pair is:

$$J = (nzev)_+ + (nzev)_- = F c \gamma (\mu_- + \mu_+) E \text{ [A/m}^2\text{]} \quad (2.1)$$

$$J = \sigma E \text{ [A/m}^2\text{]} \quad (2.2)$$

Equation (2.2) is very important and fundamental; it is the Ohm's law version for volume conductors. It is valid under the assumption of a homogeneous and isotropic medium when the current density and E-field directions are coinciding. Note that current is not the quantity used in this version of Ohm's law, but current *density* J . As J may vary according to the local E-field strength, current must be found by integrating current density over a cross-sectional area. Current (A) is the sum of charges passing a freely chosen cross section (e.g. of a copper wire) per second (flux) while current density (A/m^2) is the sum of charges passing per *unit* area per second (flux density). Current is a scalar sum of charges per second passing some area not entering the equation (*scalar flux*), it has no direction in space. Current density is defined by an area oriented in space, and is therefore itself a vector in space (*vector flux density*).

The current density J of eq. (2.2) must be summed up with contributions from each negative and positive ion species. v is the velocity of the ion (m/s). γ is the activity coefficient: not all the electrolyte may be dissociated, and this is taken care of by the activity coefficient γ having a value between 0 and 1. Note that it may be difficult to find the activity coefficients of individual ion species because of electroneutrality: an electrolyte cannot consist of only anions or cations.

The contribution to the total conductivity will come from all free ions according to their concentration, activity, charge and mobility. The *transference number* of an ion species is its percentage contribution to the total conductivity.

In the bulk of a solution with free ions there is *electroneutrality*: in a volume V [m^3] the sum of charges is zero:

$$V \sum (nze)_+ + V \sum (nze)_- = 0 \quad (2.3)$$

If this were not the case, a space charge would build up driving excess ions out of the volume. During current flow, equal amounts of charge must enter and leave a solution volume. Electroneutrality is valid for a volume much larger than ionic dimensions. Electroneutrality does not prevail at boundaries with space charge regions (cf. Section 2.4.3 on electrical double layers).

The current density according to eq. (2.1) must be summed for all free ions present, for example for NaCl eq. (2.1 and 2.2) may be written as:

$$\sigma = F (c\gamma)_{\text{NaCl}} (\mu_{\text{Na}} + \mu_{\text{Cl}}) \text{ [S/m]} \quad (2.4)$$

⁶Friedrich Wilhelm Georg Kohlrausch (1840–1910), German physicist. Author of “Lehrbuch der Praktischen Physik.”

TABLE 2.4 Molar conductivity Λ_0 [Scm^2/mol] in aqueous solution at infinite dilution and 25°C

Cation	Λ_0	Hyd	Anion	Λ_0	Hyd
$\text{H}^+/\text{H}_3\text{O}^+$	350	—	OH^-	198	
Na^+	50	5	Cl^-	76	0
K^+	74	4	HCO_3^-	45	0
Ca^{2+}	119	10	CO_3^{2-}	72	0

Hyd is the average number of water molecules in the hydration sheath.

The *molar conductivity (equivalent conductance)* Λ is conductivity per mole of solute per volume:

$$\Lambda = \sigma/c = \gamma F(\mu_+ + \mu_-) [\text{Sm}^2/\text{mol}] \quad (2.5)$$

The molar conductivity is therefore a parameter directly linked with the mobility and not with concentration. The basic unit is (S/m) per (mol/m^3), or Sm^2/mol . The mobility μ is related to the random molecular collisions and corresponding frictional force (viscosity η) experienced by the migrating ion. Ideally, the frictional force \mathbf{f} is related to the hydrodynamic radius a of the ion according to Stoke's law:

$$\mathbf{f} = 6 \nu \pi \eta a [\text{newton}] \quad (2.6)$$

The bulk electrolyte solution obeys the linear Ohm's law (eq. 2.2). The force on a charge q in an \mathbf{E} -field is proportional to the electric field strength according to $\mathbf{f} = q\mathbf{E}$. The linear Ohm's law therefore shows that ions are not formed by the external field; they are in existence already without a field.

Equation (2.2) is valid also for DC, under the condition that electrochemical changes occurring at the electrodes do not spread to the bulk. σ is also considered frequency independent up through the whole kHz frequency range (Cooper, 1946).

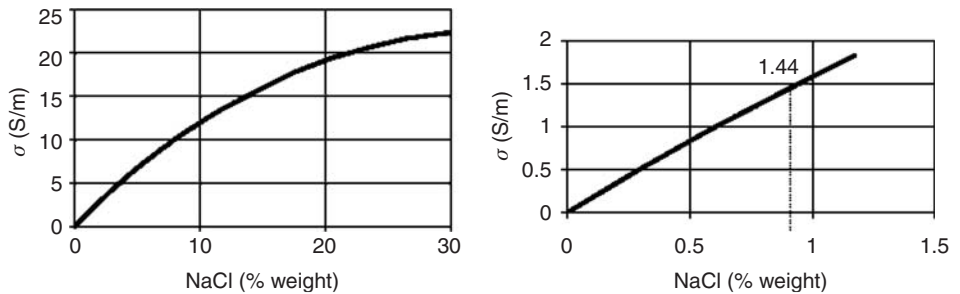
The diameter of many ions has been determined by X-ray diffraction of ionic crystals (dry), (Tables 2.1 and 11.2). From Table 2.4 we see that the number of water molecules bound in the sheath around an ion (the *hydration number*) has a certain correlation with the molar conductivity, and therefore according to eq. (2.5) to the mobility (Ca^{2+} value must be halved for this comparison). This is so because a stronger hydration increases the effective radius of the ion and therefore the friction, and also reduces the effective charge of the ion. Both hydration and the ionic atmosphere reduce the molar conductivity.

Electrolytic concentrations are in practice often given by weight (g), for example 0.9% NaCl in water meaning $9\text{g}/1000\text{g} = 9\text{g/L}$. From the relative atomic mass (Table 2.5), the molar concentration can be found. For instance, $23.0 + 35.5 = 58.5\text{g} = 1\text{mol NaCl}$. 0.9% NaCl is therefore equal to 154 mmol/L.

The conductivity of a given electrolyte solution can be found from the tables of molar conductivity, at least for low concentrations (Table 2.4).

TABLE 2.5 Relative Atomic Mass = Gram Weight per 1 mol (gram mole)

	Protons	Gram weight per mol		Protons	Gram weight per mol
H	1	1.0	F	9	19.0
Li	3	6.9	Na	11	23.0
B	5	10.8	Cl	17	35.5
C	6	12.0	K	19	39.1
N	7	14.0	Ca	20	40.1
O	8	16.0			

**Figure 2.3** Conductivity of NaCl aqueous solution (20°C).**Example**

The conductivity of 0.9% NaCl at 25°C is according to eq. (2.5):
 $\sigma = \Lambda c = (50 + 76) 0.0154 \times 10^{-1} = 1.94 \text{ [S/m]}.$

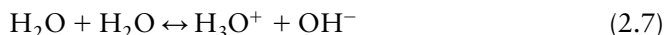
Figure 2.3 shows how the actual conductivity may be lower, because the dependence is not linear. Molar conductivity Λ_0 relates to the limiting value at low concentrations. For NaCl the relationship is quite linear up to the physiological concentration of 0.9% by weight. Sweat concentrations are somewhat lower, urine concentrations vary but may be higher, seawater concentrations are around 3.5%. Much higher concentrations are sometimes used for contact electrolytes (cf. Section 7.4.3).

At high concentrations the interaction between ions reduces their mobility. The ions are so tightly packed that their fields interact, for example so that ions of opposite charge form *ionic pairs* (with lower mobility, they become quasi-dipoles). This effect is dependent on solvent permittivity, because the lower the permittivity, the stronger the electrostatic force between charges and the formation of ionic pairs (eq. 3.1). Also higher kT gives less coherent ionic atmospheres. Higher temperature and permittivity therefore gives less friction and higher conductivity. According to the

*Onsager*⁷ theory, molar conductivity Λ is dependent on \sqrt{c} according to $\Lambda = \Lambda_0 - b\sqrt{c}$, where b is dependent on, for example, temperature and viscosity.

Conductivity of Water Itself

Water, hydroxyl and hydrogen ions have very special electrical properties. Water is strongly polar, but is also to a small extent an electrolyte in itself. From Table 2.7 we see that the intrinsic conductivity is low, but not zero. The small rest conductivity is due to a protonic self-ionizing process: there is a small statistical chance that a water molecule transfers one of its protons to another water molecule in the following way:



The traditional description of the hydrogen ion H^+ alone is not correct. Actually the proton, the hydrogen ion H^+ , cannot exist as such in water. Without the electron it only consists of the nucleus with a radius of perhaps 10^{-14}m , about four decades smaller than an ion with electrons in orbit. The electric field near the naked proton is extremely strong, and polar water molecules are immediately attracted, the proton is hydrated and the *oxonium* (also called *hydroxonium* or *hydronium*) ion H_3O^+ is formed. This is also strongly polar and attracts new water molecules forming H_5O_2^+ and H_9O_4^+ in a dynamic and statistical way. For simplicity, they will all be called a *hydrogen ion* in this book when it is not necessary to differentiate.

A small naked proton would have had a high mobility and therefore high molar conductivity. The oxonium ion is of more ordinary size, and so the molar conductivity actually measured should be in a normal range. However, hydrogen (and OH^-) ions have irregular high molar conductivity (Table 2.4). This is due to a special *proton hopping* mechanism which is different from ordinary migration (Grotthuss mechanism) illustrated in Fig. 2.4. The protons are transferred by hopping directly from water molecule to water molecule by a tunneling effect instead of being slowed by viscous forces. The speed limiting process is believed to be a

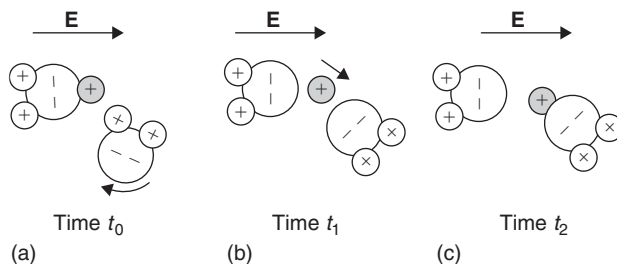


Figure 2.4 Proton hopping conductance, same molecules at three different moments: (a) water molecule rotation; (b) hopping; (c) new proton position.

⁷Lars Onsager (1903–1976), Norwegian/American chemist. 1968 Nobel prize laureate in chemistry for his work on irreversible thermodynamics.

necessary rotation of a neighbor water molecule before it can accept a proton; a statistical process. The proton can be considered to hop along a string of water molecules with a statistical net flow in the direction of the E-field. Parallel to the hopping conductance there is of course the ordinary migrational conductance.

Because of their high molar conductivity, the hydrogen ions will often dominate the conductance found. Because of electroneutrality there are, for instance, equal numbers of H^+ ions and Cl^- ions when the strong acid HCl dissociates. But the electrolytic conductivity contribution from the hydrogen ions is about 5 times as large as that of Cl^- . From Table 2.4 it is seen that for NaCl the contribution is largest from the Cl^- ions, for KCl the contributions from each ion are approximately equal.

Conductivity of Weak Acids

The electrolytes do not only determine conductivity, they are also strongly related to the acid–base balance and the $\text{pH} = -\log[\text{H}_3\text{O}^+]$ of the tissue; $[\text{H}_3\text{O}^+]$ here means the concentration in mol/L.

With salts and strong acids, water dissociates all molecules. With weak acids the situation is different, some of the acid molecules stay undissociated. An example is the conductivity due to dissolved CO_2 gas in water. Some of the CO_2 physically dissolved is transformed to H_2CO_3 , which is a weak acid. The Guldberg–Waage^{8,9} law (mass action law) is useful for the calculation of ionic concentrations in such cases. In its original form it states that the rate of a chemical reaction is proportional to the *mathematical product* of the mass of the reacting substances, and that equilibrium can be expressed by an equilibrium constant characterizing the chemical reaction. In the particular case of a dissociation process, electroneutrality also imposes the ionic concentrations to be equal (for unity valence ions). In the case with dissolved CO_2 the equilibrium dissociation constant can be set to $K_1 = 10^{-6.3}$; the Guldberg–Waage law therefore gives:

$$[\text{H}_3\text{O}^+][\text{HCO}_3^-]/[\text{H}_2\text{CO}_3] = K_1 = 10^{-6.3}$$

For such a weak acid, a doubling of the concentration $[\text{H}_2\text{CO}_3]$ leads to $\sqrt{2}$ increase in $[\text{H}_3\text{O}^+]$, because $[\text{HCO}_3^-]$ must also increase by $\sqrt{2}$ (electroneutrality) so that the product increases by 2. Because of the high molar conductivity of hydrogen ions, the total conductivity of such a solution is dominated by the hydrogen ions and is therefore roughly proportional to $\sqrt{[\text{CO}_2]}$ or the square of the partial pressure of the carbon dioxide gas in equilibrium with the solution.

Accordingly, when water is in equilibrium with air in nature, H_3O^+ and HCO_3^- ions will contribute to an additional DC conductivity as well as a reduction of pH. Actually the reduction in pH is substantial, the pH of pure (non-polluted) water is down to 5.7 (acid) when in equilibrium with the normal atmospheric CO_2 concentration levels (0.03%).

⁸Cato Maximilian Guldberg (1836–1902), Norwegian mathematician, particularly interested in physical chemistry.

⁹Peter Waage (1833–1900), Norwegian chemist, particularly interested in practical applications of chemistry.

Water itself is very weakly self-ionized, with a low equilibrium constant K_w :

$$[\text{H}_3\text{O}^+][\text{OH}^-] = K_w = 10^{-14}$$

For electroneutrality $[\text{H}_3\text{O}^+] = [\text{OH}^-]$, which then is equal to 10^{-7} , corresponding to $\text{pH} = 7$. The conductivity according to eq. (2.5) is:

$$\sigma = (\Lambda_+ + \Lambda_-)c = (350 + 198) \times 10^{-7} \times 10^{-1} = 5.5 \times 10^{-6} \text{ [S/m]}$$

cf. Table 2.7.

Other Factors Influencing Conductivity

The *temperature* dependence of conductivity of most ions in aqueous solution is about $+2.0\%/^\circ\text{C}$. This high temperature dependence results from the decrease in viscosity of water with temperature. The temperature coefficient of H_3O^+ ($1.4\%/^\circ\text{C}$) and OH^- ($1.6\%/^\circ\text{C}$) are important exceptions, and are the result of the different conduction mechanisms of these ions. Viscosity increases with increasing *pressure*, and the conductivity is reduced.

The conductivity increases at high *frequency* ($>3\text{--}30\text{ MHz}$, Debye–Falkenhagen effect). It takes about $0.1\text{--}1\text{ ns}$ to form an ionic atmosphere, the time is dependent on the ion concentration. The literature is not clear as to the conductivity frequency dependence of electrolytes such as NaCl , but Cooper (1946) found no variations in the concentration range $1\text{--}4$ (weight%) and frequency range $1\text{--}13\text{ MHz}$.

As shown, pure de-ionized water has a low conductivity, but the permittivity is constant up to the lower GHz range with a relaxation frequency around 20 GHz (Section 4.1.1).

Special Electrolytes

Some substances are completely ionized in water (strong acids), others are only partly ionized, for example weak acids. Water is often necessary for the ionization or molecule split; pure HCl liquid is for instance an insulator. Many substances dissolved in water are not ionized at all, and therefore do not contribute to electric conductivity. They are true non-electrolytes, such as sugar/glucose. The molecules of such substances are not split up (ionized, dissociated) by water. Some may have a symmetrical distribution of charges with the center of positive and negative charges coinciding. However, many molecules have centers not coinciding, forming permanent dipoles with zero net charge, such substances are called *polar*. Water itself is polar, and actually a substance has to be polar in order to be soluble in water.

In a solution with colloidal particles a charged double layer will surround each particle, and the particle may be regarded as a macro-ion. The colloidal particles free to migrate contribute to the solution's electrical DC conductance and may be regarded as a *colloidal electrolyte*. Particles are called colloidal when two of the dimensions are in the range $1\text{ nm}\text{--}1\text{ }\mu\text{m}$ (the third dimension does not have this constraint, e.g. a very thin string).

Electrolyte classification

NaCl as a dry salt at room temperature is not an electrolyte. The DC conductance is negligible, still the Na and Cl atoms are ionized, but “frozen” so that they cannot migrate.

NaCl dissolved in water is the true electrolyte, and the Na and Cl ions are split and free. Even if NaCl is the true electrolyte, the whole electrolyte solution is often also called just “the electrolyte.”

A *solid electrolyte* is also possible. In liquids, ions generally are more free to move (have a higher mobility) than in solids. Solid electrolytes at room temperature therefore have a relatively low conductivity.

AgCl is an important molecule for electrode surfaces. The chloride ions Cl^- are bound, but the silver metal ions Ag^+ are genuine charge carriers giving a certain electrolytic ionic conductivity.

The dry glass core in a pH electrode exhibits solid electrolytic conductance, not semiconductive. The electrode is proton sensitive, but the small conductivity in the glass core stems from ions of Li^+ , Na^+ and K^+ , which have mobilities 10^3 – 10^4 larger than the protons. Water is absorbed in the leached surface layers of the glass, however, and there the proton mobility is high and contributes to local DC conductance in an important way.

NaCl as a solid crystal has atoms in ionized form. But neither the Na^+ nor the Cl^- ions nor any electrons are free to migrate (at room temperature). There is no DC conductivity: NaCl is an insulator. When solid NaCl is dissolved in water, water splits the NaCl molecules into free Na^+ and Cl^- ions: NaCl is *dissociated*. NaCl is the electrolyte when dissolved in water, but we can hardly call solid NaCl an electrolyte, even if its atoms are in ionized form. However, if NaCl is heated to 800°C it melts, the ions are free to migrate with small friction (high mobility), and we have a strong *ionic liquid* or *fused electrolyte*.

There are also *mixed conductors* with both ionic and electronic conductance. The sulfides, selenides and tellurides of silver and lead are examples of this. New plastic materials with ionic conductance have been discovered in polymer chemistry. Nafion is a polymer with ionic conductivity; it is already much used in multigas analyzers in anesthesia, where the special high permeability to water is useful.

Some polymers have mixed electronic and ionic conductivity, and some are purely electronic conductors with free electrons like a metal or electrons locally linked to centers with electron-donor properties. Carbon as a most basic element for all biochemistry, is a very special element that deserves attention also as an electrode material. In the form of graphite it is an electronic conductor, but as diamond it is an almost perfect insulator.

Proteins in the body liquids may be considered as a colloidal electrolyte solute in a water solvent. Contact with water is the natural state of a protein. In more or less

TABLE 2.6 Concentration of Electrolytes in Body Liquids (meq/L) is Ion Concentration in Milliequivalents (mmole \times valency z) per Liter

	Cations (meq/L)		Anions (meq/L)		
	Plasma	Intracellular		Plasma	Intracellular
Na ⁺	142	10	Cl ⁻	103	4
K ⁺	4	140	HCO ₃ ⁻	24	10
Ca ²⁺	5	10 ⁻⁴	Protein ⁻	16	36
Mg ²⁺	2	30	HPO ₄ ²⁻ + SO ₄ ²⁻ + organic acids	10	130
H ⁺ (pH = 7.4)	4 \times 10 ⁻⁵	4 \times 10 ⁻⁵			
Sum	153	180	Sum	153	180

0.9% NaCl is 154 mmol/L.

dry form a protein loses some of its electrolytic character; it loses the charged double layer on the surface, and behaves electrically very differently from protein with water. Such materials may well be mixed conductors: electronic in the dry state, and ionic with water content. Keratin is a more or less dry protein found in the natural state of not-more-living biological materials such as hair, nail and stratum corneum. The water content of such materials is dependent on the relative humidity of the ambient air. The question of ionic or electronic conductivity in proteins is important, and an electronic conduction mechanism must be considered in many cases.

Body Liquid Electrolytes

The by far most important ions for extracellular conductance are Na⁺ and Cl⁻ (Table 2.6). Note that free protein in plasma are charge carriers with a negative charge (anions), and in this context can be regarded as macro-ions and a conductance contributor. This charge is also the basis of DC electrophoresis as an important analytical tool in clinical chemistry (Section 2.4.5). In order to maintain electroneutrality, increased protein concentration must increase the concentration of cations or reduce the concentration of other anions. The anion HCO₃⁻ is the bicarbonate related to the transport of carbon dioxide (CO₂) in the blood. A change in, for example, bicarbonate concentration (anion) will therefore have consequences for the cation concentration.

Ionic and Electronic Conduction with Respect to Semiconductor Theory

The charge carriers in metals are electrons that are free to migrate in the energy band called the conduction band (Fig. 2.5).

In semiconductors there is a special valence energy band under the conduction band. With pure (intrinsic) semiconductors the energy levels in between are forbidden levels, and at room temperature very few electrons statistically have sufficient

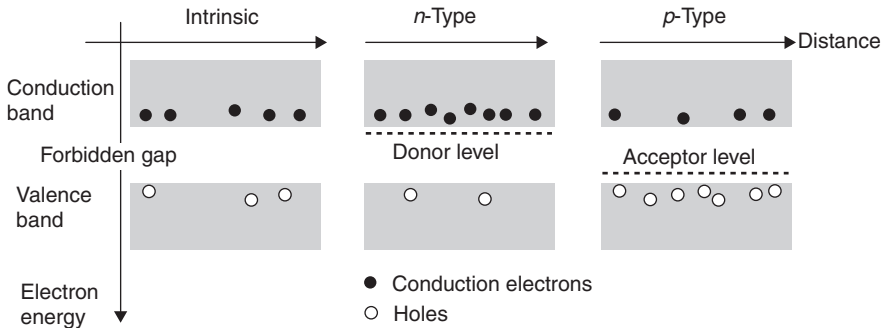


Figure 2.5 Energy levels in a semiconductor without (left) and with impurities. Local impurities create local energy levels (energy wells) as local reservoirs in the forbidden energy gap.

energy to cross the forbidden band and reach the conduction band; the conductivity is low. The energy gap is, for example, 0.7 eV (germanium) or 1.1 eV (silicon) or 5.2 eV (diamond, an insulator).

However, with *local impurities* in the material, *local* energy centers may exist in the forbidden gap. Here electrons reside on energy levels that may be characterized as local energy *wells*. With a certain amount of added energy electrons can come up from the well and reach the conduction band (*n*-type impurities). This can increase conductivity considerably (extrinsic conduction). According to the nature of the impurities, this added conduction may be by electrons or holes as charge carriers.

The idea of a possible semiconductive mechanism (electrons and holes) in biomaterials is old, as illustrated by the book by Pethig (1979). Later Takashima (1989) did not mention semiconductivity as a possible mechanism. Indications of an electronic, semiconductive conduction for the DNA molecule have appeared again (Fink and Schönenberger, 1999). Such experiments are performed under non-physiological conditions in vacuum, which implies that every water molecule free to do so has disappeared.

Ions do not obey these laws of semiconductors. However, the concept of local energy wells can also be adapted to ionic conduction. Debye (1929) proposed a model where an ion may be translocated between a pair of neighboring energy wells by an applied electric field. With an applied AC field, an ion can be made to hop between these two wells.

Materials Classified According to Conductivity

Materials are often classified according to their DC conductivity (Table 2.7): conductors, semiconductors (electronic), and insulators. According to Eq. 2.1, conductivity is determined both by the concentration of the charge carriers n and their mobility μ . For electronic conductors (charge carriers: electrons) this classification is based on energy levels and Fermi–Dirac statistics of the free electrons. A division between metals and semiconductors is sometimes based on the temperature coefficient of the conductivity σ : semiconductors (as for ionic conductors) have a positive $d\sigma/dT$, while metals have a negative $d\sigma/dT$.

TABLE 2.7 Electronic (e) or Ionic (i) DC Conductivity σ at 20°C

		σ [S/m]
Superconductors (low temperature)	e	∞
Silver	e	61×10^6
Copper	e	58×10^6
Aluminum	e	35×10^6
Steel (hard)	e	2×10^6
Mercury	e	1×10^6
Coal	e	17×10^3
Graphite	e	100×10^3
NaCl, fused, 800°C	i	300
NaCl in water, 25%	i	22
NaCl in water, 5%	i	7
NaCl in water, 0.9% 37°C	i	2
NaCl in water, 0.9%	i	1.3
Whole blood 37°C	i	0.7
Muscle, 37°C	i	0.4
Germanium (pure semiconductor)	e	2
Silicon (pure semiconductor)	e	300×10^{-6}
Bone, living	i	10×10^{-3}
Tooth (human enamel)	i?	5×10^{-3}
Ethyl alcohol	i	330×10^{-6}
AgCl	i	100×10^{-6}
Water, de-ionized	i	4×10^{-6}
Bone, dry	e?	100×10^{-12}
Transformer oil	i?	10×10^{-12}
Mica	e?	10×10^{-15}
PTFE (teflon)	e	10×10^{-15}
Diamond	e	10×10^{-15}

For ionic conductors the classification is a little more problematic; they are in the conductivity range of pure semiconductors, but the charge carriers and therefore the conduction mechanism is very different. It is often found with liquid and solid electrolytes that the difference in conductivity is the result of different *mobilities* and not so much of different number of charge carriers.

2.4. INTERPHASE PHENOMENA

We have pointed out that the processes in the bulk of the solution (*ionics*) are very different from the processes at the electrodes (*electrodics*). Since tissue is the material of interest and from a number of perspectives it is electrolytic, the field of bioimpedance and bioelectricity is much concerned with ionics. On the other hand tissue is full of

membranes, and each membrane shows distinct surface phenomena. The smaller the cells, the more important is the surface phenomena.

In addition the electrodes also form interphases with the tissue. The electrodes usually represent tools only, and our main interest is to be able to minimize or at least control their influence on the tissue data. With current carrying electrodes, the polarization processes represent special interphase phenomena.

2.4.1. Faraday's Law

In the solution there is a two-way flow of ions and there are charge carriers of both signs. In the metal wires of the electrodes there is only one type of charge carriers of one sign, the electrons. The charge of one electron is exactly equal to that of one proton (with opposite sign): 1.6×10^{-19} C, the smallest known charge called the *elementary charge*.

In the solution the current spreads out from the current carrying electrodes, and we must use *current density* (ampere/m²) as quantity instead of current (cf. eq. 2.3). A *flux* is the flow rate through a cross-sectional area, so current density is a flux density. But the total sum of ionic charges passing through the solution is the current density integrated over the whole cross-sectional area, and per second this must equal the electronic current I in the external electrode wire.

A sum of electric charges q is also a *charge* and is also called a *quantity of electricity* Q , with the unit [coulomb]. If 1 A flows through a cross-sectional area in 1 second, 1 C has passed. Faraday¹⁰ found that the reaction products are proportional to the quantity of electricity passed. The Faraday constant F is the charge of 1 mol of electrons. 1 mol is the number 6×10^{23} , and as the elementary charge is 1.6×10^{-19} C the Faraday constant $F = 96472$ C/mol. *Faraday's law of electrolysis* links the amount of reaction products at the electrode to a quantity of electricity Q :

$$M = Q/Fz \text{ [mol]} \quad (\text{Faraday's law}) \quad (2.8)$$

where M is the substance produced and z is the valency of the element produced.

Faraday's law of electrolysis defines the term *electrolytic* as follows: an electrolytic system is a system that basically is characterized by Faraday's law. A current creating a reaction at an electrode according to Faraday's law is called a *faradaic current*.¹¹ The quantity of electricity may be obtained with a DC current or a current pulse. A DC current implies faradaic current only. A pulse current has an additional capacitive, non-faradaic current component.

¹⁰Michael Faraday (1791–1867), English physicist and chemist (natural philosopher), found the laws of electromagnetic induction and of electrolysis. A self-educated man who knew very little mathematics.

¹¹*Faradic* current is the pulse current from an induction coil used for muscle stimulation.

2.4.2. Migration and Diffusion

The electrode is the final boundary for ionic migration. Here some of the ions started, and here they meet a physical hindrance. The metal of an anode may furnish metal ions to the solution, crossing the interphase.¹² Depletion or accumulation of matter and charge may occur at the electrodes, as well as chemical reactions. An electrode may also exchange electrons with *neutral species*, for example the reduction of dissolved oxygen at a cathode. The transport of neutral species in the bulk of the electrolyte is not by ionic migration, but by a diffusion transport process caused by a concentration gradient. *Diffusion may be an as important transport mechanism as migration in an electrolytic cell.*

Equations (2.1) and (2.2) are to be interpreted according to the kinetic molecular theory of the transport properties of liquids. The charge carriers do not move in an orderly, linear fashion through the liquid. *Diffusion* is the process resulting from random motion of molecules by which there is a net flow of matter from a region of high concentration to a region of low concentration. This process is related to the concepts of Brownian motion, molecular collisions and mean free path between collisions. The *migration* of charge carriers in an electric field may be regarded as a special case of diffusion caused by an external influence, not driven by an internal concentration gradient. The transport of charged molecules/ions may be due both to concentration gradients and electric fields; *electrodiffusion* is the general term for both these transport processes. The migrational part is dependent on the electric field. In order to reduce the migrational effect, an indifferent electrolyte not intervening in the process to be studied may be added to increase conductivity and reduce the electric field. Generally transport caused by electricity is classified as *electrogenic* transport.

Molecular diffusion is described by *Fick's laws*. Consider a simple system in the form of a compartment with unity width and height dimensions, and a concentration gradient in the infinite length x -direction. Fick's first law is:

$$M = -D \frac{\partial c}{\partial x} \quad [\text{mol/m}^2\text{s}] \quad (2.9)$$

where M is the molar flux density (mol per s and m^2) and D is the diffusion coefficient (m^2/s). The minus sign indicates that the transport is toward *lower* concentration. During stationary diffusion, for example in a tube, eq. (2.9) shows that a linear concentration will be set up in the diffusion zone out from the electrode surface. Fick's second law is:

$$\left(\frac{\partial c}{\partial t} \right)_x = D \frac{\partial^2 c}{\partial x^2} \quad [\text{mol/m}^3\text{s}] \quad (2.10)$$

Warburg solved this equation already in 1899, finding the concentration waves into the electrolyte at a distance from an AC-polarized electrode surface (cf. Section 2.5.3).

¹²*Interface* is a surface that forms the boundary between two materials (sharp transition). *Interphase* is diffuse transition zone between two phases (e.g. solid/liquid).

Here is another example: consider a diffusion process starting in a specified compartment with an infinitely thin (x -direction) band of solute S (mol per unit width y and depth z) released in the middle of the compartment at $x = 0$ and $t = 0$. By solving Fick's second law under these boundary conditions, the concentration as a function of position x and time t is:

$$c(x, t) = \frac{S}{\frac{x^2}{e^{4Dt}} \sqrt{4\pi Dt}} \quad [\text{mol/m}^3] \quad (2.11)$$

The initial conditions correspond to $c(0, 0) = \infty$. \sqrt{Dt} has the dimension of meter, and corresponds to the net distance diffused by a molecule in 1 second. Such time dependence is due to the random walk of the molecule. With time the solute spreads out, and the concentration at the band position ($x = 0$) decreases according to $1/\sqrt{t}$. At a distance x the concentration at first is extremely small, but then reaches a maximum and thereafter follows the falling and uniform concentration around the origin (Fig. 2.6). With $t \rightarrow \infty$, $c \rightarrow 0$ because the compartment is considered infinite in the x -direction. An electrolytic cell of finite dimensions corresponds to different boundary conditions, and a different equation. This is of importance when considering increasing t and the approach toward DC conditions. When the diffusion reaches the boundary of the cell compartment in the x -direction, the process no longer follows eq. (2.11). With diffusion-controlled processes, new frequency-dependent parameters enters at very low frequencies with a measuring cell of small dimensions (cf. the Warburg impedance, Section 2.5.3).

Equation (2.11) and Fig. 2.7 illustrate the diffusion process from an electrode surface positioned at $x = 0$, whether it is the export of reaction products or the

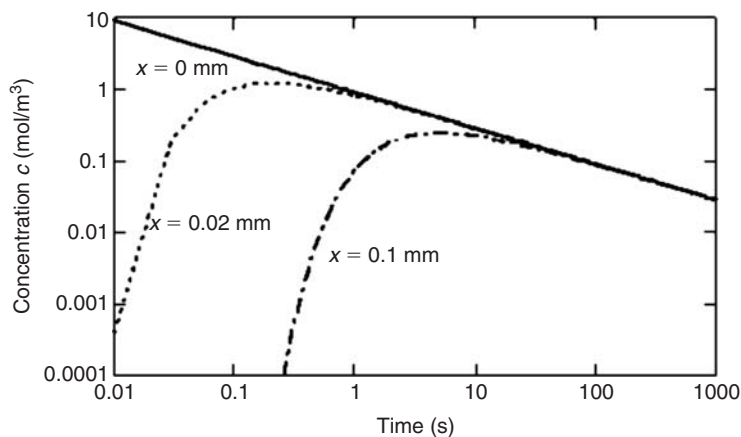


Figure 2.6 Diffusion of a thin strip of solute from position $x = 0$ at $t = 0$ according to eq. (2.11). Concentration as a function of time with position as parameter. $D = 10^{-9} \text{ m}^2/\text{s}$, $S = 10^{-4} \text{ mol/m}^2$.

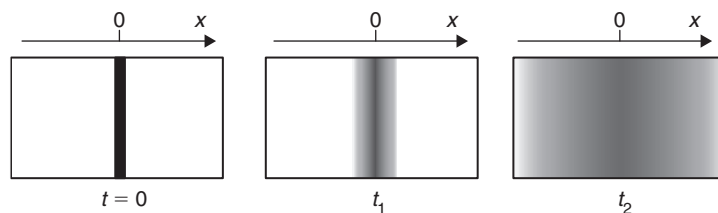


Figure 2.7 Spread of a thin strip of solute by pure diffusion.

import of reactants the other way. Equation (2.11) also illustrates that physical processes in electrochemistry do not necessarily follow exponential laws. This is an important reason why it is often difficult to model electrolytic cells with ideal electronic components.

The diffusion constant D in aqueous solution is of the order of 10^{-11} (m^2/s) for large molecules to 10^{-9} for small molecules. This means that the spread of just 1 mm in liquids will take hours for larger molecules, whereas small molecules will diffuse about 0.1 mm in 1 second. In gases the values of D are higher. For instance, for water molecules in air $D = 0.24 \times 10^{-4}$ at 1 bar and 20°C , and without any convection water molecules will therefore have moved about 5 mm in 1 second. The spread or mixture of gases in a room across a meter or more is therefore purely convection controlled.

2.4.3. The Electric Double Layer, Perpendicular Fields

At the electrode/liquid interface the conversion from *electronic* to *ionic* conduction occurs. The electrode metal is the source or sink of electrons, and *electron transfer* is the key process whereby the electrode exchanges charges with the arriving ions, or ionizes neutral substances (a second mechanism of charge transfer is by oxidation of the electrode metal, the metal leaves the surface as charged cations and enters the solution.) Without electron transfer there is no chemical electrode reaction, and no DC electrode current and no faradaic current. In the solution at the electrode surface an electric *double layer* is formed as soon as the metal is wetted. Electron transfer takes place somewhere in that double layer.

In all interphases, such as the transition zone between the metal of an electrode and the electrolyte, tissue or gel, or at a cell surface, there will be a non-uniform distribution of charges. Hence there will be an electrical potential across the interphase according to the Poisson equation (8.5). This effect is particularly pronounced at the interphase between a solid and a polar medium, like for example water, where the surface charges of the solid will attract counterions from the polar medium. When the polar medium is liquid and the ion mobility is high, the formation of an electric double layer will therefore take place in the liquid phase.

In this chapter the double layer charge will be treated as a function of the distance *perpendicular* to the surface. In Section 2.4.4 we will treat counterion movements *lateral* along the surface.

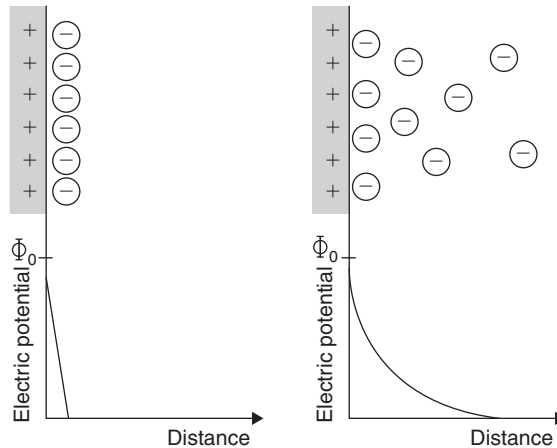


Figure 2.8 Helmholtz' (left) and Gouy–Chapman's (right) model of the electric double layer and electric potential as a function of distance from the electrode surface.

Simple Helmholtz Layer

The double layer can be thought of as a molecular capacitor, where one *plate* is represented by the charges in the metal, and the other *plate* by the ions at a minimum distance in the solution. The distance between the “plates” is of the order of only 0.5 nm, so the capacitance values are enormous. This simple model of the electric double layer was introduced by Helmholtz in 1879, and is *valid only for rather high concentration* electrolyte solutions (Fig. 2.8(left)). In this simplest model the double layer is depleted from charges. In more dilute solutions the transition will not be so abrupt and the thickness of the double layer will *increase*. The thickness is related to the distance from the metal surface at which the ions can escape to the bulk by thermal motion. In that case, the counterion atmosphere will be more like the ionic atmosphere around an individual ion, and this is commonly referred to as the *diffuse electric layer*.

General Theory of Gouy–Chapman

In the combined theory of Gouy and Chapman, the exchange of counterions between the double layer and the bulk solution due to thermal motion is taken into account. Both coulombic forces and thermal motion hence influence the equilibrium distribution of counterions in their model for the diffuse double layer (Fig. 2.8(right)).

The assumptions for their theory are, among others:

1. The surface charge is continuous and uniform.
2. The ions in the solution are point charges.

The electric potential in the double layer is given by the Poisson equation:

$$\nabla^2 \Phi = - \frac{q_{vf}}{\epsilon} \quad (2.12)$$

where Φ is the electric potential, q_{vf} is the volume density of free charges and ε is the permittivity of the medium, and furthermore by the Boltzmann equation:

$$n_i = n_0 \exp\left(\frac{-W_{el.}}{kT}\right) \quad (2.13)$$

where n_i is the concentration of an ion “ i ” at a given point, determined by coulombic forces and thermal motion, n_0 is the concentration in the bulk solution and the electric work $W_{el.} = z_i e \Phi$, where z_i is the charge per ion. The Poisson equation for the diffuse double layer will then be:

$$\nabla^2 \Phi = \frac{2ze n_0}{\varepsilon} \sinh(ze\Phi/kT) \quad (2.14)$$

We then introduce:

$$\kappa = \sqrt{\frac{2z^2 e^2 n_0}{\varepsilon kT}} \quad [1/m] \quad (2.15)$$

where $1/\kappa$ is referred to as the thickness of the double layer (also called the Debye length), and is used in the decision between simplifications of eq. (2.14). In physiological electrolyte solutions it is about 10 nm, smaller the higher the electrolyte concentration.

Debye–Hückel Approximation

The Debye–Hückel approximation may be used if the surface potential is small:

$$\Phi_0 \ll \frac{kT}{ze} \quad (2.16)$$

(approximately 25 mV for a monovalent electrolyte at 25°C). The simplification will then be made by replacing $\sinh(x)$ with x .

For a spherical double layer, the solution using Debye–Hückel approximation will be:

$$\Phi = \Phi_0 \frac{a}{r} \exp[-\kappa(r - a)] \quad (2.17)$$

For a flat double layer, that is, when $a \gg 1/\kappa$, the solution will be

$$\Phi = \Phi_0 \exp(-\kappa x) \quad (2.18)$$

General Theory of Stern

The theory of Gouy–Chapman becomes inadequate when κ and/or w_0 is large. The theory of Stern takes the finite size of the counterions and their binding properties at the surface into account. The diffuse layer is divided into an inner layer (the Stern layer) and an outer layer (the Gouy layer), as shown in Fig. 2.9. The Stern layer includes any adsorbed layer of ions. It is separated from the Gouy layer at the

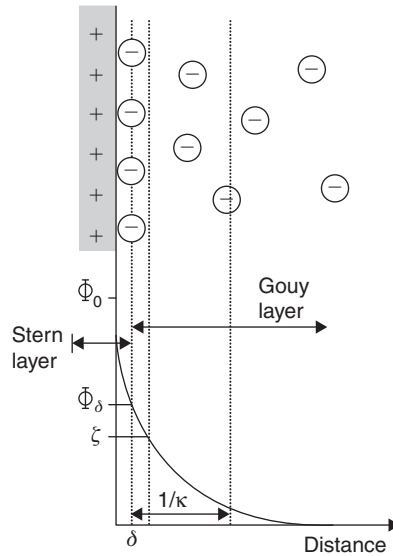


Figure 2.9 Stern's model of the diffuse electric double layer.

Stern plane at a distance δ from the surface. This distance corresponds roughly to the radius of a hydrated ion. The ions are adsorbed in the Stern layer according to the Langmuir adsorption isotherm. The theory of Gouy–Chapman is still applicable in the Gouy layer, but Φ_0 is replaced by Φ_δ which is the potential at the Stern plane. In case of strong specific adsorption in the Stern layer, Φ_0 may be smaller than Φ_δ , or they may have opposite polarity. The potential at the Stern plane, Φ_δ , may in most cases be assumed to be equal to the so-called zeta (ζ) potential, which is the electrokinetic potential which can be determined experimentally by means of, for example, electrophoresis or streaming potential measurements. The zeta-potential is the potential at the shear plane between the charged surface and the liquid, that is the potential at the boundary of, for example, a moving particle with its adsorbed ions. The Stern theory is complicated and will not be treated in any detail in this book. Stern theory should be used when the surface potential is high, or when the solution is concentrated so that a significant part of the potential drop occurs in the Stern layer. Gouy–Chapman theory may be adequate also at higher concentrations if the surface potential is small.

Grahame made a further division of the Stern layer into the inner Helmholtz layer and the outer Helmholtz layer. These layers are separated by the inner Helmholtz plane at a distance from the surface corresponding to the radius of non-hydrated specifically adsorbed ions. These ions are smaller than the counterions, and the inner Helmholtz plane is hence located between the Stern plane and the surface. The outer Helmholtz layer is limited by the outer Helmholtz plane, which is identical to the Stern plane.

2.4.4. The Electric Double Layer, Lateral Fields

Schwarz Theory for a Suspension of Spheres

Schwarz wanted to use the theories of electric double layers to describe the measured α -dispersion of particle suspensions. He considered the case of an electric double layer at the surface of a spherical particle as shown in Fig. 2.10.

The counterions will be electrostatically bound to the surface charges of the sphere, but will be free to move laterally along the surface. When an external field is applied, the positive counterions in Fig. 2.10 will move toward the cathode, but without leaving the surface of the sphere (this polarization effect is largely exaggerated in Fig. 2.10). The re-establishment of the original counterion atmosphere after the external field is switched off will be diffusion controlled, and the corresponding time constant according to Schwarz theory is:

$$\tau = \frac{a^2}{2D} \quad (2.19)$$

where $D = \mu kT/e$ and a is the particle radius.

Later improvements of Schwarz Theory

Schwarz theory provides a practical tool for analyzing measured data, but the theory has been criticized for neglecting the diffusion of ions in the bulk solution near the surface. Efforts have been made by, among others, Dukhin, Fixman, and Chew and Sen to employ Gouy–Chapman theory on particle suspensions, but the resulting theories are very complex and difficult to utilize on biological materials. Mandel and Odijk (1984) have given a review of this work.

Simplified models that use the Gouy–Chapman theory have been presented by, for example, Grosse and Foster (1987), but the assumptions made in their theory limits the utility of the model.

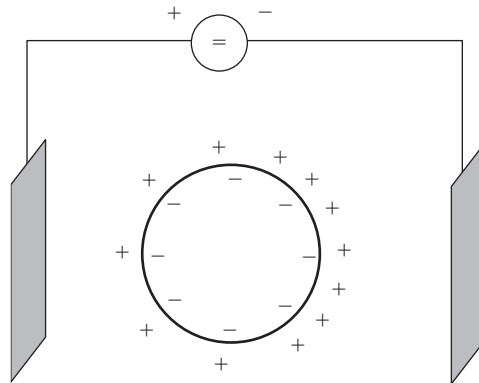


Figure 2.10 Counterion polarization near the surface of a spherical particle.

Effect of Hydration and Specific Adsorption

Hydration of ions is due to the dipole nature of water. In the case of a cation in water, the negative (oxygen) end of the neighboring water molecules will be oriented toward the ion, and a sheet of oriented water molecules will be formed around the cation. This sheet is called the primary hydration sphere. The water molecules in the primary hydration sphere will furthermore attract other water molecules in a secondary hydration sphere, which will not be as rigorous as the primary sphere. Several sheets may likewise be involved until at a certain distance the behavior of the water molecules will not be influenced by the ion.

Specific adsorption (chemisorption) is the process of ions that are chemically bound to, for example, the metal surface of an electrode. These ions are not counterions, and are hence bound to the surface by chemical bonds and not primarily by coulombic (van der Waals) forces. Specifically adsorbed ions will not be hydrated since the layers of water molecules would impede the chemical interaction with the solid surface. Counterions may be hydrated, however, and the corresponding effect will be that the counter charges are moved away from the solid surface. Models have also been presented which include the possibility that the solid surface is also hydrated, thus involving a monolayer of water molecules between the surface and the counterions.

The adsorption or desorption may occur at very sharply defined potentials, and result in a charging current in the external measuring circuit. The process may be quick or slow, and therefore frequency dependent in the case of AC. As long as there is no electron transfer, there is no electrode reaction and no faradaic current, the current is capacitive (with losses).

The hydration sheet on an electrode surface and around an ion will not stop the electrode process, but will increase the activation energy of the electron transfer. The reason being that the average distance of the water molecules from the ion will change when the ion, for example, accepts an electron. The reduced charge of the ion will increase the distance of the hydration sheet, and additional energy is required to stretch the sheet to its new position.

The increased activation energy will increase the voltage needed to sustain a faradaic current, and also influence on the faradaic impedance of the electrode (both the electron transfer resistance and the slow process impedance will be affected – see Section 2.5). It is moreover likely that hydration of the electrode surface and of the counterions will reduce the double layer capacitance.

The effect that specifically adsorbed ions may have on the overall electrode impedance is complex and only a brief discussion will be given here. If the ion is involved in the electron transfer process, a multistep reaction must be taken into account, where, for example, an electron is transferred from an ion in the solution to the adsorbed ion, and subsequently transferred from that ion to the electrode surface. This will most likely change the activation energy for the electron transfer, and hence influence on the faradaic impedance of the electrode as discussed above. Adsorbed species that do not take part in the electron transfer like, for example, neutral molecules, may block reaction sites on the electrode surface and thereby affect the faradaic current. The double layer capacitance will also be reduced as a result of reduced effective electrode area.

2.4.5. The Net Charge of a Particle

The charged double layer at the surface of colloidal particles (metallic, semi-conductive, non-conductive) and living cells in aqueous solution make them behave as macro-ions and migrate in an electric field. The net charge of a particle is related to the electrokinetic potential (zeta-potential), which is described in Section 2.4.6. This is what occurs by *in vitro* electrophoresis. In human body liquids, the range of pH is very narrow: 7.35–7.45. But *in vitro* it is usually possible to find a pH value at which an amino acid, a protein or a cell does not migrate. This pH at which no migration occurs is the *isoelectric point*, or sometimes it is a pH *range*. If the particle is conductive, there is a common charge for the whole particle, with a sheath of counterions around. When the total charge is 0, no migration occurs. If the particle is not conductive, we are dealing with local charges and counterions, and when the net migrational forces of these are 0, we are at the isoelectric point. The isoelectric point is dependent on the solution used for the examination.

The charge of proteins or cells is the basis for the reciprocal repulsion of particles in a suspension. Loss of charge means losing repulsive forces and implies *clotting* and *precipitation*. Blood coagulation is the result of such a process.

Osmosis is the transport of a solvent through a semipermeable membrane into a more concentrated solution. Reverse osmosis is applying a sufficiently high pressure on the more concentrated side to reverse the transport direction. *Dialysis* in medicine is the *separation* of suspended colloidal particles from dissolved ions or molecules of small dimensions by means of their unequal rates of diffusion through the pores of semipermeable membranes. If charged carriers are involved, applying an electric field can accelerate the process: *electrodialysis*.

Usually an *ion exchanger* is packed into a tube or column through which a solution is made to flow in order to capture anions or cations. The column arrangement forces the ion-exchange reaction, which is intrinsically reversible, to be completed. The solution flowing down the column continually meets fresh exchanger. When the exchangeable ions do start to emerge from the end of the column, the column has become completely saturated. The column may be regenerated by passing through it a solution of the ions that it originally contained.

2.4.6. Electrokinesis

There are four electrokinetic effects due to the electric charge of the double layer at the solid/liquid interphase. In an E-field, *electrophoresis* is the migration of charged particles through a liquid, and *electro-osmosis* is a bulk liquid flow through a pore caused by a migrating ionic sheath. Furthermore, a current and a potential difference is *generated* due to falling charged particles (*sedimentation* potential), and when a liquid is pressed through a pore (*streaming* potential).

The conductivity of the solution involved is of general interest in connection with these effects. High conductivity results in a high current density for a certain E-field strength, with a possible temperature rise problem. High conductivity also results in small generated potentials.

Electrokinetic effects are not restricted to charged particles, however. Field-induced polarization will make *uncharged* particles move in inhomogeneous or moving electric fields. The resultant forces increase with the volume of the particle, and are therefore called “body” or “*ponderomotive*” forces. These forces are the basis of phenomena and techniques like *electrorotation*, *levitation*, *dielectrophoresis (DEP)*, *pearl chain* formation and *traveling wave DEP* (Fuhr et al., 1996). Electrorotation and traveling wave DEP are techniques where angular or linear movement of the field relative to the particle produces the desired movement of the particle. Inhomogeneous fields on the other hand, can cause levitation, DEP and pearl chain formation, although pearl chain formation will also occur in homogeneous fields. Ponderomotive effects will be described in the next chapter.

Transport Caused by Applied Electric Field.

Electrophoresis

Free amino acids, proteins, ions, colloidal particles, bacteria and cells are possible charged particles migrating in an electric field, and can therefore be studied by electrophoresis. As described in Section 2.4.3, some molecules of the solvent are attached to charges on the particle, and hence some solvent will move together with the particle. This is a part of the electrophoretic effect.

Electrophoretic flux could be calculated from the zeta-potential, the permittivity and the viscosity. As these quantities are difficult to estimate, electrophoretic mobility is a more practical quantity (Table 2.8). Migration velocity is simple to measure and the different electrophoretic mobilities are the basis of a very powerful in vitro analytical tool for amino acids and proteins in clinical laboratories.

Electro-Osmosis

Electro-osmosis is the transport of bulk liquid through a pore under the influence of an electric field. The volume of solution transported per unit time, \dot{V} is:

$$\dot{V} = A\zeta\epsilon E/4\pi\eta L \text{ [m}^3/\text{s]} \quad (2.20)$$

TABLE 2.8 Electrophoretic Mobility ($10^8 \text{ m}^2/\text{Vs}$) at pH 7.0

Particle	Mobility
Human blood cells	-1
Streptococcus	-1
Methicillin-resistant staphylococcus	-1.5
Proton	+37
Cl ⁻	-7
Colloidal gold	-3.2
Oil droplets	-3.1

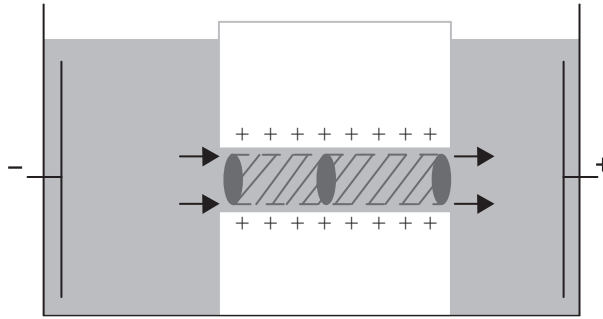


Figure 2.11 Electro-osmosis in a capillary. The double layer ion sheath migrates, and this brings the inside bulk capillary volume in motion.

where A is the effective total area of pores, L is the pore length and ζ is the double layer zeta potential.

Electro-osmosis is a kinetic process that is used for the determination of the zeta-potential of a surface/electrolyte solution interphase (Fig. 2.11). It is also a process found in the sweat pores of the human skin. A dry cathode at a skin surface will fill the ducts with liquid/sweat from deeper skin layers.

Flow-generated potentials

Sedimentation Potential

Charged particles falling through a column filled with an electrolyte solution set up a potential difference between column ends. The falling charge carriers directly represent an electric current flow, which results in a potential difference and hence a flow of charge carriers in the opposite direction, opposing the motion of the falling particles. High conductivity solutions result in small generated potentials.

Streaming Potential

When a liquid is forced through a capillary tube of length L , a potential difference $\Delta\Phi$ is generated between the ends of the capillary: $\Delta\Phi = \zeta\epsilon\Delta p/4\pi\eta\sigma$. Here Δp is the pressure difference and ζ is the zeta potential. Using the Poiseuille flow formula we get:

$$\Delta\Phi = \frac{2\zeta\epsilon\rho L}{\pi^2 r^4} \dot{V} \quad (2.21)$$

which shows that the potential difference is proportional to the volume flow \dot{V} , the capillary length and the liquid resistivity. The core electrolyte is neutral and no electromotive voltage is generated from the bulk flow, but only from the ion sheath migration.

Ponderomotive Effects

Dielectrophoresis

Dielectrophoresis (DEP) is the movement of non-charged dielectric particles in an inhomogeneous electric field. The force \mathbf{f} on a charge is $\mathbf{f} = q\mathbf{E}$, so if the net

charge is zero, there is no force. A dipole has a net charge zero and will experience a torque in an electric field, but no translational force. However, in an inhomogeneous field, there is also a translational force on a dipole. Consider a spherical non-charged particle in a medium. It is polarized in an electric field and if there is a field gradient ∇E , there is a force \mathbf{f} on the particle (Pethig, 1979) given by:

$$\mathbf{f} = (\mathbf{p} \cdot \nabla)\mathbf{E} = 2\pi a^3 \Re[\varepsilon_2(\varepsilon_1 - \varepsilon_2)/(\varepsilon_1 + 2\varepsilon_2)] \nabla E^2 \quad [\text{N}] \quad (2.22)$$

where \mathbf{p} is the induced dipole moment, subscript 1 is for the particle and 2 for the medium. Equation (2.22) is the basic equation for DEP and shows that depending on the relative polarizability of the particle with respect to the medium, the particle will move either in the direction of the field gradient (positive DEP) or in the opposite direction (negative DEP). The electrophoretic and dielectrophoretic mechanisms can be completely separated and Pohl (1958) adopted the term DEP to identify this distinction. Only DEP gives a net force in an AC electric field, the E^2 term has no polarity dependence. One problem with eq. (2.22) is that it does not account for surface- and double layers on wet surfaces.

Electrorotation

Particles suspended in a liquid will experience a torque in a rotating E-field (Arnold and Zimmerman, 1982). A dipole is induced in the particle. As the polarization process (redistribution of charges) is not immediate, the induced dipole will lag the external field and a frequency-dependent torque will exist. It can be shown that the torque is dependent on a relaxation time constant identical to the time constant in the theory of β -dispersion (Schwan, 1985). Cell rotation is therefore a direct physical manifestation of dispersion. Theory predicts that the torque may have two maxima, usually of opposite signs (co-rotation and anti-rotation) and is given by (Zhou et al., 1995):

$$\Gamma = -4\pi a^3 \Im[\varepsilon_2(\varepsilon_1 - \varepsilon_2)/(\varepsilon_1 + 2\varepsilon_2)] \nabla E^2 \quad (2.23)$$

Rotation also occurs in non-rotating external fields, and onset is often at a sharply well-defined frequency. The rotation is therefore also called *cellular spin resonance*. One possible mechanism is the dipole–dipole interaction between neighbor cells. The peak rotation frequency is many decades lower than the excitation frequency, the latter being in the β -dispersion range (MHz).

Cellular spin resonance indicates various physiological states of living or dead cells, and also represents a method for cellular manipulations. It should, for example, be possible to rotate intracellular organelles with respect to the whole cell.

Levitation

Negative DEP causes particles and cells to be repelled from regions of high electric field strength. This effect can be used to levitate particles over, for example, a planar array of electrodes. A common geometry is a four-electrode field trap with electrodes forming the sides or corners of a square and with the particle levitated over

the center of the square. The viscous forces from the medium will damp the motion of the particle.

Traveling Wave DEP

If the E-field in an electrorotation chamber was made to move in a linear rather than an angular manner, an interesting combination of dielectrophoretic and electrorotation effects will occur. The principles are shown in Fig. 2.12 where phase-shifted cosine voltages are applied to facing electrodes along an array of such electrodes. Only particles experiencing negative DEP will move along the inter-electrode channel. They will otherwise be trapped at the electrodes by positive DEP.

As shown above, the dielectrophoretic effect depends on the real part of the induced dipole moment and the electrorotation effect on the imaginary part of the induced dipole moment. Both these effects contribute to the motion of the particle in the traveling wave chamber. Viable cells will typically exhibit negative DEP at low frequencies (typically $<10\text{kHz}$) and in a frequency window below this frequency, where the imaginary part of the induced dipole moment is positive, the cell will move in the opposite direction of the traveling electric field. Below this frequency window, the cell will be levitated over the electrode array. For non-viable cells, the negative dielectrophoretic effect will typically occur at high frequencies over 1MHz . The corresponding imaginary part of the dipole moment will be negative and the cell will hence travel in the direction of the moving field (Wang et al., 1993).

Pearl Chain Formation

A dielectric particle disturbs the local E-field, so even in a homogeneous external field there is a local gradient. Two neighboring dielectric particles will therefore be attracted to each other. They form a dipole and will be oriented in the direction of the E-field. In a homogeneous field, cells will therefore tend to form pearl chains in the direction of the E-field. In a gradient field the pearl chains will protrude from the electrode surface (Schwan and Sher, 1969)

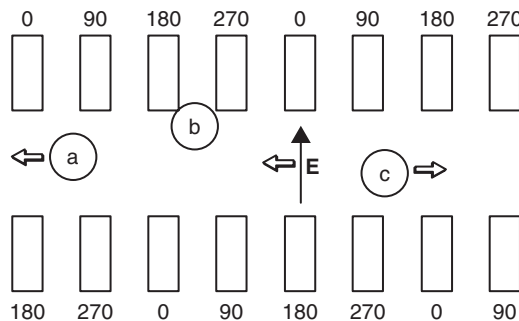


Figure 2.12 Traveling wave DEP achieved by using cosine voltages with the indicated phase relationships as excitation on each pair of facing electrodes. The electric field will travel from right to left in this example. Particle *a* could be a non-viable cell, *b* a cell trapped by positive dielectrophoresis and *c* a viable cell.

2.5. ELECTRODICS AND AC PHENOMENA

The *half-cell* concept is often used for analyzing an electrode with its surrounding solution. However, we do not have access to one half-cell, so a real electrolytic cell consists of two half-cells. Often the second electrode is considered to be a reference electrode.

2.5.1. Electrode Equilibrium DC Potential, Zero External Current (cf. Section 7.4.4)

Metal/ion and Redox Systems

According to Nernst, metals have a tendency to send their ions into a solution as solvated particles. The potential difference arises from this transfer of positive metal ions across the double layer, with a resulting negative potential on the metal electrode. The standard potential of such a *metal/ion* half-cell is shown in Table 2.9, the reference electrode here is the hydrogen electrode. Volta's original findings were in rough accordance with this table. The least noble metals have the most negative values. For the noble metals the number of metal ions sent out in the solution may be small, and the potential must then be measured under strict zero current conditions.

With an external DC power supply connected to the electrolytic cell, the applied voltage which gives *no DC current flow* in the external circuit corresponds to the *equilibrium potential* of the half-cell (or actually the cell). It is the same voltage as read by a voltmeter with very high input resistance and virtually no current flow (pH meter). In electrochemistry, *potentiometry* is to measure the potential of an electrode at zero current flow, that is when the cell is not externally polarized. In order to

TABLE 2.9 Metal/ion Equilibrium Potentials

Metal/ion	V_0 (volt)
Li/Li ⁺	-3.05
K/K ⁺	-2.93
Na/Na ⁺	-2.71
Al/Al ³⁺	-1.66
Zn/Zn ²⁺	-0.76
Fe/Fe ²⁺	-0.44
Ni/Ni ²⁺	-0.25
Sn/Sn ²⁺	-0.14
Pb/Pb ²⁺	-0.13
H ₂ /H ⁺	0
Carbon	dependent on structure
Cu/Cu ²⁺	+0.34
Ag/Ag ⁺	+0.80
Pt/Pt ²⁺	+ ~1.2
Au/Au ³⁺	+1.50

TABLE 2.10 Standard Equilibrium Electrode Potentials for Some Redox Systems

Electrode	Electrode reaction	V_0 (volt)
Pt	$2\text{H}_2\text{O} + 2\text{e}^- \leftrightarrow \text{H}_2 + 2\text{OH}^-$	-0.83
Pt	$\text{O}_2 + 2\text{H}_2\text{O} + 2\text{e}^- \leftrightarrow \text{H}_2\text{O}_2 + 2\text{OH}^-$	-0.15
Pt	$2\text{H}^+ + 2\text{e}^- \leftrightarrow \text{H}_2$	0
Carbon	$\rightarrow ?$?
AgCl	$\text{AgCl} + \text{e}^- \leftrightarrow \text{Ag} + \text{Cl}^-$	+0.22
Calomel		+0.28

understand the equilibrium potential with zero external current, we must introduce the concept of electrode reaction, and link it with an electric current in the external circuit. An electrode reaction going rapidly both ways (ionization–de-ionization, reduction–oxidation) is called *reversible*. A pure redox system presupposes an inert electrode metal, for example platinum, with no electrode metal ion transfer. At the electrodes the redox system is:

anode is the *electron* sink, where ions or neutral substances lose electrons and are oxidized: $\text{red} \rightarrow \text{ox} + n\text{e}$.

cathode is the *electron* source where ions or neutral substances gain electrons and are reduced: $\text{ox} + n\text{e} \rightarrow \text{red}$.

The metal/ion half-cell generates a potential by the exchange of *metal ions* between the metal and the electrolyte solution. In contrast, a *redox* half-cell is based on an exchange of *electrons* between the metal and the electrolyte solution. So actually there are two sets of standard potential tables, one for metal/ion half-cells (Table 2.9), and one for redox half-cells. The half-cell potential is of course *independent* of the interphase area, because equilibrium potential is without current flow. As soon as the cell is externally polarized and a current is flowing, electrode area is of interest (current density).

Table 2.10 shows some typical half-cell standard potentials for redox systems.

The Nernst Equation

The Nernst equation relates the redox processes and the potential to the concentration/activity of the ions in the solution of an electrolytic cell. It indicates the *redox equilibrium potential V with no DC current flow*:

$$V = V_0 + (RT/nF) \ln(a_{\text{ox}}/a_{\text{red}}) \quad (\text{The Nernst equation}) \quad (2.24)$$

Here V_0 is the standard electrode potential of the redox system (with respect to the hydrogen reference electrode at 1 mol concentration), n is the number of electrons in the unit reaction, R is not resistance but the universal gas constant, and F is the Faraday constant. a_{ox} and a_{red} are *activities*, $a = \gamma c$, where c is the concentration and γ is the activity *coefficient*. $\gamma = 1$ for low concentrations (no ion interactions),

but <1 at higher concentrations. The half-cell potentials are referred to standardized conditions, meaning that the other electrode is considered to be the standard hydrogen electrode (implying the condition: $\text{pH} = 0$, hydrogen ion activity 1 mol/L). The Nernst concept is also used for semipermeable membranes with different concentration on each side of the membrane (Section 4.5.1).

In eq. (2.24) RT/nF can be substituted with -61 mV for room temperature and using the common instead of the natural logarithm. Then the Nernst equation becomes:

$$V = V_0 - 0.061 \log(a_{\text{ox}}/a_{\text{red}})$$

The Nernst equation presupposes a *reversible* reaction: that the reaction is reasonably fast in both directions. This implies that the surface concentration of reactants and products are maintained close to their equilibrium values. If the electrode reaction rate is slow in any direction, the concentration at the electrode surface will not be equilibrium values, and the Nernst equation is not valid. Then the reactions are *irreversible*.

For metal cathodes the activity of the reduced forms a_{red} is 1, and the equation, for example, for an AgCl electrode is:

$$V = V_{\text{AgCl/Ag}} - (RT/F) \ln a_{\text{Cl}^-} \quad (2.25)$$

where R is the universal gas constant.

According to eq. (2.25) the DC potential is only dependent on the activity of the Cl^- anion in aqueous solution (and temperature). The silver–silver chloride electrode is an example of an “electrode of the second kind”: the electrode metal (Ag) is in equilibrium with a low solubility salt of its ions (Ag^+).

Total Galvanic Cell DC Voltage

According to Tables 2.9 and 2.10, two different electrode materials in the same electrolyte solution may generate 1 V or more DC. Superimposed on signals in the microvolt range, this may create noise and be a problem for the input amplifiers. If both electrode surfaces are of, for example, stainless steel in saline, there are not necessarily any redox reactions at the surface at all. The voltage is not well defined and may easily attain 100 mV or more, the system is highly polarizable and the output voltage noisy (cf. Section 7.4). Even strongly polarizable electrode metals like stainless steel, platinum or mercury have an electrode reaction if the applied DC voltage is high enough. This is both on the anodic and cathodic sides, but the reactions are irreversible and therefore not redox reactions.

Under zero current condition, many metal electrodes are of interest in biological work. The platinum electrode, for instance, becomes an interesting redox potential recording electrode. An inert platinum electrode may actually be used in potentiometry in the bulk of a redox system during titration or in, for example, sea water analysis. With zero current the inert platinum will pick up the redox equilibrium potential of the process.

Poisson’s law (eq. 8.5) defines the relationship between the potential function (representing a possible emv source to the external circuit) and the charge distribution

in an electrolytic volume. A change in the charge distribution near the electrode surface results in a changed potential function, and consequently a changed half-cell potential (see Section 2.4.3). A polarizable electrode therefore implies a current-induced change of charge distribution near the electrode surface, and a changed half-cell potential.

The Liquid Junction Equilibrium DC Potential

Between two dissimilar electrolyte solutions a potential difference is created, just like between a metal and an electrolytic solution. By Brownian motion the ions randomly walk with a velocity proportional to the Boltzmann factor kT . The corresponding E-field will have a direction to slow down the rapid ions and accelerate the slow ones in the interface zone. The resulting potential difference is called the *liquid junction potential* (Φ_{lj}), and follows a variant of the Nernst equation called the *Henderson equation*:

$$\Phi_{lj} = \frac{\mu^+ - \mu^-}{\mu^+ + \mu^-} \frac{RT}{nF} \ln \frac{c_1}{c_2} \quad (2.26)$$

where R is the universal gas constant and μ^+ and μ^- are the mobilities of cations and anions, respectively.

The liquid junction potential is usually less than 100 mV. For instance, for a junction of different concentrations of NaCl and with $c_1 = 10c_2$, the dilute side is 12.2 mV negative with respect to the other side.

The K^+ and Cl^- ions have about the same mobilities, and therefore KCl creates a lower liquid junction potential than, for example, NaCl. The liquid junction DC potential can be kept small by inserting a *salt bridge* between the solutions, so that there will be two junctions instead of one. By using a concentrated solution of KCl in the bridge, it can be shown that the two junction potentials will tend to be equal and be dominated by the concentrated salt solution, but with opposite signs so that they more or less cancel.

Membrane Equilibrium Potentials (Donnan Potentials)

The liquid junction potential was defined with no membrane separating the two media. A membrane separating an electrolyte into two compartments is often selectively permeable, for example rather open to water, but less permeable to certain ions or larger charge carriers. The selectivity may be due to the mechanical dimensions of pores, or charge-dependent forces.

With different concentrations on each side, such membranes generate an osmotic pressure difference. With different ionic concentration also an electrical potential difference is generated. This is called the *Donnan potential difference*, Φ_d :

$$\Phi_d = (RT/F) \ln a_1/a_2 \quad (2.27)$$

where a_1 is the activity of a specified ion on compartment side one, and R is the universal gas constant.

2.5.2. The Monopolar Basic Experiment with DC Current Flow

When we are to study electrode reactions a little further, we must be able to differentiate between cathodic and anodic processes. We therefore change the set up shown in Fig. 2.1 a little. Instead of two equal electrodes, we reduce the area of one of them to be, for example, $<1/100$ of the other (Fig. 2.13).

With no current through the electrolytic cell, it does not matter whether the electrodes are large or small; the equilibrium potentials are the same. But with current flow, the current density and therefore the voltage drop and the polarization, will be much higher at the small electrode. An increased potential drop will occur in the constrictional current path near the small electrode, and in general the properties of the small electrode will dominate the results. The small electrode will be the electrode studied – the *working electrode*. It is a *monopolar* system, meaning that the effect is determined by *one* electrode. The other electrode becomes the *indifferent* or *neutral* electrode. Note that this division is not true in potentiometry, electrode area is unimportant under no-current conditions.

We let the external DC voltage change slowly (e.g. ramp voltage from a polarograph), and we record the DC current (Fig. 2.14). In electrochemistry this is called *voltammetry* (volt-am-metry), the application of a varying voltage with the measurement of current. *Ampereometry* is more generally the measurement of current with a constant amplitude voltage.

Polarography is voltammetry, preferably with the dripping mercury electrode and with a diffusion-controlled current in a monopolar system.

The electrolyte (Fig. 2.13) is as usual NaCl 0.9% in water. With a *platinum* working electrode there will be no DC current over a rather wide voltage range

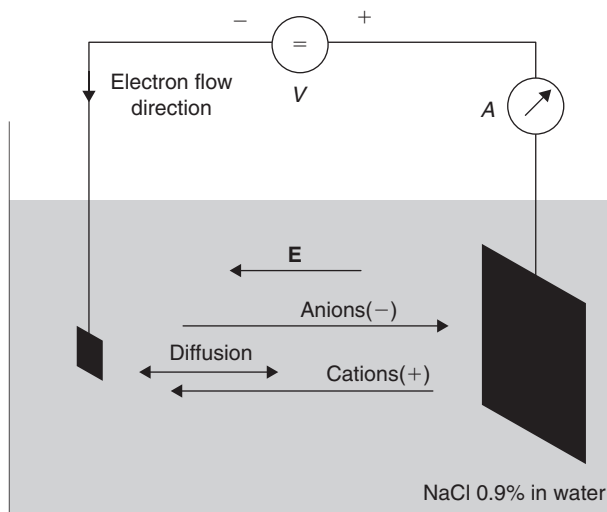


Figure 2.13 Monopolar electrode system (cf. Fig. 2.1).

(Fig. 2.14(a)). The *incremental* DC resistance $R = \Delta V/\Delta I$ is large in this range ($\Delta I \approx 0$). With beginning oxygen reduction R is much smaller, but at the current plateau (diffusion-controlled oxygen transport to the cathode) R is again large. With silver–silver chloride (Fig. 2.14(b)) R is small, even at zero DC current. The system is non-linear, and care must be taken with regard to the use of linear models.

With a sufficiently large voltage of any polarity, DC faradaic current flows and we have an *electrode reaction* at the platinum surface. R falls to smaller values. Evidently large *activation energy* is necessary to obtain electron transfer and an electrode reaction. It is not likely that this reaction involved chemical reaction with platinum, or that platinum metal entered the solution as ions. However, in our basic experiment of Fig. 2.1 we did consider the effect of dissolved oxygen. With a suitable negative voltage the neutral oxygen is reduced at the cathode, left curve stippled. This reaction causes a faradaic current. However, when the negative voltage is large enough, we reach a *current plateau*, again with a large incremental R . Then the electron transfer is no longer the rate limiting factor, but the diffusion of oxygen to the cathode. At the cathode surface the concentration of oxygen is approximately zero, all available oxygen is reduced immediately. *The current is diffusion controlled*. The oxygen molecules are neutral in the solution and are not migrating in the electric field, they move because of the concentration gradient. At the platinum surface they are ionized (reduced), accepting electrons. This is the principle of the polarographic oxygen electrode. If we increase the voltage to about -1.4 V, a much large DC current flows, and the decomposition of water with bubbles of H_2 appears.

Now let us change to a small *silver–silver chloride* working electrode (Fig. 2.14(b)). Even with a small deviation ΔV from the equilibrium voltage with zero current, the ΔI will be large, and will be in either direction. Even at the equilibrium voltage, R is rather small. We have an immediate, large electrode reaction. This is the non-polarizable electrode; even with relatively large DC currents the charge distribution does not change very much, neither do the DC potential. With a positive overvoltage on the electrode, the $AgCl$ layer thickens, with a negative overvoltage it becomes thinner and is at last stripped off. Then we have changed the electrode surface to a pure silver electrode with a different equilibrium potential.

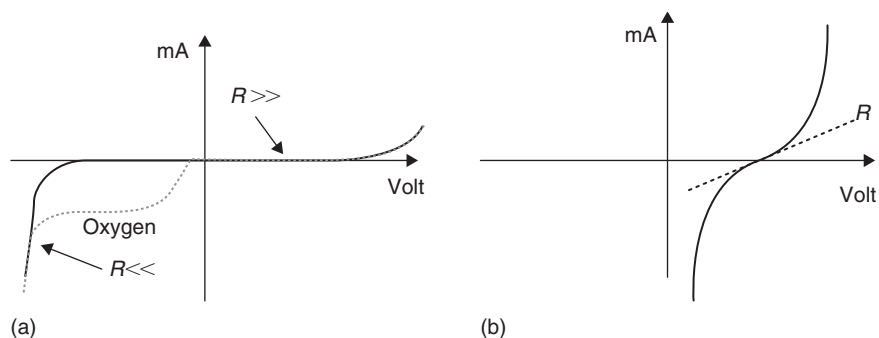


Figure 2.14 DC monopolar electrode current. Working electrode: (a) platinum, (b) silver–silver chloride.

Suppose a small AC signal is superimposed on the DC voltage. At equilibrium DC voltage with no DC current, the AC current will flow in both directions because it is a reversible redox electrode process at the AgCl surface. With a DC current, the small AC current will be superimposed on the larger DC current, and thus just change the reaction rate by a small amount.

As seen in Fig. 2.15 the resultant AC current will depend on the local slope of the DC current curve. The slope defines the *incremental resistance*:

$$R = \Delta V / \Delta I \text{ } [\Omega] \quad (2.28)$$

The incremental resistance varies according to the DC (*bias*) level. As the DC current curve is not linear, it is clear that with large amplitudes the current response will not be a sine wave even if the superimposed AC voltage is a pure sine wave. Because of the capacitive properties of the cell, the current will not be in phase with the applied sine voltage.

From the curves in Fig. 2.15 it is clear that by changing the frequency and recording the AC current it is possible to examine electrode processes and find out how quick they are. By studying the harmonic content of the current waveform as a function of DC voltage and AC amplitude/frequency, non-linearity phenomena can also be studied.

With no redox reactions, for example by using a platinum electrode in saline, the small AC voltage will result in an AC current dependent on double layer capacitance and other components (cf. Section 2.5.3).

The voltage deviation ΔV from equilibrium necessary for a certain DC current flow is called the *overvoltage*. With small deviations there is a linear relationship between ΔV and electrode current I , but with larger ΔV it is strongly non-linear. An overvoltage is linked with an external current and therefore the electrode is externally *polarized*.

In *cyclic voltammetry* the voltage is swept like in polarography, but at a pre-determined voltage level the sweep is reversed and the cycle ends at the starting voltage. More than one cycle may be used, but usually the recorded current curve changes for each cycle. The single cycle experiment must therefore not be confused with a steady-state AC condition. Two examples are shown in Fig. 2.16.

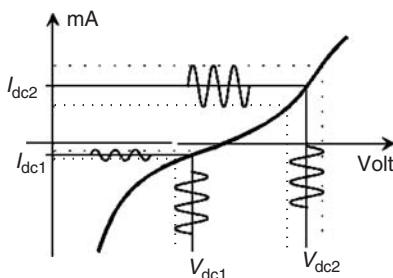


Figure 2.15 DC (bias) voltage with superimposed AC. The resulting AC current is dependent on the slope of the DC current curve.

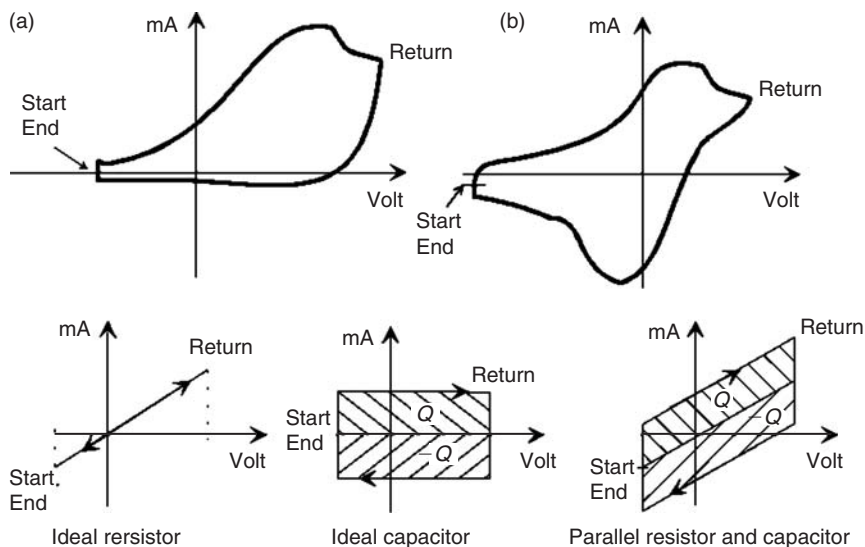


Figure 2.16 Cyclic voltammograms. Top: Electrolytic cell – (a) irreversible reaction, (b) reversible. Bottom: with ideal components.

As the sweep is linear, the x -axis is both a voltage and time axis. The charge transferred from the sweep generator to the cell is therefore proportional to the area under the curve and the x -axis ($=0$ mA). If the enclosed areas over and under the x -axis are equal, no net charge is supplied to the system. The currents may be due either to double layer charging, sorption at the metal surface or electrode reactions.

The electrolytic cell voltammograms in Fig. 2.16 are with (a) irreversible and (b) reversible processes. The irreversible process represents a net charge transfer to the cell, because very little reverse current is present. During voltage sweep a non-faradaic charge current will also flow to or from the double layer capacitance. The current steps at the sweep ends represent the reversal of such a capacitive charging current. In the reversible process most of the charge is returned, the redox reaction is reversed.

With an ideal resistor instead of the electrolytic cell, the current curve is the same straight line, and a charge transfer equal to the double of the area under the line is transferred. With an ideal capacitor the charging current I is $I = C dV/dt$. When dV/dt is constant, I is constant, when dV/dt changes sign, I changes sign. The area under the current curve is Q , and the same charge $-Q$ is returned at the return sweep. No net charge is transferred to the capacitor. The current to the parallel RC components is then the sum of the separate R and C currents (right).

One type of electrode has no defined DC voltage at all, the ideally *polarizable electrode*. It can attain any potential, it is just a double layer capacitor which can be charged to any voltage if the necessary charging current is supplied. No electron transfer occurs, no free charge carriers cross the double layer or flow in the solution. With a real electrode this implies virtually zero DC current within a certain range

of applied voltage. A platinum electrode in NaCl aqueous solution is a practical example. As a current carrying DC reference electrode in NaCl electrolyte, the platinum electrode is the worst possible choice. Another example is dropping mercury electrode in an indifferent electrolyte, with a perfectly smooth surface continually renewed. No reversible charge transfer occurs within a rather broad range of DC voltage (oxygen-free solution).

To obtain a well-defined potential *also with a variable DC current flowing*, a reversible electrochemical reaction is necessary at the electrode. Usually this implies that there must be redox reactions, with easy both way electron transfer. Such an electrode with easy electron transfer is called a *non-polarizable electrode*.

A redox reaction is not only dependent on the electrode material, but also on the electrolyte solution. As we have seen, platinum was highly polarizable in NaCl solution. However, if the surface is saturated with dissolved hydrogen gas, a redox system is created (H/H^+), and then the platinum electrode becomes a *non-polarizable reference* electrode. Surface oxidation, adsorption processes and organic redox processes may reduce the polarizability and increase the applicability of a platinum electrode in tissue media.

2.5.3. DC/AC Equivalent Circuit for Electrode Processes

The faradaic polarity-dependent DC currents just described are not only dependent on the applied DC voltage, but also on elapsed time. With a small change in excitation voltage, it takes a certain time to reach a new current level. The four processes to be considered are:

1. A faradaic component: the rate of *electron* transfer to the electro-active species of the solution (occurring near/at the electrode surface in the double layer).
2. A faradaic component: the amount of species that can be *transported* to the reaction site from the bulk of the electrolyte, and the amount of reaction products that can be transported away *from* the reaction site.
3. The electric *charging* of the double layer.
4. The *sorption* of species at the electrode surface.

The mechanisms and speed of the *electron transfer process* have long been discussed. Does it take the electron long time to meet the particle, or is the particle immediately ready to donate or accept an electron? When a chemical reaction is to occur, the species approach one another to a necessary close distance. In an electrode reaction, the ions enter the outer part of the double layer, and the chance of gaining or losing electrons increases. If the electroactive species are ions, what is the effect of the hydration sheath and ionic atmosphere surrounding them? Must a part of it be stripped off? The reacting partners must possess sufficient energy (translational, vibrational, rotational) to obtain reaction. The concept of necessary *activation* energy is therefore important. Sodium is very electropositive (cf. Table 2.2), thus tending to get rid of electrons. From these scales the most probable electrode reactions can be predicted.

A possible but rough electrical DC/AC equivalent circuit for the electrode processes is shown in Fig. 2.17. The electrodic part consists of three principal current paths in parallel. The elements are Cole-like as discussed in Section 8.2, and some of the used component symbols indicate that their values are non-ideal, frequency dependent.

As for the electrode processes, DC parameters are actually contraindicated, because a DC study should be performed with virtually zero applied overvoltage in order to be in the linear region (Section 7.2.1). By using a superimposed AC signal of sufficiently small amplitude at $f > 0$, the model may be a linear model, and the values of the components of the equivalent circuit may vary according to the applied DC voltage or current.

The Series Resistance

The bulk of the electrolyte obeys Ohm's law (eq. 2.2). Accordingly, the bulk electrolyte is modeled as an ideal resistor R_{sol} in series with the electrode components. This is to indicate that bulk electrolytic conductance is considered frequency independent, but dependent on the geometry and possible current constrictional effects (Fig. 6.3). If the bulk electrolyte is replaced by tissue, a more complicated equivalent circuit must replace R_{sol} , and we are confronted with the basic problem of division between tissue and electrode contributions.

The series resistance causes an overvoltage due to a simple IR -drop ($\Delta V = IR_{sol}$) in the solution. Actually this is not due to a polarization process. However, it is often practical to include it in the total overvoltage and the electrode polarization concept. The IR -drop is proportional to current and can be reduced by the addition of a suitable strong electrolyte not intervening with the processes of interest (*indifferent* electrolyte). It can also be reduced by introducing a reference electrode reading the potential very near to the working electrode, and connecting all three electrodes to a potentiostat (see Fig. 6.22).

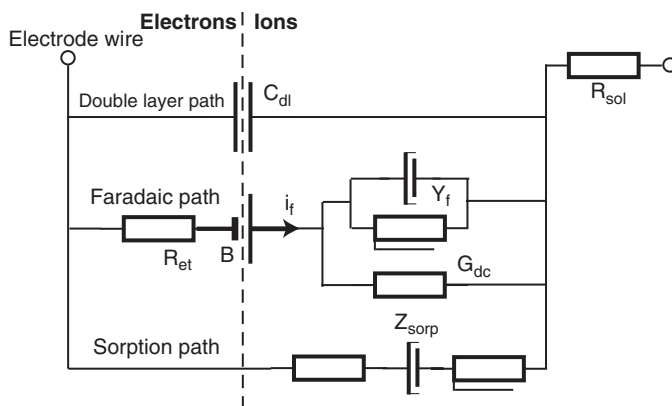


Figure 2.17 Electric equivalent circuit for the three electrode processes.

Double Layer Path with Leakage

With a dripping mercury electrode the surface is ideal and the double layer is modeled as a pure, frequency independent capacitor, somewhat voltage dependent. The capacitance values are very high because of the small double layer thickness – C_{dl} is about $20 \mu\text{F}/\text{cm}^2$. With solid electrode materials the surface is of a more fractal nature, with a distribution of capacitive and resistive properties. The actual values are dependent on the type of metal, the surface conditions, the type of electrolyte and the applied voltage. The capacitance increases with higher electrolyte concentration (cf. Section 2.4.3). The double layer capacitor is inevitable; it is there as long as the metal is wetted. C_{dl} may dominate the circuit if there are no sorption or electrode reaction processes.

Surface Sorption AC Path

The additional capacitive impedance Z_{sorb} is due to the adsorption and desorption of species at the electrode surface. These species do not exchange electrons with the electrode surface, but changes the surface charge density and therefore cause a pure AC current path. A current limiting resistor in series may model the processes with a Cole-like element without DC conductance (drawn as a series constant phase element because it is in series with a resistor, cf. Section 8.2.7). Z_{sorb} may dominate the circuit in the middle and higher Hz and lower kHz frequency range. Sorption currents are AC currents, and as the adsorption/desorption may occur rather abruptly at a certain DC voltage, these currents may be much dependent on the applied DC voltage. Sorption currents may dominate noble metal electrodes, so the measurement of their polarization impedance must be performed under controlled DC voltage.

Electrode Reaction DC/AC Path (Faradaic)

The metal and the electrolyte also determine the DC half-cell potential modeled by the battery B. If there is no electron transfer, R_{et} is very large and the battery B is decoupled, the electrode is then polarizable with a poorly defined DC potential. But if there is an electrode reaction, R_{et} has a lower value and connects an additional admittance in parallel with the double layer admittance. This current path is through the *faradaic admittance* Y_f , and the current is the faradaic current i_f . Faradaic current is related to electrode reactions according to Faraday's law (see Section 2.4.1). The faradaic impedance may dominate the equivalent circuit in the lower Hz and sub-Hz frequency range and at DC. The faradaic impedance is modeled by a complete Cole-like series system. It consists of the resistor R_{et} modeling the electron transfer, in series with a Cole-like parallel element of *admittance* Y_f related to slow processes (mass transport and slow electrode reactions) and therefore introducing time delays necessitating an equivalent admittance and not just a conductance.

The electron transfer resistance R_{et} is related to the activation energy and to the extent electroactive species have reached sufficiently near the electrode surface so that acceptance or donation of electrons can occur. If the electrode voltage is not sufficient to create electron transfer and an electrode reaction, R_{et} will be very large. R_{et} is purely resistive, which means that there is little transfer time delay. The process is

almost immediate, but energy dependent and therefore probability dependent. R_{et} is clearly current dependent, and for non-polarizable electrodes it is small for all DC current values. For polarizable electrodes it is very large at zero DC current. R_{et} is clearly a non-linear element. It only dominates to the extent that electron transfer is the current limiting process. Under that condition, the concentration of active species at the electrode is independent of current flow. Then the relationship between the overvoltage ΔV and the electrode current I is given by the *Butler–Volmer* equation:

$$I = I_0[\exp(\psi k\Delta V) - \exp(-(1 - \psi)k\Delta V)] \quad (2.29)$$

where I_0 is the exchange current present when the external current is zero, the exponent ψ is called the *transfer coefficient*, and $k = zF/RT$. At equilibrium voltage with no external current, there may actually still be large reducing and oxidizing local currents that externally cancel, this is I_0 .

The slow process *admittance* Y_f is related to reactions that are rate limited by the necessary time of transport to or from the electrode active sites, and the time of accompanying chemical reactions. If the faradaic current is limited by *diffusion alone*, the immittance is called *Warburg* immittance. R_{et} is then negligible, and the current is determined by Y_f . The electron transfer flux and the chemical reaction rate are so high that the process is controlled by diffusion alone. Diffusion is a transport process only dependent on concentration gradients (cf. Section 2.4.2). The diffusion may be of reactants to the electrode, or reaction products *away* from the electrode, both influencing Y_f . Warburg (1899) was the first to solve Fick's second law (eq. 2.10) for an electrolytic cell under AC conditions. He presumed a diffusion-controlled process with negligible migrational effects. He found that under ideal conditions the concentration at the electrode surface is $+45^\circ$ and the voltage -45° out of phase with the applied current, independently of the applied frequency. Such an ideal and purely diffusion-controlled electrolytic cell is therefore a perfect model for a constant phase element (CPE). He found that the concentration wave spreads out longer in the electrolyte the lower the applied frequency (Fig. 2.18).

The penetration will be delayed and can be described by a damped sine wave, so that both lower and higher than the bulk concentration may exist. It is like the slow penetration of changing cold and warm weather into a housing wall or the ground. Warburg found the diffusion zone, defined as the distance δ from the electrode at which the concentration wave is reduced to $1/e$ of its value at the electrode, to be:

$$\delta = (2D/\omega)^{1/2} \text{ [m]} \quad (2.30)$$

where D is the diffusion constant. The diffusion zone length δ may therefore extend all the way to the counter current carrying electrode at low frequencies. With $D = 10^{-9} \text{ m}^2/\text{s}$ and at $10 \mu\text{Hz}$, δ is 14 mm. In order to introduce negligible phase distortion, the cell length should then be several centimeters long. Pure 45° properties will only be found if convection effects are negligible during the period. A purely diffusion-controlled electrode reaction has an *infinite length Warburg admittance* with a constant (frequency independent) phase angle $\varphi = 45^\circ$. A more general

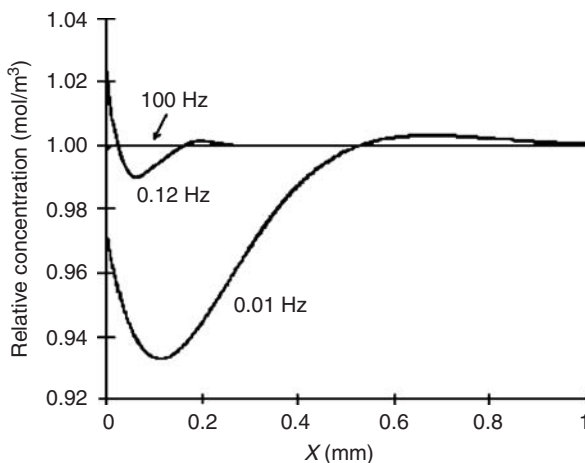


Figure 2.18 Concentration wave into the electrolyte as a function distance from electrode surface, with the frequency of the applied current as parameter: $D = 10^{-9} \text{ m}^2/\text{s}$, arbitrary current and zero current concentration.

finite length Warburg admittance does not have the same constant phase character (MacDonald, 1987).

The thickness of an electric double layer is about 0.5 nm with strong electrolytes, about the same size as the ions, and perhaps 10 nm in dilute solutions (diffuse double layer). The thickness of a diffusion zone in unstirred solutions is enormously much larger. The diffusion zone length is not dependent on concentration (as long as D is constant).

The influence of the electron transfer resistor R_{et} and the slow process admittance Y_f is determined by which factor is reaction rate limiting. It is possible to study this by plotting the faradaic impedance as a function of frequency in a log-log plot, or in the Wessel diagram and look for circular arcs (see Section 8.2).

The term *electrode polarization immittance* is sometimes related to the total immittance of the equivalent circuit of Fig. 2.17, but it is sometimes useful to exclude the series resistance R_{sol} if it has the character of being an access resistance to the electrode processes. Without electrochemical reactions, measured currents are due to double layer components and sorption. The term electrode polarization immittance should more often either be avoided or defined. The processes involved are of a very different nature, and in a measuring setup different variables must be controlled dependent on what effects are to be studied. The electrode immittance of an electronic conductor in contact with 0.9% NaCl is of special interest to us. Data for such interfaces are found in Section 7.4.5.

2.5.4. Non-linear Properties of Electrolytics

In a linear system an applied sinusoidal current results in a sinusoidal voltage response.

Electrolyte

The bulk electrolyte solution obeys Ohm's law (eq. 2.2), which is linear. If the E-field changes the viscosity η in eq. (2.6) or the number of ions per volume n in eq. (2.1), then the system is non-linear and does not obey Ohm's law (Wien, 1928; Onsager, 1934). This will be the case at very high electric field strengths. According to the Debye-Hückel theory the ionic atmosphere is symmetrical about the ion in the absence of an external electric field. In an electric field the ion migrates, but its atmosphere (ionic and hydrational) is retarded by friction and is no longer symmetrical about the ion (asymmetry effect). Accordingly, at high electric fields the conductivity increases because the ions move so fast that the retarding ionic atmosphere does not have time to form, it is stripped off (Wien¹³ effect, see Wien, 1931).

Electrode Processes

From Fig. 2.15 and the Butler-Volmer eq. (2.29) it is clear that the DC resistance is strongly dependent on the DC current through the electrode. With an AC superimposed on a DC, the resultant AC is dependent on the incremental resistance/conductance of the DC curve. If excitation is sinusoidal, and the measured AC voltage or current also is sinusoidal, then the system is linear with the amplitudes used. By increasing the amplitude, there will be a level when non-linearity is reached.

A DC or pulse current polarizes the electrode, and from the electrolytic basic experiment described in Section 2.2 it is also clear that faradaic current flow changes the chemical environment at the electrode surface. Current carrying electrodes are used in different applications such as nerve stimulation, pacemaker catheter stimulation and defibrillation with 50 A passing for some milliseconds. Often a square wave pulse is used as stimulation waveform (e.g. pacemaker), and the necessary overvoltage is of great interest (cf. Section 2.5.3). In such applications a clear distinction must be made between tissue non-linearity (Section 4.3.4.) and electrode non-linearity (this section). Non-linearity network theory is treated in Section 7.1.5. Non-linear behavior in suspensions has been studied by, for example, Block and Hayes (1970) and Jones (1979); for electroporation see Section 9.14.1.

For the electrode polarization impedance it has been shown that it was possible to state a frequency independent *voltage* amplitude limit for linear behavior (Onaral and Schwan, 1982). This limit is about 100 mV (average, corresponding to about 300 mV p-p) AC. The corresponding *current* limit will of course be frequency dependent, and be as low as $5 \mu\text{A}/\text{cm}^2$ in the lower MHz range and as high as $100 \text{mA}/\text{cm}^2$ in the higher kHz range. A typical current limit for a platinum black electrode in saline is $1 \text{mA}/\text{cm}^2$ at 1 kHz (Schwan, 1963). It is reasonable to believe that as the frequency approaches zero, the current limit of linearity flattens out around $5 \mu\text{A}/\text{cm}^2$ where the electrode impedance becomes resistive (Onaral and Schwan, 1982).

¹³Max Karl Werner Wien (1866–1938), German physicist. Brother of Wilhelm Wien (1864–1928), famous for the Wien displacement law, 1911 Nobel prize laureate in physics.

With composite waveforms the electrode may therefore operate in the non-linear region for the low frequency components, and in the linear region for the high frequency components.

The current density under a surface plate electrode is not uniform, with larger densities at the edges. The fractal properties of the electrode surface also create local areas of high current densities. The onset of non-linearity may therefore be gradual, and starts very early at very limited areas on the electrode surface. By harmonic analysis (see below) it has accordingly been found that very weak non-linearity is measurable at much lower voltages than 100 mV.

In a practical case when current carrying electrodes are used with tissue, it may also be difficult to differentiate between the non-linearity of the electrode processes and the tissue processes.

Electrode behavior in the non-linear region may be studied by electrode polarization impedance $Z = R + jX$ measured as a function of sinusoidal amplitude. The limit current of linearity i_L may, for instance, be defined as the amplitude when the values of R or X deviate more than 10% from low current density values. Often i_L is increasing with a frequency proportional to f^m (Schwan's law of non-linearity; Onaral and Schwan, 1982; McAdams and Jossinet, 1991a, 1994). m is the constant phase factor (as defined in this book) under the assumption that it is obeying Fricke's law and is frequency independent (see Section 8.2.4). When measuring current is kept less than i_L they showed that Fricke's law is valid down to 10 mHz. The limit current of linearity will usually be lower for X than for R .

PROBLEMS

1. What is the electronegativity of an atom?
2. What is covalent bonding?
3. What is the hydration of an ion?
4. What is the current density at a position in an electrolyte solution where the electric field is 2 V/m and the conductivity is 0.3 S/m.
5. What is a faradaic current?
6. What is a double layer? Does it have capacitive properties?
7. With a Pt wire and a gold wire as electrodes in the same solution, what is the voltage generated by the electrode pair?
8. What are the four electrokinetic effects?
9. What is incremental resistance?
10. A sinusoidal current waveform generates potential differences which are also sinusoidal if the system is linear. Is the current amplitude for onset of non-linearity dependent on the sine frequency?

This page intentionally left blank

3 DIELECTRICS

Chapter Contents

3.1 Polarization in a Uniform Dielectric

- 3.1.1 Coulomb's Law and Static Electric Fields
- 3.1.2 Permanent and Induced Dipole Moments
- 3.1.3 Charge–Dipole and Dipole–Dipole Interactions

3.2 The Basic Capacitor Experiment

3.3 Complex Permittivity and Immittivity

3.4 AC Polarization and Relaxation in a Uniform Dielectric

- 3.4.1 Relaxation and Dispersion
- 3.4.2 Debye Relaxation Model
- 3.4.3 Joule Effect and Temperature Rise

3.5 Interfacial Polarization

- 3.5.1 Maxwell–Wagner Effects
- 3.5.2 Adsorbed Counterions and Lateral Diffusion (MHz– kHz Region)

3.6 The Basic Membrane Experiment

3.7 The Basic Suspension Experiment

3.8 Dispersion and Dielectric Spectroscopy

Problems

We have heard that tissue electrolytes are electrolytic *conductors*, with ions free to migrate, and with considerable DC conductivity. In Chapter 2 a purely electrolytic system was characterized with immittance variables. But the same system may as well be considered as a *dielectric* and characterized with another set of variables. If the dielectric and the electrodes are dry with no free ions, there are no galvanic contact with the electrodes, and accordingly no electrode polarization impedance in series with the dielectric. Dielectric theory is well adapted to such dry systems. Biomaterials can of course be studied in the dry state, but the structure of complex molecules will usually be very different from the natural or living state. With living tissue and the electrolytic conductance of the extracellular fluids the situation is more complicated and hydration, double layer formation and electrode polarization

must be accounted for. *Then both electrolytic and dielectric theories are relevant for the study of biomaterials.*

A dielectric may be defined simply as any material placed between the plates of a capacitor for examination by an applied electric field. Traditionally it is an important difference between dielectric and bioimpedance measurements caused by water. A dielectric is often dry, and no electrode polarization occurs. An electrolytic conductor is wet, and there is an electrode polarization process at the electrode surface. Etymologically a *dielectric* is a material that the electric field penetrates (Greek *dia* meaning through), conductors do not allow static electric field penetration. Basically, a perfect dielectric is a substance without free charges. Synonyms for a perfect dielectric may then be an insulator or non-conductor, antonyms may be conductor or electrolyte. A more direct definition is a material where the capacitive (displacement) current is larger than the in-phase current, $\omega C > G$ or $f > \sigma/2\pi\epsilon$. According to this definition, saline ($\sigma = 1 \text{ S/m}$, $\epsilon = 80 \times 8 \times 10^{-12}$) is a conductor for $f < 250 \text{ MHz}$, and a dielectric for $f > 250 \text{ MHz}$. At sufficiently high frequencies even a metal becomes a dielectric. The definition is frequency dependent, and this is not very practical for a general grouping of materials. In any case, a material is classified as a dielectric if it has an ability to *store energy* capacitively, not just dissipate it.

Thus tissue may be regarded as a conductor or a dielectric, the choice is ours. An electrolytic conductor is characterized by immittance, a dielectric by permittivity or capacitance. However as we shall see, the conductivity may be complex and thus take care of a capacitive component as well, and permittivity and capacitance may be complex and also take care of a conductance. Muscle tissue is more a conductor with certain capacitive properties; stratum corneum is more a dielectric with certain conductive properties. We are in a situation that is confusing for users of bioimpedance data (e.g. medical doctors). Some bioimpedance groups characterize tissue by *immittance* terminology, others by *dielectric* terminology. A dermatologist is confronted with skin characterized by a number of parameters such as capacitance, permittivity, impedivity, impedance, resistivity, resistance, reactance, admittivity, admittance, conductivity, conductance or susceptance. They are different, but possibly correct, ways of describing a biological material.

There have been two main stream traditions in the development of dielectric theories for biomaterials: the Debye tradition of regarding biomolecules as polar materials, and the even elder tradition of regarding them as inhomogeneous materials with important interfacial polarization contributions. As the dielectric theory for polar biomaterials cannot explain many of the experimental findings, interfacial polarization theory has come into focus.

3.1 POLARIZATION IN A UNIFORM DIELECTRIC

Polarization is a difficult concept, widely but differently used. It is a key concept in understanding the electrical properties of tissue, because it covers some very important and characteristic phenomena. We will start with the most general definition of polarization, and then differentiate.

Definition:

Polarization is the electric field induced disturbance of the charge distribution in a region.

The polarization may be *endogenic* (produced by the body itself) or *exogenic* (produced by an externally applied field). Bioimpedance methods are *exogenic* and in general we *apply energy* in order to polarize a system from the outside, for instance by light which is electromagnetic radiation, or from an externally applied electric field. The exogenic energy may be stored or dissipated in the dielectric. The membrane of a living cell is polarized, because the energy-consuming sodium–potassium pump transfers ions across the membrane so that the cell interior is negatively charged with respect to the extracellular fluid. This is an *endogenic* polarization mechanism in living tissue.

All materials are polarizable, but vacuum is not (though it can hardly be called a material). With only bound ions, an electric field displaces the charges, dipoles are formed and the material is polarized. However, with free ions there are important additional effects from the migration of these ions in an electric field. With free ions, their migration in the *bulk* of a homogeneous electrolyte implies *no change in the local charge distribution* (equal amounts of charge entering and leaving a volume), and therefore no polarization strictly speaking according to the definition above. However, the E-field in the bulk also causes a local static displacement of *bound* charges, and this represents a polarization at an atomic level.

In electrochemistry an electrolytic cell may be said to be polarized if a DC current flows through the cell. In potentiometry there is zero DC current, and the recording electrodes are not considered to be polarized. A metal electrode may be positioned in a region which is not isoelectric, or the metal surface properties may vary. The result is local current flow and endogenic polarization without any current in the electrode wires.

3.1.1 Coulomb's Law and Static Electric Fields

Coulomb's law describes the mechanical force F between two charges q_1 and q_2 at distance L :

$$F = q_1 q_2 / L^2 \epsilon_s \quad \mathbf{F} = q_1 q_2 \mathbf{L} / 4\pi L^3 \epsilon_s \text{ [newton]} \quad (3.1)$$

ϵ_s is the static *permittivity*, expressing a property of the material surrounding the charges. Coulomb's law is a most fundamental law in electrostatics, and it is *empirical*. The force will try to unite charges of opposite sign (even if other forces hinder it at the closest distance in an atom). Note that the *coulomb force values are smaller the larger the permittivity of the medium*. If the medium is water with the

large relative permittivity of around 80, the forces are relatively small, and water will tend to break up (dissociate) solute molecules held together by coulomb forces.

From Coulomb's law the concept of the *electric field* is derived. There is an electric field at a location if a charge there is influenced by a mechanical force f (space vector) proportional to the charge:

$$E = f/q \quad (3.2)$$

A free *positive* charge is migrating in the same direction as the E-field. The unit for E is (V/m). $E(x, y, z)$ defines a vector field not linked to a material since it is also defined for vacuum. The work (energy) to bring a charge q from infinity to a location is equal to $q\Phi$, Φ is the potential at that location, and zero potential is by convention infinitely far away in a space without charges. A *potential difference is work per charge*, $1 \text{ V} = 1 \text{ [joule/coulomb]}$. This is the basis for defining potentials in electrolytic systems and in the electric double layer at electrode or cell membrane surfaces.

The equipotential lines will be perpendicular to the E and J vectors, but potential Φ itself is not a vector and has no direction (even if the *change* of Φ has a direction, so Φ has a *gradient* vector, $E = -\nabla\Phi$). Vector quantities being perpendicular at all points in space are treated with what mathematicians call *conformal mapping*.

3.1.2 Permanent and Induced Dipole Moments

In dry materials without free charges (e.g. Teflon or dry NaCl) there is no DC conductance and no local buildup of free charges at dielectric interfaces, no electrolytic polarization, either in the bulk or at the electrodes. However, a local disturbance of the distribution of bound charges will occur. The bound ions of the dielectric can only move (translate, rotate) locally and under strong confinement. *No electric charges are leaving the electrodes entering the dielectric*. Current passage is only possible with AC as a capacitive displacement current.

Suppose that two charges are equal but of opposite sign, kept at a small distance and thus hindered to recombine. Such an electric doublet is called a *dipole* (cf. Fig. 6.4). An atom with the electrons at a distance from the positive nucleus does not necessarily form a net dipole: the center of the electron cloud may coincide with that of the nucleus. However, every such atom is polarizable, because the electrical centers of the charges will be displaced by an *external electric field*. As positive and negative charges move in opposite directions, *dipoles* are formed (*induced*) and the material *polarized*. In addition, molecules may form *permanent* dipoles, which of course also will be influenced by an externally applied electric field. A polyatomic molecule is non-polar if it fulfils certain symmetry criteria. Water molecules are asymmetrical and therefore polar.

In electrostatic theory a dipole is characterized by its electrical *dipole moment*, the space vector p :

$$p = qL \text{ [Cm]} \quad (3.3)$$

The unit for p is coulomb meter, or outside the SI system: the *Debye unit* ($D = 3.34 \cdot 10^{-30} \text{ Cm}$). A pair of elementary charges $+e$ and $-e$ held at a distance of 0.1 nm

has a dipole moment of 4.8D, a water molecule has a *permanent* dipole moment of about 1.8D.

The dipole moment \mathbf{p} may be the resultant dipole moment of a molecule, many molecules or a whole region. Polarization \mathbf{P} [$\text{Cm/m}^3 = \text{C/m}^2$] is the electrical dipole moment *per unit volume* (dipole moment volume density). It is therefore a more macroscopic concept than the dipole moment of molecules or atoms. \mathbf{P} is a space vector having the same direction as the \mathbf{E} vector in isotropic materials:

$$\begin{aligned}\mathbf{P} &= \mathbf{D} - \epsilon_0\mathbf{E} = (\epsilon_r - 1)\epsilon_0\mathbf{E} = \chi\epsilon_0\mathbf{E} \\ \mathbf{D} &= \epsilon\mathbf{E} = \epsilon_0\mathbf{E} + \mathbf{P}\end{aligned}\quad (3.4)$$

\mathbf{D} (either as a surface charge density q_s [C/m^2], or dipole moment volume density [Cm/m^3]) is called the *electric flux density*, ϵ_r is called the *relative permittivity* or *dielectric constant* (dimensionless) of the material. $\chi = \epsilon_r - 1$ is called the *electric susceptibility*¹ of the material.

Equation (3.4) shows the relationship between polarization and permittivity. High polarization means high permittivity, $E = 0$ means $P = 0$ and no polarization. Permittivity is a measure of the amount of dipole moment density created (induced) by an electric field. Bound charges which can be displaced a long distance L , cause a larger dipole moment (eq. 3.3) resulting in a higher permittivity. A substance in the liquid state is therefore more strongly polarized than in the solid state, ice has lower permittivity than water. Tissue components such as the proteins are characterized by particularly long distances between charges, and can thus have a surprisingly high permittivity. Polarization effects actually are net effects of a constantly changing charge distribution, the degree of disorder increases with temperature according to the Boltzmann factor kT .

Polarization P cannot itself be measured. Dielectric theory is therefore invariably linked with the concept of a capacitor formed by two plates with a dielectric in between (Fig. 3.1). The capacitance of this capacitor can be measured, and the polarization *calculated*.

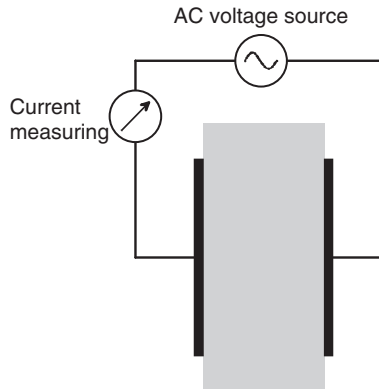


Figure 3.1 The basic capacitor experiment.

¹ Not to be confused with susceptibility in the relation: admittivity, conductivity and susceptibility.

Some molecules are *polar* (e.g. in water and many proteins). The *permanent* dipole moments are oriented at random, but with an externally applied electric field they reorient statistically. *Induced* dipoles have the direction of the applied \mathbf{E} -field, but if the medium is *polar*, the polarizing \mathbf{E} -field also *rotates the permanent dipoles* already in existence (orientational polarization). Polar materials have a large permittivity in addition to the permittivity caused by the induced dipoles of the non-polar molecules present. The permanent dipoles will experience a rotational force, defined by the *torque* $\boldsymbol{\tau}$:

$$\boldsymbol{\tau} = \mathbf{p} \times \mathbf{E} \quad [\text{Nm}] \quad (3.5)$$

If the charges are bound, the torque will result in a limited rotation. The positions and angles are statistically distributed with less ordering the higher the temperature. As we see in Section 2.4.6, in a *rotational* \mathbf{E} -field the *induced* dipoles may lag the external field, and thus also give rise to a torque and continuous rotation.

In some polar media the dipole moments are “frozen” in positions that statistically results in a net component in a given direction. They are called *electrets*, and they have a net internal \mathbf{P} -field in the absence of an externally applied field. An electret is the electrical equivalent of a permanent magnet. In the form of a thin sheet, the resultant equivalent surface charge density may be of the order of $50 \times 10^{-3} \text{ C/m}^2$. Slowly the polarization will diminish, but the process may take many years.

The polarization vector \mathbf{P} is composed of all three components:

1. An external field produces new dipoles (induced dipoles).
2. An external field orients the permanent dipoles already there.
3. Without an external field electrets have a permanent net dipole moment.

Susceptance χ is a macroscopic parameter and is correlated with a microscopical factor called the *polarizability* α (Cm^2/V) so that $\mathbf{p} = \alpha \mathbf{E}_L$ where \mathbf{E}_L is the local electric field strength. Then macroscopically $\mathbf{P} = N\alpha \mathbf{E}$, where N is the volume density of atoms or molecules. In non-polar media there is a simple relationship between the polarization and the molecular structure, the *Clausius–Mosotti* equation:

$$\frac{\epsilon_r - 1}{\epsilon_r + 2} = \frac{N\alpha_e}{3\epsilon_0} \quad (3.6)$$

Equation (3.6) can be extended to also comprise the contribution from polar molecules, the *Debye* equation:

$$\frac{\epsilon_r - 1}{\epsilon_r + 2} = \frac{4\pi N_A \left(\alpha^2 + \frac{p^2}{3kT} \right)}{\nu_m} \quad (3.7)$$

where ν_m is the molar volume and N_A is Avogadro's constant. The kT -factor is due to the statistical distribution of polar molecules causing the orientational polarization. Equations 3.6 and 3.7 are in best agreement with gases, in less agreement

in liquids and least in solids. For the last-mentioned cases Onsager and Kirkwood have extended the theory.

Polarization linked with bound charges is usually divided in three components; the total polarization is the sum of the three:

Electronic Polarization

Dipole moment density as a result of very small translational displacements of the electronic cloud with respect to the nucleus, whether in single atoms or in molecules. Displacement of electrons are very fast (picosecond), and the dispersion is in the gigahertz region. Induced dipoles will have the direction of the local E-field, and undergoes no rotation.

Orientalional Polarization

Rotational movement caused by the torque experienced by *permanent* dipoles in an electric field. The effect is seen only in polar materials.

Ionic Polarization

This is displacement of positive ions with respect to negative ions. To clarify the division between electronic and ionic polarization: electronic polarization is the displacement of the electron cloud with respect to the nucleus, ionic polarization is the displacement of ions relative to each other. The hydrated sheath around an ion at rest is symmetrical (not really at rest, everything is bumping around at room temperature, we are talking statistically). When current flows, the sheath will lag behind the migrating ion, and the sheath is no longer symmetrical to the ion (cf. the Wien effect (Section 2.5.4)). This is local polarization of charges bound to each other.

A molecule with a net charge $\neq 0$, will experience a translational force and therefore try to migrate in a *homogeneous* electric field. A dipole with net charge = 0, will *also* experience a translational force, but *only* in a *non-homogeneous* field.

3.1.3 Charge–Dipole and Dipole–Dipole Interactions

Equation 3.3 defines the electrostatic dipole moment $\mathbf{p} = q\mathbf{L}$. The potential field $\Phi(x, y, z)$ from such a dipole is given by:

$$\Phi(x, y, z) = \mathbf{p} \cdot \hat{\mathbf{r}} / 4\pi\epsilon_0 r^2 \quad (3.8)$$

where $\hat{\mathbf{r}}$ is the unit vector from the dipole to the point (x, y, z) where the potential is to be defined. A prerequisite for this equation is that the dimension of the charges is much smaller than the distance L between them (cf. Section 6.3.3). The potential field is visualized in Fig. 6.4. According to eq. (3.8) the potential falls off as $1/r^2$. Then the E-field must fall off as $1/r^3$.

In a molecule there may be local dipoles and single charges in the meaning that the counter charge is far away. Electrostatic forces will occur which basically are of a charge-to-dipole or dipole-to-dipole nature. These forces will be intermolecular and intramolecular and will therefore influence the geometrical form of the molecule.

TABLE 3.1 Energy Dependence on Distance Between Ions/Dipoles

Interaction	Distance dependence of \hat{E}
Ion–ion	$1/r$
Ion–dipole	$1/r^2$
Dipole–dipole	$1/r^3$
Dipole–dipole (random rotation)	$1/r^6$

The static energy \hat{E} related to a point charge q at a distance r from an ideal dipole is:

$$\hat{E} = -pq/4\pi\epsilon_s r^2 \text{ [joule]} \quad (3.9)$$

Table 3.1 shows the static energy dependence on the distance between ions/dipoles. Note that the energy falls off more rapidly when two dipoles rotate at random than under stationary non-thermal conditions (cf. Table 6.2).

3.2 THE BASIC CAPACITOR EXPERIMENT

Set Up

In Chapter 2 we treated the electrolytic cell. Now we will introduce a similar cell: the capacitor with two plates. The substance we placed between the electrode plates is called an electrolyte (in a solution), the substance between the plates of a capacitor is called a *dielectric* (Fig. 3.1). In one sense the difference between Fig. 2.1 and Fig. 3.1 is not very large. In Fig. 2.1 we considered a liquid between metal plates, and we studied DC conductance. The material between the plates had a *high* volume density of free charges. In Fig. 3.1 we consider a dry solid material such as Teflon with a *low* volume density of free charges, but many bound charges between the metal plates. Both DC and AC current is measured, with a phase sensitive voltmeter/ammeter or displayed on a two-channel oscilloscope.

Findings

Applying a DC voltage of even 10–20 V does not lead to a DC current. Applying an AC sinusoidal voltage leads to an AC sinusoidal current, and the current is proportional not only to voltage amplitude, but also to the signal frequency. The current top comes earlier than the voltage top, the current leads the voltage by almost 90°. As long as this is the case, even large currents do not warm up the dielectric.

Discussion

A capacitive current is an AC current. It is not an electron current of free charges passing between the plates through the dielectric. It is a true current of electrons charging the capacitor plates, but without electrons leaving or entering the plates.

It is a simple relationship between the charge Q [coulomb] on the plates, the voltage (V) between the plates, and the capacitance C [F] of the capacitor:

$$Q = VC \quad [\text{coulomb}] \quad (3.10)$$

The capacitance C of the capacitor is dependent on the plate area A [m²], the distance between the plates d [m], and a property of the dielectric between the plates defined already in Section 3.1.1. as *permittivity* ϵ [farad/m]:

$$C = (A/d)\epsilon \quad [\text{farad}] \quad (3.11)$$

If we apply a sinusoidal AC voltage to the plates as shown in Fig. 3.1, the AC current flowing as electrons in the capacitor metal wires will not have its maximum current value at the same time as the voltage maximum occur. The current is *phase shifted* in time. We measure the phase shift in degrees, defining one complete cycle of the AC sinusoidal voltage as 360° or 2π radians. An ideal, steady state sinusoidal capacitive current is 90°*ahead* of the sinusoidal voltage. It is possible by suitable electronic circuitry to separately measure the *in-phase* (conductive) current (or voltage) component, and the 90° out-of-phase (*quadrature*) (capacitive) current (or voltage) component. It is not sufficient to characterize an AC current only with one number, the amplitude. The current must be characterized by *two* numbers, with the additional number giving information about the phase. The sum of two equal amplitude sine waves is the double amplitude if they are in phase, but constant equal to zero if they are 180° out of phase.

The electric flux density D introduced in Section 3.1.2 represents a displacement of *bound* charges in the bulk of the dielectric. At the capacitor metal plates, D is also the charge per plate area: q/A , but there it is related to the *free* (electron) charge flow corresponding to the measured current in the capacitor leads. The status in the volume of the dielectric is not directly noticeable from the capacitor plates. For the capacitor, the effect of the whole dielectric volume can be reduced to the two layers of bound charges at the surface of the dielectric, each in (almost) contact with the metal plates. These charged layers are “the ends” (this must not be taken too literally, e.g. the charge separation at ordinary field strengths with electronic polarization is very, very small and less than the electron diameter) of the surface dipoles in the dielectric, induced by the external field but bound in the dielectric.

The E-field strength in the dielectric is reduced by the bound charges at the surface of the dielectric. The higher the permittivity, the lower the bulk E-field. The E-field is *discontinuous* at the dielectric surface. The electric flux density D is *continuous* at the dielectric surface as long as there are no free charges there.

3.3 COMPLEX PERMITTIVITY AND IMMITTIVITY

We revert to the basic capacitor model of Fig. 3.1. The *admittance* Y of the capacitor is (sinusoidal AC voltage u , homogeneous dielectric and no edge effects):

$$Y = G + j\omega C = (A/d)(\sigma' + j\omega\epsilon') \quad (3.12)$$

The current in the capacitor wire $\mathbf{i} = u\mathbf{Y} = uG + j\omega C$. The conductance G and the current uG comprises all components which are in phase with u . G is due to a direct DC conductance of free charges and the AC losses of bound charges in the dielectric. The j indicates that the $u\omega C$ current is in quadrature (90° phase shifted) with u , it is a displacement current. AC losses and the permittivity ϵ are usually frequency dependent, but even then \mathbf{Y} is usually equal to $(A/d)\sigma'$ at low frequencies.

Different uses of the symbol ϵ are found in the literature. Often it is not clear whether ϵ is the relative permittivity ϵ_r (dimensionless, often called the *dielectric constant*), or (as in this book) the complete expression $\epsilon_r\epsilon_0$. The epsilon subscripts are complicated: ϵ_s means static permittivity. This is not the same as ϵ_{DC} because static is electrostatic with no current flow. DC means current flow but zero frequency. ϵ_0 does not mean permittivity at zero frequency, but the permittivity of vacuum. ϵ_∞ is the permittivity at very high frequencies. And indeed here it may be high frequencies up in the optical range. The relationship between the optical refractive index n and the permittivity is roughly $n = \sqrt{\epsilon_r}$.

As seen from Table 3.2, the permittivity of water is reduced by the addition of electrolytes. This *dielectric decrement* $\Delta\epsilon_r$ is for 1 mole/L concentration -17 for

TABLE 3.2 Relative Permittivity

	10^2 [Hz]	10^6 [Hz]	10^{10} [Hz]
Gases			
Air (100 kPa)	1.00054		
Liquids			
Carbon tetrachloride	2.2	2.2	2.2
Benzene	2.28	2.28	2.28
Olive oil	3.1		
Chloroform	4.8		
Ethanol	25.7		
Water (0°C)	87.7		
Water (20°C)	80.1		
Water (25°C)	78.5	78.5	65
Water (25°C KCl-0.5 mol/L)	75	75	
Water (37°C)	74.3		
Hydrogen cyanide	116		
Solids			
Teflon	2.1	2.1	2.1
Polystyrene	2.6	2.6	2.6
Plexiglas	3.1	2.76	
Ice		4.15	3.2
Glass (Pyrex)	5	4.8	4.8
NaCl		5.9	5.9
KCl	5		
AgCl	11		

H^+ , -8 for Na^+ and K^+ , -3 for Cl^- and -13 for OH^- . It is directly related to the hydration of the ion, because these water molecules are more tightly bound and therefore not so easily polarized as free water molecules. The number of hydrated water molecules around a monovalent ion is of the order of 6 (cf. Table 2.4).

Complex Permittivity and Conductivity

It may be useful to treat σ and ε as complex quantities in the time domain, for example, in order to incorporate dielectric losses and frequency dependence. We then define:

$$\boldsymbol{\sigma} \equiv \sigma' + j\sigma'' \quad [S/m] \quad (3.13)$$

$$\boldsymbol{\varepsilon} \equiv \varepsilon' - j\varepsilon'' \equiv (\varepsilon'_r - j\varepsilon''_r)\varepsilon_0 \quad [F/m] \quad (3.14)$$

Note the minus sign in eq. (3.14) (complex conjugate).

Accordingly eq. (3.12) was written: $\mathbf{Y} = (A/d)(\sigma' + j\omega\varepsilon')$. Tissue data is often given with ε' and σ' parameters. But instead tissue data may be given with either *only* complex conductivity or complex permittivity. All three ways are in common use.

Complex Permittivity

Complex permittivity is used when the material is considered as a dielectric (an insulator) with losses. The capacitor is characterized with a complex capacitance and a complex permittivity:

$$\begin{aligned} \mathbf{Y} &= (A/d)(\sigma' + j\omega\varepsilon') = j\omega\mathbf{C} = j\omega(A/d)\boldsymbol{\varepsilon} \\ &= j\omega(A/d)(\varepsilon' - j\varepsilon'') = (A/d)(\omega\varepsilon'' + j\omega\varepsilon') \end{aligned} \quad (3.15)$$

Therefore:

$$\varepsilon'' = \sigma'/\omega \quad [F/m] \quad (3.16)$$

σ' is proportional to energy loss per *second* (power loss), ε'' to energy loss per *cycle* (*period*). Frequency independent DC conductivity σ' implies constant energy loss per second and therefore an energy loss per cycle is inversely proportional to frequency (eq. 3.16). Therefore ε'' diverges when the (angular) frequency approaches zero if σ' is frequency independent. This is why the use of ε'' for electrolytic materials may be less attractive.

Complex Conductivity

Complex conductivity is according to the basic capacitor model shown in Fig. 3.1, where capacitance and conductance are physically in parallel. Complex conductivity is used when the material is considered as a conductor with capacitive properties. The medium is characterized with a complex conductivity:

$$\mathbf{Y} = (A/d)(\sigma' + j\omega\varepsilon') = \mathbf{G} = (A/d)\boldsymbol{\sigma} = (A/d)(\sigma' + j\sigma'') \quad [S] \quad (3.17)$$

Usually G is a real number in the equation $\mathbf{Y} = G + jB$, but now G is considered complex = $\mathbf{G} = \mathbf{Y}$, thus taking care also of B . Then $\sigma'' = \omega\epsilon'$ [S/m], diverging as $f \rightarrow \infty$ (in contrast to ϵ'). This is why σ'' in electrolytic materials may be a less attractive parameter.

Complex Resistivity²

Complex resistivity is not according to the basic parallel model of Fig. 3.1, it is linked with impedance and the series equivalent model. Complex resistivity is the inverse of complex conductivity:

$$\rho = \rho' - j\rho'' = 1/\sigma = (\sigma' + j\sigma'')/|\sigma|^2 \quad [\Omega\text{m}] \quad (3.18)$$

Pay attention³ to the fact that $\rho' \neq 1/\sigma'$, but $\rho = 1/\sigma$ in the meaning $|\rho| = 1/|\sigma|$.

Losses

$\epsilon_r'' = \sigma'/(\epsilon_0\omega)$ is sometimes called the loss *factor*. The loss *angle* δ of a capacitor is defined so that the ideal capacitor with zero losses also has zero loss angle. This means that $\delta = 90^\circ - \varphi$:

$$\begin{aligned} \varphi &= \arctan \epsilon'/\epsilon'' \\ \delta &= \arctan \epsilon''/\epsilon' = \operatorname{arccot} \epsilon'/\epsilon'' \end{aligned} \quad (3.19)$$

$\tan \delta$ is also called the loss *tangent* or *dissipation factor*. $\tan \delta$ is energy lost per cycle divided by energy stored per cycle (rms or peak values).

Care must therefore be taken with regard to the term “phase angle.” In ordinary immittance texts it is always the tangent of the out-of-phase component divided by the in-phase component. However, in many classical presentations the loss angle is used instead for characterizing the polarization properties of an electrode: (Fricke, 1932: symbol ψ ; Schwan, 1963: symbol δ). Also in the classical Warburg (1899) paper: his angle ψ is the loss angle. Sometimes the loss angle is called the loss angle, sometimes it is called the phase angle.

Modulus Function

It may be useful to have a parameter for the inverse of the permittivity. This is the *modulus function* \mathbf{M} :

$$\mathbf{M} = 1/\epsilon = M' + jM'' \quad [\text{m/F}] \quad (3.20)$$

²Use of “specific resistance” and “specific conductance” for resistivity and conductivity is not recommended. Resistivity has the unit $[\Omega\text{m}]$, but “specific” means a quantity per mass, so specific resistance should then have been $[\Omega/\text{kg}]$.

³Historically there was no problem when only real quantities $\rho = 1/\sigma$ were used. However, with complex quantities, if ρ' is called resistivity, then σ' has no name because $\sigma' = \rho'/|\rho|^2 \neq 1/\rho'$!

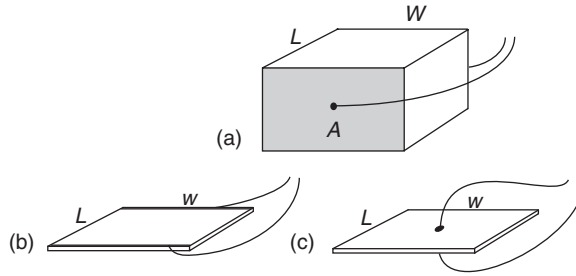


Figure 3.2 Geometrical models: (a) volume immittivity; (b) surface lateral immittivity; (c) surface perpendicular immittance.

Immittance and Material Constants, a Survey

Impedance [Ω] and admittance [S] are quantities dependent on sample and electrode geometries. Immittivity (impedivity [Ωm], admittivity [S/m]) and permittivity (F/m) are material constants.

Impedivity and complex resistivity [Ωm] are synonyms. Admittivity and complex conductivity [S/m] are synonyms. With a sample in a measuring *in vitro* cell like Fig. 3.1 or Fig. 3.2(a), the material constant admittivity = complex conductivity can be found from measured admittance \mathbf{Y} : $\sigma = \mathbf{Y}(d/A)$. The relationship between impedivity = complex resistivity and measured impedance \mathbf{Z} is: $\rho = \mathbf{Z}(A/d)$. *In vivo* measurements are difficult to perform in a measuring cell, and it is much more difficult to go from measured immittance to immittivity with the electric field distribution unknown. Tissue anisotropy and inhomogeneity add to the problems.

In a text it is often not clear whether ϵ is scalar or complex. If σ or ϵ are complex they are printed in bold in this book: $\boldsymbol{\epsilon}$ or $\boldsymbol{\sigma}$. If the parameters are not printed in bold, there may be an ambiguity: Y, Z, σ and ϵ may mean $|Y|, |Z|, |\sigma|$ and $|\epsilon|$, or the real values Y', Z', σ' and ϵ' .

$\sigma', \sigma'', \epsilon'$ and ϵ'' are components of the complex quantities $\boldsymbol{\sigma}$ and $\boldsymbol{\epsilon}$, their somewhat bewildering frequency dependent relationships are:

$$\begin{aligned} \boldsymbol{\sigma} &= j\omega\boldsymbol{\epsilon} \\ \sigma' &= \omega\epsilon'' = G(d/A) & \sigma'' &= \omega\epsilon' = \omega C(d/A) = B(d/A) \\ \epsilon' &= \sigma''/\omega = Cd/A = (B/\omega)(d/A) & \epsilon'' &= \sigma'/\omega = (G/\omega)(d/A) \end{aligned} \quad (3.21)$$

If the capacitance of the empty cell is C_e , (no dielectric, pure capacitance) it is possible to express some interesting relationships:

$$\mathbf{Y} = j\omega C_e \boldsymbol{\epsilon}_r \quad \mathbf{M} = j\omega C_e \mathbf{Z} \quad \mathbf{M} = j\omega C_e / \mathbf{Y} \quad (3.22)$$

Surface Lateral Immittivity

Usually a material is characterized with quantities for volume properties. However, an epithelium or antistatic coating may have a high resistivity with respect to the

substrate, combined with known area but unknown thickness. Then surface parameters may be useful see Fig. 3.2 (w = sample width):

$$\begin{aligned} \text{Surface lateral conductivity} \quad \sigma_{sl} &= G L/w \quad [\text{S}] & (3.23a) \\ \text{Surface lateral resistivity} \quad \rho_{sl} &= R w/L \quad [\Omega] \end{aligned}$$

Note that the surface lateral quantities have units just in [siemens] or $[\Omega]$, as L/w is dimensionless. The surface lateral parameters are pseudomaterial constants because they characterise a given surface or membrane presupposing a given, constant but unknown thickness (e.g. a tissue membrane), and with negligible influence e.g. from a substrate underneath. If these conditions are not fulfilled, surface lateral parameters are not recommended.

Like the volume material constants the surface pseudomaterial constants may be extended to be complex, e.g. surface lateral admittivity $\sigma_{sl} = Y L/w$ [S] being composed of surface lateral conductivity $\sigma'_{sl} = G L/w$ and surface lateral susceptibility $\sigma''_{sl} = B L/w$.

Surface perpendicular immittance

$$\begin{aligned} \text{Surface admittance density} \quad Y_{sd} &= G / Lw \quad [\text{S/m}^2] & (3.23b) \\ \text{Surface impedance density} \quad Z_{sd} &= RLw \quad [\Omega\text{m}^2] \end{aligned}$$

These parameters are in particular useful when dealing with high impedivity layers like human skin. Such parameters may also be given as e.g. admittance [S] *normalized* to 1 cm^2 , and preferably adding information about the actual surface area used.

3.4 AC POLARIZATION AND RELAXATION IN A UNIFORM DIELECTRIC

3.4.1 Relaxation and Dispersion

In Section 3.1 about polarization we considered polarization as a static state of a material, dependent not on time, but only on the externally applied field. In an electric field of time varying strength or direction, the charge positions were considered to be in time phase with the instantaneous values of the applied field. However, polarization and the displacement of charges in a material do not occur instantaneously. If the measuring frequency is low enough so that all charges are allowed the necessary time to change their position, polarization is maximal. But with increasing frequency the polarization and permittivity will decrease.

This time dependence may be characterized by introducing the concept of *relaxation*. It was first used by Maxwell in connection with the elastic forces in gases. Later Debye used it referring to the time required for dipolar molecules to orient themselves. Instead of applying a sinusoidal AC measuring signal and measure, for example, admittance and phase shift, the concept of relaxation is linked with a *step function* excitation signal. After a step has disturbed a system under investigation, the system is allowed to *relax* to the new equilibrium, this is the relaxation process.

Relaxation occurs in the *time* domain, after a step increase or decrease in the E-field strength. It is described by the parameter: *relaxation time*, different from the parameter immittance as a function of the frequency of a sine wave excitation.

It is often stated that all electrical properties of biological materials are due to relaxation phenomena. However, the concept of relaxation is not so meaningful with frequency independent DC conductance; the conductance is constant with time and does not relax.

Relaxation theory often does not include resonance phenomena, as these are usually not found in macro tissue samples in the frequency range from μHz to MHz.

Relaxation time is dependent on the polarization mechanism. Electronic polarization is the fastest mechanism, with relaxation in the higher MHz and GHz region. Large organic molecules like proteins may have a particular large permanent dipole moment because of the large distance L between the charges. Because they are so large and with a complex bonding, the rotation and twist can be relatively slow. However, interfacial relaxation may be the most important process and with the longest mean relaxation times of the order of seconds.

Dispersion (frequency dependence according to the laws of relaxation) is the correspondent frequency domain concept of relaxation: permittivity as a function of frequency. Even if the concept of relaxation is linked with step functions, it can of course be studied also with sine waves. An ideal step function contains all frequencies, and dispersion can be analyzed with a step function followed by a frequency (Fourier) analysis of the response signal, or with a sinusoidal signal of varying frequency.

As we shall see in the next section: in a simple case of a *single dispersion* with a single relaxation time constant there will be one permittivity level at low frequencies (time for complete relaxation), and a second *lower* level at higher frequencies (not sufficient time for the relaxation process studied). It will be a transition zone characterized by a frequency window with a characteristic center frequency. Therefore dispersion in relaxation theory often has a somewhat more precise meaning than just frequency dependence. *Simple dispersions are characterized by a permittivity with two different frequency independent levels, and a transition zone around the characteristic relaxation frequency.* In biomaterials these levels may be found more or less pronounced.

3.4.2 Debye Relaxation (IR-2C) Model

Let us assume a dielectric with only bound charges placed between two capacitor plates, and that a step increase of DC voltage is applied at $t = 0$ (Fig. 3.3). *Let us assume that the material has only one relaxation process with a single characteristic time constant*, and that the polarization increases according to an exponential curve as a function of time. This is called a *Debye single dispersion*. As a result of the polarization in the dielectric, the surface free charge density $D(t)$ ($= q_s$) at the capacitor plates will increase from one value (D_∞) to another (D_0) according to the equation:

$$D(t) = D_\infty + (D_0 - D_\infty)(1 - e^{-t/\tau}) \quad (3.24)$$

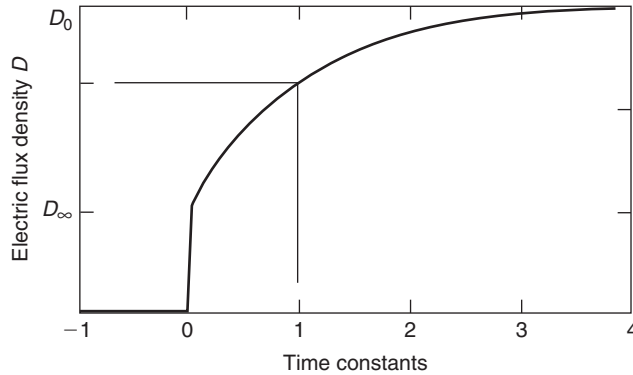


Figure 3.3 Capacitor plate surface free charge density q_s (electric flux density D) after an applied voltage step.

The subscripts refer to frequency, a sine wave parameter. D_∞ is the surface charge density at $t = 0+$ that is after the step but so early that only apparently instantaneous polarization mechanisms have come to effect (high frequency, e.g. electronic polarization). The capacitor charging current value at $t = 0$ is infinite, so the model has some physical flaws. D_0 is the charge density after so long time that the new equilibrium has been obtained and the charging current has become zero. With a single Debye dispersion this low frequency value is called the *static* value (cf. Section 7.2.1). τ is the *time constant* of the relaxation process.

By Laplace transforming eq. (3.24) it is possible to find the response in the frequency domain. With $\epsilon' = D/E$, and $C = \epsilon'A/d$, it is possible to show that:

$$\epsilon(\omega) = \epsilon'_\infty + \Delta\epsilon'/(1 + j\omega\tau) \quad \text{Debye single dispersion equation} \quad (3.25)$$

$$C(\omega) = C_\infty + \Delta C/(1 + j\omega\tau) \quad (3.26)$$

Here ϵ and C are vectors in the time domain. We have already seen the ambiguity that ϵ may mean $|\epsilon|$ or ϵ' . In dispersion theory this is less a problem, because the parameters used are at frequency extremes, where $\epsilon_s = \epsilon'_s$ and $\epsilon_\infty = \epsilon'_\infty$.

At low frequencies we measure a frequency independent capacitance $C_0 = C_\infty + \Delta C$. The frequency must be low enough to guarantee that the polarization process can follow. In a sufficiently higher frequency range we measure another frequency independent capacitance C_∞ , lower than C_0 . The frequency must be sufficiently high so that the polarization process in question cannot follow.

The best equivalent circuit for such behavior is shown in Fig. 3.4. Figure 3.4 is the circuit of Fig. 8.12(a) and Fig. 11.5. With $\tau = R\Delta C$, the complex admittance and capacitance of this equivalent circuit are:

$$\begin{aligned} Y &= j\omega C = j\omega C_\infty + j\omega\Delta C/(1 + j\omega\tau) \\ C &= C + \Delta C/(1 + j\omega\tau) \end{aligned} \quad (3.27)$$

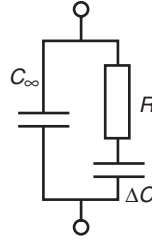


Figure 3.4 Dielectric 1R-2C model circuit for a Debye single dispersion. No DC conductance.

The *quadrature* components of eq. (3.27) are:

$$\begin{aligned} Y'' &= \omega[C_\infty - \Delta C\omega\tau/(1 + \omega^2\tau^2)] \\ C' &= C_\infty + \Delta C/(1 + \omega^2\tau^2) \\ \epsilon' &= \epsilon'_\infty + \Delta\epsilon'/(1 + \omega^2\tau^2) \end{aligned} \tag{3.28}$$

The *in-phase* loss components are:

$$\begin{aligned} Y' &= \Delta C\tau\omega^2/(1 + \omega^2\tau^2) \\ C'' &= \Delta C\tau\omega/(1 + \omega^2\tau^2) \\ \epsilon'' &= \Delta\epsilon'\tau\omega/(1 + \omega^2\tau^2) \end{aligned} \tag{3.29}$$

The quadrature component dependence with increasing frequency is from a higher level to a lower, the in-phase component goes through a maximum. C_∞ and ΔC are ideal capacitors. At very high frequencies C_∞ dominates the total admittance and capacitance. At very low frequencies R is negligible with respect to the impedance of ΔC , and the two capacitors C_∞ and ΔC are effectively in parallel. So both at high and low frequencies the circuit is purely capacitive. Correspondingly, ϵ'_∞ and $\Delta\epsilon'$ are real values associated with ideal capacitors. ϵ' is the parameter used, because at very high and very low frequencies $\epsilon'' = 0$ and ϵ is real with values not influenced by R . The *characteristic relaxation frequency* ω_c is the frequency corresponding to $\omega\tau = 1$ and the maximum ϵ'' . The characteristic relaxation time constant is $\tau = R\Delta C$, and therefore $\omega_c = 2\pi/\tau$. The value of ϵ' and maximum ϵ'' are found from eqs. (3.28) and (3.29).

$$\begin{aligned} \epsilon'_{\omega\tau=1} &= \epsilon'_\infty + \Delta\epsilon'/2 \\ \epsilon''_{\omega\tau=1} &= \Delta\epsilon'/2 \end{aligned} \tag{3.30}$$

Maximum value of ϵ'' is therefore not related to the resistor R , but R determines at what characteristic frequency the maximum value will occur.

The power loss W_L in the circuit is (constant amplitude sinusoidal *voltage* = v) (cf. Section 11.2):

$$W_L = v^2 Y' = v^2 \Delta C \omega^2 \tau / (1 + \omega^2 \tau^2) \quad [\text{watt}] \tag{3.31}$$

The power loss W_L (constant amplitude sinusoidal *current* = i) is:

$$W_L = i^2 Z' = i^2 \Delta C \omega \tau [(C_\infty + \Delta C)^2 + C_\infty^2 \omega^2 \tau^2] \quad [\text{watt}] \quad (3.32)$$

The power loss and heat dissipation do only occur in the resistor, the two capacitors are ideal components. The frequency dependence of the power loss is dependent on how the circuit is driven. With constant amplitude *voltage*, the power loss goes from zero level at very low frequencies to a defined level v^2/R at high frequencies (like σ' , see below). With constant amplitude *current*, the power loss goes from zero level at very low frequencies, through a maximum at the frequency determined by the time constant $\tau = R\Delta C$, and back to zero (like ϵ'' , see below).

Calculating the complex *conductivity* σ , the difference between high and low frequency conductance $\Delta\sigma'A/d$ must be $1/R$. $Y = (A/d)(\sigma' + j\sigma'')$, and this must be compared with Y' eq. (3.29), and Y'' eq. (3.28):

$$\begin{aligned} \sigma' &= \Delta\sigma'\omega^2\tau^2/(1 + \omega^2\tau^2) && \text{in-phase (lossy) component} \\ \sigma'' &= \omega C_\infty + \Delta\sigma'\omega\tau/(1 + \omega^2\tau^2) && \text{quadrature (capacitive) component} \end{aligned} \quad (3.33)$$

The in-phase component σ' dependence with increasing frequency is from zero to a finite level, in contrast to ϵ'' which returned to zero at high frequencies. The last term of the quadrature component equation goes through a maximum, but the first term is proportional to frequency and diverges, just like a capacitive susceptance $B = \omega C$. It is not very logical to characterize a capacitive material with conductivity variables, and some training is necessary for interpreting quadrature conductivity data for dielectrics. $\Delta\sigma'$ is a real number associated with the ideal conductor R . $\Delta\sigma'$ is the parameter used in eq. (3.33), because at very high and low frequencies σ' and the last part of the equation for σ'' both are real and not influenced by the two capacitors.

Control Equation

It is an interesting and useful link between three of the variables of eqs (3.28) and (3.29). If $\tau = R\Delta C = R\Delta\epsilon'A/d$ and $\Delta\sigma'A/d = 1/R$, the scalar relationship between $\Delta\epsilon'$, τ and $\Delta\sigma'$ is very simple:

$$\Delta\epsilon' = \tau\Delta\sigma' \quad (3.34)$$

This equation is valid only if there is no DC conductance in parallel with the equivalent circuit and C_∞ . If it is, that part must first be subtracted. σ' is limited to the AC lossy part of the dielectric.

Equation 3.34 represent an efficient tool for a control of measurement results, for example, of the data presented in Figs. 3.5 to 3.8. It is a special case of the more general Kramers–Kronig transform, interconnecting, for example, permittivity and losses as demonstrated in Fig. 3.5 and described in Section 7.1.7.

EXAMPLE: 1R-2C CIRCUIT

Figure 3.5 shows data based on the circuit of Fig. 3.4 and eqs (3.28) and (3.29) with chosen values: $\epsilon_{r\infty} = 1000$, $\Delta\epsilon_r = 9000$, $\tau = 1,592$ ms. With a ratio $A/d = 20$, this corresponds to $C_\infty = 0.18 \mu\text{F}$, $\Delta C = 1.6 \mu\text{F}$ and $R = 1004 \Omega$.

Almost 80% of the ϵ' -dispersion takes place within one frequency decade, more than 98% in two decades. The ϵ'' -dispersion is broader. It is easy to see that the data is purely capacitive at high and low frequencies.

In the Wessel diagram, the locus of the permittivity is a complete half circle (Fig. 3.6). Also here it is easy to see that the data is purely capacitive at high and low frequencies.

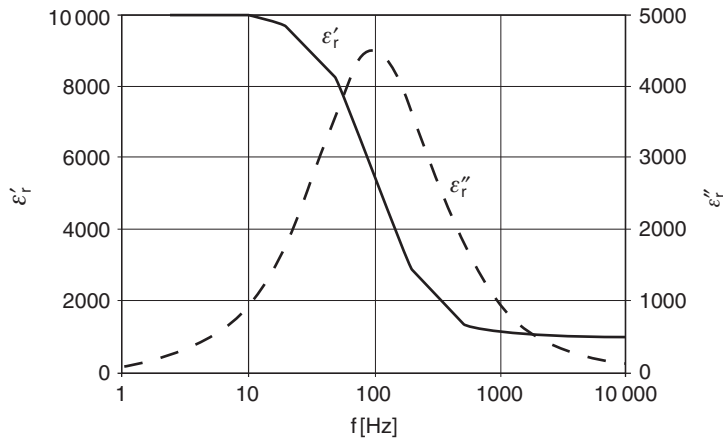


Figure 3.5 Debye single dispersion relaxation, relative permittivity. Values found in the text.

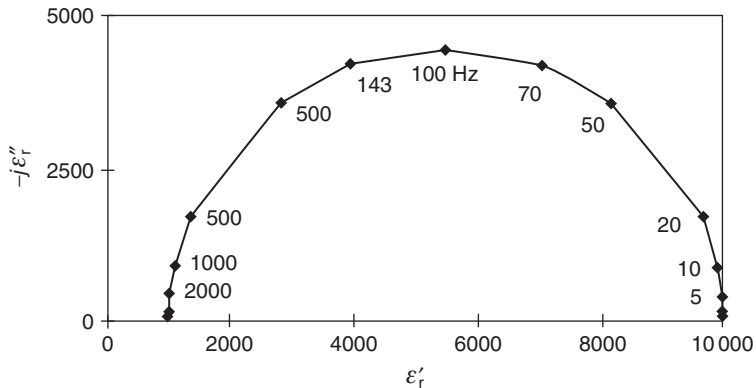


Figure 3.6 Relative permittivity plotted in the Wessel diagram, same data as Fig. 3.5.

The complex conductivity (same component values) has been plotted as a function of $\log f$ in Fig. 3.7. In-phase conductivity σ' increases to the plateau corresponding to $\Delta\sigma = d/RA$.

Figure 3.8 shows the conductivity σ locus in the Wessel diagram. Also here the characteristic frequency is $>100\text{Hz}$, and in contrast to the permittivity plot with a complete semicircle locus, there is a strong deviation with the σ'' diverging proportional to frequency. *In conclusion*, the complex conductivity

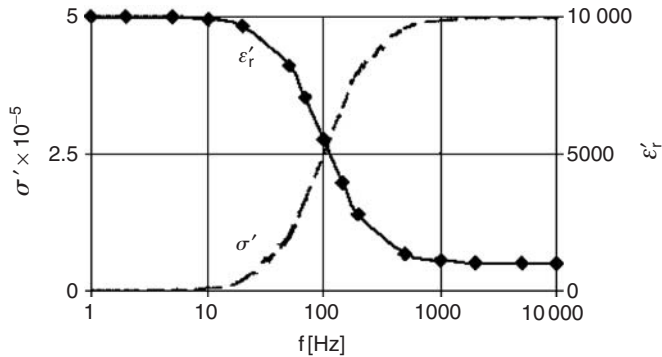


Figure 3.7 Combined permittivity and conductivity plot, same data as for Fig. 3.5.

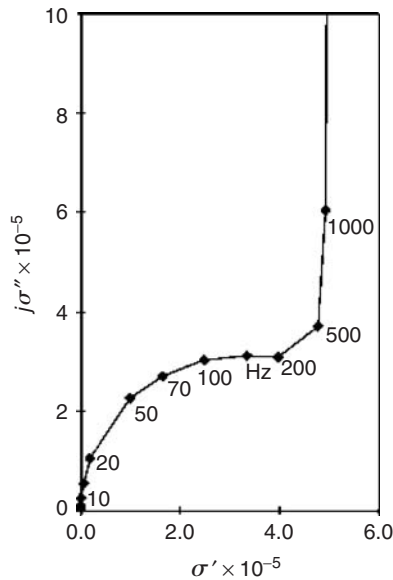


Figure 3.8 Complex conductivity (siemens) in the Wessel diagram. A diagram with admittance variables G and B would be similar. Same data as for Fig. 3.5.

semicircle is disturbed by the parallel capacitor C_∞ . In order to obtain a circle this capacitor must be omitted in the *conductivity* Wessel diagram. Correspondingly, a *permittivity* semicircle would have been disturbed by a parallel conductance G (cf. Fig. 8.13) mechanism.

The time constant and characteristic relaxation frequency can be defined in more than one way:

From the transient response (eq. 3.25)

From the midpoint of the $\Delta\varepsilon$ or $\Delta\sigma$ plotted as a function of $\log f$ (Fig. 3.5).

From the apex of the circular locus of ε or σ in the Wessel diagram (Fig. 3.6)

Conductance in Parallel, 2R–2C Model

The dielectric Debye equivalent circuit of Fig. 3.4 is basically for dry biomaterials without free charge carriers and DC conductance. The in-phase component is the lossy part of the relaxation. If it is living tissue it actually has free charge carriers and an ionic DC conductance path in parallel with C_∞ in Fig. 3.4. For DC conductance there is no relaxation process, but even so it is not unusual to add this conductance to some of the equations. In the in-phase part of eq. (3.33) a factor $\sigma_{\text{DC}}/\omega\varepsilon_0$ (diverging as $f \rightarrow 0!$) is for instance added to ε'' . The total in-phase component may then be written on the form:

$$\sigma' = \sigma_{\text{DC}} + \Delta\sigma'\omega^2\tau^2/(1 + \omega^2\tau^2) \quad (3.35)$$

Relaxation of Permanent Dipoles (MHz–GHz Region)

The permanent dipoles in a polar dielectric experience a torque by an applied electric field (cf. eq. 3.5). The actual position of each dipole is determined by this externally created torque and the thermal motion of the dipoles. The polarization P is found to be:

$$P = Np^2F/3kT \quad (3.36)$$

Viscosity effects in the dielectric are considered to hinder the rotational movement, and Debye has given the relaxation time τ of this process based on Stoke's law (eq. 2.6):

$$\tau = 4\pi\eta a^3/kT \quad (3.37)$$

The relaxation time for proteins in water is typically in the micro- to picosecond range (MHz–GHz), and the dielectric decrement of the order of ε_0 per gram per liter.

3.4.3 Joule Effect and Temperature Rise

With current flow, an ideal resistor *dissipates* heat energy; the energy is lost as electrical energy. However, an ideal capacitor *stores* electrical energy. In a non-ideal capacitor there are dielectric losses and perhaps losses from a DC current. The stored energy may be partially lost, and completely lost with time (relaxation). As long as a device, a black box or real tissue, has the ability to store energy, it contains some form of capacitors (or inductors).

Energy is the ability for doing work. Potential difference is energy per charge [joule/coulomb]. Energy is measured in *wattsecond* or *joule* which is the same; or *electron volt* [eV]. Power is the rate of doing work or transferring energy, and is measured in *watt*. Current flow through a copper wire is a flow of electric charge. If the flow occurs with negligible voltage drop, the charge undergoes no energy change. There is no voltage difference, $\Delta V = 0$. A potential difference must be defined in order to define the energy of a charge. Power is defined as the product of electric current and voltage difference.

As seen from the outside of the dielectric in the external leads, the instantaneous power W_i delivered from a sinusoidal AC supply to the parallel combination of a capacitor (susceptance B) and a conductor (G), is the instantaneous AC supply voltage multiplied by the instantaneous current in the copper leads:

$$W_i = vi = V_{\text{peak}} \sin \omega t V_{\text{peak}} Y \sin(\omega t + \phi) \quad (3.38)$$

The instantaneous power W_i is linked with a real electronic current in the copper leads. However, some of this sine wave current is in phase with the applied voltage, and some of it is 90° out of phase. The instantaneous in-phase power W_h is the instantaneous voltage multiplied by the instantaneous in-phase current component. The instantaneous out-of-phase power W_r is the instantaneous voltage multiplied with the instantaneous 90° out-of-phase (*quadrature*) current. To obtain the average power (rate of energy transfer) of the quadrature current ($\phi = 90^\circ$) (called *reactive power*) over the period T (one cycle), we integrate the instantaneous power over the period (=average energy), and divide by the period (=average power):

$$\begin{aligned} W_i &= 1/T \int [V_{\text{peak}} \sin \omega t (V_{\text{peak}} B) \cos \omega t] dt \\ &= 1/T (V_{\text{peak}}^2 B/2\omega) [\sin^2 \omega t]_0^T = 0 \end{aligned} \quad (3.39)$$

The *reactive* power W_r is pumped to and from the capacitor each quarter period, but the net supplied energy is zero. The capacitive, quadrature current just pumps electrons *charging* the plates. The quadrature current causes no heating of the dielectric, but the current in the leads is real and causes heat losses if the *wires* are non-ideal.

In the same way the power loss W_L is:

$$\begin{aligned} W_L &= 1/T \int [V_{\text{peak}} \sin \omega t (V_{\text{peak}} G) \sin \omega t] dt \\ &= 1/T (V_{\text{peak}}^2 G) [t/2 - (1/4\omega) \sin 2\omega t]_0^T = \frac{1}{2} V_{\text{peak}}^2 G \end{aligned} \quad (3.40)$$

To find a *root-mean-square (rms)* value of a function of time the function is first squared, then the mean value is taken, and then the root of the mean. The rms value must be used when power and heat effects are of interest ($W = v_{\text{rms}}^2/R$). From eq. (3.40) it is clear that the rms value of a sine wave is $1/\sqrt{2}$ of the peak value. Dealing with other waveforms, the relationships between peak, mean and rms values will depend on the waveform. Many AC voltmeters *display* rms voltage, but actually *measure* the mean value. Such practice introduces errors for non-sine waveforms.

In the *dielectric* there is ionic or electronic conduction. In a metallic conductor the free, migrating electrons collide with the lattice of the bound ionized metal atoms, and the electrons transfer their excess energy to the lattice. With electrolytes the charge carriers are ions, and ordinary migration or local displacement is hindered by viscosity-based friction. In both cases the dielectric is heated up and energy dissipated, that is the *Joule* effect.

The energy \hat{E} stored in a capacitor is given by:

$$\hat{E} = \frac{1}{2} CV^2 \quad [\text{J}] \quad (3.41)$$

In an ideal dielectric, all this energy is stored, and there is no Joule heating. In a non-ideal AC-polarized dielectric, there is an in-phase current causing Joule heating. The power loss density (W_v , watt/m³) in a homogeneous and isotropic dielectric is:

$$W_v = EJ = \sigma'E^2 \quad [\text{W/m}^3] \quad (3.42)$$

This is a DC equation. With AC, E and J are time vectors and the *dissipative* power density and dielectric temperature rise is dependent only on the local in-phase components. In vacuum the current density $J = \epsilon_0 \partial E / \partial t$ is a pure displacement current. The power density in vacuum is not zero, but the dissipated power density is zero.

The corresponding adiabatic temperature rise per second $\Delta T/t$ in the dielectric is:

$$\Delta T/t = J^2 / \sigma' c d \quad (3.43)$$

where d is mass density (for water: 1000 kg/m³), and c the heat capacity (for water: 4.2 kJ/kg and °K). In tissue, the temperature rise will be smaller than predicted from eq. (3.44). The conditions are not adiabatic because of the thermal contact with the surroundings, and blood perfusion will also cool the site considerably. In electrosurgery (Section 9.13) or with electromagnetic fields imposed on tissue (Section 7.4.8.), only the local *in-phase* components contribute to the local diathermy effect.

3.5 INTERFACIAL POLARIZATION

Biomaterials are inhomogeneous dielectrics. In general the smaller the particles, the larger the surface-to-volume ratio, and the larger the interfacial effects. In contrast to the theories of molecules forming a homogeneous material presented up to now, the relaxation mechanisms to be presented in this chapter are linked to heterogeneity

and interfaces: the classical Maxwell–Wagner effects and the counterion polarization theories.

3.5.1 Maxwell–Wagner Effects

Maxwell–Wagner effects deal with processes at the interface between different dielectrics (Maxwell 1873, Wagner 1914, Fricke 1953). Maxwell–Wagner effects are also present with dry but lossy dielectrics, with wet surfaces additional double layer effects occur. There may be free or bound surface charges at the interface. The potential Φ at the interface must be continuous, or else the E-field strength had to be infinite there. If there is no DC conductance (no free charges) in neither of the two dielectrics, the interface cannot be charged by free charges migrating in the applied field. It can be shown that the normal D-field and the tangential E-field components are unchanged across such a boundary. If there is a DC conductance in one or both dielectrics, the interface generally will be charged by free charges, and the normal D-component will not be continuous. Let us analyze Maxwell–Wagner relaxation in a simple model.

Capacitor with Two Dielectric Layers

Consider two materials, each homogeneous, as two dielectric slabs between the capacitor plates. The models with equivalent circuits are shown in Fig. 3.9. Let us consider ideal components and therefore the resistors with frequency independent values from DC.

Slabs in Parallel

On Fig. 3.9(b), the two slabs are in parallel, and the result becomes very simple as a parallel summation of $G_1 + G_2$ and $C_1 + C_2$.

Slabs in Series

The case becomes quite different and much more complicated (cf. Section 11.2.3). The total immittance, and also the voltage at the interface between the two dielectrics, will be determined by the resistors at low frequencies, but by the capacitors at high

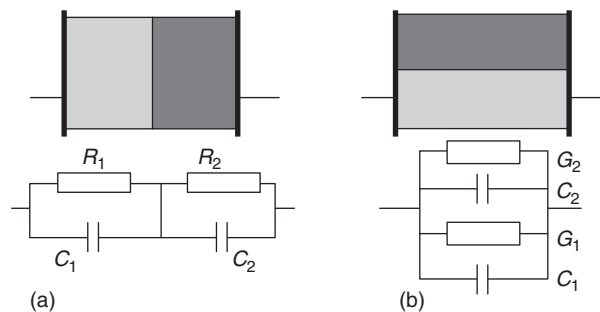


Figure 3.9 Equivalent circuits for the Maxwell–Wagner effect in a simple dielectric model: (a) the slabs in series, the resistors cause the interface to be charged; (b) the slabs in parallel.

frequencies. The analysis of Fig. 3.9(a) will be very different dependent on whether a series (impedance) or parallel (admittance) model is used.

If the externally seen *series* capacitance C_{sext} is calculated, it is the series coupling of the two capacitances C_1 and C_2 at high frequencies, but at low frequency the value of C_{sext} diverges and become infinite.

If the resultant *parallel* capacitance C_{pext} is calculated, (Section 11.2.3), we get:

$$\begin{aligned} C_{\text{pext}} &= (\tau_1 R_1 + \tau_2 R_2)/(R_1 + R_2)^2 & f \rightarrow 0 \\ C_{\text{pext}} &= C_1 C_2 / (C_1 + C_2) & f \rightarrow \infty \end{aligned} \quad (3.44)$$

Both values converge, at high frequencies with values smaller than at low frequencies. Thus with the parallel model of the two slabs in series, we have a classical Debye dispersion, with a capacitive decrement ΔC or $\Delta \epsilon'$. This is without postulating anything about dipole relaxation in the dielectric. Debye dispersion appears and is modeled by two capacitors and two resistors, or even with two capacitors and one resistor (one layer without conductivity) as shown in Section 11.2. If the components are ideal (frequency independent), the dispersion will be characterized by one single relaxation time constant.

Maxwell–Wagner dispersion is due to a conductance in parallel with a capacitance for each dielectric, so that the interface can be charged by the conductivity. With zero conductivity in both dielectrics there is no charging of the interface from free charge carriers. If side one of the dielectric is without conductivity ($\sigma_1 = 0$ and $R_1 = \infty$), then C_{pext} at very low frequencies becomes equal to C_1 . At very high frequencies the conductivities are without influence.

In an interface without *free* charges, the dielectric displacement \mathbf{D} is continuous across the interface according to Poisson's equation (cf. Section 4.3.2) on the continuity across interfaces. Since $\mathbf{D} = \epsilon \mathbf{E}$, this indicates that the \mathbf{E} -field strength will be smaller on the high permittivity side. Then the ratio of the current densities on side 1 and 2 is:

$$\frac{J_1}{J_2} = \frac{\sigma_1 E_1}{\sigma_2 E_2} = \frac{\sigma_1 \epsilon_2}{\sigma_2 \epsilon_1} \quad (3.45)$$

On the other hand, if $\sigma_1 \epsilon_2 \neq \sigma_2 \epsilon_1$, the difference in current densities indicates that the interface actually is charged. If $\sigma_1 = 0$ and $\sigma_2 > 0$, the interface will be charged.

The conductive path in parallel with the dielectric capacitance causes the Maxwell–Wagner surface charge. *This interface single layer surface charge must not be confused with the double layer charge formed at a wet interphase.* With liquid interphases such as with particles or cells in aqueous media, the double layer counterion effects are additive to the Maxwell–Wagner effects.

Suspension of Spherical Particles

This is a model, for example, for blood or cell suspensions, and the electrolytic solution of interest may then have a considerable ionic conductivity. An analytical

solution (Maxwell, 1873) is relatively simple for a *dilute* suspension of spherical particles, and with DC real conductivity as parameters (σ is for the total suspension, σ_a for the external medium and σ_i for the particles) the relation is (*Maxwell's spherical particles mixture equation*) (Foster and Schwan, 1989):

$$(\sigma - \sigma_a)/(\sigma + 2\sigma_a) = p(\sigma_i - \sigma_a)/(\sigma_i + 2\sigma_a) \quad (3.46)$$

where p is the particle volume fraction. Wagner (1914) extended this to AC cases and the use of complex parameters. Fricke (1924, 1925) extended it for the cases of oblate or prolate spheroids (*Maxwell-Fricke equation*):

$$(\sigma - \sigma_a)/(\sigma + \gamma\sigma_a) = p(\sigma_i - \sigma_a)/(\sigma_i + \gamma\sigma_a) \quad (3.47)$$

where γ is a shape factor and equal to 2 for spheres and 1 for cylinders normal to the field. From such equations $\Delta\sigma = \sigma_s - \sigma_\infty$ or $\Delta\varepsilon = \varepsilon_s - \varepsilon_\infty$ can be found (subscript s for static values), but the permittivity decrement $\Delta\varepsilon$ is often rather small, of the order of a few ε_0 . If the particles have a DC conductivity, Maxwell-Wagner effects cause ε' as a function of frequency to have an additional slope downwards.

As for the relaxation time, Debye derived a simple expression for a viscosity determined relaxation time of a sphere of radius a in liquid (eq. 3.38): $\tau = 4\pi a^3 \eta / kT$. The relaxation time is therefore proportional to the volume of the sphere and the viscosity of the liquid.

Maxwell's equation (3.46) is rigorous only for dilute concentrations, and Hanai (1960) extended the theory for high volume fractions:

$$\frac{\varepsilon - \varepsilon_i}{\varepsilon_a - \varepsilon_i} \sqrt[3]{\frac{\varepsilon_a}{\varepsilon}} = 1 - p \quad (3.48)$$

Hanai's equation gives rise to dispersion curves that are broader than the Maxwell-Wagner equation (Takashima, 1989).

Dilute Suspension of Membrane-Covered Spheres

Equation 3.48 can be extended to comprise spheres in spheres, or sheath-covered spheres. If sheath thickness d is much less than large sphere radius a , the complex conductivity of one sphere inside another sphere is:

$$\sigma = (\sigma_i - (2d/a)(\sigma_i - \sigma_{sh}))/((1 + d/a)(\sigma_i - \sigma_{sh})/\sigma_{sh}) \quad (3.49)$$

where the subscript i is for sphere material, and sh for the sheath membrane. Equation (3.49) is valid for a sphere without external medium. In order to have the complete description the conductivity value from eq. (3.49) is therefore inserted in eq. (3.47) for the complex conductivity of the sphere.

For a *cell suspension* with cell membranes dominated by a membrane capacitance C_m , the equations can be simplified using certain approximations (Schwan, 1957, Foster and Schwan, 1989):

$$\Delta\varepsilon = 9paC_m/4\varepsilon_0 \quad (3.50)$$

$$\sigma_s = \sigma_a(1 - 3p/2) \quad (3.51)$$

$$\tau = aC_m(1/2\sigma_a + 1/\sigma_i) \quad (3.52)$$

The full equations (*Pauly-Schwan* equations) are found in Pauly and Schwan (1959). They correspond to a large dispersion due to membrane charging effects and a small dispersion at higher frequencies due to the different conductivity of the cytoplasm and extracellular liquids. Schwan and Morowitz (1962) extended the theory to small size vesicles of radii 100 nm. With even smaller particles the two dispersion regions overlap in frequency (Schwan et al., 1970).

3.5.2 Adsorbed Counterions and Lateral Diffusion (MHz–kHz Region)

In Section 2.4.3 we analyzed the double layer charge in the solution as a function of the perpendicular distance from the solid surface. No double layer formations are considered in the Maxwell–Wagner theory (Section 3.5.1). However, in *wet* systems and in particular with a high volume fraction of very *small* particles, the surface effects from counterions and double layers usually dominate. This was shown by Schwan et al. (1962). By dielectric spectroscopy they determined the dispersion for a suspension of polystyrene particles (Fig. 3.10). Classical theories based on polar media and interfacial Maxwell–Wagner theory could not explain such results, the measured permittivity decrement was too large. The authors proposed that the results could be explained in terms of surface (*lateral*) admittance.

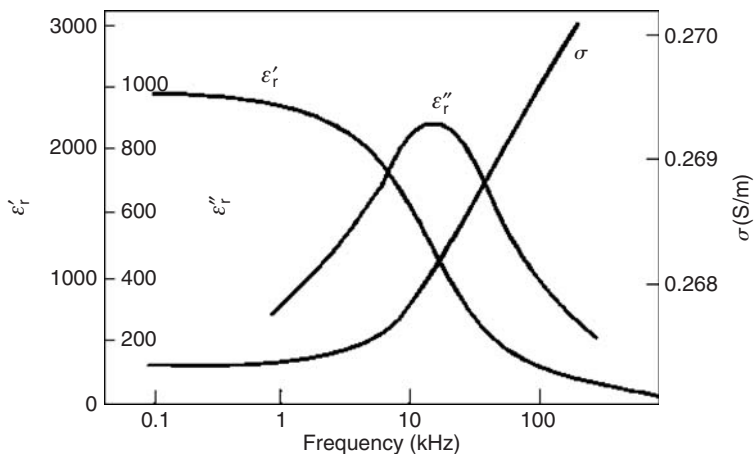


Figure 3.10 Permittivity for a suspension of polystyrene particles. *Source:* Redrawn from Schwan et al. (1962) by permission.

Counterion Diffusion, Schwarz's Theory

Schwartz (1962) proposed a model with a tightly bound layer of adsorbed counterions on the sphere surface to explain the high permittivity increment found (hundreds of ϵ_0) in a suspension of colloidal particles. Diffusion, and not migration may govern ionic motion in a double layer. Diffusion processes are not necessarily exponential, but as an approximation the time constants of such effects are according to the term L^2/D , where L is the diffusion length and D the diffusion coefficient (cf. eq. 2.19). This is in contrast to Maxwell–Wagner relaxation, where the RC product, that is resistance and capacitance, determines the time constant. The corresponding relaxation frequencies may be low, in the Hz and kHz range. Schwarz developed a theory based on counterion relaxation, where:

$$\tau = a^2 \epsilon_0 / 2 \mu k T \quad (3.53)$$

$$\Delta \epsilon = (9p / (2 + p)^2) (e^2 a q_s / \epsilon_0 k T) \quad (3.54)$$

where a = particle radius, μ = counterion mobility, q_s = surface density of charged groups on the particle surface.

In Schwartz' theory, the ions were bound to the double layer and lateral motion within it. A theory is also possible allowing ions to enter or leave the layer from the bulk.

Counterion Diffusion in Pores

Takashima (1989) deduces the expression for the dielectric increment of a suspension of long cylinders by transforming the relations for ellipsoids from rectangular to cylindrical coordinates:

$$\Delta \epsilon = \frac{e^2 q_s a^2}{b k T} \frac{9 \pi p}{2(1 + p)^2} \frac{1}{1 + j \omega \tau} \quad \text{if } a \gg b \quad (3.55)$$

where a is cylinder length and b is cylinder radius. This equation has been found to be applicable also to pores (Martinsen et al., 1998) and will give a rough estimate of the rate of dielectric dispersion to be expected in sweat ducts and other pore systems.

The electrical properties of microporous membranes in 1 mM KCl solution was investigated in the frequency range 1 mHz–1 kHz by Martinsen et al. (1998), using a four-electrode measuring cell (Fig. 3.11).

An α -dispersion centered around 0.1 Hz was detected and this was assumed to be caused by counterion relaxation effects in the pores of the membrane. The membranes used were 6 μm thick Nuclepore polycarbonate membranes. These membranes have 3×10^8 pores/cm² with a pore diameter of 100 nm. The pores are cylindrical with a length equal to the membrane thickness. The surface density of charged groups of the membranes were calculated using streaming potential

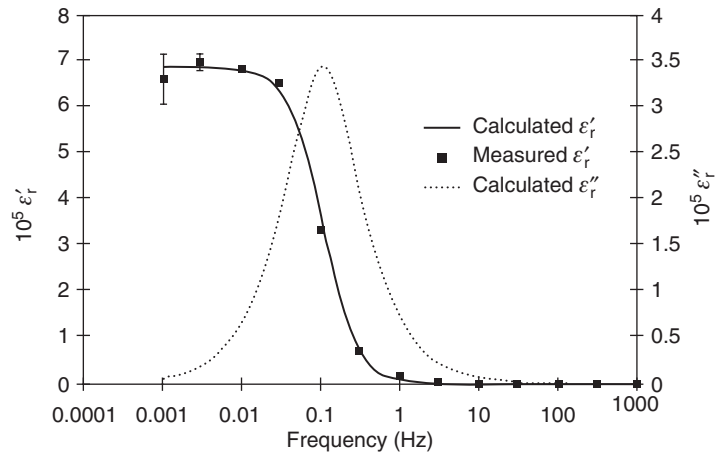


Figure 3.11 Dielectric dispersion of a polycarbonate membrane with pore diameters 100 nm; 1 mM KCl solution; measured and calculated values; DC conductivity omitted. *Source:* From Martinsen et al. (1998) by permission.

measurements (see Section 2.4.6) which enabled the use of eq. (3.55) for calculation of the dielectric increment. Figure 3.11 shows the measured dispersion together with the calculated real and imaginary part from eq. (3.55). Other mechanisms which may contribute to the relaxation (e.g. the influence from diffusion of ions in the bulk electrolyte) were not considered in the study.

3.6 THE BASIC MEMBRANE EXPERIMENT

Set Up

Let us again consider the electrolyte container with a NaCl 0.9% aqueous solution, but this time it is divided into two compartments by a membrane (Fig. 3.12). A sinusoidal AC current is applied to the large current carrying electrodes. Two additional voltage pick-up electrodes (no current flow in their leads) are placed on each side of the membrane, and a phase sensitive voltmeter or a two-channel oscilloscope measures the voltage. This four-electrode system eliminates any influence from electrode polarization impedance: The potential drop at the current carrying electrodes does not intervene, and the recording electrodes do not carry any current, so the potential drop in their polarization impedances is zero.

Without Membrane

Without a membrane an AC voltage Δv is measured. This voltage is proportional to the current through the system, it is in phase with the current, and the amplitude is independent on frequency. The solution behaves “ohmic,” obeying Ohm’s law

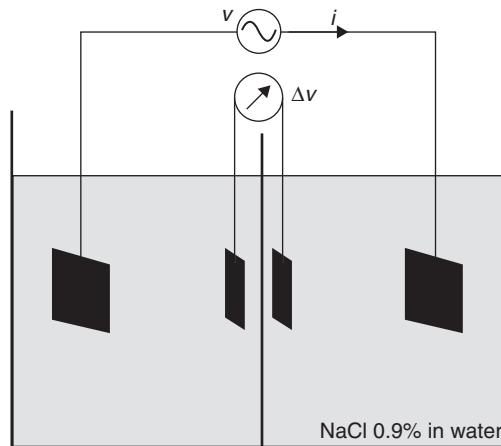


Figure 3.12 The basic membrane experiment.

(eq. 2.2) like a perfect resistor. The voltage is due to the ohmic voltage drop caused by the current density in the bulk volume between the recording electrodes.

Thin Metal Membrane

Then the measured voltage increases, the phase of the recorded voltage lags behind the current, and the amplitude is frequency dependent.

The conductivity of the metal is more than 1000 times that of the electrolyte, and the metal is thin. The voltage drop in the metal itself must be very small, and the increased measured voltage must be caused by the two double layers formed on each side of the metal plate. These double layers clearly have capacitive properties, and they are in series with the metal.

Let us suppose that there is a thin pore in the membrane. The walls of the pore must also be covered by a double layer. Will counterions in that double layer, and ordinary ions in the pore volume, migrate with the AC E-field? No, because of the high conductivity of the metal the local E-field strength along the axis of the pore will be very small.

Thin Membrane of Insulating Material (No Pores)

The measured voltage difference is very large at low frequencies. At higher frequencies (e.g. >1 kHz), measured voltage is smaller and almost 90° after the applied voltage.

With an insulating material in the membrane, no DC current can flow through the cell. An AC current will flow through the three series coupled capacitors: two double layer capacitors at each side of the wetted membrane, and the capacitor with the membrane itself as dielectric. The measured voltage difference will consist of the voltage drop in the solution between the measuring electrodes, plus the voltage drop across the three capacitors. Most of the reactance will stem from the membrane, because its capacitance will be far lower than that of the double layers. At sufficiently

high frequencies, the reactance of the membrane capacitors will be so small that the effect of the membrane will disappear, and the phase angle will approach 0° .

Membrane of Insulating Material with Pores

This time the voltage is not so high at low frequencies (e.g. $<10\text{Hz}$). There is a very small phase shift, less than 5° . At higher frequencies the voltage difference is falling with frequency and with a 90° phase shift.

The pores form a DC current path. The sum of their conductances is so large that the capacitive effect of the membrane as a dielectric is small at low frequencies. If there are not too many pores, most of the potential difference is over the membrane pores, and the E-field strength in the pores will be high. The counterions of the double layer on the pore walls will migrate synchronous with the E-field, and the solution inside the pore will be pumped back and forth by electro-osmosis. At higher frequencies the membrane susceptance will shunt the pores, and voltage across the pore will be reduced.

Discussion

The most interesting membranes in the field of bioimpedance are of course the membranes in the living body, the cell membranes: the excitable ones in the muscles and the nerve system, and the less excitable ones. In addition, there are membranes both *inside* and *outside* the cells. Inside the cells there are membranes around some of the organelles. Outside there are thick, solid macromembranes around all organs such as the heart, the lungs, the brain, the intestines (mediastinum), etc.

In tissue the cell membranes are very small and a part of a living system, quite different from the basic *in vitro* model just shown. However, our simple model is well suited for artificial membranes. With a special technique it is useful for artificial bilayer lipid membranes (BLM) very much like the cell membranes. The membrane pore is then closed with a lipid droplet. The droplet gradually becomes thinner, until it turns from multi-molecular thickness into a single bilayer covering the orifice of the pore. Such a bilayer lipid membrane has important similarities with real cell membranes.

A better model for tissue is the suspension-measuring set-up to be presented in the next Section 3.7.

3.7 THE BASIC SUSPENSION EXPERIMENT

Set Up

Let us consider our electrolyte container again, but let us fill it with a suspension of particles as shown in Fig. 3.13, instead of the separating membrane. The electrolyte is still NaCl 0.9% in water. The particles used are small insulating glass or plastic beads. If the particles are sufficiently small ($<0.5\mu\text{m}$) the solution is optically clear, and the particles will be evenly but randomly distributed in the volume by Brownian movements according to the Boltzmann factor kT . A *suspension* is usually defined as a liquid with *larger* particles. Then gravitational energy will dominate the kT -factor, and a sedimentation process will go on so that the

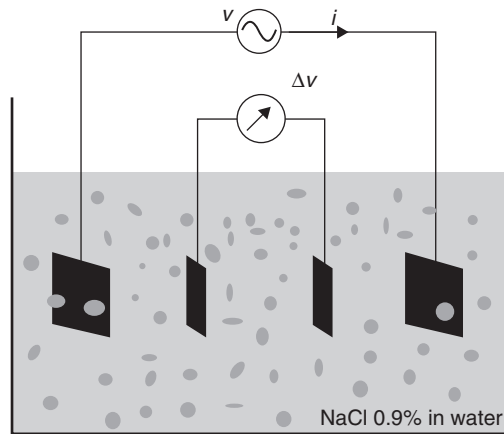


Figure 3.13 The basic suspension experiment.

particles will sink to the bottom. The system is unstable, and the concentration in bulk will fall with time. These definitions are rather broad, and several subgroups may be formed. Many molecules are for instance known to *associate* (molecules of *same* kind forming more complex structures, e.g. water molecules) in solution, and particles may form *aggregates* if their charges are small enough. Macromolecules may form *colloids* with properties dominated by surface properties.

Findings

A voltage is measured almost like that found for the basic setup without a membrane (Section 3.6). However, a small phase lag is measured, and the voltage decreases somewhat with frequency. The voltage increases with increased particle concentration.

With a high voltage applied, and at a very low frequency < 1 Hz, it is possible with a magnifying glass to see the particles moving back and forth synchronously with the AC.

Discussion

In general, the double layer on each particle surface will add capacitance to the system, and therefore the measured voltage will decrease with frequency and lag the current. Note that some of the current passes perpendicular to the double layer of the particles, but some of the current passes parallel to the double layers. Smaller particles have increased surface to volume ratios, and therefore result in higher capacitance.

If the particles are *highly conductive* with respect to the solution (metal), this metal is not directly accessible for the current; the double layer must be passed 2 times. If the concentration of metal particles (fill factor) is increased, the measured voltage will not necessarily decrease, that depends on metal/solution impedance and therefore also the frequency. Above a certain particle concentration there will

be a sharply increased probability of a direct contact *chain* of particles throughout the measured volume segment, the segment will be short-circuited.

If the particles are low conductive (*glass*), the resistance of the suspension at low frequencies will be higher than without particles. Measured voltage is increased, and in addition it will lag the current by a certain phase angle. If the frequency is increased, the susceptance of the sphere volume capacitors will be higher and in the end be determined by the permittivity of the spheres with respect to the solution. With cells the cell membrane surface properties will complicate the case further.

With a sufficiently low frequency the particles can follow, and we witness how the particles of the suspension are pumped back and forth by *electrophoresis* as a sign of their net electric charge.

3.8 DISPERSION AND DIELECTRIC SPECTROSCOPY

Schwan emphasized the concept of *dispersion* in the field of dielectric spectroscopic analysis of biomaterials. Dispersion has already been introduced in Section 3.4.1: dispersion means frequency dependence according to relaxation theory. Biological materials rarely show a single time constant Debye response as described in Section 3.4.2. They are also often not in accordance with a pure Cole model, but exhibit a certain non-symmetrical distribution of relaxation times (DRT). All such models are covered by the dispersion concept.

Dispersion is therefore a broad concept, and many types of DRTs are possible. The Cole brothers proposed a certain DRT corresponding to the apparently simple Cole–Cole equation (Section 8.2). The Cole–Cole equation presupposes a constant phase element (CPE). However, other distributions than the Cole–Cole type are also found to be in agreement with measured tissue values. The Cole–Cole model is however attractive because the mathematical expressions are so simple. Dispersion models as described below therefore pertain to many types of dispersion mechanisms, amongst those also Cole–Cole systems.

Dispersion data is based on the electrical examination of a biomaterial as a function of frequency, that is, dielectric spectroscopy. Schwan (1957) divided the relaxation *mechanisms* in three groups, each related to, for example, cell membranes, organelles inside cells, double layer counterion relaxation, electrokinetic effects, etc. He called them α -, β -, and γ -dispersions (cf. Fig. 3.14). The permittivity of muscle tissue decreases in three major steps corresponding to these dispersions, roughly indicated by Schwan (1957) to correspond to 100 Hz, 1 MHz and 10 GHz. In the data of Gabriel et al. (1996b) they are situated at lower frequencies: 1 Hz, 1 KHz and 1 MHz (Fig. 4.10). Later a fourth δ -dispersion has been added in the lower GHz range. There are two possible interpretations of these dispersions:

1. The dispersions are linked with defined frequency ranges.
2. The dispersions are linked with defined relaxation mechanisms.

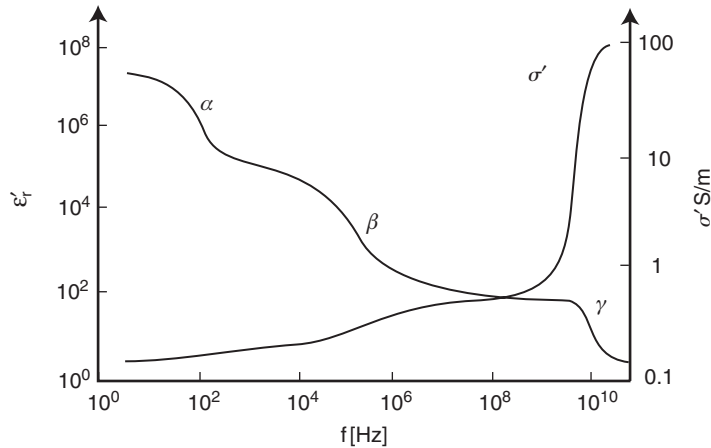


Figure 3.14 Dispersion regions, idealized. *Source:* Modified from Schwan (1988).

TABLE 3.3 Dielectric Dispersions

Type	Characteristic frequency	Mechanism
α	mHz–kHz	Counterion effects (perpendicular or lateral) near the membrane surfaces, active cell membrane effects and gated channels, intracellular structures (e.g. sarcotubular system.), ionic diffusion, dielectric losses (at lower frequencies the lower the conductivity).
β	0.001–100 MHz	Maxwell–Wagner effects, passive cell membrane capacitance, intracellular organelle membranes, protein molecule response.
γ	0.1–100 GHz	Dipolar mechanisms in polar media such as water, salts and proteins.

Sometimes dispersions are related to defined frequency ranges, and to a lesser extent to possible relaxation mechanisms. Newer findings have shown that the α -dispersion must be extended down to the millihertz frequency range (see Table 3.3).

Dispersions may be described with permittivity or immittivity parameters. Complex permittivity or complex immittivity may be presented in Wessel diagrams as shown in Chapter 8. Wessel diagrams focus data in a narrow frequency range, for broad band spectroscopic data logarithmic frequency scales are better suited (Fig. 3.14). Figure 3.14 shows that the permittivity in biological materials typically diminishes with increasing frequency, little by little the charges (dipoles) are not quick enough to follow the changes in the E-field. The dispersion regions are here

shown as originating from clearly separated Cole–Cole-like systems. Such clearly separated single dispersions can be found with cell suspensions. In tissue the dispersion regions are much broader and overlap, sometimes as a continuous fall almost without levels and over many decades of increasing frequency (cf. Chapter 4 on tissue properties and Section 8.2.14 on multiple Cole systems).

A problem with a purely dielectric approach is how to treat the free charge carriers and the corresponding DC conductivity found with living tissue. The conductivity of saline alone is without dispersions below 10 MHz. Equation (3.16) ($\epsilon'' = \sigma'/\omega$) shows that with constant conductivity the quadrature permittivity diverges at lower frequencies. The interpretation for living tissue is therefore easily distorted using the ϵ'' variable. There are two ways out of this: (1) The measured DC conductivity can be subtracted as a non-dispersion parameter. (2) Quadrature permittivity is replaced by in-phase conductivity, as shown in Fig. 3.14. With subtracted DC conductance the ϵ'' waveforms would have been peaks (cf. Fig. 3.5). The conductivity waveform has a continuously increasing level (cf. Fig. 3.7), and no DC conductance subtraction is necessary when presenting the data. However, the underlying models are different. The electric equivalent circuit for the permittivity parameter is a 1R–2C model, for the conductivity parameter a 2R–1C model (cf. Section 8.2.6).

The permittivity ϵ'_r for tissue may attain values larger than 10^6 at low frequencies. This does not imply that the capacitive properties of living tissue are dominating at low frequencies (cf. Table 4.1). The admittance of living tissue is actually dominated by the conductive properties of liquids, and the out-of-phase current is very much smaller than the in-phase current. These effects could not be measured without the introduction of high resolution measuring bridges, taken into use by Schwan and pioneers before him (cf. Section 7.3.1). Dispersion is the most common model for explaining the electric behavior of biomaterials, even if electrolytic theory with DC conductivity and electrode phenomena are important factors. The strength of the dispersion concept is that it is very broadly phenomenological, not forcing anybody to consider detailed mechanisms. It is very much Schwan's merit that this field was opened in such a broad way. But the generality is also a problem: dispersion and relaxation concepts can easily be taken as explanations of the machinery behind the phenomena, and they are not. Dispersion relates to the electrical and physical *behavior* of molecules, somewhat opposed to analytical methods such as NMR or light spectroscopy more examining molecular *structure*. This is partly due to the techniques in analytical chemistry, which are based on resonance phenomena, while dielectric spectroscopy below about 1 GHz is concerned with relaxation, usually presented as a non-resonance phenomenon. However, in the lower GHz region sharp resonance phenomena are observed for DNA molecules (Takashima, 1989, p.214).

PROBLEMS

1. At which frequency may copper be considered as a dielectric defined as $B = G$? For copper use $\epsilon_r = 3$ and $\sigma = 6 \times 10^6$.
2. What is the force between two opposite charges of 1 C at distance 1 m?

3. How large is the polarization \mathbf{P} (Cm/m^3) in a dielectric with relative permittivity equal to 3?
4. What is the complex admittance Y of an ideal capacitor with dimensions area 1 cm^2 and thickness 1 mm , and with a dielectric with $\epsilon_r = 3$ and $\sigma = 2\text{ S/m}$ at 1 MHz ?
5. What is the complex impedance Z of the same capacitor?
6. An ideal capacitor with dimensions area 1 cm^2 and thickness 1 mm is measured to have a frequency independent resistance $10^6\Omega$ and a capacitance of $15 \times 10^{-12}\text{ F}$. Find the complex permittivity, conductivity and resistivity of the dielectric at 1 MHz .
7. Sketch Fig. 3.14 by replacing the σ sigma parameter with the ϵ_r'' parameter.

4 PASSIVE TISSUE ELECTRICAL PROPERTIES

Chapter Contents

4.1 Basic Biomaterials

- 4.1.1 Water and Body Liquids
- 4.1.2 Proteins
- 4.1.3 Carbohydrates (Saccharides)
- 4.1.4 Lipids and the Passive Cell Membrane

4.2 Tissue and Organs

- 4.2.1 Tabulated Tissue Conductivity Data
- 4.2.2 Muscle Tissue
- 4.2.3 Nerve Tissue
- 4.2.4 Adipose and Bone Tissue
- 4.2.5 Blood
- 4.2.6 Human Skin and Keratinized Tissue
- 4.2.7 Whole Body
- 4.2.8 Post-excision Changes, the Death Process
- 4.2.9 Plant Tissue

4.3 Special Electrical Properties

- 4.3.1 Tissue Anisotropy
- 4.3.2 Continuity Across Interfaces
- 4.3.3 Tissue DC Properties
- 4.3.4 Non-linear Tissue Parameters, Breakdown
- 4.3.5 Piezo- and Triboelectric Effects

Problems

4.1 BASIC BIOMATERIALS

Hydrogen (63% of the human body's number of atoms), oxygen (25%), carbon (9%) and nitrogen (1.4%) are the four most abundant atoms of the human body. They are all able to form covalent bonds (e.g. water) based on the sharing of electron

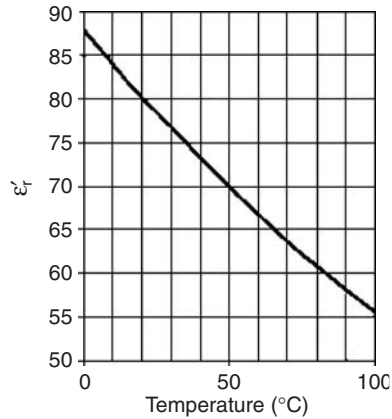


Figure 4.1 Relative permittivity of pure water, temperature dependence. *Source:* Data from CRC (1998).

pairs by two atoms with unpaired electrons in their outer shells (cf. Section 2.1). Most biomolecules are compounds of carbon, because of the bonding versatility of this element. Nearly all the solid matter of cells is in the form of: *water, proteins, carbohydrates and lipids*.

4.1.1 Water and Body Liquids

A short repetition from Chapter 3: water is a polar liquid with a static relative permittivity of about 80 (20°C), falling to 73 at 37°C (Fig. 4.1).

The addition of electrolytes such as NaCl or KCl lowers the permittivity proportionally to concentration (e.g. with a dielectric decrement $\Delta\epsilon_r$ of about 4 for 250 mmol/L concentration of KCl (cf. Section 3.3)).

The high permittivity is one reason for the dissociative power of water. Ionic bonds are split up so that ions exist in aqueous solutions in a free, but hydrated form. Because of the strong dipolar electric field, water molecules are attracted to ions and local charges, forming a hydrated layer (sheet) which tends to neutralize the charge and increase the effective dimensions of the charged particle. The binding of water to protein molecules may be so strong that the water is better characterized as *bound* water. Bound water has different properties than liquid water and must be considered to be a part of the solid and not the liquid phase. A range of bonding energies may be present corresponding to a scale from free water molecules as liquid, via more loosely bound molecules to a very tight bonding when it is very difficult to extract the last water molecules.

Hydrogen ions in the form of protons or oxonium ions contribute to the DC conductivity of aqueous solutions both by migration and hopping.

Pure water exhibits a single Debye dispersion with a characteristic frequency of about 17 GHz (Fig. 4.2).

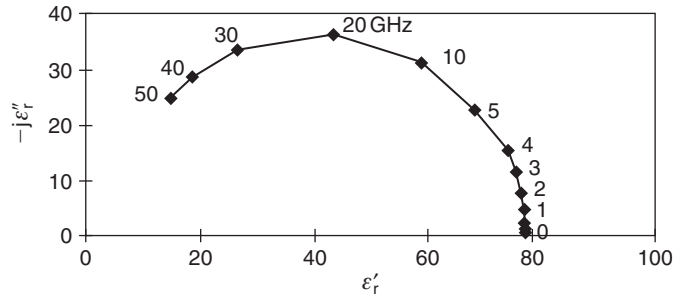


Figure 4.2 Complex relative permittivity of pure water, 25°C. Source: Data from CRC (1998).

Ice has a static relative permittivity of about 92 at 0°C (at low frequencies, but fallen to <10 already at 20 kHz), slightly anisotropic (~14%), and increasing with lower temperature. The characteristic frequency of the relaxation is much lower than for water, around 3 kHz, and with disturbing conductive effects <500 Hz (Hasted, 1973).

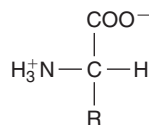
The *living* cell must contain and be surrounded by aqueous electrolytes. In human blood the most important *cations* are: H⁺, Na⁺, K⁺, Ca⁺⁺, Mg⁺⁺; and *anions*: HCO₃⁻, Cl⁻, protein⁻, HPO₄⁻, SO₄⁻. Note that protein in the blood is considered as a negative (macro)-ion.

The electrolytes both intra- and extracellular are listed in Table 2.6. They cause an electrolytic conductivity of the order of 1 S/m. Up to at least 10 MHz it is considered to be frequency independent (Cooper, 1946).

Most of the cells of the body undergo mitosis only if they are attached to a surface. Cancer cells are not dependent on such attachment. Blood containing erythrocytes is the best example of a natural cell suspension.

4.1.2 Proteins

Proteins are the most abundant macromolecules in living cells, and 65% of the protein mass of the human body is intracellular. Proteins are the molecular instruments through which genetic information is expressed. All proteins are constructed from 20 *amino acids*, joined by covalent bonds. All 20 amino acids have the following group in common:



This common group is shown in ionized form as would occur at pH 7, the amino group has acquired a proton (NH₃⁺), and the carboxyl group has lost one (COO⁻). The charges are separated and represent a permanent dipole with zero net charge,

and such substances are *polar*. At pH 7 all amino acids are more or less polar. Even so, the common group is also paradoxically called a “dipolar ion” or a *zwitterion*, because at other pH values it attains a net charge: at low pH values, the NH_3^+ group dominates and the acid is a cation with a net positive charge. At high pH values, the COO^- group dominates and the “acid” is an anion with a net negative charge. Clearly, the term amino acid may be misleading, because in water solution they actually can be an acid (proton donor) or a base (proton acceptor). Even if these conditions mostly are non-physiological, the acid–base behavior in vitro is valuable for the examination and mapping of amino acids.

The R symbolizes a side chain that determines the properties of each amino acid. The electrical properties of the protein are also strongly dependent on this R-group, but only if it is polar or charged. The amino acids are classified according to their R-groups, but the properties of an R-group and therefore the amino acid are very dependent on pH and molecule configuration, so the classification differs in the literature. The following classification for the 20 amino acids may be used at a physiological pH around 7.4:

Eight of the amino acids are *hydrophobic* and therefore the R-groups are grouped as *non-polar*: they are without net electric charge and have a negligible dipole moment. The net dipole moment of all eight amino acids is equal to that of the common group.

Seven are *hydrophilic* and the R-groups are therefore grouped as *polar*. These polar R-groups have an expected large influence on dielectric permittivity. Some of them tend to dissociate H^+ ions so that the amino acid also becomes charged and ionic.

Two are with negatively charged R-groups and therefore have a net negative charge.

Three are with positively charged R-groups and therefore have a net positive charge.

Those amino acids having a net electric charge do migrate in a homogeneous electric field and thus have an electrophoretic mobility. As explained, at $\text{pH} \neq 7$ all amino acids may be charged. The pH of zero net charge is the *isoelectric point*. For example, glycine has no net charge in the pH range 4–8, so this is the *isoelectric range*.

Attempts to interpret the measurements with aqueous solutions of amino acids and peptides with the Clausius–Mosotti equation fail (Section 3.1.2). Instead, it is a usual practice to characterize the polarizability with of biomolecules by a *dielectric increment* δ . At low concentration there is a proportionality between the concentration and the permittivity increase for many biomolecules:

$$\epsilon_r = \epsilon_{\text{rps}} + \delta c \quad (4.1)$$

where ϵ_{rps} is the relative permittivity of the pure solvent. The unit for the dielectric increment δ is c^{-1} . The dielectric increment for many amino acids is in the range 20–200, with dipole moments in the range 15–50 Debye units (D), (Pethig, 1979).

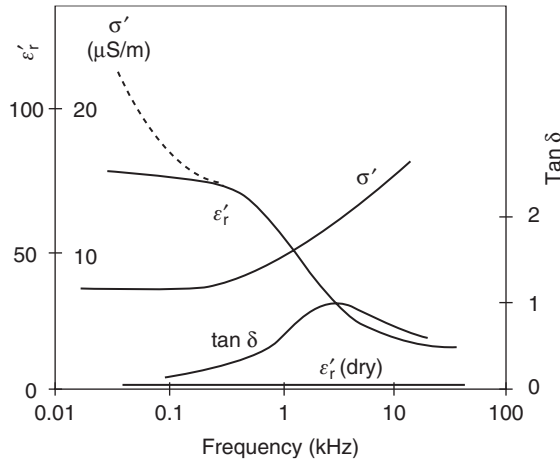


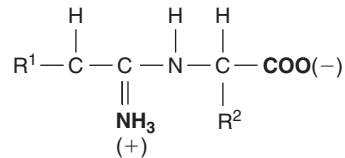
Figure 4.3 Dielectric dispersion for glycine crystals, with water content (0.67% and 0%) as parameter. Two-electrode method, dashed line without correction for electrode polarization. *Source:* From Takashima and Schwan (1965) by permission.

Electrical Properties of Isolated Amino Acids

In dry form the polar amino acids may crystallize as a hard material like NaCl. With non-polar types the dry crystal lattice is softer. The electric properties of dry and wetted amino acids are dramatically different. Glycine is the simplest amino acid with only one hydrogen atom as the R side chain. The R-chain is uncharged, but polar, so glycine is hydrophilic. In dry form it forms hard crystals, and Fig. 4.3 shows the dielectric dispersion of glycine powder in dry form and with a small (0.67%) water content. The permittivity of dry powder is very low and frequency independent (at least down to 20 Hz). With water a clear dispersion is apparent with a characteristic frequency around 1 kHz. The size of the crystals has no effect on high and low frequency permittivity levels, but the larger the particle size, the lower the characteristic frequency. Protons are believed to play an important role in the water dependent conductivity of relative dry materials (South and Grant, 1973), due to the hopping conductance mechanism (Fig. 2.4).

Peptides are small groups of amino acids, and *polymers* are even more complicated forms of peptides forming *proteins*. A polymer is a general term covering any material built up from a series of smaller units (monomers). Proteins differ from each other because each has its own amino acid *sequence*. Like the amino acids, many proteins can be isolated in crystalline and dry forms. A protein may be in the form of a loose strand or a rigid structure. Cross bindings and foldings are very important for the geometrical form, size and rigidity, and also for the function and the electrical properties. Bonds and links are strengthened or weakened according to the charges and distances involved. A change in water solvent concentration may change the electrostatic forces because they are permittivity dependent (cf. Section 3.1.1), whereby the protein will swell or shrink.

A protein may have a very regular form like an α -helix, or a chaotic morphology by *denaturation* at high temperatures or extreme pH values. The denaturation of a protein reduces the solubility in water, and heat coagulation of tissue is therefore accompanied by water liberation. The denatured protein nearly always loses its characteristic biological activities, and the electric properties are often completely changed. This shows the importance of the higher orders of the geometrical (secondary) structure of a protein. A simple peptide may for instance have the form:



As the forms become more complex, very different forms of charge distributions and bonds are possible. The rigidity of the bonds will be important for the electrical relaxation phenomena. In comparison with the displacement of electrons and nuclei during atomic polarization (10^{-15} m), the distance between the charges in a macromolecule can be very large (10^{-8} m). Therefore the dipole moment of proteins could be very large. But the symmetry of the electric charges in protein molecules is also surprisingly high. Even with a large number of ionized groups, the dipole moment often corresponds to only a few unit charges multiplied by the length of the molecule. Some proteins actually have a negligible dipole moment and must be regarded as non-polar.

A protein with a large number of ionized groups is a *polyelectrolyte* if it has a net electric charge. If it is free, it will migrate in an electric field. Usually it is not free, and may therefore only undergo local polarization. Because a polyelectrolyte has distributed charges all over the molecule, each charge is sufficiently isolated to attract ions of an opposite charge. A local ionic atmosphere is formed, just like the one formed around ions in strong electrolytes, or even a better analogy: they are *counterions* just like the counterions forming the electrical double layer. The counterions decrease the DC mobility, and counterion polarization is believed to be very important in many proteins in water solution.

Electrical Properties of Isolated Amino Acids, Peptides and Proteins

Figure 4.4 shows Cole–Cole plots for glycine (amino acid), glycyglycine (peptide) and albumin (protein). As a biomolecule becomes more and more complicated and large (amino acid–peptide–protein), the frequency exponent $1-\alpha$ of the Cole–Cole equation becomes higher (α lower), indicating a broader distribution of time constants.

A *DNA molecule* consists of two polynucleotide chains (helices). The two chains intertwine with a fixed pitch of 3.4 nm. Two types of base pairs bridge the two helices at a fixed distance of 0.34 nm. The phosphate groups in the nucleotide chains carry negative electric charges in water solution. Because of the bridges the double helix

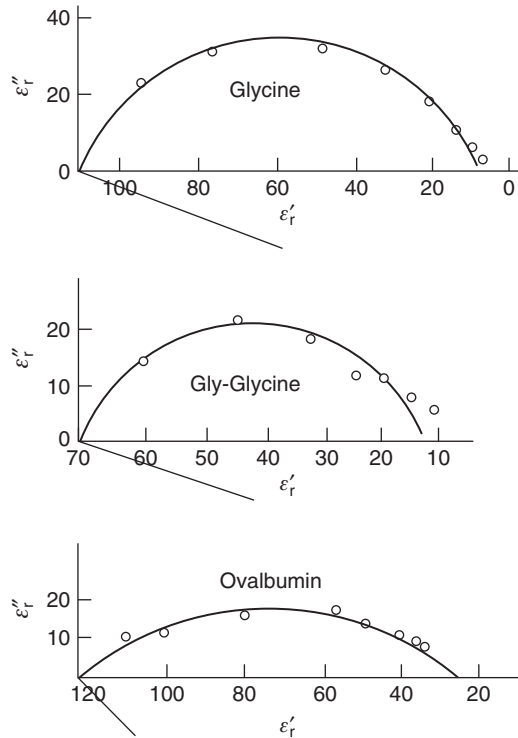


Figure 4.4 Cole-Cole plots for an amino acid (glycine with 1.5% water), a peptide (glycylglycine with 1% water) and a protein (albumin with 11% water). *Source:* From Takashima and Schwan (1965) by permission.

demonstrates considerable rigidity, and may be considered as a charged rigid rod. When a DNA solution is heated higher than about 80°C, the two strands unwind and the DNA is changed from a double helix to random coils. The denatured form may in some cases revert to the natural form by a slow cooling process. The dielectric dispersion is shown in Fig. 4.5, and is very different in natural and denatured forms. The polarization found may be due to either the movement of charges along the rod, or the turning of the whole molecule. However, the polarization has been shown to be more due to counterion polarization than the orientation process of the permanent dipole. The electrical properties of DNA were also studied by Mandel (1977) and Maleev et al. (1987). A possible resonance phenomenon was discussed by Foster et al. (1987) and Takashima (1989).

4.1.3 Carbohydrates (Saccharides)

These are the fuels for the cell metabolism. They also form important extracellular structural elements, like cellulose (plant cells) and have other specialized functions.

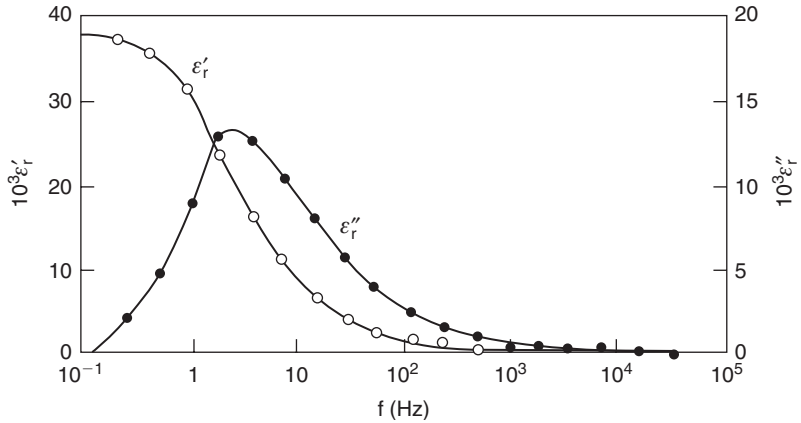


Figure 4.5 Dielectric dispersion of DNA molecules in dilute suspension. *Source:* From Takashima (1989) by permission.

Bacterial cell membranes are protected by cell walls of covalently bonded polysaccharide chains. Human cell membranes are coated with other saccharides. Some saccharides form a jellylike substance filling the space between cells. Some polysaccharides may have a negative charge at pH 7, but many carbohydrates are not believed to contribute dominantly to the admittivity of tissue.

4.1.4 Lipids and the Passive Cell Membrane

Lipids are water insoluble, oily or greasy organic substances. They are the most important storage forms of chemical energy in the body. In our context a group of lipids is of particular importance: the *polar* lipids. They are the major component of the passive cell membranes, and an important basis for the capacitive nature of cells and tissue. Polar lipids form micelles (aggregates of molecules, e.g. formed by surface active agents), monolayers and bilayers. In aqueous systems the polar lipids spontaneously form micelles, whereby the hydrophobic hydrocarbon tails are hidden from the water. On the water surface they form monolayers with the hydrophobic tails pointing out toward the air.

The cell membrane is an absolute condition for life, because by it the cell can control its interior by controlling the membrane permeability. If the membrane is destroyed the cell dies. The membrane is a layer that separates two solutions, and forms two sharp boundaries toward them. The cell membrane consists of *phospholipids* that form a bilayer lipid membrane (BLM) about 7 nm thick (Fig. 4.6). Each monolayer has its hydrophobic surface oriented inward and its hydrophilic surface outward toward either the intra- or extracellular fluids. The inside of such a bilayer is hydrophobic and lipophilic. A BLM is a very low electric conductivity membrane and is accordingly in itself closed for ions. It let lipids pass, but not water. However, water molecules can pass specialized membrane channels (cf. Chapter 5). The intrinsic

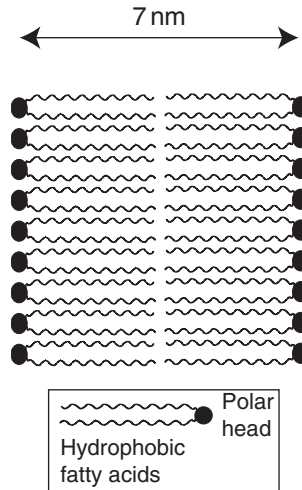


Figure 4.6 BLM, the main component of the cell membrane.

conductance is of the order of 10^{-6} S/m, and a possible lipophilic ionic conductivity contribution can not be excluded.

Even if the conductivity of the BLM itself is very low, the membrane is so thin that the capacitance is very high and the breakdown potential low. The electric field strength with 70 mV potential difference and thickness 7 nm is 10 kV/mm. This represents a large dielectric strength, but not larger than, for example, Teflon. And as we shall see this is not the potential across the bilayer itself, but the potential of the bilayer + the potential difference of the two electric double layers formed on each surface of the membrane.

A complex coating of special carbohydrates covers the external cell membrane surface, the *glycocalyx*, strongly modifying surface properties. Many of the glycocalyx carbohydrates are normally negatively charged, so that living cells repel each other. During fever the blood sedimentation (mm/h) is increased because the electric charge of the erythrocytes is diminished so that they lump together. According to Stokes law (eq. 2.6) flow friction is proportional to sphere radius a , while the weight is proportional to a^3 : the larger the sphere, the higher the sedimentation velocity (cf. also the electrokinetic effects described in Section 2.4.6).

Some of the carbohydrates are receptor substances binding, for example, hormones, and some are important for the immunological properties of a cell.

An electric double layer covers the wetted outer cell membrane surface. The total cell has a net charge revealed by its electrophoretic mobility. The cell membrane capacitance with the thickness of about 7 nm is of the order of $1 \mu\text{F}/\text{cm}^2$. The frequency dependence of the membrane capacitance has been a subject of dispute (Cole, 1972), but often the BLM as such is considered to have a frequency independent membrane capacitance.

When the potential difference is increased >150 mV, the *membrane* breaks down (cf. Section 9.4.1) on electroporation. This must not be confused with the

excitation process, when the ionic *channels* of the membrane suddenly open (cf. Chapter 5).

An artificial BLM may spontaneously take the form of a sphere, enclosing a solution at the inside. Such a sphere is called a *liposome*, and has important similarities with a cell. Agitated by ultrasound during formation they may have a diameter of 10–100 nm, and are thus smaller than most living cells. Agitated by hand they may be in the micrometer range.

4.2 TISSUE AND ORGANS

Tissue is a very heterogeneous material, and interfacial processes are very important. The cells are of uneven size and with very different functions. There is a large difference between the tissue conductivity: from the liquid tissue flowing through the blood vessels to the myelin sheaths as insulators surrounding the axons of the nerve cells, from connective tissue specialized to endure mechanical stress to bones and teeth, muscle masses, the dead parts of the skin, gas in lung tissue and so on. From an electrical point of view, it is *impossible* to regard tissue as a homogenous material.

Let us consider a simple case with a volume of many cells in interstitial fluids (Fig. 4.7).

The cell membranes are considered to have a high capacitance and a low but complicated pattern of conductivity. At DC and low frequencies current passes around the cells. Lateral conductance in the double layers is also possible. Cell interior does to a smaller degree contribute to current flow. At higher frequencies the membrane capacitance let AC current pass. The membrane effect disappears, and the current flows everywhere according to local ionic conductivity.

All interfaces give rise to Maxwell–Wagner and counterion polarization effects as described in Section 3.5.

In general tissue is an anisotropic medium because of the orientation of cells, macromembranes and organs (Figs 4.30–4.32). Such an anisotropy is a low frequency phenomenon if it is due to membranes, but not if it is due to, for example, air. Organs are very often compartmentalized, with *macromembranes as compartment walls*. The lung, the heart, the brain and the stomach all have multi-layer membranes, but the largest is the abdominal membrane, *peritoneum*. These membranes may have large influence on current flow, and also endogenic currents between the organs. The gradients of ionic concentration develop electromotive voltages (emv's) that influences current flow (Nordenstrøm, 1983).

Electrical tissue data is tabulated in Table 4.1. The maximum magnitudes for the different tissue dispersion regions are shown in Table 4.2 (cf. Section 3.8).

Usually extracellular liquids dominate the in-phase conductivity. The low frequency *temperature coefficient* is therefore that of electrolytes, around +2%/°C. The quadrature ϵ' or Y'' components have a smaller temperature coefficient (around –0.5%/°C), but dependent on the measuring frequency in relation to the characteristic frequencies of the dispersions. The effect of hyperthermia and freezing on tissue impedance was studied by Yu et al. (2004).

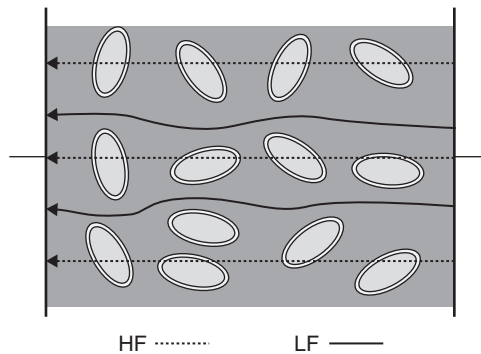


Figure 4.7 Low and high frequency current paths in tissue.

TABLE 4.1 Tissue Conductivity, LF and 1 MHz

Tissue	σ (S/m) 1 Hz–10 kHz	σ (S/m) ca 1 MHz	φ_{\max} @ <10 MHz	anisotropy
Human skin, dry	10^{-7}	10^{-4}	80°	?
Human skin, wet	10^{-5}	10^{-4}	30°	?
Bone	0.005–0.06		20°	Strong
Fat	0.02–0.05	0.02–0.05	3°	Small
Lung	0.05–0.4	0.1–0.6	15°	Local
Brain (grey matter)	0.03–0.4	0.15	15°	Small
Brain (white matter)	0.03–0.3			Strong
Liver	0.2	0.3	5°	?
Muscle	0.05–0.4	0.6	30°	Strong
Whole blood	0.7	0.7	20°	Flow dependent
Urine	0.5–2.6	0.5–2.6	0°	0
CSF	1.6	1.6	0°	0
Saline, 0.9%, 20°C	1.3	1.3	0°	0
Saline, 0.9%, 37°C	2	2	0°	0
Seawater	5	5	0°	0

TABLE 4.2 Maximum Dispersion Magnitudes According to Schwan (1963)

	α	β	γ
$\Delta\epsilon_r$	5×10^6	10^5	75
$\Delta\sigma$	10^{-2}	1	80

4.2.1 Tabulated Tissue Conductivity Data

It is very difficult to tabulate tissue conductivity, in particular living tissue. Traditionally tissue is classified into four groups in medicine: epithelium, muscle, connective tissue and nervous tissue. Text books in histology may list about 35

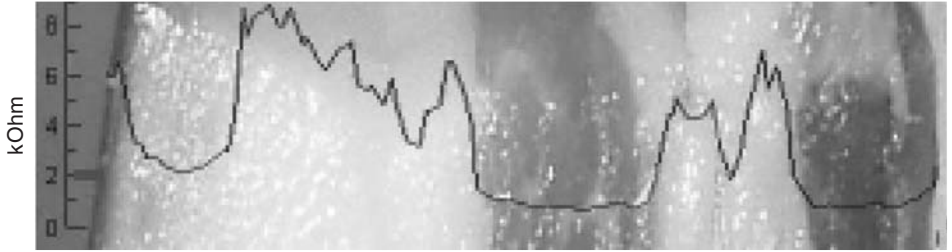


Figure 4.8 Measured modulus of impedance at 10 kHz plotted as a function of insertion depth in a piece of bacon. The mark at about 2 k Ω indicates the starting point of the horizontal needle insertion path. *Source:* Courtesy of Håvard Kalvøy.

classifications, Gabriel et al. (1996a) identified over 30 tissue types according to electrical properties. If we leave the macro view and approach cellular levels and the basic tissue building blocks, the tissue parameter values may change a decade from micrometer to micrometer penetration depth. This can be illustrated by a thin needle with an insulated shaft and a small exposed tip. Figure 4.8 shows the measured monopolar impedance as a function of insertion depth in a piece of bacon. There are large differences within apparent similar tissue, what volume shall a quoted conductivity value be valid for?

Furthermore the values are dependent on frequency, temperature, water content, blood perfusion, the status of the body. The difference between data from human and mammalian animal tissue is usually considered small. The biomaterial may be in vivo or ex vivo tissue, excised material from freshly killed animals, human autopsy material obtained a day or two after death. Electrical tissue data has been tabulated by many authors in many review articles and book chapters: Schwan and Kay (1957), Schwan (1963), Geddes and Baker (1967), Foster and Schwan (1986), Duck (1990), Stuchly and Stuchly (1990), Holder (2005). Gabriel et al. (1996a) made a literature survey. Their own measurements, Gabriel et al. (1996b), were made with two-electrode technique and a coaxial probe in the frequency range 10 Hz–20 GHz. In that way the transfer impedance component was eliminated.

Problems with tabulated values are therefore:

- What is the tissue volume the data is averaged over?
- Is the anisotropy given?
- Is it human tissue?
- Are the values valid for living tissue, in vivo, ex vivo or newly excised; or for dead tissue? Is the temperature given?
- Is the frequency dependence given?

In Section 3.8 about dispersions the use of permittivity or conductivity parameters was discussed. From Section 2.3 we know that conductivity is dependent both on the density of charge carriers and their mobility. In the frequency range <10 MHz, tissue admittance is usually dominated by the conductivity of the body electrolytes, at higher frequencies by the dielectric constant. The electrolytes without

cells, in particular urine and cerebrospinal fluid (CSF), have the highest low frequency conductivity. The higher the cell concentration, the lower the low frequency conductivity. Tooth, cartilage and bone, lipids, fat, membranes such as skin stratum corneum, connective tissue, may contain much inorganic materials with low conductivity but very dependent on body liquid perfusion.

In Vitro Data

Let us recall that tissue can be characterized by permittivity or admittivity. In a unity measuring cell ($A/d = 1$ (m)) the permittivity is: $\epsilon' = C_p$ and $\epsilon'' = G/\omega$. The conductivity is: $\sigma' = G$ and $\sigma'' = \omega C_p$.

The poorly conducting membranes of the body and the interfacial polarization therefore cause the permittivity corresponding to α -dispersion in the mHz–kHz range (cf. Section 3.8). At frequencies <1 Hz, the capacitive current component vanishes, and the admittivity is purely conductive determined mostly by the liquids outside the outermost membranes. In a frequency range 0.1–10 MHz, the phase angle is maximum (except for human skin where it is at much lower frequencies). This is also the Maxwell–Wagner β -dispersion range for the dielectric interfaces, where the susceptance of the cell membranes becomes large, and their influence more and more negligible. If there is an anisotropy at lower frequencies, it has disappeared in this frequency range. The dipolar dispersion of the proteins also appears in this frequency range, and it is still active above 100 MHz. This is the γ -dispersion range extending all the way up to the single Debye characteristic frequency of water, centered on 18 GHz. The susceptance is dominating at these high frequencies, and the phase angle may be $>80^\circ$.

In Vivo Data

Magnetic Resonance Electrical Impedance Tomography (MREIT) is a new and promising non-invasive method for finding conductivity data in vivo, Oh et al. (2005). Other techniques are invasive, by needle or surgical opening measuring in situ or excised ex vivo. The spatial resolution of the measuring electrodes is important with respect to tissue data averaging. In medicine the *parenchyma* is the typical tissue of the functional element of an organ, in contrast to its framework (stroma). With a needle electrode with insulated shaft the size and cutting properties of the tip are important. With a blunt needle the tissue is pushed during the advancement until the tip suddenly penetrates and the tissue moves back. Thin membranes and tissue interfaces may generate large differences within a fraction of a millimeter (Fig. 4.8).

Tissue immittivity is dependent on body liquid perfusion or tissue ischemia and pathological processes. Local tissue may be living for a considerable time also after the body as such is dead. Hair and nail is dead tissue and the stratum corneum of the skin is already dead in its “in vivo” position.

4.2.2 Muscle Tissue

Muscle tissue exhibits a large α -dispersion, and as shown in Fig. 4.9 it may be strongly anisotropic with a low frequency conductance ratio of about 1:8 between

transversal and longitudinal directions. In the longitudinal direction the high conductance is not very frequency dependent, indicating that direct free liquid channels dominate the current path. It has been proposed that the α -dispersion arises from interfacial counterion polarization, or from sarcotubular membrane systems in the interior of the muscle fiber. The transversal properties are presumably more dominated by interfacial β -dispersion of the Maxwell–Wagner character.

Figure 4.10 shows another data set presented with permittivity and conductivity. In the transversal situation 3–4 dispersions are clearly seen. The longitudinal data illustrates how dispersion levels may be almost non-existent. Dispersion may take the character of one single straight line through many decades of frequency.

4.2.3 Nerve Tissue, Linear Properties

The brain is the only tissue with a large volume of nerve tissue. Nerve tissue elsewhere may be regarded as cables, and electrical cable theory is often applied. The insulating properties of the myelin sheath increase the impedance for myelinated nerves.

Macroscopical data for brain tissue is shown in Fig. 4.11. Measurements in vivo through the low conductivity scalp will show quite different data.

4.2.4 Adipose and Bone Tissue

Figure 4.12 shows the dispersion of adipose tissue. Adipose tissue and in particular bone and bone marrow have a wide spread of permittivity and conductivity, very dependent on the degree of blood and other liquid perfusion.

4.2.5 Blood

Whole blood consists of erythrocytes (containing the hemoglobin) and other cells in plasma. Blood may be studied as whole blood in vivo, erythrocytes in suspension, lysed erythrocytes in suspension, as plasma, etc. The erythrocytes are formed as doughnuts with an outer diameter of about 10 μm . Plasma is the liquid part with electrolytes and large organic electrically charged molecules. Lysed erythrocytes are destroyed cells with their intracellular material (hemoglobin) emptied into the liquid. The electrical properties of whole blood and lysed blood are of course very different, Figs. 4.13 and 4.14. From Maxwell–Wagner theory it is possible to find an expression for the conductivity of a suspension of membrane-covered spheres (Section 3.5.1).

Whole blood exhibits β -, γ - and δ -dispersion, but curiously enough no α -dispersion, Foster and Schwan (1989). The β -dispersion has a dielectric increment of about 2000 centered around 3 MHz (hematocrit 40%). Erythrocytes in suspension have a frequency independent membrane capacitance with very low losses (Schwan, 1957). The impedance of lysed erythrocytes in suspension shows two

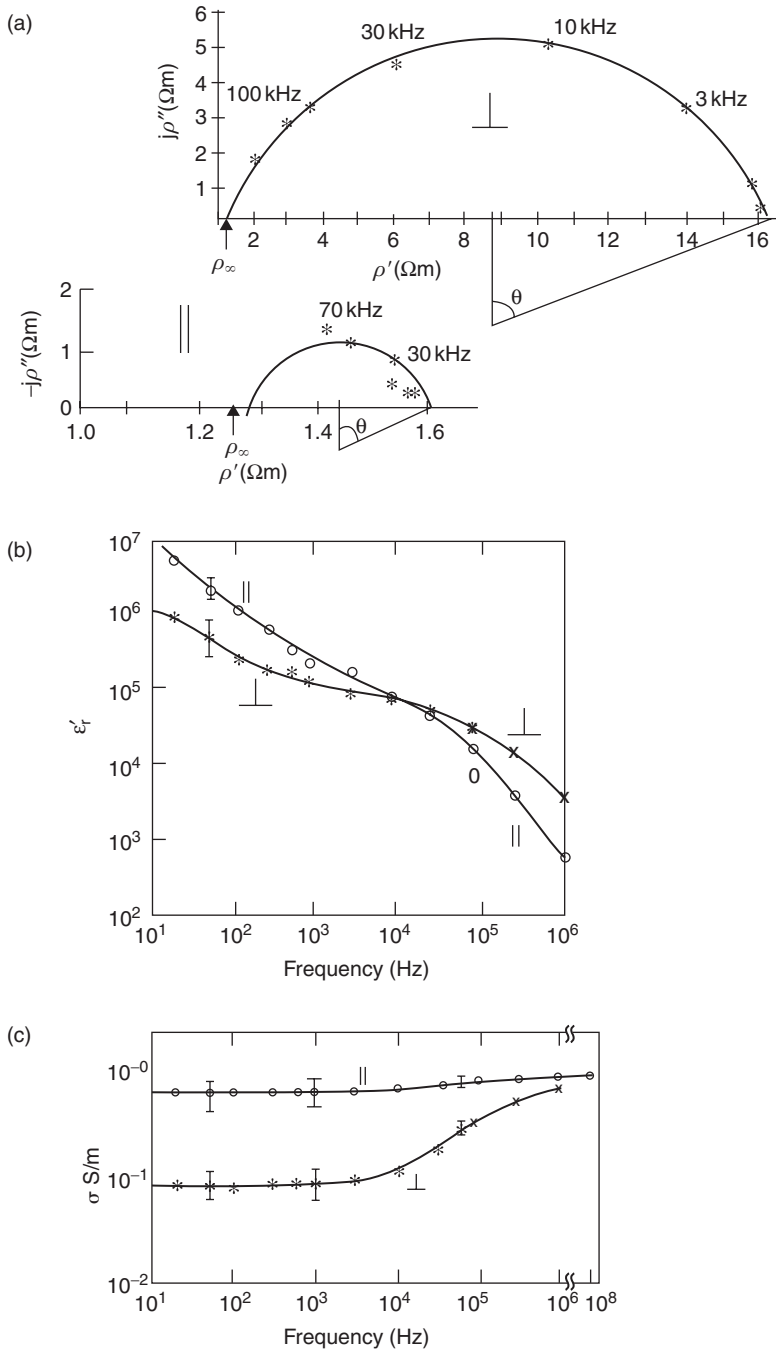


Figure 4.9 Dog excised skeletal muscle (37°C), frequency dependence and anisotropy. Current path: \perp transversal, \parallel longitudinal to muscle fibres. (a) Complex resistivity in the Wessel plane; (b) Relative permittivity; (c) Conductivity. Redrawn from Epstein and Foster (1983), by permission.

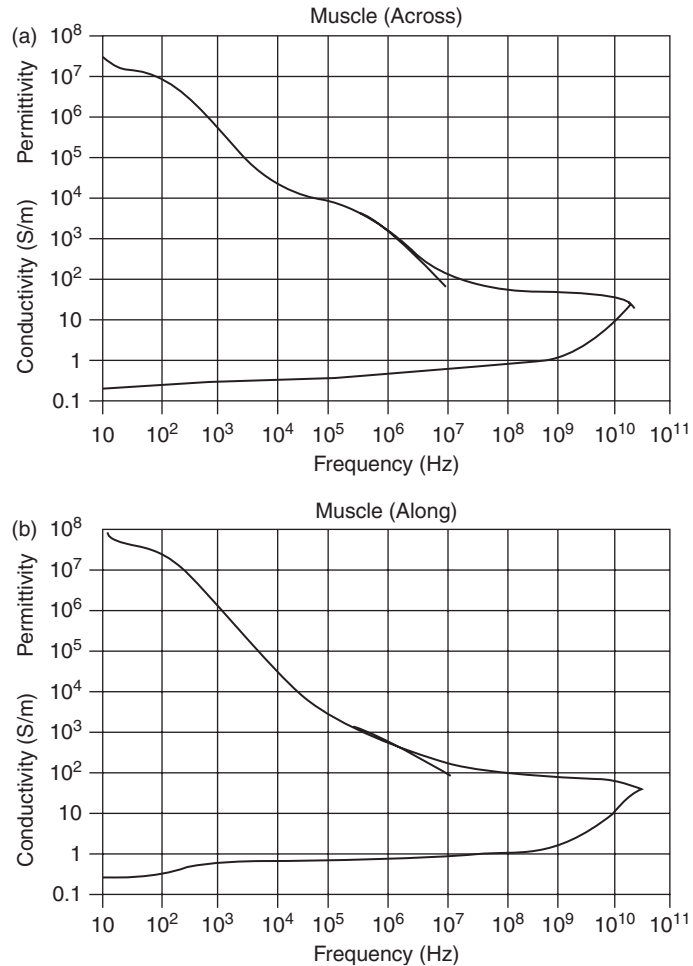


Figure 4.10 Dispersion of muscle tissue. (a) transversal; (b) longitudinal. *Source:* From Gabriel et al. (1996b) by permission.

clearly separated single relaxation frequencies (Debye dispersions). The α -dispersion is in the lower kHz range and the β -dispersion in the lower MHz range (Schwan, 1957; Pauly and Schwan, 1966).

Figure 4.13 presents an example of the dielectric constant and conductivity of a suspension of *lysed* erythrocytes, the characteristic frequency is low, approximately 1.5 kHz. Figure 4.13 shows the admittance of erythrocytes in natural condition during sedimentation.

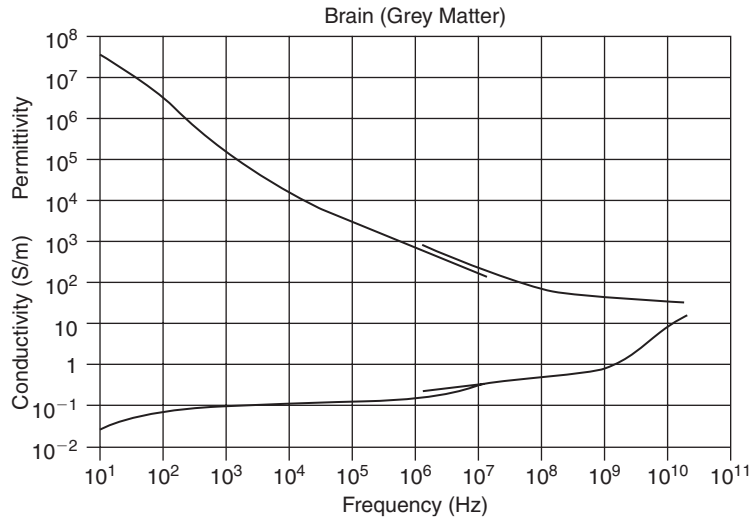


Figure 4.11 Dispersion of brain tissue. *Source:* From Gabriel et al. (1996b) by permission.

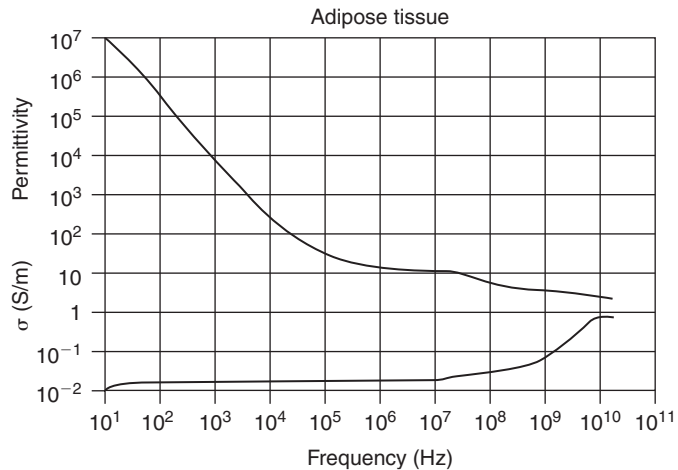


Figure 4.12 Dispersion of adipose tissue. *Source:* From Gabriel et al. (1996b) by permission.

The use of dielectric spectroscopy to characterize living cells and the possible derivation of cellular parameters like living cell volume concentration, complex permittivity of extracellular and intracellular media and morphological factors, is discussed by Gheorghiu (1996). Another possible application is the electrical measurement of erythrocyte deformability (Amoussou-Guenou et al., 1995).

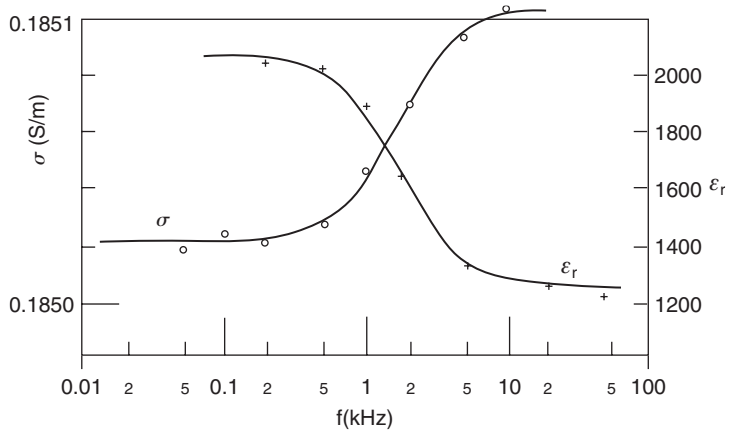


Figure 4.13 Dielectric constant and conductivity of a suspension of lysed erythrocytes. Characteristic frequency low, approximately 1.5 kHz. Note high resolution conductivity scale. *Source:* From Schwan (1957) by permission.

4.2.6 Human Skin and Keratinized Tissue

Epithelia are cells organized as layers, skin is an example. Cells in epithelia form *gap junctions*. Particularly in tight membranes these junctions are special *tight junctions*. The transmembrane admittance is dependent both on the type of cell junctions and to what extent the epithelium is shunted by channels or specialized organs (e.g. sweat ducts in the skin).

The impedance of the skin is dominated by the stratum corneum at low frequencies. It has generally been stated that skin impedance is determined mainly by the stratum corneum at frequencies below 10 kHz and by the viable skin at higher frequencies (Ackmann and Seitz, 1984). This will of course be dependent on factors like skin hydration, electrode size and geometry, etc. but may nevertheless serve as a rough guideline. A finite element simulation on a concentric two-electrode system used by Yamamoto et al. (1986) showed that the stratum corneum accounted for about 50% of the measured skin impedance at 10 kHz, but only about 10% at 100 kHz (Martinsen et al., 1999).

Stratum corneum may have the thickness of from about 10 μm (0.01 mm) to 1 mm or more under the foot. The stratum corneum is a solid state substance, not necessarily containing liquid water, but with a moisture content dependent on the surrounding air humidity. Stratum corneum is not soluble in water, but the surface will be charged and a double layer will be formed in the water side of the interphase. Stratum corneum can absorb large amounts of water (e.g. doubling its weight). Stratum corneum may be considered as a solid state electrolyte, perhaps with few ions free to move and contribute to DC conductance. The stratum corneum contains such organic substances as proteins and lipids, which may be highly charged but bound, and therefore contributing only to AC admittance.

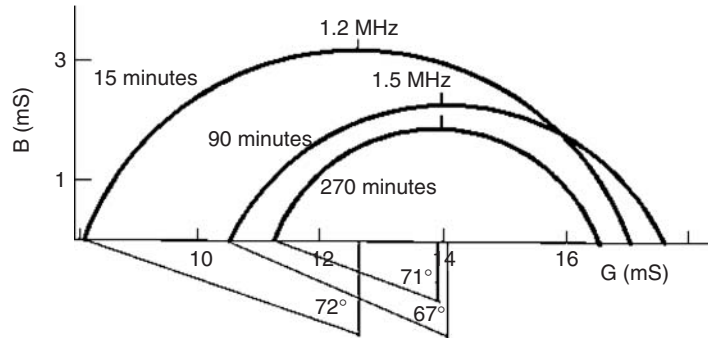


Figure 4.14 Admittance of erythrocytes in natural condition during sedimentation. *Source:* From Gougerot and Fourchet (1972) by permission.

An open question is whether the conductance in stratum corneum in addition to the ionic component, also has an electronic component (e.g. as a semiconductor).

The stratum corneum has been shown to display a very broad α -dispersion (Fig. 4.15) that presumably is mainly caused by counterions. Viable skin has electrical properties, which resembles that of other living tissue, and hence displays separate α - and β -dispersions. The interface between the stratum corneum and the viable skin will also give rise to a Maxwell–Wagner type of dispersion in the β -range. While the impedance of the stratum corneum is much higher at low frequencies than the impedance of the living skin, the differences in dispersion mechanisms make the electrical properties converge as the frequency is increased. This is the main reason why increased frequency in general leads to measurements at deeper layers in the skin.

Yamamoto and Yamamoto (1976) measured skin impedance on the ventral side of the forearm with a two-electrode system and an AC bridge. They used Beckman Ag/AgCl electrodes filled with gel and measured 30 minutes after the electrodes had been applied. The skin was stripped with cellulose tape 15 times, after which the entire stratum corneum was believed to have been removed. Impedance measurements were also carried out between each stripping so that the impedance of the removed layers could be calculated. The thickness of the stratum corneum was found to be $40\ \mu\text{m}$, which is more than common average values found elsewhere in the literature. Therkildsen et al. (1998) found, for example, a mean thickness of $13.3\ \mu\text{m}$ (minimum $8\ \mu\text{m}$ /maximum $22\ \mu\text{m}$) when analyzing 57 samples from non-friction skin sites on Caucasian volunteers. However, the moisture increase caused by electrode occlusion and electrode gel has most certainly increased the stratum corneum thickness significantly.

Knowing the stratum corneum thickness enabled the authors to calculate the parallel resistivity and relative permittivity of the removed stratum corneum. Furthermore, the resistivity and relative permittivity of the viable skin was calculated by assuming homogenous electrical properties and using the formula for the constrictional resistance (cf. Fig. 6.3). The resistance of disk surface electrode is

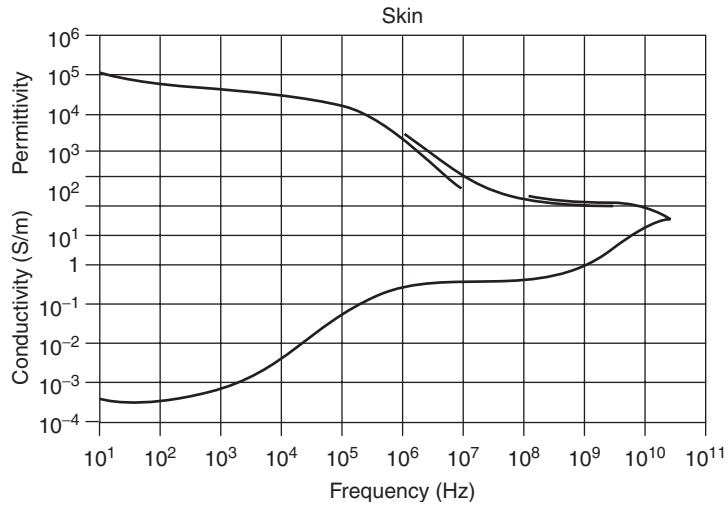


Figure 4.15 Dispersion of skin tissue. Source: From Gabriel et al. (1996b) by permission.

(eq. 6.17): $R = \rho/4a$. Since $RC = \rho\epsilon_r\epsilon_0$, the relative permittivity of the viable skin can be calculated from the measured capacitance with a similar formula:

$$C = 4a \epsilon_r \epsilon_0$$

The calculated data from Yamamoto and Yamamoto (1976) are presented in Fig. 4.16.

These data can also be presented as conductance and susceptance versus frequency as in Fig. 4.17. The very broad nature of the dispersion can easily be seen in this figure. The conductance levels out at low frequencies, indicating the DC conductance level of the skin. The susceptance seems to reach a maximum at approximately 1 MHz, which should then correspond to the characteristic frequency of the dispersion. This frequency response is difficult to interpret and the apparent broad dispersion is most probably a composite of several dispersion mechanisms. The highly inhomogeneous nature of the stratum corneum with a significant hydration gradient in brick-like layers of dead, keratinized cells should produce significant dispersion mechanisms both in the alpha and beta range.

The frequency response shown in Fig. 4.17 can be compared with the admittance data from a 180 μm thick sample of palmar stratum corneum in vitro as shown in Fig. 4.18 (Martinsen et al., 1997a). These measurements were performed with two-electrode system and hydrogel electrodes at 50% relative humidity (RH). The DC level of this stratum corneum sample is much lower than the one shown in Fig. 4.17, even after adjusting for the 4.5 times greater thickness of the in vitro sample. This is easily explained from the difference in hydration for the two samples. Stratum corneum in vivo is hydrated by the underlying viable skin and in this case, also by the

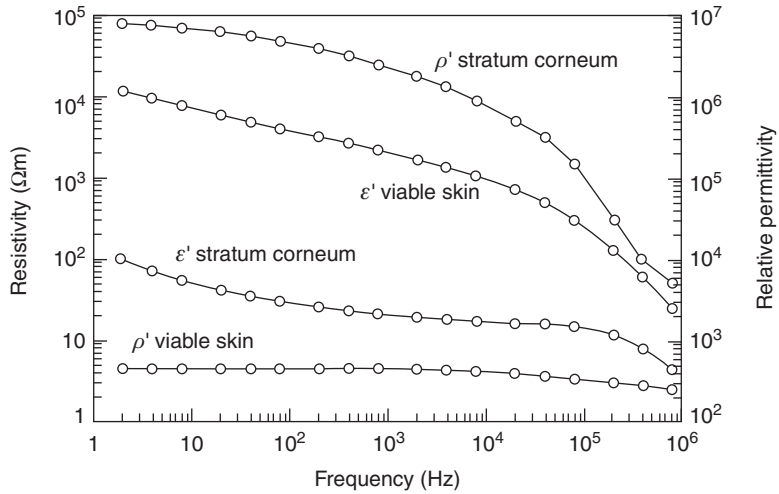


Figure 4.16 Average resistivities and relative permittivities in stratum corneum and viable skin. Source: Redrawn from Yamamoto and Yamamoto (1976).

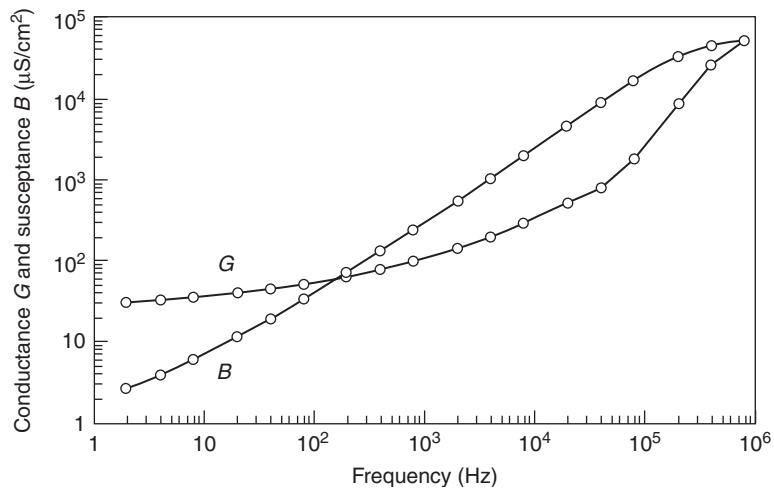


Figure 4.17 Surface admittance density of the stratum corneum as calculated from data presented in Fig. 4.16.

electrode gel. The *in vitro* skin is in balance with the ambient RH and the hydrogel electrodes do not increase the hydration (Jossinet and McAdams, 1991).

An important finding by Yamamoto and Yamamoto (1976) was that the impedance of the removed stratum corneum layers did not produce a circular arc in the complex impedance plane. This is obvious from Fig. 4.19 where the admittance data from Fig. 4.17 have been transformed to impedance values and plotted in the complex plane.

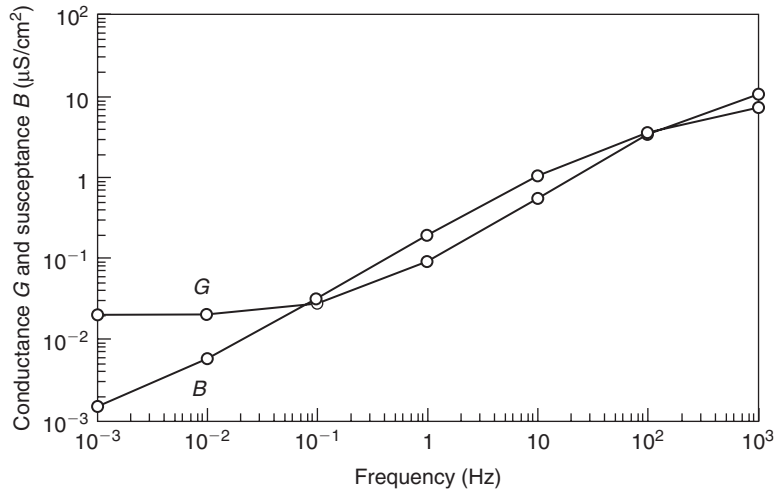


Figure 4.18 Surface admittance density of palmar stratum corneum in vitro. *Source:* From Martinsen et al. (1997a) by permission.

Hence, if one plots the data from multi-frequency measurements on skin in vivo in the complex plane and use a circular regression in order to derive, for example, the Cole parameters one must be aware of the following: Stratum corneum alone does not necessarily produce a circular arc, and as described earlier in this chapter, the measured volume or skin layer is highly dependent on frequency. The derived parameters therefore represent a mixture of different skin layers and different dispersion mechanisms and are thus totally ambiguous when used for characterizing conditions of specific skin layers.

Skin admittance varies greatly both between persons and between different skin sites on the same person. Changes in, for example, sweat gland activity and ambient RH during the day or year season is also reflected by large variations in skin admittance, mainly because of changes in skin hydration.

Table 4.3 shows the results from impedance measurements at 10 Hz on different skin sites as measured with a 12 cm² ECG dry metal plate electrode positioned directly on the skin site after a short breath had been applied to the skin surface (Grimnes, 1983a). The first column presents measurements immediately after the electrode had been applied, and the two subsequent columns gives the values after 2 and 4 hours respectively. The first column shows a large variation in the control impedance, which was interpreted as unstable sweat duct filling during the measurement. The two other columns show stable results at two different levels of control. The values in Table 4.3 clearly demonstrate the large variability in skin impedance on different skin sites, and how this changes during a period of skin occlusion.

The sweat ducts of the skin introduce electrical shunt paths for DC current. Although lateral counterion relaxation effects have been demonstrated in pores,

TABLE 4.3 Site Dependence of Skin Impedance ($k\Omega\text{ cm}^2$) at 10 Hz. Initial Values and Values Obtained After Two Intervals of 2 hours. Each Measurement is Compared with the Value ($k\Omega$) Obtained from a Control Pre-gelled ECG Electrode on the Ventral Forearm. Reproduced from Grimnes (1983a)

	$k\Omega\text{cm}^2/k\Omega$		
	Start	2 hour	4 hour
Hand: – dorsal side	720/80	210/17	300/33
Forearm: – ventral – distal	250/80	240/17	190/35
Forearm: – ventral – middle	840/80	230/17	360/36
Forearm: – ventral – proximal	560/80	180/17	260/36
Upper arm: – dorsal	840/75	260/16	660/36
Upper arm: – ventral	1000/70	300/16	780/34
Forehead	60/70	36/16	48/35
Calf	325/45	375/17	325/36
Thorax	130/37	110/16	130/35
Palm	200/80	150/17	200/33
Heel	120/60	180/15	120/35

this effect is presumably negligible in sweat ducts, and sweat ducts are hence predominantly conductive (Martinsen et al., 1998). The DC conductance measured on human skin is not only due to the sweat ducts, however. Measurements on isolated stratum corneum as well as nail and hair, reveal conductance values comparable to those found on skin in vivo (Martinsen et al., 1997a, b).

Since sweat duct polarization is insignificant, the polarization admittance of the skin is linked to the stratum corneum alone. This implies that measurements of capacitance or AC conductance at low frequencies only reflect the properties of the stratum corneum.

The series resistance (i.e. the limiting impedance value at very high frequencies) is very small for the stratum corneum. In a practical experimental set-up, the impedance of the viable skin will in fact overrule this component. The value of this effective series resistance is typically in the range 100–500 Ω .

Skin Penetrated by External Electrolytes

In low frequency applications $<100\text{ Hz}$, the skin impedance is very high compared to the polarization impedance of wet electrodes and deeper tissue impedance. The stratum corneum consists of dead and dry tissue, and its admittance is very dependent on the state of the superficial layers and the water content (humidity) of the surrounding air in contact with the skin prior to electrode onset. In addition, the sweat ducts shunt the stratum corneum with a very variable DC conductance. Sweat fills both the ducts and moisturizes the surrounding stratum corneum. The state of the skin and measured skin admittance at the time of electrode onset is therefore very variable. With low sweat activity and dry surroundings the skin admittance may easily attain values $<1\ \mu\text{S}/\text{cm}^2$ at 1 Hz.

From the time of onset of a *dry* metal plate, the water from the deeper, living layers of the skin will slowly build up *both* a water contact with the initially dry plate *and* water content in the stratum corneum. A similar process will take place in the skin with hydrogel as contact medium (but here the metal/gel interphase is already established). The processes may take a quarter of an hour or more. The water vapor pressure of the hydrogel may be such as to supply or deplete the stratum corneum of water, dependent on the initial skin conditions.

To avoid the long period of poor contact, a skin drilling technique may remove the stratum corneum. Even mild sandpaper rubbing may reduce the initial impedance considerably.

To shorten the long period of poor contact, an electrolytic solution or wet gel is often applied to the skin. The electrolyte concentration of the contact medium is very important. By using high salt concentration, the water *osmotic pressure* in the deeper layers will strongly increase the water transport up through the skin to the high concentration zone. This may be admissible for short time use (e.g. <0.5 hour). For prolonged use, skin irritation may be intolerable. For long term use the concentration must be reduced to the range of a physiological saline solution (around 1% of electrolytes by weight).

A surface electrode with contact electrolyte covering a part of the skin may influence measured skin immittance by four different mechanisms:

1. Changing the water partial pressure gradient in the stratum corneum.
2. Osmotic transport of water to or from the contact electrolyte.
3. Penetration of substances from the electrode gel into the stratum corneum.
4. Changing the sweat duct filling

With a dry electrode plate, the moisture buildup and admittance increase in the stratum corneum start at the moment of electrode onset. With a hydrogel, admittance may increase or decrease. With wet gel or a liquid, the initial admittance is high, and with strong contact electrolytes the admittance will further increase for many hours and days (Fig. 4.20). As the outer layers of stratum corneum may be wet or dry according to the ambient air, it will not be possible to find a general contact medium which just stabilizes the water content in the state it was before electrode onset, the onset of the electrode will generally influence the parameters measured.

With dry skin the admittance may be $<1\ \mu\text{S}/\text{cm}^2$ at 1 Hz. A typical admittance of $>100\ \mu\text{S}/\text{cm}^2$ is possible when the stratum corneum is saturated by electrolytes and water. The conductivity is very dependent on water content and believed to be caused, for example, by protons (H^+) and charged, bound proteins that contribute only to AC-admittance.

Figure 4.21 shows the dominating effect of sweat duct filling on skin *admittance*, and shows clearly how skin capacitance is in parallel and therefore unaffected by the parallel conductance change.

Hair and Nail

Hair is compactly cemented keratinized cells, and grows in *hair follicles* that essentially are invaginations of the epidermis into the dermis. The *sebaceous glands* are

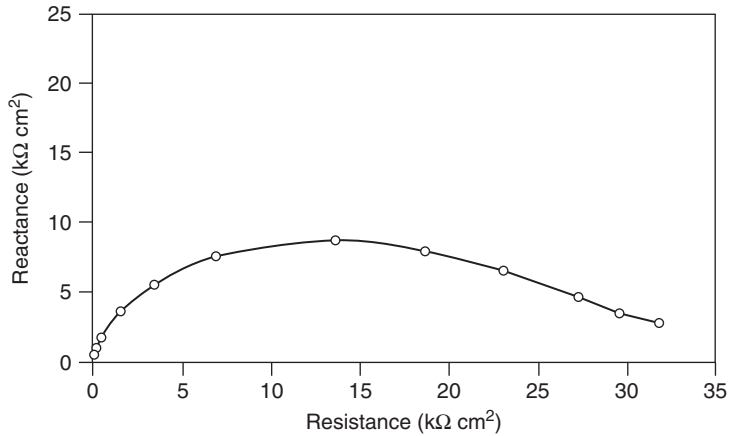


Figure 4.19 The stratum corneum data from Fig. 4.17 plotted in the complex impedance plane.

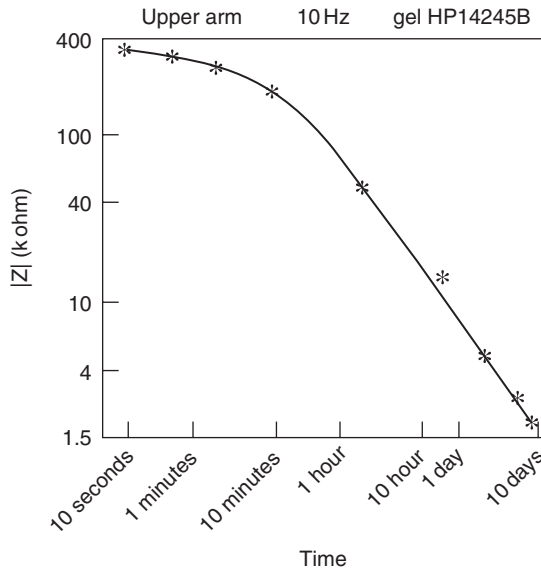


Figure 4.20 Skin impedance as a function of time for an ECG electrode of type: commercial, long term, wet gel, strong electrolyte. *Source:* From Grimnes (1983a) by permission.

located on the sides of the hair follicles. They secrete *sebum* to the skin surface, but the purpose of this secretion is unclear, apart from the fact that it gives a scent that probably is unique to each human being. The problem of *Acne vulgaris*, well known to most young people, is connected to these glands.

The frequency response of hair is not unlike the properties of skin, but typical measured admittance values are of course very small, which makes these measurements

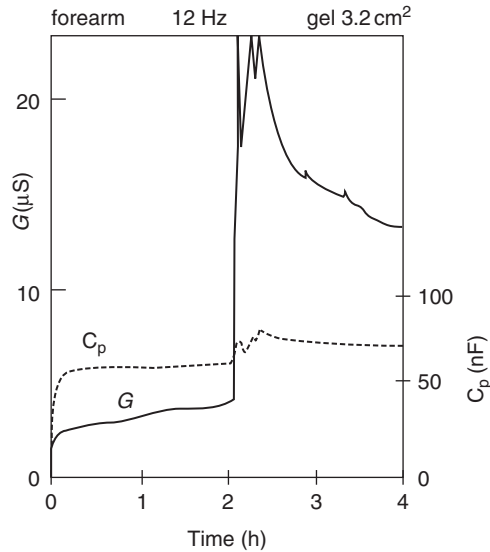


Figure 4.21 In vivo skin conductance and parallel capacitance during abrupt sweat duct filling (sudden physical exercise) and emptying. *Source:* From Grimnes (1984) by permission.

complicated to perform. Figure 4.22 shows measurements on 100 hair fibers in parallel at different ambient relative humidities (Martinsen et al., 1997b). Hair length was approximately 2 cm.

At 86% RH the conductance is almost frequency independent (dominated by DC properties) up to 1 kHz, and at 7% and 62% only a small increase at the highest frequencies can be detected. The susceptance is increasing linearly at the highest frequencies, but levels off at the lowest frequencies. The frequency at which this flattening starts increases with RH.

Adsorption of water into hair is a very slow process. Robbins (1979) found that the hydration of hair fibers had stabilized after a period of 18–24 hours after being introduced to an increase in ambient RH. Martinsen et al. (1997b) found that the conductance continued to increase for several days after such a step in RH and concluded that a possible cause of this is that adsorbed water molecules regroup in a way that increases their contribution to the conductivity. They furthermore found desorption to be a very quick process where the main change in conductance appeared during the first minutes after reducing ambient RH, but also with minor changes in conductance for the succeeding few hours.

The electrical admittance of keratinized tissue is typically logarithmically dependent on water content or ambient RH. An example from human hair is shown in Fig. 4.23 where the 1 Hz conductance of 50 fibers in parallel is plotted against ambient RH (Martinsen et al., 1997b).

Nail is also keratinized tissue but is harder than stratum corneum. This is partly due to the “hard” α -keratin in nail as opposed to the more “soft” β -keratin in stratum corneum (Baden, 1970; Forslind, 1970).

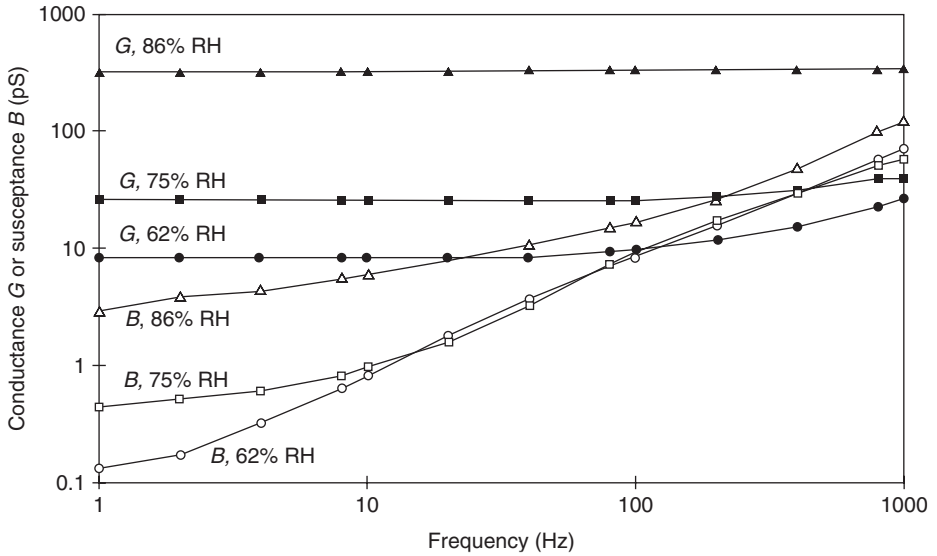


Figure 4.22 Electrical admittance of 100 hair fibers in parallel as function of RH. Source: Martinsen et al. 1997b.

Even though nail is readily available and easy to perform electrical measurements on, the electrical admittance of human nail have not been extensively investigated. Figure 4-24 shows the conductance and susceptance of a 450 μm thick nail at 38% RH, measured with a two-electrode hydrogel system (Martinsen et al., 1997a).

The electrical properties of nail resemble those of stratum corneum and hair. Note, however, that the low frequency susceptance plateau in Fig. 4.24 represents a deviation from a simple model with a distribution of relaxation times for a single dispersion mechanism (cf. Section 8.2), and must be due to another dispersion mechanism such as electrode polarization, skin layers, etc. The admittance of nail is also logarithmically dependent on water content as shown in Fig. 4.25 (Martinsen et al. 1997c)

4.2.7 Whole Body

Resistance

The value of the impedance between two skin surface electrodes is usually dominated by the contribution of the skin. However, the skin impedance may be negligible if:

1. the voltage is high enough for skin electrical breakdown;
2. the skin is thoroughly wetted;
3. the skin is perforated;

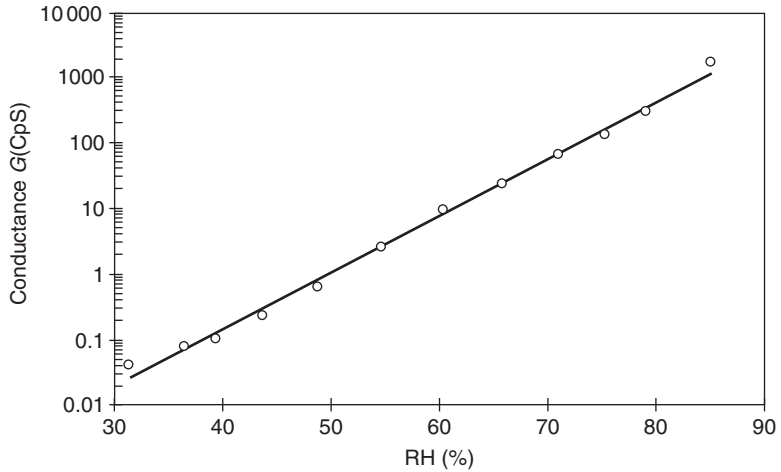


Figure 4.23 Electrical admittance of 50 hair fibers as a function of RH at 1 Hz. Circles are measured values and line is logarithmic regression. *Source:* Martinsen et al. 1997b.

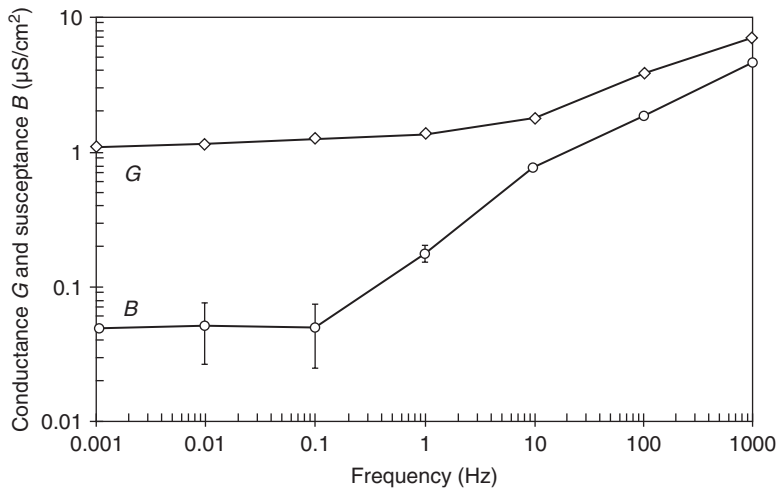


Figure 4.24 Electrical admittance of human nail. Error-bars show uncertainty in low frequency susceptance data. *Source:* Martinsen et al. 1997a.

- 4. effective skin contact area is very large;
- 5. the signal frequency is sufficiently high.

Without the skin and with the living body tissue considered purely resistive, the resistance R of a body segment is determined by the mean resistivity ρ , mean length L and mean cross sectional area A according to $R = \rho L/A$. The resistance can be measured by a four-electrode technique (Freiberger, 1933; Grimnes, 1983a).

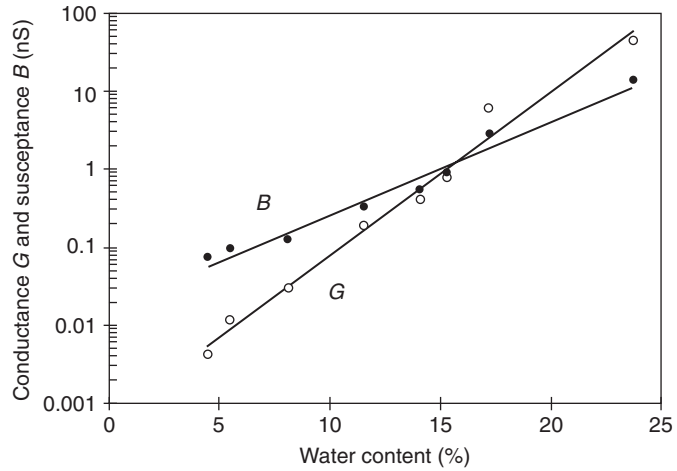


Figure 4.25 Electrical admittance for nail at 80 Hz as function of absolute water content (% weight). Area is 3.14 mm² and thickness is 0.34 mm. Circles are measured values and line is logarithmic regression. Source: Martinsen et al. 1997c.

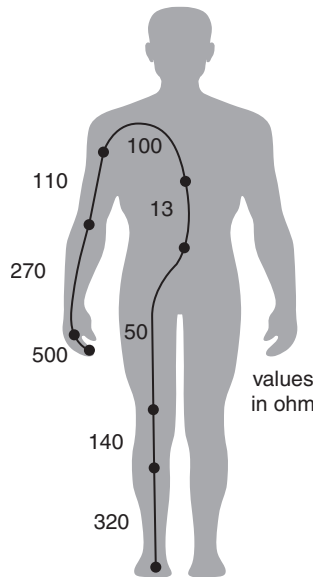


Figure 4.26 Body segment resistance distribution (no skin contribution, no current constriction). Values as found with four-electrode technique. 500 Ω is a one finger contribution. Linear values according to eq. (2.2), not very dependent on current density levels.

In Fig. 4.26, notice the importance of the cross sectional area. The resistance is dominated by the contribution from a finger, underarm and leg, while the influence from the chest is negligible. In addition the current flow may be constricted near the electrodes if the electrodes are small, and an additional *constrictional resistance*

must be accounted for (cf. Fig. 6.3). Higher resistance values may also be due to the relatively small well-conducting tissue cross sectional areas in such joints as the hand/wrist, elbow and knee.

When skin electrical protection has been broken down during an electrical accident, the volume segment resistance is the current limiting factor (cf. Section 9.17).

Body immittance data used for the estimation of body composition (see Section 9.10).

4.2.8 Post-excision Changes, the Death Process

Tissue metabolism decreases after the tissue has been excised. Often the temperature falls, and measured variations must account for such possible variables. If the tissue is supported by temperature and perfusion systems, the tissue may be stabilized in a living state *in vitro* (*ex vivo*).

If the tissue is not supported, irreversible changes will occur followed by cell and tissue death. If blood flow is interrupted, the metabolism continues, but in an anaerobic way. Osmosis will cause cell swelling and tissue damage and a consequence of this is the narrowing of extracellular pathways which typically gives an increase in the low frequency (<10 kHz) impedance. A steep increase in low frequency impedance is also found in tissue with gap junctions when these gap junctions are closed after a certain duration of ischemia. Gap junctions can also produce an additional dispersion at very low frequencies (e.g. in porcine liver at about 7 Hz) which vanishes completely when the gap junctions close. Since metabolic products are no longer removed, one will sometimes find a decrease in impedance at high frequencies (e.g. 10 MHz) (Gersing, 1998). In brain tissue, irreversible changes may occur within 5 minutes at 37°C and in cardiac tissue after 20 minutes. Impedance spectroscopy has been shown to be of great value for the monitoring of these processes and for the assessment of organ state (Gersing, 1998; Casas et al., 1999).

Figure 4.27 shows the time courses of the electrical resistance at 100 Hz and 10 MHz, measured on canine heart muscle treated by perfusion with Custodiol® (Gersing, 1998).

The initial drop in resistance is due to the warming up of the cool tissue sample, and the subsequent drop in 10 MHz resistance is probably caused by accumulation of metabolic products in the tissue (as mentioned above). The 100 Hz resistance rises steeply after a period of about 3 hours indicating the onset of tissue damage. This damage is non-reversible when the upper plateau is reached and the organ cannot be revived. Also Salazar et al. (2004) found that bioimpedance measurements enabled differentiation between normal, ischemic and infarcted myocardium.

In keratinized tissue such as the outer layers of the human skin, in hair, nail and horn, the change and ultimate death of the cells are genetically programmed to occur during a period of about 30 days. The dead keratinized cells need no intra- or extracellular fluids, and may be in a dry state with low admittance values.

Bozler and Cole (1935) measured the electrical impedance of frog sartorius muscle from 1.1 kHz to 1.1 MHz. Measurements were first done approximately 2 hours after dissection. The tissue was then stimulated in order to induce contraction, and

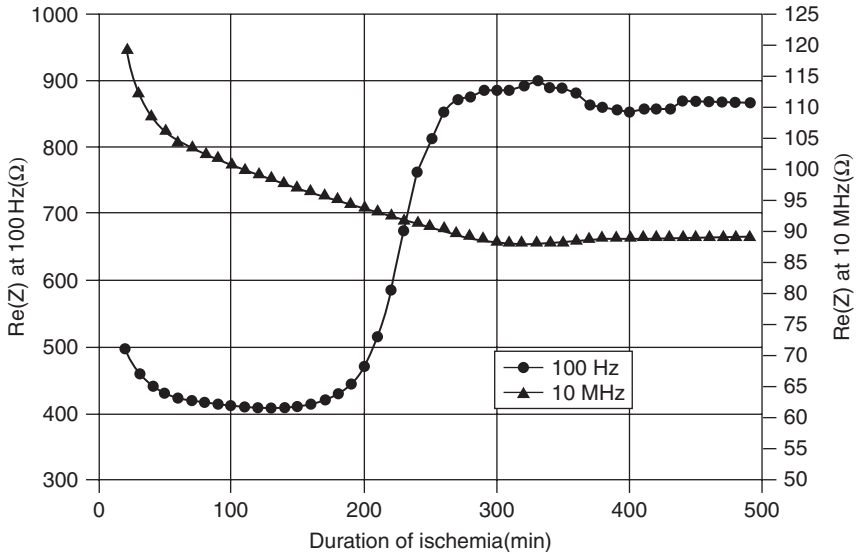


Figure 4.27 Resistances at 100 Hz and 10 MHz of a Custodiol® perfused canine heart muscle at 25°C. Source: From Gersing (1998) with permission.

the tissue was measured again, approximately 3 hours after dissection. They found a minor arc of a circle when the data were plotted in the complex impedance plane. Between the relaxed and contracted state, R_0 was found to increase by 75%, while R_∞ increased only 2%. R_0 and R_∞ denote as usual the resistances measured at very low and very high frequency, respectively. The significant increase in R_0 was interpreted as a reduced ionic conduction through the cell membranes.

Schäfer et al. (1998) measured on skeletal muscle of rabbits and dogs from 100 Hz to 10 MHz and found a β -dispersion whose characteristic frequency in the impedance plane, typically moved from 20 to 10 kHz and then back to 20 kHz during ischemia. They furthermore found the low frequency resistance to increase during the first 300 minutes of ischemia, subsequently decreasing up to 850 minutes and then increasing again. The initial increase in resistance is explained as being due to increasing edema because of osmotically induced water shifts, which reduce the extracellular volume. This effect continues also after 300 minutes but is surpassed by a reduced membrane resistance caused by the opening of ion channels, leading to a net reduction of the low frequency resistance. In their model, the membrane resistance reaches a constant level after about 850 minutes while the extracellular resistance continues to increase, resulting in a net increase of resistance after 850 minutes.

Martinsen et al. (2000) presented measurements of the electrical properties of haddock muscle from 1 Hz to 100 kHz as a function of time after the fish was sacrificed (Fig. 4.28). Clear α - and β -dispersions were found. Most of the α -dispersion disappeared after a few hours. The low frequency resistance of the β -dispersion increased during the first 5 hours as the fish went into rigor, and then decreased as cell destruction developed.

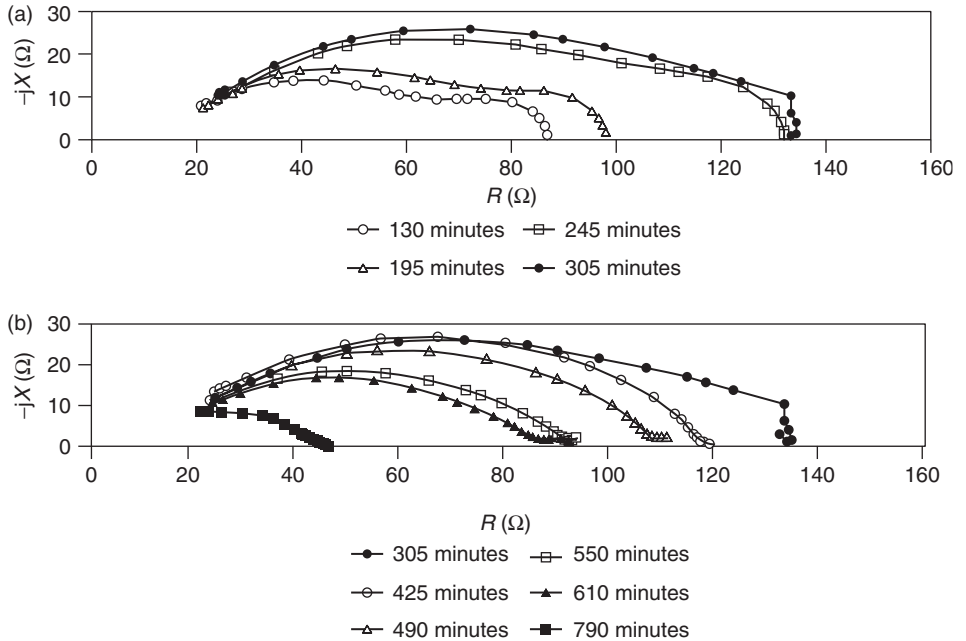


Figure 4.28 Post-mortem ZPLOT for fish muscle. (a) First 5 hours after death; (b) Next 7 hours. Source: Martinsen et al. (2000) by permission.

4.2.9 Plant Tissue

In general, plant tissue impedance data are not in accordance with Cole–Cole system models. Non-symmetrical models of the Davidson–Cole and Havriliak–Negami types have been used (Zhang et al., 1995). Figure 4.29 shows a Z-plot with data from Scots pine needles obtained with a two-electrode technique. Air spaces in the needles were believed to have an important influence both on the α of the Cole equation and the skewness of the arc. High temperature dependence has also been reported for plant tissue. Chilcott and Coster (1991) found that a 10°C increase resulted in more than a doubling of the conductance of *Chara Corallina* (an aquatic plant).

4.3 SPECIAL ELECTRICAL PROPERTIES

4.3.1 Tissue Anisotropy

Electrical properties such as permittivity or conductivity are usually direction dependent in tissue. This is due to morphological patterns in the tissue such as for instance structural lines of muscle fibers, tendons, nerve fibers, blood vessels. The patterns may be regular or have so small dimensions that the tissue may be defined as macroscopically homogeneous. The properties of tissue vary strongly according to the dimensional scale; there are heterogeneities at all levels from, for instance, the muscle

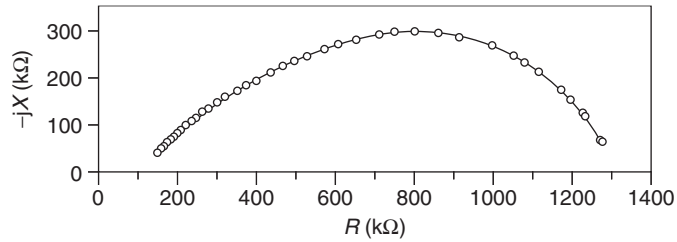


Figure 4.29 Impedance plot for Scots pine needles. *Source:* From Zhang (1995) by permission.

as an organ between other organs down to the atomic dimensions of its cell components. All parameter values are actually averaged values of a certain tissue volume.

Dielectric Microscopic Anisotropy

Microscopic means that the anisotropy is due to non-symmetrical structures very small relative to the dimension of the prescribed tissue volume. In the classical electrostatic model there are no free charge carriers, they are all bound to their atoms or molecules. With an applied electric field the electron cloud is displaced and a dipole moment is generated (cf. electronic polarization Section 3.1.2). The electric charges are very small (e.g. electrons 10^{-15} m) and their displacement caused by polarization is extremely small ($\approx 10^{-17}$ m). In the capacitor model of Fig. 3.1 the applied E-field is therefore not disturbed macroscopically by the induced dipoles, only at an atomic scale. However, in a solid dielectric the charge carriers may be bound differently in different directions (e.g. crystalline solids), thus resulting in net permittivity anisotropy. In a dielectric with anisotropy the three vectors of eq. (3.4) $\mathbf{D} = \epsilon_0 \mathbf{E} + \mathbf{P}$ are therefore not necessarily parallel.

Permittivity is usually higher in liquids than in solids (e.g. water/ice) because the charges are more loosely bound in a liquid. A liquid such as water is polar but isotropic when all molecules are free to find their statistical positions.

Bioimpedance Macroscopic Anisotropy

In bioimpedance theory there are free charge carriers and the current density is $\mathbf{J} = \sigma \mathbf{E}$ (eq. 2.2). The dimensions of interest are usually much larger than in the dielectric polarization cases, and the applied field is macroscopically disturbed by the anisotropy. Take, for example, a cubic model of a homogeneous biomaterial as shown in Fig. 4.30. In the middle is shown an insulating spheroid implant which results in a clearly lower net conductivity in the vertical electrode pair (hindering current flow in the constrictional zones of the electrodes, shadowing effect) and a slightly lower net conductivity in the horizontal pair. To the right a metal implant results in a corresponding anisotropy but with higher net conductivity in the vertical electrode pair. Thus both implants introduce macroscopical anisotropy.

Figure 4.31 shows how the macroscopical E-field is disturbed and goes parallel to the insulator surface (left), but perpendicular to the metal surface (middle).

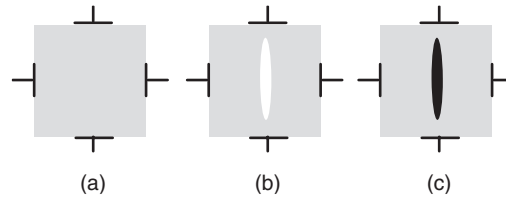


Figure 4.30 Anisotropy created by *macroscopic* inhomogeneity. (a) Uniform biomaterial; (b) with one spheroid of low conductivity; (c) or high conductivity.

To the right a model is shown with small tubes implanted in the biomaterial. If the tubes are of metal there is no E -field inside the tubes, and zero current density there. With insulating walls the E -field direction inside the tubes is tube axial and so is the direction of the current density. Outside the tubes the local E -field is also parallel with the tube axis. The direction of the local E -field is varying, but macroscopically eq. (2.2) is correct so that the local current density direction is equal to the local E -field direction. In order to take care of direction dependence the conductivity σ may be extended to be a tensor. A tensor is a generalization of a vector, and in general it has nine directional components. Only six of them are independent, and by choosing the best coordinate axes with respect to, for example, crystal axes they reduce to three.

Figure 4.32 illustrates macroscopic anisotropy in a simplified tissue model. In living tissue, conductivity may be 10 times larger in one direction than another. At low amplitude levels the tissue is still linear, and the principle of superposition and the reciprocity theorem are still valid. However, Ohm's law for volume conductors $\mathbf{J} = \sigma\mathbf{E}$ is not necessarily valid even if it is still linear, the current density direction will not coincide with the E -field direction if the anisotropic structures are sufficiently small.

Frequency Dependence

The models of Figs. 4.30–4.32 will exhibit Maxwell–Wagner dispersion. The anisotropy of Fig. 4.32 disappears at high frequencies because the capacitive membranes are short-circuited. When anisotropy is caused by, for example, air in the lungs, the anisotropy may persist at virtually all frequencies.

Conclusion

Anisotropy implies that the possible selective measurement of defined tissue volumes is disturbed. This leads to serious objections and problems in impedance tomography, finite element methods (FEM) and immittance plethysmography.

4.3.2 Continuity Across Interfaces

In tissue an implant may be conductive (metallic) or insulating (Dacron). Tissues of different electrical properties may result in the bending of current density field

lines. At a sharp interface the following rules applies:

1. Potential
The potential is continuous across any interface.
2. Tangential component of \mathbf{E}
The tangential component of \mathbf{E} is continuous across any interface.
3. Normal component of \mathbf{D}
If there are no free charges at the interface the normal component of \mathbf{D} is continuous. If there is a surface charge density q_s then $q_s = \Delta\mathbf{D}$ where $\Delta\mathbf{D}$ is the difference in the normal component of \mathbf{D} across the interface.

Bending of \mathbf{J} in Conductive Materials

A bending of current density field lines occurs at the interface between two homogeneous materials of different conductivity as shown in Fig. 4.34. Let θ be the angle between a line of \mathbf{J} and a line perpendicular to the interface (Fig. 4.34), then:

$$\sigma_2 \tan \theta_1 = \sigma_1 \tan \theta_2 \tag{4.2}$$

The field of, for example, region 1 is not an independent variable. Irrespectively of how the field was initially the introduction of, for example, a piece of metal in tissue changes the original field so that all field lines become oriented perpendicular

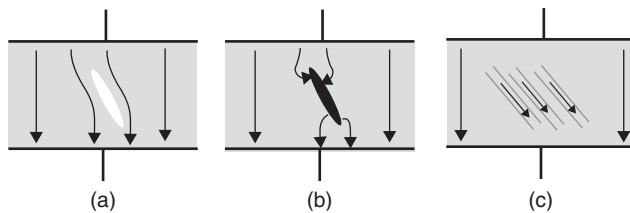


Figure 4.31 Capacitor model with homogeneous conductive biomaterial. (a) With insulating implant; (b) with metal implant; (c) with, inserted well conducting tubes, cf. Fig. 6.28.

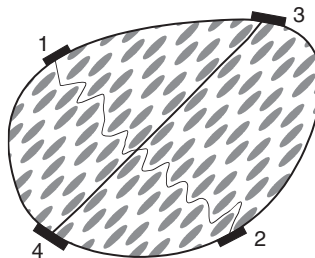


Figure 4.32 Anisotropy in a simplified tissue model. Each ellipse is a cell with cell membranes (cf. Fig. 4.7).

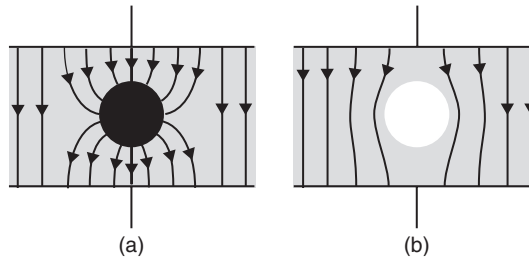


Figure 4.33 (a) Conductive (b) and insulating sphere implanted in a homogeneous material. The current density (electric field) lines are always perpendicular to the metal surface and parallel to the insulator surface.

to the metal surface. There are some similarities between optical refraction and such line bending; the refraction occurs when light crosses an interface between two optical materials of different refractive index. But the bending is in some respect quite different: in optics the introduction of a lens does not change the electromagnetic field in front of the lens.

Examples

If region 2 is a metal so that $\sigma_2 \gg \sigma_1$ then according to eq. (4.2) $\theta_1 \approx 0^\circ$, showing that the current enters the metal perpendicularly to the surface. Therefore the tangential **E**-field strength in the region 1 side of the interface is small and according to rule (2) above the tangential **E**-field strength must be equally small on the region 2 side. The small **E**-field strength in region 2 is due to the high conductivity there.

If region 2 is an insulator so that $\sigma_2 \ll \sigma_1$ then $\theta_1 \approx 90^\circ$, showing that the current avoids the insulator and flows parallel to the insulator surface. Therefore the tangential **E**-field strength in the region 1 side of the interface is high and according to rule (2) above the tangential **E**-field strength must be equally high on the region 2 side. The high **E**-field strength in region 2 is due to the low conductivity there.

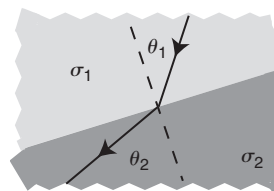


Figure 4.34 Bending of current density field lines.

4.3.3 Tissue DC Properties

Endogenic DC Potentials/currents

The Nernst equation 2.24 defines potential differences as a function of ionic activities, and the Maxwell–Gauss equation 8.1 defines potential changes as a function of charge densities. We may hypothesize that there are DC potential differences between some of the organs of the body, and that accordingly there may be large endogenic electric DC currents flowing between organs. Imagine, for example, the stomach with its large content of concentrated HCl (Nordenstrøm, 1983).

The most basic DC potential difference is the polarization potential of about -70 mV in the cell interior with reference to the extracellular fluids. Also the palmar and plantar skin sites are at a negative potential with respect to other skin sites, by a magnitude up to -30 to -40 mV DC. It is created by a difference in ionic activities across the skin barrier, with a possible addition of streaming potential waves from sweat propelled up the sweat ducts. The skin potential is shunted by skin sweat duct conductance. Increased sweat activity, as occurring during a *galvanic skin response* (GSR), therefore reduces the magnitude of the DC voltage (GSR-DC-wave). GSR is the DC part of the more general concept: *electrodermal response* (EDR) (cf. Chapter 9.15.4).

On the surface of the body DC recording is moreover used in electro-oculography (EOG), in order to determine the position of an eye behind a closed eyelid. Together with GSR this is one of the few electrophysiological methods making use of DC potentials.

For DC measurement it is important that the two electrodes are reference electrodes. If the electrodes are made of different metals or surfaces, a large exogenic DC voltage (possibly >1 V) may be generated. Often the best choice is two AgCl reference electrodes. They can be coupled to the skin or tissue via electrode gel as shown in Fig. 7.42, or via a salt bridge to reduce the DC offset from liquid junction potentials. An *invasive* electrode as neutral electrode is the most stable DC reference with a unipolar skin potential recording system.

Remember that with an exogenic DC source, it is not possible from a pure DC measurement to discern between changes in emv's and resistance/conductance (cf. Section 7.2.6). Measured DC voltage is not necessarily proportional to the DC resistance of the unknown if a DC constant current is passed through the unknown.

Closed Electric Circuits in the Body

As explained there are endoelectrogenic sources in the cell membranes. But it is quite likely that some macroscopic membranes around organs also are the sites of electricity sources. Nordenstrøm (1983) proposed that there are closed DC circuits in the body with the well-conducting blood vessels serving as cables (e.g. a vascular–interstitial closed circuit). These DC currents can cause electro-osmotic transport through capillaries.

Dental galvanism is the production of electricity by the metals in the teeth.

DC Conductivity

Living tissue is surrounded by extracellular liquids, and these liquids have a DC conductivity around 1 S/m (Section 4.2.1). However, all organs in the body are surrounded by epithelia, and epithelia with tight junctions between the cells have very low DC conductance. Measured DC conductivity is therefore very dependent on what sorts of epithelia and lipid bilayers the current has to cross.

Injury Potentials, Bone Fracture Growth

It is well known that the zone of tissue injury is the source of DC potentials. It has often been postulated that bone growth is enhanced if a DC current is supplied to each side of the fracture. Nordenstrøm used DC in an electrochemical treatment of tumors.

4.3.4 Non-linear Tissue Parameters, Breakdown

At sufficiently low volume power density, every biomaterial is linear. At sufficiently high volume power density, every biomaterial is non-linear. Many applications make use of the non-linear region, where the principle of superposition no longer is valid. The non-linearity may be a property of the biomaterial, or of the electrode/electrolytic systems used (cf. Section 2.5.4) about the non-linearity of electrolytics, and the Section 7.1.5 on measuring principles for non-linear systems.

At the *atomic and molecular* level, some of the charge displacements will reach saturation at high E-field strength levels (cf. Section 2.5.4). The alignment of dipoles in a polar dielectric will reach a maximum when the field energy is of the same order of magnitude as the Boltzmann factor kT .

At the *cellular* level the cell membranes of polarized cells are of the order of 10 kV/mm, and additional field strengths may easily bring the membrane into a non-linear region even without cell excitation. Cell excitation, the opening of membrane channels and the creation of an action potential are the result of non-linear processes. Electroporation and electrofusion of cells in vitro (Section 9.14.1) are also processes in the non-linear region.

In human *skin* Yamamoto and Yamamoto (1981) found the upper limit of linearity to be about $10 \mu\text{A}/\text{cm}^2$ at 10 Hz and $100 \mu\text{A}/\text{cm}^2$ at 100 Hz. Ionic flow through human skin in vivo is probably constrictional through special zones of high conductance (Grimnes, 1984). Thus non-linear phenomena may occur at such low average current densities.

They ascribe this phenomenon to the ionic conduction in the keratins of the stratum corneum. Electro-osmosis in the sweat ducts causes strong non-linear effects with only a few volts DC (Grimnes, 1983b) (Fig. 4.35). A dielectric breakdown will occur at very high electrical fields in the stratum corneum. Grimnes (1983c) found that dry skin on the dorsal side of the hand did withstand 580 V DC for more than 3 seconds, but that breakdown was immediate at 935 V. These are astonishingly high values remembering that the skin often is of the order of $20 \mu\text{m}$ thickness (Figs 4.35 and 36).

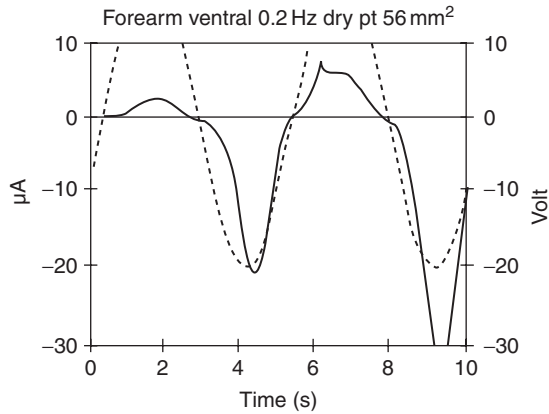


Figure 4.35 Voltage-currents curves showing electro-osmosis and strong non-linearity in human skin in vivo. *Source:* From Grimnes (1983b) by permission.

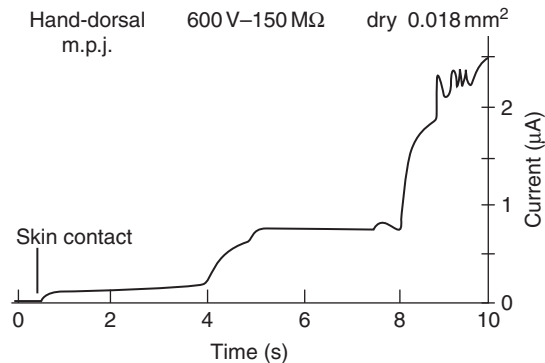


Figure 4.36 Thin stratum corneum dielectric strength, human skin in vivo. *Source:* From Grimnes (1983c) by permission.

Figure 4.36 shows that dry human stratum corneum in vivo could withstand a positive polarity DC voltage of 600 V for 4 seconds. With negative polarity the breakdown is much more pronounced caused by electro-osmotic transport of electrolyte solution from deeper living parts of the skin.

There are some important *clinical* applications involving non-linearity:

Defibrillator current of >50 A over 60 cm^2 electrode area implies a current density around 1 A/cm^2 (Section 9.12). This is clearly in the non-linear region both for skin and living tissue, and actually the skin is reddened particularly under the electrode edge after a shock has been given. Geddes et al. (1976) reported that the resistance found from measured peak voltage with a 20 A peak current pulse with two 60 cm^2 electrodes corresponded with the small signal impedance measured at 30 kHz. During successive defibrillator shocks, a decrease in transthoracic impedance has been reported (Geddes et al., 1975b). After ten 400 J shocks, the impedance fell to

80% of the initial value. These effects must probably be contributed to cell membrane and myocardium damage. Because of the current constriction near the electrodes the highest current densities and largest effects are presumably there.

In *electrosurgery* the current density near the electrode is much higher than during defibrillation, and current duration is much longer. In cutting mode the cell interior is brought up to 100°C in just a few milliseconds, and the cells explode. Tissue destruction is the goal (Section 9.13).

Iontophoresis for sweat sampling using DC current through the skin is presumably carried out in the non-linear region (Section 9.15).

An *electrostatic discharge* with an electric arc as contact medium may imply very high current densities on the affected area (cf. Section 9.17) on threshold of perception.

Incremental Impedance for Non-linear, Time-Variant Objects

The impedance is usually measured by means of small voltage and current to ensure a linear behavior of the material under test. Many of the biological objects show active electrical behavior interfering with impedance measurements. The simple ratio between voltage and current becomes meaningless. This for instance happens when the impedance of single membranes are assessed. Especially, if these membranes are excitable or contain any voltage controlled ionic channels, they show non-linear and time variant passive electrical properties. The adequate parameter describing this is the small signal response or the incremental impedance. Since it adds a degree of freedom (voltage at operating point or offset), its result is a field of spectra (Fig. 4.37). For instance, at cell membranes, the most important spectrum is at the resting voltage.

For resistance or impedance measurements at materials driven into a non-linear voltage region it is often more informative to calculate the dynamic impedance dU/dI (also incremental impedance or small signal behavior). Since the voltage is a parameter, it should be known for any dynamic impedance measured.

Non-linearity of Membranes at Low Electric Field

Lipid Membrane

The biological membrane bases on a lipid bilayer. The polar head groups of the lipids are hydrophilic, thus they are arranged to contact the water. Since the aliphatic tails are hydrophobic they face each other in the inner of the membrane, thereby minimizing the energy of the entire system (Alberts et al., 2007). Because of the hydrophobic interior of the membrane, hydrated charged ions cannot cross this structure, which yields insulating behavior. However, since the membranes are a 2D liquid, meaning that a lipid molecule is highly mobile within the xy -layer but almost fixed along the z -axis, there is still a probability to find defects which can permit the passage of ions. Since this probability is very small, lipid membranes show a resistivity up to $G\Omega\text{cm}^2$.

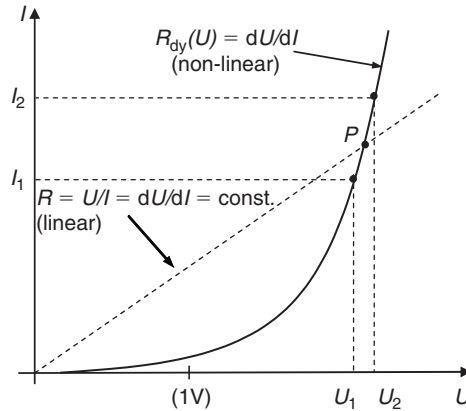


Figure 4.37 Linear and non-linear behavior of a material under test.

An additional driving force like an electric field can enhance the probability for the ion passage. This results in progressive increasing of the current with increased transmembrane voltage even for a pure lipid membrane.

Most of the biological membranes carry charges at the head groups, responsible for the appearance of an electric double layer in contact with electrolytes. This incorporates two parts, the directly adsorbed layer (Helmholtz-layer) and a more diffuse layer (Guy–Chapman-layer). The entire arrangement is called Stern layer (Fig. 4.38).

The outer electric field can modulate the behavior of the Stern layer, which has implications for impedance measurements with respect to the voltage applied but also to the frequency. The ions within the double layer are less mobile, therefore increasing the resistance of the entire system. The mobility increases with higher field strength, thereby increasing the probability of ions reaching the cell membrane and in rare cases crossing it. This effect is more pronounced at higher frequency where a net transport across the membrane is not necessary. The increased mobility of ions within the double layer will considerably decrease its resistance.

The capacity of the membrane is governed by the high electric resistance of the aliphatic tails within the membrane. The electric thickness of the membrane depends on the region without mobile charges as well. If this thickness decreases due to the outer electric field or even more pronounced, if ions are driven into the region of the head groups, this thickness decreases, resulting in increased capacitance of the membrane. Although this effect is not important for DC measurements, it will influence the AC measurements.

Cell Membrane

The membranes surrounding each cell (plasma membrane) and the intracellular structures (endoplasmatic reticulum, Golgi-apparatus, nuclear membrane, mitochondria membranes, other organelle membrane) are not only composed of lipids

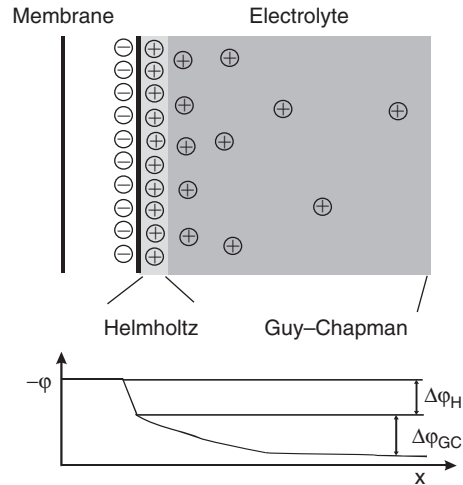


Figure 4.38 Electric double layer at a cell membrane. The potential across the Helmholtz-layer drops linearly while the further drop in the Guy–Chapman-layer is exponential.

but incorporate proteins and steroids as well. Besides this, adsorbed proteins will greatly influence the functionality of the membrane. Integral proteins can span the entire membrane. A considerable fraction of these proteins facilitates transmembrane transport of species usually not permeating the membrane. The transport mechanism may be very different. One group involves carriers which need several steps of structural changes for the transport. Some carriers are powered externally (i.e. by dephosphorylation of ATP) and can facilitate transport against the electrochemical gradient (i.e. Sodium–potassium-ATPase, Sodium–potassium-pump).

Other proteins build up channel structures providing access to a number of ions. Most of these channels are ion selective (Na^+ , K^+ , Cl^- , Ca^{2+}) and can be controlled by external forces like ligand binding (acetylcholine receptor), mechanical (sensing cell in the ear), or electrically (Na-channels in excitable cell membranes).

Because of a great number of voltage sensitive channels, they are mostly responsible for non-linear properties of cell membranes at low voltage (<100 mV).

Since many cells are arranged in series and parallel by measurements in a tissue it is vague to get information about single cell membranes in an electrode arrangement cm-dimension.

A suitable method to study non-linear behavior of cell membranes is the whole cell path technique (Fig. 4.39): (a) the cell in suspension is clamped by a micropipette (opening $\approx 1 \mu\text{m}$). To avoid electrode polarization both electrodes are silver–silver chloride-electrodes consisting of chloridized Ag-wire. The counter electrode is immersed in 3M KCl which is arranged as gel in another pipette with bigger opening. Since the electrolyte of the suspension medium has a constant Cl^- concentration, the potential drop at the electrode is constant as well and can be compensated, either by adjusting the equipment or mathematically. (b) CHO cell (Chinese hamster ovary cell) attached to the micropipette. The cell diameter is about $16 \mu\text{m}$.

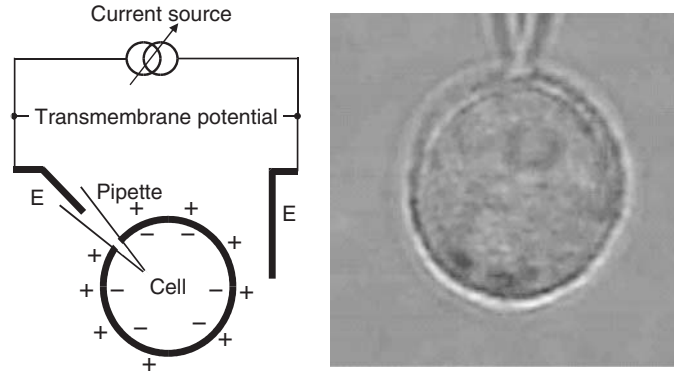


Figure 4.39 Arrangement for whole cell clamp. *Source:* Frantescu et al., 2004.

To test the electrical behavior of the cell, one can apply a voltage stimulus (i.e. voltage ramp or step) and monitor the current (voltage clamp). Other than in technical systems, the application of a current ramp (or step) and monitoring the voltage (current clamp) yields different results and therefore additional information (Pliquett et al., 2005).

The slope of the ramp applied is critical since biological membranes show PI-behavior. This means, the response to a stimulus is only partly proportional to the stimulus. Another, often greater part, is an integrating response (dose effect).

The result shown in Fig. 4.40 is within the limits where all changes are fully reversible and are only interpreted as happening without structural changes of the membrane itself (i.e. it is most likely (but not only) a result of manipulating the open/closed state of channels).

4.3.5 Piezo- and Triboelectric Effects

In Chapter 3, we have learnt that an applied electric field induces dipole moments in a dielectric. Such a displacement of charges generally generates a dimensional change in the material. This is called *electrostriction*.

Vice versa mechanical stress changes the dimensions of the material. Usually this does not result in an electrical polarization of the material, because most materials have a so-called center of symmetry canceling opposite charge displacements. However, crystals lack such a center of symmetry, and they generate an internal polarization \mathbf{P} when mechanically deformed. These materials are called *piezoelectric*, with a direct conversion from mechanical to electrical energy.

In human hair and other keratinized materials, piezoelectric properties have been found. This is also the case for bone and tendon. Bone remodeling has been attributed to piezoelectricity. The theory is that the mechanical stress on a bone generates bioelectricity that in turn influences bone growth. As most biomaterials

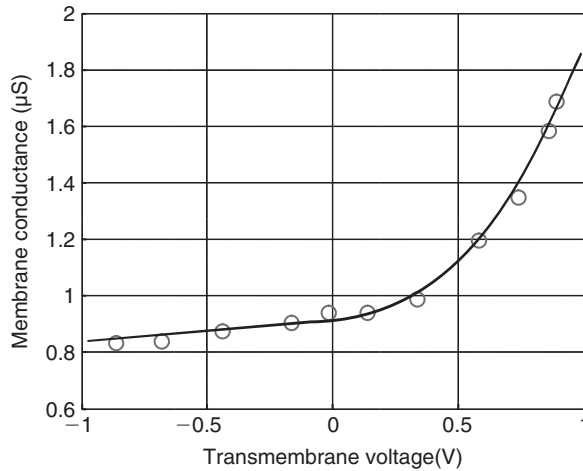


Figure 4.40 Membrane conductance depending on the voltage applied to a CHO cell membrane. The stimuli were 1 ms long rectangular current pulse. The figure shows an average (current and voltage) over a greater number of experiments with always new cells. Error-bars would be on the order of $0.4 \mu\text{S}$ and are omitted for showing a nicer picture. It should be noted that CHO-cells do not have an excitable membrane.

exhibit piezoelectric properties, it is not strange that there is an abundant number of theories postulating piezoelectric effects in tissue (e.g. that the transducer mechanism in the inner ear) in the hair follicles, of the touch and vibrational sensitivity, is piezoelectric. Results in the literature are often with dry sample, and the question remains as to the importance of piezoelectricity in living, highly conductive tissue.

Triboelectricity (frictional charging) is the generation of charges when two materials suddenly are separated. All materials, solids and liquids, isolators and metals, display this phenomenon. A *triboelectric series* is often set up, but as the position is very dependent on surface properties, the series often differ. Humidity and cleanliness affect the series drastically. Here is one such series:

$++ \leftarrow$ rabbit's fur, bakelite, glass, *wool*, silk, cotton, wood, metals, polystyrene, teflon $\rightarrow --$

Presumably *human hair*, and perhaps dry *stratum corneum*, has a position not too far from wool.

During wintertime, triboelectricity may generate several kilovolt on an insulated person during walking, or by blanket movements when the patient's bed is made. If the patient is monitored, noise will appear on for instance the ECG recordings (Gordon, 1975). But the seriousness of the electrostatic problem is linked not only with the generation mechanism, but also with the *discharge* mechanism. The conductivity, both volume and surface, of the materials is of uttermost importance, because it determines the discharge time constant. If a person is charged by walking on a floor or taking off some clothing, the person's capacitance to earth (e.g.

150 pF) together with the resistance to earth (e.g. $8\text{ G}\Omega$, $\tau = 1.2$ seconds), determines the time constant. If the time constant is several seconds, problems will occur because the charge will stay long enough to cause an electric arc discharge at for instance the touch of a metal object. If it is in the millisecond region the person is rapidly discharged, and no arc discharge will occur at the touch of a metal object. The conductance of many low conductivity materials is very humidity dependent, so the problems are much larger at low ambient RH. This occurs indoors in cold countries during the winter. Under these conditions, cotton is better (have higher conductivity), than most synthetic materials.

Triboelectricity is of great practical interest because it is the basis of all the problems associated with *electrostatic* discharges. Such discharges represent a risk, because they may excite nerves or ignite flammable vapors. The discharge may be perceptible (Sections 9.17). Some of the electricity generation is due to the rubbing and separation of skin with textile clothing. The triboelectric properties of skin and hair are therefore of interest (combing the hair). When the RH in a room has been 10% for some time, a person can easily be charged to 30 kV with respect to earth just by walking or rising from a chair. During walking, the electricity generation is determined by the materials of the shoe soles and the floor.

PROBLEMS

1. From data found in Section 4.1, what is roughly the permittivity of water at 37°C ?
2. Are the electrical properties of amino acids dependent on the water content?
3. With a membrane capacitance of $1\ \mu\text{F}/\text{cm}^2$ and a membrane thickness of 7 nm, what is the permittivity of the membrane material?
4. How large is the conductivity anisotropy at low frequencies in muscle tissue (Fig. 4.9)?
5. Sketch roughly the corresponding ϵ'' curve on Fig. 4.13.
6. Figure 4.26 indicates that the resistance of a finger is about $500\ \Omega$. Calculate the mean resistivity of the finger tissue modeled as a cylinder. Use the dimensions of your own longest finger.

This page intentionally left blank

5 EXCITABLE TISSUE AND BIOELECTRIC SIGNALS

Chapter Contents

5.1 Cell Polarization

5.2 Action Potential

- 5.2.1 Ion Channels
- 5.2.2 Channel Gating
- 5.2.3 Cell Potential Model
- 5.2.4 Cell Oscillator

5.3 The Neuron

- 5.3.1 Motor Neuron
- 5.3.2 Brain and Neurons

5.4 Axon Transmission

- 5.4.1 Excitation from the Soma
- 5.4.2 Exogenic Excitation
- 5.4.3 Moving Current Dipole
- 5.4.4 Myelinated Axons
- 5.4.5 The Nerve
- 5.4.6 Synapses
- 5.4.7 Excitation
- 5.4.8 External Current Excitation

5.5 Receptors

- 5.5.1 Patch Clamp Technique

Problems

In living tissue important communication control is implemented by hormones and nerves. Hormones are slow broadcasting information carriers; nerves are quick pre-wired point-to-point information carriers. Some cells are not excitable, for instance the cells of adipose and connective tissue or blood. They are passive, not under nerve control, and only weakly polarized. However, nerve, muscle and gland

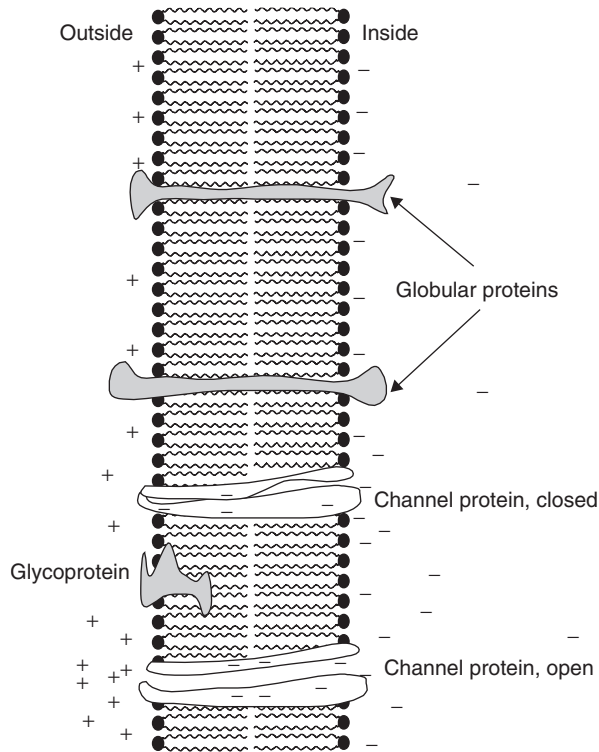


Figure 5.1 BLM with embedded proteins. A channel macroprotein may form a water channel, an ion channel or an ATP-driven ion pump.

cells are polarized and excitable; within a 1/1000 second such cells may react on trigger signals such as electrical, mechanical or chemical energy. The excitation of a cell is accompanied by an *action potential*. The action potential is the basic bioelectric event and signal source in the body.

In Section 4.1.4 the passive cell membrane was described. The membrane is a bilayer lipid membrane (BLM) shown in Figs. 4.6 and 5.1. The membrane of a living cell is a most complex and dynamic system. The cell membrane itself is a major barrier to ion flux, but embedded in the membrane are *channels*, *transporters* and *ion pumps*. Electrically, they represent shunt pathways in parallel with the BLM (Figs 5.1 and 5.3). The *water channels* are a special class of channels selectively allowing water flux (but without electric charge: no proton, no ion flux) in response to osmotic gradients and therefore regulating cell volume swelling or shrinking.

5.1 CELL POLARIZATION

Cell polarization is generated by the *ion pumps* (Fig. 5.3) using the energy of ATP hydrolysis to drive ions against the electrochemical gradient. This energy-consuming mechanism *polarize* the cell so that the interior of excitable cells has a potential of

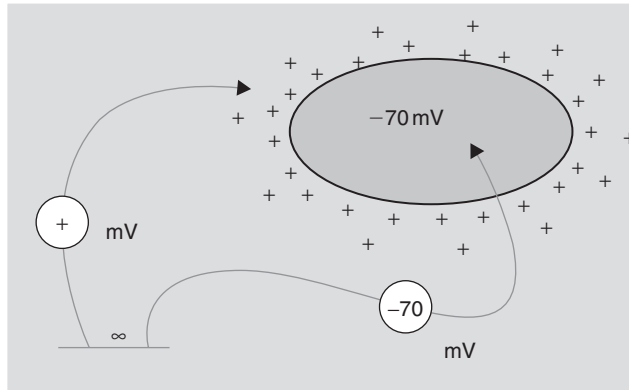


Figure 5.2 The polarized excitable cell.

about -70 mV with respect to the extracellular electrolytes (Fig. 5.2). Such a pump is a molecular device, embedded in the cell membrane, capable of generating a net electric current across the membrane and thus *electrogenic*.

The *sodium pump* ($\text{Na}^+ - \text{K}^+ - \text{ATPase}$) is the most important ion pump and in nerve cells about 70% of its ATP is consumed to fuel sodium pumps. Instead of a direct channel across the membrane, the sodium pump is equipped with a special “box” with a special “door” (Fig. 5.3). Initially the door is open toward the inside so that three intracellular Na^+ ions with bound ATP enter the box. The door is closed, the box is turned around and the enclosed ions are released to the outside. There the pump binds two extracellular K^+ ions with ATP. The pump reorients and releases K^+ into the cell interior. A full cycle has then been completed so that the channel is never open in its total length.

The sodium pump consists of two subunits: The alpha subunit binds ATP and both sodium and potassium ions. The smaller beta subunit determines the position and activation of the alpha subunit. The sodium pump translocates a greater electric charge in one direction than in the other. Per cycle, it exports three sodium ions (Na^+) and imports two potassium ions (K^+) resulting in a net electric current flow out of the cell of one positive ion. Millions of such pumps in one cell membrane polarize the cell to steady state so that the cell is fully polarized and ready to be triggered. The whole polarization process such as the number of pumps, their position and activity is under control from, for example, aldosterone, catecholamines, insulin and thyroid hormones.

The Nernst equation (2.24) was presented as an equation valid for redox electrode processes in electrochemistry. The Nernst concept is also used for the calculation of the potential difference across a membrane which separates two electrolyte compartments with different ion concentrations. Exchanging the natural logarithm with the common logarithm and putting $n = 1$ and temperature 37°C , eq. (2.24) becomes:

$$V = -61 \log \frac{c_e}{c_i} \quad (\text{mV}) \quad (5.1)$$

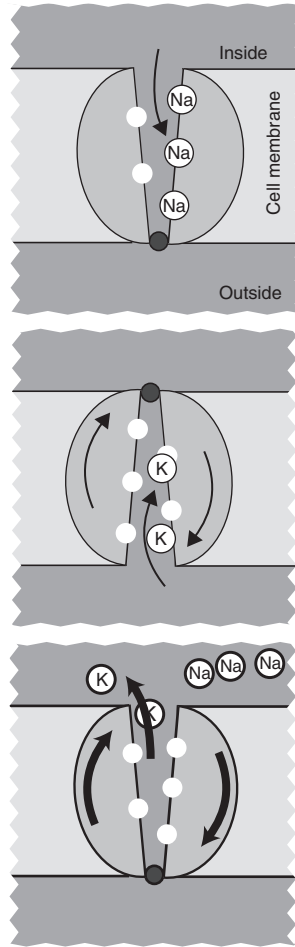


Figure 5.3 Na⁺-K⁺-ATPase pump embedded in a cell membrane.

where c_i and c_e are the intracellular and extracellular concentrations of one ion species. With an external concentration of, for example, K⁺ 10 times larger than the internal concentration the intracellular potential is -61 mV.

With more than one ion species present the extension of Goldman (1943) is used, for example, with Na⁺, K⁺ and Cl⁻ ions:

$$V = -61 \log \frac{c_{iNa^+} P_{Na^+} + c_{iK^+} P_{K^+} + c_{iCl^-} P_{Cl^-}}{c_{eNa^+} P_{Na^+} + c_{eK^+} P_{K^+} + c_{eCl^-} P_{Cl^-}} \quad (\text{mV}) \quad (5.2)$$

where P is the permeability (m/s).

The *Donnan* effect is a special case for the use of the Nernst concept on membranes. Consider a membrane permeable to all inorganic ions but not to charged macromolecules (proteins) or charged colloidal particles. The presence of such

macromolecules on only one side of the membrane will change the distribution of the small ions free to cross the membrane (cf. Section 2.5.1).

The polarized potential of excitable human cells is found in the range -40 mV to -90 mV.

Some of the organelles inside the cell such as mitochondria have their own membranes presumably built in the same way as the cell membrane with BLM and membrane channels.

5.2 ACTION POTENTIAL

A polarized and excitable cell may suddenly become *depolarized*. *Gates* in ion selective channels suddenly open, and ions flow passively with the electrochemical gradient through the channel until the intracellular charge is more or less neutralized and the gate is again closed. *Cole* and *Curtis* studied the non-linear effects of excitable membranes in the late 1930s. In 1939 *Hodgkin* and *Huxley* succeeded in measuring the voltage inside a nerve cell for the first time. They showed that during a nerve impulse the intracellular voltage reversed, for example, from -70 mV to $+30$ mV. Therefore this could not be due to a simple short circuiting effect caused by increased membrane conductance; it must be due to an ion flux phenomenon. In a series of five remarkable articles in 1952, they and Bernhard Katz gave the current classical description of the voltage sensitive opening and closing of separate channels for Na^+ and K^+ in the cell membrane. This achievement was awarded with the Nobel Prize in 1963.

5.2.1 Ion Channels

An ion channel is a protein embedded in the cell membrane. The protein consists of an ion filter and a gate. Channels are usually described in terms of their selectivity and gating mechanism. Due to the selective permeability to ions the cell membrane may be described as an *electrochemical* membrane. An open channel is *highly selective*, the permeability for K^+ may, for instance, be 1000–10 000 times higher than for Na^+ . The *anion* channel macroprotein for Cl^- is very different from the *cation* channel protein of, for example, Na^+ or K^+ (Jentsch, 2002). The selectivity is not due to ion size but due to the charge spatial distribution in the filter part of the protein. The channel capacity is high, a K^+ channel can let through 200 million ions per second. But if the channel is open only 1 ms then 0.2 million ions are let through in each trigger event. As a monovalent ion corresponds to an electric charge of 0.16 aC (1 attocoulomb = 10^{-18} C), this corresponds to a charge of 32 fC. If one cell membrane has 10 million channels a charge of $0.32 \mu\text{C}$ flows out of the cell into the extracellular gel.

5.2.2 Channel Gating

Normally channels have closed gates. A gate can be opened by a *voltage* change or by the arrival of a *ligand*. If it is voltage gated it is the voltage across the cell membrane

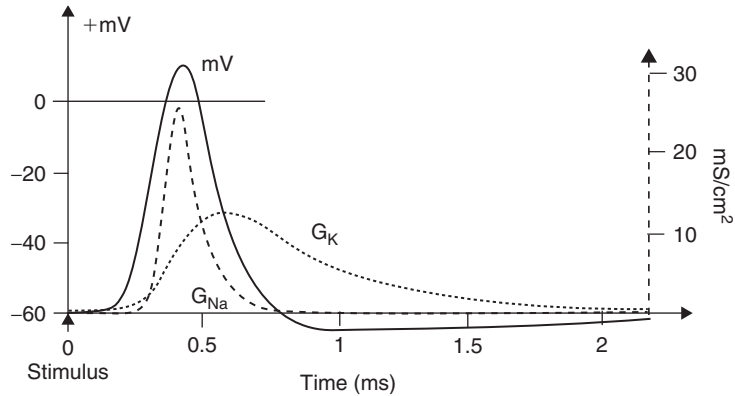


Figure 5.4 Intracellular potential and cell membrane surface conductance density during cell excitation, mammalian neuron.

that determines whether a channel is opened or remain closed. The motor nerve axon has voltage gated sodium and potassium channels.

Figure 5.4 shows the potential and conductance waveforms after stimulus application. There is a delay before the potential starts to increase in the positive direction. Then the sodium channel gate opens and Na^+ flows into the cell and the cell is depolarized. The potential crosses the zero line and soon reaches its maximum positive potential. The opening of the K^+ gate is slower and the opening time is longer than for Na^+ . After gate closing the cell repolarizes and the potential goes negative and even more negative than the initial level. During depolarization the cell cannot be re-triggered (the *refractory period*) before the cell is repolarized. Figure 5.4 shows the most basic and fastest signal source in the human body, the action potential and the sudden change in channel conductance. The frequency content of the signal is up to a few kHz, but this can only be recorded very near the cell. At larger distance the geometry may act as a low-pass filter (cf. Section 6.5.1).

Each gated channel may be modeled by an emv in series with an electrical resistance (Fig. 5.5). The BLM membrane capacitance of about $1 \mu\text{F}/\text{cm}^2$ is in parallel and is an important time constant parameter of the system. The changes in intracellular potential mean that the membrane capacitance is charged and discharged.

If suddenly the channels (Fig. 5.4) open so that the intracellular potential changes abruptly, the ions must also supply a transient discharge current of the membrane capacitance. At the extracellular side the current is not with respect to a far away reference electrode, but concentrated to an interstitial fluid zone near the cell. The current flow can be modeled with local current dipoles, and is clearly measurable with unipolar or bipolar pick-up electrodes in the interstitial liquid. When the cell is depolarizing, cations and anions flow in all directions through the open channels, but it must be a net flow of anions out of the cell. If the internal mechanical pressure is not to fall or rise, neutral water molecules must also have their gated transport channels.

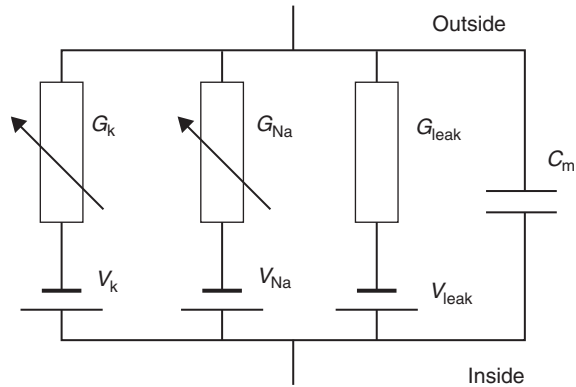


Figure 5.5 A simple electrical model of a cell membrane. *Source:* From Hodgkin and Huxley (1952) by permission.

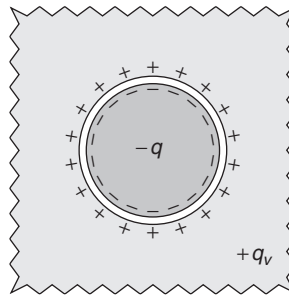


Figure 5.6 Static cell model with perfect insulating tight membrane and conductive electrolytes. Initially some intracellular cations have been transported out of the cell into the extracellular infinite volume.

In the actual situation there are many channels, they may be represented by a surface layer of distributed dipoles. This layer can at a distance be simplified to one net dipole representing one or more cells.

5.2.3 Cell Potential Model

Consider a cell model like in Fig. 5.6 with the cell interior completely insulated from the outside by a perfect membrane without channels. The intracellular and extracellular electrolytes are well conductive. The interior has been polarized by an initial transport of some cations out from the interior and into the extracellular volume.

The interior has a well-defined electrical capacitance with respect to the outside. Double layers are formed in the electrolyte/membrane interphase both internally and externally. The measured intracellular potential includes the potential of these charged double layers (cf. Section 2.4.3). A double layer has a thickness of the order of

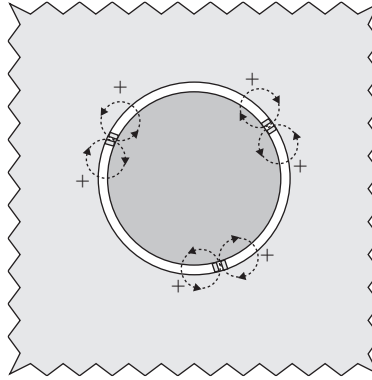


Figure 5.7 Polarized cell just after the opening of three ionic channels resulting in a sudden inflow of cations.

0.1–10 nm, and the cell membrane about 7 nm. The total measured BLM capacitance, double layers included, is about $1 \mu\text{F}/\text{cm}^2$. The charge q necessary to obtain a voltage U across a capacitor is $q = CU$ (C). With a cell radius of $2 \mu\text{m}$ the membrane area is $A = 4\pi r^2 = 50 \times 10^{-12}$ (m^2). With $v = 60 \text{ mV}$ the charge is $q = 0.5 \text{ pC}$ and as a monovalent ion has a charge of 0.16 aC , this means that about 3 million monovalent ions must have been removed from the cell interior to obtain 60 mV . This calculation is not based on the Nernst concept because the permeability of the membrane is zero. The calculation is based on the charge of the membrane capacitance.

The basic capacitor model (Fig. 3.1) is a dielectric between two metal plates with free electrons. In the cell model the metal plates are replaced by electrolytes with free ions. In the static case with no leakage across the membrane there is no current flow inside or outside the cell. At the inside membrane a surface charge density q_{sf} of free ions neutralizes the electric field in the membrane plus the double layer charges so that the cell interior has $E = 0$ and no current flow. There is electroneutrality in the bulk, but surface charges at the interphase. The intracellular bulk volume has a potential, but zero electric field strength. The membrane has a bound surface charge density q_{sb} which will reduce the membrane E-field to $(q_{\text{sf}} - q_{\text{sb}})/\epsilon_0$. Thus the E-field in the membrane is *less* than the potential difference divided by the membrane thickness.

Can the intracellular static voltage be measured from the outside without a unipolar electrode penetrating the membrane? The intracellular net charge creates a charged layer at the outside surface of the cell. In this way the cell will migrate into an applied extracellular electric field, and this migration can be measured (electrophoresis). The charges are very near the cell membrane surface, and in the extracellular bulk electrolyte no potential related to the intracellular charge can be measured.

Now let us introduce passive ion channels in the membrane of a polarized cell (Fig. 5.7). The channels are normally closed, but now suddenly opened. Due to the potential difference, cations will immediately start to migrate into the negative cell interior. A current density field is suddenly created both intra- and extracellularly.

The extracellular current density vector field \mathbf{J} and the potential field Φ are related: $\nabla\Phi = -\mathbf{J}/\sigma$. The current is generated by the ionic flow, and it terminates on the membrane capacitor in a discharge/charge process.

An *action potential* can accordingly be measured by nearby electrodes with unipolar or bipolar technique.

The cell potential models of Figs 5.6 and 5.7 are very simplified in order to obtain a basic understanding of the current density and potential fields. They represent a macro view of a system with very small dimensions; in particular the thickness of a human cell membrane is only about 7 nm and the channel protein charge positions accurate to within an ångström (0.1 nm). In addition the real cell membrane is covered by a very dynamic system of receptor molecules and other components. Also electrolytes in contact with proteins have thin charged double layers formed at the interphase.

5.2.4 Cell Oscillator

Figure 5.5 shows a leakage conductance in parallel with the other ion channels. If the leakage current is larger than the net pumping current, the cell is slowly depolarized and if it is voltage gated it may reach the trigger level. The cell has become a free running oscillator with a frequency determined by the trigger level, the membrane capacitance and the balance between the polarizing and leakage currents.

5.3 THE NEURON

A neuron consists of: (1) soma (cell body), (2) dendrites, (3) transmission part (fiber) and (4) output terminals (synapses). The cell nucleus and organelles are in the soma, and organelles are also spread out along the axon. Dendrites represent the neuron input and a single long axon, the output. Neurons have very different forms and sizes with respect to axon length (up to 1 m), number of dendrites, size and position of the soma and number of presynaptic terminals (up to 100 000).

Figure 5.8 shows some typical neuron morphologies. The motor neuron is found in the spinal cord. It is an efferent type bringing information from the central nervous system (CNS) to, for example, a muscle or gland. The receptor type is an afferent neuron with a special direct axon coupling between the receptor and the CNS. The pyramid morphology is found in the cortex of the brain.

5.3.1 Motor Neuron

Figure 5.9 shows an example of a motor neuron. *Presynaptic terminals* from other neurons are connected to the dendrites and also directly to the soma. Presynaptic terminals on the dendrites are *excitatory*; about 5% of all dendrites are directly on the soma and most of them are *inhibitory*. One neuron has one soma and one axon. The change-over zone between the axon and the soma is the *hillock*. The inhibitory

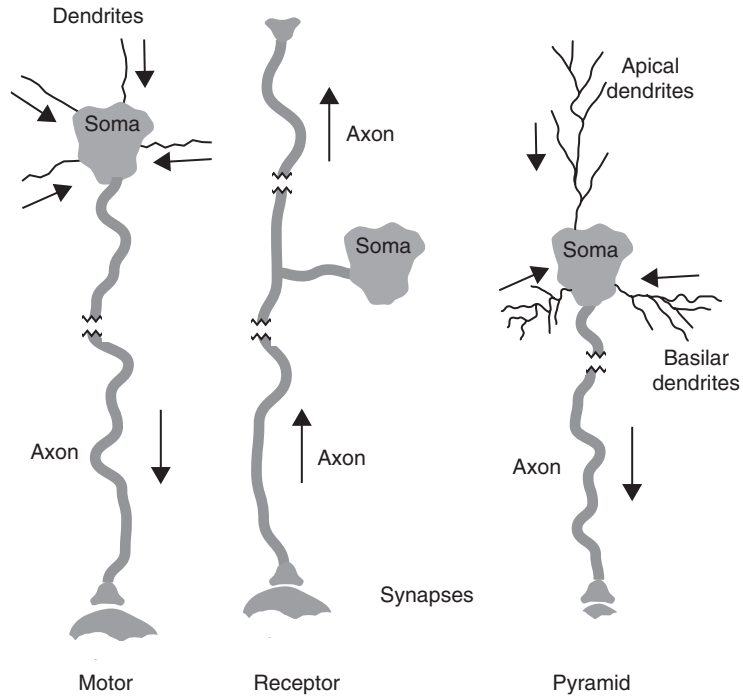


Figure 5.8 Typical neuron morphologies.

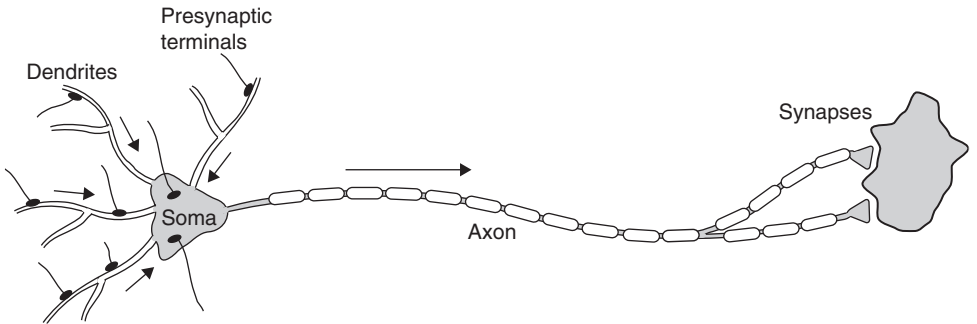


Figure 5.9 Motor neuron with myelinated axon.

presynaptic terminals on the soma are almost a gate for the excitatory signals from the dendrites on their way to the hillock. The soma integrates all inputs, and the response is all or nothing. If the neuron is triggered, the action potential starts in the hillock. The excitation then spreads down the axon to the end where the axon terminates in one or more synapses coupled, for instance, to a muscle, gland or another neuron.

The neuron may respond not only to electrical input, also mechanical pressure and chemical substances may act as input signals. The difference between a neuron and a receptor (cf. Section 5.5) may thus be small.

5.3.2 Brain and Neurons

The three most important parts of the brain are the cerebrum, brainstem and cerebellum. They are covered by several membranes: between the skull and the brain there are three membranes (meninges): dura mater (two layers), arachnoid (resembling a spider's web) and pia mater. The pia mater is in direct contact with the cortex, and between the pia mater and the arachnoid there is space for the highly conductive cerebrospinal fluid (CSF).

The *cortex* is the outer part of the cerebrum. The phylogenetic newest part is the human cortex, the *neocortex*. It is 2–5 mm thick, covers all convolutions of the cerebrum and probably comprises about 10 billion neurons with about 1000 billion connections. The cells of the cortex are of three types: *granular*, *fusiform* and *pyramidal*. Cortical neurons are strongly interconnected and are the principle source for the EEG signals registered on the head. The superficial layer is often referred to as *gray* matter. The cells there are of two types: pyramidal and non-pyramidal. The next layer is *white* matter and consists of axons and connective tissue. Cortex is organized vertically (*z*-direction) in six layers (lateral *x*–*y* direction) and in the sensory cortex also in vertical columns. A neocortical column may have a diameter of about 0.5 mm. The neurons in a column communicate in short range *x*–*y* directions and longer range *z*-directions. Axons may be oriented vertically through some of these layers, or laterally to neighboring areas. Some cortical areas have primary somatic sensory functions (e.g. vision or hearing) and other primary motor functions (e.g. hand skills). Large areas cannot be assigned to any specific function.

The brainstem is a prolongation of the spinal cord and is the eldest part of the brain, taking care of basic functions necessary in all vertebrates.

The cerebellum is a motion computer optimized for rapid and smooth movement control in animals and humans.

Electrical Properties

Section 4.2 and Table 4.1. give some basic electrical properties of tissue relevant for the brain. Figure 5.10 shows a simple model of the brain with the layers to be passed by an electrical current. It is the cortical brain with its neurons which is the main endogenous signal source. The pia mater and the skull have low conductivities, while the brain and scalp have medium conductivity and the blood and CSF have high conductivities. The skull is a mechanically strong bone structure with relatively low electrical conductance estimated as being about 20 times lower than that of the scalp or the brain (Oostendorp et al., 2000). This ratio is important because it determines, for instance, the current path between current carrying scalp electrodes. If the CC electrodes are near to each other a large part of the current may flow in the scalp with a

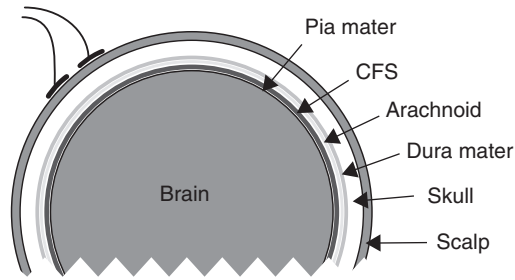


Figure 5.10 Model of the brain with membranes, skull and scalp.

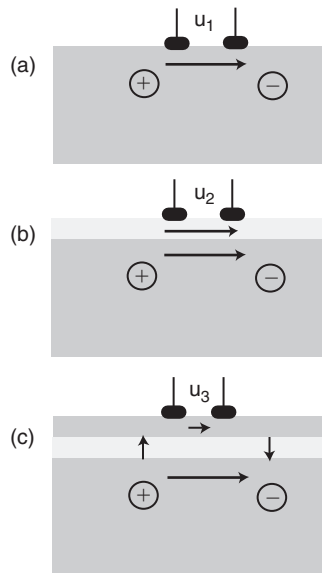


Figure 5.11 Signal transfer from deep current dipole to surface PU electrodes and the effect of layers: (a) without layer; (b) with poorly conducting layer; (c) with well conducting layer on top of the poorly conducting layer. Arrows represent direction and magnitude of E-field.

small penetration into the brain. These two layers result in substantial signal attenuation from the endogenous sources to the surface pick-up electrodes.

Figure 5.11 illustrates the signal attenuation effect of layers between the pick-up electrodes and a current dipole volume. Let the dipole be supplied by a constant current. The arrows symbolize the magnitude and direction of the electric field generating potential differences at the electrodes. Figure 5.11(a) illustrates the direct contact with the cortex resulting in a rather high pick-up voltage u_1 . Figure 5.11(b) shows that with a poorly conducting layer (e.g. skull) the current density in the skull will be small, but the resistivity is high so that $u_2 \approx u_1$ as long as the layer is thin with respect to dipole length. Figure 5.11(c) shows that a second well conducting layer (e.g. scalp) has been added. Current will pass perpendicularly through the skull into the scalp

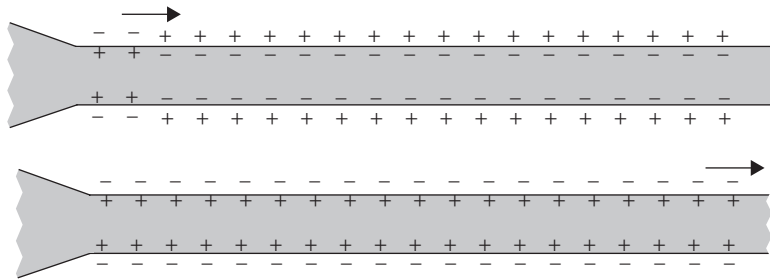


Figure 5.12 The soma at the left initiates an action potential transmission along the axon.

and easily pass the scalp and then return through the skull to reach the minus pole. However, the current density in the top layer will be small and as the resistivity also is low, u_3 will be smaller than u_1 . The skull/scalp combination has a signal attenuation effect dependent on the conductivity ratio between the layers and the thickness of the layers.

5.4 AXON TRANSMISSION

The brain is the only organ with a large volume of nerve tissue. Nerve tissue elsewhere may be regarded as cables with coupling nodes (plexus), and electrical cable theory is often applied. The naked axon diameter is of the order of $20\ \mu\text{m}$, and the length can be 1 m.

5.4.1 Excitation from the Soma

The excitation front shown in Fig. 5.12 is initiated at the soma, enters the axon and propagates to the right. The velocity in a naked, non-myelinated axon is low (C-fiber) and of the order of 1 m/s. If the sum of the depolarization and repolarization times is 1 ms the length of the depolarized part is thus 1 mm and outside the drawing in Fig. 5.9 (bottom). It is clear from Fig. 5.12 that the border line between polarized and non-polarized parts of the axon can be treated as the orientation of a dipole field generated by the membrane current. In the extracellular electrolyte current flows from the positive (polarized) part to the negative (depolarized) part as shown in Fig. 5.14 and according to the usual convention in the literature. The current is accompanied by a potential field, and therefore the action potential can then be measured by extracellular electrodes.

5.4.2 Exogenic Excitation

The axon has no unidirectional mechanism, and if triggered by an external current anywhere between its ends the impulse propagation will go in both directions as shown in Fig. 5.13. How will the soma react?

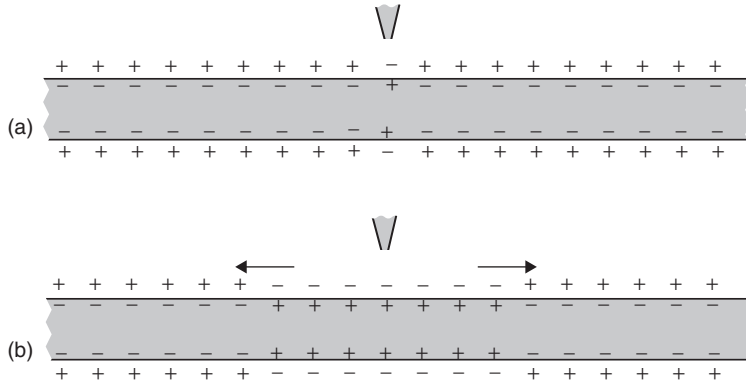


Figure 5.13 (a) Initial external excitation by a unipolar electrode and (b) propagation in both directions.

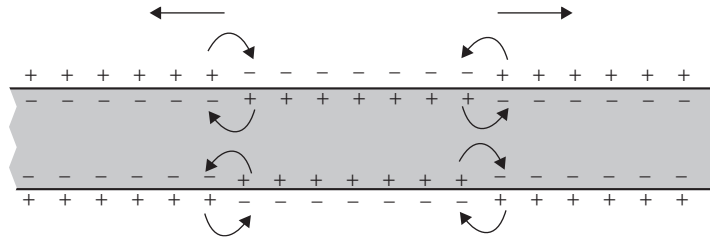


Figure 5.14 Moving dipoles in both directions as a result of an exogenic excitation. Arrows symbolize conventional current direction from plus to minus (direction of cation flow).

5.4.3 Moving Current Dipole

The propagation of the action potential signal through tissue is occurring with an accompanying low-pass filtering effect (cf. Section 6.5.1).

The current flow directions indicated in Fig. 5.14 are so that the intracellular flow is in the direction of the impulse propagation. When making an equivalent electric circuit for the process (Fig. 5.15), the thin axon interior has a much larger resistance R_a than the large volume extracellular resistance, which is therefore omitted. The current is the charging/discharging current of the membrane capacitance. The propagation velocity is to a large extent determined by the time constant of the axon resistance and the membrane capacitance: $\tau = R_a C_m$.

5.4.4 Myelinated Axons

The propagation velocity in a nerve fiber can be increased by myelination of the axon. For unmyelinated fibers the propagation velocity increases with the square root of the fiber diameter, and in thin fibers it can be as low as 0.5 m/s (Table 5.1).

TABLE 5.1 Nerve Diameter and Propagation Velocity

		Diameter (μm)	Velocity (m/s)	Example of function
α	Myelinated	15–20	60–100	Skeletal muscle
β	Myelinated	5–15	30–90	Vibration, high-precision touch
γ	Myelinated	1–10	6–60	Muscle spindle
δ	Myelinated	1–5	6–30	Deep pressure
C	Unmyelinated	0.5–2	0.5–2	Sympathetic, pain, tickle, crude touch and pressure

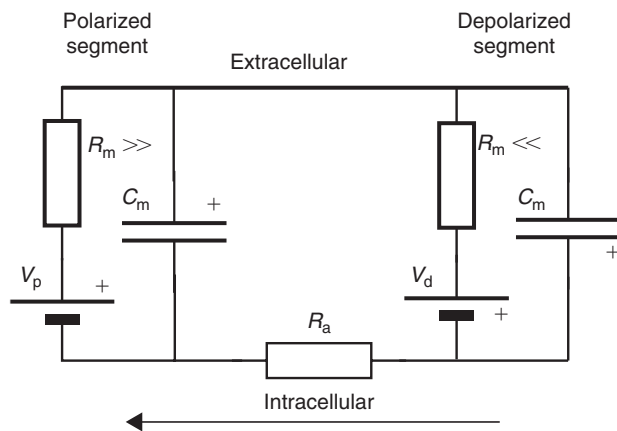


Figure 5.15 Equivalent circuit for the axon action potential propagation process in the direction of the arrow. Per axon length R_a is the intracellular resistance, R_m is the membrane resistance and C_m is the membrane capacitance. V is the Goldman related emv (Eq. 5.2).

The myelin sheath surrounds the axon like the insulation of an electric cable. The myelin may be thicker than the axon itself (about $20\mu\text{m}$) and is made of a lipid with very low conductivity. The axon membrane thickness is effectively increased, and the effective capacitance decreased. The myelin sheath is interrupted about every millimeter by a *node of Ranvier*. The result is a higher velocity, up to 100m/s . A Ranvier node is a few microns of naked cell membrane. The result is propagation in a saltatory way from node to node (Fig. 5.16).

5.4.5 The Nerve

A *nerve* is a collection of nerve fibers (fascicles). Axons must be electrically isolated from each other to maintain channel separation. Each axon, naked or with myelin, is therefore spirally wrapped by a thin sheath or membrane (*neurilemma*). Axons

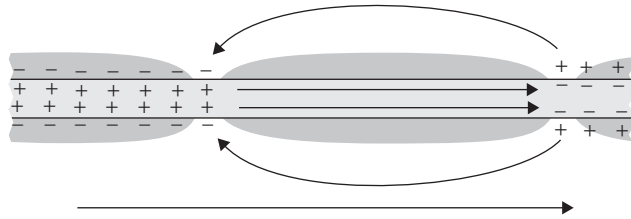


Figure 5.16 Myelinated axon, saltatory propagation from node to node.

are grouped in a *bundle (funiculus)* surrounded by its own sheath of connective tissue (*perineurium*). Within a bundle the fibers are packed with interstitial connective tissue (*endoneurium*). Many bundles constitute a nerve. The outermost part of a nerve is a sheet of connective tissue (*epineurium*). A nerve bundle usually contains both efferent fibers (motor fibers, signal direction toward periphery) and afferent fibers (receptor signals toward CNS).

As each of these sheets and membranes have different thicknesses and conductivities they play an important role in determining current density fields and the exogenic excitation threshold.

5.4.6 Synapses

The synapse is the region where signal coupling between, for example, two neurons takes place. In the synapse the signal may pass, may be blocked or may be modified. In the animal world there are two types of synapses: the *chemical* and the *electrical* synapses.

Chemical Synapses

Most of the synapses in the CNS are chemical. A ligand-gated membrane channel may be directly activated by *neurotransmitters* secreted at the synapse by the transmitting neuron. The neurotransmitter acts on receptor proteins called *ligands* on the surface of the receiving neuron. The chemical synapse allows only unidirectional traffic. The neuron that secretes the neurotransmitter is *presynaptic*, the signal receiving neuron is *postsynaptic*. The chemically activated ion channels in the postsynaptic neuron are called *ligand* activated channels. Over 30 different neurotransmitters are known and they have excitatory or inhibitory effect dependent on the receptor properties. Neurotransmitters are substances such as adrenaline, acetylcholine or dopamine conveying signal transmission across the synapses.

Electrical Synapses

In the electrical synapse the distance between the cell membranes is just a few nanometers and much shorter than in the chemical synapse. The joining membranes open a direct channel between the intracellular compartments in the form of

small tubules (*gap junctions*) allowing direct ionic flow. Gap junctions are found in the visceral smooth muscles and in the cardiac muscle. Gap junctions allow direct signal transmission in both directions between neighboring muscle cells so that each cell does not need a direct innervation.

Target Tissue

Target tissue is typically the other neurons. The action potential arrives along an axon, which may split up into several synapses. These act as presynaptic terminals on other neurons. Other target tissue types are muscle, blood vessels, intestines and glands.

5.4.7 Excitation

Neuron excitation is dependent on the total information entering from all presynaptic terminals. As the number of inputs are many thousand no single input has any decisive influence. The inhibitory inputs have largest influence because there are much fewer inhibitory than excitatory presynaptic terminals.

In the nerve system there is a summation both *spatial* and *temporal*. This is easily illustrated with skin receptors. If a variable skin contact area electrode is used for the examination of electric current perception it is found that the current density threshold is dependent on the contact area. As the area is increased the current density threshold is lower because of the summation effect of the receptor responses in the skin (Martinsen et al., 2004). Because of the temporal summation the excitatory signals must be synchronized in order to trigger the neuron. However, slow changes of the presynaptic DC levels may also make a cell more or less excitable. Such level shifts are according to the Nernst concept and are also under hormonal control.

Trigger Parameter

The choice of the best parameter for defining a trigger level is difficult. The level may be expressed as current (mA), current density (mA/mm²), voltage, charge (C), energy (J or Ws) or power (W).

We have seen that a cell basically must move a net number of ions in order to approach the trigger level (Fig. 5.7). For a single cell the charge was calculated to be of the order of 0.5 pC. The polarized cell is positively charged at the external cell surface. It is therefore reasonable to believe that a short negative polarity pulse from an external electrode would decrease the membrane potential and therefore be excitatory. This is according to experimental evidence: the trigger level is lower with negative pulses.

Basically we may guess that the preferred parameter is electric charge (C), being the membrane capacitance charge. However with extracellular electrode we do not have direct access to the cell interior, and most of the charge supplied by the electrodes is lost in the tissue volume far from the cell. It is the current density near the cell surface which is therefore the basic parameter. As the current density

usually is unknown it is a common practice to use accessible parameters, that is, those which can be measured in the electrode lead wires: current, charge, energy or power. Usually a current-controlled rectangular pulse generator is used. The pulse duration and current level are selected, which then actually is the charge $q=It$. If the generator voltage waveform is also measured the power or energy can be determined. A defibrillator pulse is defined with the energy parameter (Ws or joule). This is, from practical reasons, because the pulse is delivered by a large charged capacitor. A pacemaker pulse is also given as current and pulse duration, that is in reality electric charge.

5.4.8 External Current Excitation

A current carrying electrode is used to trigger (excite, pace) a nerve. The electrode may be on the skin (transcutaneous excitation), as a needle inserted through the skin, as a catheter electrode, as a part of an active implant, or as a microelectrode into an exposed nerve or axon.

The most used current waveform is rectangular monophasic or biphasic, cf. Fig. 7.7. With defined electrode/tissue geometry there is a relationship between the pulse duration and the current level necessary for nerve excitation. Figure 5.17 shows an example: as the pulse duration increases the necessary current approaches asymptotically a baseline current called the *rheobase*. The *chronaxie* is the pulse duration with the double rheobase current.

Weiss (1901) and Lapicque (1907) presented slightly different models of current–duration relationships for rectangular pulses (Reilly, 1998). Weiss used the equation

$$I = I_0 \left(1 + \frac{\tau}{t} \right) \quad (\text{hyperbolic}) \quad (5.3)$$

and Lapicque used

$$I = I_0(1 - e^{-t/\tau})^{-1} \quad (\text{exponential}) \quad (5.4)$$

where I is the minimum current for excitation with a pulse width t , τ is a time constant characteristic for the nerve tissue and electrode geometry, and I_0 is the rheobase current. τ for motor nerves may be about 0.3 ms and for myocard 3 ms.

Figure 5.17 shows a calculated current–duration graph with linear scales based on the hyperbolic model with normalized values: rheobase current 1 mA and chronaxie 1 ms. In the hyperbolic model the chronaxie is equal to the time constant. The charge necessary for triggering is constant at short pulse durations and increasing with longer pulses. The energy necessary for triggering goes through a minimum near the chronaxie.

The *empirical* current–duration relationship is in somewhat better accordance with the hyperbolic model than the exponential, but the exponential model is directly derived from the electric circuit model with a current source supplying

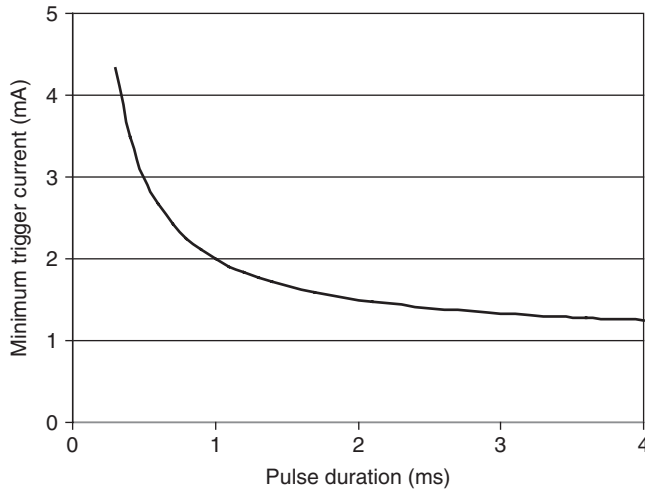


Figure 5.17 Current level versus pulse duration, according to the hyperbolic rheobase model.

an ideal resistor and capacitor in parallel. The empirical current–duration relationship is different for myelinated and naked axons. Also it must be remembered that the excitation process is non-linear and not easily modeled with ideal electronic components.

Electrotonus and rheobase are further treated in Section 9.7.

5.5. RECEPTORS

Receptors transduce specific types of received energy into a nerve signal. They are selective and have a narrow range of stimulus energy levels. There are five types of receptors:

1. Mechanoreceptors (skin, joint, ear, vessel, muscle)
2. Thermal receptors (warm and cold)
3. Chemical (itch, taste, smell, carbon dioxide, oxygen)
4. Pain (nociceptors)
5. Electromagnetic (eye)

A receptor may consist of free nerve endings or specialized organelles. Some of them couple to axons, not dendrites. Nociceptors are coupled to slow, thin, non-myelinated axons (C-fibers). Muscle spindle receptors monitor the muscle tension and the electrotonus. Some receptors are sensitive to static energy levels; others monitor the rate of change of stimulus energy, for instance the Pacinian corpuscles which are sensitive to vibration.

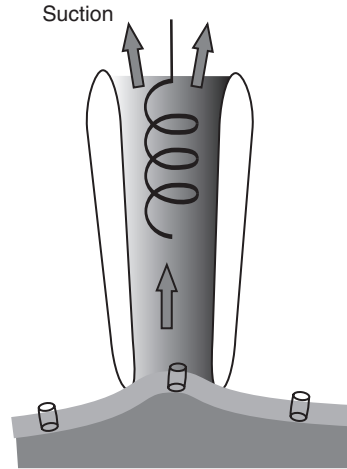


Figure 5.18 Patch clamp technique.

5.5.1. Patch Clamp Technique

The patch clamp technique with its great versatility has been a most important tool in the study of excitable cells. Figure 5.18 illustrates the main components of the technique. A glass pipette with a very small opening (diameter $\approx 1 \mu\text{m}$) is filled with an electrolyte in contact with a metal electrode for current and potential recording. The pipette is brought in contact with a cell membrane and suction applied to make a tight seal around a tiny area (patch) comprising, for example, one membrane channel. The suction brings the pipette-extracellular liquid resistance up, e.g., from $50 \text{ M}\Omega$ to $50 \text{ G}\Omega$; the suction creates a *gigaseal*. When a channel opens all ions therefore flow through the pipette and are measured as electrons in the electrode wire. The arrangement shown in Fig. 5.18 is called the *cell-attached patch clamp technique*.

Local membrane destruction can be made by suddenly applying a short strong burst of suction. A hole is created in the cell membrane so that the pipette is in direct electrolytic contact with the cell interior. Electrical potentials and currents from the entire cell are measured and this is therefore called the *whole-cell recording technique*. The hole may also be used to inject substances into the interior of the cell.

The *inside-out patch technique* is to retract the pipette that is in the cell-attached configuration so that a small vesicle of membrane remains attached. By exposing the tip of the pipette to an external electrolyte it is possible to control the medium to which the intracellular surface of the membrane is exposed. Alternatively, if the pipette is retracted while it is in the whole-cell configuration, the membrane's ruptured ends at the tip of the pipette can anneal so that a membrane patch is produced that has its extracellular surface exposed. This arrangement, called the

outside-out patch technique, is optimal for studying how channel activity is influenced by extracellular chemical signals, such as neurotransmitters.

PROBLEMS

1. Use the Nernst equation to find the potential difference across a cell membrane where the concentration of potassium on the outside is five times higher than on the inside. Should the calculation have been done with the Goldman equation?
2. Calculate the change in intracellular potential if 2 million Na^+ ions are transported out of the cell. Data: Cell diameter $10\ \mu\text{m}$, membrane capacitance $1\ \mu\text{F}/\text{cm}^2$, ion charge $1.6 \times 10^{-19}\ \text{C}$, $q = UC$.
3. Find the difference between the Weiss and Lapique equations if $t/\tau = 10$.
4. Define an action potential. Must it be measured with an intracellular microelectrode?

This page intentionally left blank

6 GEOMETRICAL ANALYSIS

Chapter Contents

6.1 Volume Conductors

- 6.1.1 Forward Problem
- 6.1.2 Inverse Problem
- 6.1.3 Boundary Value Problem

6.2 Two-electrode Systems

6.3 Sphere Sources, Ideal 3D Models

- 6.3.1 Sphere Monopole Source
- 6.3.2 Constricting/dispersing Zone
- 6.3.3 Bioelectric Dipole, Two Equal Spheres
- 6.3.4 Disc Monopole Source
- 6.3.5 Ellipsoidal Needle Source

6.4 Line Sources, Ideal 2D Models

- 6.4.1 Cylinder and Stripe Monopolar Sources
- 6.4.2 Two Parallel Cylinders
- 6.4.3 Ring Monopolar Source
- 6.4.4 Distance from Source Dependence

6.5 Signal Transfer in Tissue Volumes

- 6.5.1 Fixed Recording Lead and Moving Source, Ideal Volumes
- 6.5.2 Two Dipoles and the Lead Vector, Ideal Volumes
- 6.5.3 Non-ideal Volumes, the Reciprocal Lead Field
- 6.5.4 Sensitivity Field

6.6 Three- and Four-electrode Impedance Systems

- 6.6.1 Three-Electrode Systems, Unipolar Recording
- 6.6.2 Four-Electrode (Tetrapolar) Systems

6.7 Finite Element Method (FEM)

6.8 Tomography (EIT)

6.9 Duality of Dielectrics and Conductors

Problems

Important electrical characteristics of an electrode/tissue system are determined solely by the geometrical configuration. To clarify this important function, the systems to be treated in this chapter are simple models suited for basic analysis and mathematical treatment as well as computational approaches such as finite element analysis (Section 6.7). In bioimpedance systems the biomaterial is usually an ionic wet conductor, and the current carrying electrodes are therefore polarized. However, in this chapter the models are idealized in several ways: Biomaterial is considered homogeneous and isotropic. An electrode is considered isoelectric (superconducting metal). Only DC systems without polarization phenomena and frequency dependence are considered. Then a *potential* difference between two points in tissue space is equal to the *voltage* difference found between two circuit wires connected to the same two points, $\Phi_{12} = V_{12}$. If the value of the potential is known everywhere in space, Φ can be interpreted as a potential *field* $\Phi(x, y, z)$, V is simply the voltage difference between two defined points in a wired electric circuit. Φ is a scalar quantity (energy per charge = volt), the current density \mathbf{J} is a space vector and has a current density vector field $\mathbf{J}(x, y, z)$.

All models are volume models, but the field from a long cylinder has no changes in the direction of the cylinder axes. For this reason or because of symmetry (e.g. spheres) simplified calculations and 2D presentations give all necessary information for many basic geometry models. This is true when the imaging plane cuts through, for example, the sphere center or the cylinder axis.

6.1 VOLUME CONDUCTORS

Figure 6.1 shows two CC electrodes connected to a tissue volume. In the electrode wires the flow of electrons is confined to the wires. When the electrode dimensions are smaller than the tissue volume dimension the ionic current spreads out from a source electrode so that the current density falls with distance from the electrode. Voltage and current in the electrode wires are measured and they define the

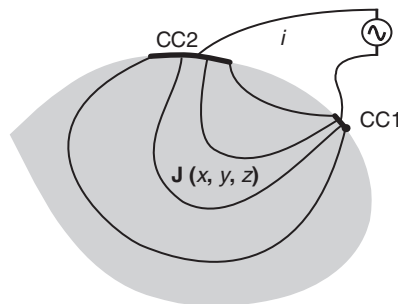


Figure 6.1 Current i (A) in the electrode wires and current density \mathbf{J} (A/m²) in the tissue volume. The lines drawn in the tissue show current flow direction, the proximity of two lines the current density magnitude. i is easily measured and known; the $\mathbf{J}(x, y, z)$ field is difficult to map and often unknown.

impedance. However, in the tissue volume the current flow must be defined with both magnitude and direction, and the parameter is current density \mathbf{J} (A/m^2), a spatial vector. The current density field $\mathbf{J}(x, y, z)$ cannot be easily measured and the current density field is often unknown.

6.1.1 Forward Problem

To find the potential field in tissue caused by a known signal current source is a *forward* problem. The tissue may be inhomogeneous, anisotropic and of finite dimensions. Examples are given in Section 6.3. Usually there is one unique solution to a posed problem.

6.1.2 Inverse Problem

In electrophysiology a body surface potential is often recorded, with the purpose of characterizing the unknown bioelectric source in position, size and direction. To go from measured potentials in a known conductive medium and calculate back to the source properties is called an *inverse* problem. Usually there are *infinitely* many possible solutions to a posed problem (cf. Fig. 7.10). Important classical patient examination methods such as ECG and EEG are aimed at characterizing properties of the source organ, and are thus based on more or less empirical solutions to the inverse problem.

6.1.3 Boundary Value Problem

In impedance tomography, the problem is a *boundary value* problem. From recorded potentials caused by exogenic current injection the distribution of conductivity is to be found.

6.2 TWO-ELECTRODE SYSTEMS

In order to obtain a current flow two electrodes are necessary in order to close the circuit; if one electrode is the *source*, the other must be a *sink*.

A clear distinction is made between *current carrying* (CC) and *pick-up* (PU) electrode systems. CC electrodes are also called current injecting, stimulating, driving or source electrodes, and the source may be *endogenic* (energy sources of the organism, i.e. bioelectric sources) or *exogenic* (energy sources outside the organism, e.g. externally applied electricity as in bioimpedance). PU electrodes are with negligible current flow and are also called signal recording, sensing, receiving, registering or lead electrodes.

CC Electrodes

CC electrodes are polarized because they are current carrying. A *dipolar* current injecting electrode pair uses two equal electrodes, each electrode contributing in the same way (current dipole). The dipole is the *most fundamental model* of a bioelectric signal source.

A *monopolar* current injecting electrode system has one small electrode as the *active (working, source)* electrode, and the other one as a large area *neutral (sink)* electrode.

Neutral CC Electrode

The neutral CC electrodes are also called indifferent, silent, passive or dispersive electrodes. Neutral means that the current density at the electrode surface is so low that the effect of current flow is negligible. The ideal CC neutral electrode is an enormous spherical electrode infinitely far away and at zero potential. In real situations it may be difficult to obtain large enough electrode areas with low enough current density, and the neutral electrode has a disturbing effect. This implies that there may be all sort of intermediate versions between true monopolar and dipolar systems. A special way of creating a more ideal neutral system with a small electrode is to use two of them in an active opamp circuit (see Section 7.2.7).

PU Electrodes (a Lead)

PU electrodes are measuring electric potential difference. They are used with negligible current flow and are therefore not polarized. A *lead* may be defined physically as two signal wires with their associated recording electrode system. It may also be defined conceptually as an information channel receiving information from a signal recording electrode system. A lead can be an electrode pair, a *bipolar* lead. A *unipolar* lead is with one PU and an indifferent electrode system.

A bipolar lead measures the local potential difference and is therefore actually also an electric field strength (V/m) probe. If the conductivity is known it is also a current density probe since $\mathbf{J} = \sigma\mathbf{E}$. Since the electric field is a vector field and the bipolar lead has an orientation being the length \mathbf{L}_{pu} between the PU electrodes, the measured voltage is the dot product: $v = \mathbf{E} \cdot \mathbf{L}_{pu} = \mathbf{J} \cdot \mathbf{L}_{pu}/\sigma$. The larger the electrode area, (a) the larger the averaging effect, (b) the lower the spatial resolution, (c) the lower the signal source impedance (less noise, better high frequency response).

However, if the tissue under an electrode is not isoelectric, exchange currents will flow between electrode surface regions and *an electrode may become polarized without current flow in the external electrode wire*.

Neutral PU Electrode

Neutral PU electrodes are also called indifferent or reference electrodes. A PU electrode may be more or less indifferent depending on its area and position with respect to signal sources. The ideal unipolar models presuppose an enormous spherical neutral electrode, infinitely far away and at zero potential. In a limited tissue volume such as the human body the ideal indifferent electrode is not feasible,

TABLE 6.1 The Number of Electrodes and Confusion from Words with Both Latin and Greek Origins

Latin (PU)	Greek (CC)	Meaning
Unipolar	Monopolar	One electrode dominant in a non-symmetrical system of two or more electrodes
Bipolar	Dipolar	Two equal electrodes in a symmetrical system
Tripolar	Tripolar	Three-electrode system
Quadropolar	Tetrapolar	Four-electrode system

and we use the concept of *quality* of an indifferent electrode. A practical approach is to take the average potential of several electrodes (e.g. Wilson's central terminal in ECG). It is not ideal to connect electrodes of different potentials resulting in exchange current flow between them, but each electrode may first be connected to a buffer amplifier.

A recording of electric biopotentials is an *electrogram*. If zero potential difference is measured in a region, the region is *isoelectric*. A line designating tissue at the same potential is an equipotential *line* and a cable connecting two electrodes in separate regions so that the regions have the same potential is called an equipotential *cable*.

Immittance and Transmittance

A one-port (dipolar) electrode system measures immittance. The two electrodes function both as CC and PU electrodes. A two-port four-electrode system measures *transmittance*: for example with current injected in one port and voltage recorded at the other port (the black box, Section 7.1). The electrode pairs of current injection and voltage recording may be interchanged: if the reciprocity theorem is valid, the transmittance is the same. For the reciprocity theorem to be valid there are no constraints on geometry, only on, for example, system linearity as outlined in Section 7.1.2. The reciprocity theorem is not based on geometry but on network theory, and is therefore treated in Section 7.1.

Monopolar-Unipolar

The terms monopolar–dipolar are of Greek origin, and are preferably used for current carrying systems in this book. The terms unipolar and bipolar are of Latin origin and are often used for signal pick-up electrode systems. The terminology in the literature is confusing (cf. Table 6.1), and it is practically impossible to be consistent.

6.3 SPHERE SOURCES, IDEAL 3D MODELS

The monopolar sphere is the most basic geometry in the sense that *any* electrode in an infinite homogeneous medium reverts to a symmetrical spherical geometry

TABLE 6.2 Parameter Dependence on Distance r from Different Sources in a Homogeneous Medium, cf. also Table 3.1

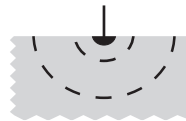
Source	Unipolar PU Φ [V]	Dipole PU $\Delta\Phi$ [V] E [V/m] J [A/m ²]	In tissue W_v [W/m ³]
Long rod	$\sim \ln(r^{-1})$	$\sim r^{-1}$	$\sim r^{-2}$
Sphere	$\sim r^{-1}$	$\sim r^{-2}$	$\sim r^{-4}$
Dipole	$\sim r^{-2}$	$\sim r^{-3}$	$\sim r^{-6}$

at sufficiently large distance. At distance any electrode geometry corresponds to an equivalent sphere radius.

The spherical coordinate system with the coordinates r , θ and ϕ is of course well suited for spherical sources. A sphere in a homogeneous medium *disperses* the current radially out in all directions. Since the surface area of a sphere is $4\pi r^2$, the current density falls proportional to r^{-2} . As we shall see, this is in contrast to a line source where the current density falls proportional to r^{-1} (Table 6.2). Because the current spreads out in all directions a 3D analysis is necessary, but in a homogeneous medium any plane through the sphere center will show the same 2D plot.

6.3.1 Sphere Monopole Source

The conductance G of a superconducting hemisphere of radius a , half-submerged in a half-infinite homogeneous biomaterial and with a concentric half-spherical reference electrode infinitely far away, is:



$$G = \sigma 2\pi a \quad (\text{S}) \quad R = \rho / 2\pi a \quad (\Omega) \quad (\text{hemisphere}) \quad (6.1)$$

In a real case with a metal electrode in an electrolyte solution, the electrode polarization impedance due to the surface layer is physically in series with the electrolytic resistance given by eq. (6.1). Equation (6.1) shows that the electrolytic resistance is inversely proportional to *radius* a (or circumference $2\pi a$) of the electrode. However, the electrode *polarization impedance* is inversely proportional to a^2 (surface area $2\pi a^2$). Therefore, the influence of the electrode polarization can be made as small as wanted by increasing the sphere radius. Alternatively, by reducing the electrode radius sufficiently, it will be possible to measure polarization or electrode surface properties selectively, without influence from the electrolytic series resistance.

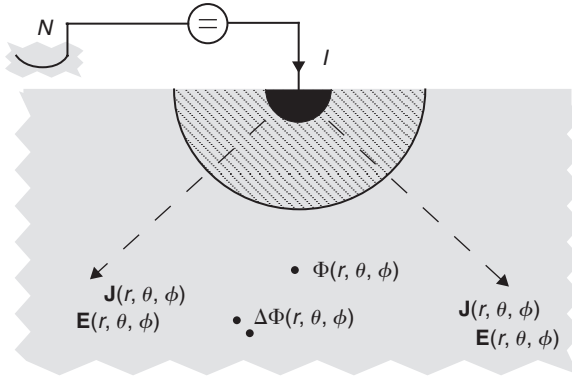
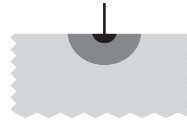


Figure 6.2 Vector fields caused by a monopolar, hemispherical surface source shown with a corresponding arbitrary equipotential hemisphere. N is an ideal neutral electrode infinitely large at infinite distance.

The resistance contribution of a finite hemispheric *shell* of radius r on the metal sphere of radius a is:



$$R = \frac{\rho}{2\pi} \left(\frac{1}{a} - \frac{1}{r} \right) \quad (\text{hemispheric shell, } r \geq a) \quad (6.2)$$

Accordingly, 99% of the total resistance is within a sphere of radius $100a$, and 90% within a sphere of radius $10a$. The resistance value measured with a small spherical monopolar electrode may therefore show good spatial selectivity. A concentric hemisphere is an equipotential surface, and the surface can therefore be covered by a thin metal sheet acting as one electrode. It is not a neutral electrode until r is large. As a neutral electrode a hemispherical electrode with $r \rightarrow \infty$ is equal to an infinite area bottom plate at infinite distance (Fig. 6.2).

Injecting a current I into a hemisphere, the current density J in the tissue volume in radial direction is:

$$J = \frac{I}{2\pi r^2} \quad [\text{A/m}^2] \quad (\text{hemisphere, } r \geq a) \quad (6.3)$$

The voltage V is applied relative to the infinitely remote reference electrode with $V = 0$ (Fig. 6.2). The current I to the hemisphere electrode is $I = V\sigma 2\pi a$. The scalar potential field Φ in the medium (forward problem) is:

$$\Phi = \frac{Va}{r} = \frac{\rho I}{2\pi r} \quad [\text{V}] \quad (\text{hemisphere, } r \geq a) \quad (6.4)$$

Notice that V is a voltage supplied by an external wire circuit, Φ is a potential in space.

From eq. (2.2) $\mathbf{E} = \mathbf{J}/\sigma$ where \mathbf{E} is the *electric field strength* (V/m). Since $I = V\sigma 2\pi a$ the electric field \mathbf{E} is from eq. (6.3):

$$\mathbf{E} = Va\hat{\mathbf{r}}/r^2 \text{ (V/m)} \quad (\text{space vector, } r \geq a) \quad (6.5)$$

where $\hat{\mathbf{r}}$ is the unity radius vector, dimension [1]. The potential difference in a pick-up dipole of length L_{pu} is:

$$\Delta\Phi = Va L_{\text{pu}} \cdot \hat{\mathbf{r}}/r^2 \text{ [V]} \quad (r \geq a) \quad (6.6)$$

Note that as sphere radius $a \rightarrow 0$, then $G \rightarrow 0$ (eq. 6.1). With applied voltage V the potential at the electrode surface $\Phi_a = V$ ($r = a$, eq. 6.4). The whole potential drop Φ occurs at the electrode if $a \rightarrow 0$, and no current flows. This is not the result of a polarization; it is a pure function of geometry. However, with applied current I and $a \rightarrow 0$, at the electrode surface $\Phi_a \rightarrow \infty$, $\mathbf{E}_a \rightarrow \infty$ and $\mathbf{J}_a \rightarrow \infty$.

Power density $\mathbf{W}_v = \mathbf{E}\mathbf{J}$ is:

$$\mathbf{W}_v = \sigma(Va)^2/r^4 = \rho(I/2\pi)^2/r^4 \quad [\text{watt/m}^3] \quad (\text{hemisphere, } r \geq a) \quad (6.7)$$

Power density falls off extremely rapid with distance from the electrode, and the equation formulates the basis of unipolar electrosurgery (see Section 9.7). It shows that the diathermy effect is concentrated to a very narrow sheath around the electrode, and with little tissue damage elsewhere in the tissue. The temperature rise ΔT in a tissue volume is:

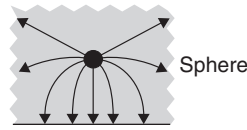
$$\Delta T = \frac{J^2}{\sigma} \frac{t}{cd} \quad [^\circ\text{C}] \quad (6.8)$$

where c is specific heat capacity (e.g. for water 4.2 kJ per kg and $^\circ\text{C}$), and d is the density. With a current density of $J = 200 \text{ mA/cm}^2$, $\sigma = 1 \text{ S/m}$ and $d = 1000 \text{ kg/m}^3$, the temperature rise in the tissue per second is 1°C . This is under adiabatic conditions, that is with no cooling effects from the surroundings (e.g. no blood flow).

Sphere and Conductive Plate

Hitherto we have analyzed the hemisphere in a half-infinite homogenous medium. The model is changed if the sphere is in a medium of limited dimensions or if homogeneity is disturbed by, for example, a conductive plate. Let us take the case of an infinite medium with a conductive plate at a finite distance from the sphere. The resistance and conductance can be found from the non-ideal current carrying

dipole solution (eq. 6.16) because the current density field is unchanged if the plane isoelectric area is replaced by a thin metal plate. With respect to the dipole solution the resistance is halved and the conductance is doubled (whole sphere and plate immersed in an infinite medium):



$$G = \sigma 4\pi a \left(1 + \frac{a}{L} + \left(\frac{a}{L}\right)^2 + \left(\frac{a}{L}\right)^3 + 2\left(\frac{a}{L}\right)^4 + 3\left(\frac{a}{L}\right)^5 + \dots \right) \quad (L > 2a) \quad (6.9)$$

where L is 2 times the distance between the sphere center and the plate, and short circuit between sphere and plate occurs at $L = 2a$.

6.3.2 Constricting/dispersing Zone

The zone near a small source or sink electrode is the *spreading, dispersing or constricting zone* of the current path (Fig. 6.3). In the spreading zone of a half-sphere the resistance R is $(\rho/2\pi)[(1/a) - (1/r)]$ according to eq. (6.2). However, $R = \rho L/A$ in the segmental zone in Fig. 6.3. With a small sphere the total resistance will be dominated by the constricting resistance, and then is a monopolar system.

6.3.3 Bioelectric Dipole, Two Equal Spheres

The dipole is the most fundamental bioelectric model of endogenic signal sources in biology; the current from the dipole spreads out in the body and must eventually return to the dipole to close the electric circuit. The living cell may be regarded as dipoles spread out on the cell surface area (cf. the cell membrane, Section 5.1). The action potential of a nerve cell may be regarded as being generated by dipoles

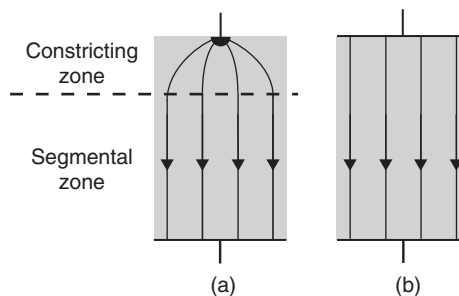
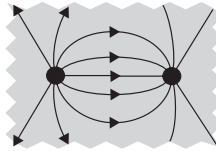


Figure 6.3 Current constricting: (a) monopolar system where the resistance is increased by the smaller electrode and current constricting geometry; (b) bipolar system.

under motion (cf. Section 6.5.1). The sum of millions of muscle cells may be considered equivalent to one single dipole (the heart vector).



The dipole is well known from *electrostatic* theory, by *duality* the electrostatic dipole equations can be used for current carrying dipoles. Such duality has a limited validity range; this is further discussed in Section 6.9. The current carrying dipole is defined with two current carrying spheres of radius a and center to center distance L_{cc} resulting in a dipole moment \mathbf{m} :

$$\mathbf{m} = I L_{cc} \quad [Am] \tag{6.10}$$

The direction of L_{cc} is the dipole axis.

Ideal Current Carrying Dipole

An *ideal* current carrying dipole mathematically defined is a dipole in an *infinite homogeneous* medium where $I \rightarrow \infty$, $a \rightarrow 0$ and $L_{cc} \rightarrow 0$, keeping m constant. However in physics and engineering the concept of infinitely small current carrying *points* with infinite current density is not ideal. *In engineering mathematics we will therefore still define the current dipole as technically ideal with $a > 0$ if $L_{cc} \gg a$ and the dimensions of the homogeneous volume are much larger than L_{cc} .*

If the superposition theorem is valid the scalar potential field can be found by simply adding the potential contribution from each sphere (a forward problem):

$$\Phi = \frac{I\rho}{4\pi} \left(\frac{1}{r_1} - \frac{1}{r_2} \right) \quad [V] \quad (\text{technically ideal CC dipole}) \tag{6.11}$$

where r_1 and r_2 are the distances from each sphere to the pick-up position of Φ .



Equation (6.11) may be expressed with the dipole moment $\mathbf{m} = I L_{cc}$ and as a vector dot product valid if $r \gg L_{cc} \gg a$:

$$\Phi = (\rho/4\pi)\mathbf{m} \cdot \hat{\mathbf{r}}/r^2 \quad [V] \quad (\text{technically ideal CC dipole}) \tag{6.12}$$

The vector dot product indicates the directional sensitivity shown in Fig. 6.4. The potential falls as r^{-2} (Table 6.2) in all radial directions except for the special case of \mathbf{r} being perpendicular to \mathbf{m} , then $\Phi = 0$ for any distance.

Equation (6.13) shows the bipolar potential pick-up from the CC dipole. r_1 and r_2 are the distance from the CC dipole to each of the PU dipole poles. In this way

the local electric field strength E (V/m) in the $\mathbf{r}_1 - \mathbf{r}_2$ direction is measured. $\mathbf{r}_1 - \mathbf{r}_2$ is actually the length of the PU dipole (L_{pu}):



$$\Delta\Phi = (\rho/4\pi r^3) \mathbf{m} \cdot (\mathbf{r}_1 - \mathbf{r}_2) \quad [V] \quad (\text{technically ideal CC dipole}) \quad (6.13)$$

Notice that eqs (6.11)–(6.13) do not refer to a co-ordinate system. Notice also that the dot product is defined with the vectors mathematically moved to obtain a common starting point, physically they are separated by the distance r .

The resistance of the ideal dipole is simply the resistance of one whole sphere multiplied by two:

$$R = \rho/2\pi a \quad G = \sigma 2\pi a \quad (\text{technically ideal CC dipole}) \quad (6.14)$$

Then a large part of the medium between the spheres does not contribute to the resistance.

Figure 6.4 illustrates the potential distribution in a plane through a current dipole axis (homogeneous infinite conductive medium). Such current flow lines and equipotential lines are of course the same for any such plane (cylinder coordinates).

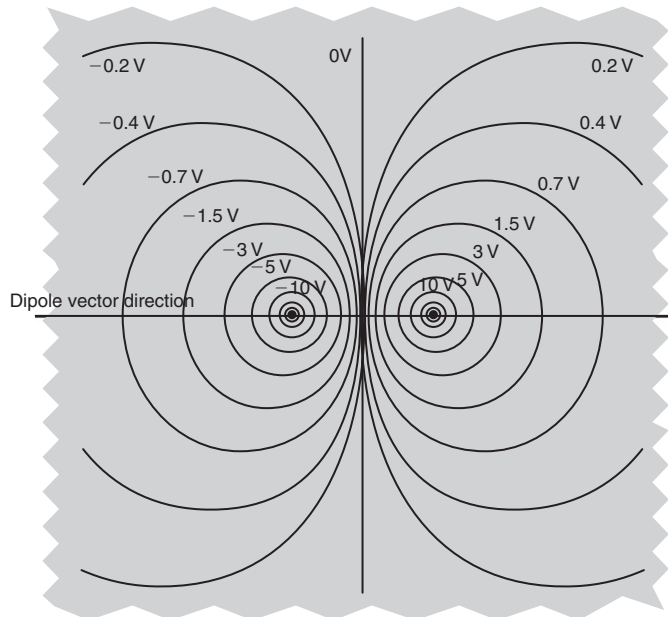


Figure 6.4 Equipotential lines in any plane through a current dipole axis, not referred to a Cartesian co-ordinate system. High density of equipotential lines in the center is only due to the arbitrarily chosen voltage range.

The model is based on two current carrying spheres at a distance L_{cc} apart. Each electrode may be regarded as a unipolar electrode in their proximity zone of the current path, with equipotential lines as concentric circles. Further away the equipotential lines are not circular. However, in cable theory (Section 6.3) with the poles of Fig. 6.4 being considered as long wires these equipotential lines are circular but eccentric.

Ideal Pick-up Dipole

Equation (6.13) gave the potential difference $\Delta\Phi$ between two points in the field of a technically ideal current dipole. This potential difference can be picked up by a recording dipole. Such a dipole is not current carrying and the dipole spheres may therefore approach points. Let the distance r between the two dipoles be large and the pick-up dipole length L_{pu} be small so that $r_1 \approx r_2 = r$. $\mathbf{r}_1 - \mathbf{r}_2 = \mathbf{L}_{pu}$ and therefore:



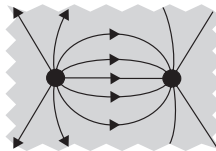
$$\Delta\Phi = (\rho/4\pi r^3) \mathbf{m} \cdot \mathbf{L}_{pu} \quad [\text{V}] \quad (\text{two technically ideal dipoles at long distance}) \tag{6.15}$$

$\mathbf{m} = I\mathbf{L}_{cc}$ is the source, and the mathematically defined ideal current dipole is with $L_{cc} \rightarrow 0$ and $I \rightarrow \infty$ while m is constant. Equation (6.15) shows that the ideal pick-up dipole is not like this: the potential difference is proportional to L_{pu} , so that sensitivity is lost if $L_{pu} \rightarrow 0$. *The ideal pick-up dipole is with point spheres but finite dipole length.*

The double dipole model with one current carrying and one pick-up dipole far away from each other is an important analytical model for studying transfer functions in media (cf. Section 6.5.3 on the lead field).

Non-ideal Current Dipole

If the condition $L_{cc} \gg a$ is not met, the superposition theorem is not valid because the introduction of a second superconducting sphere disturbs the current density lines from the first sphere. The conductance of two spheres immersed in an infinite homogeneous medium is:



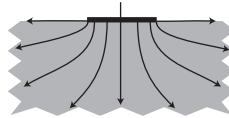
$$G = \sigma 2\pi a \left(1 + \frac{a}{L} + \left(\frac{a}{L}\right)^2 + \left(\frac{a}{L}\right)^3 + 2\left(\frac{a}{L}\right)^4 + 3\left(\frac{a}{L}\right)^5 + \dots \right) \quad (\text{two whole spheres, } L > 2a) \tag{6.16}$$

This equation takes care of the effect that each sphere has on the other. Half-immersed in the surface of a semi-infinite medium the conductance according to eq. (6.16) is halved. If $L \gg a$ eq. (6.16) simplifies to eq. (6.1). Using the factors written out in eq. (6.16) the error of eq. (6.16) is $<1\%$ at the length $L = 3a$ ($L = 2a$ represents short circuit). At $L = 4a$ the ideal dipole solution (eq. 6.1) gives only 75% of the true value obtained with eq. (6.16).

If the conductivity of the spheres is equal to the conductivity of the medium, the current density field is not disturbed, but we still have the problem of how to connect the end of the wire to the sphere.

6.3.4 Disc Monopole Source

The disc can be regarded as a flattened sphere (*oblate* ellipsoid of revolution), the needle as a stretched sphere (*prolate* ellipsoid of revolution). A spheroid is the same as an ellipsoid of revolution.



Analytical solutions are possible because by letting the length of the axis of revolution tend to 0 we end up with a disc. If positioned on the surface it is the most common of all electrode geometries. We then discover the often overlooked fact that current is not injected evenly under the surface of such a plate electrode.

Figure 6.5 shows a 2D cut through the center of a surface disc electrode on a conducting homogenous medium. It shows the potential field with a current injecting electrode plate of radius $a = 5$ units. The equipotential lines are themselves spheroids, at a distance $>2a$ they rapidly approach a spherical shape. But near the electrode edge the distance to an equipotential spheroid is much smaller than at the center, indicating a higher current density at the edge.

Each confocal spheroid in Fig. 6.3 is an equipotential surface and may be regarded as a possible electrode, with unchanged equipotential lines outside the

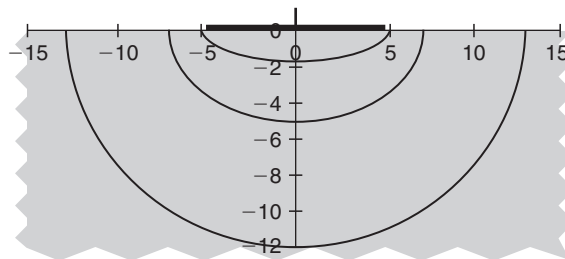


Figure 6.5 Equipotential lines caused by a current carrying disc electrode at the tissue surface.

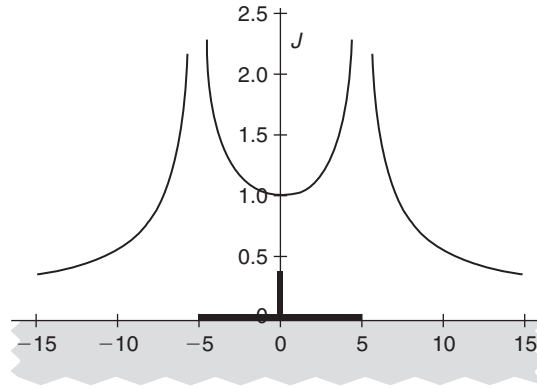


Figure 6.6 Current density in the tissue surface layer caused by a disc electrode. $J = 1$ corresponds to the current density of a spherical electrode with the same radius, half-immersed in the tissue.

electrode. The only difference is that the conductance G of such a spheroid will increase with size. The conductance of the surface disc with radius a is found to be:

$$G = \sigma 4a \quad R = \frac{\rho}{4a} \quad (\text{one side}) \quad (6.17)$$

Comparing with eq. (6.1), a disc has therefore only $2/\pi$ times less conductance than a sphere of the same radius, independently of a . As for the sphere, the conductance is proportional to the electrode circumference, not the area (Fig. 6.6).

At the surface of a disc electrode (Fig 6.6) the current density J as a function of the radius r is:

$$J = \frac{I}{2\pi a \sqrt{a^2 - r^2}} \quad (r < a, \text{ one side}) \quad (6.18)$$

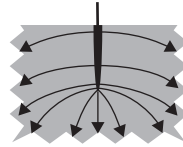
The direction of J is perpendicular to the metal surface except at the edge, which is a singular curve where the current also leaves the edge in directions of the tissue surface. Current density therefore diverges at the edge. The edge is therefore outside the zone of linearity. There are many misconceptions in the literature, with current density under a surface electrode considered uniform. The current density in the disc center is the same as on the surface of a sphere of the same radius a . The potential field in the tissue is:

$$\Phi = \frac{2V}{\pi} \arctan \frac{\sqrt{2}a}{\sqrt{(r^2 - a^2 + \sqrt{(r^2 - a^2)^2 + 4a^2z^2})}} \quad (6.19)$$

when the disc is lying in the xy -plane symmetrical to the origin. The tissue surface potential ($z = 0$) is then $(2V/\pi)\arctan((r/a)^2 - 1)^{-0.5}$.

6.3.5 Ellipsoidal Needle Source

This geometry is important as a model for invasive electrodes, often used in neurophysiology with insulated shaft and an open half-ellipsoid-like end as the active electrode. The conductance of a half-ellipsoid of revolution in a half-infinite homogeneous medium is:



$$G = \sigma \frac{2\pi\sqrt{L^2 - a^2}}{\ln \frac{L + \sqrt{L^2 - a^2}}{a}} \quad (\text{half ellipsoid of revolution}) \quad (6.20)$$

where a = rotational radius and L = half long axis.

Equation (6.20) is for a non-insulated half-ellipsoid inserted from the surface. When the needle shaft is insulated, so that when the needle is inserted from the surface and penetrates deeper into the tissue the model may be regarded as a gradual change toward a full-length ellipsoid in an *infinite* medium. The conductance given by eq. (6.20) would then be doubled. A slightly different model is to consider the half-ellipsoid positioned at the end of an insulating rod.

For needles the diameter d is a more practical dimension than radius a , so if $d = 2a$ is inserted in eq. (6.20) and if $L \gg d$, the equation simplifies to:

$$G = \sigma \frac{\pi 2L}{\ln \frac{4L}{d}} \quad R = \rho \frac{\ln \frac{4L}{d}}{\pi 2L} \quad (L \gg d) \quad (6.21)$$

Figure 6.7 shows how small influence the needle diameter has on the needle conductance (due to the logarithmic factor in eq. 6.20). An equivalent sphere is a sphere with the same conductance as a given needle. The equivalent sphere to a non-insulated needle of diameter $0.1 L$ and needle length $L = 0.5$ has a diameter of about $0.3 L$. Reducing the needle diameter further down to three decades ($0.0001 L$) only reduces the equivalent sphere diameter to $0.1 L$. Needle length is the dominant factor. This is a general rule for the electrical properties of electrodes: it is the largest dimension that is the determining factor.

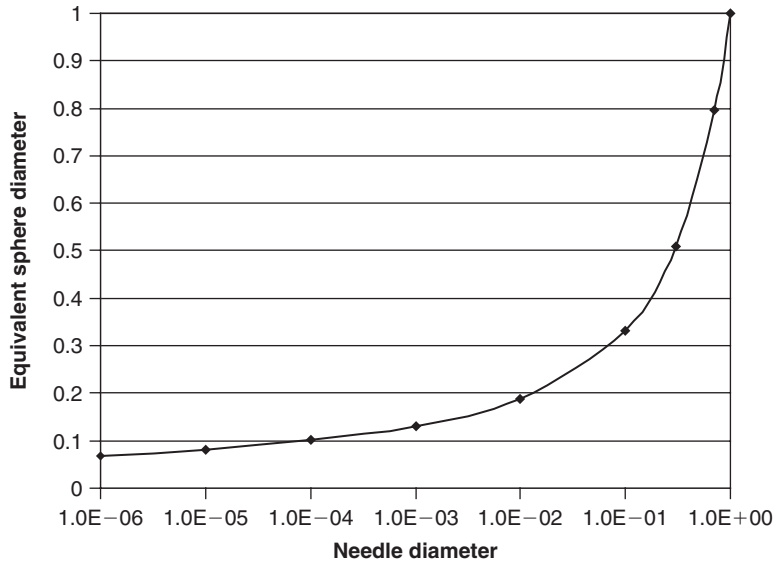


Figure 6.7 Equivalent sphere diameter as a function of needle diameter, equivalent sphere and ellipsoidal needle having equal conductance. Needle half-axis length $L = 0.5$.

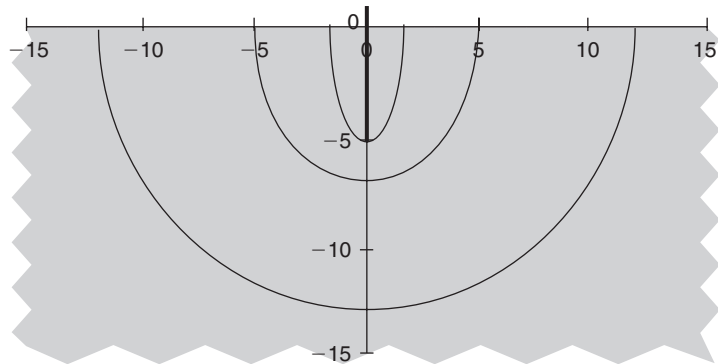


Figure 6.8 Equipotential lines of a non-insulated current injecting needle (prolonged spheroid of maximum radius 0.2 units and length 5 units).

Figure 6.8 shows the equipotential field lines caused by a current carrying needle electrode having the form of a long, thin ellipsoid. The potential drop is very important near the needle tip.

Figure 6.9 shows the needle surface current density as a function of depth, normalized with $J = 1$ at the electrode tip. If such a non-insulated needle is used for nerve excitation most of the current will be injected from the shaft, but at threshold the excitation occurs only at the tip.

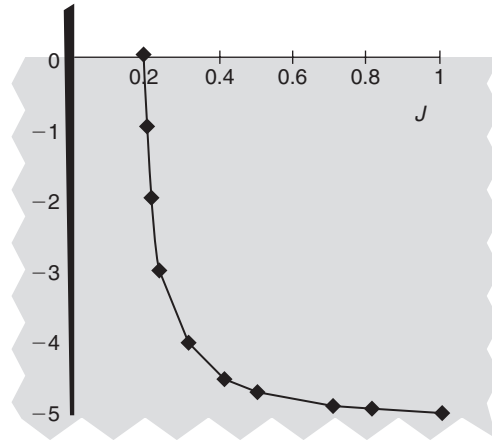
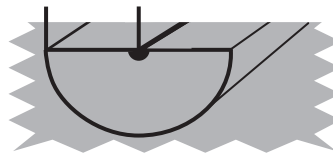


Figure 6.9 Needle surface current density as a function of depth. Needle dimensions: maximum diameter 0.4 units, length 5 units.

6.4 LINE SOURCES, IDEAL 2D MODELS

Like the sphere, a cylinder of infinite length also spreads the current radially, but not in the length direction. The cylindrical coordinate system with the coordinates z , r and ϕ is of course well suited for line sources. The sphere has double curvature, while the cylinder has single curvature geometry. The surface area of a cylinder segment of length L is $2\pi rL$ and the current density accordingly falls proportional to r^{-1} (sphere: r^{-2} , Table 6.2). The line source spreads the current deeper than a sphere of the same radius.



A cylinder of length L and limited by two insulating plates perpendicular to the cylinder axis has the same electrical properties as the infinitely long cylinder per length L .



6.4.1 Cylinder and Stripe Monopolar Sources

Figure 6.2 is relevant, but this time the black electrode must be interpreted not as a sphere but a cut through an infinitely long half-immersed cylinder. The resistance and conductance of a half-immersed cylinder is:

$$R = \frac{\rho}{\pi L} \ln \frac{r}{a} \quad \frac{G}{L} = \frac{\sigma \pi}{\ln \frac{r}{a}} \quad (r \geq a, \text{ hemicylinder, infinitely long}) \quad (6.22)$$

Here L is not the cylinder length because that is infinite: L is the length of a cylinder segment. The radius of the half-immersed cylinder is a , and r is the radius of a chosen outside concentric hemicylinder in the tissue volume. R is the resistance between two cylinders and in contrast to the sphere, R *diverges* if $r \rightarrow \infty$.

The surface of a cylinder segment is $2\pi rL$, and if I is the current fed into that cylinder segment the current density in tissue is:

$$J = \frac{I}{L} \frac{1}{\pi r} \quad [\text{A/m}^2] \quad (r \geq a, \text{ hemicylinder}) \quad (6.23)$$

It is not possible to define a finite potential at $r = \infty$ because a certain current I then results in an infinite potential as R diverges. With an infinitely long cylinder only potential *differences* can be defined and eq. (6.24) describes a quantity often called the “logarithmic potential” for this difference between two points at distances r_1 and r_2 :

$$\Delta\Phi = \frac{I\rho L}{\pi} \ln \frac{r_1}{r_2} \quad [\text{V}] \quad (r \geq a, \text{ hemicylinder}) \quad (6.24)$$

If the surface of the cylinder is defined as $r_1 = a$, the potential at distance r in the tissue is:

$$\Phi = \frac{I\rho L}{\pi} \ln \frac{a}{r} \quad [\text{V}] \quad (r \geq a, \text{ hemicylinder}) \quad (6.25)$$

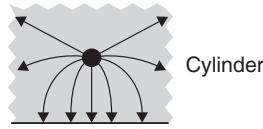
According to eq. (6.25) the potential at $r = \infty$ is $-\infty$ V and at the cylinder surface 0 V. In comparison the potential of a sphere is zero at infinite distance.

Since the current density field has no changes in the axial direction, the calculations are simplified to 2D problems. Around the ends of a *finite* length rod in an infinite conductive medium the problem is no longer 2D, and the best analytical approach is to turn to an ellipsoid geometry (cf. Section beneath on finite length rod).

Infinite Cylinder and Conducting Plate

The two parallel cylinder solution is directly applicable to a complete cylinder above, for example, an infinite metal plate, because the current density field

is unchanged if the isoelectric plane surface is covered by a thin metal sheet. The resistance is halved and the conductance is doubled (cf. eq. 6.27):



$$R = \frac{\rho}{2\pi L} \ln \left\{ \frac{D}{2a} + \sqrt{\left(\frac{D}{2a}\right)^2 - 1} \right\} \quad \frac{G}{L} = \frac{2\sigma\pi}{\ln \left\{ \frac{D}{2a} + \sqrt{\left(\frac{D}{2a}\right)^2 - 1} \right\}} \quad (6.26)$$

where D is 2 times the sphere center to plane distance. If $D \gg a$, this simplifies to

$$\frac{G}{L} = \frac{2\sigma\pi}{\ln \frac{D}{a}} \quad (6.26a)$$

Finite Length Rod

The needle equations (6.20) and (6.21) are also valid if a needle ellipsoid with full length $2L$ is turned 90° so that its long axis is parallel to the surface and with the ellipsoid half-immersed. This is perhaps the best analytical model for a finite length rod.



6.4.2 Two Parallel Cylinders

The resistance and conductance of two half-immersed cylinders are:



$$R = \frac{2\rho}{\pi L} \ln \left\{ \frac{D}{2a} + \sqrt{\left(\frac{D}{2a}\right)^2 - 1} \right\} \quad \frac{G}{L} = \frac{\sigma\pi}{2 \ln \left\{ \frac{D}{2a} + \sqrt{\left(\frac{D}{2a}\right)^2 - 1} \right\}} \quad (6.27)$$

where D is the distance between the cylinder centers. If $D > 20a$, this is equal to the double resistance of the single cylinder (eq. 6.22) to an accuracy better than 0.1%.

6.4.3 Ring Monopolar Source

The conductance of a ringformed cylinder of ring radius R and cylinder radius a in a half-infinite volume is:



$$G = \sigma \frac{2\pi^2 R}{\ln \frac{8R}{a}} \quad (\text{half immersed}) \quad (6.28)$$

Just as for the ellipsoid needle we see that the conductance is not much dependent on cylinder radius a , it is the length $2\pi R$ which is important.

6.4.4 Distance from Source Dependence

Table 6.2 shows distance from source dependences. Important consequences of the values are: the current density falls less rapid from a cylinder than a sphere source. Power density and therefore temperature rise falls extremely rapid with distance from a CC sphere.

6.5 SIGNAL TRANSFER IN TISSUE VOLUMES

The basic bioelectric model is the dipole. In *ideal volumes* (homogenous infinite size, tissue with linear isotropic electrical properties) analytical solution can be found as already shown. Even if analytical solutions cannot be found with finite volumes and heterogeneous tissue, transfer functions may be determined from measurements or calculations, cf. section 6.5.3. The dipole is well suited for analytical models.

6.5.1 Fixed Recording Lead and Moving Source, Ideal Volumes

The basic model for signals derived from the action potential of a nerve cell axon is a *free* current carrying dipole vector with fixed moment $\mathbf{m} = I\mathbf{L}_{cc}$ (eq. 6.10)

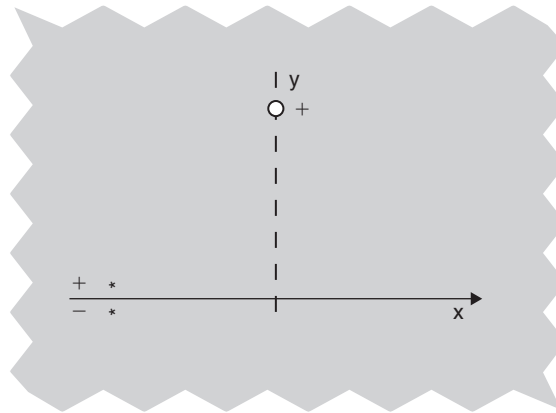


Figure 6.10 Moving current dipole (* *) model with unipolar pick-up fixed position electrode.

(Fig. 6.10). We will now go into a more detailed description of the axon model because it so clearly demonstrates how the registered waveforms are so dependent on the PU electrodes lead, and how the geometries, the axon included, act as a low-pass filter.

An ideal (Section 6.3.3) current dipole with constant moment moves with constant velocity along the x -axis in an ideal volume (Fig. 6.10). The monopolar and bipolar potentials are calculated at a fixed point on the y -axis at distances $5L_{cc}$ and $10L_{cc}$, respectively. The monopolar and bipolar potentials are calculated using eq. (6.11) with $I\rho = 2000\pi$. The potential values in Figs 6.11 and 6.12 can therefore be compared.

Unipolar Recording

The potential contribution from each dipole sphere is added according to eq. (6.11). Equation (6.12) shows that with the dipole moment \mathbf{m} and the distance \mathbf{r} in the same direction the potential falls off as r^{-2} . This is in accordance with the maximum amplitudes at Fig. 6.11(b) for the recording electrode distances $5L_{cc}$ and $10L_{cc}$. At Fig. 6.11(a) however the r^{-2} agreement is not so precise because the maxima do not occur at the same x value for the two distances.

Bipolar Recording

Bipolar PU electrodes actually measure the electric field strength. The potentials are calculated at each PU electrode and subtracted. Equation (6.13) indicates that the potential difference $\Delta\Phi$ falls off more rapidly with distance than in the unipolar case. From Fig. 6.12 the $\Delta\Phi$ fall is between r^{-2} and r^{-3} . This is confirmed by Fig. 6.12, showing a large positional discriminative property. The waveform in

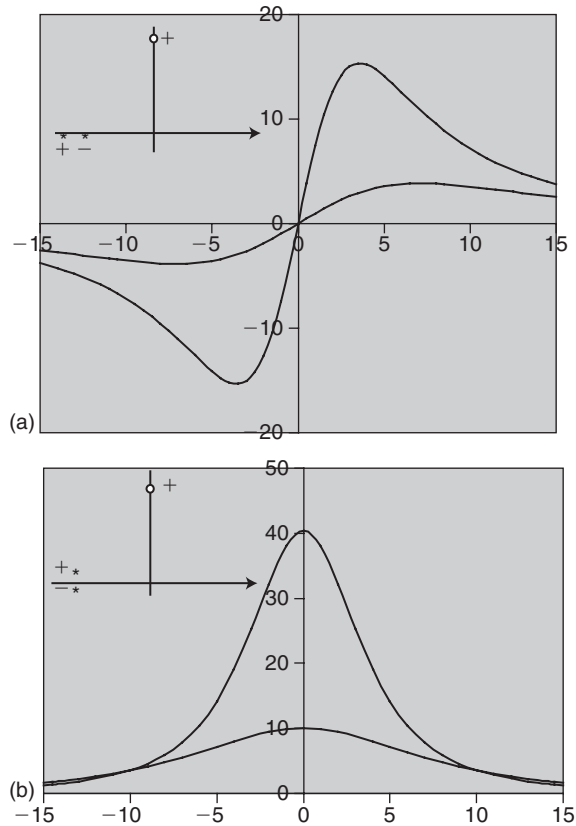


Figure 6.11 Unipolar potentials from a current dipole moving along the horizontal x -axis. Dipole length is L_{cc} , the unit of the x -axis is L_{cc} . The recording electrode is at distance $5L_{cc}$ and $10L_{cc}$: (a) horizontal dipole orientation, biphasic waveforms and high spatial resolution; (b) vertical dipole orientation, monophasic waveforms and largest signal amplitude of all geometries.

Fig. 6.12(c) is even triphasic. Figure 6.12 (a) and (b) show biphasic waveforms with a large high frequency content, but the recorded voltage difference is small.

Spatial Resolution and Frequency Content, the Passage Effect

All the bipolar recordings show higher discriminative power than the unipolar recordings. The bipolar waveforms therefore have higher frequency components.

The curves at distance $10d$ are less steep and with less high frequency components. *The distance to the signal source acts as a low-pass filter.* This is not due to tissue electrical properties, but only to different geometrical angles of view. It is in

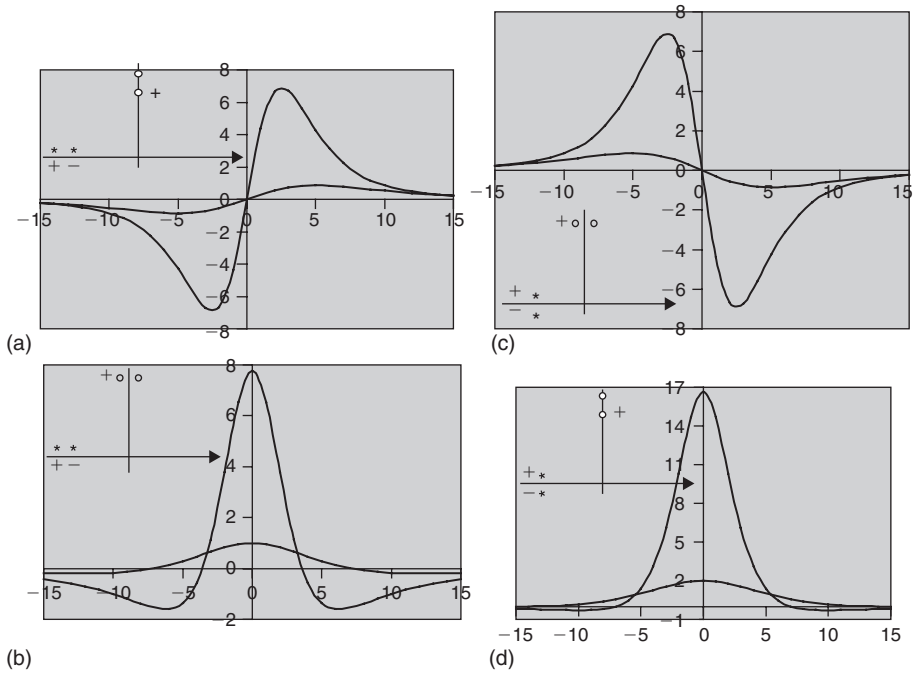


Figure 6.12 Bipolar potentials from a current dipole source. Conditions as for Fig. 6.11 with the recording dipole length $L_{pu} = L_{cc}$.

accordance with, for example, the high content of high frequency signals found in EMG signals obtained with recording electrodes near to a large muscle mass. It is like standing at a distance from a road where cars pass. The near you are to the road, the more intense is the noise at car passage, but the shorter the noise duration. At long distance from the road a low noise starts early, but do not reach a high noise maximum at passage.

6.5.2 Two Dipoles and the Lead Vector, Ideal Volumes

We have just calculated the pick-up potential from a moving dipole source in an ideal infinite volume. The potential recorded from an endogenic electrical source is, as we have seen, much dependent on the position of the electrodes with respect to the source (Figs 6.11 and 6.12). We will now analyze signal transfer between two ideal dipoles more in detail.

Figure 6.13 shows a general model with two technically ideal dipoles in an infinite, homogeneous medium. One dipole is current carrying (dipole length L_{CC}); the other is for signal pick-up (dipole length L_{PU}). Their axes need not cross each other.

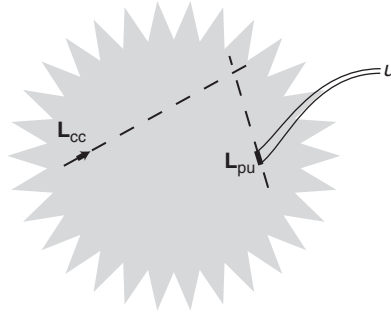


Figure 6.13 Two ideal dipoles far away from each other in an infinite, homogeneous conductor volume. Their axes need not cross each other. The left dipole is current carrying (\mathbf{L}_{cc}), the right dipole (\mathbf{L}_{pu}) picks up signals transferred from L_{cc} .

Equation (6.15) gave the potential difference from a current carrying ideal dipole. Putting $\mathbf{m} = I\mathbf{L}_{cc}$ we have:

$$\Delta\Phi = u = (I\rho/4\pi r^3) \mathbf{L}_{pu} \cdot \mathbf{L}_{cc} \quad [\text{V}] \quad (\text{technically ideal dipoles}) \quad (6.29)$$

It is clear from this equation that it does not matter which dipole is current carrying and which is pick-up, in accordance with the principle of reciprocity. We separate the part of eq. (6.29) associated with the PU dipole and call it the *lead vector* \mathbf{H} :

$$\mathbf{H} = (\rho/4\pi r^3) \mathbf{L}_{pu} \quad [\Omega/\text{m}] \quad (\text{Lead vector of technically ideal pick-up dipole}) \quad (6.30)$$

The lead vector¹ defines the pick-up part of a transfer factor between the CC and PU dipoles. It depends on the resistivity ρ of the medium, the distance r between the dipoles, the pick-up dipole length vector \mathbf{L}_{pu} . The scalar signal u created by a current dipole $\mathbf{m} = I\mathbf{L}_{cc}$ is:

$$u = \mathbf{H} \cdot \mathbf{m} \quad [\text{V}] \quad (\text{technically ideal dipoles}) \quad (6.31)$$

Vector \mathbf{H} has a free starting point but fixed magnitude and direction according to eq. (6.30). The current dipole \mathbf{m} is bound, but may vary in current I and length \mathbf{L}_{cc} .

The transfer impedance Z_t is defined as u/i in the external wires, so from eq. (6.29):

$$Z_t = (\rho/4\pi r^3) \mathbf{L}_{pu} \cdot \mathbf{L}_{cc} \quad [\Omega] \quad (\text{technically ideal dipoles}) \quad (6.32)$$

¹Schmitt (1957) called the lead vector \mathbf{H} transfer impedance. This may be misleading both because impedance is a spatial scalar while \mathbf{H} is a spatial vector and with dimension (Ω/meter).

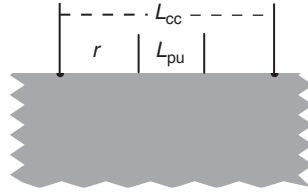


Figure 6.14 Two dipoles oriented in-line on a plane, infinite tissue surface.

Z_t is a scalar in space, but may be a time vector \mathbf{Z}_t related to a frequency dependence of ρ . Both the lead vector \mathbf{H} and the scalar transfer impedance Z_t are transfer factors between the current carrying and pick-up dipoles. The relationship between them is: $Z_t = \mathbf{H} \cdot \mathbf{L}_{cc}$ [Ω].

The Einthoven triangle is an example of a recorded voltage u (the ECG signal) modeled as the dot product of the *lead vector* of a bipolar PU electrode pair and the bound *heart dipole vector* \mathbf{m} (cf. Section 9.1).

In-line Surface Dipoles

For surface electrodes simple analytical solutions can be found if we return to eq. (6.11). Equation (6.11) is valid for all technically ideal current carrying dipoles without any restrictions on the distance to the potential pick-up positions. Let us call the two current carrying electrodes CC1 and CC2 with dipole length L_{cc} , and the two pick-up electrodes PU1 and PU2 with dipole length L_{pu} . If the two dipoles are on the same plane surface, the geometry is completely determined by three vectors: the two dipole vectors and one vector giving the distance between them. If they are in line three scalars must be known (Fig. 6.14).

Since the upper half-infinite volume is taken away, the potential of eq. (6.11) for a given current is doubled. For the in-line geometry of Fig. 6.14 the voltage difference is:

$$\Delta\Phi = \frac{I\rho}{2\pi} \left(\frac{1}{r} - \frac{1}{L_{pu} + r} - \frac{1}{L_{cc} - r} + \frac{1}{L_{cc} - L_{pu} - r} \right) \quad \begin{array}{l} \text{(ideal surface} \\ \text{dipoles in line)} \end{array} \quad (6.33)$$

If the electrodes are equally spaced with distances d , the voltage difference is:

$$\Delta\Phi = \frac{I\rho}{2\pi d} \quad \text{(ideal surface dipoles in line)} \quad (6.34)$$

and the transfer impedance Z_t is:

$$Z_t = \frac{\rho}{2\pi d} \quad \text{(ideal surface dipoles in line)} \quad (6.35)$$

The model of Fig. 6.14 is based on contact hemispheres for the PU electrodes with radius $a \rightarrow 0$, but for the current carrying electrodes $a > 0$ according to our

definition of an ideal current carrying dipole. The system is therefore not necessarily reciprocal if the two dipoles are swapped. In Fig. 6.14 therefore $r \geq a$.

Equations (6.29)–(6.35) are the basic equations for three- and four-electrode systems according to the model of two ideal dipoles. Notice that all these analytical models presuppose ideal dipoles, that is, electrode sphere radii much smaller than dipole length, distance between dipoles much larger than dipole lengths, infinite homogeneous isotropic medium.

6.5.3 Non-ideal Volumes, the Reciprocal Lead Field

Figure 6.15 illustrates a situation with a finite and inhomogeneous volume where \mathbf{m} is the dipole source, symbolizing, for instance, the heart vector. Under such conditions the dipole equations are not exact solutions, and a more realistic approach according to limited conductor volumes and inhomogeneous tissue must be found. In order to find the lead vector \mathbf{H} under more realistic conditions, the concept of *reciprocal* excitation was introduced (McFee and Johnston, 1953). Reciprocal excitation is to let the PU electrodes be current carrying with a unity current of 1 A (in contrast to their intended use as zero current PU electrodes). The current density vector field $\mathbf{J}'_{\text{reci}}(x, y, z)$ generated by a unit current excitation is called the *reciprocal lead field*, dimension $[1/\text{m}^2]$.

Initially the lead field is often unknown, but may be found by FEM modeling to the extent that the volume dimensions and resistivity distribution are known. The lead *field* illustrates the sensitivity distribution of the pick-up electrodes for current carrying electrodes or biological processes somewhere in the finite volume. The measured signal u is:

$$u = \iiint \rho \mathbf{J}_{\text{cc}} \cdot \mathbf{J}'_{\text{reci}} dv \quad [\text{V}] \quad (\text{The general transfer signal equation}) \quad (6.36)$$

u is of course proportional to the excitation current density J_{cc} , so J_{cc} has the dimension $[\text{A}/\text{m}^2]$. In order to get rid of the unit current concept we may equally

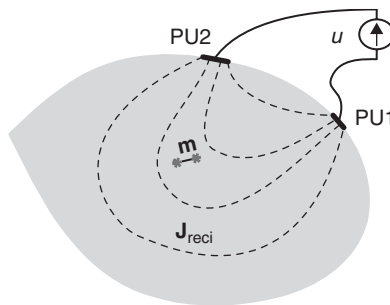


Figure 6.15 Sensitivity of a PU electrode pair to a dipole source \mathbf{m} is directly related to the reciprocal current density generated by the PU electrodes at the source position.

well use $J' = J/I_{\text{reci}}$ [$1/\text{m}^2$] where I_{reci} is any current level supplied in the pick-up electrode wires. The equation is then:

$$u = I_{\text{reci}}^{-1} \iiint \rho \mathbf{J}_{\text{cc}} \cdot \mathbf{J}_{\text{reci}} \, dV \quad [\text{V}] \quad (6.37)$$

If $\mathbf{J} = \sigma \mathbf{E}$ (isotropic case) we may equally well express u as a function of the two electrical fields:

$$u = I_{\text{reci}}^{-1} \iiint \sigma \mathbf{E}_{\text{cc}} \cdot \mathbf{E}_{\text{reci}} \, dV \quad [\text{V}] \quad (6.38)$$

The transfer impedance Z_t between the current carrying and pick-up electrodes is:

$$Z_t = \iiint \rho \mathbf{J}'_{\text{cc}} \cdot \mathbf{J}'_{\text{reci}} \, dV \quad [\Omega] \quad (\text{The general transfer impedance equation}) \quad (6.39)$$

It is still possible to use the lead vector concept, for example, from the example shown in Fig. 6.15. The lead vector of the PU dipole is not a vector field, it is the total sensitivity of a lead under ideal (homogeneous, infinite, isotropic) conditions. However, in real cases the PU electrodes may be at large distance from each other on the body surface, and it is less evident that they shall be considered as a dipole. But even with the highest geometrical and tissue complexities, the tissue can always be considered linear with the current and voltage levels generated by life processes. Therefore the principle of superposition is valid, and any space vector can be decomposed into its Cartesian x - y - z components. Each direction can be treated separately and later added to form one resultant vector. For instance, the relation $u = \mathbf{H} \cdot \mathbf{m}$ may still be useful if two sets of PU electrodes are used with individual lead vectors and simultaneous measurement of the two lead voltages from the same source. The individual vectors are added so that the direction of the source dipole vector \mathbf{m} can be determined. This is used for the determination of the electrical axes of the heart (see Section 9.1).

A lead vector \mathbf{H} is determined by the geometry and conductivity distribution of the signal pick-up system, and is valid for one tissue volume and one set-up with all electrode and source positions and distributions defined and constant. Changing one PU electrode or source position leaving all other factors constant, results in another lead vector \mathbf{H} .

Optimum electrode configuration is crucial in order to focus the measurements on the desired tissue volume (see e.g. Song et al., 2005). The sensitivity of a transfer impedance measurement in a limited volume with four surface electrodes can be determined by studying the dot product according to eq. (6.39) (cf. Fig. 6.16). In some volume positions where the vectors are perpendicular to each other the measured impedance is insensitive to local resistivity changes. In other positions the angle is $>90^\circ$; in those positions the sensitivity is reversed. Again we must point out that *the transfer impedance is not an ordinary impedance, it is a transfer factor between an input port and an output port. If, for example, $Z_t = 0$ this is not because the tissue is so well conducting, it is because there is no signal transmittance from the source dipole to the PU dipole. It is only with the one-port*

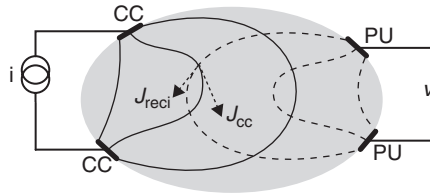


Figure 6.16 Four-electrode system with current density and reciprocal current density lines. Sensitivity is illustrated at one point, the dot product, and therefore the sensitivity there is small because the two current density vectors are almost perpendicular to each other.

two-electrode technique that tissue immittance is measured without influence from transmission properties.

Swapping the PU and CC pairs does not change the transfer impedance as long as the system is electrically linear (reciprocity). This is valid for both tripolar and tetrapolar electrode systems.

6.5.4 Sensitivity Field

The lead vector \mathbf{H} is a transfer factor determining signal amplitudes in a pick-up electrode pair from, for example, a certain biological source activity in a fixed position. So H is a *sensitivity parameter* of the whole lead system, a larger lead vector means larger signal transfer. From Fig. 6.15 it is clear that higher signal amplitudes are recorded from a dipole source near the electrodes and their constricted current zones of high current density. If the reciprocal current density is negligible in a volume, dipole sources in that volume do not contribute to the recorded signal.

The transfer impedance Z_t between the current carrying electrode pair and the pick-up electrode pair is given by eq. (6.39). The contribution of each voxel is $\rho \mathbf{J}'_{\text{reci}} \cdot \mathbf{J}'_{\text{cc}}$, and we define the sensitivity S of a tissue voxel as:

$$S = \mathbf{J}'_{\text{reci}} \cdot \mathbf{J}'_{\text{cc}} \quad [1/\text{m}^4] \quad (6.40)$$

The sensitivity S is a factor determining the influence of the local resistivity on the total result, the impedance contribution of a voxel is $\rho S dv$. If an interesting physiological process is going on somewhere in the tissue, the pick-up electrode pair should be situated so that the volume is in a high sensitivity zone of the PU electrodes. In Section 9.2 on plethysmography, for instance, the sensitivity for detecting small local changes in tissue conductivity is discussed.

In a two-electrode system (bipolar or monopolar) the forward and reciprocal current densities are identical, so therefore:

$$Z = \iiint \rho |J'|^2 dv \quad S = |J'|^2 \quad (6.41)$$

where J' is the unity current density ($1/\text{m}^2$). If the medium is homogeneous the resistivity ρ is constant and can be placed outside the integration sign, then the contribution of a voxel is simply a function of $|J'|^2$.

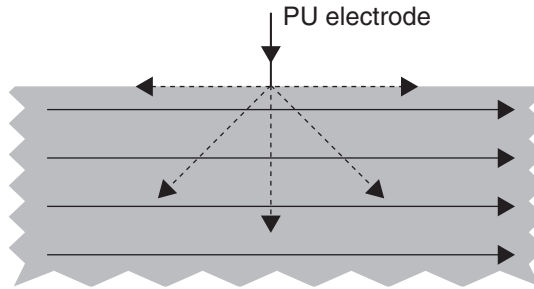


Figure 6.17 Sensitivity of a PU electrode in a uniform current density field.

Sensitivity may be defined according to any transfer function; our interest is on impedance sensitivity. The spatial variation of S is the *sensitivity field*. At the neutral electrode in a unipolar system J is low, so the contribution of the tissue there will be negligible. In a tube with cross-sectional area A and $J = I/A$ constant, eq. (6.41) reverts to the well-known $R = \rho L/A$. For the unipolar hemisphere on the tissue surface eq. (6.3) shows that J is proportional to r^{-2} . From eq. (6.41) Z is proportional to $|J'|^2$, and the contribution of a voxel falls very rapidly as r^{-4} . However, at the same time the *number* of voxels in a spherical shell increases as r^2 , so the contribution of a shell falls as r^{-2} . It is of course a general phenomenon that the number of voxels increases in a current spreading geometry with falling J and falling contribution of each voxel.

Zero Net Sensitivity, the Symmetry Paradox

Figure 6.17 illustrates reciprocal current injection by a small contact area PU electrode into an infinite volume of homogeneous and isotropic material with uniform current density J'_{cc} . From the reciprocally excited PU electrode the current spreads out in a hemispherical symmetrical geometry in accordance with Fig. 6.1. The reciprocal current density J'_{reci} near the electrode is very high, and one may be led to believe that the sensitivity is high in this zone. The voxels lying in the vertical line from the pick-up electrode have zero sensitivity because the reciprocal current line is perpendicular to the horizontal current lines. Near the surface the dot product $J'_{reci} \cdot J'_{cc}$ is very high near the PU electrode. However, as long as we are inside the symmetrical zone of reciprocal current density the contributions from the left- and right-side volumes with respect to the PU electrode position are equal but with opposite signs. The volume of the symmetrical zone is dependent on the reciprocal current path, for example whether it is a bipolar or unipolar PU electrode system. The paradox is that if the symmetrical very high sensitivity region has zero net sensitivity, all contributions cancel. In conclusion, such an electrode configuration will be very sensitive to asymmetry in the tissue near the PU electrode, and the recording may easily be unstable and noisy. Increased PU electrode contact area will reduce the problem, but this implies current disturbance of the J'_{cc} field.

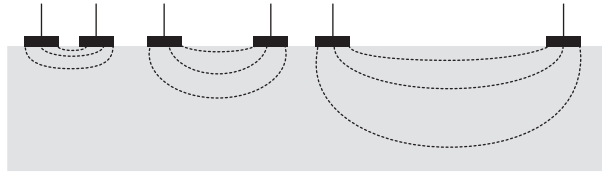


Figure 6.18 Measuring depth as a function of spacing distance between equal electrodes.

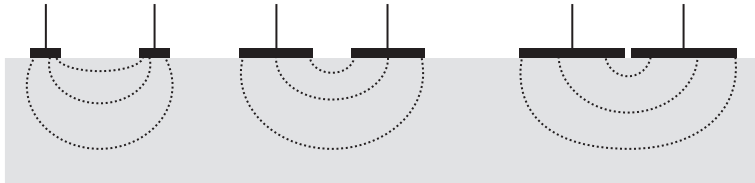


Figure 6.19 Measuring depth as a function of electrode dimensions, constant distance between electrode centers.

Bipolar Impedance Measurement, Measuring Depth

Constant Area Discs, Varying Distance

The distance between two surface electrodes will influence measuring depth (Fig. 6.18). If the bipolar electrodes are driven from a constant amplitude voltage source, the total current and in particular the current density will decrease with increasing distance. In addition, the relative contribution of the deeper layers will increase. Even so, the sensitivity is proportional to the current density squared, so a given volume of tissue proximal to the electrodes is more important for the result than the *same volume* in the deeper layers. By varying the distance between the electrodes, it is therefore possible to control the measuring depth. Ollmar and Nicander (1995) varied the measurement depth by inserting a third active current carrying electrode between the two measuring electrodes.

Constant Distance, Varying Disc Area

Measuring depth is not so dependent on electrode dimensions. This is illustrated in Fig. 6.19 with equal electrode center distances. With the narrow gap in the right figure, the sensitivity in the gap will be high. On the other hand the number of voxels there is small and the number of low sensitive voxels is very high. The local gap sensitivity can be increased much more by keeping the narrow gap, but reducing the electrode areas.

By using multiple surface electrodes it is possible to reduce the measuring depth somewhat (Fig. 6.20). Such electrodes are often made in the form of metal strips, not discs. Measuring depth is determined *both* by the strip width and the distance between the strips.

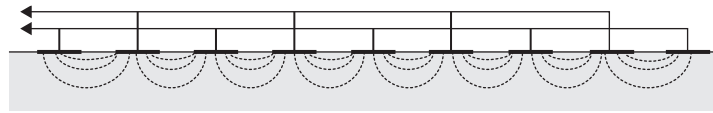


Figure 6.20 Multiple surface electrodes.

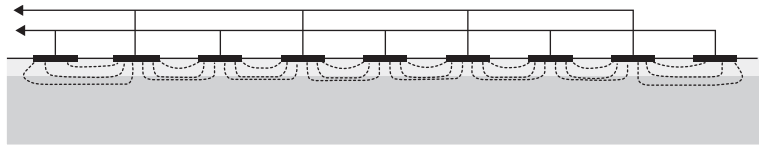


Figure 6.21 Surface electrodes on poorly conducting surface layer.

Surface Layer

If a homogenous volume is covered by a poorly conducting homogenous layer, the current will go more or less perpendicular right down to the well conducting layer (Fig. 6.21). The whole volume of the poorly conducting layer will dominate measuring results. Dependent on the conductivity ratio and upper layer thickness/edge to edge distance, a certain part of the current will still go the shortest way through the poorly conducting layer.

6.6 THREE- AND FOUR-ELECTRODE IMPEDANCE SYSTEMS

6.6.1 Three-Electrode Systems, Unipolar Recording

Three-electrode systems correspond to a *two-port, three-terminal network* equivalent (cf. Section 7.1). Since there are two ports it is the *transfer parameters* which are measured even if one CC and one PU electrode are the same. Figure 6.22 shows the principle (Grimnes, 1983a). The current flows between the M and C electrodes, the R electrode is a PU electrode without current flow.

In a two-electrode unipolar impedance system it may be difficult to estimate a possible contribution from the neutral electrode. Often only a zone of the current path proximal to the measuring electrode is of interest, for example, when measuring skin admittance. In such cases the distal volume segment of the current path is a disturbing part. It may also be difficult to work with a sufficiently large neutral electrode in some situations. By adding a third electrode, it becomes easier to control the measured tissue zone. The set-up has the measuring electrode M common both for current injecting and voltage recording.

With just the measuring electrode M and the electrode C the resultant current is dependent on the impedance of both electrodes plus the tissue in between. By measuring the voltage u on a potential recording electrode R (no current flow and no polarization) with respect to M, the admittance Y of M is: $Y = i/u$. In a practical

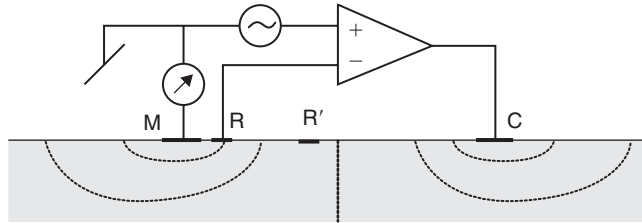


Figure 6.22 Three-electrode geometry and circuit, equipotential lines shown in tissue are for homogeneous biomaterial. The position of electrode R determines the sensitivity field of the electrode system.

set-up this is effectively done with an operational amplifier as shown. The circuit guarantees that the potential on R is equal to the excitation voltage, so it is a constant voltage, admittance reading circuit. What is then included in measured Y ?

1. The polarization impedance of electrode M.
2. A tissue volume zone proximal to M, with gradually reduced contribution (sensitivity) at increasing distance from M. Negative sensitivity in the volume between the R and C electrodes.

One interesting feature with this circuit is that if there is a capacitively coupling of 50/60 Hz mains leakage current to the patient, the necessary AC current is supplied by the current carrying counter electrode. This current is supplied by the operational amplifier, which does not pass the measuring electrode, and is therefore not recorded by the transresistance amplifier.

The circuit of Fig. 6.22 shows also the principle of a *potentiostat*, with the reference electrode controlling the voltage of the electrode M.

From Fig. 6.3 we know that a spherical electrode alone has a larger sensitivity in the constricted zone of the electrode for purely geometrical reasons. Using a surface disc M electrode, tissue near the electrode edge also influences the result to a larger extent than tissue elsewhere (see Section 6.3.4).

If the geometry is fixed, the electrodes included, the R and the C wires may be swapped with no change in measured admittance (reciprocity). This is an important circuit quality test. The polarization impedance of C and the impedance of R should not influence the results, but if any of the electrodes is too small that electrode may be in the nonlinear region so that the reciprocity test fails.

The metal of the R electrode should be recessed (Fig. 6.25), or the metal should be narrowed in the current flow direction, to impede current flow from being attracted away from the lower admittivity tissue surface layers.

The three-electrode op-amp circuit of Fig. 6.22 has a problem if the M and R electrodes are of different metals and so generates a DC voltage difference (Section 2.5.1). The same problem occurs if the tissue generates an endogenic DC voltage. The palmar sites may, for instance, generate up to -50 mV with respect to the underarm. The op-amp will generate a DC current to drive the op-amp inputs to 0 V difference, and the whole system may inadvertently be under steady polarization.

Example: Three-Electrode Intracellular Voltage Clamp

Figure 6.23 shows a similar three-electrode voltage intracellular clamp circuit. A problem with the circuits is that two microelectrodes must be introduced through the cell membrane.

A single invasive electrode may be used, with constant current injection simultaneously with the voltage recording by the same electrode. Electrode polarization will be included in the voltage reading. Here it is also likely that the M and R electrodes are dissimilar and may generate a DC voltage. To diminish this problem a sample-and-hold circuit can be used, so that a reference voltage is read before current is switched on. In current flow mode the sampled reference voltage is subtracted from the instantaneously recorded voltage, and the voltage clamp circuit drives a current necessary to obtain a clamp to the voltage difference.

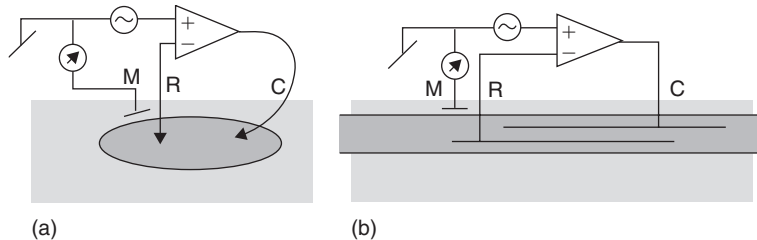


Figure 6.23 Intracellular three-electrode voltage clamp circuits: (a) ellipsoid cell form; (b) nerve cell axon.

6.6.2 Four-Electrode (Tetrapolar) Systems

If the effect of the zones proximal to the current carrying electrodes and the polarization impedance of the electrodes themselves are to be reduced, the four-electrode system is preferred. Such four-electrode systems correspond to a *two-port, four-terminal network* equivalent (cf. Section 7.1). Since there are two ports, these systems actually measure *transfer parameters* between the ports. This means that if, for instance, impedance is measured to 0Ω , this does not necessarily imply high conductivity tissue, but rather no signal transfer from CC to PU electrodes.

Example: In Vitro Tube

An *in vitro* example is shown in Fig.6.23 with a tube filled with a homogeneous electrolyte. The PU electrodes are recessed and connected to the tube via two salt bridges. Let us calculate the transfer signal from eq.6.36, and call the cross-sectional area of the tube A and the distance between the

equipotential surfaces of the PU electrodes L. From the geometry we consider the current density \mathbf{J}_{CC} uniform with a direction parallel to the tube axis \mathbf{z} . With $\hat{\mathbf{z}}$ as the unity vector $\mathbf{J}_{CC} = \hat{\mathbf{z}}i/A$. The reciprocal current density field \mathbf{J}'_{reci} is not easily found as the PU electrodes are connected to the tube with salt bridges. However, under the condition that the equipotential lines of the salt bridges have the same potential as the electrodes, these lines can be represented by thin metal plates, and the reciprocal excitation can be applied to those. We consider that the current flows only between the plates so that $\mathbf{J}'_{reci} = 1/A$. The integrand of eq.6.36 is accordingly $\rho(i/A)\hat{\mathbf{z}} \cdot \hat{\mathbf{z}}/A = \rho(i/A)$. With the reciprocal current density outside the plates equal to zero the volume of integration is restricted and $dv = AL$. Therefore $u = i \rho L/A$ and the transfer resistance according to eq.6.39 is $R_{tr} = \rho L/A$.

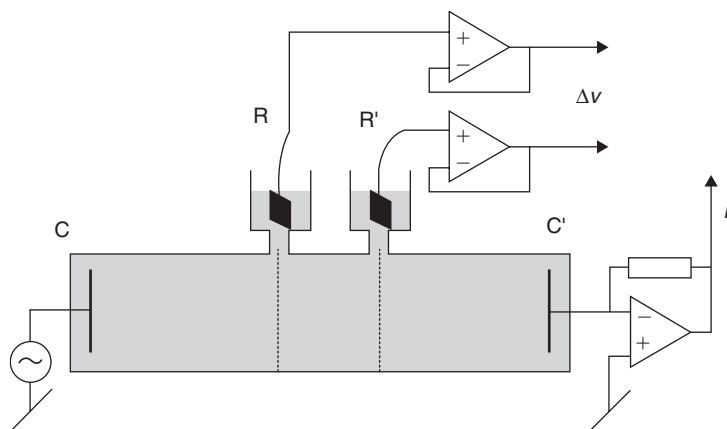


Figure 6.24 Four-electrode system, tubular in vitro version.

Current is recorded with a current reading operational amplifier. The PU electrodes are connected to one buffer amplifier each. No current is flowing in the electrode leads, and the electrodes can therefore not be externally polarized (but internal currents may polarize them, see below). Electrolyte/salt bridge connections are used in order to be able to increase the electrode metal area to increase electrode admittance and reduce noise (Fig. 6.24).

Large electrodes directly into the measuring cell will disturb ionic current flow pattern, and polarization will occur on the metal surface. The electrode metal should not be in direct contact with the electrolyte, but should be recessed (Fig. 6.25). The electrolyte is contained in a tube with isolating walls, and if a part of this wall is substituted by electrode metal, the current will prefer the high conductivity path of the metal. The current lines will deviate from the path parallel to the tube walls, and in one part of the area the current will enter, in the other part it will leave. Thus

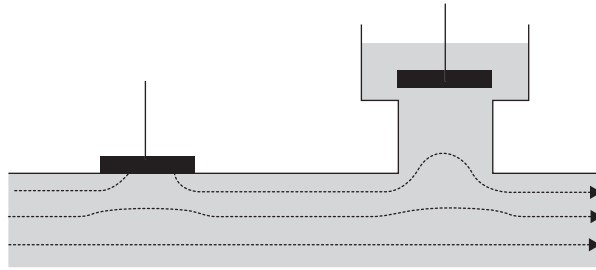


Figure 6.25 The non-recessed electrode to the left implies polarization from the current entering and leaving the metal.

the electrodes *are* polarized, but not by a current in the external leads. The polarization may not be uniform over the electrode surface area, and the polarization will occur according to local current direction and polarization admittance. When the metal is recessed, the current will also deviate into the electrolyte of the bridge path, but the current will not pass any metal surface, and no polarization will occur.

In Vivo Example 1

Figure 6.26 shows a four-electrode in vivo skin surface version. The two recording electrodes define to a certain extent the measured segment. When the geometry is analyzed with eq. (6.39) it will be seen that the sensitivity is negative in the zone between the M and R electrodes and positive between the R and R' electrodes. The zones are not sharply delimited, and it is only the sensitivity field together with the resistivity distribution which gives all necessary information about the contribution of each voxel. There

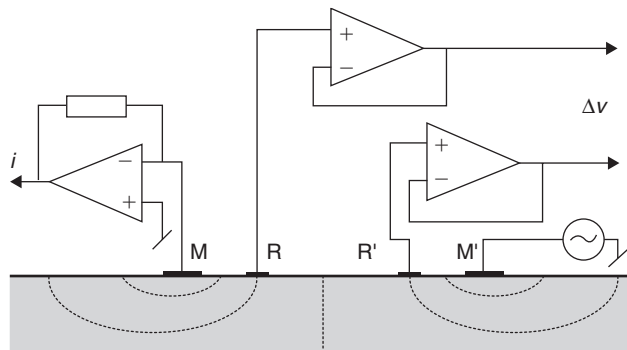


Figure 6.26 Four-electrode system, in vivo version. Equipotential lines dotted. The position of R-R' determines the tissue segment measured and the size of the proximal zones measured by M and M'.

is, for example, no contribution from voxels where \mathbf{J}_{rec} and \mathbf{J} are perpendicular to each other.

To reduce the proximal zone contribution, and sometimes for anatomical reasons, it may be advantageous to place the R electrodes *outside* the M electrodes, instead of inside as shown in Fig. 6.26. If the system is linear, transfer immittance should be the same if the CC and PU electrodes are swapped (cf. the reciprocity theorem).

In Vivo Example 2

Fig 6.27 shows an in vivo transfer impedance spectrum obtained with four electrodes positioned on the forearm.

The spectrum shows two dispersions plus an inductive dispersion which drives the phase positive at 1 MHz (Fig. 6.27). Both the current density field, \mathbf{J}_{CC} and the reciprocal lead field \mathbf{J}'_{CC} of the pick-up electrodes, are unknown.

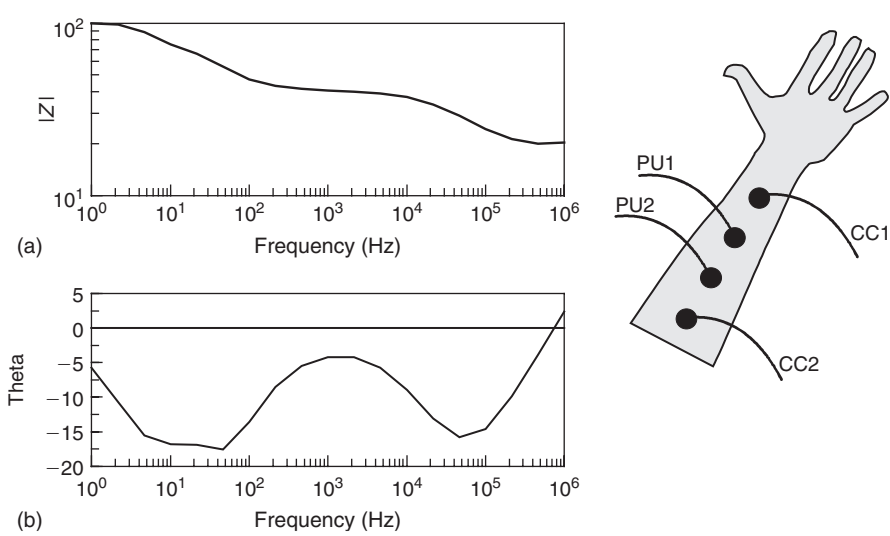


Figure 6.27 Transfer impedance frequency spectrum from forearm.

6.7 FINITE ELEMENT METHOD (FEM)

Maxwell's equations are discussed in Section 8.2.1. Any problem in regard to the distribution of current or electric field in a homogeneous or composite material can be solved with these equations if the excitation and electrical properties of the materials are known. There are in general two different types of problems to be solved in

differential equations, *initial value* problems and *boundary value* problems. Initial value problems arise when the values of the unknowns are given at a particular point, for example at a given time, and the values at future times are to be computed. Boundary value problems arise when the values on the boundary of a material are known, and the values of the interior are to be computed. The latter is a common situation in bioimpedance research where, for example, the current distribution in tissue is to be computed from a given excitation from surface electrodes.

Since the differential equations that describe the behavior of our system, in this case the Maxwell equations, basically describe an infinite-dimensional object, we must use a finite-dimensional approximation to represent the solution. There are two main forms of such approximation: *finite differences* and *finite elements*. In the finite difference method, the differential equation describing the continuous change of the values can, for example, be replaced with an approximation describing the slope of change between a finite number of discrete points, called mesh points.

The FEM involves dividing the modeled geometry into small subregions called elements. The unknown solution is then expressed as the weighted sum of basis functions, which are polynomials in each element. The differential equation is then used in each element to compute the weight used for the basis function of that particular element in the total sum. Each calculation introduces a small error but the errors will in the ideal case diminish as the number of points or elements is increased. There is no guarantee however, for some ill-posed problems, that the sum of an increasing number of diminishing errors will not have a large effect. It is therefore highly recommendable to verify any algorithms or computer software of the sort before use by first solving similar problems that have an analytical solution.

Earlier in Chapter 6 we have treated some simple electrode/tissue geometries with mathematical analytical solutions. Of course, tissue morphology and composition is so that analytical solutions most often cannot be found. It is therefore necessary to take a more engineering approach: to make a realistic geometrical model of the tissue and electrode system, immittance distribution is included. Then let a computer calculate current density vectors and equipotential lines on the basis of a chosen mesh.

In principle, the computer programs may calculate complex 3D models with frequency-dependent tissue parameters. However, the computing time may be long, and accordingly time consuming to experiment with the model. It is important to define the problem in the simplest possible way, and in a way adapted to the software used. If the 3D problem can be reduced by symmetry to two dimensions, and if a DC/purely resistive problem definition can be used, results are more easily obtained (Fig. 6.28).

In Fig. 6.28(a) we see a conducting rectangle with a circular area of higher conductivity placed inside the rectangle. The arrows inside the rectangle are current densities calculated by means of the FEM. The results show how current is attracted to the area of higher conductivity. In Fig. 6.28(b), a diagonal slice of the circular area has the same conductivity as the rest of the rectangle, while the remaining part of the circular area has lower conductivity. It is now obvious how the current is attracted to the well conducting channel, and that the direction of the current in this channel, due to the geometry of the medium, is different from the main current direction.

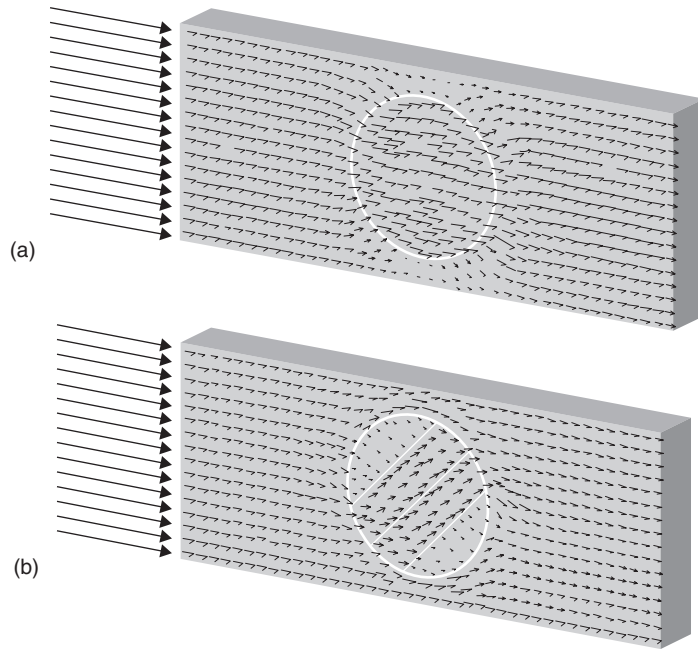


Figure 6.28 Current density field in a uniform medium, disturbed by a homogeneous but well conducting cylinder (a), and an anisotropic cylinder (b). Both models bend the lines of the current density and the \mathbf{E} -field, but in the homogeneous cylinder the \mathbf{E} -field direction is the same as the externally applied field (Knudsen, 1999).

This simple example elucidates a general problem discussed by Plonsey and Barr (1982). In their study of the four-electrode technique utilized in cardiac muscle conductivity measurements, they point out that one does not directly measure conductivity along each axis in turn when measuring along the x -, y - and z -axes. Due to anisotropy the current will not necessarily follow the direction of the measured axis and hence, the measured electrical properties will be influenced by the conductivity in all directions. Plonsey and Barr (1982) used an anisotropic *bidomain* (considers both intracellular and interstitial conductions) model and showed that if the ratios of intracellular to interstitial conductivity are equal along each of the three coordinate axes, then all six conductivities can be calculated from measurements along the three axes.

6.8 TOMOGRAPHY (EIT)

A mapping of the immittance distribution in a tissue layer (tomography) or a tissue volume is possible with a surface multiple electrode system. In electrical impedance tomography (EIT), current (about 1 mA) is typically injected into one electrode pair and the voltages between other electrodes are recorded (Rosell et al., 1988b).

Current injection is then successively shifted so that all electrode pairs are used. The reciprocal theorem will be a sort of a control of system linearity. A frequency in the order of 50 kHz is commonly used, so a complete set of measurements with, for example, around 50 electrodes can be performed in less than 0.1 s. The images obtained have a resolution of about 1 cm at 10 cm tissue depth.

One of the fundamental problems of anatomical imaging based on single frequency impedance measurements is that the absolute impedance is difficult to determine accurately because of the uncertainty in the position of the electrodes. Impedance imaging has hence until recently mainly been concerned with impedance changes due to physiological or pathological processes. With the introduction of multifrequency EIT, the possibility of tissue characterization based on impedance spectroscopy has been realized (Riu et al., 1992, 1995). If the frequency response varies significantly between different organs and tissues, it will be easier to achieve anatomical images because the images will be based on characteristic changes of impedance with frequency rather than the absolute value of the impedance. Indexes such as the relation between measured data at two frequencies may be used, but, because of the differences in characteristic frequencies for the dispersions of different tissues, it has been proved difficult to choose two frequencies to match all types of tissues. Hence, typically 8–16 frequencies are used. Brown et al. (1994a) used seven frequencies from 9.6 kHz to 614 kHz in a 16-electrode thorax measurement and computed from the measured data several parameters from a three-component electrical model. They also adapted the measured data to the Cole impedance equation (see Section 8.2.7). Indexes were furthermore made by using the 9.6 kHz data as a reference and they concluded that it may be possible to identify tissues on the basis of their impedance spectrum and the spectrum of the changes in impedance. Blad (1996) proposed another approach in a preliminary study on imaging based on the measurement of characteristic frequency.

In principle, the method of mapping tissue immittance distribution is not limited to a slice. By increasing the number of electrodes, volume acquisition is equally possible. One of the potential benefits from 3D EIT is that it could take into account the fact that the current spreads out of the imaging plane of 2D EIT. However, the complexity of both the EIT hardware and software will increase considerably by introducing this third dimension. Some important achievements in the pursuit of 3D EIT were, for example, presented in Nature in 1996 (Metherall et al., 1996).

Typical EIT systems involve 16–32 electrodes in any one plane and operate at frequencies between 10 kHz and 1 MHz. The Sheffield Mark III system (Brown et al., 1994a,b) uses 16 electrodes and injects current and measures potential drop between interleaved neighboring electrodes in order to reduce cross-talk (Fig. 6.29). It measures on frequencies between 9.6 kHz and 1.2 MHz and use a current of 1 mA p-p. A total of 64 measurements are made at each frequency when driving odd numbered electrodes and measuring at even numbered electrodes.

As explained in Sections 6.5.4 and 9.2.3, the sensitivity of the measurement to a given local change in admittivity is given by the dot product of the current density vectors resulting from injecting current through the two pairs of current and potential

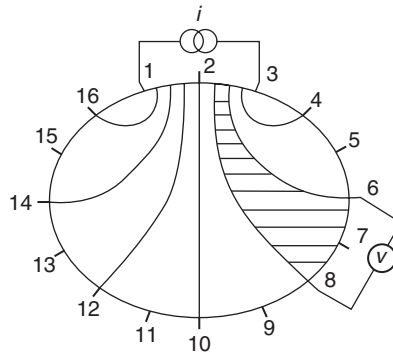


Figure 6.29 Applying current and measuring potential difference between interleaved electrodes in a homogenous medium.

electrodes, respectively. The sensitivity may be highest close to the current injecting or potential pick-up electrodes and lowest toward the center of the medium, depending on the size of the electrodes and the distance between them.

Some of these problems have also been addressed by the adaptive current tomographs (ACT) systems of the group at Rensselaer Polytechnic Institute (Gisser et al., 1987). They have built 32- and 72-electrodes systems with as many independently controllable sources as electrodes. This allows all electrodes to excite the unknown region. Measurements are also obtained from all electrodes simultaneously. This scheme allows many different patterns of current to be applied, some of which have low spatial frequencies, which are relatively insensitive to small errors in electrode placement. It also permits higher current densities in the body interior without excessive currents at any skin site, increasing the distinguishability of small inhomogeneities at greater depth from the electrodes. Isaacson has shown how to generate the best sets of current patterns to apply to the unknown region.

Recent work of this group has focused on imaging breasts using radiolucent electrodes attached to a mammography machine (Kao et al., 2007; Saulnier et al., 2007). This allows accurate control of electrode placement, which is important for making static images. The reconstruction algorithms designed by Isaacson permit static image reconstruction with good fidelity. The algorithms also reconstruct a full 3D volume in a few slices of tissue between the electrode planes. The system now used is a 72-electrode system capable of imaging at seven frequencies in the band from 3.3 kHz to 1 MHz, acquiring and displaying all seven images in 6 seconds. Off-line analysis of these spectra has developed a scheme that can distinguish malignant tissue from normal and benign abnormalities with promising sensitivity and specificity.

Contactless data acquisition techniques are also utilized in EIT. Such systems may involve coils for inducing currents and electrodes for measuring voltage, or they may be totally contactless when magnetic coils or capacitive coupling are used both for the current excitation and for measuring the voltage response (Scaife

et al., 1994; Gencer and Ider, 1994). Tozer et al. (1998) described a system where currents at 10 kHz, 100 kHz and 1 MHz are passed axially in the body (between head and feet) and the resulting magnetic field in the body is measured by means of small search coils. The measured magnetic fields are related to current distribution by the Biot–Savart² law, which, among other things, states that the intensity of the magnetic field set up by a current flowing through a wire is inversely proportional to the distance from the wire. Korjenevsky and Cherepenin (1998) presented an all-magnetic system that comprises coils both for inducing current and for measuring voltage. Their system works in the frequency range 10–20 MHz and measures phase shifts between excitation and response, which is found to be proportional to the integral of the conductivity of the medium. The high frequency typically used for such all-magnetic systems have, however, so far reduced their clinical utility.

This has been challenged by the Graz group, which is developing both hardware and image reconstruction algorithms for simultaneous multifrequency magnetic induction tomography (MIT) at a low frequency band (50 kHz to 1 MHz) (Scharfetter et al., 2003; Hollaus et al., 2004). The latest system consists of 16 transmitter coils and 16 planar gradiometers as receiver coils with an analog bandwidth of 50 kHz to 1.5 MHz, which covers a good part of the β -dispersion of many tissues (Rosell et al., 2001). At each acquisition time 8 of the 16 excitation coils are simultaneously driven by individual power amplifiers with up to 3 A_{ss} at multiple frequencies. These amplifiers are configured as current sources so that every coil termination is high enough so as not to perturb the field of all other coils. For encoding the excitation coils their individual carrier frequencies differ by 200–500 Hz. In this way every excitation frequency is split into eight subcarriers within a bandwidth of 1.6–4 kHz so that they can be approximately considered as a single peak in the comparatively flat tissue spectrum. The theoretical acquisition speed is up to 10 frames/s. Image reconstruction is carried out either from state differential or from frequency differential datasets with a regularized one-step Gauss–Newton approach (Merwa et al., 2003; Scharfetter et al., 2006a,b; Brunner et al., 2006). Iterative solutions have been tested but not yet evaluated with real data.

Cross-talk is by no means the only instrumentation problem experienced in EIT. Rosell and Riu (1992) discussed the significant common-mode voltage sensed by the potential measuring electrodes. They proposed a method called common-mode feedback and obtained an improvement of 40 dB in the measurements at frequencies up to 10 kHz. Bragos et al. (1994) designed wideband single and floating current sources for EIT based on current-mode components and with DC feedback, and the effect of electrode size on images of different objects in saline tanks was described by Newell et al. (1998).

The methods for constructing images from immittance measurements may be divided into *single-pass* and *iterative* processes. In single-pass methods, a single

²Jean-Baptiste Biot (1774–1862) and Félix Savart (1791–1841). French scientists. Biot was author of “Traité élémentaire d’astronomie physique” (1805) and accompanied J.-L. Gay-Lussac in 1804 on the first balloon flight undertaken for scientific purposes.

mathematical operation is performed on the measured data. Although the conceptual simplicity of the method makes it unsuitable for static imaging where the images are based on the absolute immittance values measured, it works well for dynamic imaging where the images are based on changes in the time or frequency domain. Single-pass methods can be further divided into backprojection and sensitivity matrix methods. Backprojection is a commonly used technique in X-ray computer tomography (CT) imaging where the values of a measured profile are distributed in pixels through the thickness of the object and the accumulated value in each pixel after profiles has been measured in different angles and is used for imaging. A high-pass filtering technique is also normally used on the image to reduce artificial blurring of the contour of the organ produced by the backprojection. The sensitivity matrix is the matrix of values by which the conductivity values can be multiplied to give the electrode voltages. The matrix describes how different parts of the measured object influence on the recorded voltages due to the geometrical shape of the object. The sensitivity matrix has to be inverted in order to enable image reconstruction. This operation is not uncomplicated and many techniques have been suggested, cf. Morucci et al. 1994.

Iterative methods are mostly used for static imaging. An intelligent guess of the distribution of, for example, conductivities in the tissue is made initially in the iterative algorithm. The forward problem (see Section 6.1.1) is then solved to calculate the theoretical boundary potentials that are compared to the actual measured potentials. The initial guess is then modified to reduce the difference between calculated and measured potentials and this process is repeated until this difference is acceptably small. The calculation for the boundary potentials may, for example, be performed by means of the FEM (see Section 6.7).

Because of poor resolution, the range of clinical applications has so far been limited. Examples are imaging of gastric function (Mangnall et al., 1987, Smallwood et al., 1994), pulmonary ventilation (Harris et al., 1987), perfusion, brain hemorrhage (Murphy et al., 1987), hyperthermia (Griffiths and Ahmed, 1987; Gersing et al., 1995), epilepsy and cortical spreading depression (Holder, 1992), swallowing disorders and breast cancer (Jossinet, 1996). EIT has also been applied to assess the unilateral pulmonary function with a standard 16-electrode system (Serrano et al., 2002) and also using reduced electrode sets (Serrano et al., 2004). Also tidal volume monitoring seems feasible, at least in healthy volunteers, with better results in men than in women (de Lema et al., 2006; Balleza et al., 2007).

A fundamental difficulty is also the considerable anisotropy found in the electrical properties of, for example, muscle tissue. No satisfactory solution of how to deal with anisotropy in EIT has yet been proposed for anisotropic electrical impedance imaging (see e.g. Lionheart, 1997). The obvious advantages of the method are speed of acquisition and relatively low-priced equipment. Two European concerted action programs on EIT (originally called Applied Potential Tomography) resulted in a high activity research period. This was described in a comprehensive review article by Boone et al. (1997), following the completion of the last program.

Impedance plethysmography is closely related to tomography since both are concerned with the recording of local tissue immittivity variations or distributions.

Impedance plethysmography is the measurement of immittance changes due to respiration or perfusion and is described in more detail in Section 9.2.

6.9 DUALITY OF DIELECTRICS AND CONDUCTORS

A biomaterial can be characterized as a conductor or a dielectric. If the system is linear, the complex conductivity and the complex permittivity contain the same information. It is therefore natural that many of the formulas of dielectrics have their corresponding conductor versions and vice versa. Dual parameters are for instance:

$$\varepsilon \Leftrightarrow \sigma$$

$$\mathbf{D} \Leftrightarrow \mathbf{J}$$

$$q_v \Leftrightarrow I_v$$

where I_v is the current source volume density.

In physics and engineering the duality has its limitations not present in the pure mathematical equations:

It is the problem of *range*: σ' may approach zero (vacuum) and infinity (superconductors), while the lowest value of ε is ε_0 (vacuum) and the highest value at least in living tissue does not approach infinity.

It is a problem with the principle of *superposition*: In electrostatic theory the charge carrier, for example electron or ion, is considered vanishingly small (point charge) so that the field from a single charge is not disturbed by the introduction of a second charge: the fields of several charges can simply be added. To measure exogenic immittivity a current flow is injected into the conductor. The current carrying electrodes cannot have to be points, they must have a certain size in order to limit the current density and the local heat dissipation. Then the introduction of a second electrode may disturb the field from the first electrode, with the consequence that the principle of superposition is no longer valid.

Electrostatic theory deals with the field of one point charge. The other charge of opposite polarity is infinitely far away. This is parallel to the situation with a monopolar CC electrode (Fig. 6.2). With the *electrostatic dipole* we have two charges of opposite polarities separated by a length L and without DC current flow. The current dipole is used in materials with free charge carriers so that DC currents can flow. The dipole moment of an *electrostatic* dipole is $\mathbf{p} = q\mathbf{d}$ (Cm). An *ideal* electrostatic dipole is a dipole where $q \rightarrow \infty$ and $d \rightarrow 0$, keeping the dipole moment constant. Many potential equations are based on the model of point charges and the principle of superposition. The *current* carrying dipole model is defined with two current carrying spheres of radius a separated by a distance \mathbf{d} resulting in a dipole moment $\mathbf{m} = I\mathbf{d}$ (Am). An *ideal* current dipole would then be a dipole where $I \rightarrow \infty$, $a \rightarrow 0$ and $d \rightarrow 0$, keeping m constant. The ideal dipole as a mathematical model is not necessarily problematic, in physics and engineering it is not “ideal,” the concept of current carrying *points* is unacceptable.

PROBLEMS

1. A sphere of radius 1 cm is positioned in an infinite medium of resistivity $1 \Omega\text{m}$.
 - a. Calculate the resistance between the sphere and an infinite large and distant counter electrode.
 - b. Calculate the resistance with a spherical counter electrode at distance 10 cm.
 - c. Calculate the resistance with an infinite area plate counter electrode at distance 10 cm.
2. Consider a large plastic cylinder of diameter 80 cm filled with saline of $\rho = 2 \Omega\text{m}$. In the center is placed an electrical equivalent heart dipole of moment 10 mA cm. Calculate the measured voltage in two pick-up electrodes 10 cm apart, parallel to the heart dipole and at distance 10 cm. Consider the case to be ideal according to Section 6.3.3.
3. Make a comparison between the two-electrode system (resistance of two hemispheres far away from each other according to eq. (6.1) is $R = \rho/\pi a$) and the four-electrode system of eq. (6.35).
4. Find the dipole current of a heart vector with the following parameters given: $u = 1 \text{ mV}$, $L_{\text{pu}} = 0.3 \text{ m}$, $L_{\text{cc}} = 1 \text{ cm}$, $r = 5 \text{ cm}$, $\rho = 2 \Omega\text{m}$. Consider eq. (6.29) is valid.

7 INSTRUMENTATION AND MEASUREMENT

Chapter Contents

7.1 General Network Theory, The Black Box

- 7.1.1 Admittance, Impedance and Immittance
- 7.1.2 The Two-Port Network and the Reciprocity Theorem
- 7.1.3 Reciprocity
- 7.1.4 Extended Immittance Concepts
- 7.1.5 The Non-linear Black Box
- 7.1.6 The Time Constant
- 7.1.7 Kramers–Kronig Transforms

7.2 Signals and Measurement

- 7.2.1 DC, Static Values and AC
- 7.2.2 Periodic Waveforms, Fourier Series of Sine Waves
- 7.2.3 Aperiodic Waveforms
- 7.2.4 Spectrum Analysis, Fourier Transforms
- 7.2.5 Signal Generators
- 7.2.6 The Basic Measuring Circuit
- 7.2.7 Operational Amplifiers and Filters
- 7.2.8 Ground, Reference and Common Mode Voltage

7.3 Bridges, Impedance Analyzers, Lock-in Amplifiers

- 7.3.1 Bridges
- 7.3.2 Digital Lock-in Amplifiers
- 7.3.3 Analog Lock-in Amplifiers
- 7.3.4 Microelectronic Mode Lock-in Amplifiers
- 7.3.5 Impedance Analyzers and LCR-Meters
- 7.3.6 Time Domain Spectroscopy
- 7.3.7 Time Domain Transmissometry
- 7.3.8 Time Domain Reflectometry

7.4 Electrodes: Design And Properties

- 7.4.1 Half-Cell Concept
- 7.4.2 Electronic Conductors
- 7.4.3 Contact Electrolytes
- 7.4.4 Equilibrium DC Properties (Negligible Current Flow)

- 7.4.5 Polarization Immittance (Linear Conditions)
- 7.4.6 Non-linear Conditions (Current Flow)
- 7.4.7 Electrode Design
- 7.4.8 Non-galvanic Coupling to Tissue

7.1 GENERAL NETWORK THEORY, THE BLACK BOX

In many cases we will regard our biological material, together with the necessary electrode arrangements, as an unknown “black box.” By electrical measurement we want to characterize the content of the box (we do not have direct access to the key to open the lid!). We want to use the data to *describe* the electrical behavior, and perhaps even *explain* some of the physical or chemical processes going on in the box, and perhaps discern the electrode and tissue contributions. The description must necessarily be based on some form of *model*, for example, in the form of an *equivalent* electric circuit, mimicking measured electric behavior. We may also want to link properties to distinct tissue parts or organ parenchyma behavior. A basic problem is that always more than one model fit reasonably the measured electric behavior. The equivalent circuit is the tool of the electronic engineers and facilitates their interpretation of the results, simply because they are trained and used to interpret such diagrams. As discussed in Section 8.1, the equivalent model may also go further and be of a more explanatory nature.

The black box may be assumed to “contain” the whole body, a part of the body, just an organ, or just a cell, together with the electrodes. It may also be assumed to contain not the real things, just the *equivalent model circuit* of the tissue of interest.

We will now give a very general description of the black box and how to characterize it electrically, irrespective of the box content. The black box may be considered to contain the real tissue with electrodes for excitation and response measurement, or our model in the form of an electric *network* as a combination of *lumped* (discrete) electrical components. The network may be with two, three or four external *terminals* (cf. the number of electrodes used). A pair of terminals for excitation or recording is called a *port*. The treatment is so general that the content can be characterized with global variables not particularly linked with electrophysiology.

A very general box is the four-terminal type with two ports shown in Fig. 7.1(a). This is the box corresponding to the four-electrode systems described in Section 6.6: two recording electrodes in the electrical field of two current carrying electrodes.

7.1.1 Admittance, Impedance and Immittance

The four external variables of a two-port black box are v_1 and i_1 (first port), v_2 and i_2 (second port). There are four possible ratios: v_1/i_1 , v_2/i_2 , v_1/i_2 and v_2/i_1 . These ratios may be inverted so actually there are eight possible ratios. If the signals are sine waves, most of them have their special names.

If a chosen ratio is current-to-voltage, the ratio is called *admittance*. It is measured in siemens (S), and can be obtained directly by reading current when a constant



Figure 7.1 Black boxes. The two boxes (a) and (b) allow for transfer parameters from one port to the other. Box (c) is a one-port, two-terminal box with only driving point parameters possible.

amplitude AC *voltage* is applied ($Y = iv$). If the ratio is voltage-to-current, the ratio is called *impedance*. It is measured in Ω , and can be obtained directly by reading voltage when a constant amplitude current is applied ($Z = v/i$).

Driving point immittance is defined with excitation and response at the same port (also as a one-port network), *transmittance* is defined with excitation and response at different ports. Transmittance may be transfer admittance or transfer impedance.

Immittance is the general term covering the duality of admittance and impedance.

A *resistor* opposes and limits current flow. This ability is characterized by the resistance R (Ω), or the conductance measured in siemens. If the resistor is considered ideal, the resistance and the conductance are equal for DC and AC irrespective of frequency.

A *capacitor* also opposes and limits current flow. This ability is characterized by the impedance Z measured in Ω , or the admittance measured in siemens. If the capacitor is considered ideal, the capacitance C is considered frequency independent, but the impedance is frequency dependent and for sine waves equal to $1/\omega C$. The impedance is therefore infinite at DC, but lower the higher the frequency.

Putting these two single components together in *series* in a two-component circuit, we obtain a more general expression for the impedance Z in complex form: $Z = R + jX$. Here X is the reactance, for an ideal capacitor $X = 1/\omega C$. For the single component ideal capacitor, $R = 0$.

Putting the two single components together in *parallel* in a two-component circuit, we obtain a more general expression for the admittance Y in complex form: $Y = G + jB$. Here B is the susceptance, for an ideal capacitor $B = \omega C$. For the single component ideal capacitor, $G = 0$.

7.1.2 The Two-Port Network and the Reciprocity Theorem

Generally a two-port, three to four terminal network can be completely defined with four ratios (constants) characterizing the network, and four variables. Here we will introduce two different equation sets:

The *admittance* equation set for a two-port network is:

$$i_1 = Y_{11} v_1 + Y_{12} v_2 \quad (7.1)$$

$$i_2 = Y_{21} v_1 + Y_{22} v_2 \quad (7.2)$$

Driving point admittance Y_{11} or Y_{22} is measured with excitation and response at the same port. The *transfer admittances* Y_{12} and Y_{21} are defined as:

$$Y_{12} = i_1/v_2 \quad (v_1 = 0, \text{ port 1 short-circuited}) \quad (7.3)$$

$$Y_{21} = i_2/v_1 \quad (v_2 = 0, \text{ port 2 short-circuited}) \quad (7.4)$$

The variables v are independent, i are dependent, and both transfer admittances are specified with one of the ports *short-circuited*.

The *impedance* equation set for a two-port network is:

$$v_1 = Z_{11} i_1 + Z_{12} i_2 \quad (7.5)$$

$$v_2 = Z_{21} i_1 + Z_{22} i_2 \quad (7.6)$$

Driving point impedance Z_{11} or Z_{22} is measured with excitation and response at the same port. The *transfer impedances* are defined as:

$$Z_{12} = v_1/i_2 \quad (i_1 = 0, \text{ port 1 open}) \quad (7.7)$$

$$Z_{21} = v_2/i_1 \quad (i_2 = 0, \text{ port 2 open}) \quad (7.8)$$

The variables i are independent, v are dependent, and both transfer impedances are specified with one of the ports *open*.

Conditions

For the network theory presented, there are certain conditions to be met if the theory is to be valid; that the network should be:

1. *Linear*. The immittances must be independent of v or i , both the principle of *superposition* and *proportionality* must hold. Most of the systems of our interest are not linear at DC, but may have a linear amplitude range at AC: sometimes a broader range the higher the frequency.
2. *Passive*. The energy delivered to the network must be positive for any excitation waveform, and all currents or voltages must be zero without excitation. As we know, tissue with electrodes does not fulfill this last requirement; we know for instance that it contains cells with endogenic ionic pumps.
3. *Causal*. The network response must be non-anticipatory, for example, there must be no response before an excitation has been applied. Important in Fourier analysis, for instance the phase response of a capacitive network at the onset of a sine wave excitation. Often phase analysis actually presupposes that the sine wave has been there long before the time of analysis.

In this book all these three conditions are considered to be valid when a system is characterized as *linear*, if not otherwise noted.

A somewhat different measuring principle is to record the voltage at a port, and record the reduced signal as a function of shunting the recording port with different load impedances (Mørkrid et al., 1980).

Many ratios may be formed between the different variables. If the circuit is a current-to-voltage amplifier, the ratio of interest is v_o/i_i , which is a resistance. Such an amplifier is therefore called a *transresistance* amplifier. In a tube or a field effect

transistor, the input voltage controls the output (anode or drain) current, the ratio i_o/v_1 is a *transconductance*.

A *transfer function* of frequency $H(\omega)$, position $H(r)$ is dimensionless and is chosen in order to emphasize signal transmission and not tissue characteristics so directly:

$$H(\omega) = v_2/v_1 \quad (\text{dimensionless}) \quad (7.9)$$

7.1.3 Reciprocity

A network is *reciprocal*¹ if the relationship between excitation and response remains unaltered when the points of excitation and response are interchanged. Then the transfer immittances are equal, $Y_{12} = Y_{21}$ and $Z_{12} = Z_{21}$. Tissue is reciprocal only if it is linear and passive. A network of passive components may be reciprocal, but the insertion of a transistor makes it non-reciprocal. The transistor is a one-direction signal device.

The reciprocity theorem is illustrated in Fig. 7.2. On top is the basic configuration with excitation input to the left and signal output recording to the right. In Reciprocal I voltage is supplied from the right and the current measured at left. In Reciprocal II the voltage source has been replaced by a current source, and the voltage measured at left. Reciprocal I is easier to understand since it copies the electrical parameters of the Direct version. The fact that all four electrodes are current carrying in Reciprocal I makes it less attractive than the Reciprocal II version. The transfer impedance $Z = v/i$ is equal in all these cases.

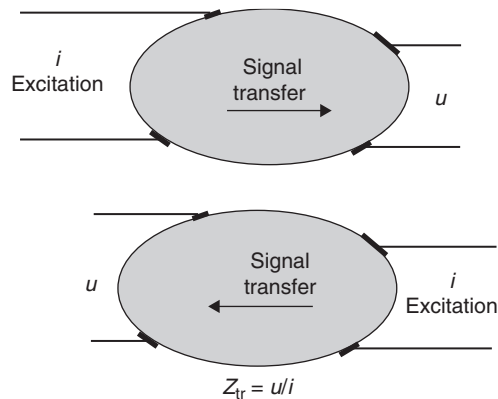


Figure 7.2 Reciprocity.

¹This is the *reciprocity* theorem, and originates from Helmholtz. In mechanical engineering a similar type is known as the *reciprocal* theorem, and originates from Maxwell.

7.1.4 Extended Immittance Concepts

The classical immittance concept is linked to sine waves. The driving point admittance of a black box port is for instance defined as the ratio $Y = i/v$, where v is a sine wave as the independent variable. However, such ratios may be defined also for other waveforms than DC or sine waves. The immittance concept may be extended by the *Laplace²transform*.

By replacing the imaginary frequency variable $j\omega$ by an extended complex frequency variable $s = \sigma + j\omega$ (here σ is not conductivity), it is possible to define, for example, impedance not only in the angular frequency ω -domain, but also in the s -domain. The impedance of a capacitor of capacitance C is, for example, in the frequency domain: $Z(\omega) = 1/\omega C$, and in the s -domain: $Z(s) = 1/sC$. The Laplace transforms of some very important excitation waveforms are very simple: for example, for a unit impulse it is 1, a unit step function $1/s$, a ramp $1/s^2$, etc. That is why the excitation with, for example, a unit impulse is of special interest examining the response of a system. In the extended immittance definition, calculations with some non-sinusoidal waveforms become very simple. Even so, Laplace transforms are beyond the scope of this book.

7.1.5 The Non-linear Black Box

The immittance concept may also be extended for *non-linear networks*, where a sine wave excitation leads to a non-sinusoidal response. Including an immittance value for each harmonic component of the response performs the necessary extension. In the linear region the principle of superposition is valid. This means, for example, that the presence of strong harmonics in the *applied* current or voltage would not affect immittance determination at the fundamental frequency or a harmonic (Schwan, 1963). The lock-in amplifiers used today are able to measure harmonic components, making possible an analysis of non-linear phenomena and extend measurement to non-sinusoidal responses.

In the non-linear region the principle of superposition is not valid. When measuring in the non-linear region, it is necessary to state whether the system uses constant amplitude current (current clamp) or constant amplitude voltage (voltage clamp). With, for example, constant amplitude voltage, the voltage per definition is sinusoidal, but the current is not. If the measuring system is able to measure selectively sufficiently many current harmonic components (and a possible DC component, *rectification*), the actual current waveform in the time domain is defined. Such a steady state non-linear analysis is well suited in the low excitation energy end of the non-linear region. At higher current densities used, for instance, in defibrillator shocks, steady state cannot be obtained (temperature rise and destruction), and all measurements must be performed during one single pulse of energy.

²Pierre Simon de Laplace (1749–1827), French mathematician. Famous for his work on differential equations and on probability, even so an extreme determinist.

7.1.6 The Time Constant

Immittance theory is based on *sinusoidal* excitation and sinusoidal response. In relaxation theory (and cell excitation studies) a *step* waveform excitation is used, and the time constant is then an important concept. If the response of a step excitation is an exponential curve, the time constant is the time taken to reach 63% of the final, total response. Let us, for instance, consider a series RC connection, excited with a controlled *voltage* step, and record the current response. The current as a function of time $I(t)$ after the step is: $I(t) = (V/R)e^{-t/RC}$, the time constant $\tau = RC$, and $I(\infty) = 0$.

However, if we excite the same series RC circuit with a controlled *current* step and record the voltage across the RC circuit, the voltage will increase linearly with time ad infinitum. The time constant is infinite. Clearly the time constant is dependent not only on the network itself, but on how it is excited. *The time constant of a network is not a parameter uniquely defined by the network itself.* Just as immittance must be divided between impedance and admittance dependent on voltage or current-driven excitation, there are two time constants dependent on how the circuit is driven. The network may also be a three- or four-terminal network. The time constant is then defined with a step excitation signal at the first port, and the possibly exponential response is recorded on the second port.

The step waveform contains an infinite number of frequencies, and the analysis with such non-sinusoids is done with Laplace transforms.

7.1.7 Kramers–Kronig Transforms

If the real part of a linear network function of frequency is known over the complete frequency spectrum, it is possible to calculate the imaginary part (and vice versa). There is a relationship between the real and imaginary parts of an immittance (or ϵ' and ϵ''), given by the Kramers–Kronig transforms (KKT). In theory there is no additional information in, for example, the real data when the imaginary data are known. Of course a double data set increases accuracy and makes a control of data quality possible.

KKT are tools brought to network theory by the work of Kramers (1926) and Kronig (1929) on X-ray optics in the late 1920s. Just as the reciprocity theorem, they are purely mathematical rules of general validity in any passive, linear, reciprocal network of a *minimum phase shift* type. By minimum-phase networks we mean ladder networks which do not have poles in the right half plane of the Wessel diagram. A ladder network is of minimum phase type; a bridge where signal can come from more than one ladder is not necessarily of the minimum-phase type. The transforms are only possible when the functions are finite-valued at all frequencies. With impedance $Z = R + jX$ the transforms are:

$$R(\omega) - R(\infty) = \frac{2}{\pi} \int_0^{\infty} \frac{fX(f) - \omega X(\omega)}{f^2 - \omega^2} df \quad (7.10)$$

If we seek DC values, ω is set to zero and we get:

$$R(0) - R(\infty) = \frac{2}{\pi} \int_0^{\infty} \frac{X(f)}{f} df = \frac{2}{\pi} \int_{-\infty}^{+\infty} X(\ln f) d(\ln f) \quad (7.11)$$

$$X(\omega) = -\frac{2\omega}{\pi} \int_0^{\infty} \frac{R(f) - R(\omega)}{f^2 - \omega^2} df \quad (7.12)$$

$$\varphi(\omega) = \frac{2\omega}{\pi} \int_0^{\infty} \frac{\ln|Z(f)|}{f^2 - \omega^2} d(\ln f) \quad (7.13)$$

The frequency of integration f is from 0 to infinite. The resistance or reactance or modulus of impedance $|Z|$ must therefore be known for the complete frequency spectrum. When the frequency range is limited and the number of measurement points is reduced, some error is committed when obtaining one impedance component out of the other (Riu and Lapaz, 1999).

Dealing with one dispersion, the spectrum of interest is limited to that of the dispersion.

With *admittance* $Y = G + jB$ the transforms are:

$$G(\omega) - G(\infty) = \frac{2}{\pi} \int_0^{\infty} \frac{fB(f) - \omega B(\omega)}{f^2 - \omega^2} df \quad (7.14)$$

If we seek DC values, ω is set to zero and we get:

$$G(0) - G(\infty) = \frac{2}{\pi} \int_0^{\infty} \frac{B(f)}{f} df = \frac{2}{\pi} \int_{-\infty}^{+\infty} B(\ln f) d(\ln f) \quad (7.15)$$

The corresponding *permittivity* KKT are:

$$\varepsilon'(\omega) - \varepsilon'(\infty) = \frac{2}{\pi} \int_0^{\infty} \frac{f\varepsilon''(f)}{f^2 - \omega^2} df \quad (7.16)$$

$$\varepsilon''(\omega) = \frac{2\omega}{\pi} \int_0^{\infty} \frac{\varepsilon'(f) - \varepsilon'(\infty)}{f^2 - \omega^2} df \quad (7.17)$$

If we seek static (DC) values, ω is set to zero and we get:

$$\varepsilon'(0) - \varepsilon'(\infty) = \frac{2}{\pi} \int_0^{\infty} \frac{\varepsilon''(f)}{f} df = \frac{2}{\pi} \int_{-\infty}^{+\infty} \varepsilon''(\ln f) d(\ln f) \quad (7.18)$$

Consequently, the area under one dispersion loss peak is independent of the distribution of relaxation times. Equation (7.18) also represents a useful check for experimental data consistency.

7.2 SIGNALS AND MEASUREMENT

7.2.1 DC, Static Values and AC

DC (direct current) is a current flowing in the same direction all the time (*unidirectional* current). The abbreviation “DC” is so much used that it is a common language to say DC current (tautology) and DC voltage (contradictory). A DC may be constant, but may also fluctuate or an AC may be superimposed, as long as the sum never changes direction. Any DC and AC signal may be added, but if the system is *non-linear* the response will not be equal to the sum of the individual signal responses. The DC current may be pulsed, but if the current changes direction in the cycle, it is an AC.

A *galvanic* current is the same as a DC current, and the term is used in particular for therapeutic applications and in electrochemistry. Anode and cathode are not defined from voltage polarity, but current direction. A galvanic (electrolytic) cell produces (passes) DC. If it does not, it is a dielectric cell and only displacement AC passes. Even so an in-phase current may pass the cell, but it is due to dielectric losses and not DC conductance. Thus in-phase components are not the same as DC components.

Stable values are constant values, the term *static* values corresponds to steady state conditions and can be used for a DC potential or voltage, but not so well for a DC current in disagreement with *electrostatic* conditions. In dielectric relaxation theory the subscripts often refer to frequency, for example, D_0 (Section 3.4.2) is the charge density at $f = 0$, that is so long time after the excitation step that the new equilibrium has been obtained and the charging current has become zero. With a single Debye dispersion this low frequency value is called the *static* value (cf. Section 3.1.4). D_0 could therefore equally well have been called D_s , with s for “static.” This is the case for the symbol of permittivity, where low frequency permittivity is ϵ_s , while ϵ_0 is the vacuum permittivity.

AC (alternating current) is a current steadily changing direction. The abbreviation is so much used that it is a common language to say AC current (tautology) and AC voltage (contradictory). We also say constant AC voltage (contradictory), but we mean constant amplitude AC voltage.

DC Compared with a Sine Wave AC with $f \rightarrow 0$

When a sine wave frequency approaches 0Hz, corresponding to a period of, for example, an hour or more, the signal may for a long time be regarded as a slowly varying DC. Strong DC polarization effects may have time to develop at the electrodes, and capacitive susceptance is very small according to $B = \omega C$.

In order to maintain linear conditions in electrolytic systems, the signal amplitude must be reduced to 0 as $f \rightarrow 0$ (cf. Section 2.5.4). Except in the bulk of an electrolyte (cf. eq. 2.2), *DC conditions are therefore virtual unobtainable in electrolytic systems* (cf. also the Warburg impedance concept described in Section 2.5.3). This

is well illustrated with the logarithmic frequency scale, where both infinitely high and infinitely low frequencies are equally off-scale and unattainable. With electronic (not ionic) conduction and ordinary resistors, perfect DC conditions represent no difficulty, and these can therefore only be idealized *models* of electrolytic systems.

7.2.2 Periodic Waveforms, Fourier Series of Sine Waves

A *periodic* waveform repeats itself exactly at regular time intervals (the period T). It is predictive: at any moment in the future we can foresee the exact value. According to Fourier, any periodic waveform can be considered to be the sum of a *fundamental* sine wave of frequency $f_1 = 1/T$, and sine waves at certain discrete frequencies, the *harmonics* ($2f_1$, $3f_1$, $4f_1$, and so on). A periodic waveform is an idealized concept, the waveform is to have lasted and to last forever. At the time we start and stop it, other frequency components than the harmonics appear as transients.

The sine wave is a very special periodic waveform in the sense that it is the only waveform containing just one frequency: the fundamental frequency. Why has just the *sine wave* such special qualities?

It is derived from the circle, Fig. 7.3, it is the projection of a rotating radius (cf. the phasor, Section 11.1.4). If the rotation is steady, the waveform is sinusoidal. A sinusoidal is characterized by its *frequency* f (Hz, periods per second) or the *period* $T = 1/f$ (second). *Angular* frequency ω must be used for trigonometric functions and to emphasize the relationship with the angle of the rotating radius. $\omega = 2\pi f = 2\pi/T$ is the number of rotations (in radians or degrees) per second. T is the time of one complete rotation. $\varphi = \omega t$ is the angle of rotation during the time t . A frequency independent phase shift or a reference value φ_0 may be added: $\varphi = \omega t + \varphi_0$.

If the sine wave is symmetrical around 0, it has no DC component and is described by the equation:

$$v(t) = V_0 \sin(\omega t + \varphi_0) \quad (7.19)$$

$$\int v \, dt = -V_0 \cos(\omega t + \varphi_0) = -V_0 \sin(90^\circ - \omega t - \varphi_0) \quad (7.20)$$

$$dv/dt = V_0 \cos(\omega t + \varphi_0) = V_0 \sin(90^\circ - \omega t - \varphi_0)$$

The time derivative as well as the time integral of a sine wave is also a sine wave of the same frequency, but phase-shifted 90° . The relationship between a sine wave and the circle is seen more directly in the complex notation of a radius \mathbf{r} rotating around the origin in the Wessel diagram:

$$\mathbf{r}(t) = r_0 e^{j(\omega t + \varphi_0)} = r_0 [\cos(\omega t + \varphi_0) + j \sin(\omega t + \varphi_0)]$$

As the time derivative of an exponential is the same exponential, then $\partial(e^{j\omega t})/\partial t = j\omega e^{j\omega t}$. That is why integration and derivation in the equations describing the behavior of electrical circuits can be replaced by algebraic operations with the $j\omega$ instead of the $\partial/\partial t$. *This is under the assumption that all signals are sine waves of the same frequency.*

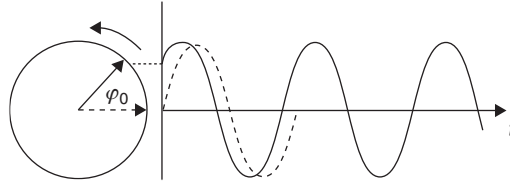


Figure 7.3 The sine wave, with a reference sine wave stippled.

A phasor and a sine wave are given with respect to some reference sine wave. In Fig. 7.3 the reference is stippled, and the waveform of interest *leads* the reference by about 45° .

The peak value is called the *amplitude* V_p , φ is the *phase angle*. To define φ we must define a reference sine wave, for instance the known excitation signal. Although the mean value of a full period is 0, it is usual to quote the mean of half a period: $2V_p/\pi$. The *rms* value is $V_p/\sqrt{2}$.

The Sum and Product of Two Sine Waves

To simplify the equations and the discussions we presuppose two sine waves of *equal amplitude*, symmetrical around zero.

The *sum* of two such sine waves of different frequencies is:

$$f(t) = \sin \omega_1 t + \sin \omega_2 t = 2 \sin \left(\frac{\omega_1 + \omega_2}{2} t \right) \cdot \cos \left(\frac{\omega_1 - \omega_2}{2} t \right) \quad (7.21)$$

The *product* of two sine waves of different frequencies is:

$$f(t) = \sin \omega_1 t \cdot \sin \omega_2 t = \frac{1}{2} [\cos(\omega_1 - \omega_2)t - \cos(\omega_1 + \omega_2)t] \quad (7.22)$$

Case 1: $\omega_1 = \omega_2 = \omega$

With a constant phase difference φ between the sine waves, $\omega_1 t = \omega t$ and $\omega_2 t = \omega t - \varphi$:

$$\text{Sum: } f(t) = \sin \omega t + \sin(\omega t - \varphi) = 2 \cos \frac{\varphi}{2} \sin \left(\omega t - \frac{\varphi}{2} \right) \quad (7.23)$$

The *sum* is as a *pure sine wave* at the fundamental frequency, phase shifted, with double amplitude when $\varphi = 0^\circ$ and zero amplitude when $\varphi = 180^\circ$. No new frequencies appear, in accordance with the law of superposition valid for a linear system:

$$\text{Product: } f(t) = \sin \omega t \cdot \sin(\omega t - \varphi) = \frac{1}{2} [\cos \varphi - \cos(2\omega t - \varphi)] \quad (7.24)$$

This is an important equation, proving the creation of a new frequency in a non-linear system where the laws of superposition are no longer valid. A DC

component and a pure sine wave of double the frequency (second harmonic component) have appeared and the fundamental frequency has disappeared. The equations are illustrated in Fig. 7.4.

Frequency spectrum analysis fundamentals (cf. eq. 7.24 and Fig. 7.4, right hand side)

- The product of two sine waves of equal frequency and phase difference not 90° contains a DC component (Fig. 7.4).
- The product of a sine wave and a cosine wave of equal frequency contains no DC component.
- Thus by multiplying a given signal function with a reference sine wave, the DC component of the product is proportional to the in-phase signal component at the reference frequency.

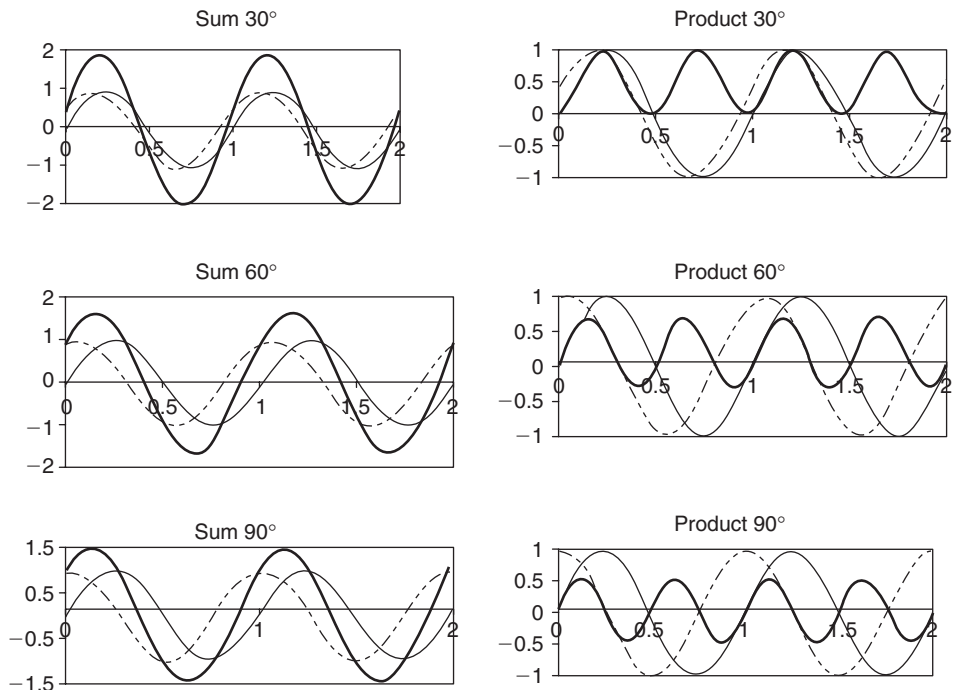


Figure 7.4 Sum and product of two equal amplitude ($=1$), equal frequency sine waves, phase shifted by various amounts: 30° (top), 60° (middle) and 90° (bottom). Notice the DC component of the product (right-hand side). Example is with amplitude = 1 (e.g. volt), $f = 1$ Hz so that the time scale is in seconds.

The low-pass filtered result is a DC voltage proportional to the cosine of the phase difference between the signals, quadrature signals ($\varphi = 90^\circ$) are thus canceled. The peak-to-peak amplitude of the second harmonic component is half the fundamental and independent of the phase.

Equation (7.24) formulates the basis for the lock-in amplifier and frequency spectrum analysis (Fourier analysis). In the lock-in amplifier one sine wave is the stable reference signal supplied by the experimental setup. The other sine wave is the measured response variable, usually containing also other non-synchronized signals and noise.

In tissue and at electrodes, the linear case corresponds to low-level excitation. The non-linear case and the creation of new frequencies correspond to high-level excitation (the non-linearity in the form of multiplication is of course only one possible form).

Input Signal with DC Component

$$f(t) = (V + \sin \omega t) \cdot \sin(\omega t - \varphi) = \frac{1}{2} [\cos \varphi - \cos(2\omega t - \varphi)] + V \sin(\omega t - \varphi) \quad (7.24a)$$

This is a realistic situation because electrodes often generate a DC offset voltage V . Equation (7.24a) shows that the fundamental frequency reappears, but does not contribute to a low-pass filtered output signal. This is because we have a true sinus multiplication. If the reference signal is a square wave as it often is in simpler chopped phase-sensitive rectifiers (cf. Fig. 7.18), the input DC appears also in the output as an error signal.

Case 2: $\omega_1 \neq \omega_2$

$$\omega_1 \approx \omega_2$$

If $\omega_1 \approx \omega_2 \approx \omega$, eqs (7.23) and (7.24) can be used by introducing a slowly varying phaseshift φ .

The most important effect for the *sum* (eq. 7.23) is the corresponding varying amplitude according to the $\cos(\varphi/2)$ factor. The sum is a sine wave of frequency ω with amplitude changing at the low beat frequency $\omega_1 - \omega_2$ from the double value to zero. The new waveform does not contain any new frequencies, and there is no DC component. This is illustrated in Fig. 7.5(a),(b). The curve is contra-intuitive because it may easily be taken as a waveform containing the sum and beat frequencies, which it does not. It is the fundamental sine wave with slowly varying amplitude at the beat frequency 0.125 Hz. The picture is different when the frequency difference is larger (Fig. 7.5(c),(d)). Now it is clearly seen that high frequency sine wave is simply superimposed on the slow sine wave.

In the *product* (eq. 7.24) waveform the DC level changes at the low beat frequency $\omega_1 - \omega_2$ according to the factor $\cos \varphi$. This is a true DC component created by the non-linear effect. However, it has zero mean value over a beat frequency period, and thus does not contribute to a DC component after low-pass filtration.

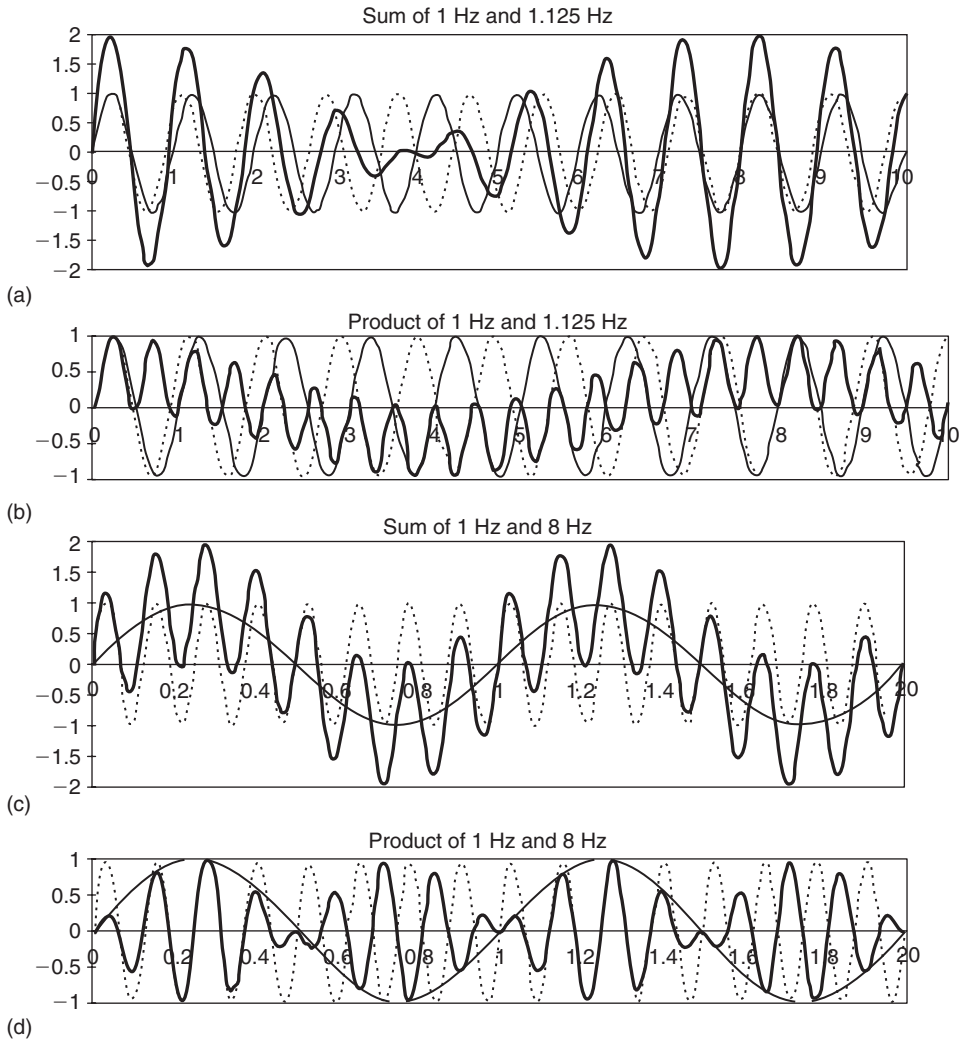


Figure 7.5 Different frequencies. Sum and product of two equal amplitude ($=1$) sine waves: (a),(b) 1 Hz and 1.125 Hz sine waves ($\omega_1 \approx \omega_2$); (c),(d) 1 Hz and 8 Hz sine waves.

The second harmonic component has constant peak-to-peak amplitude but a phase varying at the beat frequency.

Large Difference Between ω_1 and ω_2

Now the discussion is based on eqs (7.21) and (7.22). It is clear from Fig. 7.5(c),(d) that the *sum* waveform is just the 1 Hz and 8 Hz signals with no phase shifts. However, the *product* waveform has a new higher frequency (the sum $8 + 1 = 9$ Hz).

When studying Fig. 7.5(c),(d), the waveform is amplitude modulated with an envelope frequency of 1Hz. The frequency difference component of 7Hz ($8 - 1 = 7\text{Hz}$) is difficult to see.

In radio communication systems the signal with frequency ω_1 is called the carrier and ω_2 the modulation, and $\omega_1 \gg \omega_2$. The amplitude modulated signal from a perfect multiplier under these conditions does not contain the low frequency signal ω_2 , but just the upper and lower sideband frequencies $\omega_1 + \omega_2$ and $\omega_1 - \omega_2$. They are very near to the carrier frequency and can therefore be transmitted through the ether.

It is clear from these discussions that the waveforms in the time domain may be difficult to interpret correctly, and it is the mathematical treatment which gives the correct answers.

The Sum of a Fundamental Sine Wave and Its Harmonic Components: Fourier Series

The only waveform containing just one frequency is the sine wave. A periodic waveform can be created by a sum of sine waves, each being a harmonic component of the sine wave at the fundamental frequency determined by the period. This is illustrated 7.6(a), showing the sum of a fundamental and its third and fifth-harmonic components. It indicates that uneven harmonic components may lead to a square wave, with a precision determined by the number of harmonic components included.

Fig. 7.6(c) shows the frequency spectrum of the waveform. It is a *line* or *discrete* spectrum, because it contains only the three discrete frequencies. Continuously repetitive waveforms have line spectra, their periodicity is composed only of the fundamental and its harmonic components.

Fourier formulated the mathematical expression for the sum of the fundamental and its harmonics. The condition is that a fundamental period of a waveform $f(t)$ can be determined, and that the waveform $f(t)$ is extended outside its defined interval so that it is *periodic* with period 2π :

$$f(t) = \frac{a_0}{2} + \sum_{n=1}^{\infty} (a_n \cos n\omega_1 t + b_n \sin n\omega_1 t) \quad (7.25)$$

where a_n and b_n are the amplitudes of each harmonic component n , a_0 is the DC component, and ω_1 the angular fundamental frequency defining the period 2π .

According to the Fourier series eq. (7.25), any periodic waveform is the sum of a fundamental sinusoid and a series of its harmonics. Notice that in general each harmonic component consists of a sine and cosine component. Of course either of them may be zero for a given waveform in the time domain. Such a *waveform synthesis* (summation) is done in the time domain, but each wave is a component in the frequency domain. The *frequency spectrum* of a periodic function of time

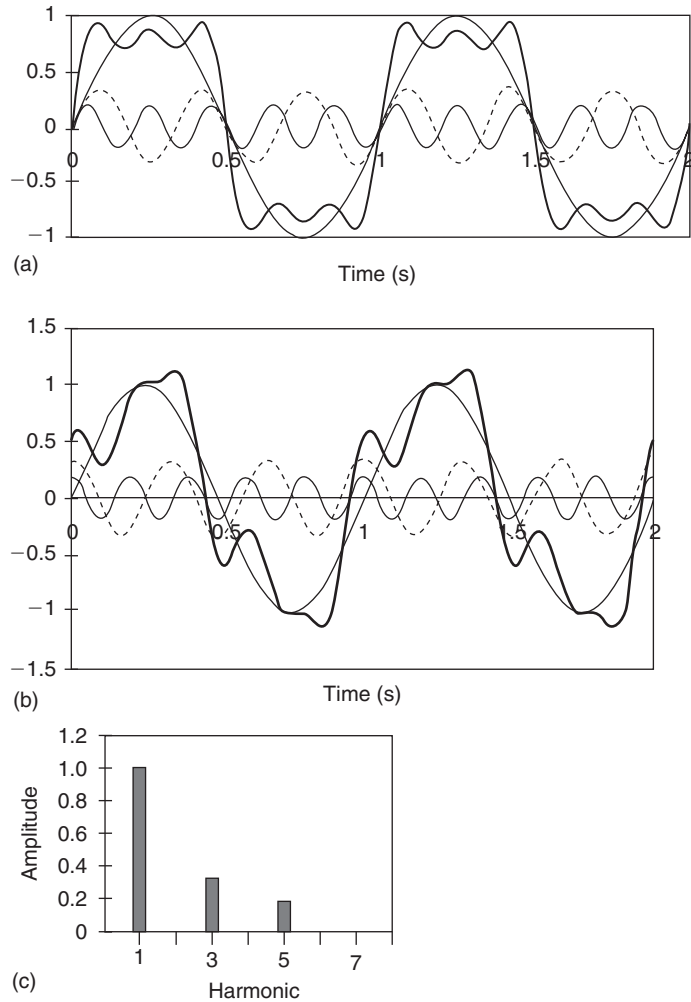


Figure 7.6 Summation of harmonic sine waves, waveform dependence of phase relationships. Amplitude of fundamental sine wave = 1. Time domain: (a) in-phase harmonics, (b) phase-shifted harmonics. (c) Amplitude magnitude line frequency spectrum, equal for both cases.

$f(t)$ is therefore a *line* spectrum. The amplitude of each discrete harmonic frequency component is:

$$a_n = \frac{1}{\pi} \int_{-\pi}^{\pi} f(t) \cos(n\omega_1 t) dt \quad (7.26)$$

$$b_n = \frac{1}{\pi} \int_{-\pi}^{\pi} f(t) \sin(n\omega_1 t) dt \quad (7.27)$$

$$\mathbf{A}_n = a_n + jb_n \quad (7.28)$$

$$A_n = \sqrt{a_n^2 + b_n^2} \quad (7.29)$$

$$\varphi = \arctan(b_n/a_n) \quad (7.30)$$

Because the waveform is periodic, the integration can be limited to the period interval 2π as defined by ω_1 . However, the number n of harmonic components may be infinite. The presentation of a signal in the time or frequency domain contains the same information; it is a choice of how data is to be presented and analyzed.

Figure 7.6 illustrates how two rather different waveforms in the time domain may have the same amplitude magnitude A_n frequency spectrum. The amplitude magnitude frequency spectrum does not contain all necessary information, the phase information is lacking. For each harmonic component both the sine and cosine (eqs 7.26 and 7.27), or the magnitude and phase (eqs 7.29 and 7.30) must be given, a magnitude and a *phase spectrum*. The amplitude \mathbf{A}_n is a vector, therefore amplitude magnitudes A_n cannot just be added as scalars. A given waveform is the sum of only one unique set of sine and cosine harmonics.

An infinite number of harmonics must be added in order to obtain, for instance, a true square wave. The Fourier series for a periodic square wave of unit amplitude is (cf. Fig. 7.6(a)):

$$f(t) = \frac{4}{\pi} \sum_{n=1,3,5,\dots} \frac{1}{n} \sin n\omega_1 t \quad (7.31)$$

This square wave can therefore be realized as the sum of only sine components.

Any waveform with sharp ascending or descending parts, like the square wave or sawtooth, may contain large amplitudes of higher harmonic components. The triangular pulses contain more of the lower harmonics. No frequencies lower than the fundamental, corresponding to the repetition rate, exist. The waveform may contain a DC component, if it is symmetrical around zero the DC component is zero. However, if the waveform is started or stopped, it is no longer periodic, and the Fourier series approach is no more valid.

By using non-sinusoids as excitation waveforms, a system is excited at several frequencies simultaneously. If the system is linear, the response of each sine wave can be added. If the system is non-linear, new frequencies are created influencing the frequency spectrum. The square wave to the left in Fig 7.7 has no DC component. One of the ramps in the middle is used in scanning devices such as polarographs. As drawn, the waveform has a DC component. The pulse to the right has a DC component dependent on the repetition frequency.

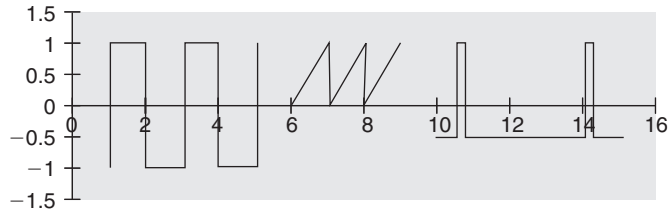


Figure 7.7 Square, ramp and pulse periodic waveforms.

7.2.3 Aperiodic Waveforms

These are the waveforms of bioelectricity, because the repetition rate of, for example, the respiration or the heart is not perfectly periodic.

Single Pulse or Step

A single pulse or a step function excitation is the basis of relaxation theory. Power dissipation and temperature rise may, for instance, impede the use of repetitive waveforms, and single pulse excitation is necessary. A single pulse is a pulse waveform with repetition interval $\rightarrow\infty$, it has a *continuous* frequency spectrum as opposed to a line spectrum. The *unit impulse* (delta) waveform is often used as excitation waveform. It is obtained with the pulse width $\rightarrow 0$ and the pulse amplitude $\rightarrow\infty$, keeping the product = 1. The frequency spectrum consists of equal contributions of all frequencies. In that respect it is equal to white noise (see below). Also, the infinite amplitude of the unit pulse automatically brings the system into the non-linear region. The unit impulse is a mathematical concept, a practical pulse applied for the examination of a system response must have a limited amplitude and a certain pulse width.

What then is the frequency content, for example, of a single rectangular pulse? It can be found from the periodic waveform by letting the period $\rightarrow\infty$. The frequency spectrum $F(\omega)$ of a positive pulse of amplitude A and duration T is:

$$F(\omega) = \frac{2A}{\omega} \sin \omega \frac{T}{2} \quad (7.32)$$

Note that the frequency spectrum as defined by $F(\omega)$ in eq. (7.32) is *amplitude per angular frequency*. Equation (7.32) defines a continuous frequency spectrum, *all frequencies* are present except the discrete frequencies $1/T$. This may be regarded as another way of saying that the periodicity of a single pulse does not exist and it has no characteristic harmonics. All these frequency components must also be a function of time: all components must be zero before the single pulse has arrived (cf. the causality criterion, Section 7.1.2). During and after the pulse the frequency spectrum components build up and decay, with time constants depending on the filters used to record them. Another illustration of a *frequency spectrum as a function of time* is the frequency analysis of speech or music. Biological events do not

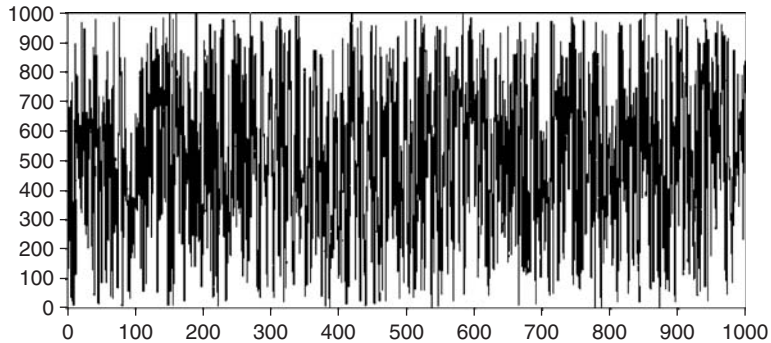


Figure 7.8 White noise in the time domain. One thousand samples of arbitrary numbers between 1 and 1000. Mean (DC) value = 500.

occur strictly periodically, and it is therefore a general need for doing a frequency analysis as a function of time. In order to have good resolution in the time domain the time interval used should be short. But a short time interval makes it impossible to analyze low frequencies. This is the basis for the special short time Fourier transform (STFT) presented by Gabor (1946).

White Noise Waveform

Like the sine wave containing only one frequency, white noise signal is the other extreme containing all frequencies of equal amplitudes. Like the sine wave or unit impulse, white noise is an ideal concept. It is a fractal curve, any enlargement will just bring up similar curves. It is an interesting excitation waveform, because the system is examined at all frequencies simultaneously. White noise is a curve where the value in the future cannot be predicted, there is an equal probability of any amplitude at any moment. Both the unit pulse and white noise are represented by a flat frequency spectrum. However, the ideal unit pulse is of infinite short time duration, while the ideal white noise is of infinite long time duration.

However, because amplitude in any system is limited, we do not have absolute white color of the noise found in a system. Also our total sampling time is limited. The curve in Fig. 7.8 is calculated for a certain time interval Δt . Based on Fig. 7.8, we evidently can say nothing about a possible periodicity for times $>\Delta t$ (frequencies below $1/\Delta t$). In general, any amplitude is possible, noise must therefore be described by a value averaged over a defined time interval. Usually the root-mean-square (rms) value is used. This is practical because noise is related to energy according to Boltzmann, Einstein and the interpretation of Brownian motions (random walks).

Figure 7.8 shows a computer generated curve, and the computer was asked to generate 512 random numbers (periodic samples at the x -axis) of values between 1 and 1000 (amplitude at the y -axis). These choices are related to the graphical limitations of the illustration. Figure 7.8 therefore does not illustrate ideal white noise, because both the number of samples and the amplitudes are limited. The waveform

is somewhat contra-intuitive, because visual inspection may easily give the impression of periodicities.

7.2.4 Spectrum Analysis, Fourier Transforms

Frequency Spectrum (Fourier) Analysis

The *time domain* is well known from daily life experience. It is, for example, the way a signal is recorded as a function of time as an ECG waveform. From the waveform in the time domain the components can be found in the *frequency domain*: a search for periodicity. In the frequency domain we have seen the line spectra of *periodic* signals. But the heart does not beat regularly. The heart rate varies both in a noisy way and by the way it is controlled by nervous and biochemical systems. Making a frequency analysis of an ECG waveform will therefore not give a *line* spectrum, the spectrum will have a more *continuous* character. Regular heartbeats at sleep correspond to more pronounced line spectra than those obtained during variable physical activity. The frequency spectrum of an electronic-driven pacemaker, however, is a line spectrum. A periodic waveform occupies a line spectrum, an aperiodic waveform occupies a continuous frequency spectrum.

There are several ways of finding the frequency spectrum of a time domain waveform, periodic or aperiodic. By sending the signal into a filter bank, the output of each filter represents the signal content as a function of time (both frequency and time domain!) within the frequency passband of the filter. The result is not optimal because the output of each filter is an amplitude magnitude, the phase information is lost. In Section 7.2.2 we have just shown that by multiplying the waveform to be analyzed by a sine wave, the DC value of the result indicates the amplitude content at that frequency. By multiplying also by a 90° phase-shifted signal, information about the phase relationships in the waveform may also be obtained. This must be repeated at each frequency of interest, and therefore is a slow procedure. Instead of these analog methods, the signal can be digitized and treated by a mathematical algorithm called a fast Fourier transform (FFT). In such ways the frequency content can be extracted, this is the Fourier³ or spectrum analysis. Such an analysis is a search for periodicities in a waveform.

The Fourier *series* with discrete harmonics were introduced in Section 7.2.2. Mathematically the Fourier *transform* of a function (periodic or non-periodic) in the time domain $f(t)$, to the corresponding function in the frequency domain $f(\omega)$, is described by:

$$F(\omega) = \int_{-\infty}^{\infty} f(t)e^{-j\omega t} dt \quad (\text{to frequency spectrum from time domain}) \quad (7.33)$$

³Joseph Fourier (1768–1830), French mathematician. Participated as scientist in the Napoleon military expedition in Egypt 1798–1801.

The inverse Fourier transform is then:

$$F(t) = \int_{-\infty}^{\infty} F(\omega)e^{j\omega t} d\omega \quad (\text{to time domain from frequency spectrum}) \quad (7.34)$$

Note that by multiplying by the complex expression $e^{j\omega t} = \cos \omega t + j \sin \omega t$, both the in-phase and quadrature components, and thus the phase information is taken care of. When dealing with signals defined, for example, as volt, $F(\omega)$ represents the signal distributed in the frequency spectrum: the *density of signal amplitude per frequency bandwidth*. The unit may be, for example, $\mu\text{V/Hz}$. In general there will be two spectra: one in-phase spectrum and one quadrature spectrum, or one amplitude spectrum and one phase spectrum. Thus $F(\omega) = F'(\omega) + jF''(\omega)$, or $|F(\omega)| = |F(\omega)|e^{j\phi(\omega)}$, and $|F| = (F'^2 + F''^2)^{1/2}$. Because of the phase dependence, the amplitudes at each frequency are not simply additive.

Equation (7.33) is the integral, and thus a more general form of eq. (7.25). The integral form can, for example, be used for periodic signals when the pulse interval $\rightarrow \infty$, that is for a single pulse (eq. 7.32). Note also the non-realistic integration over the complete frequency spectrum from $-\infty$ to $+\infty$, and that the frequencies are not limited to the harmonics. As we have seen, the integration interval is not a problem with periodic waveforms, the waveform can easily be extended without limitation. With aperiodic waveforms, approximations introducing errors must be made, see below.

According to eq. (7.33), there may be a non-zero signal density at any frequency, thus a *continuous spectrum* is possible. With periodic waveforms only *line spectra* were possible and this is illustrated in Fig. 7.9.

The *energy* of a waveform pulse is proportional to the square of voltage or current in a time interval. According to Plancherel's theorem (a special case of the more general Parseval's theorem⁴), the *energy* corresponding to an ideal resistor and a voltage or current waveform $f(t)$ computed in the time domain is equal to the energy computed in the frequency domain:

$$\int_{-\infty}^{\infty} f^2(t) dt = \int_{-\infty}^{\infty} |F(\omega)|^2 d\omega \quad (7.35)$$

For steady state conditions the integral diverges and *power* (energy per time interval) spectra are used. Note that the magnitude $|F(\omega)|$ used in eq. (7.35) implies that the information contained in the phase relationships is lost in the power spectrum. Or stated more positively, power spectra are not sensitive to phase relationships and values may just be added.

When dealing with power spectra related to, for example, rms voltage v_{rms}^2 according to $W = v_{\text{rms}}^2/R$, $|F(\omega)|^2$ represents the distributed power spectrum: the *density of signal power per frequency bandwidth*. The unit for $F(\omega)$, for example

⁴Parseval des Chênes (1755–1836), French mathematician. Forced to flee France after writing poems critical to the Napoleonic government.

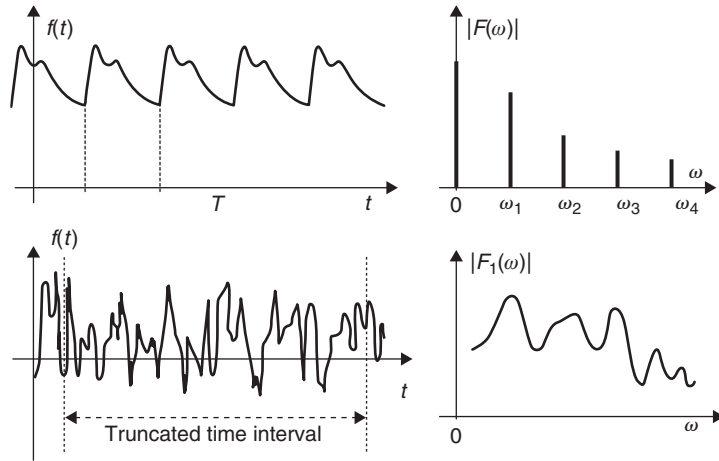


Figure 7.9 Top: Periodic waveform with a line harmonic frequency spectrum. Bottom: Non-periodic waveform has a continuous frequency spectrum. Line spectrum amplitude [volt]. Continuous spectrum amplitude [volt \sqrt{sec}].

when dealing with noise spectra, may be $\mu V_{\text{rms}}/\text{Hz}$. When the spectrum is plotted with amplitude per $\sqrt{\text{Hz}}$ on the y -axis and frequency on the x -axis and scaled so that the area under the $F(\omega)$ curve is equal to the total rms value in the time domain (Plancherel's theorem), the spectrum is called a *power density spectrum*. A less stringent definition is simply that a spectrum is called a *power spectrum* when the function is squared before analysis.

Aperiodic Signal in a Limited Time Interval

With a recorded waveform, we generally must assume that it represents the sum of non-synchronized aperiodic signals, for example, from exogenic sources and endogenic activities such as respiration, peristaltic movements, heart beats and nerve activities. In addition, there may be wideband noise and noise at discrete frequencies, for example, from the power line 50 or 60 Hz fundamentals.

In a practical case, the waveform to be analyzed must be of a limited time duration. This is particularly clear when the analog signal has been digitized for computer analysis. Thus a long-lasting waveform must be *truncated* with a finite sampling time. Errors are introduced when such a waveform is analyzed, because the Fourier transform (eq. 7.33) presupposes that the integration interval is infinite. When the end value (trailing edge) is not equal to the start (leading) value, the abrupt change of level corresponds to high frequency components introduced by the truncation. Generally truncation results in sharp discontinuities in the time domain, and the additional frequency components in the frequency spectrum are called *leakage*.

To reduce the leakage effect, the signal can be amplitude weighted around the leading and trailing edges, so that the signal starts and ends near zero value. A Hanning or Blackman truncation function is often used for this purpose.

The truncated time interval also defines the lowest frequency that can be analyzed, nothing can be said about sine wave components with half-periods longer than the time analyzed.

In conclusion the truncation introduces errors due to leakage, and the (totally sampled) interval limits the lowest frequency analyzed. In addition, the limited sampling frequency may also introduce errors when an analog waveform is to be digitized. The sampling frequency must be higher than twice the highest frequency to be analyzed (*Nyquist criterion*). If this is not the case, *aliasing* errors (frequency folding) are introduced. If the sampling frequency cannot be increased, the signal must be low-pass filtered before analysis, so that the Nyquist criterion is met for all signal components reaching the analyzer.

Correlation and Convolution

In electroencephalogram (EEG) waveforms, it may not be easy to visually estimate whether there is interdependence between the waveforms from two different leads. *Correlation* analysis is used to find common periodicities of two functions (waveforms) $f_1(t)$ and $f_2(t)$. We have seen that if we multiply two sine waves of the same frequency, the DC value of the product is proportional to the cosine of the phase difference φ between them (eq. 7.24). We can therefore calculate the product as a function of delaying one of the waveforms with respect to the other, and look for maxima corresponding to $\varphi = 0$. Mathematically, for each time t , the correlation value $c(t)$ can be found by summing up the products of one of the waveforms and a time displaced version of the other:

$$c_{\text{cor}}(t) = \int_{-\infty}^{\infty} f_1(\tau)f_2(t + \tau) d\tau \quad (7.36)$$

The correlation will be maximal if one signal can be displaced with respect to the other until they fluctuate together. The correlation function $c(t)$ will be a more or less noisy sine wave symmetrical around $t = 0$. The decay of the amplitude envelop from $t = 0$ indicates the degree of correlation: the slower the decay, the higher the correlation. If $f_1(t) = f_2(t)$, *autocorrelation* is done by delaying a copy of the function itself and performing the integration of eq. (7.36). The process will be much the same as a Fourier analysis, a search for periodicity.

For the sake of completeness, the *convolution* transform shall also be mentioned because it is so closely related to crosscorrelation:

$$c_{\text{con}}(t) = \int_{-\infty}^{\infty} f_1(\tau)f_2(t - \tau) d\tau \quad (7.37)$$

The plus/minus sign in the integrand is the only difference between the integrals of crosscorrelation and convolution. Convolution is a powerful mathematical tool strongly related also to the Fourier transform. By performing a usual logarithmic transform, a multiplication is simplified to a summation, and then the anti-logarithmic

transform brings up the result. In a similar way, *convolving* two functions in the time domain corresponds to a *multiplication* of the same functions in the frequency domain. The convolving action implies a folding in the frequency domain, represented by the term $(t - \tau)$. In the integrand of the correlation transform there is no folding process in the term $(t + \tau)$.

Signal Averaging

If a synchronization signal is available from the stimulus source, special noise reducing techniques are available. The response of an organism to a stimulus is called an *evoked potential* or *event-related* signal. The technique is somewhat similar to the principle of a lock-in amplifier (Section 7.3). By recording the response as a function of time after a stimulus, store it, repeat the stimulus many times, each time sum the response with the last sum, we gradually increase the signal to noise ratio (SNR). Non-synchronized waveforms will cancel out in the long run. It can be shown that the SNR increases with \sqrt{N} , where N is the number of stimuli (cf. eq. 7.45 in Section 7.3.2). The SNR limits are related to the variability of the responses, both with respect to amplitude and time. Applications are, for example, within hearing, brain stem evoked potentials, EEG with visual stimuli, electrodermal response (EDR).

Other Forms of Signal Processing

- An important *time domain* analysis method is the *probability density function* of finding a certain signal amplitude value. This is simply histograms of the amplitude window values versus the number of counts in each amplitude window.
- Recording the number of *zero crossings* per time interval.
- *Bispectral* analysis. Instead of phase spectra obtained in Fourier analysis where the phase relates to the start of the epoch, the bispectrum correlates the phase between different frequency components. Used in EEG.
- *Wavelet analysis*. This is treated in Section 8.4.5.

7.2.5 Signal Generators

The Constant Amplitude Voltage Output (Voltage Clamp)

From the mains and our use of batteries we are well acquainted with the constant amplitude voltage supply. The ideal voltage supply has zero internal resistance. It supplies the set voltage from no load (load resistance ∞ , open circuit) to full load (minimum load resistance and maximum current). Two ideal voltage sources cannot be coupled in parallel. In series the voltages are added.

With $V = \text{constant}$, Ohm's law $I = V/R = VG$ shows that the current is proportional to G , not to R .

The Constant Amplitude Current Output (Current Clamp)

There are no constant amplitude current supplies in our daily life surroundings, so we are not so well acquainted with this sort of supply. It may be constructed in two ways: either by electronic circuitry or by a voltage supply with a large series resistance.

The ideal current supply has infinite internal resistance. It supplies the set current from no load (load resistance 0, short circuit) to full load (maximum load resistance and maximum voltage). To leave a current supply open-circuited is the same as leaving a voltage supply short-circuited. Two ideal current sources cannot be coupled in series. In parallel the currents are added.

With $I = \text{constant}$, Ohm's law $V = RI = I/G$ shows that the voltage is proportional to R , not to G .

Choice of Supplies

The power dissipated as a function of load resistance R is:

$$W(R) = RI^2 = V^2/R \quad (7.38)$$

We realize from these equations the important difference between using a constant amplitude current or a constant amplitude voltage supplying a variable load resistance. The current-voltage characteristic of the black box may decide the choice of constant amplitude voltage or current.

7.2.6 The Basic Measuring Circuit

Let us consider a black box containing some series combination of ideal components: one resistor, one or no battery, and one or no capacitor. By external measurements we shall find the component values in three different cases.

First, we are told that there is only one resistor in the black box. To find the resistance value R we apply a known DC voltage V , Fig. 7.10(a). From measured current I the resistance is calculated: $R = V/I$. Now let somebody go into the black box and add the ideal battery B in series with the resistor, Fig. 7.10(c). The DC current will of course change. How can we from the outside know whether the DC current change was due to a change in resistance, or an additional emf in the black box? *We can not.*

In order to find out, we must add something to the measurement. For instance, by varying V , the current I also varies. By applying $V = 0$, we still have a current flowing, which must be $I = V_B/R$. We can then assume that there must be a battery in the circuit.

To obtain this information, we actually had to superimpose a varying signal, an AC voltage, on the DC voltage. In addition, this manual method cannot be used if we want to continuously monitor changing values of V_B and R .

If R and B are non-ideal with current depending values, as in an electrolytic electrode system, the approach cannot be used. A better approach is to superimpose a *small, continuous* sine wave voltage on the applied DC voltage. Our current

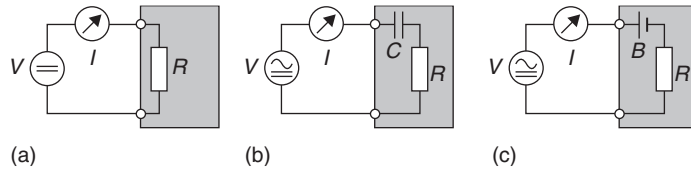


Figure 7.10 Basic black box measuring problems.

measuring device must then be able to measure both AC currents with phase, and DC. The battery (being ideal with zero internal resistance) will not influence the AC current, and we consequently measure the resistance of R at AC, but a different “ R ” at DC. As there is no phase shift, we then know that the battery is in the circuit. If we repeat the measurement on many frequencies and the results are identical, we know that there is no capacitor inside the black box.

What if the battery B is replaced by a capacitor C ? (Fig. 7.10(b)) With the sine wave superimposed, the current will be phase shifted. From a single frequency measurement, we can find the R - C values by the impedance formula $Z = R + 1/j\omega C$.

The DC current will decay from the value found when the applied voltage was switched on. The voltage V_c on the capacitor depends on the charge and the capacitance according to $V_c = Q/C$. Just like the battery it stores energy, and it can give this energy back. The capacitor voltage represents a voltage that changes the current I in the same way as a battery. The AC current will not change during the charging of the capacitor, so constant impedance reveals that the DC current decay must be caused by a gradually increased capacitor charge.

If the battery also is inserted, it cannot necessarily be detected from the outside because it is blocked by the capacitor. A battery *may be* regarded as a very large capacitor with a nearly constant charge and voltage, so large a capacitance that its reactance ($1/\omega C$) is negligible. Also an ideal battery has zero internal resistance (reactance). However, the battery generates an electromotive voltage (emv) from a chemical reaction. The capacitor is a dry system with energy stored in the dielectric, and a voltage according to $V = Q/C$. It is a matter of definition whether the capacitor voltage shall be called a counter-emv; in this book only emv from electrolytic net charge distributions will be regarded as such.

Measurement of Immittance with an Endogenic Signal Source

It is possible to determine the immittance of an electrode system without the use of exogenic signal sources. An endogenic signal is recorded, and the electrode system is loaded with a known admittance in parallel. The *reduction* in signal amplitude is measured as a function of the admittance load. The source immittance can be then be calculated. The method has been used for checking the influence of a limited input impedance of ECG amplifiers (Geddes and Valentinuzzi, 1973), and the estimation of signal source impedance of implanted pacemaker electrodes (Mørkrid et al., 1980).

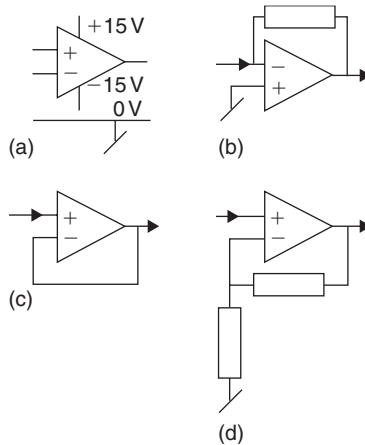


Figure 7.11 Operational amplifier circuits. The details shown in (a) are always present but usually omitted.

7.2.7 Operational Amplifiers and Filters

The Operational Amplifier

The operational amplifier is an amplifier with two inputs (inverting and non-inverting), always used with negative feedback, and having so large amplification that the voltage difference between the inputs is negligible. It may be used as single ended voltage amplifier (negligible input current) Fig. 7.11(d)), as a current amplifier (negligible voltage drop (b), called a *transresistance* amplifier), or for making a constant amplitude voltage or constant amplitude current output. It is not suited to measure a differential voltage without loading the measured circuit, this is done by a special circuit (often composed of three operational amplifiers) called an *instrumentational amplifier* Fig. 7.11(a).

These amplifiers are active devices, and the inputs need a certain bias current and must be within the limits of the power supply voltage. The power supply leads and the reference lead (0 V) as illustrated in Fig. 7.11 (a) are omitted on most circuit diagrams. Notice that the inputs are galvanically separated neither from the output, nor from the power supply. Transformers or opto-couplers are needed if galvanic separation is necessary (Fig. 7.11).

Fig. 7.11(c) shows the voltage follower, it is just a buffer with amplification approximately equal to 1. It is also the principle of a constant amplitude voltage supply. The purpose is to read a voltage without loading (drawing current) from the measured point. Often the op-amp may be brought as near the recording electrode as possible. Then the output lead is not critical and need not necessarily be shielded. A shield for the input lead may preferably be connected to the output instead of ground, because the capacitance between inner lead and shield is then eliminated (bootstrapping). By adding two resistors (d) it is possible to obtain amplification.

The current measuring circuit is very attractive instead of introducing a current reading shunt resistor with the necessary (even if small) voltage drop. The voltage drop in this circuit is virtually zero.

The circuit of (b) can be used also as a constant amplitude current circuit. A constant amplitude voltage and a resistor are used to supply the input current. The load is the feedback resistor, the constant input current will pass the resistor for any resistance value up to the voltage limit of the operational amplifier output circuit (a few volts below the power supply voltage to the op-amp).

Frequency Filtering

High-Pass Filter

To eliminate DC from an AC signal a blocking capacitor is inserted. Together with a resistor they form a high-pass filter (Fig. 7.12(a)). The time constant is RC , and the so-called 3-dB *corner frequency* f_0 is $1/2\pi RC$. At that frequency the phase shift is 45° , and the amplitude has dropped to 63%. This is clear from the transfer function:

$$H(\omega) = v_0/v_i = (\omega^2 R^2 C^2 + j\omega RC)/(1 + \omega^2 R^2 C^2) \quad \varphi = \arctan 1/\omega RC \quad (7.39)$$

The phase shift is: At f_0 , $\varphi = 45^\circ$; at $10f_0$, $\varphi = 5.7^\circ$ and at $100f_0$, $\varphi = 0.57^\circ$. The phase shift in a filter is thus substantial even far away from the corner frequency in the passband, and the frequency must be much higher than the corner frequency to ensure negligible phase shift.

If a repetitive signal is applied to the tissue electrodes via a high-pass filter, no DC polarization is possible.

Low-Pass Filter

The low-pass filter (LPF, Fig. 7.12(b)) is passing low frequencies and DC. The transfer function is:

$$H(\omega) = v_0/v_i = (1 - j\omega RC)/(1 + \omega^2 R^2 C^2) \quad \varphi = \arctan -\omega RC \quad (7.40)$$

The same precaution holds for the phase shift: to ensure low phase shift, the frequency must be much lower than the corner frequency. Such low-pass filtering effects are an important source of error when reading signals through high impedance systems such as insulated microelectrodes due to inevitable stray capacitance between the inner conductor and the surrounding tissue.

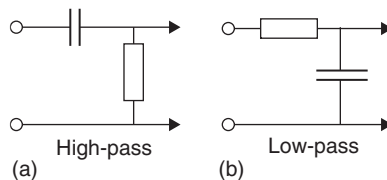


Figure 7.12 High-pass and low-pass filters.

The LPF is also easily realized with a capacitor in parallel with the feedback resistor of the op-amp circuits of Fig. 7.11 (b and d).

7.2.8 Ground, Reference and Common Mode Voltage

In a building there are building materials forming the ceiling, floor and walls of a room. The materials used may have a certain electrical conductivity. We must remember that the dimensions are very large, so that even a small conductivity may result in appreciable conductances according to $G = \sigma A/L$. These materials form a Faraday cage around the room, and it is of interest to have electrical access to this cage. That is one of the functions of the household *ground wire*. In our context the importance of the ground wire is not that it is connected to the earth, but to the building and the room we are in. The ground wire is of interest not only with respect to noise (*functional grounding*), but also with respect to safety (*safety grounding*). Therefore the net plug of electromedical class I equipment contains three wires: the two power line wires and the ground wire with the color yellow/green according to the international standard IEC-60601. Electromedical equipment may also be of class II with *double insulation*, then there is no safety ground wire in the power cable.

For safety reasons, we ideally wish to have a floating (not grounded) patient (person), because if the patient by accident has a potential with respect to ground, no current flows. Therefore modern electromedical equipment is usually designed with a *floating applied part* of type BF or CF (cf. Section 9.17.5). The applied part is the part of the equipment that by intention is in physical contact with the patient. *B* means body, *C* cardiac and *F* floating. The *F*-type equipment is designed with a *galvanic separation* between the applied part and the rest of the equipment. Some equipment still grounds the patient, type *B*.

Electronic circuitry with operational amplifiers is usually supplied from a symmetrical power supply, for example, $\pm 12\text{V}$. This implies three leads to the amplifier: $+12\text{V}$, 0V and -12V . The 0V lead is also called the *reference* lead or chassis lead. The reference lead is used for connecting local shields of, for example, cables or chassis. The reference lead is often floating, that is not connected to ground. The symbols for reference and ground are shown in Fig. 7.13(d). It may also be grounded to reduce noise (functional grounding), or to increase safety (protective grounding).

The signal input of electronic amplifiers may be designed single ended or differential. *Single ended* input Fig. 7.13(b) is an asymmetrical two-lead input circuit, one lead for the signal plus the reference lead. The reference lead, grounded or not, is common for the input, output and power supply. The circuit is a two-port, three-terminal device.

Differential input (upper left) is a symmetrical three-lead input circuit, two leads for the input signal (+lead in phase, -lead 180° out of phase with the output) plus the reference lead. The signal between the differential leads v_i is the differential, wanted signal. The voltage between the differential inputs leads (together) and the reference lead, is the *common mode voltage* (CMV, Fig. 7.13(c)). The amplifier should be as insensitive to CMV as possible, and this is expressed by the amplifier's *common mode rejection ratio* (CMRR), usually given in decibel (dB). A CMRR of

100 dB ($=10^5$) means that, for example, a CMV input signal of 1 V (between the two input leads connected together and the reference lead) is equivalent to a differential input signal of $10\ \mu\text{V}$. The CMRR is always strongly frequency dependent, with the highest value at DC. In the left circuit an ordinary operational amplifier is used, in the right circuit the special *instrumentational amplifier* is used. That circuit is a two-port, five-terminal device. However, two of the terminals are connected together.

The CMV must usually be within limits set by the power supply of the amplifier. If the supply is $\pm 12\text{V}$, the CMV input range is perhaps $\pm 9\text{V}$. For this reason the patient/test person usually must have a third electrode connected to the reference lead of the input amplifier. Without this third lead, the input amplifier's CMV range may easily be exceeded. Both DC and AC must be considered in this respect. In type BF and CF equipment the third electrode is a floating reference electrode, in type B equipment it is a ground electrode (Fig. 7.13(d)).

An operational or instrumentation amplifier of the applied part is usually *galvanically coupled* to the patient. If it has infinitely high CMRR, then with respect to CMV noise cancellation it would be the same as if input and output were galvanically separated. But with respect to safety it is not ideal, because the CMV input range is restricted to less than the power supply voltage to the amplifier. Outside that linear range, the junctions of the input transistors may enter a non-linear breakdown region. To keep it inside the CMV range, a third electrode is usually necessary. An input circuit is therefore only *galvanically separated* if its energy supply is from batteries or transformers, and if the signal output is by optical, transformer or radio signal (telemetry) coupling. Then the allowed CMV may be in the kilovolt range. A transformer winding input is the nearly perfect input both for safety and DC CMV cancellation, but unfortunately not for broadband amplification and high input impedance.

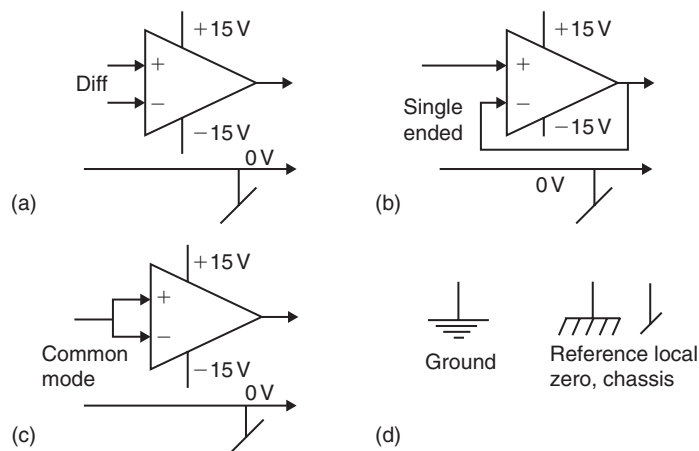


Figure 7.13 (a) Differential (instrumentational amplifier) input. (b) Single ended input. (c) Common mode coupled input. (d) Symbols for ground and local reference.

Mains Noise Reduction Methods

Fig. 7.14 shows three situations of power line capacitively coupled noise voltage. Suppose first (left) that leakage current is passing through a grounded electrode on the patient. The skin impedance under such electrode may easily attain $100\text{ k}\Omega$ at $50/60\text{ Hz}$. With a leakage current of $1\text{ }\mu\text{A}$, the voltage on the patient with respect to ground is 100 mV . With a single ended signal amplifier (two electrodes on patient: signal and ground), the 100 mV is superimposed on the signal of interest. To reduce the influence of the noise voltage, either the coupling to the mains (increase distance to source, shield, Faraday cage) or the impedance of the ground electrode (dominated by skin impedance) must be reduced.

Another approach (middle) is to convert the noise voltage to a common voltage by applying an instrumentational amplifier (two measuring electrodes on patient). With a floating patient the voltage may be about 10 V , so a common mode rejection factor of 120 dB (10^6) would be needed to reduce the noise contribution to $10\text{ }\mu\text{V}$. In addition, the CMV must be within the linear range of the instrumentational amplifier. By *also* grounding the patient (three electrodes on patient), the CMV range is better controlled.

A third approach (right) is to clamp the patient to ground potential by an active operational amplifier circuit (two electrodes on patient), Fig. 7.14(right). The reference electrode picks up the voltage of the deeper skin layers (skin impedance independent: no current flow and no voltage drop in the stratum corneum). The operational amplifier sets up a current in the current carrying electrode to just counterbalance the capacitively coupled noise current, the reference electrode is virtually grounded. It is also possible to put in safety resistors (R_1 and R_2) without reducing the effect of the circuit. In that way the patient is not directly grounded even if the semiconductor circuits break down. Of course this is also possible to do in the instrumentational amplifier input leads. The signal amplifier may be single ended – ground referenced (totally three electrodes on patient) or differential (totally four electrodes on patient).

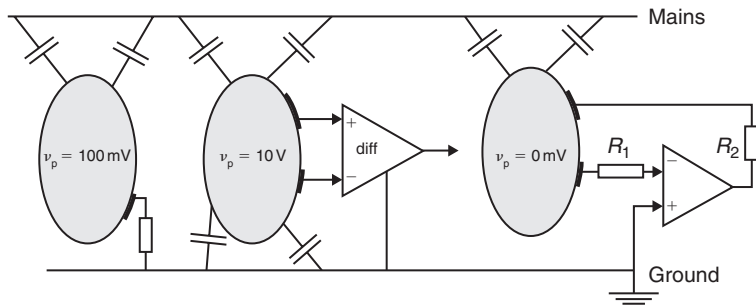


Figure 7.14 Three noise reduction approaches. *Left*: grounded patient. *Middle*: floating patient with instrumentational amplifier. *Right*: ground-clamping circuit. v_p is typical patient AC voltage with respect to ground. v_p is in practice non-sinusoidal. Because of the high-pass filtering effects, the harmonics of the mains supply are expanded.

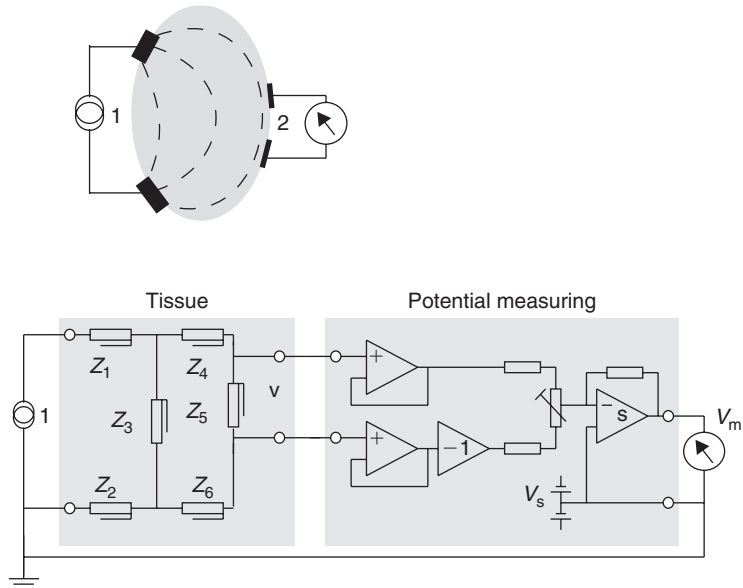


Figure 7.15 Equivalent circuits for tissue and a potential amplifier. The impedance symbols are for frequency-dependent components.

The patient has been considered equipotential in this analysis. From the human body segmental resistances described in Fig. 4.26, the chest has a segmental resistance of the order of $10\ \Omega$. With $1\ \mu\text{A}$ flowing the voltage difference is of the order of $10\ \mu\text{V}$. In the limbs the segmental resistances are much higher. If this is critical, care must be taken as to where to locate the reference and current carrying electrodes of the clamping circuit, and where to locate measuring electrodes with respect to noise current flow paths.

Figure 7.15 illustrates how the common mode voltages are controlled in an often used configuration, by grounding one side of the signal source. (Grimnes and Martinsen, 2007b) In medical instrumentation terms this means that the instrument is a class B device (Section 9.17.5).

7.3 BRIDGES, IMPEDANCE ANALYZERS, LOCK-IN AMPLIFIERS

Circuitry for impedance measurements has changed dramatically since the first measurements were performed on biological tissue. The development of digital electronics and the incorporation of computer power in almost all instruments have had an important impact on the possibilities of studying the passive electrical behavior of biomaterials over a wide frequency range, and with a speed which was not feasible only a few years ago. Only a brief summary of some of the techniques will be given in this section. In low frequency measurements on tissue with a

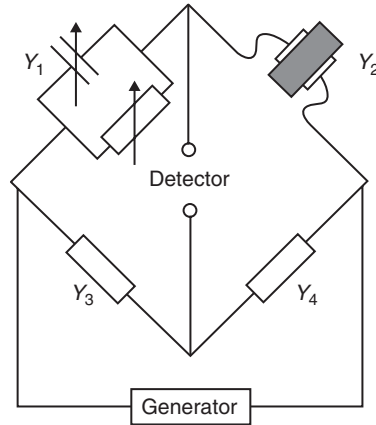


Figure 7.16 Admittance measurement with an AC bridge.

large DC conductivity from body fluids, high-resolution methods are of particular interest.

7.3.1 Bridges

A variety of bridges have been used for immittance measurements for a long time. The general principle of an AC bridge is illustrated as an admittance bridge in Fig. 7.16, where $Y_1 = 1/Z_1$ is a parallel circuit of a variable resistor and a variable capacitor, and $Y_2 = 1/Z_2$ is the measured sample.

By balancing the bridge so that the signal measured by the detector is equal to zero, the unknown admittance Y_2 can be calculated using the relation $Y_1 Y_4 = Y_2 Y_3$.

The advantage of bridges is their high-resolution capabilities, a feature very important for extending dielectric measurements to low frequencies in tissue (cf. Section 3.8). Blood, for instance, has a conductivity of about 1 S/m and ϵ'_r of 1500, frequency independent up to 100 kHz. A conduction resolution of about 10^5 is necessary for a precision of 10% at 1 kHz (Schwan, 1963). Schwan discussed both low and high frequency bridges, and Schwan and Ferris (1968) discussed high-resolution tetrapolar bridges. Hayakawa et al. (1975) have further increased the precision of bridge instrumentation.

However, manual bridges are slow, and not suited for measurements on dynamic systems. Although automated bridges are commercially available, they have given way to other methods for bioimpedance measurements, such as for example, lock-in amplifiers.

The lower practical frequency limit for an AC bridge is about 10 Hz if it is transformer coupled, and down to DC if it is directly coupled. The upper frequency limit may be high in the MHz region with special constructions.

7.3.2 Digital Lock-in Amplifiers

Lock-in amplifiers are commonly used to detect minute signals buried in noise. This can only be accomplished, however, if the signal of interest appears as an amplitude modulation on a reference frequency. The ideal lock-in amplifier will then detect only the part of the input signal having the same frequency and phase as the reference frequency. This technique is ideal for immittance measurements, since admittance appears as an amplitude modulation on the measured current, and impedance appears as an amplitude modulation on the measured voltage.

Lock-in amplifiers can be basically digital or analog. Analog amplifiers will be treated in the next section.

Digital lock-in amplifiers are based on the multiplication of two sine waves, one being the signal carrying the amplitude modulated information of interest, and the other being a reference signal with the chosen frequency and phase. If the reference signal is given (assuming amplitude of unity) by:

$$v_r = \sin(\omega_r t) \quad (7.41)$$

and the input signal is:

$$v_i = v_1 \cdot \sin(\omega_i t + \varphi) \quad (7.42)$$

the output signal will be (cf. eq. 7.24 and 7.24a):

$$\begin{aligned} v_0 &= v_1 \cdot \sin(\omega_i t + \varphi) \cdot \sin(\omega_r t) \\ &= \frac{v_1}{2} [\cos((\omega_i - \omega_r)t - \varphi) - \cos((\omega_i + \omega_r)t + \varphi)] \end{aligned} \quad (7.43)$$

A low-pass filter will follow this multiplier module, and the right-hand cosine expression may therefore be ignored. In fact the only DC signal that will appear at the low-pass filter output, will be the one corresponding to $\omega_i = \omega_r$, which gives:

$$v_0 = \frac{v_1}{2} \cdot \cos \varphi \quad (7.44)$$

A lock-in amplifier is perfect for immittance measurements. Two amplifiers should be used, one with a reference signal identical to or in phase with the excitation signal, and one with a reference signal 90° out of phase with the excitation signal. If the excitation signal is a voltage, the measured current should be converted to a voltage using, for example, a transresistance amplifier. In that case the DC outputs from the lock-in amplifiers will be proportional to the parallel admittance values of the measured object, i.e. conductance and susceptance, respectively. Using a current as excitation will correspondingly produce a measured voltage that can be separated into signals proportional to the series impedance values, which are resistance and reactance.

Total suppression of noise in this system is of course only possible if the integration time is infinite, that is the multiplication is carried out over an infinite number of signal cycles. Gabrielli (1984) showed that the suppression of random (white) noise is given by an equivalent filter function with a bandwidth Δf given by:

$$\Delta f = \frac{f_r}{N} \quad (7.45)$$

where f_r is the analyzed frequency and N is the number of cycles. Hence, in a 10 Hz measurement, the bandwidth is 0.1 Hz when integrating over 100 cycles, but only 2 Hz when integrating over only five cycles of the signal. The corresponding transfer function is given by:

$$|\mathbf{H}(\omega)| = \frac{2}{\pi N} \left[\frac{\sin(N\pi\omega/\omega_0)}{1 - (\omega/\omega_0)^2} \right] \quad (7.46)$$

where ω/ω_0 is the normalized angular frequency. The transfer function is also shown in Fig. 7.17 as a function of number of integration cycles.

Digital lock-in amplifiers have virtually no low frequency limitations. Commercial amplifiers typically operate down to 1 mHz, but, for example, the Solartron 1260 is constructed for measurements down to 10 μ Hz (corresponding to a period of about 28 hours!). The upper frequency limit is about 100 kHz mainly limited by the conversion time in the analog to digital converters (ADCs). Above this frequency, heterodyne sampling can be used as described in Section 7.3.5 which extends the range of Solartron 1260 to 32 MHz. Another example of a radio-frequency digital lock-in amplifier is the SR844 from Stanford Research Systems. It has a frequency range from 25 kHz to 200 MHz with an *absolute* phase error better than 2.5° below 50 MHz, increasing to a maximum of 10.0° at 200 MHz. The *relative* phase error is less than 2.5°, however, which can be utilized in a practical

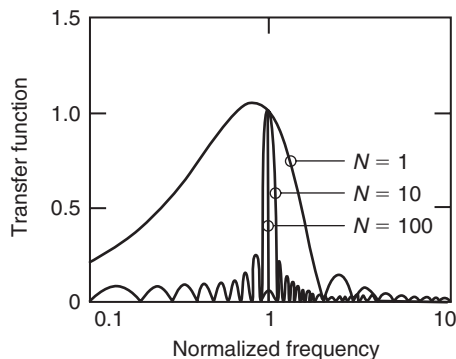


Figure 7.17 Absolute value of transfer function for digital lock-in amplifier as a function of normalized frequency and number of integration cycles.

experimental situation by measuring, for example, before and after the biomaterial is added to an electrolyte solution. Those interested in constructing their own digital lock-in amplifier should read, for example, Vistnes et al. (1984).

7.3.3 Analog Lock-in Amplifiers

The heart of the analog lock-in amplifier is the synchronous rectifier that includes a phase sensitive detector (PSD) and a low-pass filter.

The PSD in Fig. 7.18 comprises an inverter and an analog switch. The switch is connected to the in-signal in the positive half-periods of the reference signal, and to the inverted in-signal in the negative half-periods. Hence, if the in-signal and reference signals are in phase, the detector will act as a full wave rectifier, providing a maximum DC signal out from the low-pass filter. If the in-signal and reference signal are 90° out of phase, the resulting signal out from the PSD will be without any DC component as shown in Fig. 7.18, and the low-pass filter will produce no output signal. A phase shift between 0° and 90° will accordingly produce a DC signal lying between these two limits. It can easily be shown that the output signal from the synchronous rectifier is given by the equation:

$$V_{out} = V_{in}(av)\cos \varphi \tag{7.47}$$

where V_{out} is the DC voltage out from the low-pass filter, $V_{in}(av)$ is the average value of the AC in-signal and φ is the phase shift between the in-signal and the reference.

As described in the previous section for digital lock-in amplifiers, the analog PSD can be mathematically described as a multiplication of the in-signal and the reference signal. Since in this case the reference signal controls a switch, it must be

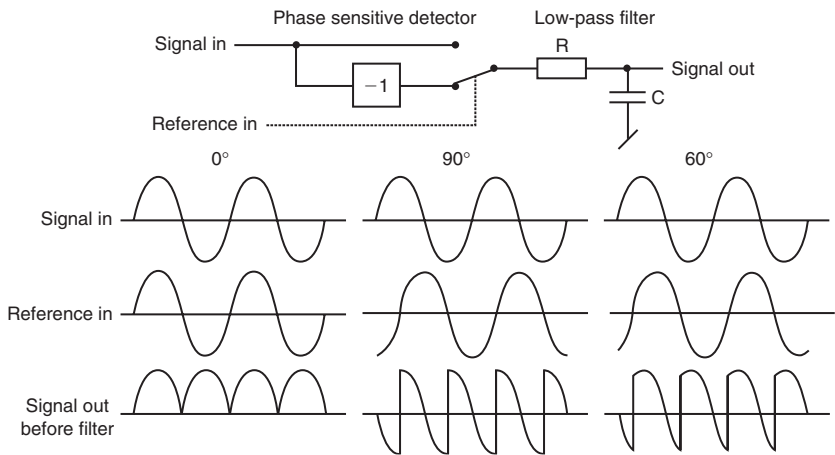


Figure 7.18 Synchronous rectifier with 0°, 90° and 60° phase shift between signal and reference.

regarded as a square wave. We should then take into account the Fourier components of this signal which include the frequency of the square wave itself as well as all odd harmonic frequencies. The synchronous rectifier will hence be sensitive to both the reference frequency and to all odd harmonic components, but with sensitivity proportional to $1/n$ where n is the odd harmonic number (cf. eq. 7.31).

Analog lock-in amplifiers have a practical lower frequency limit of about 1 Hz, owing to the necessity of AC coupled inputs. Since any DC signal will influence the results, the method requires pure AC signals. The upper frequency limit of the analog lock-in technique is about 100 kHz, and is mainly due to problems of stray capacitance.

7.3.4 Microelectronic Mode Lock-in Amplifiers

Most signal processing has traditionally been confined to manipulating electrical voltages, and current signals are typically transformed into voltages in electronic instruments. However, in semiconductor devices currents are fundamentally controlled, and it has proved to be advantageous to use current mode signal processing in modern applications, for example in integrated circuits for biomedical applications, see Grimnes and Martinsen (2006), but especially in low power implantable medical devices as described by Silveira and Flandre (2004).

The basic idea for using current mode analog lock-in technique, for example for RF measurements, is that currents may be driven with relatively low voltages in discrete-time switching circuits. Thus, high-level continuous-time signals are not expressed through higher voltages, but through the level of currents, which remains relatively low, for example within the microampere range. As a result, battery supplied low voltage (1.0–2.5 V) and low power (microwatt range) microelectronic circuits can be designed and fabricated. Also the charging time of stray capacitance is reduced, which shortens signal propagation time, enabling precision measurements at higher frequencies. A low-cost current mode lock-in amplifier has been presented by Min and Parve (1996, 1997).

As shown in Fig. 7.19, it comprises a programmable oscillator that provides a symmetrical controlled current through the specimen of interest, Z_X . The voltage across the same specimen is again converted into a current by a differential input voltage-to-current converter (VCC), which is also termed as a transconductance amplifier or transor (see Grimnes and Martinsen, 2006). The current from the transconductance amplifier is then decomposed into its in-phase and quadrature components by means of current mode switches that are driven by the reference signal from the programmable oscillator. Hence, to measure the quadrature component, the oscillator must provide also a second reference signal that is 90° out of phase with the excitation signal. A differential input current-to-current converter (\pm CCC) produces the output current i_o , which is filtered and converted into an output voltage V_o by the LPF.

To avoid aliasing, the measured signal, which is synchronously rectified, is filtered by the LPF before reaching an ADC. The final averaging of the result is performed using digital signal processing. The system has an upper practical frequency limit of about 10 MHz.

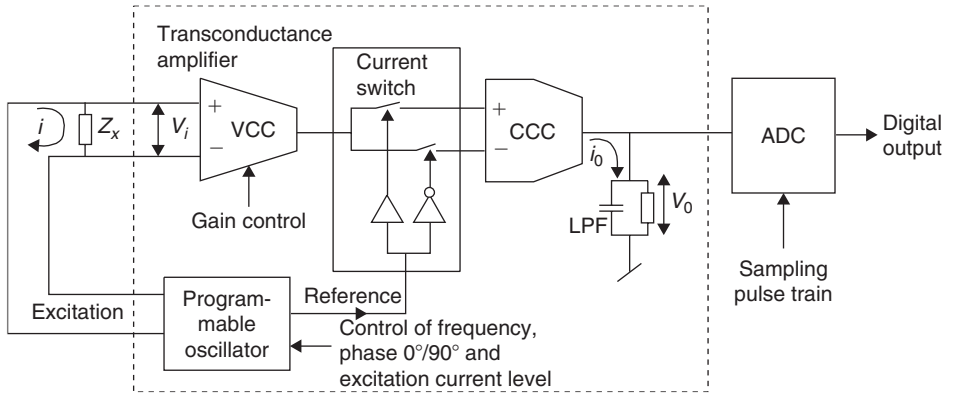


Figure 7.19 On-chip current mode lock-in amplifier.

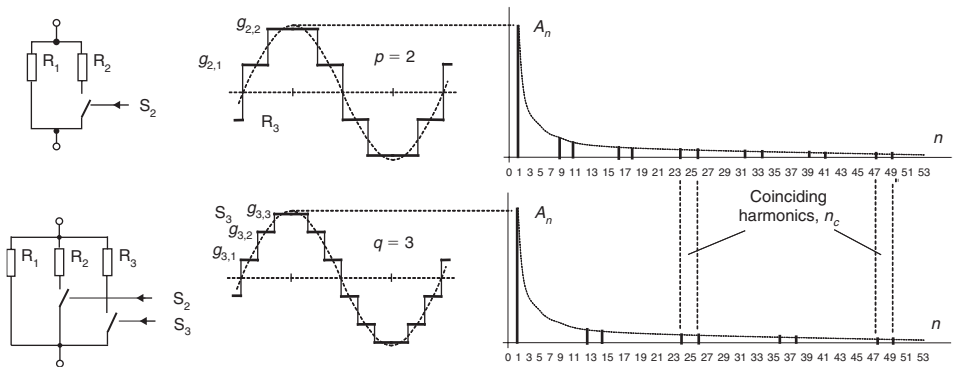


Figure 7.20 Two-level ($p = 2$) and three-level ($q = 3$) approximations of sine waves and their spectra.

To achieve full vector operation (detection of both the in-phase and quadrature components simultaneously), two identical lock-in channels are needed, one driven by the 0° reference signal and the other by the 90° reference.

Significant efforts have been devoted to suppressing the sensitivity of synchronous rectifiers to higher odd harmonics, proportional to $1/n$, where n is the order number of the odd harmonics (cf. eq. 7.3.1). Min et al. (2002) described a solution, in which a very rough approximation of sine waves with only some single discrete levels is used in both the excitation and reference signals. It is important that the excitation and reference signals should be approximated differently. The idea is based on the fact that the synchronous rectifier is sensitive only to these higher harmonics, which are present simultaneously in both the excitation and reference signals. In Fig. 7.20 is shown the case where two-level ($p = 2$, levels $g_{2,1}$ and $g_{2,2}$) and three-level ($q = 3$, levels $g_{3,1}$, $g_{3,2}$, and $g_{3,3}$) approximations are used by switching on and off the parallel connected current limiting resistors.

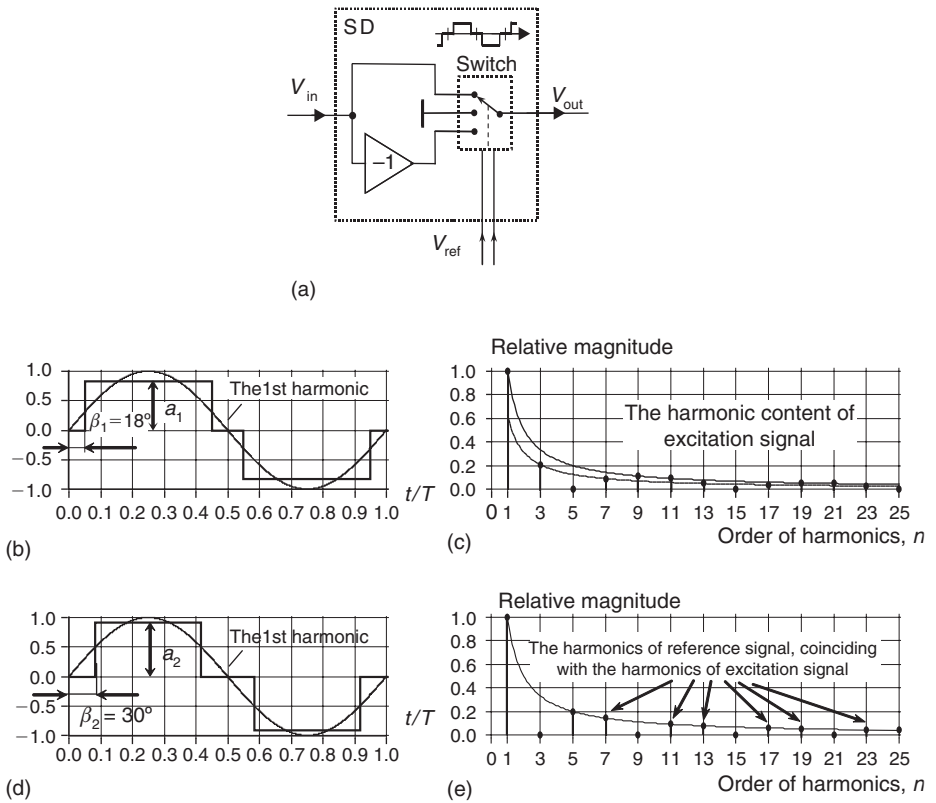


Figure 7.21 Circuit diagram of the modified synchronous detector (a), and the approximated sine waves with suppressed 5th harmonic (b) and its spectrum (c), and with suppressed 3rd harmonic (d) and its spectrum (e).

The spectra in Fig. 7.20 show that the harmonic contents of differently approximated waveforms ($p = 2$ and $q = 3$) are also different, though the most significant odd harmonics (the 3rd and 5th) are absent in both. The orders of higher harmonics (n_c) which coincide in the excitation ($p = 2$) and reference ($q = 3$) signals, and to which the instrument is sensitive, can be found from the general equation:

$$n_c = (4p \cdot q)i \pm 1, \quad i = 1, 2, 3, 4, \dots$$

In our case, where $p = 2$ and $q = 3$, the orders of common harmonics $n_c = 23; 25$ ($i = 1$), $47; 48$ ($i = 2$), $71; 73$ ($i = 3$), etc. The residual sensitivity to these harmonics is very low, proportional to $1/(n_c)^2$.

An even simpler solution is described in Min and Parve (2007), where only $+1, -1$ and 0 levels are used for approximations of the sine waves. Figure 7.21 shows a practical case where the two 0 -level sections, lasting $1/6$ of each half-period $T/2$ ($\beta_1 = \pi/6 = 30^\circ$) remove the 3rd harmonic, and lasting $1/10$ of the half-periods $T/2$ ($\beta_1 = \pi/10 = 18^\circ$) remove the 5th harmonic. As the result, the synchronous

rectifier will not be sensitive to the 3rd and 5th harmonics any more, only the degraded sensitivity remains to the 7th, 11th, 13th, 19th, etc., odd harmonics.

Publication by Min et al. (2007a) describes the digital version of a similar device, which uses synchronous sampling of the response voltage.

A fast impedance spectrometer may use generation of several sine wave excitations simultaneously and also simultaneous processing of the response signals during a short observation time. One effective solution is given by Min et al. (2007b), where the synchronous sampling performs the spectral analysis without any multiplication. Sorting and grouping of samples and the groupwise summing of their values enable to obtain the short time spectrograms, whereas restrictions on choosing of excitation frequencies must be taken into account.

7.3.5 Impedance Analyzers and LCR-Meters

There are several different kinds of automated instruments for impedance measurements, which can be divided into two general categories: LCR-meters and impedance analyzers. LCR-meters use the auto-balancing bridge technique to measure the impedance of materials. They can generally be used in a frequency range roughly between 5 Hz and 1 GHz. Low cost meters are also available, like the SR720 or HP4263B which measure at five pre-defined frequencies from 100 Hz to 100 kHz.

Impedance analyzers are also called *frequency response analyzers* and are in most cases combined instruments employing two or more different techniques to cover a larger frequency range. One example is the HP4294A, which covers a frequency range from 40 Hz to 110 MHz. It can be used for impedance or gain-phase measurements and has four terminals for impedance measurements. Proper four-electrode measurements are not available because the voltage and current electrodes must be connected together at the device under test. However, Gersing (1991) designed a special pre-amplifier for these analyzers which gives separate connections for the voltage and current electrodes. Such front-end amplifiers for increased measurement accuracy have also later been designed by, for example, Yelamos et al. (1999).

Another example is the Solartron 1260 which uses digital correlation techniques for measurements in the range 10 μ Hz to 32 MHz. The ADCs used have a resolution of 16 bits and the basic accuracy is 0.1% for magnitude and 0.1° for phase measurements. The 1260 has three channels measuring in parallel (two voltage and one current measurement channel) and ordinary digital lock-in technique is used after the ADCs. For the highest frequency range (65.5 kHz to 32 MHz) an analog phase-locked loop system is used that generates both the high frequency output waveform to the sample under test and an internal high frequency reference signal, which is arranged to be at a slightly different frequency than the output waveform. The input waveform is mixed (heterodyned) by this reference waveform to produce a sum and difference frequency. The sum frequency is filtered leaving the low frequency waveform, which can then be analyzed using the ADC. A digital heterodyning process is used for measurements in the mid-frequency band (300 Hz

to 65.5 kHz) to mix the input signals down to low frequency. Low frequency measurements up to approximately 300 Hz are measured directly by the ADC.

The 1260 has a generator, a current measurement input and two differential voltage inputs. This allows the instrument to be used either in two- or four-terminal connection mode. In order to further improve the instrument's performance in four-electrode bioimpedance measurements, the 1294 impedance interface has been developed by Solartron as a pre-amplifier for the 1260 impedance analyzer (or any other frequency response analyzer). The 1294 makes use of driven shields, balanced generator and high input impedance voltage sense inputs in order to minimize stray currents to ground and hence maximize accuracy when measuring in difficult four-terminal conditions. In addition, this interface has been developed to comply with the IEC-60601 standard for connection of electrical equipment to live subjects. The 1294 can also be used for two- or three-electrode measurements.

Frequency domain techniques like, for example, *spectrum analyzers* and *Fourier analyzers* can also be used for impedance measurements at audio and higher frequencies. A variety of excitation functions may be chosen and the transfer function of the measured object can hence be found by analyzing the response spectrum. Spectrum analyzers are typically swept-tuned, superheterodyne receivers that display amplitude versus frequency. However, unlike the Fourier analyzers, spectrum analyzers do not provide phase information. Fourier analyzers use digital sampling and mathematical algorithms to form a Fourier spectrum of a signal, and they can be used for both periodic and transient signals.

Another type of instruments that can be used for impedance measurements are *network analyzers* which are typically used in a frequency range between 100 kHz and 100 GHz. Measurements of the transmission through and/or reflection from a material are used together with information about the physical dimensions of the sample to characterize the electrical properties. Careful calibration and correction procedures must be utilized when measuring in this frequency range since even minor changes in the measuring setup may largely influence the results.

7.3.6 Time Domain Spectroscopy

The time domain approach is advantageous for fast measurement requirements. Given the hardware available today, the accuracy can compete with that of measurements in the frequency domain Feldman et al. 2003. The most important excitation signal in the early days was either a pulse (square or Dirac) or a rectangular wave. Today new concepts like multi-sinus excitation, ultra wide band pseudo noise sequences (Sachs, 2007) or wavelets emerge. The purpose of the new concepts is to emphasize important regions of the spectrum while maintaining a low crest factor.

An advantage of time domain based measurements is the option to compensate for parasitic reflections and transmission losses at specific parts of the measurement arrangement, like connectors or cables. In the frequency domain, the excitation frequency sweeps over a range which can be over eight decades for some commercial devices. The sweep time depends on the range and numbers of frequencies. This can be easily tens of seconds up to several minutes.

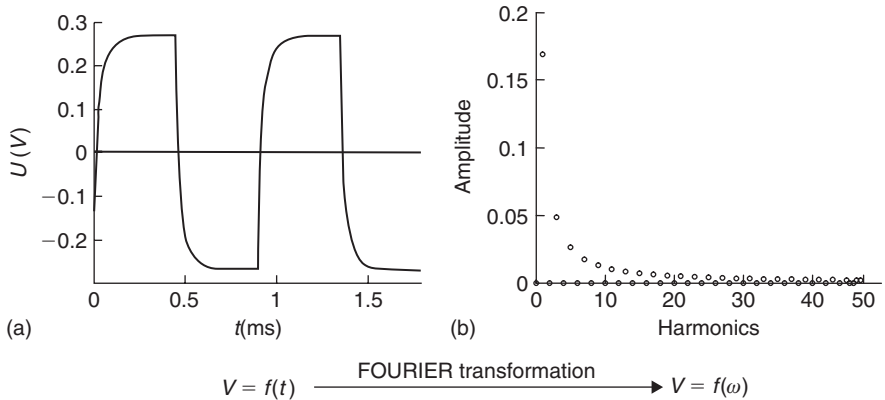


Figure 7.22 Basics of transformation from time to frequency domains.

The basic feature of time domain spectroscopy (TDS) is the application of a broad bandwidth signal containing all the frequencies together. A typical signal with broad bandwidth is the square wave. Other popular signals are the Dirac pulse, the multi-sinusoidal excitation, and the Gaussian pulse or wavelets.

Using Fourier transformation (or even better the FFT) the signal can be transformed into the frequency range, yielding the phase-sensitive amplitude for discrete frequencies (Fig. 7.22).

Thus, a broad frequency range (several decades) can be obtained at once. Since the amplifiers need to have this high bandwidth, other than the selective amplifiers used in frequency domain measurements, a noisy signal results in many cases. For the highest speed, a single shot monitoring is feasible. However, the noise will limit the bandwidth. If the time requirements are not too strict, averaging is possible, thereby greatly enhancing the SNR.

7.3.7 Time Domain Transmissometry

For low frequency applications (mHz–MHz) the classical approach using two or four electrodes interfaces are commonly used. Three electrodes interface is usually employed in conjunction with active electrical properties at surfaces, like sensor surfaces. Since the behavior within the immediate vicinity of the working electrode overwhelms the measurement, the results are compatible with monopolar measurements. The front end is similar to that employed in frequency domain measurements. The marked difference is the application of a broadband signal and monitoring of the time function of the response.

A very simple approach is shown in Fig. 7.23. The material under test (MUT), which may be, for instance, a cell suspension or needle electrodes inserted into a tissue, is in series with a resistor. It should be noted that the electrodes for such a simple arrangement should be large. If not, the electrode polarization will dominate in the result.

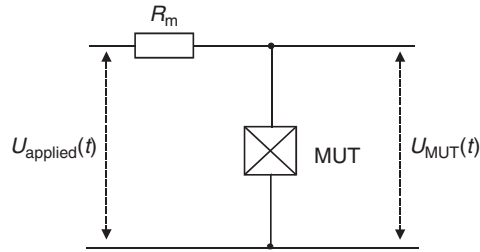


Figure 7.23 Simple arrangement for time domain measurement.

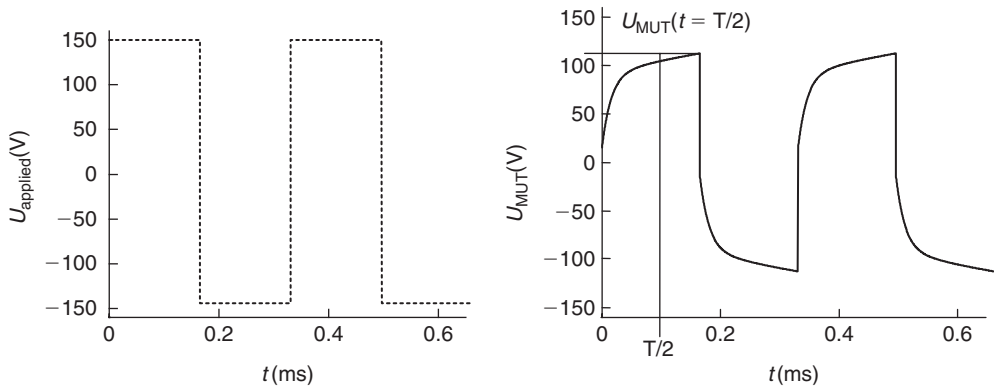


Figure 7.24 The rectangular wave (left) is applied to the voltage divider of the measuring resistor R_m and the MUT while the deformed waveform appears across the MUT.

The broad bandwidth signal, which may be simply a rectangular wave, is applied to the MUT and its deformation is then measured (Fig. 7.24).

Because of capacitance such as from charging of cell membranes, the voltage across the MUT is deformed (Fig. 7.24). If the applied rectangular wave and the measured deformed signal are both measured over time, collected with a digital oscilloscope and fed to a computer which can perform a Fourier transform, then these time domain signals can be converted to the frequency domain using standard engineering calculations. Thus, the resistance and capacitance values for the elements of a simple equivalent circuit (R-RC) can be directly calculated from the deformed time domain signal.

One half wave of the deformed signal can be described as $V_{\text{MUT}}(t) = A_0 - A_1 e^{t/\tau}$. A_0 , A_1 and τ can be fitted using non-linear methods like the Marquard-Levenberg algorithm.

The resistor R_{ext} can be immediately calculated using A_0 :

$$R_{\text{ext}} = \frac{R_m A_0}{(U_{\text{applied}} - A_0)}$$

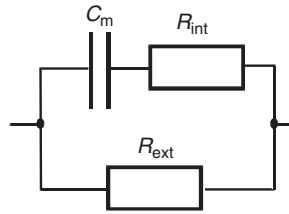


Figure 7.25 Model for biological object, where R_{ext} is the resistance of the extracellular space, R_{int} arises from the cytosol and C_m mimics the capacitor due to the cell membranes.

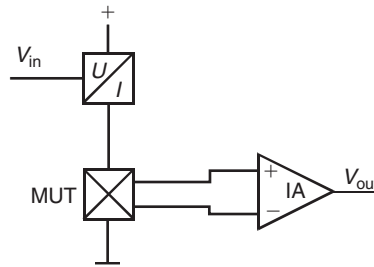


Figure 7.26 Impedance measurement using current excitation and tetrapolar interface. The U/I converter supplies the current while the high ohmic instrumentation amplifier yields the voltage difference across the inner electrodes.

where R_m is the resistance of the measuring resistor in Fig. 7.23. To make further calculations simpler, R_{mp} is introduced as the equivalent resistance of the parallel combination of R_m and R_{ext} . Then,

$$R_{me} = \frac{R_m R_{ext}}{(R_m + R_{ext})}$$

It may be interesting to note that A_0 and R_{me} model a voltage source with an open circuit voltage of A_0 and an internal resistance of R_{me} .

The calculation of the rest of the elements (R_{int} , C_m) is straightforward using the following equations:

$$R_{int} = \frac{2A_0}{A_1 + A_1 e^{-T/2\tau}} R_{me} - R_{me} \quad \text{and} \quad C_m = \frac{\tau}{R_{ext} + R_{me}}$$

This simple approach relies on some assumptions. First, the rectangular wave is nearly ideal with instantaneous rise and quite stable during a half-period. Secondly, the electrodes are big enough to keep electrode polarization at a minimum.

A more sophisticated approach is the application of a current signal with monitoring of the voltage developed across the MUT. Moreover, the use of a second pair of electrodes for voltage monitoring reduces greatly the electrode polarization (Fig. 7.26).

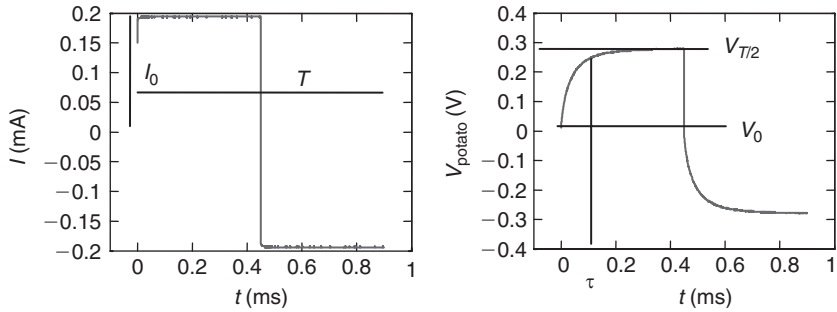


Figure 7.27 Typical signal captured by the oscilloscope. The applied current I_0 is $\pm 190 \mu\text{A}$ and the period is 0.9ms.

A sample measurement on potato is shown in Fig. 7.27. The electrode system consists of four needles (20-mm long, inner electrodes 20-mm apart, diameter of one needle 3 mm).

The calculation of the equivalent circuit becomes simple when the period is much larger than the time constant for charging the membranes, $T \gg \tau$, that is at $t, T/2$ s is already a steady voltage reached:

$$R_{\text{ext}} = \frac{V_{T/2}}{I_0} \quad R_{\text{int}} = \frac{R_{\text{ext}}(V_{T/2} + V_0)}{V_{T/2} - V_0} \quad C_m = \frac{\tau}{R_{\text{ext}} + R_{\text{int}}}$$

This, however, is finally a rough approximation for the impedance. It is more accurate and therefore favored to calculate the impedance as the ratio between the Fourier-transformed voltage and current:

$$Z(j\omega) = \frac{F(V(t))}{F(I(t))}$$

In the special case with no DC offset we find the zeroth coefficient (DC component) zero as well. Because of the symmetry each even coefficient will also be zero. Note that several programs, like Matlab (The Mathworks Inc), start with the first coefficient which is then the DC-part (Fig. 7.28).

7.3.8 Time Domain Reflectometry

The MUT is placed at the end of a transmission line (i.e. coaxial cable). The cable has a characteristic impedance (Z_0) while the MUT in case of biological matter shows capacitive behavior (Fig. 7.29).

An incident wave (E_{INC}) propagates through the transmission line up to a point where the dielectric behavior is changing (end of the line). This yields reflection and the reflected wave (E_{REF}) travels back.

The reflection coefficient is:

$$r = \frac{E_{\text{REF}}}{E_{\text{INC}}}$$

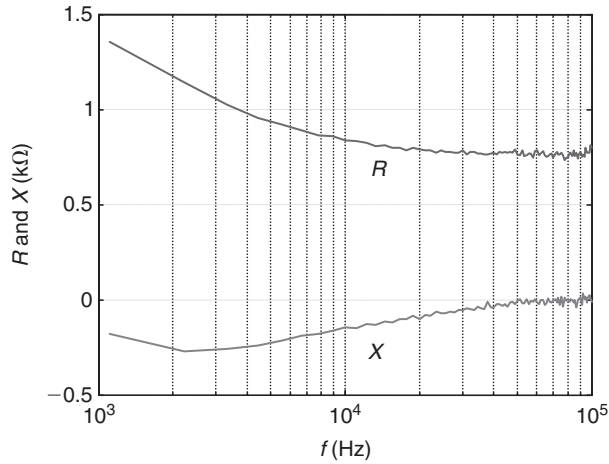


Figure 7.28 Impedance spectrum of a potato measured in time domain.

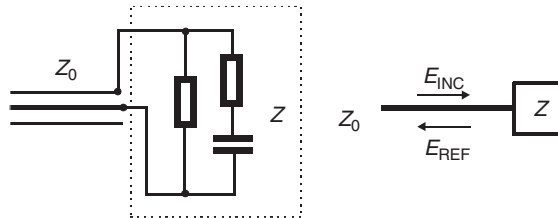


Figure 7.29 Coaxial transmission line connected to a complex impedance. The incident wave E_{INC} is applied while the reflected wave E_{REF} is reflected at the MUT.

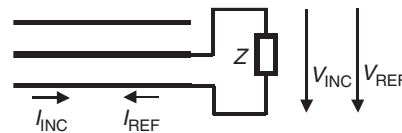


Figure 7.30 Voltage and current at the object and inside the transmission line.

which in terms of voltage monitored at one point of the line is:

$$r = \frac{V_{REF}}{V_{INC}}$$

The voltage at any point of the line is the sum of both, the voltage of reflected (V_{REF}) and the incident (V_{INC}) wave (Fig. 7.30):

$$V = V_{INC} + V_{REF}$$

But, since the direction of both waves is opposite, also the currents (I_{INC} , I_{REF}) have opposite direction. Therefore, the current is:

$$I = I_{\text{INC}} - I_{\text{REF}}$$

According to Ohm's law, the impedance of the MUT is:

$$Z = \frac{V}{I} = \frac{V_{\text{INC}} + V_{\text{REF}}}{I_{\text{INC}} - I_{\text{REF}}}$$

Since the current at the transmission line is

$$I = \frac{V}{Z_0} = \frac{V_{\text{INC}} - V_{\text{REF}}}{Z_0}$$

we find

$$Z = \frac{V_{\text{INC}} + V_{\text{REF}}}{V_{\text{INC}} - V_{\text{REF}}} Z_0 \quad \text{or in terms of } r \quad Z = Z_0 \frac{1+r}{1-r}$$

It should be noted at this point that this simple approach is only valid for MUT with no spatial distribution. If the chamber does not have negligible geometrical length or the measurement aims in the assessment of higher frequencies one has to account for the field distribution within the chamber. For more information refer to Cole et al. (1989).

There are three special cases, the open line, the short circuit and the termination with a matching resistor.

Open line $\lim Z \rightarrow \infty$:

In case of an open line no energy can be dissipated at the end of the line, thus all energy is reflected and the reflected voltage equals the voltage of the incident wave: $V_{\text{REF}} = V_{\text{INC}}$. The reflection factor is $r(Z \rightarrow \infty) = V_{\text{REF}}/V_{\text{INC}} = 1$.

Matched line $Z = Z_0$:

If the impedance of the MUT equals the characteristic impedance of the cable, all the energy is dissipated by the MUT. Since nothing is reflected, r becomes zero.

Short circuit $Z = 0$:

Since no voltage drops across an open circuit, no energy is dissipated by the MUT. Therefore, all energy is reflected but with the opposite polarity: $V_{\text{REF}} = -V_{\text{INC}}$. Therefore the superposition of the incident and the reflected voltage is zero. In case of sinusoidal voltage, the reflected wave shows a phase jump of 180° at the MUT. The reflection factor is $r(Z = 0) = V_{\text{REF}}/-V_{\text{INC}} = -1$.

Measurement Using Time Domain Reflectometry

We consider a transmission line consisting of a $50\ \Omega$ coaxial cable (RG58, RG174) which is terminated by different loads. A square pulse ($50\ \text{mV}$, $200\ \text{ns}$) travels along the cable (Fig. 7.31). To make things simple, we are not going to consider any distortion caused by the cable itself.

The reflected voltage at a certain distance is shifted along the time axis since the speed is limited to $v = (c_0/\sqrt{\epsilon})$ where c_0 is the speed of light in vacuum and ϵ is the permittivity of the material between the inner and the outer conductors of the cable.

The simulation shows the voltage at the entry of a 3-m long cable terminated with a three-element impedance consisting of a $100\ \Omega$ resistor in parallel with a serial combination of a $20\ \Omega$ resistor and a $1\ \text{nF}$ capacitor (Fig. 7.31). The excitation pulse (dotted) has an amplitude of $50\ \text{mV}$ and a rise time of $4\ \text{ns}$. The delay between the signals is caused by the delay time along the cable. First the reflected voltage becomes negative because of the impedance at high frequency ($100\ \Omega$ parallel to $20\ \Omega$) is less than the characteristic impedance of the cable resulting in a negative reflection factor. With proceeding pulse the capacitive elements become increasingly charged. This lowers the current through the MUT and thus the impedance becomes bigger than that of the cable and the reflected wave becomes positive. The voltage monitored, for instance, by an oscilloscope at the entry of the cable is the sum of the incident and the reflected voltages as seen in the right panel of Fig. 7.31.

Electrode Polarization

A conductive sample yields electrode polarization which is evident even at frequencies above $10\ \text{kHz}$. A simple correction is the modeling of electrode behavior using a capacitor for the double layer. Since the current will be known, one can calculate the voltage across the capacitor and correct the voltage across the MUT. For more sophisticated procedures consult the literature (Schwan, 1992a).

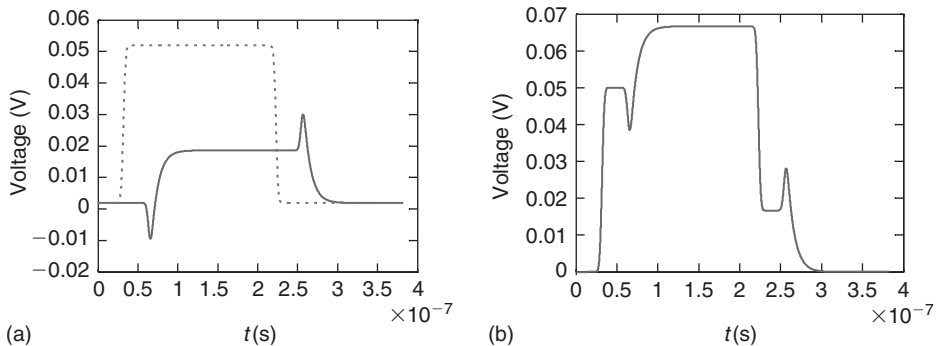


Figure 7.31 (a) Incident (dotted) and reflected (solid) waveform for the three-element impedance and (b) the corresponding voltage at the monitor.

Besides partly mathematical correction of the electrode polarization it is a challenge to find the right electrode configuration and the right electrode material. A widely used electrode is the open ended coaxial probe. Besides this, coaxial chambers (see example) are often used, especially for cell suspensions. This works well up to the frequency where the center electrode acts as antenna and disturbs the impedance due to its resonance behavior. The correction of this can be found in Cole et al. (1989). Another approach is the use of antennas which needs some more attention because of multiple reflection and the relatively weak reflected signal.

7.4 ELECTRODES: DESIGN AND PROPERTIES

In this book we use the terms electrode, transducer, sensor and probe. *Probe* is perhaps the most general term comprising sensing components, housing and cable, for example ultrasound probe. *Sensor* may be the same or only the sensing components, for example temperature sensor. *Biosensor* is a sensor using biomaterials as one of the sensing components. *Medical sensor* is a sensor made for use in medicine. *Transducer* is the part converting a physical quantity into an electric signal, for example pressure transducer or electrode.

Definition

Electrode in our context is strictly speaking the site of shift from electronic to ionic conduction.

However, bioimpedance electrodes need not have such a *galvanic* contact with tissue, the contact may be by displacement (capacitive) currents via a thin teflon or glass membrane; or air coupled. An electrode functions by *electric* fields. Time varying *magnetic* fields may also produce electric currents in tissue, stimulating nerves or producing potential differences which can be picked up by electrodes.

An electrode *pair* may be used for (1) current carrying, (2) measuring a potential difference without current flow and (3) both.

- *Polarized electrode*: polarized by a current flow in the electrode wire. *Polarizable electrode*: considerable changes in its half-cell potential as a function of current flow. *Non-polarizable electrode*: only small changes in its half-cell potential as a function of current flow.
- *Unpolarized electrode*: in equilibrium with no current flow.
- *Polarization impedance*: degree of hindrance of AC current flow across the interface metal–electrolyte. *Linear case*: use of so small AC voltage amplitudes or high frequencies that the effects of electrolytic or tissue reactions are negligible. *Non-linear case*: use of so large AC voltage amplitudes or low frequencies that electrolytic or tissue reactions are noticeable.

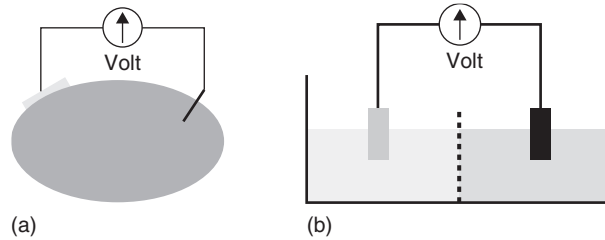


Figure 7.32 (a) Body with one invasive monopolar electrode (needle). (b) Electrolytic cell model: two half-cells and one membrane voltage.

7.4.1 Half-Cell Concept

The body is an ionic conductor. In order to pick up a potential or apply a current *two* electrodes are necessary (Fig. 7.32). One such electrode together with its electrolyte is the *half-cell* of the electrode pair (Fig. 7.32(b)). The DC voltage measured is the sum of the equilibrium potentials of the two electrodes and the membrane. The membrane potential is, for instance, the skin DC potential. If the two electrodes are made of different metals (e.g. steel and platinum) a DC voltage of hundreds of millivolt may be generated (battery effect).

If impedance is measured the electrodes must also be connected to a current source. The two electrodes, the membrane and the electrolytes all contribute. As they are physically in series the contributions can be added (preferably as vectors).

7.4.2 Electronic Conductors

Current Carrying Properties

The polarization properties of different metals can be tested in a setup as shown on Fig. 7.33 (Cooper, 1980)(see Table 7.1). Pulses of 1-second duration and a controlled current of $10\ \mu\text{A}$ are supplied to a current carrying electrode pair in a saline solution. The polarization properties of these current carrying electrodes do not matter as long as the generator is of a controlled current type. Two equal metal electrodes are used as pick-up electrodes, and it is this electrode pair which is studied in the setup of Fig. 7.33. They are loaded with a resistor of $750\ \text{k}\Omega$, so they are actually slightly current carrying and therefore polarized. The equivalent electric circuit (Fig. 7.33(b)) comprises the parallel coupling of a resistor R_{pol} and a capacitor C_{pol} . A non-polarizable electrode has a much smaller R_{pol} , while a polarizable electrode has much larger R_{pol} than the load $750\ \text{k}\Omega$.

Figure 7.34 shows the pick-up voltage obtained with six different electrode metals. The silver chloride electrode pair is the best one ($R_{\text{pol}} \sim 75\ \text{k}\Omega$), pure silver is much worse ($R_{\text{pol}} > 10\ \text{M}\Omega$): the square wave form is totally distorted. The transfer resistance between the pick-up and current carrying electrodes is $R = V/I = 100\ \mu\text{V}/10\ \mu\text{A} = 10\ \Omega$. For platinum the time constant is roughly 0.5 second, so that $C_{\text{pol}} = 0.5\ \text{s}/0.75\ \text{M}\Omega = 0.7\ \mu\text{F}$. Highly polarizable electrodes are dominated by C_{pol} with little influence from a large R_{pol} . As soon as the capacitor is charged, no more

TABLE 7.1 Electrode Conductor Materials

Metal	Properties	Use
Silver–silver chloride	Stable DC reference, low DC polarization, not biocompatible	Skin surface ECG, EMG
Platinum metals	Non-corrosive, biocompatible, polarizable	Needles, implants
Gold	Non-corrosive, less biocompatible than platinum	Needles
Titanium	Highly biocompatible	Implants
Stainless steel	Mechanically strong, non-corrosive, highly DC polarizable and noisy, very alloy dependent	Needles
Tin, lead	Low noise, soft and moldable	EEG
Nickel	Thin flexible plates, skin allergic reactions	Skin surface
Silver, zinc, iron, aluminum	Pharmaceutical or bactericidal properties	DC therapy and skin iontophoresis
Carbon	X-ray translucent, soft and flexible multiuse rubber plates	Skin surface ECG, EMG
Polymers	Also found as ionic or mixed versions, special consideration must be taken for the ionic contact medium. May be a part of the contact electrolyte.	Skin surface

Metals listed are usually alloys. In practice, oxides are formed covering the surface, also on the noble metals and their alloys. Use of different metals may generate large DC voltages which may saturate the input stage of biopotential amplifiers.

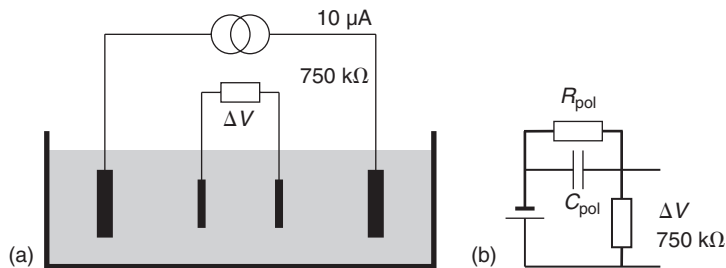


Figure 7.33 (a) Four-electrode system in 0.9% saline. Potential pick-up electrode pair of different metals as shown in Fig. 7.34. (b) Equivalent electric circuit for the loaded pick-up electrode pair.

current flows and the output voltage is zero. According to Fig. 7.34 silver, gold and stainless steel are highly polarizable. But notice that replacing the load resistance of $750\text{ k}\Omega$ with a much higher resistance will reduce the polarizing current through the pick-up electrodes, reduce the polarization and reduce the waveform distortion.

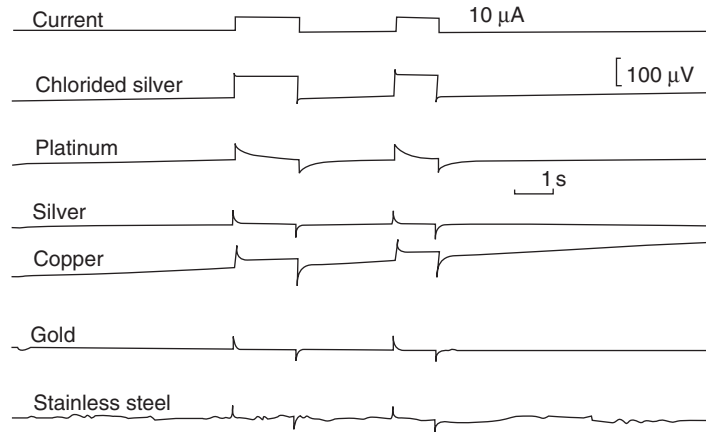


Figure 7.34 Measured voltage ΔV with six different pick-up electrode metals (cf. Fig. 7.33).
 Source: Cooper et al. (1980).

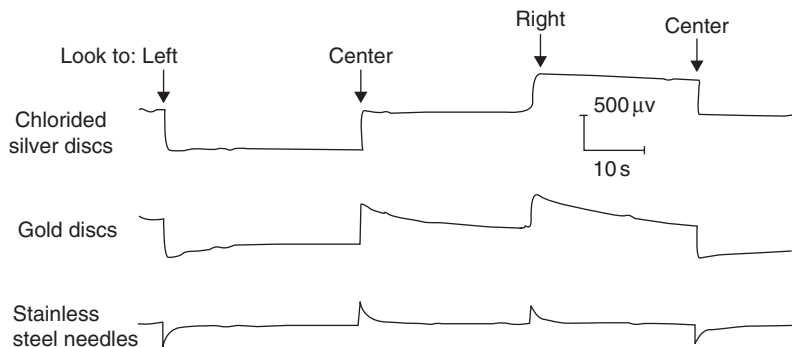


Figure 7.35 Recording of eye movements for different electrode metals. Electrode positions: 1 cm from the outer canthus of each eye. Source: Cooper et al. (1980).

Figure 7.35 shows the metal dependence with an endogenous signal source (EOG). EOG registrations are measured with DC response biopotential amplifiers.

Silver–Silver Chloride

This is a much used electrode metal (and metal chloride) in biology and medicine for DC applications both because it is simple and because it has a well-defined DC potential not very dependent on DC current flow (small overvoltage, cf. Chapter 2). It is therefore a non-polarizable DC reference electrode. It usually consists of silver covered by an AgCl layer, often electrolytically deposited. Ag and AgCl are toxic and cannot be used for long-term tissue contact. A salt bridge is often used in order to remove the electrode metal from direct tissue contact.

Wet AgCl is a solid ionic conductor (cf. Chapter 2). With DC current flow, the AgCl layer will increase in thickness if the electrode is the anode. The polarization

impedance will go through a minimum and thereafter increase as a function of AgCl layer thickness, see below. As a cathode with DC current flow, the layer will diminish and eventually be stripped off. We are left with a pure silver surface with quite different properties, for example with much higher polarization impedance and a different equilibrium potential (Fig. 7.34) and Section 2.5.1.

To produce an AgCl electrode the silver is placed as the anode in a solution of, for example, 0.9% NaCl. The optimum result is dependent on both the current density and quantity of electricity used; often the current density is of the order of 1 mA/cm^2 , and the quantity of electricity is 1000 mAs/cm^2 (Geddes, 1972). Optimum values are not necessarily the same for minimum impedance and maximum DC voltage stability, and they are dependent on actual electrode surface area. The best AgCl layer thickness also depends on the desired mechanical durability, and the possible quantity of electricity that may be passed in the opposite direction without stripping off the AgCl layer during use. A monopolar nerve stimulating electrode is nearly always used as cathode, and will therefore gradually strip off an AgCl layer. AgCl may also be *sintered* to form bulk AgCl, the surface can then be rubbed and thus be used many times.

Platinum Metals

Platinum electrodes are in certain ways the opposite of AgCl electrodes. Platinum is biocompatible and therefore highly suitable for invasive electrodes and implants. Even if it is DC polarizable it is still suitable for DC potential measuring applications under strict zero DC current conditions. Together with other noble metals and their alloys, they are also preferred as current carrying electrodes in contact with living tissue, in particular, for pacemaker implanted catheter electrodes. For pacing electrodes Greatbatch (1967) found large differences between the pure noble metals and their alloys, except for Pt and Pt 90%, Ir 10%.

The platinum electrode can be improved by an active electrolytic process forming a platinum black surface. The reduced polarization impedance is due to an increased effective metal surface area (fractal surface). The electrode is prepared in an electrolyte containing, for example, 3% platinum chloride, with the platinum as the cathode. Platinum black is deposited on the surface, and also here there are optimum values for current density and quantity of electricity: a current density of about 10 mA/cm^2 and a quantity of electricity (charge) of about $30\,000 \text{ mAs/cm}^2$ is recommended (Schwan, 1963). Best results are obtained if the platinum surface is sandblasted before platinum black deposit. However, the surface may be fragile, and a protein layer formed with tissue contact may easily smooth the micro-rough surface and increase polarization impedance. Platinum black electrodes are best stored in distilled water and short-circuited (Schwan, 1963).

Titanium Alloys

Typically, titanium alloys have been the materials of choice for medical implants. The Ti-6Al-4V alloy is generally considered chemically inert, compatible with human tissue and resistant to corrosion by human body fluids. However, the small percentages of vanadium and aluminum contained in the alloy are potentially toxic.

Pure titanium is chemically and biologically more compatible with human fluids and tissue, but it is too weak for prostheses that must bear heavy loads, such as leg or hipbone implants.

7.4.3 Contact Electrolytes

The contact medium is an ionic conductor positioned between the electronic conductor and the tissue. Insulating materials such as glass which depend purely on displacement currents are a special group. The purpose of the contact electrolyte is to:

- control the metal–electrolyte interface
- form a high conductance salt bridge from the metal to the skin or tissue
- ensure small junction potentials
- enable the metal–electrolyte interphase to be kept at a distance from the tissue
- fill out spaces between an electrode plate and tissue
- moisten a poorly conducting skin with electrolytes

The contact medium represents an electrolytic volume DC resistance in series with the polarization and tissue impedances. Ionic contact media of special interest are:

1. wet gel or paste with electrolytes
2. solid gel (hydrogel) with electrolytic conductance, with or without adhesive properties
3. saline (e.g. physiological 0.9%) or salt bridge electrolytes
4. body fluids
5. tap water
6. ionic polymers
7. electric arcs

Skin Surface Contact Electrolytes

The stratum corneum layer of non-wetted human skin is strongly variable and may be very poorly conductive. As we shall see the skin is often dominating the electrical properties of an electrode used for recording endogenic signal sources such as the ECG. This skin influence is therefore treated here (for additional information on skin electrical properties, see Chapter 4).

Wet Gel Electrolytes

The mechanical or viscous properties of the contact medium are important, and often the electrolyte is thickened by a gel substance or contained in a sponge or soft clothing. Commercial ECG electrodes are often delivered as pre-gelled devices for single use, and must then be stored safely to prevent bacterial growth or drying out. The medium may also contain preservatives to increase storage life, or quartz particles for abrading purposes on the skin.

Generally, the ionic mobility and therefore the conductivity in a high viscosity paste are lower than in a liquid. Wet electrolytes of high concentration (>1%)

penetrates the skin actively, with a time constant often quoted to be of the order of 10 min (Tregear, 1966; Almasi and Schmitt, 1970; McAdams et al., 1991b). However, actually the process is not exponential (as diffusion processes are not), and may go on for hours and days (Grimnes, 1983a), cf. Fig. 4.20. The penetration is stronger the higher the electrolyte concentration, but also more skin irritating. NaCl is better tolerated by human skin at high concentration than most other electrolytes. Figure 7.36 shows the electrolyte penetration into the skin the first 4 hours after electrode onset to the skin. Impedance at 1 Hz is dominated by stratum corneum electrolyte content, with less than 1% contribution from the electrode's own small signal polarizing impedance.

The conductivity σ of some often used contact cremes/pastas: Redux creme (Hewlett Packard) 10.6 S/m, Electrode creme (Grass) 3.3 S/m, Beckman-Offner paste 17 S/m, NASA Flight paste 7.7 S/m, NASA electrode creme 1.2 S/m.

In comparison, 0.9% NaCl (by weight) physiological saline solution has a conductivity of 1.4 S/m, and muscle tissue less than half of this but very anisotropic. Most gels are therefore strong electrolytes. NASA Flight paste, for instance, contains 9% NaCl, 3% KCl and 3% CaCl, in total 15% (by weight) of electrolytes. Thick EEG paste may contain as much as 45% of KCl.

Skin impedance is usually much higher than electrode polarization impedance (Grimnes, 1983a). Physically as they are in series, Fig. 7.37, electrode polarization impedance can often be neglected in skin applications. In Fig. 7.37 R_{cnstri} is related to the current constricting zone of the electrode (cf. Fig. 6.3).

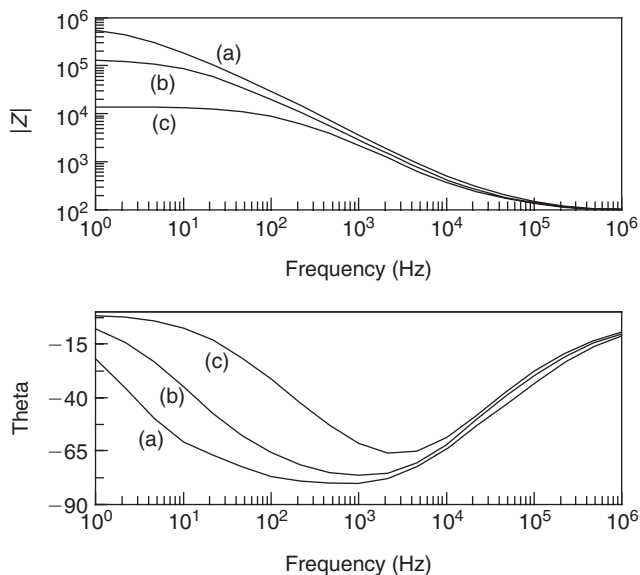


Figure 7.36 Spectra of human skin plus polarization impedance and the effect of contact electrolyte skin penetration. Values just after electrode onset (a) and after 1 (b) and (c) 4 hours. One commercial ECG electrode, skin wetted area 3 cm².

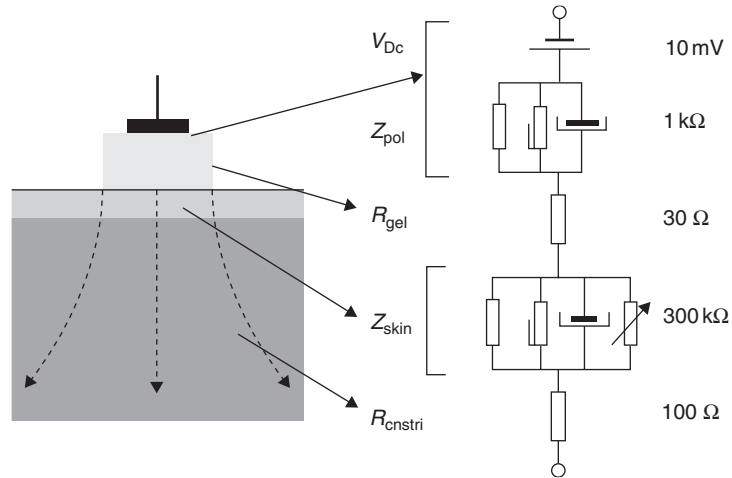


Figure 7.37 Skin surface electrode geometry and its equivalent electric model. *Right:* Typical values at 10Hz for a commercial wet gel ECG electrode. Note that Z_{skin} before contact electrolyte penetration is >99% of the total impedance.

In some skin applications the electrode polarization impedance may still be a source of error. With solid gel contact electrolyte the series resistance of the contact medium may be disturbing at higher frequencies. When the stratum corneum is highly penetrated by electrolytes (Fig. 7.36) the skin impedance is so low (50 k Ω) that the electrode polarization impedance becomes important.

Skin impedance is of great concern both for recording and current carrying applications. The frequency band and the resolution both in space and time may depend on the skin impedance. High electrode impedance and relatively low amplifier input impedance has been a problem in ECG right from the time of Einthoven, who used large electrolyte containers with the limbs deeply immersed. A classical study for ECG applications is by Geddes and Baker (1966). Rosell et al. (1988a) measured the impedance of skin coated with gel, but otherwise unprepared, and found that for 1 cm², the impedance at 1 Hz varied from 10 k Ω to 1 M Ω and at 1 MHz was always close to 120 Ω . They measured at sites typically used for ECG, impedance plethysmography, impedance cardiography and electrical impedance tomography and stressed the importance of considering these values for designers of biopotential amplifiers. Also McAdams and Jossinet (1991b) re-examined the problem with respect to the increased demands posed by the renewed interest in high-resolution ECG recording. See Chapter 4 for more information on skin electrical properties.

“Dry” Skin Contact

Putting a dry metal disc on non-wetted human skin results initially in a very rapid admittance rise as the natural water of the skin gradually wets the dry metal surface. Before disc onset the water content of the superficial layers of the stratum corneum

is determined by the partial pressure of water vapor in the surrounding air, and on the recent sweat activity. After some hours the conditions may become more like the applied wet gel case.

Solid Gel (Hydrogel)

A solid gel may constitute both the contact electrolyte and the adhesive surface. Solid gels are with natural or synthetic hydrocolloids (McAdams et al., 1991b). They do not wet the skin, and when applied to the skin the gel may moisten the skin or the skin may moisten the gel. Water transport is diffusion controlled to the material with the lowest partial pressure of water. In contrast to wet gels, the effective electrode area when applied to the skin is rather constant and well defined. Hydrogels as skin contact medium have been found to give smaller parallel DC conductance and higher capacitance coupling than wet contact media (McAdams et al., 1991b). This implies less wanted properties the lower the frequency of interest, but desired properties in high frequency applications such as for electrosurgery plate electrodes.

Skin Abrasion and Carbon Tattooing

Even a rather light abrasion of the skin surface is surprisingly effective in taking away the surface layers and obtaining direct access to the deeper part of the stratum corneum with higher water content.

Other methods have also been tried to avoid the high impedance of the skin. Vitreous carbon buttons have been implanted in the skin, and tattooing techniques have been used for depositing colloidal carbon in skin (Hoenig et al., 1978). Black dot areas of about 8 mm in diameter showed reduced impedance at 1 Hz. The effect was reported to be equally active after more than 2 years.

Tissue Liquid Electrolytes

Invasive electrodes usually have metal in direct contact with the tissue. The metal must then be biocompatible for the duration of tissue contact. The electrical properties will be dependent on the metal and the tissue.

Electric Arc

A special ionic contact medium, to skin or any tissue surface, is the gas *plasma*. Plasma is an ionized, and therefore conductive, gas. The ionization process is high electric field induced, and the process is enhanced in inert gas atmospheres such as argon.

In its simplest form, an arc may be drawn from a needle electrode to the skin surface. The arc will seek high conductive spots like the sweat duct orifices. The arc may be DC or AC driven, and in air about 2000 V per millimeter distance is necessary for ignition with a steady state current in the micro-ampere range.

A single spark is the usual contact medium with electrostatic discharges in daily life situations (Section 9.29).

In electrosurgery, argon is used as a gas medium for RF coagulation of tissue surfaces. The argon gas flow guides the arc and facilitates the spread coagulation

over a larger area. At the same time oxygen reactions are impeded, and thus the carbonization of tissue.

7.4.4 Equilibrium DC Properties (Negligible Current Flow)

At zero current conditions the electrode is at equilibrium, and the polarization still existing is therefore endogenic. Endogenic polarization is important and manifests itself by a polarization immittance measured with low AC currents so that the system is linear (cf. Section 2.5.4). However, even with zero current flow in the electrode wire local currents may flow caused by inhomogeneities of the metal surface or contact with a non-isoelectric tissue area.

Electrode Pair DC Voltage and Noise

If different metals are used in an electrode pair, the different half-cell potentials may easily create a DC voltage output of >1 V. This may represent a source of noise and may saturate the input stage of the biopotential amplifier used. Inhomogeneous surfaces may create local potential differences, local DC current flow and local corrosion, even with zero current flow in the external circuit. If an AgCl surface is partly stripped its coating so that some pure silver surface appears, the DC voltage will change and the noise level will increase (cf. Table 2.9 half-cell potentials).

Two equal AgCl plates immersed in a homogeneous chloride electrolyte, will in practice generate <1 mV DC, under well-controlled conditions just some few microvolts.

The *noble metals* in saline solution are highly polarizable, and the DC voltage will be unstable and poorly defined unless under strict zero current conditions. Metal alloy inhomogeneity will create noise as a function of local current flow between different parts of the metal surface. The noise generation of stainless steel electrodes is very dependent on the alloy composition.

Liquid-Liquid Potentials (Salt Bridge Function)

It is useful to consider a contact electrolyte as a salt bridge, emphasizing the physical separation between the metal-electrolyte interphase and the electrolyte-tissue contact zone. Just like a metal-electrolyte junction generates a DC potential, so does the junction of two different liquids. This potential is called a *liquid junction potential* (Φ_{lj}):

$$\Phi_{lj} = \frac{\mu^+ - \mu^-}{\mu^+ + \mu^-} \frac{RT}{nF} \ln \frac{c_1}{c_2} \quad (7.48)$$

where μ^+ and μ^- are the mobilities of cations and anions, respectively. In biological application it must be remembered that adsorbed species at the electrode surface may change the half-cell potentials.

The liquid potential of a junction of different concentrations of NaCl is for instance: with $c_1 = 10c_2$ the dilute side is 12.2 mV negative with respect to the

other side. The salt bridge usually represents a low resistance bridge to the tissue, and makes an effective contact with only a small liquid junction potential. The solution may be in the form of a liquid, a paste, a gel or a hydrogel. The ionic mobilities are less the higher the viscosity of the medium, and the liquid junction potential thus changes according to eq. (7.48).

The liquid junction DC potential generated by a salt bridge is minimized if the mobilities of the ions used are as equal as possible (cf. eq. 7.48). This is, for instance, the case for K^+ and Cl^- , a salt bridge therefore often contains a strong KCl electrolyte. Then it may be necessary to impede the strong electrolyte from reaching the tissue or measuring cell, by introducing a rather tight plug or filter. The influence of the cations Na^+ , K^+ and Ca^+ is different on living cells and tissue, so the choice between NaCl, KCl or CaCl may be very important.

In electrophysiology requiring DC stability, AgCl electrodes are widely used. They may be used with a salt bridge filled with saturated KCl. Even if the salt solution is immobilized with agar gel at the tissue side, potassium is known to influence excitable cells, and it may be preferable to use NaCl 0.9% instead. A liquid junction DC potential must then be accounted for.

DC measurements of skin potentials are of particular interest. Often palmar skin is at about -20mV with respect to an invasive electrode or a non-palmar skin surface electrode. Such a voltage is very dependent on the contact electrolyte used, and on the liquid junction potential between the salt bridge and the natural electrolytes (sweat) of the skin. It is found that the measured DC voltage is very dependent not only on the concentration of the salt, but also on the cations (e.g. Na^+ , K^+ or Ca^+) used.

Reference Electrodes

In the field of bioimpedance the by far most important non-polarizable electrode for stable DC potential measurement is the *AgCl electrode*. This is because all tissue liquids contain some Cl^- ions, and because the electrode can be made very small, for example with just a small chlorided silver wire. The half-cell potential relative to a standard hydrogen electrode at 25°C in an aqueous solution is $+0.222\text{V}$. Under ideal conditions such an electrode can be reproducible to $\pm 20\mu\text{V}$. Thus two equal electrodes in the same solution should have zero potential difference to within $\pm 40\mu\text{V}$. This precision is quoted under the assumption of virtually no DC current flow.

The most cited reference electrode is the *platinum-hydrogen* electrode, and electrode DC potentials are often given relative to such an electrode. It is an important electrode for absolute calibration, even if it is unpractical in most applications. The platinum electrode metal is submerged in a protonic electrolyte solution, and the surface is saturated with continuously supplied hydrogen gas. The reaction at the platinum surface is a hydrogen redox reaction: $H_2 \leftrightarrow 2H^+(\text{aq}) + 2e$, of course with no direct chemical participation of the noble metal. Remember that the standard electrode potential is under the conditions $\text{pH} = 0$ and hydrogen ion activity 1mol/L at the reference electrode. Thus the values found in tables must be recalculated for other concentrations. Because of the reaction it is a hydrogen electrode, but it is also a platinum electrode because platinum is the electron source or sink, and perhaps a catalyst for the reaction.

Noise

Noise is an AC voltage superimposed on the equilibrium DC potential. The noise can take the form of pulse noise, white noise or $1/f$ noise. The frequency range is therefore important; the generated noise is defined in rms values, for example $\mu\text{V}/\sqrt{\text{Hz}}$, but often also given as peak-to-peak (p-p) values. There are three rules:

1. Less noise the larger the electrode area, because of the averaging effect.
2. More noise the more polarizable electrode (poorly defined half-cell potential).
3. More noise the more diluted contact electrolyte.

With a usual ECG signal bandwidth of 0.1–100 Hz, an AgCl electrodes in 0.9% saline may generate of the order of $10\ \mu\text{V}$ p-p. A pure silver plate may easily generate 10 times this amplitude. Also sudden spikes of millisecond duration and hundreds of microvolt amplitude may be generated. An important noise source is a non-uniform electrode surface, with local current exchanges between impurity centers as local corrosion processes.

Stirring is another noise source, due to a mechanical disturbance of the concentration gradients in the double layer. To minimize this effect it is important to stabilize the solution with respect to the metal surface. A protection cup or a salt bridge separation to the tissue is often used in order to minimize the metal–electrolyte interphase movements.

7.4.5 Polarization Immittance (Linear Conditions)

By electrode polarization immittance we mean the immittance of the electronic/ionic interface as described earlier in Section 2.5. In this interphase many of the processes occur physically in *parallel* (Fig. 2.17), and it is a good reason to study them by also using *admittance*. As the electrode is *in series* with the biomaterial of interest, it is also a good reason to focus on electrode *impedance* as a source of error in tissue characterization.

The metal–electrolyte interface area is called the *electrode area* (EA). EA may be the plane area, or include a surface roughness or fractal factor. The interface area of the contact medium and the tissue is called the *effective electrode area* (EEA). With skin surface electrodes often $\text{EEA} > \text{EA}$ (Fig. 7.42). With electrolyte-filled glass microelectrodes often $\text{EEA} < \text{EA}$ (Fig. 7.48). *On tissue*, the contact area is very important:

1. Large EA implies low electrode polarization impedance.
2. Small EEA may imply geometrically dependent current constriction effect (cf. Fig. 6.3) and a larger influence from the tissue or electrolyte volume near the electrode.
3. Large EEA for *recording* electrodes implies an averaging effect and loss of spatial resolution.
4. Large EEA for *stimulating* electrodes implies higher excitable tissue volume and a summation effect in the nerve/muscle system.

The immittance per EA is dependent on double layer capacitance, possible redox reactions and sorption processes at the interface, as well as diffusion processes in the electrolytic solution (cf. Fig. 2.17). In series with the interface impedance there is the bulk volume resistance of the contact medium obeying Ohm's law $\mathbf{J} = \sigma \mathbf{E}$. By determining and then subtracting this series resistance, the polarization immittance properly speaking appears.

Platinum Black Electrode

The impedance is shown in Fig. 7.38 for black platinum in a physiological saline solution, one of the lowest polarization impedance systems known. Schwan's data are for a 1.4-mm² platinum disc, but here recalculated for 1 mm² and given as impedance series values. If inversely proportional to EA, the values correspond to an impedance $|Z|$ less than 1 Ω for 1 cm² at 1000 Hz. The exponential factor for the reactance X is $m = -0.61$ ($R^2 = 0.996$). If Fricke's law is valid, this corresponds to a phase angle $\varphi = m \times 90^\circ = -54.9^\circ$ and a loss tangent $\tan \delta = 0.39$. The resistance R exponent factor for the whole frequency range is $m = -0.55$ ($R^2 = 0.998$), corresponding to a phase angle $\varphi = -49.5^\circ$. As is easily seen in Fig. 7.38, the ratio X/R and therefore also $|\varphi|$, diminish with increasing frequency. Instead of whole range exponents, local exponents for a limited frequency range may be examined, and a useful accordance with Fricke's law is found even if φ is a function of frequency (Schwan, 1963).

The parallel capacitance calculated from the data of Fig. 7.38 is not a pure double layer capacitance, it is too frequency dependent. It must be due to redox or sorption processes at the platinum surface. Under optimum conditions it is possible to obtain capacitance values of the order of 500 $\mu\text{F}/\text{mm}^2$ at 20 Hz (Schwan, 1963). A polished and etched platinum surface has a capacitance of the order of 0.5 $\mu\text{F}/\text{mm}^2$ at 20 Hz, 1/30 of the value for the platinum black surface shown in Fig. 7.38.

AgCl Wet Gel Electrode

Figure 7.38 showed that platinum black is a preferred electrode metal element with respect to low polarization impedance. However, it may easily be polarized by a DC current, and for such cases a silver-silver chloride electrode is usually preferred. Typical immittance plots for one pre-gelled silver-silver chloride ECG electrode obtained from two electrodes in front to front contact (no tissue in between) is shown in Fig. 7.39. The data were obtained with a constant amplitude current of 1 $\mu\text{A}/\text{cm}^2$ rms, corresponding to a single electrode maximum (1 mHz) voltage of 2.5 mV rms.

A possible interpretation of these data is: At high frequencies the series resistance of the electrolyte dominates (frequency independent value of about 5 Ω , Fig. 7.40(a)) and the low value indicates a strong, high conductivity electrolyte. At low frequencies the parallel admittance of the polarization process at the AgCl surface dominates. Accordingly the *high frequency* results must be analyzed from the *impedance* plot. The low frequency admittance plot (right) indicates a DC leakage parallel to the polarization process of approximately 0.3 mS. In the medium frequency range from about 0.1 Hz to 100 Hz (three decades), the phase angle is constant equal to about 43°, so the polarization immittance is dominated by a CPE. The frequency

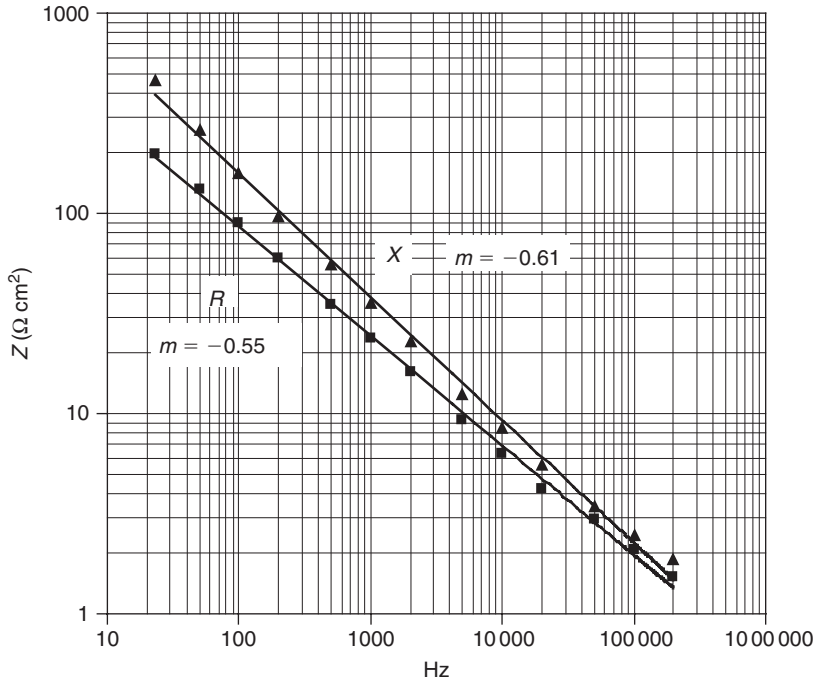


Figure 7.38 Polarization impedance for monopolar platinum black electrode in physiological saline solution. Constrictional series resistance subtracted. Data from Schwan (1963), by permission.

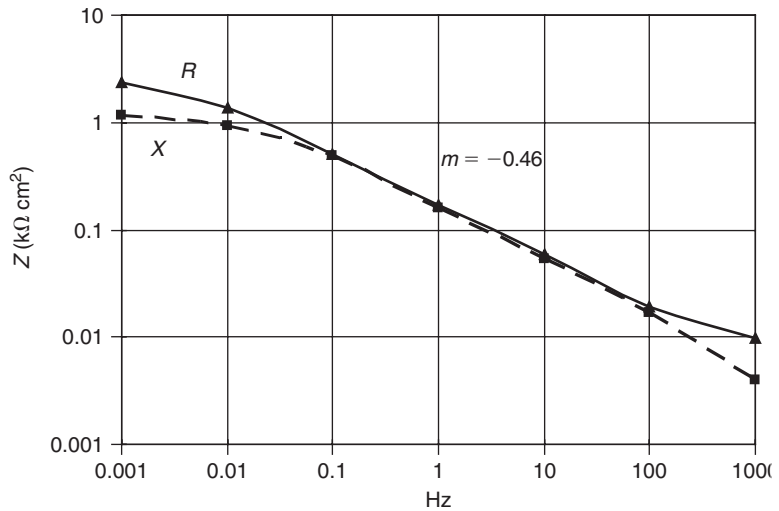


Figure 7.39 AgCl pre-gelled wet electrolyte electrode polarization impedance. Two ECG commercial electrodes measured front to front, contribution of one electrode. Gel area 3 cm^2 .

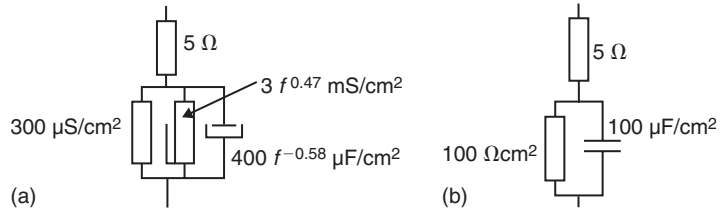


Figure 7.40 Equivalent circuits for the electrode polarization impedance found with one AgCl/wet-gel electrode: (a) with frequency-dependent CPE components ($m = 0.47$); (b) more simplified version with ideal components, valid around 10 Hz (ECG).

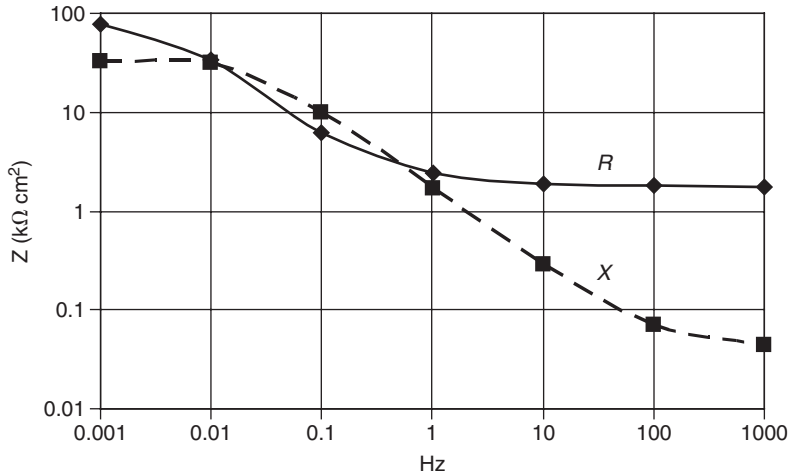


Figure 7.41 Hydrogel–aluminum electrode, 5 cm² skin contact area, polarization impedance. Two ECG commercial electrodes front to front, contribution of one electrode.

exponent m of the admittance in the same range is found to be 0.47, which multiplied by 90° is also about 43° . The CPE is therefore of a Frick type.

Two possible electrical equivalent circuits are shown in Fig. 7.40. Such equivalent circuits are often given in the literature in the most simplified way with static components as shown for 10 Hz in Fig. 7.40(b). Important characteristics of an electrode are lost by such a simplification. For two-electrode tissue measurements, the immittance of the equivalent circuits of Fig. 7.40 are a source of error physically in series with the tissue, and must either be negligible, or be subtracted as impedance from the measured impedance.

Hydrogel–Aluminum Electrode

Figure 7.41 shows the same data as Fig 7.39 but for hydrogel and aluminum electrode metal. Series resistance flattens out at about 1500 Ω at higher frequencies. This corresponds to a conductivity of the hydrogel equal to $\sigma = 6 \text{ mS/m}$ (gel thickness 1 mm). Accordingly the polarization impedance down to about 0.1 Hz of this

hydrogel electrode is resistive and dominated by the frequency independent resistance of the gel.

The conductivity of the hydrogel contact medium is much smaller than for the wet gel (Fig. 7.39 showing a series resistance of only about $5\ \Omega$). With such a high series resistance, the visible constant phase frequency range of the CPE is reduced to a small zone around 0.1 Hz. The polarization admittance $|Y|$ of the metal–electrolyte interphase is about $20\ \mu\text{S}/\text{cm}^2$ at 0.01 Hz, and consequently much lower than for the AgCl/wet-electrolyte case with about $600\ \mu\text{S}/\text{cm}^2$ at 0.01 Hz. At the lowest frequencies B is almost proportional to frequency, indicating a relative static capacitance ($B = \omega C$). Because of the large series resistance, it is difficult to assess accordance with Fricke's law directly. However, it is possible to subtract the presumed static series resistance from measured R , and then proceed the analysis from there.

The series capacitances of some other metal–electrolyte interfaces are given by Geddes (1972). They are always lower than the AgCl or platinum black electrodes in 0.9% NaCl. For stainless steel it was given as $40\ \mu\text{F}/\text{cm}^2$ at 20 Hz ($\approx 500\ \mu\text{S}/\text{cm}^2$).

The series resistance in these models may be regarded as an access resistance to the electrode interface, dependent on electrolyte conductivity and geometry, but not linked to the polarization processes. As such it belongs to the chapter on contact media and should be subtracted from measured electrode impedance when analyzing polarization immittance.

The series resistance may often be regarded as a short salt bridge with a high conductivity electrolyte solution. The salt bridge resistance may be a problem at high frequencies. Electrodes for plethysmography, for instance, are used around 50 kHz, and the polarization impedance is then so low that the series resistance may be the dominant factor. This is particularly true with hydrogel contact media as shown in Fig. 7.41.

Difference Between Electrolyte and Tissue as Contact Media

A contact electrolyte is a homogeneous material. The current distribution may be uniform with the metal closing the cross-sectional area of a measuring cell tube. Otherwise it will be a current spread from the electrode with a constrictional effect near the electrode, perhaps with an edge effect if it is a surface plate electrode. Even if the current density always may be unevenly distributed, there is however one fundamental difference if the metal is in direct contact with tissue. At low frequencies the cells will have a shadow effect because the poorly conducting cell membranes force the current to go around the cells in the interstitial liquid. The current density may vary locally and have much higher values than the average. The effective polarization impedance may be higher than the values found with a homogeneous electrolyte. Schwan (1992a) found that electrode polarization impedance increased with higher concentration of cells in suspension.

Electrolyte Concentration

A polarization ratio can be defined as the ratio of polarization impedance to the bulk resistance of the electrolyte. Mirtaheri et al. (2005) measured the ratio as a function

of frequency (10^{-2} – 10^3 Hz) and NaCl concentration (2.4–77.0 mmol/L), and found that the polarization ratio diminished as a function of concentration regardless of electrode material. Medical stainless steel ratio was concentration independent but had high electrode polarization impedance values compared to the other metals studied. Aluminum showed small ratio changes at low concentrations. However, the changes were more pronounced at higher concentrations. Gold, platinum and silver showed a moderate concentration dependency at low concentrations.

7.4.6 Non-linear Conditions (Current Flow)

With a current flow in the electrode wire the electrode is polarized by that current, this is an exogenic polarization. Non-linearity phenomena may then occur at the electrode or in the tissue. Here we concentrate on electrode properties.

DC polarization may be caused by the average component of a pulse- or sine wave form or by continuous unidirectional current flow.

Pulse polarization non-linearity may occur during a single pulse if it lasts long enough to cause irreversible electrolysis. Pulses <1 ms are mostly transferred to the tissue by capacitive current paths not implying electrolysis (non-faradic current). The same rules are valid for *large AC current polarization*, the higher the frequency, the better the linearity.

A fractal model was used by Ruiz et al. (2005) to explain the non-linear behaviour of an electrode–electrolyte interface.

Metal–Liquid Overvoltage

During exogenic current flow, an overvoltage is created as well in the double layer, the diffusion layer and the resistance in the bulk electrolyte. Many applications are in the non-linear region of current–voltage ratios. With DC currents the overvoltage may increase gradually and attain many volts with polarizable electrodes, accompanied by several possible effects of electrolysis at the electrode surface.

Neurostimulation is usually performed with needles, and square wave pulses of amplitude <5 mA and duration <1 ms are common. With skin surface electrodes the current used may be larger.

Pacemaker pulses are usually short AC pulses with a zero DC component, and the overvoltage is mainly determined by the double layer capacitance. Nerve stimulators may be with or without a net DC component.

In *iontophoresis* or *anti-hyperhidrosis* treatment, electrodes are used with continuous DC current. During such conditions the volume of the electrolyte compartment is of interest with respect to the buffering capacity for the products of electrolysis.

Defibrillator shocks are usually monophasic (Fig. 9.17) with a large DC component. Geddes et al. (1975a) measured the current–voltage characteristics with a 5-ms duration heavily damped sinusoidal defibrillator pulse. Standard defibrillator electrodes 3.5" in diameter (60 cm^2) were used with current pulses up to 80 A. The electrodes were face-to-face at 1 cm distance with the space filled with a $8.4\text{ }\Omega\text{-cm}$ electrode paste. It was found that the impedance of both electrodes (defined as the ratio of *peak* voltage to *peak* current) at such current levels was only a fraction of

1Ω . With the usual thorax tissue impedance of about 50Ω , little energy is therefore lost in electrode polarization processes. The 0.01Hz impedance of the same electrode pair at small linear AC current levels was found to be about $2\text{k}\Omega$.

7.4.7 Electrode Design

Skin Surface Electrodes

The most used skin surface electrode is the recessed type (see Fig. 7.42). The metal plate is at a certain distance from the tissue surface. The electrolyte is guarded in a rigid container for mechanical support and to minimize evaporation. The electrolyte solution is often supported or contained in a sponge. In this way the metal–solution interphase is clearly defined, and the total electrode impedance can easily be measured by connecting two electrodes face-to-face. Streaming potentials (electrokinesis) can be annoying if the solution is moved with respect to the metal during patient movements, but with the recessed electrode the interphase is stabilized and motion artifacts minimized.

The area of the skin wetted or in contact with the electrolyte solution is called the EEA of the electrode. EEA is the dominating factor determining electrode/skin impedance. EEA may be much larger than the metal area in contact with the solution (EA), which determines the polarization impedance. The electrode is fixed with a tape ring outside the EEA. Electrolyte penetrating the tape area increases EEA, but reduces the tape sticking area. Pressure on the electrode does not squeeze electrolyte out on the skin surface, because of the rigid container construction.

The right-hand side of Fig. 7.42 shows an electrode with solid contact gel. The gel is sticky and serves both as contact electrolyte and electrode fixation. For this electrode, $\text{EEA} = \text{EA}$. The electrolyte conductivity is rather low because the solution is a gel with low ionic mobilities. Electrolyte series resistance may be the dominating factor of electrode–skin impedance at high frequencies. This may introduce problems for use, for example for impedance plethysmography around 50kHz . With this electrode type the skin is not wetted. With such constructions it is possible to make an electrode with a very large $\text{EEA} > 100\text{cm}^2$, and obtain efficient skin contact over the whole contact area by using a rather thick gel. For neutral electrode plates in high frequency electrosurgery the conductivity of the gel may deliberately be chosen low, so that the electrode functions mostly by capacitive coupling.

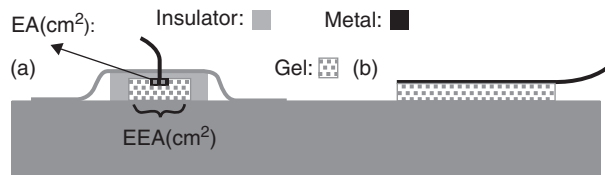


Figure 7.42 Skin surface electrode designs: (a) recessed metal with gel in stiff cup; (b) electrode with hydrogel contact electrolyte.

Band electrodes are used as large surface, low impedance electrodes with the additional attractive feature of *reducing the current constrictional effect* found with smaller disc electrodes. This is important in two-electrode applications such as impedance plethysmography and body composition estimation. In Fig. 7.43 the usual configuration is shown with the current carrying electrodes C and C' as the outer electrodes. Consider the difference of swapping the current carrying and recording electrodes.

Multiple Point Electrodes

The problem with a plate electrode in some applications is the covering effect on the tissue. With a multiple point electrode humidity, for instance, can escape from the surface. Dependent on tip sharpness and electrode pressure the points may penetrate the superficial layers.

Concentric Ring Electrodes

Barnett (1937) used a three-electrode system with a 6 cm² ring electrode as measuring electrode on the upper arm (Fig. 7.44). He used monel metal covered by flannel soaked in normal saline. The current carrying counter electrode was positioned symmetrical on the other side of the arm. The reference electrode was concentric to the measuring ring electrode. This is an efficient geometry for eliminating much of the deep tissue series impedance. He measured in the frequency range 2–42 kHz. With a four-electrode technique he also measured deep tissue contribution.

Yamamoto et al. (1986) used a two-electrode quasi bipolar system, with the large electrode having about 10 times the area of the small one. The concentric electrodes were positioned spring mounted in a tube in order to secure a constant electrode mechanical pressure on the tissue surface. With a third current carrying electrode it has also been used as a part of a three-electrode system (Martinsen et al., 1996).

Martinsen and Grimnes used a three-electrode concentric ring system with the outer ring split into two parts, one used as reference electrode (R) and the other as current carrying (C) electrode (Fig. 7.44). In this way the reference electrode picks up a potential more near to that of the measuring electrode, so that deeper tissue series impedance contribution is reduced.

Invasive Needle Electrodes

Electrodes as shown on Fig. 7.45 and 7.46 are used for EMG and in neurology. They may be of stainless steel, with outer diameter around 1 mm or less. As seen the shaft may be used as a reference electrode. Because of small EA and according

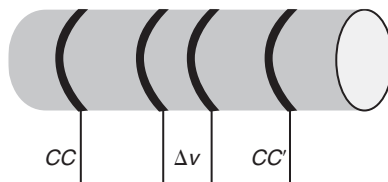


Figure 7.43 Band electrodes.

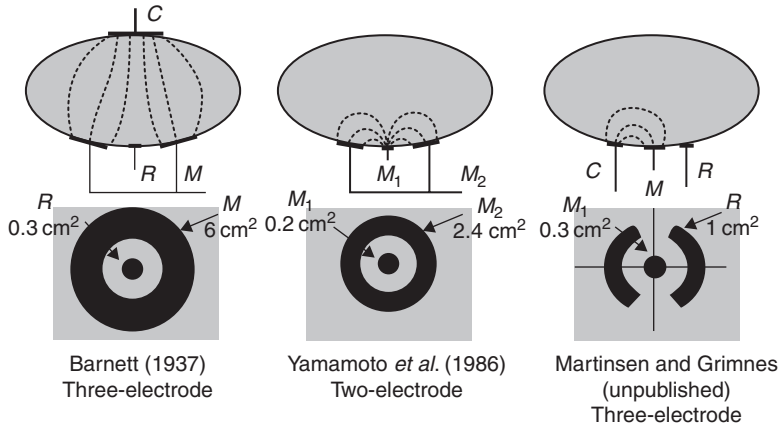


Figure 7.44 Concentric ring electrodes.

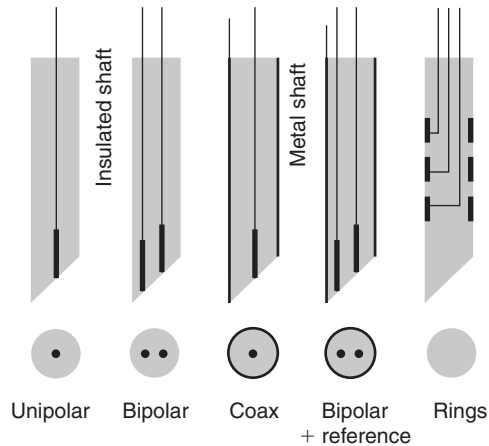


Figure 7.45 Needle electrode cross-sections.

to eq. (6.1 and 6.17), the total electrode impedance may be high and dominated by electrode polarization impedance.

Hollow needles are used for injection or aspiration of liquid samples. The external shaft is insulated by, for example, lacquer layer insulation; the internal tube is usually not insulated. The tip of the needle is exposed as an oval ring or a small tip area (Fig 7.46).

Impedance of Needle Electrode in Living Tissue

Figure 7.47 shows the monopolar impedance spectrum measured with a thin insulated needle inserted in porcine living tissue. The 90% sensitivity zone is roughly a sphere of about 3 mm centered at the exposed needle tip. Above ≈ 10 kHz the data is dominated by tissue properties, below ≈ 1 kHz by electrode polarization impedance.

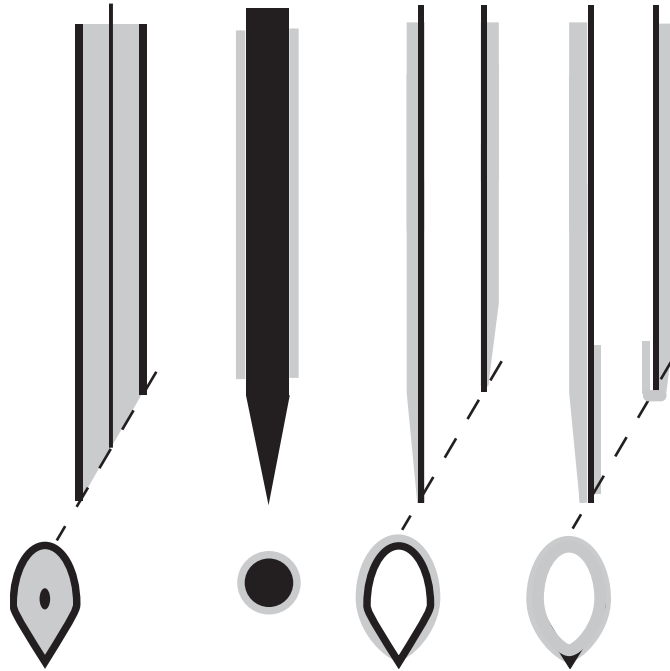


Figure 7.46 Needle models. From left: Coaxial small EA with exposed metal shaft, massive needle with insulated shaft, hollow injection needle with internal metal contact, hollow injection needle with internal end insulation.

Tissue Dependence of Polarization Immittance

An important finding from Fig. 7.47 was that the polarization impedance was tissue dependent, in accordance with the findings of Schwan (1992a).

With such data combined with multivariate analysis it is possible to determine the type of tissue that surrounds a needle tip, and also the position of the needle tip.

Microelectrodes for Intracellular Recordings

Monopolar recordings are made with a small transmembrane electrode in contact with the cytoplasm, and a larger extracellular electrode in the interstitial liquid. The tip of the electrode must be small enough to penetrate the membrane without too much damage and not too much plasma–electrolyte leakage. Squid giant axons have diameters up to 1000 μm , and in such studies the diameter of the penetrating part may be of the order of 50 μm . For ordinary cell sizes tips down to 1 μm diameter are used.

The electrode itself may be the end of a *metal needle* or the end of a fluid-filled *glass capillary (micropipette)*. The electrical characteristics of these two types are very different, and they have their characteristic application areas. The metal electrode has poor DC properties, and is best for recording fast action potentials. The micropipette electrode is better suited for recording DC or slowly varying DC potentials (Fig. 7.48).

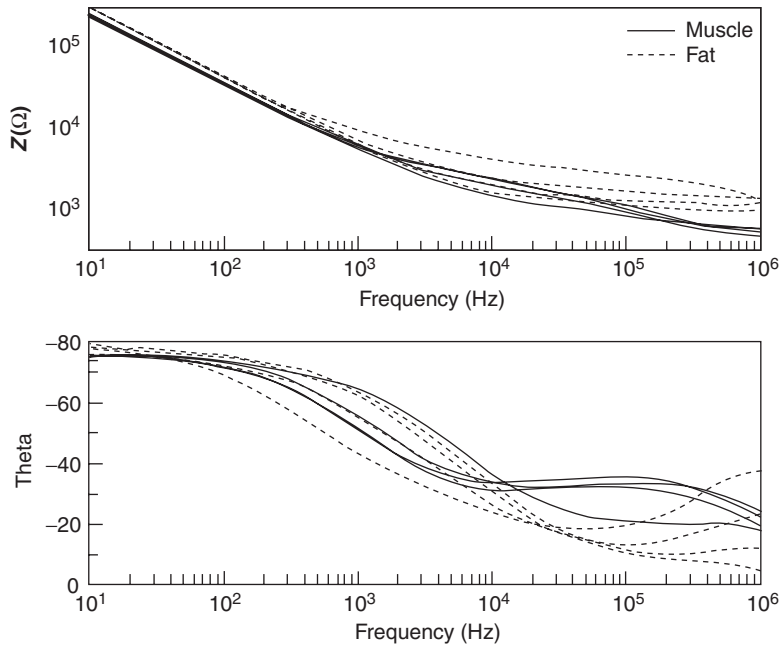


Figure 7.47 Monopolar impedance of insulated needle with exposed tip in situ in living porcine tissue. Impedance data dominated by electrode polarization below ≈ 1 kHz. Notice however polarization impedance dependence on tissue type. *Source:* Courtesy of Håvard Kalvøy.

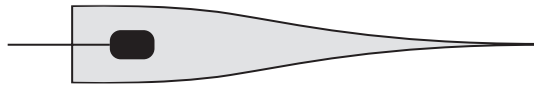


Figure 7.48 Glass micropipette electrode.

The *metal needle* can be made of tungsten, stainless steel, platinum alloys, etc., and it is possible to fabricate tip diameters down to $1\ \mu\text{m}$. It is necessary to isolate the shaft except the tip. A lacquer or glass coating can do this. A description of how to make them can be found in Geddes (1972). The metal surface exposed to the electrolyte is very small (of the order of $10\ \mu\text{m}^2$), and accordingly the polarization impedance may be several megaohms, increasing at lower frequencies and making the electrodes less suited for DC measurements. The frequency response is dependent on the polarization impedance and the distributed stray capacitance. The stray capacitance depends on the length of the needle shaft in contact with fluids and the thickness of the isolating layer.

The glass *micropipette* electrode is filled with an electrolyte, usually 3 M KCl. Such a high concentration is used to lower the electrode resistance, but the infusion of this electrolyte into the cell must be minimized. A liquid junction potential of some mV will be generated by the concentration gradient at the tip.

The electrode is fragile. During muscle studies the glass capillary end may easily break when the cells are excited. The micropipette electrodes are made with orifice diameters down to $1\ \mu\text{m}$. The small tip and its length and diameter determine to a large extent the electrical properties of the electrode, and its resistance may easily attain $100\ \text{M}\Omega$. The electrode surface is often AgCl , and the EA can be easily made so large that electrode polarization impedance error is negligible. It is a purely resistive electrode, however with distributed stray capacitance due to the glass dielectric in contact with the inner electrolyte and external tissue liquids.

The ordinary use of a micropipette electrode is monopolar. Double pipette electrodes are sometimes used with only one penetration of the cell membrane. One pipette is current carrying and the other is recording in a three-electrode setup.

Cellular Patch Clamp

Instead of introducing microelectrodes into the cell, a part of the cell membrane (a patch) may be attached to the electrode (glass pipette) by suction. cf. Section 5.5.1.

In Vitro Measuring Cells

Some material constants with a homogeneous cylinder of biomaterial are: $\sigma = GL/A$, $\varepsilon = CL/A$ and the resistivity $\rho = RA/L$. The ratio A/L (dimension m) or L/A (dimension $1/\text{m}$) is the *cell constant* of a measuring cell. In general the cell constant can be determined for other geometries than the cylinder, so that it is easy to derive the unknown conductivity, permittivity or resistivity from measured results. In the latter case it is of course important that the measuring cell is completely filled with the sample biomaterial. If sample size varies, it is easier to use a *guard ring* (Fig. 7.49(c)) around the measuring electrode kept at the same voltage. The effect of stray fields or current constriction is then reduced.

If the measurement is to be performed under *ex vivo* conditions, the tissue is to be kept alive by controlling the temperature and the extracellular fluids. Also with dead samples temperature and extracellular liquid control may be necessary. For “dry” dead samples control of the *ambient air humidity* may also be necessary.

One way of reducing the effect of electrode polarization is to increase the impedance of the sample by increasing its length. In order to compensate for the polarization impedance further, several methods are possible:

1. Four-electrode system (tetrapolar) (cf. Section 6.6.2).
2. Measure electrode polarization impedance separately and subtract.
3. Substitute the unknown with a known sample for calibration.
4. Vary the measured sample length, for example, in suspensions.

Methods 2 and 3 are based on the assumption that the metal–liquid interphase and thus the polarization impedance is invariable. This is not always the case. Measuring on “dry” samples, for instance, implies poor control of the contact electrolyte. Also a sample may contain local regions of reduced conductivity near the electrode surface. The currents are then canalized with uneven current density at the metal surface (shielding effect). Electrode polarization impedance, in particular at low frequencies, is then dependent on the degree of shielding (Fig. 7.47).

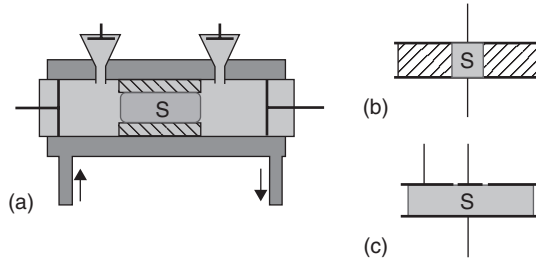


Figure 7.49 Measuring cells for tissue samples (S): (a) four-electrode liquid-filled system, temperature controlled; (b) sample confined by insulating material; (c) guard ring (kept equipotential with center electrode).

7.4.8 Non-galvanic Coupling to Tissue

Magnetic Field Coupling to Tissue

Magnetic Nerve Stimulation

A time varying magnetic field causes an induced electromotive voltage (emv) in a conducting medium according to *Faraday's law of induction* (more generally formulated in Maxwell's equation 8.2):

$$v = -\partial\phi/\partial t \quad (7.49)$$

where ϕ is the magnetic flux (in weber or volt-seconds) through a closed loop, and v is the voltage between the loop ends if the loop is open. In volume conductors the loops are effectively closed and the induced potential causes a flow of electric current. Such currents induced by time varying magnetic fields are called *eddy currents*. The induced eddy current density will be higher, the higher the medium conductivity. Induced low frequency currents will therefore follow high conductive paths (blood vessels), and avoid low conductivity areas (lung and bone tissue, myelin). With the fast switching ($100\mu\text{s}$) of the high gradient magnetic fields (25 mT/m) used in MRI, the current density in the body is approaching the threshold of perception. This is analogous to the use of skin surface coils for the stimulation of superficial nerves. Bickford and Fremming (1965) demonstrated the feasibility of magnetic nerve stimulation. Barker et al. (1985) found that it is possible to stimulate the human motor cortex. With a suitable skin surface coil of a diameter of about 10 cm, a short millisecond pulse with a peak current of the order of 5000 A creates a local maximum field of a few tesla. Even if the magnetic field strength falls off with distance, the induced current in a nerve just under the coil is sufficient for excitation. The excitation threshold is dependent on the magnetic field direction. The ordinary single coil construction gives maximum field strength distributed over the whole circle corresponding to the coil windings, with only a small contribution in the coil center. Double coils are used in order to focus the field strength. The inductance of the coil and the high current level and short pulse time correspond to a high voltage across the coil ends and thus a high local electric field in addition to

TABLE 7.2 Skin Depth δ as a Function of Frequency and Material

σ (S/m)		δ @60Hz	δ @1 kHz	δ @1 MHz	δ @3 GHz
5.8×10^7	Copper	8.5 mm	2 mm	66 μ m	1.2 μ m
1×10^5	Graphite	210 mm	50 mm	1.6 mm	29 μ m
5	Sea water	30 m	7 m	2 m	4 mm
1	Physiological saline	67 m	16 m	4.5 m	8.9 mm

the magnetic field. The mechanical forces acting on the coil windings are considerable, and with repeated pulses heat development must also be considered.

Eddy currents will set up their own magnetic fields, *opposing the external field*. The magnetic field will therefore be attenuated as function of depth (*skin effect*). The *skin depth* (depth of penetration) δ in the case of a uniform, plane electromagnetic wave propagating in a volume conductor with a magnetic permeability μ is:

$$\delta = \frac{1}{\sqrt{\pi f \sigma \mu}} \quad (7.50)$$

As the wave may be reflected at the surface, the initial value corresponds to the value just inside the medium. Equation (7.50) must be used with care, because the far-field conditions of a *wave* are not fulfilled at lower frequencies.

The skin depth will be high if the conductivity is low and the frequency is low. According to Table 7.2, magnetic alternating fields are not very much attenuated by the presence of a human body at frequencies below 1 MHz. Casañas et al. (2004) used a frequency of 28 kHz to measure iron overload in the human liver. At frequencies used in MRI, for example 60 MHz for 1.5 T systems, the attenuation and phaseshift are considerable.

Magnetic Resonance Imaging

In magnetic resonance imaging (MRI) the field coupling to the body is as purely magnetic as possible. It is obtained by three sets of coils: the static main field coils (e.g. 1 T), the gradient coils (e.g. 30 mT/m with rise and fall times in the microsecond range) and the RF coils (e.g. with separate transmitting, e.g. peak power of 10 kW at 60 MHz, and receiving coils).

In a superconducting coil the voltage across the coil ends is zero, and so there are no additional E-field applied to the patient. Gradient coils and RF coils however have a considerable voltage difference between the coil ends in order to drive the necessary current. If not shielded such coils therefore produce an electric field in addition to the magnetic field.

Magnetic Fields from Endogenic Current Sources

All electric currents are accompanied by magnetic fields. With the invention of the superconducting quantum interference device (SQUID) as an extremely low magnetic field (10^{-9} T) detector, it has become possible to measure the magnetic fields

from the small endogenous currents of the body, even from the small sources in the heart and the central nervous system. This has opened up a whole new field of measurements analogous to their electric counterparts: MKG (EKG), MEG (EEG) and so on. However, these interesting subjects are outside the scope of this book, and the reader is referred to the book by Malmivuo and Plonsey (1995).

Electric Field Coupling to Tissue

A non-galvanic electric field coupling to tissue is a capacitive coupling. Accordingly it is more efficient the higher the signal frequency used, according to $B = \omega C$. For low frequencies, for example $<1\text{ Hz}$ and at DC, non-galvanic coupling cannot be used. However, for example, the coupling from the power lines is of interest in hazard analysis, even when the coupling is at several meters distance and the frequency is only 50/60 Hz.

Static Electric Field Coupling to Tissue

An ideal dielectric is a material, which allows internal E-fields because the material has no free charge carriers and therefore no DC conductivity. A conductor like the human body, being exposed to an external static field, does not allow internal static E-fields, the charges on the surface are rearranged so that the internal E-field strength is zero. *An externally applied static E-field to the human body therefore has no effect on internal organs, only on the skin.* However, applied *alternating* E-fields result in tissue currents and internal E-fields. At high electric fields corona discharge will occur.

Low Frequency Electric Field Coupling to Tissue

Humans are exposed to electric fields from power lines in their daily life. The power lines inside buildings expose us to 50/60 Hz E-fields, and in a usual situation some tenths of a microampere is measured if a well-insulated person is grounded via an ammeter. Such small currents are perceptible for humans under certain conditions (*electrovibration*, Section 9.17.1). Outdoors a much higher current can be measured if the person is under a high voltage power line. Calculations show that at low frequencies (e.g. power line frequencies 50/60 Hz), the field strength in a human's interior is far smaller than the external field strength (Foster and Schwan, 1989). Except for the skin, the tissues of the body to the first approximation may be considered to be equipotential. However, this is not true for small signal measurements: $1\ \mu\text{A}$ 50/60 Hz through, for example, an arm with a total resistance of about $500\ \Omega$ (Fig. 4.26) results in a voltage difference of 0.5 mV. This is certainly not a negligible signal when ECG signals of the same magnitude are to be measured (cf. Section 9.1). The current density distribution in such cases, was studied by Guy et al. (1982).

The effect of an applied alternating E-field may be analyzed as an ordinary capacitor coupled system (Chapter 3). The tissue of interest may be modeled as a part of the dielectric, perhaps with air and other conductors or insulators. The analysis of simple geometries can be done according to analytical solutions of ordinary electrostatic equations as given in Chapter 6. Real systems are often so complicated that analysis preferably is done with a FEM (Section 6.7).

A simple first approximation calculation can be done, for example, with a model consisting of a conductor cylinder of radius a at distance $D/2$ from an infinite plane conductor. The capacitance per meter conductor is (cf. eq. 6.26):

$$C = \frac{2\pi\epsilon}{\ln\frac{D}{a}} \quad (7.51)$$

With $D = 2\text{ m}$ and $a = 1\text{ mm}$, C is of the order of 7.6 pF/m (and not very dependent neither on a nor on D !). The current is $i = u\omega C$ per meter, and with 60 Hz and 130 V this gives $0.35\text{ }\mu\text{A}$ per meter wire. Such a simplified model with a person as the plane conductor is therefore in rough agreement with measured currents from power cord couplings found in actual situations. With a completely insulated person, the AC voltage of the person is the mains voltage with respect to ground reduced by the voltage division caused by the power cord/person and person/ground capacitances. If the person is grounded, the system can be regarded as a monopolar system. The grounding point is the point of high current density (active electrode). The whole body skin surface area is the low current density capacitively coupled neutral plate. Possible effects are to be found at the active electrode site.

For bioimpedance measurements a bipolar electrode may be used covered by an insulating layer of teflon or glass. This is further analyzed by FEM (see Section 6.7). Another example of capacitive electrode coupling is diathermy, see below.

High Frequency Electric Field Coupling to Tissue

Short wave diathermy utilizes a frequency around 27 MHz , corresponding to a wavelength of about 12 m . The tissue is placed in the near-field of an applicator capacitor (or coil), and the local power density $W_v[\text{watt/m}^3]$ is everywhere given by the equation 3.42 $W_v = \sigma E^2 = J^2/\sigma$. Eq. 3.43 gives the corresponding temperature rise as a function of current density (or E-field strength) under adiabatic conditions.

A certain selectivity between tissue doses is of interest, and from these equations it may be deduced that with constant amplitude voltage (E-field strength), the tissue of highest conductivity has the largest power dissipation and temperature rise. This is true in a homogeneous medium, but in the inhomogeneity of real tissues the opposite may also be true. Consider a capacitor with two equal slabs of materials with unequal conductivities *in series*. With DC parameters it is easy to show that the ratio between the power densities in slabs 1 and 2 when $\sigma_1 \ll \sigma_2$, is:

$$\frac{W'_1}{W'_2} = \frac{\sigma_2}{\sigma_1} \gg 1$$

The current density is the same in the two slabs, and it is determined by the slab with lowest conductivity, σ_1 . Slab 1 with the *lowest* conductivity also has the highest E-field strength, and will therefore have the highest power density.

If the two slabs are side by side *in parallel*, the situation will be opposite. The E-field strength is the same in both slabs, but the current densities are not. The

material with *highest* conductivity will have the highest current density and the highest power density.

With an *inductive* coil coupling, the circulating currents in the tissue are eddy currents, which are proportional to tissue conductivity, see later in this Section. The corresponding rules for inhomogeneous materials can easily be worked out.

2000 MHz = 2 GHz corresponds to a wavelength of about 15 cm, and the tissue is partly in the near-field and partly in the far-field. At higher microwave frequencies the conditions are more and more of a far-field type, so we are dealing with electromagnetic *radiation* properly speaking, cf. below. The electromagnetic fields of microwave diathermy are determined not only by incident radiation, but also on reflected energy from interface zones of changing impedance, for example at skin, fat and bone surfaces.

Non-galvanic Coupling by Electromagnetic Waves (Far-Field Radiation)

The electromagnetic fields at a distance from the source larger than about 10 times the wavelength propagate as a far-field electromagnetic *wave*. Near-field components have vanished. More than 3 m away from a 1 GHz antenna the fields thus are dominated by the electromagnetic wave. Examples of electromagnetic wave coupling to tissue are, for example, microwave heating or a person in front of a radar antenna.

Even higher frequencies correspond to IR, visible and UV light. In this range electromagnetic waves more and more behave like a stream of photons, particles without charge and rest mass. Planck's law $\Delta E = h\nu$ defines the correspondence between photon energy ΔE and frequency ν . The higher the frequency, the higher is the photon energy. In the UV spectrum the photon energy has increased to about 5 eV, enough to excite the outer electrons of an atom. The radiation is then *ionizing*, representing a rather well-defined hazard to living tissue. Even higher energy photons, partly absorbed by tissue, are used in diagnostic X-ray, but these subjects are outside the scope of this book.

Passing through homogenous tissue attenuates an electromagnetic wave, Table 7.3. Fat with low conductivity has least attenuation.

In addition, reflection and scattering occur in tissue. For lower frequency, frequencies <100 GHz and wavelengths >3 mm, the wave obeys the laws of reflection and not scattering. *Rayleigh* scattering is the dispersion of electromagnetic radiation by *small* particles having a radius less than approximately 1/10th of the wavelength of the radiation. Rayleigh scattering is strongly frequency

TABLE 7.3 Depth of Penetration of an Electromagnetic Wave into Tissue

	Saline	Muscle	Fat
433 MHz	2.8 cm	3 cm	16 cm
2.5 GHz	1.3 cm	1.7 cm	8 cm
10 GHz	0.2 cm	0.3 cm	2.5 cm

dependent: the higher the frequency, the more powerful the scattering. When the radius of curvature of tissue is *larger* than the wavelength, geometrical scattering (planar reflection) occurs. This effect is frequency independent, and the basis of lenses and the laws of reflection, cf. Section 4.3.2.

The reflection and transmission of a plane wave at a planar tissue interface depend on the frequency, the polarization and angle of incidence of the wave, as well as the complex dielectric constant of the tissue. The reflection coefficient R from (and the transmission T through) an interface of two media with intrinsic impedances Z_1 and Z_2 are:

$$R = \frac{Z_2 - Z_1}{Z_2 + Z_1}$$

$$T = \frac{2Z_2}{Z_2 + Z_1}$$
(7.52)

The specific absorption rate (SAR) of non-ionizing electromagnetic radiation with frequencies <100 GHz is defined (sine waves, W/kg) as:

$$\text{SAR} = \frac{\sigma' + \omega\varepsilon''}{\rho} \cdot E_{rms}^2 [\text{W/kg}]$$
(7.53)

Where ρ is mass density [kg/m^3]. This equation does not take into account possible absorption of magnetic energy related to the magnetic permeability of tissue. It also does not necessarily relate ε'' and all the absorbed power to heat and temperature rise.

PROBLEMS

1. What is transfer impedance?
2. What is reciprocity?
3. Why is eq. (7.24) important for understanding lock-in amplifiers and Fourier analysis?
4. What is a polarized electrode? Give an example.
5. What is a non-polarizable electrode? Give an example.
6. What is a typical dry skin impedance modulus at 10 Hz?
7. What is a typical wet skin impedance modulus at 10 Hz?
8. What is a typical wet gel electrode polarization impedance modulus at 10 Hz?
9. What is a typical solid gel electrode polarization impedance modulus at 10 Hz?

This page intentionally left blank

8 DATA AND MODELS

Chapter Contents

8.1 Models, Descriptive and Explanatory

8.2 Equations and Equivalent Circuits

- 8.2.1 Maxwell's Equations
- 8.2.2 The Bidomain Model
- 8.2.3 Two-Component Equivalent Circuits, Ideal Components
- 8.2.4 Constant Phase Element
- 8.2.5 Augmented Fricke CPE_F
- 8.2.6 Three- and Four-Component Equivalent Circuits, Ideal Components
- 8.2.7 Cole Equations (Cole 1940)
- 8.2.8 Cole–Cole Equations (Cole and Cole 1941)
- 8.2.9 Control of Fricke Compatibility
- 8.2.10 The α Parameter
- 8.2.11 Dispersion Model in Accordance with Relaxation Theory
- 8.2.12 Symmetrical DRT
- 8.2.13 Non-symmetrical DRT
- 8.2.14 Multiple Cole Systems

8.3 Data Calculation and Presentation

- 8.3.1 Measured Data, Model Data
- 8.3.2 Indexes

8.4 Data Analysis

- 8.4.1 Multivariate Analysis
- 8.4.2 Clinical Performance
- 8.4.3 Neural Networks
- 8.4.4 Chaos Theory and Fractals
- 8.4.5 Wavelet Analysis

Problems

8.1 MODELS, DESCRIPTIVE AND EXPLANATORY

We will see in Section 8.2.3 that when measuring on a parallel circuit with controlled voltage, the real part of the resulting current will be proportional to the conductance, and the imaginary part will be proportional to the susceptance. And furthermore, that if the physical reality is a series circuit, this simple proportionality will be absent, and the values must be mathematically calculated in each case. The same proportionality is also present for controlled current measurements on a series circuit. Values for conductance and susceptance of the skin are thus always related to an opinion on whether these phenomena electrically exist in series or parallel.

The problem when trying to make an electrical model of the physical or chemical processes in tissue is that often it is not possible to mimic the electrical behavior with ordinary lumped, physically realizable components such as resistors, capacitors, inductors, semiconductor components and batteries. Let us mention three examples: (a) the constant phase element (CPE), not realizable with a finite number of ideal resistors and capacitors. (b) The double layer in the electrolyte in contact with a metal surface. Such a layer has capacitive properties, but perhaps with a capacitance which is voltage dependent or frequency dependent. (c) Diffusion-controlled processes (cf. Section 2.4.2). Distributed components such as a CPE can be considered composed of an infinite number of lumped components, even if the mathematical expression for a CPE is simple.

In this section we will use electrical models for human skin as examples in a general discussion on the use of electrical models. An electrical model of the skin with only two components will obviously not be able to simulate the frequency response measured on skin – it is certainly too simple compared to the complex anatomy of human skin. We suggest three different solutions to this problem, which would result in the following archetypes:

Model 1: One solution is to make complete distinction between the different structures of the skin, and hence make an electrical model as complex as the skin itself. Lipid membranes would then typically be replaced by capacitors, electrolytes by resistors and semipermeable membranes by voltage sources. The model will, without compromise on the cellular level, aim to reflect the electrical properties of the various *microanatomical* structures.

Model 2: A different solution would be to focus on those structures of the skin that make the largest contributions to the electrical properties, decide whether each of these structures should be represented by a resistor or a capacitor, and finally find the simplest electrical equivalent that comprises all these structures. This *organ-oriented* model is thus a simplified version of model 1.

Model 3: A third solution would be to consider the skin as a *black box*, make extensive measurements on it, and find the electric circuit that matches the admittance levels and frequency response measured. The anatomy of the skin is not considered in this model.

These three models will appear very different, but they are all electrical models of the skin. Is one of them more “correct” or “better than” the other models – and in that case, why?

The Model Concept

The word *model* is ambiguous. A model can be a three-dimensional representation of an object, but it can also be a person presenting fashion clothing, an object used to produce casting molds, a person who is portrayed, an instrument for physical model experiments, a substitute for something, an illustration of a mathematical expression, etc. The word *model* has essentially two different interpretations; *prototype/picture* and *equivalent/substitute*. Mathematical models should also be mentioned, which are a sort of predictive substitutes for reality. A characteristic of models is that they represent selected properties of the reality they reflect.

Models that serve as visual pictures of reality, have a geometric resemblance to the original, but can be scaled compared to it. The substitute models depict other properties than the visual. They can, with regard to these properties, act as substitutes for the original. (As an alternative, one could claim that the pictorial models serve as substitutes with regard to visual properties, and include them also in this group.) Their predictive function is of great interest, because they are often used to investigate a specific side of the functionality or structure of the original, or its response to given stimuli. Such models might be flight simulators, models of the hull of a ship, miniature railroads, mathematical models, electrical models or maps. Hence, for each of these models, one has chosen to emphasize one or more attributes from the original, and has thus made them selective acting substitutes. The models to be discussed here are substitute models, where the electrical properties are important.

Description or Explanation?

Let us return to the question of which model is the best or most correct. The question as posed is obviously not precise enough to be given an exact answer. What is required from a good or correct model?

The term “electrical equivalent” is as frequently used as “electrical model” in the literature. The more rigorous word “equivalent” has a more precise meaning than “model.” An electrical equivalent is a circuit that electrically behaves exactly like the original when studied from predefined terminals. Model 3 is in this respect the best electrical equivalent, and consequently also the best model, if the overall object is to describe the electrical properties of the skin. The descriptive models should therefore in this context be separated from the explanatory.

The descriptive models characterize the skin electrically by means of both known electric components and algorithms. The models reflect primarily the phenomena, that is the measured values and time courses, and the theories are not to any great extent connected to the microanatomy of the skin. The entities of the model do not necessarily exist as isolated biologic structures, and even though the model includes known electric components, they do not necessarily resemble corresponding electrophysiological processes in the skin.

The explanatory models are based on the basic concepts of electrical theory – potential, conductance, polarization, induction, etc. Knowledge about the physical mechanisms behind these phenomena is used to provide understanding of similar phenomena in biologic materials, and the models are largely influenced by theories

concerning the relationship between microanatomy and fundamental electrical properties. It is vital that these models only include discrete electric components for which the essential mode of operation is known. The models are explanatory because one believes that the components of the model represent isolated anatomical structures or physical processes, such that the dominating electrical property can be explained by means of the properties of the component.

The Most Correct Model

The most correct model takes all recent knowledge about relaxation processes, frequency dispersion, diffusion, fractals, etc. into account. It is an electrical equivalent to the skin, that is it has the same frequency response. It is furthermore simple and uses symbols in a way that makes it easy to understand the outlines of the electrical properties of the different substructures of the skin. The model takes care of all requirements of an electrical model of the skin – but unfortunately it does not exist! The most correct of the existing models is therefore the one best adapted for the target group.

The realism of the lumped element models is not easy to assert in view of modern theories and measurement techniques, and these models can be regarded as pragmatic explanatory models. They are, however, the only models that differentiate between substructures of the skin, and have clinical value in that they aid in choosing measuring technique.

The pure instrumentalism of the descriptive models is also questionable. There is an obvious need to correlate the parameters τ and α with well-defined mechanisms in the skin, particularly regarding the use of skin admittance measurements as a diagnostic tool. The descriptive models can therefore be considered as essential intermediate stages in the development of better explanatory models. The new explanatory models will comprise discrete, passive components, but there will be a change in the use of symbols compared to the descriptive models, as the relationship between anatomical structure and electrophysiological mechanisms are revealed. These new models should be able to explain the so far empirically disclosed connections between skin diseases and the frequency response of the skin, by showing how changes within a substructure in the skin influence one or more of the components of the model, and hence how this can be detected by choosing the appropriate measuring technique.

8.2 EQUATIONS AND EQUIVALENT CIRCUITS

A mathematical equation is also a model, and a very ideal one. There is an important interaction between these two model forms: the mathematical equation and the equivalent circuit diagram, with respect to the phenomena to be described.

8.2.1 Maxwell's Equations

Maxwell's famous four equations are found in many versions, for example in differential or integral form and with different parameters involved. Equations (8.1)–(8.4)

show one example set (the Minkowski formulation). The differential form relates the time and space derivatives at a point (in an infinitesimal small *volume*), to the current density at that point. The integral form relates to a defined finite *volume*. Ideal charge distributions are often discontinuous, and so not differentiable, *therefore the integral form is a more generally applicable form*.

	Differential form	Explanation by integral
Equation (8.1) Gauss law	$\nabla \cdot \mathbf{E} = q_v/\epsilon_0$	Flux of \mathbf{E} through a closed surface = net enclosed charge/ ϵ_0
Equation (8.2) Faradays law	$\nabla \times \mathbf{E} = -\partial\mathbf{B}/\partial t$	Line integral of \mathbf{E} around a loop = $-$ rate of change of flux of \mathbf{B} through the loop
Equation (8.3)	$\nabla \cdot \mathbf{B} = 0$	Flux of \mathbf{B} through a closed surface = 0
Equation (8.4) Amperes law	$\nabla \times \mathbf{H} = \mathbf{J}_f + \partial\mathbf{D}/\partial t$	Line integral of \mathbf{H} around a loop = current density of free charges through the loop + rate of change of flux of \mathbf{D} through the loop

Local symbols in this chapter are: c = velocity of light (m/s), \mathbf{B} = magnetic flux density [Vs/m^2], \mathbf{H} = magnetic field strength [A/m]. q is charge [C], q_v is charge density [C/m^3], q_{vf} is density of free charges not including dipole charges bound (q_{vb}) in the material, $q_v = q_{vf} + q_{vb}$.

∇ is the differential *vector operator* called *nabla* or *del*: $\nabla = \mathbf{i}\partial/\partial x + \mathbf{j}\partial/\partial y + \mathbf{k}\partial/\partial z$, where \mathbf{i} , \mathbf{j} and \mathbf{k} are unity vectors in a Cartesian coordinate system.

$\nabla\Phi$ is the *gradient* of Φ (the gradient of a scalar is a vector), $\nabla \cdot \mathbf{B}$ is the *divergence* of \mathbf{B} (the divergence of a vector is a scalar) and $\nabla \times \mathbf{B}$ is the *curl* of \mathbf{B} (the curl of a vector is a vector).

These four equations go back to Maxwell¹ himself and the year 1873. Maxwell's four equations describe almost all known electrical effects in one complete, concentrated, powerful set. They were very much based on Faraday's discoveries; for example, eq. (8.2) is a more general formulation of Faraday's law of induction. The equations state that a *variable* electrical field can only exist together with a magnetic field, and vice versa. They are based on the presupposition that a charge cannot be created anywhere, charges can just be moved. They apply to any inertial reference frame: the *charge* of a particle moving at an increasing velocity is constant, while the *mass* increases. The Maxwell equations themselves are linear: they do not contain products of two or more variables. They are extremely robust valid also for non-linear, non-homogenous and anisotropic systems.

Maxwell used the concept of quaternions, and the equations did not have the modern form of compactness. It was *Oliver Heaviside* (1850–1925) who first expressed them in the form we know today. It was also Heaviside who around 1886 coined the terms *impedance*, *conductance*, *permeability*, *admittance* and “permittance” which later became *susceptance*.

¹James Clark Maxwell (1831–1879), British mathematician and physicist, founder of the electromagnetic field theory and the kinetic theory of gases.

Most other equations describing electrical effects are derivable from the Maxwell's equations. In bioimpedance Gauss law is important, describing how the E-field is changed by the existence of net space charges. It is equally valid for net free or bound charges. However, $\nabla \cdot \mathbf{D} = q_{vf}$ is related to free charges, meaning that the flux of \mathbf{D} through a closed surface = net enclosed free charges inside. If we replace E by $-\nabla\Phi$, we obtain the *Poisson* equation:

$$\nabla^2 \Phi = -q_v/\epsilon_0 \quad \text{or} \quad \partial^2 \Phi/\partial x^2 + \partial^2 \Phi/\partial y^2 + \partial^2 \Phi/\partial z^2 = -q_v/\epsilon_0 \quad (8.5)$$

∇^2 is called the *Laplacian*. The special case of the volume charge density q_v being zero is called the Laplace equation:

$$\nabla^2 \Phi = 0 \quad (\text{Laplace equation}) \quad (8.6)$$

From eq. (8.1) the following relationship can be deduced: $\mathbf{D} = \epsilon_0 \mathbf{E} + \mathbf{P}$ (eq. 3.4), it is valid also for non-isotropic, non-linear materials. Other equations derivable from the Maxwell's for linear and isotropic materials are, for example, Ohms law $\mathbf{J} = \sigma \mathbf{E}$, the power density law (Joule heat) $W_v = \sigma' E^2$ (watt/m³), the stored energy density law $\hat{E}_v = \frac{1}{2} \mathbf{E} \cdot \mathbf{D}$ (joule/m³). Maxwell's equations are valid for all kinds of electromagnetic radiation, and contain the speed of light in the eq. (8.4) (in another version than Minkowski's).

Maxwell introduced the term *displacement current* for the current through free space and the local displacement of the *bound* charges (dipoles) in the dielectric, as opposed the movement of *free* charges.

From Maxwell's equations the fundamental difference between static near fields (electromagnetic *fields*) and radiation (electromagnetic *waves*) is demonstrated. In Section 6.3 we treated the dipole. Consider that the dipole moment vary as a sine function with time. Now if the frequency is very high, the time delay will be noticeable if we are at a distance much longer than the wavelength $\lambda = c/f$ from the dipole.

In the *near field* (distance to the source $\ll \lambda$), electric and magnetic fields are independent of each other, it is possible to have, for example, a pure 50Hz electric field with a negligible magnetic field.

Bioimpedance and the Maxwell's equations

The Maxwell equations most relevant to bioimpedance are eqs (8.4) and (3.4): $\mathbf{D} = \epsilon_0 \mathbf{E} + \mathbf{P}$. If the magnetic component is ignored, eq. (8.4) is reduced to:

$$\partial \mathbf{D} / \partial t = -\mathbf{J} \quad (1)$$

Equations (1) and (3.4) are extremely robust and also valid both under *non-homogeneous, non-linear and anisotropic* conditions. To be more useful for bioimpedance four restrictions are introduced:

1. Use of sufficiently small voltage amplitude across the material so the system is *linear*.

2. Use of *sinusoidal* functions so that in complex notation a derivative, for example $\partial E/\partial t$, is simply the product $j\omega E$ (j is the imaginary unit and ω the angular frequency, cf. Section 11.1).
3. Use of $\mathbf{D} = \varepsilon \mathbf{E}$ (space vectors), where the permittivity $\varepsilon = \varepsilon_r \varepsilon_0$. This implies that D , P and E all have the same direction and therefore that the dielectric is considered isotropic.
4. No fringe effects in the capacitor model of Fig. 3.1.

Let us now apply eq. (1) on the capacitor model of Fig. 3.1 with the metal area equal to A and the dielectric thickness equal to L . However, eq. (1) is in differential form, and the interface between the metal and the dielectric represents a discontinuity. Gauss law as an integral form is therefore used, and we imagine a thin volume straddling an area of the metal/dielectric interface. According to Gauss law the outward flux of D from this volume is equal to the enclosed free charge density on the surface of the metal. With an applied voltage v , it can be shown that $D = v\varepsilon/L$. By using eq. (1) we then have $\partial D/\partial t = j\omega v\varepsilon/L = J$, and $i = j\omega v\varepsilon A/L = vj\omega C$.

We now leave the dielectric and take a look at the external circuit where the current \mathbf{i} and the voltage \mathbf{v} (time vectors) are measured and the immittance determined. The admittance is $\mathbf{Y} = \mathbf{i}/\mathbf{v}$. With no losses in the capacitor, \mathbf{i} and \mathbf{v} will be phase shifted by 90° (the quadrature part). The conductance is $G = \sigma' A/L$ and the basic equation of bioimpedance is then (time vectors):

$$\mathbf{Y} = G + j\omega C \quad (2)$$

Three important points must be made here:

Firstly, eq. (2) shows that the basic impedance model actually is an *admittance* model. The conductive and capacitive (quadrature) parts are physically in parallel in the model of Fig. 3.1.

Secondly, the model of Fig. 3.1 is predominantly a dielectric model with *dry* samples. In bioimpedance theory the materials are considered to be *wet*, with double layer and polarization effects at the metal surfaces. Errors are introduced, which however can be reduced by introducing three- or four-electrode systems (Section 6.6). Accordingly, in dielectric theory the dielectric is considered as an *insulator* with dielectric losses, in bioimpedance theory the material is considered as a *conductor* with capacitive properties. Dry samples can easily be measured with a two-electrode system. Wet, ionic samples are prone to errors and special precautions must be taken.

Thirdly, the Maxwell equations used are valid at a point. With a homogeneous and isotropic dielectric material in Fig. 3.1 the variables have the same values all over the sample. With inhomogeneous and anisotropic materials the capacitor model implies values averaged over the volume. Then under *linear* (small signal) conditions the equations are still correct, but the measured values are difficult to interpret. The capacitor is basically an *in vitro* model with a biomaterial placed in a measuring chamber. The average anisotropy can be measured by repositioning the sample in the capacitor. *In vivo* measurements must be analyzed with sensitivity fields as shown in Section 6.5.

As we have seen a biomaterial can be characterized as a conductor or a dielectric. If the system is linear, the complex conductivity and the complex permittivity contain the same information. It is therefore natural that many of the formulas of dielectrics have their corresponding conductor versions and vice versa. In Section 6.9 this duality is further discussed.

8.2.2 The Bidomain Model

Equation (2.2) $\mathbf{J} = \sigma \mathbf{E}$ is not valid in anisotropic materials if σ is a scalar. Tissue as a rule is anisotropic. Plonsey and Barr (2000) discussed some important complications posed by tissue anisotropy and also emphasized the necessity of introducing the concept of the *bidomain* for cardiac tissue. A bidomain model is useful when the cells are connected by two different types of junctions: tight junctions and gap junctions with the cell interiors directly connected. The intracellular space is one domain and the interstitial space the other domain.

8.2.3 Two-Component Equivalent Circuits, Ideal Components

We will now discuss the simplest equivalent circuits mimicking the immittance found in tissue measurements. In this section the R–C components are considered *ideal*, that is frequency independent and linear. Immittance values are examined with sine waves, relaxation times with step functions. A sine wave excitation results in a sine wave response. A square wave excitation results in a single exponential response with a simple R–C combination.

The two-component model with one resistor and one capacitor is a one-port network, and is the simplest and most important model because every measurement on a specific frequency is reduced to such a circuit. The results are given as complex immittance values with two figures corresponding to the two components: one resistor and one capacitor. Inductive properties and corresponding resonance phenomena are possibilities that are found, for example, in membranes, but here we limit the treatment to capacitive systems.

Admittance and the Parallel Model

In the parallel two-component model circuit it is direct access to both components from the external terminals, Fig. 8.1. Therefore the voltage can be externally controlled, but not the current division. Accordingly, a *constant amplitude voltage* v is applied across the model parallel circuit, and the current i is measured. The admittance Y has a direct relationship with a parallel G–C circuit, the real part Y' is G , and the imaginary part Y'' is $B = \omega C$.

The parallel values are measured directly because it is proportionality between admittance Y and measured i . v is the independent reference sine wave, with zero phase shift per definition, and therefore here designated as a scalar:

$$Y = i/v \quad (8.7)$$

$$Y = G + j\omega C_p \quad (8.8)$$

$$\varphi = \arctan \omega C_p / G \quad (8.9)$$

$$\varepsilon' = C_p \quad (\text{unity cell})$$

$$\varepsilon'' = G/\omega \quad (\text{unity cell})$$

$$\tau = C_p / G \quad (8.10)$$

The circuit has some very characteristic properties:

1. The admittance diverges at higher frequencies (eq. 8.8), here the model is not in agreement with biomaterial properties.
2. It does let DC current pass.
3. The phase angle is positive; meaning the current (dependent variable) is leading the voltage. Since i is the dependent variable, for causality it cannot lead the start of the sine wave, only after steady state conditions have been obtained.
4. The time constant τ of eq. (8.10) is not found with a controlled step voltage excitation as shown in Fig. 8.1, the capacitor will be charged in zero time during the voltage step. The characteristic time constant of the parallel circuit alone *can only be found* with a *constant amplitude current* ($R_i = \infty$) excitation.

Time Constant of the Parallel G-C Circuit

The time constant τ of the parallel circuit depends on how it is driven. With a controlled step *current* across the circuit (not constant amplitude voltage as shown in Fig. 8.1), the voltage across the G-C combination increases exponentially from zero to $V = I/G$. The time constant is $\tau = C_p/G$. Driven by a controlled *voltage* step V , the starting current is infinitely high, and the time constant is zero.

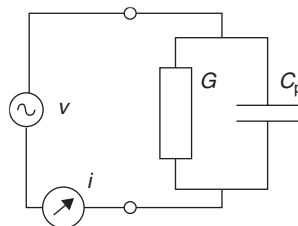


Figure 8.1 Parallel circuit driven from an ideal voltage source ($R_i = 0$), the response recorded by an ideal current reading device ($R_i = 0$).

If the Parallel Model Is to be Characterized with Impedance

We may express the impedance Z of the parallel circuit using the parallel values G and C_p , $Y^2 = G^2 + B^2$ and $\tau_Y = C_p/G$ (Y^2 means $|Y|^2$):

$$\begin{aligned} R &= G/Y^2 \\ X &= -B/Y^2 \\ Z &= 1/Y = (1/G)(1 - j\omega\tau_Y)/(1 + \omega^2\tau_Y^2) \\ Z' &= (1/G)/(1 + \omega^2\tau_Y^2) \\ Z'' &= -(1/G)j\omega\tau_Y/(1 + \omega^2\tau_Y^2) \\ C_s &= C_p(1 + 1/\omega^2\tau_Y^2) \end{aligned} \quad (8.11)$$

Equation (8.11) illustrates the extreme importance of choosing the best model circuit:

- Z' will be frequency dependent, even if G is not.
- The series capacitance C_s *diverges toward infinite capacitance values at low frequencies*. This will for instance be experienced with a measuring bridge if an unknown parallel combination is to be zeroed by a series combination in the balancing arm (Section 7.3.1).

Impedance and the Series Model

In the series two-component model circuit there is no direct access to both components from the external terminals, Fig. 8.2. Since the two components are in series, the current can be externally controlled, but not the voltage division. Accordingly, a *constant amplitude current* i is applied across the model series circuit, and the voltage v is measured. The impedance Z has a direct relationship with a series R-C circuit, because the real part Z' is R , and the imaginary part Z'' is $X = -1/\omega C$. The series values are measured because it is proportionality between impedance Z and

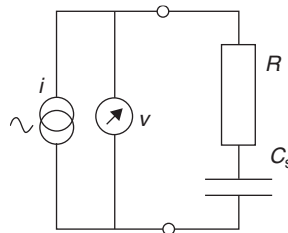


Figure 8.2 Series circuit driven from an ideal current source ($R_i = \infty$), the response recorded by an ideal voltage reading device ($R_i = \infty$).

measured v . i is the independent reference sine wave, with zero phase shift per definition, and therefore here designated as a scalar:

$$\mathbf{Z} = \mathbf{v}/i \quad (8.12)$$

$$\mathbf{Z} = R - j/\omega C_s \quad (8.13)$$

$$\varphi = \arctan(-1/\omega\tau) \quad (8.14)$$

$$\tau = RC_s \quad (8.15)$$

Important properties of the series circuit are:

1. The impedance converges at higher frequencies (eq. 8.13).
2. It does not allow the passage of DC current.
3. The phase angle is negative. This means that the voltage as dependent variable is lagging the current (cf. current leading in the parallel circuit).
4. The time constant τ of eq. (8.15) is not found with constant amplitude current excitation as shown in Fig. 8.2, the capacitor will be charged at infinity during the current step. The characteristic time constant of the parallel circuit alone *can only be found with a constant amplitude voltage* ($R_i = 0$) excitation.

Time Constant of the Series R-C Circuit

The time constant τ of the series circuit depends on how it is driven. With a controlled step *voltage* V across the circuit (not controlled current as shown in Fig. 8.2), R is effectively in parallel with C_s , and the current decays exponentially from an initial value of $i = V/R$ to $i = 0$ with a time constant $\tau = RC_s$. The voltage across the capacitor increases exponentially with time from $v = 0$ to $v = V$ with the same time constant. Driven by a controlled *current* step I , the total series resistance is effectively infinite, and the voltage across the circuit (after a transient period) increases linearly with time with a velocity $\Delta v/\Delta t = I/C_s$. The time constant is therefore infinitely large.

If the Series Model Is to be Characterized with Admittance

We may express the admittance \mathbf{Y} of the series circuit with the series values R and C_s , $Z^2 = R^2 + X^2$ and $\tau_Z = RC_s$ (Z^2 means $|Z|^2$)

$$G = R/Z^2$$

$$B = -X/Z^2$$

$$\mathbf{Y} = 1/\mathbf{Z} = (\omega^2 C_s \tau_Z + j\omega C_s)/(1 + \omega^2 \tau_Z^2)$$

$$\begin{aligned}
 Y' &= (1/R) \omega^2 \tau_Z^2 / (1 + \omega^2 \tau_Z^2) \\
 Y'' &= C_s \omega / (1 + \omega^2 \tau_Z^2) \\
 C_p &= C_s / (1 + \omega^2 \tau_Z^2) \\
 \varepsilon' &= C_s / (1 + \omega^2 \tau_Z^2) \quad (\text{unity cell}) \\
 \varepsilon'' &= \omega C_s \tau_Z / (1 + \omega^2 \tau_Z^2) \quad (\text{unity cell})
 \end{aligned} \tag{8.16}$$

Equation (8.16) illustrates the extreme importance of choosing the best model circuit:

- Y' will be frequency dependent, even if R is not.
- The parallel capacitance C_p will be frequency dependent, even if C_s is not. C_p converges to zero at high frequencies. C_p is now the capacitance as seen from the outside (C_{ext}), different from C_s because we do not have direct access to C_s from the model terminals.

Bode and Wessel Diagram Presentations

Figure 8.3 shows an example of how a model series circuit will look like in a Bode diagram. Most of the phase shift is within a frequency range of two decades, centered on the characteristic frequency 1.592 Hz where $\varphi = 45^\circ$. $|Z|$ however has hardly started to increase at the characteristic frequency when passing toward lower frequencies.

Figure 8.4 illustrates the *parallel* circuit in the Wessel diagram. In a Y -plot representation the locus is a straight line. Because of the frequency scale direction, it is reasonable to interpret this as an infinitely high characteristic frequency or an infinitely small time constant, as if the circuit was voltage driven. However, *in the impedance plane (Z-plot), the parallel circuit has a half circle locus*. Then the characteristic frequency of the apex is $f_c = G/2\pi C_p$, as if the circuit were current driven.

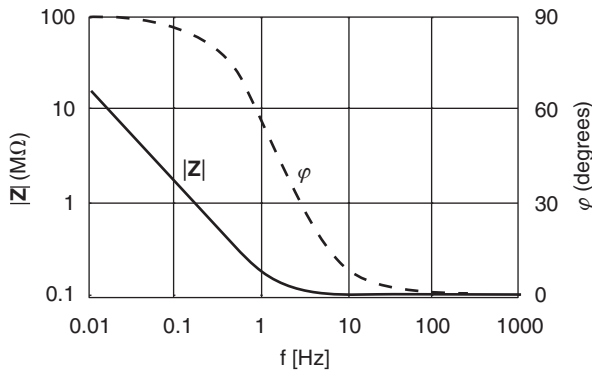


Figure 8.3 Impedance of the series model of Fig. 8.2 presented in a Bode diagram: frequency and impedance scales logarithmic, phase scale linear. $R = 0.1 \text{ M}\Omega$, $C_s = 10^{-6} \text{ F}$ ($\tau = 0.1$ second, $f_c = 1.6 \text{ Hz}$).

Notice how the Z-plot enlarges the low frequency part and the Y-plot the high frequency part.

Figure 8.5 illustrates the *series* circuit in the Wessel diagram. In a Z-plot representation the locus is a straight line. Because of the frequency scale direction, it is reasonable to interpret this as zero characteristic frequency or an infinitely high time constant, as if the circuit were current driven. However, *in the admittance plane (Y-plot), the series circuit has a half circle locus*. Then the characteristic frequency of the apex is $f_c = 1/2\pi RC_s$, as if the circuit were voltage driven. Notice how here also the Z-plot enlarges the low frequency part and the Y-plot the high frequency part.

In conclusion, the parallel and series two-component circuits are *complementary models* and very different from each other. A choice of model is unavoidable when electrical data is to be analyzed and presented. The choice must be based on a presumption on the actual physical arrangement in the biomaterial/electrode system to be modeled.

Parallel- and series-equivalent circuits contain the same information in ideal systems. *The choice is often actually done in the measurement setup*: by choosing constant amplitude voltage or current modus from the signal generator, or by choosing parallel or series coupling in the bridge arm.

Of course it is also possible to use non-ideal sources, and measure both voltage and current at the terminals of the system under examination. By special feedback

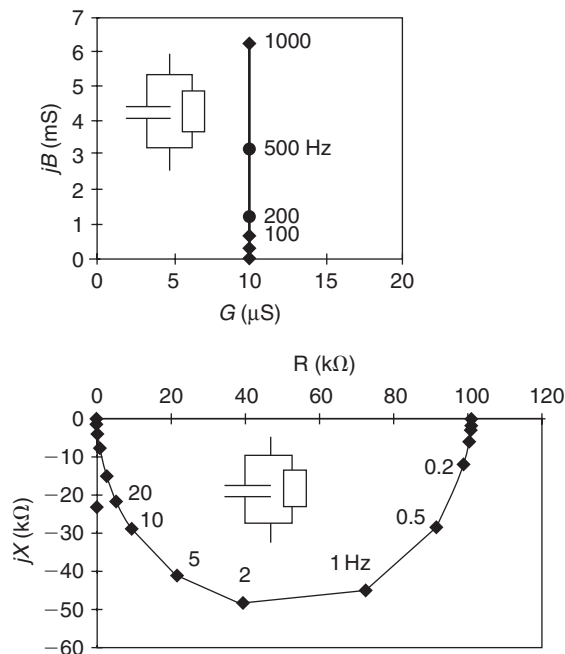


Figure 8.4 Wessel diagrams for the parallel model circuit. $G = 10 \mu\text{S}$, $C_s = 10^{-6}\text{F}$ ($\tau = 0.1$ second, $f_c = 1.6\text{Hz}$).

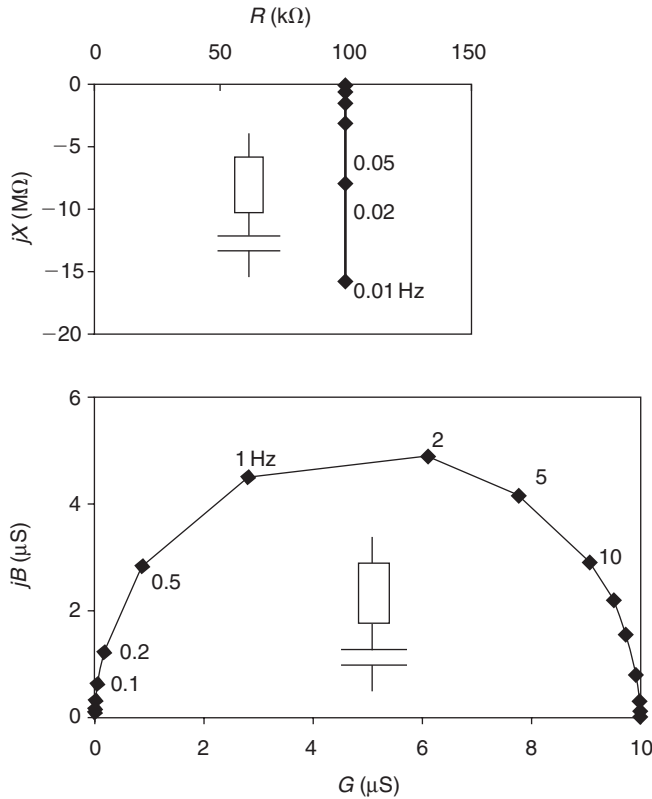


Figure 8.5 Wessel diagrams for the series model circuit. $R = 100\text{ k}\Omega$, $C_s = 10^{-6}\text{ F}$ ($\tau = 0.1$ second, $f_c = 1.6\text{ Hz}$).

circuits it is also possible to control, for example, the power dissipation in the unknown (e.g. isowatt modus). It must still be decided whether admittance or impedance values are to be calculated and presented.

If the system under examination is non-linear, the information in the parallel and series models is not equal. Series values cannot be calculated from parallel values and vice versa, and the actual measuring circuit determines the variables and the model chosen.

8.2.4 Constant Phase Element

The two-component equivalent circuit models presented in the last section are of course too simple to mimic the admittance found with real biomaterials at all frequencies. A much better agreement can often be obtained by allowing the components to be non-ideal, that is frequency dependent. In particular, the frequency dependence can be modeled so that the *phase* of the immittance is *independent* of frequency.

Let us calculate the characteristic properties of a general CPE as a conductor and a suscepter in parallel, both frequency dependent. The frequency dependence of the admittance $\mathbf{Y} = G + jB$ is sought so that the phase angle ($\varphi_{\text{cpe}} = \arctan B/G$) becomes frequency *independent*:

$$B_{\text{cpe}}/G_{\text{cpe}} = k \quad (8.17)$$

From eq. (8.17) it is clear that in order to keep the phase angle constant, both G and B must be dependent on the frequency in the same way:

$$G_{\text{cpe}} = G_{\omega=1}\omega^m \quad B_{\text{cpe}} = B_{\omega=1}\omega^m \quad (8.18)$$

The dimension of G_{cpe} and B_{cpe} is siemens (S), so the dimension of $G_{\omega=1}$ and $B_{\omega=1}$ is not so simple: $[S/\omega^m]$ or $[S \cdot s^m]$.

Here the introduction of a parameter τ with the dimension of time and forming the product $\omega\tau$ is of interest for two reasons:

1. τ represents a useful frequency scale factor.
2. The product $\omega\tau$ is dimensionless (an angle).

Equation (8.18) is then changed to (G_1 and B_1 are values at $\omega\tau = 1$):

$$G_{\text{cpe}} = G_1(\omega\tau)^m \quad B_{\text{cpe}} = B_1(\omega\tau)^m \quad (8.19)$$

The introduction of τ has the interesting consequence that it changes the dimension of G_1 and B_1 to be that of an ideal conductance: siemens.

$$\mathbf{Y}_{\text{cpe}} = (\omega\tau)^m(G_1 + jB_1) \quad (8.20)$$

$$\varphi_{\text{cpe}} = \arctan B_1/G_1 \quad (8.21)$$

Equations (8.20) and (8.21) define a general CPE, determined by $\omega\tau$, m , G_1 and B_1 . *There is no correlation between m and φ_{cpe}* , and there are no restrictions to the value of m . m does not determine the constant phase value, but it defines the frequency dependence of the \mathbf{Y}_{cpe} and the frequency scale together with τ .

If the m -values are restricted to positive values in the range $0 \leq m \leq 1$, then the admittance \mathbf{Y}_{cpe} is increasing with frequency, in accordance with what is found for tissue. As can be seen from eq. (8.20), this also implies the intrinsic property of zero DC conductance and susceptance. By also specifying the susceptance to be capacitive, obeying the equation $B = \omega C$ and therefore $B_1 = (1/\tau)C_1$ ($C_1 = C_{\omega\tau=1}$), we get for the *admittance parallel* version:

$$\mathbf{Y}_{\text{cpe}} = (\omega\tau)^m G_1 + j\omega^m \tau^{m-1} C_1 \quad 0 \leq m \leq 1 \quad (8.22)$$

$$\varphi_{\text{cpe}} = \arctan C_1/\tau G_1 \quad (8.23)$$

$$C_{cpe} = C_1(\omega\tau)^{m-1} \quad \text{(falling with increasing frequency)} \\ \text{when } 0 \leq m \leq 1 \tag{8.24}$$

Let us examine the extreme values of frequency:

When $f \rightarrow \infty$, $Y_{cpe} \rightarrow \infty$ (eq. 8.22), even when $C_{cpe} \rightarrow 0!$ (eq. 8.24).

When $f \rightarrow 0$, $Y_{cpe} \rightarrow 0$, even when $C_{cpe} \rightarrow \infty!$

Let us examine the extreme values of $m = 0$ and $m = 1$:

$m = 0$: $G_{cpe} = G_1$, an ideal (frequency independent) resistor.

$C_{cpe} = C_1/\omega\tau$, a very special capacitor.

$m = 1$: $G_{cpe} = G_1\omega\tau$, a very special resistor.

$C_{cpe} = C_1$, an ideal (frequency independent) capacitor.

In both cases the constant phase character is valid with $\varphi_{cpe} = \arctan C_1/\tau G_1$, not necessarily 0° or 90° . But with $G_1 = 0$: $\varphi_{cpe} = 90^\circ$; and with $C_1 = 0$: $\varphi_{cpe} = 0^\circ$.

The *impedance, series* version show similar properties. The equivalent circuits are shown on Fig. 8.6.

In the Wessel diagram of Fig. 8.7 the loci of the Y_{cpe} and Z_{cpe} , both the parallel and series circuits, are straight lines, with no circular arcs as seen in Figs 8.4

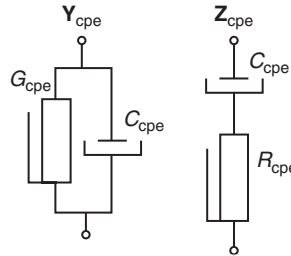


Figure 8.6 Equivalent circuits of parallel and series CPEs. The symbols are for non-ideal, frequency-dependent components.

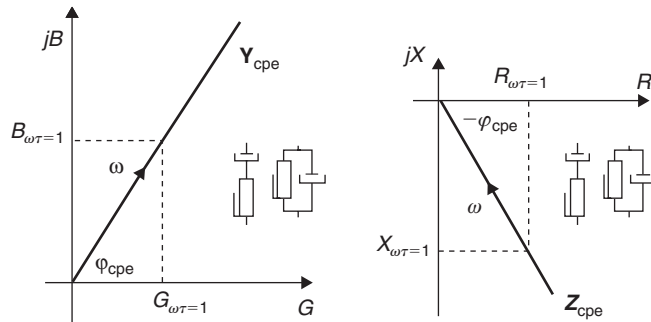


Figure 8.7 Immittance of an isolated CPE. There is no difference between series and parallel representation, in contrast to Figs 8.4 and 8.5.

and 8.5. *The choice between parallel or series representation is not important for a CPE, and using a series or parallel circuit as shown in Fig. 8.6 is arbitrary.* In particular, by inverting, for example, the admittance of a parallel CPE into an impedance Wessel diagram, the locus will still be a line (Fig. 8.7), not a circular arc.

A CPE comprises a frequency dependent capacitor and resistor. From an electronic point of view a CPE is a two-component descriptive model. If the mechanism behind is seen as one process, it is a one-component explanatory model.

CPE in Accordance with Fricke's Law (CPE_F)

According to Fricke's law, *there is* a correlation between the frequency exponent m and the phase angle φ in many electrolytic systems: when experiments show that $C = C_1 f^{m-1}$, then $\varphi = m\pi/2$. As pointed out by Fricke (1932), m is often also found to be frequency dependent. However, it can be shown that Fricke's law is not in agreement with the Kramers–Kronig transforms *if m is frequency dependent* (Daniel, 1967). If we therefore also presuppose m and φ to be frequency independent, we have a CPE. For such a Fricke CPE_F it is usual practice to use the exponent symbol α ($m = \alpha$). The immittance of a Fricke CPE_F can then be written in a very simple way in complex notation (remembering that $j^\alpha = \cos \alpha\pi/2 + j \sin \alpha\pi/2$, cf. eq. 11.6):

$$\begin{aligned} Y_{\text{cpeF}} &= G_1(j\omega\tau)^\alpha = \omega^\alpha \tau^\alpha G_1(\cos \alpha\pi/2 + j \sin \alpha\pi/2) \\ Z_{\text{cpeF}} &= R_1(j\omega\tau)^{-\alpha} = \omega^{-\alpha} \tau^{-\alpha} R_1(\cos \alpha\pi/2 - j \sin \alpha\pi/2) \end{aligned} \quad (8.25)$$

The factor α intervenes *both* in the constant phase expression ($\cos \alpha\pi/2 + j \sin \alpha\pi/2$) *and* the frequency exponent, in accordance with Fricke's law. The dimension of Y_{cpeF} and G_1 is siemens [S] and R_1 ohm [Ω]. The values of Y_{cpeF} at extreme frequencies are like the general CPE: zero DC conductance and no admittance limit at very high frequencies. The admittance at the extreme values of $\alpha = 0$ and $\alpha = 1$ must not be confused with the extreme values of m given in the general discussion of eqs (8.22)–(8.24) above:

$\alpha = 0$: $\varphi_{\text{cpeF}} = 0^\circ$. $Y_{\text{cpeF}} = G_1$: the Fricke CPE_F is an ideal conductance.
 $\alpha = 1$: $\varphi_{\text{cpeF}} = 90^\circ$. $Y_{\text{cpeF}} = j\omega\tau G_1$: the Fricke CPE_F is an ideal capacitor, with $C = \tau G_1$.

A CPE_F has the locus of a straight line through the origin in the Wessel diagram, just as the general CPE, Fig. 8.7. Notice that the factor $(j\omega)^\alpha$ implies a Fricke-compatible CPE_F, but the factor $j^\alpha \omega^m$ ($m \neq \alpha$) implies a Fricke (and Cole) non-compatible CPE.

In conclusion: For a general CPE there is no correlation between the frequency exponent m and the constant phase angle φ_{cpe} . However for a Fricke CPE_F, $\varphi_{\text{cpeF}} = m\pi/2 = \alpha\pi/2$.

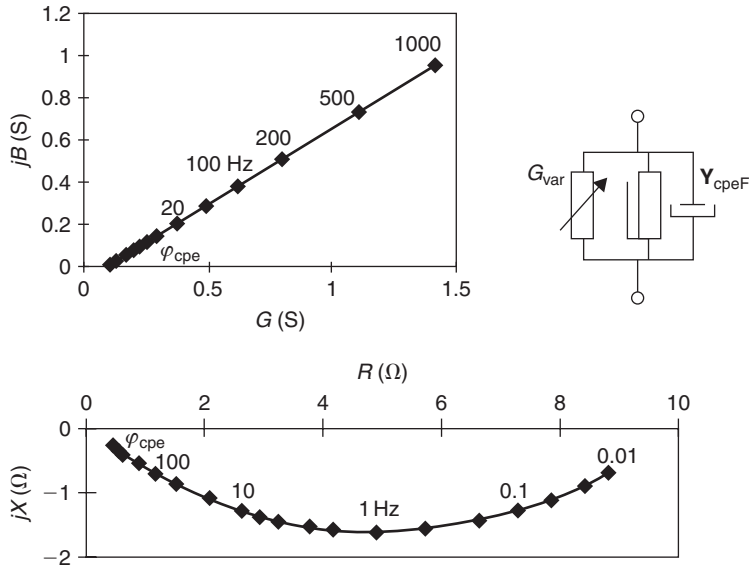


Figure 8.8 Y-plot and Z-plot for a CPE_F with a freely chosen $G_{var} = 0.1$ (S). $\alpha = 0.4$ ($\varphi = 36^\circ$), $G_1 = 0.1$ (S), $\tau = 0.1$ (s).

8.2.5 Augmented Fricke CPE_F

Freely Chosen Augmenting Ideal Resistor

We may *augment* the Fricke CPE_F by adding a resistor G_{var} (an ideal, frequency independent DC conductance) to a CPE_F. Let us consider the case with G_{var} in *parallel* with the CPE_F (eq. 8.26). With an ideal resistor augmenting a CPE in *series*, the case will be similar.

The *admittance* locus will still be a line, but not through the origin (Fig. 8.8):

$$Y_{cpeFA} = G_{var} + G_1(j\omega\tau)^\alpha \tag{8.26}$$

In the admittance plane the parallel combination will not have a finite characteristic time constant, and τ has the character of being just a frequency scale factor. Inverted to the *impedance* plane *the added conductor* G_{var} *causes the locus to be a circular arc* with a characteristic time constant $\tau_c = \tau_Z$ and frequency ω_c corresponding of the apex (the point of maximum magnitude of reactance) of the arc.

In general τ_Z will be dependent on G_{var} , this easily shown by programming these equations in a spreadsheet, an example is illustrated in Fig. 8.9.

This model with a free variable conductance in parallel with a CPE or CPE_F is often found in the literature and analyzed as if being in agreement with the Cole

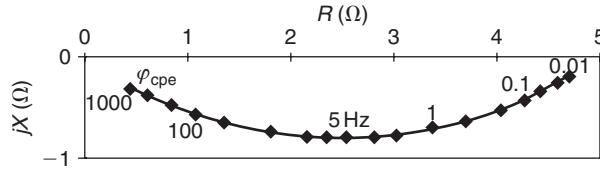


Figure 8.9 Demonstration of τ_z being dependent on the augmenting conductor G_{var} : higher conductance leads to higher characteristic frequency. Parameters as for Fig. 8.8 except that $G_{\text{var}} = 0.2$ (S).

model (cf. Section 8.2.7), which it is not. Equation (8.26) is a non-Cole-compatible model which can be used if both conductance and characteristic frequency or time constant are found to *vary during an experiment* (cf. Section 8.2.11).

Cole-Compatible Augmented CPE_F

Restricting the value of G_{var} ($=1/R$) so that it is equal to the G_1 of the CPE_F element, gives a special case with different properties. The impedance of such a Cole element is:

$$Z_{\text{Cole}} = R/[1 + (j\omega\tau_z)^\alpha] \quad (8.27)$$

Equation (8.27) describes a parallel Cole element (cf. eq. 8.29), G_{var} is now a dependent variable. With ideal components the time constant of a parallel circuit is $\tau = C/G$, and thus dependent on the parallel conductance. In eq. (8.26) the characteristic time constant is dependent on the parallel conductance G_{var} . However, in the special case of eq. (8.27), the parallel conductance *does not* influence the characteristic time constant. τ_z and the characteristic frequency ω_c corresponding to the apex of the ZARC is determined by the equation $\omega_c\tau_z = 1$ and is independent of $G_{\text{var}} = G_1$ and α . This is the Cole case and has been obtained by linking the DC conductance value G_{var} to the magnitude of the immittance value of the CPE. The case is illustrated in Fig. 8.10.

Equation (8.27) is a part of the Cole equation (cf. Section 8.2.7). *If the characteristic frequency ω_c is found to vary during an experiment and it is reasonable to believe that this is due to an independent parallel conductance, the process cannot be modeled with eq. (8.27), and the process is Cole incompatible.*

In conclusion, a circular arc locus in the immittance Wessel diagram can:

1. not be due to a CPE alone;
2. be due to a general CPE augmented by an ideal resistor in parallel or series (not Fricke, not Cole compatible);
3. be due to a Fricke CPE_F augmented by an ideal resistor of freely chosen value in parallel or series (not Cole compatible);
4. be due to a Fricke CPE_F augmented by an ideal resistor of a particular value in parallel or series (Cole compatible).

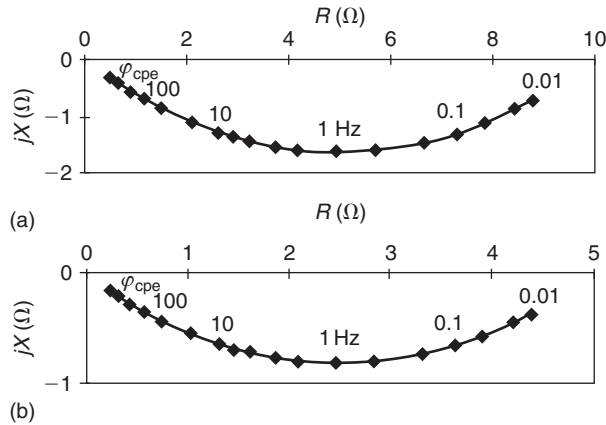


Figure 8.10 Demonstration of τ_z being independent of the augmenting conductor (Cole case). Z-plot for a CPE_f with a Cole-compatible parallel conductor. No change of characteristic frequency, the only changes are the scales on the axes. (a) $G_{var} = G_1 = 0.1$ (S); (b) 0.2 (S); other parameters as for Fig. 8.8.

8.2.6 Three- and Four-Component Equivalent Circuits, Ideal Components

Usually, the two-component circuit is too simple to mimic with sufficient precision the frequency dependence of the variables measured. The three-component model combines features of both the series and parallel models. It may consist of two capacitors and one resistor (dielectrics with bound electric charges), or two resistors and one capacitor (conductors with free charge carriers). Detailed equations can be found in Section 11.2.

Two Resistors–One Capacitor Circuits (2R–1C, Conductors)

The only two basically different versions are illustrated in Fig. 8.11. Both allow DC current, and both guarantee current limitation at high frequencies. The detailed equations are found in the appendix (Section 11.2). The two circuits are very similar because *it is possible to obtain the same immittance values for all frequencies with only one set of component values*. As we have seen, this was not possible with the two-component series and parallel circuits. Their descriptive powers are therefore identical, and a choice must be made on the basis of their explanatory possibilities. However, the choice is important because the component values for the same frequency dependence are not identical. It is easy to see that the limiting cases at very low and very high frequencies determine the resistor values.

The *parallel* version is best characterized by admittance because the *time constant then is uniquely defined* (Section 11.2). It has been used for cells and living tissue, with C for cell membranes, R for intracellular and G for extracellular liquids.

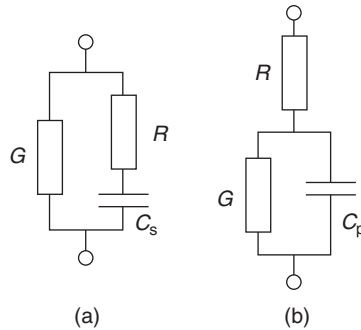


Figure 8.11 Conductor 2R-1C models: (a) parallel version and (b) series version.

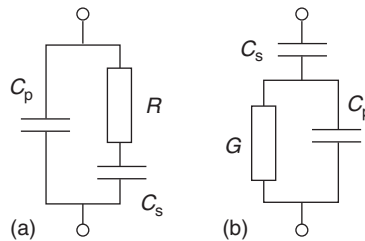


Figure 8.12 Dielectric 1R-2C models: (a) parallel version (b) series version.

The *series* version is best characterized by impedance because the *time constant then is uniquely defined* (Section 11.2). It has often been used as a skin electrical equivalent, with R for deeper tissue in series and the skin composed of G and C in parallel.

Two Capacitors–One Resistor Circuits (2C-1R, Dielectrics)

Detailed equations for such circuits with ideal components are found in Section 11.2. The only two basically different versions are illustrated in Fig. 8.12. Neither allows DC current, and neither guarantees current limitation at high frequencies. The two circuits are similar because it is possible to obtain the same immittance values for all frequencies with only one set of component values. With one set of component values, they cannot be made equal to the 1C-2R models at more than one frequency. Their descriptive powers are identical, and a choice must be made on the basis of their explanatory possibilities. However, the choice is important because the component values for the same frequency dependence are not identical. It is easy to see that the limiting cases at very low and high frequencies determine the capacitor values. The parallel version is an important model for a simple relaxation process. It is the preferred version because it can be defined *with one unique time constant* (Section 11.2), and is according to the Debye equation (3.25) treated in Section 3.4 on relaxation.

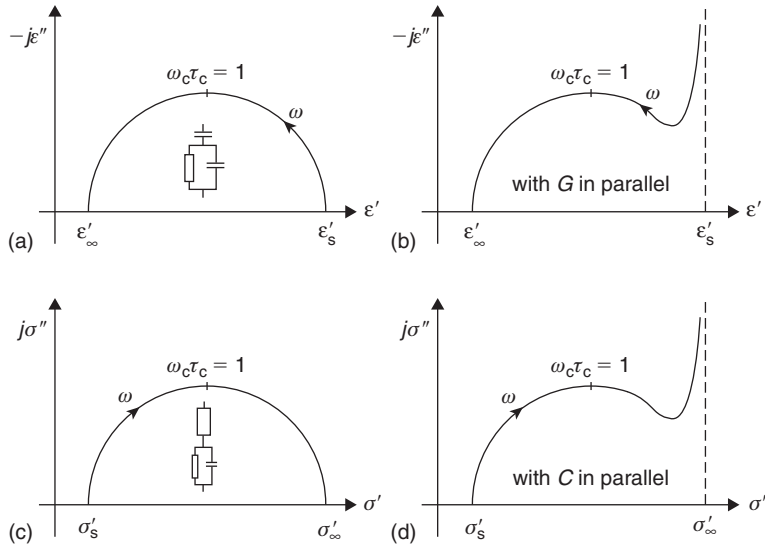


Figure 8.13 (a),(b) The effect of a parallel conductor added to the 2C–1R dielectric circuit of Fig. 8.12. (c),(d) The effect of a parallel capacitor added to the 2R–1C conductor circuit of Fig. 8.11.

The Effect of Additional Parallel Conductors and Capacitors

The permittivity locus of a Debye dispersion in the Wessel diagram is a complete half circle with the center on the real axis (Fig. 8.13(a)). An ideal resistor in parallel destroys the circle at low frequencies (Fig. 8.13(b); cf. Fig. 3.8). The conductivity locus is equally sensible for an ideal capacitor in parallel at high frequencies (Fig. 8.13(d)).

8.2.7 Cole Equations (Cole 1940)

Impedance is the dependent variable in the Cole equations. For most biologic systems it is observed that the center of the impedance circular arc locus is situated below the real axis in the Wessel diagram. This was clear from the late 1920s, and Cole and Fricke published diagrams and equations based on a frequency independent phase angle. But in 1940 Kenneth S. Cole proposed the following empirical equation: $z = z_{\infty} + (r_0 - r_{\infty})/(1 + (j\omega\tau)^{\alpha})$ to describe tissue impedance. The basis was findings he presented in 1928 and onwards. In 1940 he explained the frequency dependence as membrane capacitive effects and not relaxation as he did one year later together with his brother. Actually the term z_{∞} is misleading and is replaced by an ideal resistor R_{∞} in the usually quoted version of the Cole_Z equation:

$$Z = R_{\infty} + \frac{\Delta R}{1 + (j\omega\tau_Z)^{\alpha}} \quad [\Omega] \quad \Delta R = R_0 - R_{\infty} \quad (8.28)$$

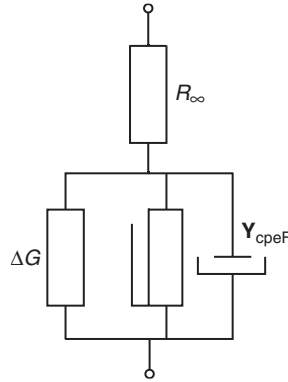


Figure 8.14 The complete Cole_Z system.

The subscripts for the resistances relate to frequency. The simplest equivalent circuit for this equation is with two ideal resistors and one CPE immittance. As shown in Section 8.2.6 there are two possible variants that may be adapted over the whole frequency range. Examining the equations in Section 11.2, we see that the *series* version has the advantage that $R = R_\infty$ and $\Delta R = \Delta R$ directly and that the circuit is characterized with only one time constant. The simplest equivalent circuit for the Cole_Z eq. (8.28) is therefore the one shown in Figs 8.14 and 8.15. Here $\Delta G = 1/\Delta R$, the symbol ΔG is preferred to G_0 because it is not the DC value of the system.

If we omit the series resistance R_∞ in eq. (8.28), we find the admittance of the remaining parallel part of the circuit to be: $Y_{\text{Cole}} = \Delta G + \Delta G(j\omega\tau)^\alpha$. This admittance is difficult to handle because it has no characteristic time constant of finite value, the admittance locus of Y_{Cole} is a line. τ is merely a frequency scaling factor (cf. Section 8.2.4). By using the impedance form, the locus becomes a circular arc with a characteristic time constant τ_Z :

$$Z_{\text{Cole}} = 1/[\Delta G + \Delta G(j\omega\tau_Z)^\alpha] \quad [\Omega] \quad (8.29)$$

Equation (8.29) describes an ideal conductance in parallel with a Fricke CPE_F, we may call it the *parallel Cole element*. Together with the series resistor R_∞ they form a *complete Cole series system*. The impedance and capacitance of the Fricke constant phase element CPE_F alone is:

$$\begin{aligned} Z_{\text{cpeF}} &= 1/\Delta G(j\omega\tau_Z)^\alpha && [\Omega] \\ C_{\text{cpeF}} &= \omega^{\alpha-1}\tau_Z^\alpha \Delta G \sin \alpha\pi/2 = (\Delta G/\omega)(\omega\tau_Z)^\alpha \sin \alpha\pi/2 && [\text{farad}] \end{aligned} \quad (8.30)$$

The Cole element is a very special combination of a Fricke CPE_F and a parallel ideal (DC) conductance ΔG so that ΔG also controls the magnitude of the CPE_F admittance. A change in a parallel conductance influences the magnitude (not the α) of the Z_{cpeF} , so the parallel conductance is not a separate mechanism, but a part

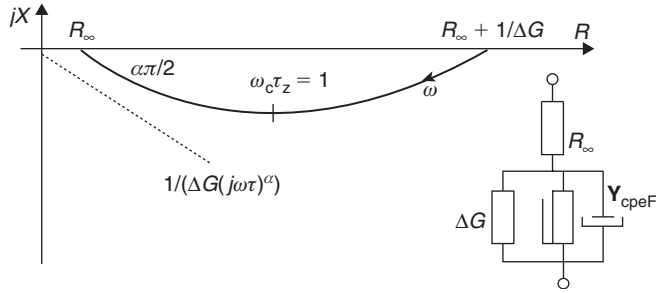


Figure 8.15 The impedance locus (ZARC) of the Cole_z system.

of the Cole dispersion mechanism. The Cole_z equation does not allow an *independent* variable DC conductance in parallel with the CPE_F without disturbing the components of the CPE. This may limit the applicability of the Cole_z equation in many real systems, because parallel processes are often independent of the CPE_F. For example in the skin, with sweat duct conductance in parallel with the capacitive properties of the stratum corneum, the series model has serious limitations. However, the series resistance R_∞ of the Cole_z equation is not correlated with the parameters of the Z_{Cole} : ΔG , τ or α . R_∞ may therefore freely be regarded as an independent *access resistance* to the parallel Cole element.

In the *impedance* (Z-plot) Wessel diagram the series resistance R_∞ of the Cole system moves the arc of the Cole element to the right along the real axis a distance equal to the value of R_∞ , and with no influence on the characteristic frequency.

Cole Equation in Admittance Form

By examining the equations for the equivalent circuits in Section 11.2, we find that it is the *parallel* 2R–1C circuit which is best suited. Then the components in the equivalent circuit are directly equal to the parameters in the equation (G_0 and ΔG). Accordingly the Cole_Y equation in admittance form is:

$$Y = G_0 + \frac{\Delta G}{1 + (j\omega\tau_Y)^{-\alpha}} \quad [\text{S}] \quad \Delta G = G_\infty - G_0 \quad (8.31)$$

Equation (8.31) may be decomposed in its real and imaginary parts:

$$Y' = G_0 + \Delta G \frac{1 + (\omega\tau)^{-\alpha} \cos(\alpha\pi/2)}{1 + 2(\omega\tau)^{-\alpha} \cos(\alpha\pi/2) + (\omega\tau)^{-2\alpha}} \quad [\text{S}] \quad (8.32)$$

$$Y'' = \Delta G \frac{(\omega\tau)^{-\alpha} \sin(\alpha\pi/2)}{1 + 2(\omega\tau)^{-\alpha} \cos(\alpha\pi/2) + (\omega\tau)^{-2\alpha}} \quad [\text{S}] \quad (8.33)$$

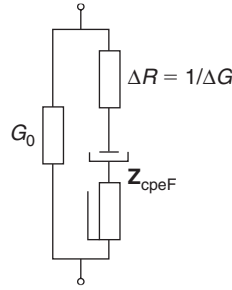


Figure 8.16 The complete Cole_Y system.

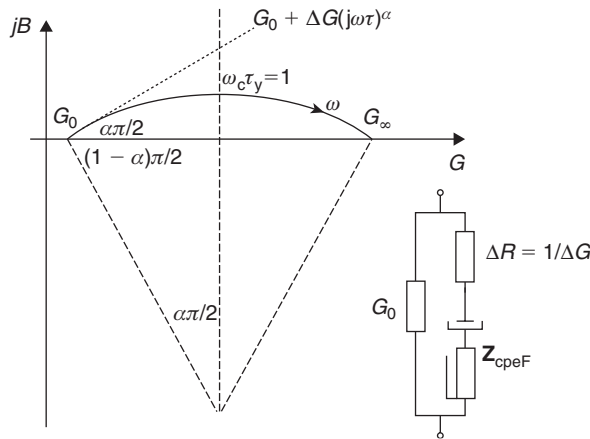


Figure 8.17 The admittance locus (YARC) of the Cole_Y system.

Such decompositions can of course also be made of the Cole impedance equation as well as the conductivity and permittivity equations. Equations (8.32) and (8.33) illustrate how extremely compact the Cole and Cole–Cole equations are.

The subscripts for the conductors relate to frequency. The best equivalent circuit is shown in Fig. 8.16. The resistor $\Delta R (=1/\Delta G)$ and the C_{peF} are now in series, and it is better to operate with the impedance of the C_{peF} :

$$\begin{aligned} Z_{cpeF} &= \Delta R(j\omega\tau_Y)^{-\alpha} = \Delta R(\omega\tau_Y)^{-\alpha}(\cos \alpha\pi/2 - j \sin \alpha\pi/2) \quad [\Omega] \\ C_{cpeF} &= \omega^{\alpha-1} \tau_Y^\alpha / \Delta R \sin \alpha\pi/2 = (\omega\tau_Y)^\alpha / (\omega\Delta R \sin \alpha\pi/2) \quad [\text{farad}] \end{aligned} \quad (8.34)$$

In the Cole parallel model, the capacitance of the Fricke element C_{cpeF} is dependent on ΔR , α , ω and τ_Y . A variable G_0 will not disturb the locus curve form in the admittance Wessel diagram, but move the arc along the real axis (Fig. 8.17). C_{cpeF} , α , ΔR , the characteristic frequency and the frequency scale on the arc will not change, but G_∞ will change.

Because $Y = \sigma A/d$, and A/d is equal for all the components, eq. (8.31) may be written:

$$\sigma = \sigma_0 + \Delta\sigma/[1 + (j\omega\tau_Y)^{-\alpha}] \quad [S/m] \tag{8.35}$$

If we omit the parallel conductance G_0 in eq. (8.31), we find the impedance of the remaining part of the circuit to be $Z_{\text{Cole}} = \Delta R + \Delta R(j\omega\tau_Y)^{-\alpha}$, or

$$Y_{\text{Cole}} = 1/[\Delta R + \Delta R(j\omega\tau_Y)^{-\alpha}] \quad [S] \tag{8.36}$$

This is a Fricke CPE_F in series with an ideal resistor, we may call it the *series Cole element*. Together with the parallel conductance G_0 they form the *complete Cole parallel system*.

The term ΔR is found *both* in the Cole CPE_F and the series resistance of eq. (8.36). A change in a series resistance influences the value of the CPE_F , so the series resistance is *not a separate mechanism*, but a part of the Cole polarization mechanism. The Cole $_Y$ equation does not allow an *independent* variable DC resistor in series with the CPE_F . This limits the applicability of the Cole $_Y$ equation in many real systems, because often series processes are processes independent of the CPE_F . However, the parallel conductance G_0 of the Cole $_Y$ equation is not correlated to ΔR , nor to τ or the α of the Z_{Cole} . G_0 may therefore freely be regarded as an *independent* parallel conductance to the series Cole element. For example in the skin, with sweat duct conductance in parallel with the capacitive properties of the stratum corneum, the parallel Cole model may therefore be a better choice than the series model.

Figure 8.18 shows the admittance locus of a Cole $_Y$ system with the u and v lengths defined (to be used for control of Fricke compatibility, cf. Section 8.2.9). Measured phase angle φ is always smaller than $\alpha\pi/2$. φ_{max} and the corresponding angular frequency are shown on the figure.

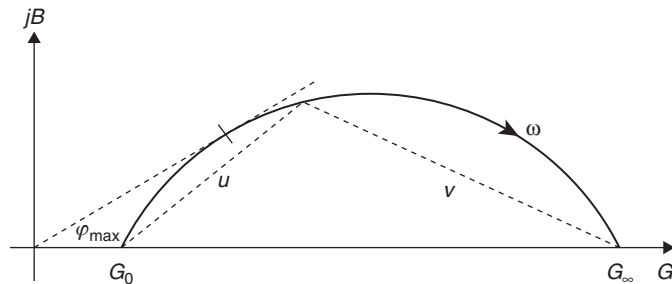


Figure 8.18 YARC plot showing the u - v variables and the maximum possible measured phase angle φ_{max} .

In Conclusion

For Cole-compatible systems, the immittance arc locus is completely defined by three parameters, for example: G_0 , ΔG and α . Vice versa, a *given* arc completely defines three parameters: G_0 , ΔG and α .

The fourth parameter is the characteristic time constant τ_c , which defines the frequency scale. Vice versa: a given frequency scale defines the characteristic time constant.

These four parameters are independent as variables. τ is so only because one of the two ideal resistors of a Cole system is correlated with the CPE.

The Cole equations are descriptive in their nature. Even so, many have tried to use them for explanatory purposes but usually in vain. If a Cole model is to be used not only for descriptive but also for explanatory purposes it is necessary to discuss the relevance of the equivalent circuit components with respect to the physical reality which is to be modeled. Because the Cole models are in disagreement with relaxation theory this is not easy. A more general dispersion model, Section 8.2.11, may help circumvent problems occurring when the characteristic frequency is found to vary and DC paths with independent conductance variables cannot be excluded.

8.2.8 Cole–Cole Equations (Cole and Cole, 1941)

Permittivity is the dependent variable in the Cole–Cole equations. In 1941 Cole and Cole proposed the following version:

$$\varepsilon = \varepsilon_\infty + \frac{\Delta\varepsilon}{1 + (j\omega\tau_0)^{1-\alpha}} \quad \varepsilon_s - \varepsilon_\infty = \Delta\varepsilon \quad [\text{F/m}] \quad (8.37)$$

Here ε_s is used for static values (and not ε_0 which is reserved for vacuum permittivity). This is in agreement with the complex permittivity as $f \rightarrow 0$: in this model (Fig. 8.19) there is no DC conduction and accordingly electrostatic conditions.

As $C = \varepsilon A/d$, the Cole–Cole equation (8.37) may equally well be written as a capacitance equation:

$$C = C_\infty + \Delta C/[1 + (j\omega\tau_0)^{1-\alpha}] \quad [\text{F}] \quad (8.38)$$

By inspection of the equations for the two-capacitor models found in Section 11.2, we find the parallel version best adapted. According to eq. (11.27) it can be characterized by one single time constant. The equivalent circuit is shown in Fig. 8.19

Notice that when $\omega \rightarrow \infty$, $C_{\text{cpeF}} \rightarrow 0$ (eq. 8.34), thus decoupling ΔC (even if the fact that $Z_{\text{cpeF}} \rightarrow 0$ (eq. 8.34) could lead to the false conclusion that ΔC actually is in the circuit).

A *Cole–Cole plot* is permittivity plotted in a Wessel diagram. If the permittivity is according to the Cole–Cole equation, the locus will be a circular arc. The permittivity used in the Cole–Cole equations implies that the model is changed from regarding tissue as a conductor (2R–1C model) to regarding tissue as a dielectric

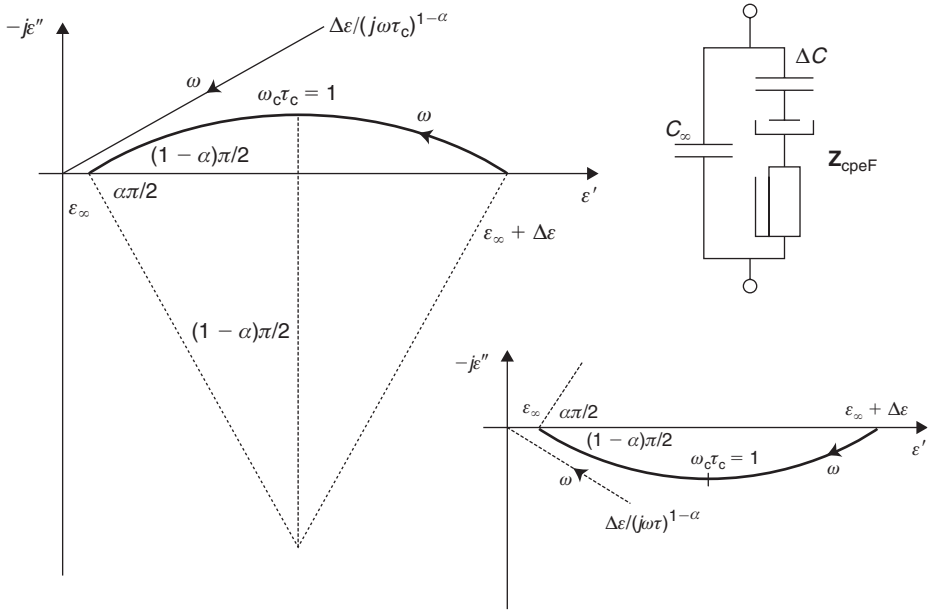


Figure 8.19 Equivalent circuit for the Cole–Cole permittivity equation.

(1R–2C model) with only bound charges and dielectric losses. A 2R–1C model cannot have the same spectrum as a 1R–2C model with a fixed set of component values, so an arc locus in one model will not result in an arc locus in the other model. In living tissue there is a substantial DC conductance. Such conductance in parallel disturbs the circular arc locus (cf. Fig. 8.13 (a),(b)) and *must be subtracted for permittivity circular arc analysis*. Vice versa: if the admittance values are represented by a circular arc locus, the permittivity derived from it *will not* be a circular arc. In conclusion: admittance is linked with a 2R–1C equivalent circuit, and permittivity is linked with a 1R–2C circuit. With fixed component values, these equivalent circuits cannot be made to have the same frequency dependence.

8.2.9 Control of Fricke Compatibility

For a data set, one procedure is to plot the data in a Wessel diagram, and then do a best fit to adapt a circular arc to the data. The extension of this arc gives, for example, G_0 , G_∞ and α . τ_c is found from the characteristic frequency f_c corresponding to the apex of the arc, from the equation $\omega_c\tau_c = 1$. *However, this is under the assumption that the data set is in accordance with Fricke’s law and a CPE*. As shown in Section 8.2.4, there are CPEs that do not have the link between the frequency exponent m and the constant phase angle φ . If the data is in disagreement with Fricke’s law, the parameters found from the arc in the Wessel diagram do not correspond to the parameters G_0 , G_∞ , α and τ of the Cole equation. A perfect

circular arc locus is not a proof of accordance with the rule of Fricke or the equations of Cole, as shown for example by eq. (8.26) and Fig. 8.8. A data check for Fricke compatibility can be done by plotting, for example, R or X or C_S or G or B or C_p as a function of log-frequency and determine the frequency exponent m , and then check whether m corresponds to the α found in the Wessel diagram. With reference to Fig. 8.18 and the ratio u/v , it can be shown that $u/v = (\omega\tau)^\alpha$ for immitance and $(\omega\tau)^{1-\alpha}$ for permittivity. $\log(u/v)$ plotted as a function of $\log(f)$ is therefore a straight line for a circular arc. α can be found from the slope being equal to $\alpha\pi/2$. The characteristic time constant τ_c can be found from the intercept of the straight line and the vertical axes at $\log(f) = 0$, this $\log(u/v)$ -value is equal to $\alpha \log(\tau_c)$.

8.2.10 The α Parameter

Characterizing tissue with the α parameter has the advantage that the parameter is not dependent on the geometry of the tissue sample as long as the measured tissue volume is constant and not a function of frequency. α is then a material constant like ϵ .

It is common observation that the value of Z for tissue decreases with frequency, Y increases with frequency and ϵ decreases with frequency. By choosing α as exponent in the Z equation (Cole, 1940), $-\alpha$ in the Y equation and $1 - \alpha$ (equivalent to the loss factor of a capacitor: the phase angle of an ideal capacitor is 90° , but the loss angle is 0°) in the ϵ equation (Cole-Cole, 1941), the correct frequency dependence is taken care of *with the same α value independently of model, α being always positive*: $1 \geq \alpha \geq 0$. It is possible to regard the parameter α in several ways:

1. As a measure of a distribution of relaxation times (DRT).
2. As not due to a DRT, but based on the theory of many-body interactions between clusters in the material. Such a non-empirical model has been developed by Dissado-Hill (1979).
3. As a measure of the deviation from an ideal resistor and capacitor ($\alpha = 0$) in the equivalent circuit.
4. According to energy models, for example charge carriers trapped in energy wells.
5. According to physical processes like Warburg diffusion.

According to the first interpretation, the spread of relaxation times may be due to: (a) different degrees of molecular interaction (no interaction $\alpha = 1$, ideal capacitor), (b) cellular interactions and properties of gap junctions, (c) anisotropy, (d) cell size and (e) fractal dimensions.

Table 8.1 shows a summary according to the first and third interpretations. $\alpha = 0$ corresponds to the lossy case, $\alpha = 1$ for the permittivity corresponds to the no loss case. α is therefore analog to the phase angle, $1 - \alpha$ to the loss angle (cf. Section 3.3).

TABLE 8.1 The Exponent α in Cole Equations

Equation	Exponent	Equivalent circuit components	
		$\alpha = 0$	$\alpha = 1$
Z	α	Ideal resistors	Ideal resistors and capacitor
Y	$-\alpha$	Ideal resistors	Ideal resistors and capacitor
ϵ	$1-\alpha$	Ideal resistor and capacitors (Debye)	Ideal capacitors

8.2.11 Dispersion Model in Accordance with Relaxation Theory

The Cole single dispersion impedance model (eq. 8.28) is based on an ideal conductance as a dependent variable (eq. 8.29) and a characteristic time constant as an independent variable. Usually however, the characteristic time constant of tissue or cell suspensions is a function of conductance according to relaxation theory (cf. Section 3.4). The Cole model is therefore not in accordance with relaxation theory.

A more general dispersion model can be deduced from the already presented eq. (8.26) and is found to be (Grimnes and Martinsen, 2005):

$$Z = R_{\infty} + \frac{1}{G_{\text{var}} + G_1(j\omega\tau_Z)^\alpha} \quad (8.39)$$

Here τ_Z is a nominal time constant according to the Cole model when τ_Z is a free variable but G_1 and G_{var} are not, $G_1 = G_{\text{var}}$. The time constant as a dependent variable is expressed by eq. (8.40). τ_{Zm} is the time constant changing with changing conductance. If G_{var} increases, the time constant τ_{Zm} decreases and this is in accordance with relaxation theory:

$$\tau_{Zm} = \frac{1}{\omega_{Zm}} = \tau_Z \left(\frac{G_1}{G_{\text{var}}} \right)^{1/\alpha} \quad \text{or} \quad G_1 = \frac{G_{\text{var}}}{(\tau_Z \omega_{Zm})^\alpha} \quad (8.40)$$

The equivalent circuit is shown on Fig. 8.20 for the impedance and admittance cases.

A consequence of the model is that the apex of an immittance locus no longer necessarily corresponds to the Cole characteristic time constant, it corresponds to τ_{Zm} (eq. 8.40).

Let us see how we proceed from measurement results to model variables. We start by making, for example, a Z-plot in the Wessel plane with measured values (Fig. 8.21), let us assume that we are dealing with a single dispersion. The three variables R_0 , R_{∞} and φ_{cpe} are determined from the arc position and geometry, and from them $G_{\text{var}} = (R_0 - R_{\infty})^{-1}$ and $\alpha = \varphi_{\text{cpe}}/90^\circ$ are calculated. The characteristic frequency ω_{Zm} is taken from the apex of the arc, and the time constant $\tau_{Zm} = 1/\omega_{Zm}$ calculated. From eq. (8.40) we can then follow variations in G_1 by choosing an arbitrary

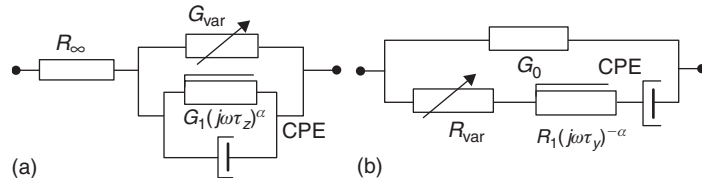


Figure 8.20 Dispersion model in accordance with relaxation theory (eq. 8.39): (a) impedance model and (b) admittance model.

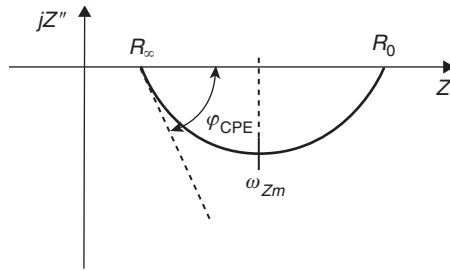


Figure 8.21 A circular arc locus in a Z-plot example is determined from measured spectrum data. The arc defines three parameters: R_0 , R_∞ and φ_{CPE} . ω_{Zm} is taken from the apex of the arc. These values are put into eq. (8.40), and variations in, for example, α and G_1 can be followed separately.

nominal time constant τ_Z , for example equal to 1 second. With the Cole model four parameters are determined from a measured data set; in the new model five parameters are determined. With the new model it is possible to test such hypothesis as whether the CPE has remained constant during an experiment or whether the free conductance G_1 value alone has changed. Such tests are impossible with the Cole model.

8.2.12 Symmetrical DRT

Perfect Circular Arcs, Cole-Compatible DRTs

The characteristic time constant τ_c in the form of τ_Z and τ_Y of eqs (8.28) and (8.31) deserves some explanation. A two-component RC circuit with ideal components has a time constant $\tau = RC$. A step excitation results in an exponential response. With a CPE the response will not be exponential. In Section 8.2.4 the time constant was introduced simply as a frequency scale factor. However, the *characteristic* time constant τ_c may be regarded as a mean time constant due to a distribution of relaxation time constants (DRT). When transforming the Cole_Z impedance Z to the Cole_Y admittance Y or vice versa, it can be shown that the alphas of the two Cole

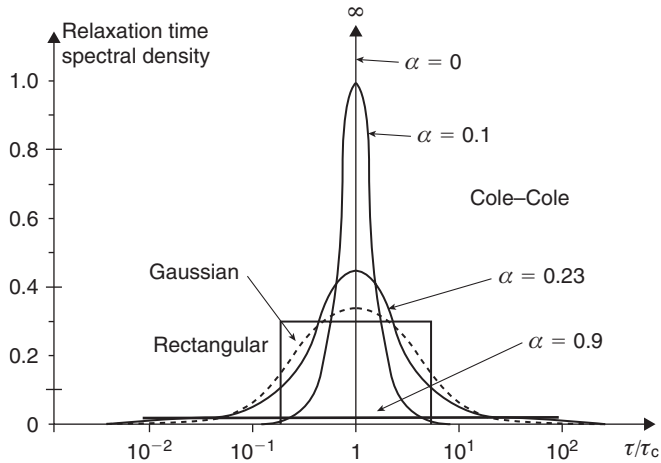


Figure 8.22 Time constant distribution for four different Cole (immittance) cases, and in addition the log-normal (Gaussian) and rectangular distributions. They are all symmetrical around the characteristic time constant τ_c , and correspond to circular arcs (Cole) or near-circular arcs. $\alpha = 0$ is a single time constant (Debye) case.

equations (8.28) and (8.31) are invariant, but the characteristic time constants τ_c are not. In fact:

$$\tau_Y = \tau_Z (\Delta G R_\infty)^{1/\alpha} = \tau_Z \left(\frac{R_\infty}{R_0} \right)^{1/\alpha} \tag{8.41}$$

$\tau_Y < \tau_Z$ because R_∞ is always less than R_0 .

It is possible to determine the relationship between the DRT and the two parameters α and τ in the Cole–Cole equation (Cole and Cole, 1941):

$$p(\ln \tau) = \frac{1}{2\pi} \frac{\sin \alpha\pi}{\cosh \left[(1 - \alpha) \ln \frac{\tau}{\tau_0} \right] - \cos \alpha\pi} \tag{8.42}$$

Where $p(\ln \tau)$ is the spectral density of time constants and τ_0 is the mean relaxation time. This Cole–Cole distribution is the only distribution corresponding to a Fricke CPE_F . The distribution is broad, allowing for a considerable density two decades away from the mean (characteristic) time constant (Fig. 8.22).

Quasi-circular Arcs

Other distributions than the Cole–Cole of eq. (8.42) are possible, for instance a constant function extending over a limited range of time constants. Such different distributions result in Wessel diagram loci surprisingly similar to circular arcs (Schwan, 1957). High precision measurements, calculations and plotting are necessary in order

to determine the type of a DRT. Actually a plot in the complex plane is much more sensitive to whether the distribution is logarithmically symmetrical. *An estimation in the Wessel diagram is therefore more on whether the time constants are logarithmically symmetrical distributed, than whether the data actually are in agreement with a Cole–Cole model.* The popularity of the Cole–Cole model is due to the fact that by *choosing* the arc as the best regression curve to the data points found, the mathematical equations become apparently simple (the Cole equations), and the corresponding equivalent circuits also become simple.

8.2.13 Non-symmetrical DRT

Davidson and Cole (1951) proposed another version of the Cole–Cole equation:

$$\epsilon = \epsilon_{\infty} + \Delta\epsilon/(1 + j\omega\tau)^{\beta} \quad (8.43)$$

Havriliak and Negami (1966) and Williams and Watts (1970) proposed even more general versions of the form:

$$\epsilon = \epsilon_{\infty} + \Delta\epsilon/[1 + (j\omega\tau)^{\alpha}]^{\beta} \quad (8.44)$$

These equations do not correspond to circular arcs in the complex plane, but a non-symmetrical DRT with a larger density of relaxation times on the low frequency side.

With measured data showing a non-symmetrical DRT the choice of model is important: for example, a model according to this section, or a model with multiple Cole systems, see next section.

Parameters similar to those, for example, of the Cole equation, can also be computed without choosing a model. Jossinet and Schmitt (1998) suggested two new parameters that were used to characterize breast tissues. The first parameter was the distance of the 1 MHz impedance point to the low frequency intercept in the complex impedance plane and the second parameter was the slope of the measured phase angle against frequency at the upper end of the spectrum (200 kHz–1 MHz). Significant differences between carcinoma and other breast tissues were found using these parameters.

8.2.14 Multiple Cole Systems

With a given data set obtained from measurements it must be decided how the data is to be interpreted and presented (cf. Section 8.1). This immediately leads to the question of which model should be chosen. The same data can be interpreted using Cole variables like α and τ , but also with many non-Cole models as explained in earlier chapters. As we shall see, many data sets can be explained with multiple dispersions, for example multiple Cole systems. As we now present multiple Cole systems it must always be kept in mind that the tissue data set

certainly could have been made to fit other models. The ability to fit the multiple Cole model to the data set *is not a proof* that this model is the best one for describing, or explaining, the data found. Skin is for instance used as an example in this chapter, and we know that skin data is not necessarily in agreement with the Cole model.

As stated in Section 8.2.7, the four-component equivalent circuit may be used as a model for the Cole equation. The Cole equation represents a single electrical dispersion with a given DRT, and can hence be an interesting model for a macroscopically homogenous tissue within a limited range of frequencies. A practical experimental setup will, however, in most cases involve a measured object that can be divided in two or more separate parts, where each of these parts can be modeled by an individual Cole equation. Furthermore, when measuring over a broader frequency range, different dispersion mechanisms will dominate in different parts of the frequency range, and each of these mechanisms should also be ascribed to an individual Cole equation. We will suggest using the phrase *Cole system* for any system comprising one predominating dispersion mechanism that is decided to be adequately represented by one single Cole equation. This section deals with the necessity and problems of identifying more than one Cole systems in a measured object.

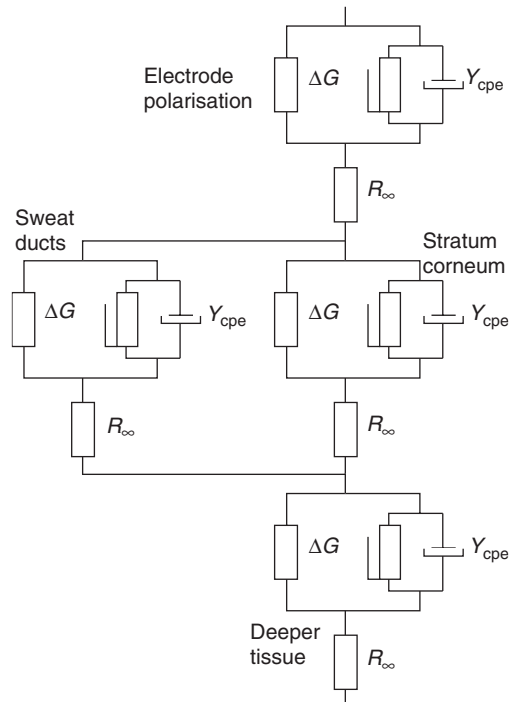


Figure 8.23 Assembly of Cole systems for measurements on skin.

Consider an assembly of Cole systems like the one shown in Fig. 8.23. This electrical equivalent corresponds with the object under investigation when doing impedance measurements on human skin. Measured data may represent contributions from electrode polarization, stratum corneum, sweat ducts and deeper tissue, and furthermore several dispersions of some of these components. Only one Cole system is shown for the electrode polarization although two dispersions have been found in some studies (Onaral and Schwan, 1982). The stratum corneum is dominated by one broad dispersion (Yamamoto and Yamamoto, 1976) and the sweat ducts may exhibit dispersion due to counterion relaxation (Martinsen et al., 1998). The viable skin will probably have several dispersions as explained in Section 4.2.6.

This rather incomprehensible equivalent circuit may of course be simplified on the basis of existing knowledge about the different parts of the circuit. The Cole system representing the sweat ducts will, for example, be reduced to a simple resistor since the polarization admittance most probably is negligible (Martinsen et al., 1998). This corresponds to α being close to zero in the Cole equation. The β and γ dispersions of deeper tissue may furthermore be dropped if the measurements are made at sufficiently low frequencies, and there may likewise be rationales for neglecting the electrode polarization in a given set of data. It is nevertheless of great importance to recognize all relevant Cole systems that may influence on the interpretation of measured data, and then carefully make the necessary simplifications. (We choose to use the Cole system as the basic model for any separate part of the measured object, since, for example, a pure resistor can readily be achieved by choosing $\alpha = 0$ in the Cole equation.)

The succeeding discussion will be restricted to the case of two Cole systems in series or parallel, and how the measured data in those two cases will appear in the complex admittance (Y -plot) or impedance (Z -plot) plane.

Consider two Cole systems in series having the following arbitrarily chosen parameters (τ is given for the impedance plane) (Table 8.2).

Each of these two Cole systems will produce a circular arc in the complex impedance plane as shown in Fig. 8.24, and when impedance measurements are done on the total system, complex values like the ones indicated by circles in the diagram will be obtained.

Measurements will hence in this case reveal the presence of two Cole systems if the measured frequency range is broad enough. Measurements up to about 1 kHz will however only disclose one circular arc, corresponding to system 2 shifted to the right approximately by the value of R_0 in system 1.

TABLE 8.2 Parameters for the Two Cole Systems in Series

	R_0	R_∞	τ_z	α
System 1	1.7 k Ω	200 Ω	20 μ s	0.55
System 2	10 k Ω	300 Ω	5 ms	0.75

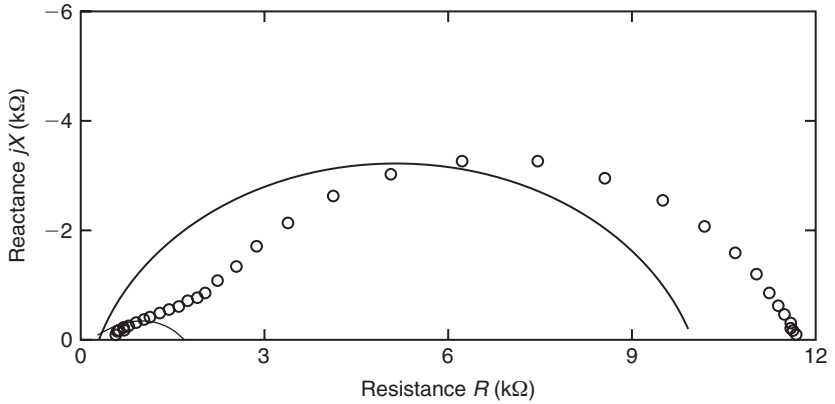


Figure 8.24 Cole plot in the impedance plane (Z -plot) for values given in Table 8.2 showing system 1 (small solid arc), system 2 (large solid arc) and measured values (circles).

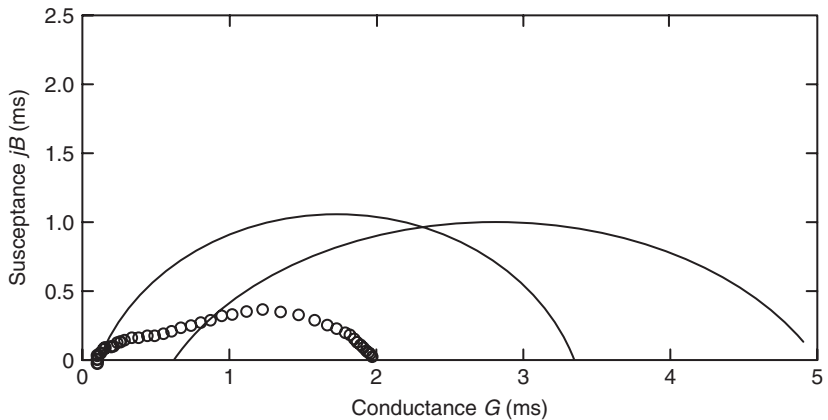


Figure 8.25 Cole plot in the admittance plane (Y -plot) for values given in Table 8.2 showing system 1 (right solid arc), system 2 (left solid arc) and measured values (circles).

The same data are plotted in the complex admittance plane in Fig. 8.25. The small arc representing system 1 in Fig. 8.24 has now become a large arc due to the low value of R_∞ . This illustrates the importance of using descriptions like “small” or “large” dispersions in connection with Cole plots with considerable care. The existence of two dispersions will be revealed in this plot also, provided the frequency range exceeds 1 kHz.

The analysis will become more troublesome if the relaxation times of the two Cole systems are closer. Consider now two new Cole systems, system 3 and system 4, having almost identical parameters to the systems in Table 8.2, but with the relaxation time of system 1 increased from $20\ \mu\text{s}$ to 2 ms as shown in Table 8.3.

TABLE 8.3 New Parameters for the Two Cole Systems in Series. As Table 8.2 except changed τ_z for System 3

	R_0	R_∞	τ_z	α
System 3	1.7 k Ω	200 Ω	2 ms	0.55
System 4	10 k Ω	300 Ω	5 ms	0.75

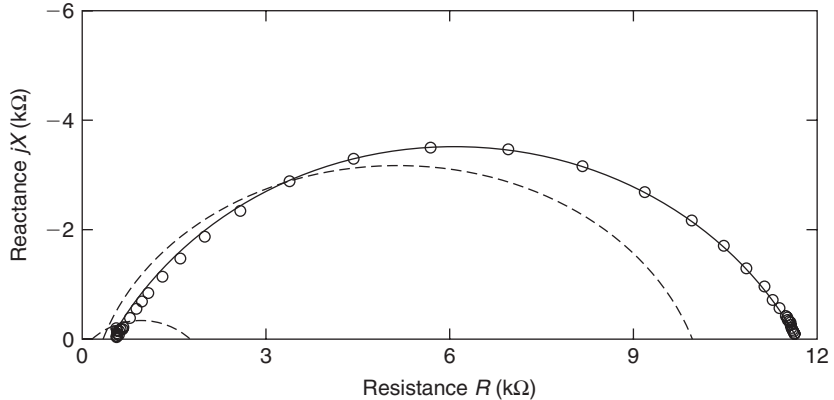


Figure 8.26 Cole plot in the impedance plane (Z -plot) for values given in Table 8.3 showing system 3 (small dotted arc), system 4 (large dotted arc), measured values (circles) and fitted circular arc (solid line).

TABLE 8.4 Parameters for Arcs Fitted to Measured Values for the Two Cole Systems in Series

	R_0	R_∞	τ	α
Fitted impedance arc	11.7 k Ω	500 Ω	~ 5 ms	0.72
Fitted admittance arc	11.7 k Ω	500 Ω	~ 5 ms	0.67
Fitted admittance arc (low frequency only)	11.7 k Ω	500 Ω	~ 5 ms	0.72

A dotted arc in Fig. 8.26 represents each of the two systems. The corresponding measured values show that *the existence of two Cole systems cannot be discovered in the diagram*. The natural thing will thus be to attempt to fit one circular arc to the measured values, as indicated by the solid line in Fig. 8.26. The parameters of this fitted arc are given in Table 8.4. The values of R_0 and R_∞ are of course the sum of the corresponding values for the two isolated systems, but the most interesting features are the values of τ_z and α . The value of τ_z will be close to the value of the dominating system, that is the largest arc in the impedance plane. (For two Cole systems in parallel, this will be the largest arc in the admittance plane.) The value

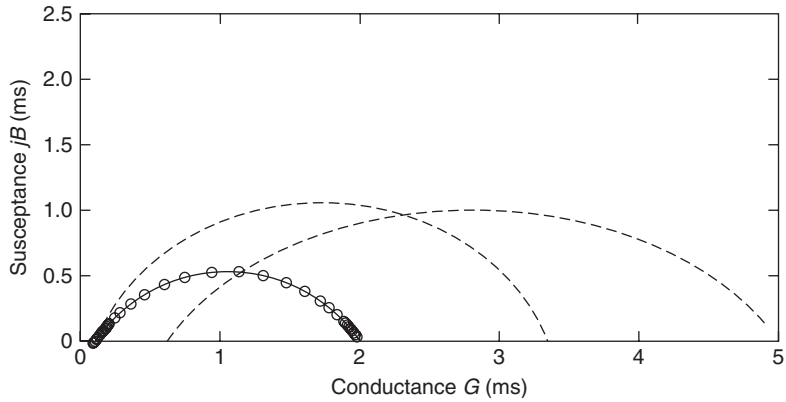


Figure 8.27 Cole plot in the admittance plane (Y-plot) for values given in Table 8.3 showing system 3 (right dotted arc), system 4 (left dotted arc), measured values (circles) and fitted circular arc (solid line).

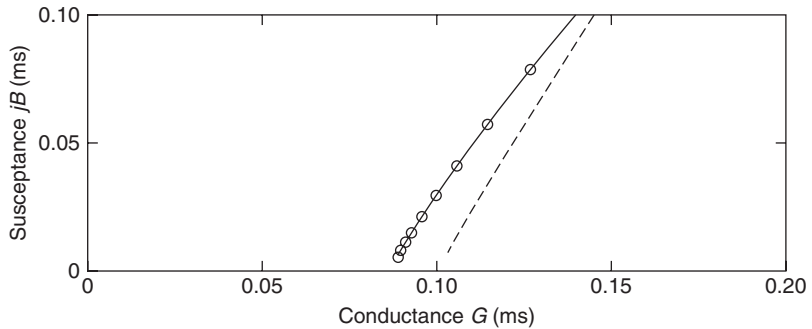


Figure 8.28 Low frequency part of Fig. 8.27, showing system 4 (dotted arc), measured values (circles) and fitted circular arc (solid line).

of α will be closer to the value of the dominating system, but may still be significantly different from either of the systems.

The same data are presented in the complex admittance plane in Fig. 8.27. In this plot, the arcs are about equal in size, but they produce total values that coincides well with a single circular arc. The parameters of this arc are given in Table 8.4, and the most interesting thing is the value of α , which is roughly the mean of the two original values.

However, when plotting only the low frequency part of Fig. 8.27, the calculated value of α will be closer to that of system 4 as shown in Table 8.4, and, in this case, equal to the value found in the impedance plane.

The preceding examples demonstrate how two Cole systems in series influence on the measured electrical data. Two parallel Cole systems will behave in a similar manner, and we leave to the reader to investigate how systems with two parallel dispersions behave. We encourage the use of simulations like this, in order to

acquire a general sense of how changing one parameter or part of a system comes out in different plots.

8.3 DATA CALCULATION AND PRESENTATION

8.3.1 Measured –, Model –, and Derived Data

Measured data and model data, the one cannot live without the other. A clear distinction is necessary between measured “raw” data, *calculated measured* data and *derived* data. All these data are both obtained and analyzed according to models, equations included, as described in Sections 7.1, 8.1 and 8.2.

The measuring setup determines what data is *raw* data. If a constant amplitude current is applied to a set of electrodes, and the corresponding voltage is measured, this voltage is directly proportional to the impedance of the unknown. Then raw data and the measured variable is impedance.

Raw data has to be presented in some chosen form. Some of the data is collected as a function of time, some as a function of frequency. If data is collected as a function of both frequency and time, the need for a three-dimensional presentation is present.

By a simple mathematical operation the inverse values of impedance may be *calculated*, the admittance values found contain no additional information, and the calculations do not contain any apparent conditions with respect to any disturbing influence like temperature, atmospheric pressure, etc.: it is a purely mathematical operation. Therefore, the admittance data is correct to the extent that the impedance data is correct, it is just two different ways presenting the measured data.

The problem of *derived* data is much larger, the variable of interest may be non-electrical, for example tissue water content, derived from electrical variables. Then a new question arises: What *other* variables do influence the correlation between the water content and the measured electrical variable? This is a *selectivity* problem, and a *calibration* problem.

If the measured volume can be defined (not always possible in measurements in vivo), admittivity may be calculated, and also permittivity. Permittivity cannot be measured, only be calculated; capacitance can be measured. If instead an index is calculated (cf. next Section) knowledge of dimensions is not needed, but it must be ascertained that measured data is from the same tissue volume.

The interpretation of the measured data is always linked to some sort of model: an equation or a black box concept. Choosing a model is a major decision, and whether it is to be a descriptive or explanatory (cf. Section 8.1). The task is to choose a productive model, for example as simple as possible but not too simple, allowing conclusions and predictions.

8.3.2 Indexes

An index is the ratio between two measurements made under different conditions but *on the same sample volume*. The index can be calculated from measurement

results with respect to the results from a “gold” standard, or be based for instance upon the same parameter measured at different energies or frequencies. Indexes can also be made by a mathematical operation on the combination of measurement results and other parameters such as, for example, height or weight of the measured person. Actually the phase angle $\varphi = \arctan(B/G)$ is an index.

An index is often useful because it is a relative parameter that becomes independent on, for example, sample dimensions (as long as it is invariable) or some invariable material property. By calculating several indexes one may be able to choose one which is particularly well correlated with clinical judgments. An index may be based on a clear understanding of the underlying physical process, for instance the admittance ratio of high frequency and low frequency values referring to the total and the extracellular liquid volumes. But indexes may also be a “blind” route when they are used without really knowing why the correlation with clinical judgments is high. It has, however, long and very positive traditions in medicine, as for instance in the interpretation of electroencephalogram (EEG) waveforms.

8.4 DATA ANALYSIS

8.4.1 Multivariate Analysis

Multivariate analysis is a set of techniques used for analysis of data sets which contain more than one variable, and the techniques are especially valuable when working with correlated variables. The techniques provide an empirical method for information extraction, regression or classification and many of these techniques have been developed quite recently because they require the computational capacity of modern computers.

As a trivial example, say that you wanted to utilize impedance measurements to assess the quality or texture of the inside matter of an apple. One approach would be to develop an electrical model for the apple and figure out how texture differences depend on things like cell structure and water content. Based on these assumptions, you could try to postulate how differences in texture will influence the impedance spectrum and then seek to have this confirmed by experiments. Referring to Section 8.1 this would be the explanatory approach, whereas a more descriptive approach could be the use of multivariate analysis.

To use a multivariate regression technique, you would need another way of measuring or assessing the apple’s texture as a golden standard to calibrate your model against. The measured impedance values will in this case often be called X -variables and the measurements from the calibration instrument is called Y -variables.

There may exist a mechanical instrument for measuring the softness of the apple material or you may simply use a taste panel to score each apple on a scale from 1 to 10. What the multivariate regression software program then will do for you is basically to produce an model, which you can use to calculate the softness of each apple (Y -variable) from the measured impedance data (X -variables) or from any data derived from the measured data, such as Cole parameters, etc.

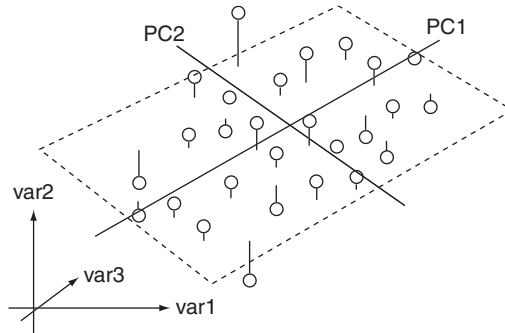


Figure 8.29 Samples plotted with each individual measured variable on orthogonal axes. The samples are projected down on the plane given by PC1 and PC2.

The main purpose of multivariate methods would be information extraction. The simplest form of information extraction and data reduction is the *Principal Component Analysis* (PCA) technique. The history of PCA can be traced to an article by Pearson (1901). It is a statistical method that can be performed in a wide variety of mathematical, statistical or dedicated computer software like for instance Matlab (The MathWorks, Inc.), SPSS (SPSS, Inc.) or The Unscrambler (Camo, Inc.). We will here give a short non-mathematical introduction to this method, and we refer the reader to one of the many available text books on this topic for a more in-depth, formal presentation.

PCA is mathematically defined as an orthogonal linear transformation that transforms the data to a new coordinate system such that the greatest variance by any projection of the data comes to lie on the first coordinate (called the first principal component), the second greatest variance on the second coordinate and so on.

In Fig. 8.29 the samples are plotted as circles according to their measured impedance values in the n -dimensional space, where n is the number of measured values in each impedance spectrum. For obvious reasons, only three orthogonal directions are shown in the figure. Hence, a frequency scan using 19 discrete frequencies (three frequencies per decade from 1 Hz to 1 MHz) measuring resistance and reactance, would give data points plotted in the 38-dimensional space. The longest axis inside the “volume” occupied by the data points in this space will be the first principle component (PC1). The second longest axis orthogonal to PC1 will be PC2, and so on. In this way a new coordinate system that emphasizes the greatest variances in the data set, is constructed.

Certain plots and graphical presentations are frequently used in multivariate analysis and the most frequently used is perhaps the *score plot*. This is a two-dimensional scatter plot (or map) of scores for two specified components (PCs), in other words a two-dimensional version of Fig. 8.29. The plot gives information about patterns in the samples. The score plot for PC1 and PC2 is especially useful, since these two components summarize more variation in the data than any other pair of components. One may look for groups of samples in the score plot and also detect outliers, which may be due to measurement error. In classification

analysis the score plot will also show how well the model is able to separate between classes. An example is given in Section 9.15.3.

The *loading plot* is the corresponding map of the variables for two specified PCs. Looking at both the score plot and the loading plot for the same two components can help you determine which variables are responsible for differences between samples. For example, samples to the right of the score plot will usually have a large value for variables to the right of the loading plot, and a small value for variables to the left of the loading plot. The score s_i for sample i for one PC is given by

$$s_i = \sum_{j=1}^n p_j x_j \quad (8.45)$$

where p_j is the loading associated with variable x_j .

Another popular method is called partial least squares (PLS) regression. This method also creates a new coordinate system based on orthogonal linear transformations, but the optimization criterion is different. While PCA maximizes the variance in X , PLS will maximize covariance between X and Y .

For classification one may use a method called Soft Independent Modeling of Class Analogies (SIMCA) where one PCA model is constructed for each class of samples, but a range of other methods are also available.

The importance of using professional statisticians in the planning of experimental studies cannot be overestimated. Many researchers find out too late that they should have designed the study differently. Statistics is a complex subject matter and a thorough understanding of the field takes years of training. If bioimpedance shall succeed in providing useful instruments to healthcare and other areas, the appropriate use of statistical methods is essential.

8.4.2 Clinical Performance

Receiver operating characteristics (ROC) graphs are useful for visualizing the performance of binary (having two possible outcomes) classifiers. It is a well-known means for evaluating diagnostic tools in medicine, but in general it can be used for evaluation of all kinds of classification algorithms (Fawcett, 2005).

The obvious example from bioimpedance applications in medicine would be the possible diagnosing or classification of human tissue as normal or cancerous from a measured impedance spectrum. After measurements and the pertinent treatment of the data, the possible outcomes from the classifier are denoted positive (p') or negative (n') with regard to cancer or not (Fig. 8.30). The true classes are correspondingly denoted p or n .

ROC graphs are commonly used to assess the performance of a classifier. Sensitivity is plotted on the y -axis and 1 -Specificity on the x -axis.

Classifiers producing results on the diagonal, dashed line in Fig. 8.31 have the same performance as random guessing or coin flipping. Results toward the upper, left corner of the graph are better and a result in the point $(0,1)$ represents a perfect classifier.

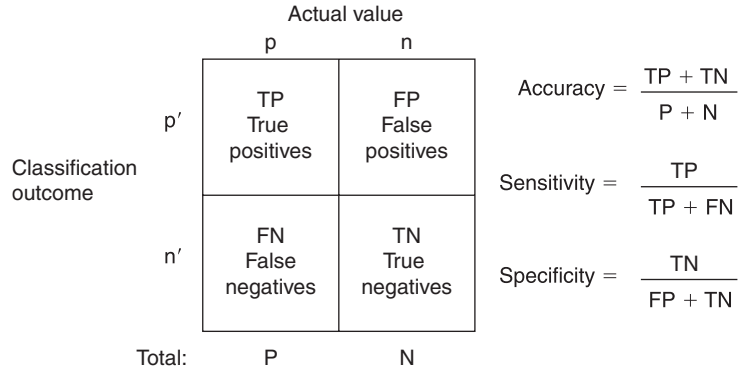


Figure 8.30 Confusion matrix showing the four outcomes of a binary classification process.

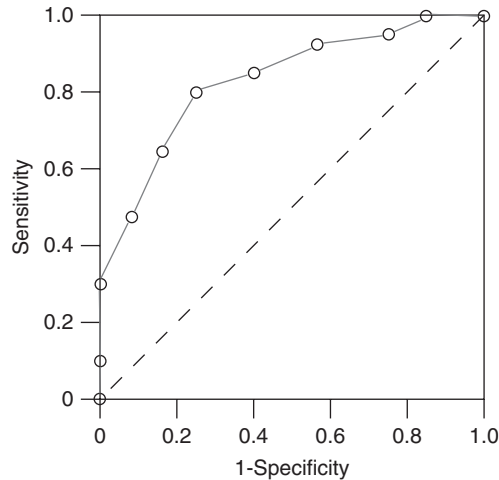


Figure 8.31 A basic ROC graph.

As an example, say that the classifier calculates a number from 1 to 10 from the measured impedance data, where low numbers represent normal tissue and high numbers cancerous tissue. In most real cases the distributions of normal and cancerous tissues will overlap on this scale. Setting the cut-off value to 6 may for instance classify 80% of the cancerous tissues correctly, but at the same time erroneously classify 20% of the normal tissue as cancerous. This corresponds to TP = 0.8 and FP = 0.2 and a point at (0.2,0.8) in the ROC graph. Changing the cut-off value from the lowest to the highest value in steps, and calculating the corresponding TP and FP for each value will produce a curve in the ROC graph, similar to the one shown in Fig. 8.31. The area under the curve is commonly used as a measure of classifier performance. An area of 1.0 indicates a perfect classifier,

whereas 0.5 is equal to random guessing. Values below 0.5 can be made equally larger than 0.5, just by negating the prediction.

8.4.3 Neural Networks

A neural network is a system of interconnected processing elements called neurons or nodes. Each node has a number of inputs and one output, which is a function of the inputs. There are three types of neuron layers: input, hidden and output layers. Two layers communicate via a weight connection network. The nodes are connected together in complex systems, enabling comprehensive processing capabilities. The archetype neural network is of course the human brain, but there is no further resemblance between the brain and the mathematical algorithms of neural networks used today.

A neural network performs parallel and distributed information processing that is learned from examples, and can hence be used for complex bioimpedance signal processing. The “learning” capabilities of neural networks are by far their most fascinating property. The processing may be simulated in a computer program, but because of the sequential nature of conventional computer software, the parallel feature of the neural network will be lost and computation time will increase. However, simulation on a computer gives the great advantage of full control over the network algorithm at any time. Physical neural networks are most often implemented as VLSI (Very Large Scale Integrated circuit) electronic circuits, and sometimes a hybrid solution is chosen.

Neural networks may be constructed in many ways, and those presented so far in the literature can be classified as follows:

1. *Feedforward networks*: These networks are usually used to model static systems. Data from neurons of a lower layer are propagated forward to neurons of an upper layer, and no feedback is used.
2. *Recurrent networks*: These networks include feedback, and are usually used to model dynamic systems.
3. *Associative memory networks*: A type of recurrent network whose equilibrium state is used to memorize information.
4. *Self-organizing networks*: The neurons are organized on a sort of dynamic map that evolves during the learning process, in a way that is sensitive to the history and neighboring neurons. Clustering of input data is used to extract extra information from the data.

The most commonly chosen approach is the feedforward network using a so-called back-propagation algorithm. The back-propagation algorithm can be thought of as a way of performing a supervised learning process by means of examples, using the following general approach: a problem, that is a set of inputs, is presented to the network, and the response from the network is recorded. This response is then compared to the known “correct answer.” The result from this comparison is then fed back into the system in order to make the network adapt

according to the information inherent in the examples. This adaptation is accomplished by means of adjustable parameters that control the behavior of the network. The act of repeatedly presenting inputs to the network, and providing it with feedback regarding its performance, is called *training*, and the network can be said to be *learning*.

8.4.4 Chaos Theory and Fractals

An exciting development has for some years been seen in the use of chaos theory in signal processing. A chaotic signal is not periodic; it has random time evolution and a broadband spectrum, and is produced by a deterministic non-linear dynamical system with an irregular behavior. The evolution in state space (also called phase space) of a chaotic signal must take place on a *strange attractor* of volume zero, which requires sensitive dependence to initial conditions. An attractor is a set of values to which all nearby values converge in an iterative process. In order to classify the attractor as strange, this set of values must be a fractal. Consider for example the sequence produced by the iterative process:

$$S_n = (\cos x)^n \quad (8.46)$$

This sequence appears when you, for example, repeatedly press the cosine button on a pocket calculator and it converges to 0.739 if x is an arbitrary number in radians. Other iterative processes do not converge to a specific number, but produce what seems like a random set of numbers. These numbers may be such that they always are close to a certain set, which may be a *fractal*. This set is called a fractal attractor or strange attractor.

Fractal patterns have no characteristic scale, a property that is formalized by the concept of *self-similarity*. The complexity of a self-similar curve will be the same regardless of the scale to which the curve is magnified. A so-called fractal dimension D may quantify this complexity, which is a non-integer number between 1 and 2. The more complex the curve, the closer D will be to 2. Other ways of defining the fractal dimension exist, such as the Hausdorff–Besicovitch dimension.

Self-affine curves resemble self-similar curves, but have weaker scale-invariant properties. Whereas self-similarity expresses the fact that the shapes would be identical under magnification, self-affinity expresses the fact that the two dimensions of the curve may have to be scaled by different amounts for the two views to become identical (Bassingthwaight et al., 1994). A self-affine curve may hence also be self-similar; if it is not, the curve will have a local fractal dimension D when magnified a certain amount, but this fractal dimension will approach 1 as an increasing part of the curve is included. Brownian motion plotted as particle position as a function of time gives a typical example of a self-affine curve.

The theory of fractal dimension may be used in bioimpedance signal analysis, for example, for studying time series. Such analysis is often done by means of *Hurst's rescaled range analysis* (R/S analysis), which characterize the time series by

the so-called *Hurst exponent* $H = 2-D$. Hurst found that the rescaled range often can be described by the empirical relation:

$$R/S = (N/2)^H \quad (8.47)$$

where R is the peak-to-peak value of the cumulative deviation from the average value of the signal, and S is the corresponding standard deviation over a time period of N sampling intervals. Natural phenomena such as temperature and rainfall figures are found to have Hurst exponents more or less symmetrically distributed around 0.73 ($SD = 0.09$) (Feder, 1988).

8.4.5 Wavelet Analysis

It is difficult to give an introduction to wavelet analysis without reference to Fourier analysis, which is discussed earlier in this chapter.

Consider the following signal:

$$f(t) = \sin(\omega_0 t) = \sin\left(\frac{2\pi}{T} t\right) = \begin{cases} \sin(\pi t), & 0 \leq t \leq 2 \\ \sin(2\pi t), & 2 \leq t \leq 3 \end{cases} \quad (8.48)$$

which is the sum of two single-period sine signals, as shown in Fig. 8.32. The Fourier transform for this signal will be

$$F(\omega) = \int_0^2 \sin(\pi t) e^{-j\omega t} dt + \int_2^3 \sin(2\pi t) e^{-j\omega t} dt \quad (8.49)$$

which solves to

$$F(\omega) = \frac{\pi}{\omega^2 - \pi^2} (e^{-j2\omega} - 1) + \frac{2\pi}{\omega^2 - 4\pi^2} (e^{-j3\omega} - e^{-j2\omega})$$

The modulus response of $F(\omega)$ is shown in Fig. 8.33.

Figure 8.33 shows that you need an infinite number of sine waves to reconstruct the original signal perfectly, or at least a large number of sine waves to get close to the original.

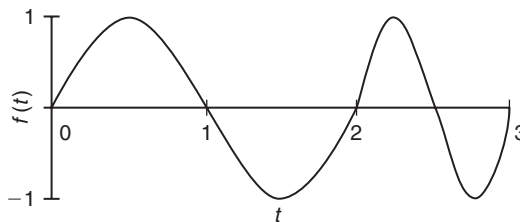


Figure 8.32 Sequence of two single-period sine wave signals.

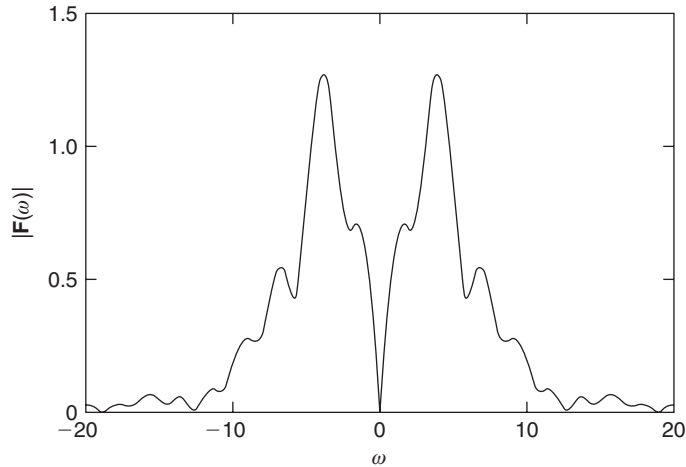


Figure 8.33 Modulus response of the signal in Fig. 8.32.

Looking at Fig. 8.33, it is obvious that the signal could be represented by only one or two frequency components if the transformation was performed within a moving time window. This kind of time–frequency analysis is available in the so-called short-time Fourier transform (STFT) (cf. Section 7.2.3). The problem with STFT is that the resolution in time and frequency is restricted once you have selected the kind of window you want to use for your analysis.

An intuitive solution to this problem would be to allow for sine waves with finite duration to appear as building blocks in the transformed data. This is the basis of wavelet analysis. The wavelet transform is based on such building blocks or elementary functions, which are obtained by dilations, contractions and shifts of a unique function called the wavelet prototype (or mother wavelet) $\psi(t)$.

There are four different types of wavelet transforms:

1. *The continuous wavelet transform*: This transform is given as:

$$\text{CWT}(a, \tau) = \frac{1}{\sqrt{a}} \int_{-\infty}^{\infty} f(t) \psi\left(\frac{t - \tau}{a}\right) dt \quad (8.50)$$

It has a parallel in the Fourier transform, and the variable t , scale a and shift τ are all continuous.

2. *The discrete parameter wavelet transform (or wavelet series)*: Here the parameters a and τ are discretized to $a = a_0^m$ and $\tau = n\tau_0 a_0^m$. The parameters m and n are integers and the function $f(t)$ is still continuous. The transform is then given as:

$$\text{DPWT}(m, n) = a_0^{-m/2} \int_T f(t) \psi(a_0^{-m}t - n\tau_0) dt \quad (8.51)$$

The wavelet prototype $\psi(t)$ is hence shifted in time by increasing n or in frequency by increasing m . An increased m will reduce the time duration and thereby increase the center frequency and frequency bandwidth of $\psi(t)$.

3. *The discrete time wavelet transform:* This is a version of the DPWT with discrete time where $t = kT$ and the sampling interval $T = 1$, given as:

$$\text{DTWT}(m, n) = a_0^{-m/2} \sum_k f(k) \psi(a_0^{-m}k - n\tau_0) \tag{8.52}$$

4. *The discrete wavelet transform:* This is defined as:

$$\text{DWT}(m, n) = 2^{-m/2} \sum_k f(k) \psi(2^{-m}k - n) \tag{8.53}$$

The discrete wavelet $\psi(k)$ can be, but not necessarily, a sampled version of a continuous counterpart.

Let us now see how discrete parameter wavelet transform can be applied to the simple example given above. The transform coefficients were given as:

$$\text{DPWT}(m, n) = a_0^{-m/2} \int_T f(t) \psi(a_0^{-m}t - n\tau_0) dt \tag{8.54}$$

Considering the signal in Fig. 8.32, one could choose the mother wavelet to be a single period of a sine wave, for example

$$\psi(t) = \sin\left(\frac{2\pi}{T}t\right) = \sin(\pi t) \tag{8.55}$$

and furthermore choose $a_0 = \frac{1}{2}$ and $\tau_0 = 2$, giving transform coefficients on the form:

$$\text{DPWT}(m, n) = 2^{m/2} \int_T f(t) \psi(2^m t - 2n) dt \tag{8.56}$$

where the baby wavelets are

$$\psi_{m,n}(t) = 2^{m/2} \psi(2^m t - 2n) \tag{8.57}$$

The procedure is then to compare the value of this wavelet with $f(t)$ for one period of the wavelet, that is $0 \leq t \leq 2$, which gives you $\text{DPWT}(0,0) = 0$. Then increase m and n individually in positive unit steps, to get $\text{DPWT}(0,0)$ equal to:

	$n = 0$	$n = 1$	$n = 2$
$m = 0$	1	0	0
$m = 1$	0	0.707	0
$m = 2$	0	0	0

Hence, $f(t)$ can be represented by two terms only:

$$f(t) = \psi_{0,0}(t) + \frac{1}{\sqrt{2}} \psi_{1,1}(t) \tag{8.58}$$

An in-depth description of wavelets and their use in biomedical signal processing is given by Akay (1998).

PROBLEMS

1. An ideal resistor of $1\text{ k}\Omega$ is coupled in parallel with an ideal capacitor with capacitance $2.2\ \mu\text{F}$. Calculate the complex impedance and the complex admittance at 314 Hz .
2. Suppose that we have obtained the measurement results shown in Table 8.5. The table contains raw data, as for instance obtained directly from a lock-in amplifier. It is admittance data according to $Y = G + jB$, and the results are given in microsiemens:
 - (a) Calculate the corresponding impedance values at each frequency.
 - (b) Plot complex admittance as a function of logarithmic frequency, with linear and logarithmic conductance/susceptance scales. Is there a second dispersion below 0.1 Hz ?
 - (c) Plot the admittance and impedance data in a Wessel diagram and compare.
 - (d) Plot of the admittance magnitude and phase (called a *Bode²plot* if it is presented with logarithmic amplitude scales, linear phase scale and logarithmic

TABLE 8.5 Measured Data

f (Hz)	G (μS)	B (μS)
0.01	23.0	0.5
0.03	23.1	0.7
0.1	23.2	0.7
0.3	23.4	1.6
1	23.8	3.7
3	25.1	7.7
10	29.8	16.4
20	36.3	23.6
50	52.5	31.8
100	68.3	32.2
200	82.0	27.0
500	92.6	17.4
1000	96.3	11.4
3000	98.7	5.6
10000	99.5	2.4
30000	99.8	1.1
100000	99.9	0.5

²Hendrik W. Bode, research mathematician at Bell Telephone laboratories, author of the book “Network analysis and feedback amplifier design” (1945).

frequency scale on the x -axis). It is important to be aware of the different curves obtained with logarithmic immittance variables. With linear scales the characteristic frequency coincides with the geometrical mean of the dispersion, this is changed with the logarithmic scales used in Bode plots.

- (e) Let us assume that we know the dimensions of the sample to be $d = 1$ mm and $A = 1$ cm². We can then calculate the relative permittivity according to the equations in Section 3.3. Calculate the complex capacitance and permittivity and plot the results in Bode and Wessel diagrams. Compare the spectra with the admittance plots.

9 CLINICAL APPLICATIONS

Chapter Contents

9.1 Electrocardiography

- 9.1.1 Three Limb Electrodes (Six Limb Leads)
- 9.1.2 Six Chest Electrodes (Six Unipolar Precordial Leads)
- 9.1.3 Standard 12 Lead ECG
- 9.1.4 Cardiac Electrophysiology
- 9.1.5 Vector Cardiography
- 9.1.6 Forward and Inverse Problem
- 9.1.7 Technology

9.2 Impedance Plethysmography

- 9.2.1 Ideal Cylinder Models
- 9.2.2 The Effect of Different Conductivities
- 9.2.3 Models with Any Geometry and Conductivity Distribution
- 9.2.4 Rheoencephalography

9.3 Impedance Cardiography

9.4 Tissue Characterization in Urology

9.5 EEG, ENG/ERG/EOG

9.6 Electrogastrography

9.7 EMG and Neurography

9.8 Electrical Impedance Myography

9.9 Electrotherapy

- 9.9.1 Electrotherapy with DC
- 9.9.2 Electrotherapy of Muscles

9.10 Body Composition Analysis

9.11 Implanted Active Thoracic Devices

- 9.11.1 Physiological Impedance Components
- 9.11.2 Fluid Status Monitoring
- 9.11.3 Cardiac Pacemakers

9.12 Defibrillation and Electroshock

- 9.12.1 Defibrillator
- 9.12.2 Electroshock (Brain Electroconvulsion)

9.13 Electrosurgery**9.14 Cell Suspensions**

- 9.14.1 Electroporation and Electrofusion
- 9.14.2 Cell Sorting and Characterization by Electrorotation and Dielectrophoresis
- 9.14.3 Cell-Surface Attachment and Micromotion Detection
- 9.14.4 Coulter Counter

9.15 Skin Instrumentation

- 9.15.1 Fingerprint Detection
- 9.15.2 Stratum Corneum Hydration
- 9.15.3 Skin Irritation and Skin Diseases Including Skin Cancer
- 9.15.4 Electrodermal Response
- 9.15.5 Sweat Measurements
- 9.15.6 Iontophoretic Treatment of Hyperhidrosis
- 9.15.7 Iontophoresis and Transdermal Drug Delivery

9.16 Non-medical Applications**9.17 Electrical Safety**

- 9.17.1 Threshold of Perception
- 9.17.2 Electrical Hazards
- 9.17.3 Lightning and Electrocution
- 9.17.4 Electric Fence
- 9.17.5 Electrical Safety of Electromedical Equipment

Bioimpedance research and development have been going on for a very long time, and the number of *clinical* applications does regularly increase but at a low rate. Bioimpedance is a general transducing mechanism for many physiological events, and the instrumentation is low cost. Basically the situation may have the aspect of a technology seeking a problem, but this must be reverted by taking another approach: go to the clinics and start with their problems and needs and see whether bioimpedance technology has a solution. Many of the transducing mechanisms can indeed offer solutions, but they must compete with the other solutions already in clinical use. Ultrasound imaging instrumentation for example can measure many of the parameters that bioimpedance can also measure. As the medical doctors already have the ultrasound probe in their hands as a multiparameter measuring device the bioimpedance technology must offer some definite advantages. The job is to find those clinical application areas.

Another job is to standardize the methods used by different models and companies. A problem related to standardization is when different models use non-scientific methods being based on non-published algorithms. Another problem is

that it is difficult to describe the clinical applications in detail because the more important they are the more patent rights and commercial interest complicate the picture.

9.1 ELECTROCARDIOGRAPHY

Electrocardiography (ECG) is an important clinical examination routinely performed with 12 leads, 9 skin surface electrodes plus a reference electrode. ECG is also important for long term monitoring in intensive care units. Also ECG control is extremely important during resuscitation and defibrillation.

During a routine ECG examination four electrodes are connected to the limbs. Three of these are for ECG signal pick up and one is a reference electrode (right leg (RL)) for noise reduction. Six electrodes are connected in the thorax region at well-defined positions near the heart.

9.1.1 Three Limb Electrodes (Six Limb Leads)

The most basic ECG examination is with three skin surface electrodes on the limbs: one at the left arm (LA), one at the right arm (RA) and one at the left leg (LL). Figure 9.1 illustrates how six limb leads are derived from these three electrodes.

It is unusual that pick-up electrodes are placed so far away from the source organ; the main reasons in ECG are standardization and reproducibility. In our language, the limbs are salt bridges to the thorax. By this, the coupling to the thorax is well defined and electrocardiograms can be compared even when recorded in different hospitals and at long intervals. The position of the electrodes on each limb is uncritical because the distal part of each limb is isoelectric (with respect to ECG, not with respect to, for example, electromyography (EMG) sources of the arm muscles). Such is the reproducibility that the bipolar leads form the basis for determining the axis of the electric heart vector.

Three Bipolar Leads: I, II, III

Channel I is the voltage difference RA–LA; channel II: RA–LL; channel III: LA–LL. Einthoven found the following relationship between the scalar lead voltages: $u_{II} = u_I + u_{III}$. Figure 9.2 shows an example of a typical ECG waveform.

The Three Unipolar Limb Leads: aVR, aVL, aVF

In the days of the first publications of Einthoven¹ no amplification tube had yet been invented, and the signal from the electrodes had to drive a galvanometer directly.

¹ Willem Einthoven (1860–1927), Dutch physician. Nobel prize laureate in medicine 1924 (on ECG).

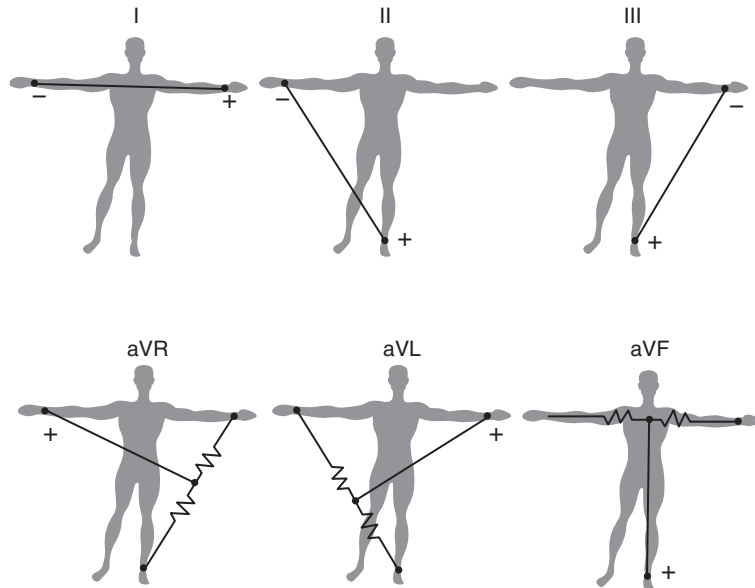


Figure 9.1 The six limb leads derived from three limb electrodes (both arms and left leg). Here a means augmented.

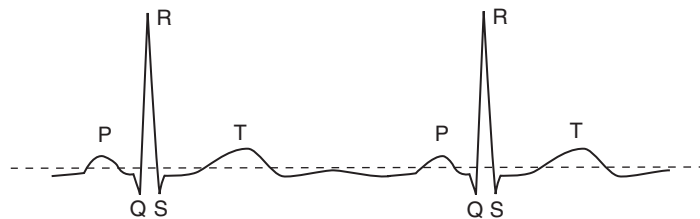
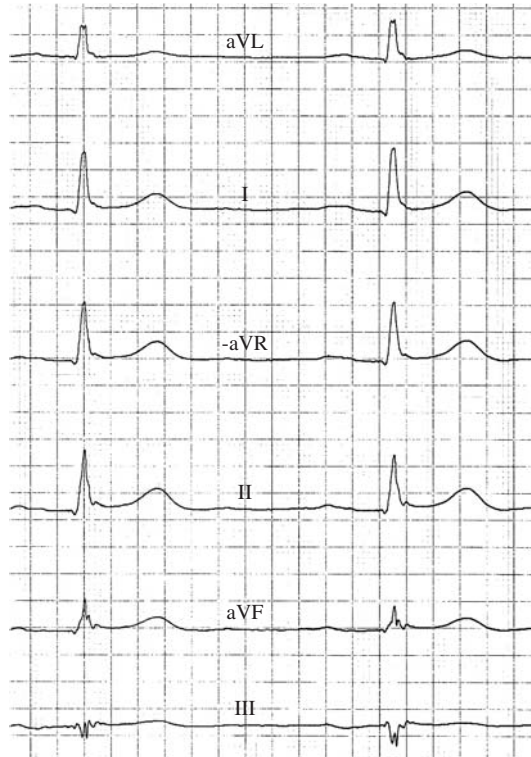


Figure 9.2 ECG waveform lead II. Dashed line is zero voltage determined by the electronic circuit high-pass filter functioning so that the negative and positive areas become equal.

Later the *unipolar augmented* leads were invented; they were called augmented because the signal amplitudes were higher. A “reference” voltage was obtained by summing the voltage from two of the limb electrodes (Fig. 9.1). More important, these vector leads have the interesting property of interlacing the vector lead angles of I, II and III (0° , 60° and 120°) so that each 30° is covered. This is shown in Fig. 9.6, where both an example of the heart vector \mathbf{m} and the six lead directions are shown. Figure 9.3 shows the six limb leads arranged in a so-called Cabrera sequence. The text box in Fig. 9.3 contains a set of data extracted from the six ECG lead waveforms.



HR 52/minute	QRS 92 ms	T axis 35°
RR 1150 ms	QT 426 ms	P(II) 0.08 mV
P 146 ms	P axis 40°	S (aVL) -1.12 mV
PR 234 ms	QRS axis 24°	R (aVF) 1.64 mV

Figure 9.3 ECG waveforms of the six standard extremity leads shown with the augmented leads interlaced between the bipolar limb leads (Cabrera sequence).

Einthoven Triangle and the Lead Vector

Einthoven (1913) proposed an equilateral triangle model with center in the heart center (Fig. 9.4). Each side of the triangle corresponded to each of the three bipolar leads I, II and III. He proposed the heart modeled as a bound dipole vector (he did not use that expression), and that a lead voltage was the projection of the heart vector on a corresponding triangle side (actually a dot product). He proposed that his model could be used for determining the heart vector axis. This means that he saw a solution to the inverse problem: from measured lead voltages to the heart vector, from measured surface potentials to source characterization. He regarded the triangle apexes as corresponding to right and left shoulder and the symphysis. The triangle is

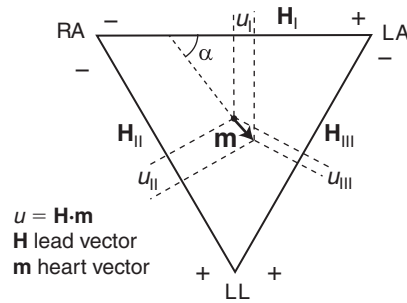


Figure 9.4 Einthoven's triangle. The triangle is in the frontal plane of the patient. \mathbf{m} is the heart vector bound to the "center" of the heart; u is the instantaneous scalar voltage measured in a respective lead; α is the instantaneous angle of the electric axis of the heart.

in the frontal plane of the patient, and the heart vector has no component perpendicular to the frontal plane. He considered the heart vector to be very short.

Burger and Milan (1946) formalized Einthoven's idea and introduced the concept of the *lead vector* (eq. 6.30). The lead vectors \mathbf{H} of the I, II and III leads correspond to the sides of the Einthoven triangle with corners corresponding to the anatomy: the shoulders and the symphysis. The measured lead voltage u (volt) is a scalar and according to eq. (6.31) $u = \mathbf{H} \cdot \mathbf{m}$ so that u is the projection of \mathbf{m} in the direction of a lead vector \mathbf{H} (Fig. 9.4). \mathbf{H} [Ω/meter] for each lead is obtained from the Einthoven triangle, and the heart vector \mathbf{m} [Am] is the unknown. The magnitude and direction of \mathbf{m} can be determined from measured potentials of at least two leads (Fig. 9.4).

\mathbf{m} represents a bound vector with the fixed origin in the "center" of the heart, the lead vectors \mathbf{H} are free vectors. Sampling the u values of the leads I, II and III at a given moment on Fig. 9.4 defines the *instantaneous* value and direction (angle α in Fig. 9.4) of the heart vector \mathbf{m} . The mean direction during the QRS complex defines the *electrical axis* of the heart. Mean direction is used because the R tags are not completely concurrent for the I, II and III leads. The electrical axes for the P, QRS and T complexes have different directions (cf. the text box of Fig. 9.3). During a QRS complex the locus of the vector arrow describes a closed loop in the frontal plane (Fig. 9.5).

The electrical axis of the heart can roughly be determined by looking at the net area of a QRS complex. A net positive area means that the heart vector has the same direction as the lead vector. A small net area means that the heart vector is perpendicular to the lead vector. A negative net area means that the heart vector has the opposite direction of the lead vector. It is interesting to compare this interpretation which is based on a bound heart vector with changing length and direction, with the model used for Figs. 6.10–6.12. The model for Fig. 6.11 is a current dipole moving but having constant length and direction. With \mathbf{m} and \mathbf{H}_{II} parallel

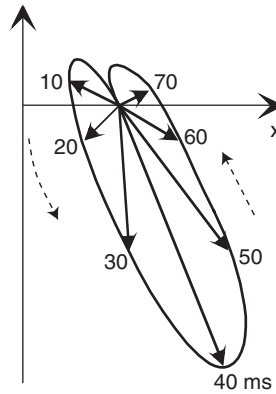


Figure 9.5 Locus of the heart vector \mathbf{m} given each 10 ms in the QRS diastole. Derived from the Einthoven triangle (Fig. 9.4). The graph is in the frontal plane and the x-axis has the direction of the lead vector \mathbf{H}_I ($\alpha = 0$).

the waveform will be monophasic, with \mathbf{m} and \mathbf{H}_{III} perpendicular the waveform will be biphasic.

The *dipole* model in ECG has been a hot topic.² Einthoven (1913) did not use the dipole concept, but referred to the potential difference [V] between two close points in the center of the heart. He thus defined a current vector with the voltage difference between its poles. There is an ambiguity here: A potential difference may be regarded as a scalar [V], but may also be regarded as an electric field [V/m] vector. A bipolar lead may be regarded as an electric field transducer with scalar voltage [V] output. Einthoven used the concept of electromotive force (EMF) which may be considered to have direction when related to the transducing mechanism of the force exercised on a charge in an electric field, but may also be regarded as a scalar potential [V]. So the heart dipole has a vector moment [Am], the heart dipole moment has a direction from plus pole to minus pole, the resulting current density in the thorax is a vector field [A/m^2], the current density \mathbf{J} and the electric field strength \mathbf{E} are in isotropic media proportional and simply related by eq. (2.2): $\mathbf{J} = \sigma\mathbf{E}$. Einthoven did not use the vector concept neither the dipole concept. He referred to the direction of maximum potential difference, and this is in accordance with the Maxwell equation $\mathbf{E} = -\nabla\Phi$.

²“Unfortunately, the application of the long known and well understood principles of potential theory to electrocardiography was not in general well received. Many of the more or less theoretical and mathematical papers along these lines aroused a storm of opposition. Some of the criticism came from physicians who felt that electrocardiography was a purely empiric science and that progress in the field could come only from comparison of the electrographical findings with clinical and post mortem data. Much opposition came from physiologists, many eminent in their field, who not only discounted any article of theoretical nature but also regarded the dipole hypothesis as rank heresy” (Wilson, 1953).

The Einthoven triangle gained more and more acceptance, but was also heavily criticized. In particular four aspects have been attacked:

1. *Redundancy*: Of course $u_I + u_{II} + u_{III} = 0$ (Kirchhoff's law) in a linear system. Because the two input wires of the amplifier of lead II are swapped lead II has changed sign so that: $u_{III} = u_{II} - u_I$. Theoretically a third lead contains no new information, in practice however it represents a quality control and eases rapid waveform interpretations.
2. It is not a great surprise that an equivalent to the electrical activity of the whole myocardium, the transmission from the sources to the different lead electrodes included, can not be modeled as one bound dipole vector alone. The surprise is that the accordance is so good. Refinements can only include expansion with spherical harmonic multipoles such as a quadrupole, not with moving dipoles, electromotive surfaces or multiple dipoles.
3. *Lack of 3D data*: The Einthoven triangle is flat as if all electrical activities in the heart occur in a thin vertical sheet. An additional back electrode would for instance represent a first primitive approach to a lead perpendicular to the classical Einthoven triangle.
4. The triangle is actually based on a model with two ideal dipoles (cf. Section 6.4.2). This presumption is broken because (1) the distance between the dipoles is not very much longer than the dipole lengths; (2) the medium is not infinite and homogeneous.

Torso models were built filled with electrolytes and with an artificial heart in the natural heart position. Burger and Milan (1946) used two copper plates 2 cm in diameter and 2 cm apart with two wires supplying a current as an artificial heart. The dipole concept was not used, but the lead vector and an oblique triangle instead of the equilateral Einthoven triangle. The heart vector was defined as the direction a heart propagates current flow; the dimension was given as $[Vcm^2]$. It is still easy to mix the dimensions, in Fig. 9.2 and 9.4 it is easy to believe that the heart vector is some strange voltage vector created by projections of the lead voltages. But the heart vector is a dipole vector according to $\mathbf{m} = iL_{cc}$ [Am]. The direction of the vector is the electrical axis of the heart, and this is clinically used. The split components of \mathbf{m} : the dipole current i and the distance vector L_{cc} are not used clinically.

Table 9.1 shows time intervals and heart vector axis as shown in Fig. 9.6.

TABLE 9.1 Normal Values of Time Intervals and Direction of the Heart Vector

Normal values		
0.12 seconds < PQ < 0.25 seconds	QRS < 0.12 seconds	$-30^\circ < \text{QRS axis} < +90^\circ$

9.1.2 Six Chest Electrodes (Six Unipolar Preordial Leads)

A larger signal with higher information content is obtained by placing surface electrodes as near to the heart as possible. The drawback is that the exact electrode positions become critical, and it is difficult to obtain the same positions next time by another person or clinic. Six unipolar pick-up electrodes are positioned on the skin around the heart in a transverse plane. The lead vector of each of the six electrodes has the direction of the line from the heart center to the unipolar electrode in the transversal plane. The “reference” electrode system may be simply the RA electrode alone (CR lead). A more common “reference” is obtained (V lead) by summing the voltage from all three extremities, this is the Wilson reference.

Other Unipolar Leads

Invasive Electrodes

During open heart surgery a net of 11 sterile electrodes are used for epicardial mapping. They have direct contact with the surface of the heart, and the spread of signal on the heart surface is examined by sampling at millisecond intervals in the systole. The signal amplitude is large, and the discriminative power also. The position of infarcted regions is revealed by abnormal epicardial potential spread.

Another invasive ECG recording is with intracardial catheter electrodes (e.g. for *His³-bundle* transmission). Both unipolar and bipolar leads are used, and the

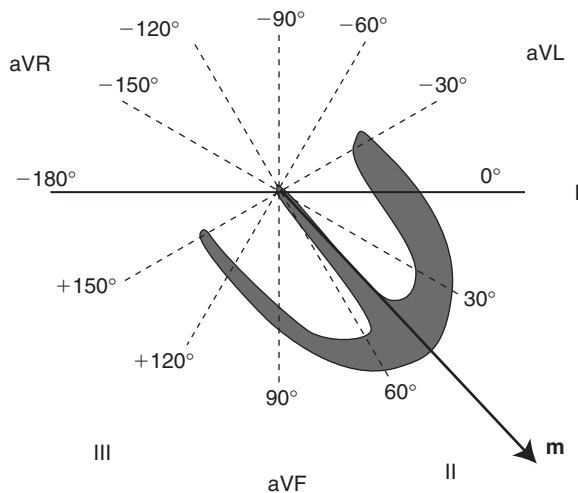


Figure 9.6 Myocard of left (thick) and right (thin) ventricles, the Einthoven triangle in the frontal plane. QRS heart vector **m**, normal angle values are between -30° and $+90^\circ$.

catheter is always advanced into the right atrium via the venous vessels. From there it is further advanced through the tricuspidal valve into the ventricle. Being so near to the source, only small position changes have a large influence on the recorded waveform. This is acceptable because usually the time intervals are of greatest interest. Since the electrodes are very near or on the myocard, the recorded signals have several millivolt of amplitude and with a frequency content up to above 500 Hz.

9.1.3 Standard 12 Lead ECG

The 12 lead ECG clinical diagnostic test is composed of the six limb leads (see Fig. 9.3) and the six unipolar precordial leads.

9.1.4 Cardiac Electrophysiology

The heart is a large muscle group (myocard) driven by a single firing unit followed by a special network for obtaining the optimal muscle squeeze and blood acceleration. It is a very important organ and a very well-defined signal source; therefore all sorts of recording electrodes have been taken into use: from invasive intracardiac catheter electrodes for local His-bundle recording, to multiple sterile electrodes placed directly on the heart surface during open heart surgery (epicardial mapping).

The cardiac cycle in the normal human heart is initiated by the sinoatrial (SA) node. The excitation wave spreads through the atria at a velocity of about 1 m/s. The electroanatomy of the heart separates the atria and ventricles (two chamber heart) so that the excitatory wave can be delayed before it reaches the ventricles. This delay of about 0.15 s is performed in the zone of the atrioventricular (AV) node, and permits a filling of the ventricles before their contraction. Beyond the AV node the excitation spreads rapidly (2–4 m/s) in the networks of His and Purkinje. These networks consist of specialized muscular (not nerve) tissue. From these networks the excitation wave spreads in the myocard at a much lower speed (0.3 m/s). The myocard cells communicate by channels that connect the intracellular electrolytes directly. Each muscle cell is therefore triggered by its neighbor myocard cell but guided by the Purkinje network. Myocard lacks direct nerve control, although the SA node is under nerve control. The intracellular volume is like one volume of cytoplasm with many nuclei (*syncytium*), and electrical models are based on the concept of the *bidomain*, the extracellular and intracellular domains. The tissue mass of the network is much smaller than the mass of the myocard and the electrical signal from myocard dominates the surface ECG.

³Wilhelm His Jr. (1863–1934), Swiss physician.

Important clinical use of ECG data is to look for beat-to-beat differences, both waveform and repetition rate (variation in the beat-to-beat Q-T interval is called *dispersion*), arrhythmias, blocks, detection of ischemia and infarcted muscle volumes and their positions.

9.1.5 Vector Cardiography

Fig. 9.5 actually shows a 2D vector cardiogram in the *frontal* plane. 3D vector cardiography according to Frank is based on the heart vector in a 3D Cartesian diagram. Five strategically positioned skin surface electrodes define the heart vector in the *transversal* plan, and two additional electrodes on the head and LL take care of the vertical vector component. The heart vector is calculated from the recorded lead voltages and projected into the three body planes. Three loci curves of the vector tip in the three planes are the basis for the doctor's description. In principle the 12 channel registration is reduced to three, even so this 3D data set contains more information than the 2D data set from lead I, II and III. However, the problem for vector cardiography is that it is very difficult to throw overboard the long tradition of interpreting curves obtained with the old standardized electrode positions. From long experience a clinical information bank has been assembled giving the relation between waveform and diagnosis. The reason for these relationships may be unknown, and is not of great concern as long as the empirical procedure furnishes precise diagnostic results. All doctors world over are trained according to this tradition (the interpretation of EEG waveforms is another striking example of such a practice). For special diagnostic problems the vector cardiograph has some distinct advantages. For example, the vector display of the QRS complex has a much better resolution than the narrow QRS waveform obtained with a standard 12 lead ECG. Also the vector cardiograph is valuable for training purposes to obtain a better understanding of the spatial distribution of the electrical activity of the heart.

9.1.6 Forward and Inverse Problem

The purpose of the ECG examination is to find the electrical properties of the heart by measuring potential differences on the skin surface. The EMFs of the heart produce currents in the surrounding tissue. The anatomy of the thorax and the conductivity distribution determine how the current flow spreads and which potential differences are to be found at the skin surface. It is generally accepted that the thorax tissue is linear with the usual endogenous current density/electrical field amplitudes generated by the heart. The different contributions of different myocard volumes can therefore simply be added. On the other hand the tissue may be anisotropic and the transfer impedance is frequency dependent. A rough demonstration

of that can be obtained by measuring the transfer impedance between the arms and a bipolar skin surface pick-up electrode pair positioned over the apex and the sternum (Fig. 9.7). Because of reciprocity the transfer impedance is the same if the current is applied to the electrodes on the thorax and the potential difference between the hands is measured. From Fig. 9.7 the frequency components of the P and T waves are not much attenuated, but the frequency components of the QRS above 50 Hz are attenuated by a factor of about 10 or more.

To find the electrical properties of the heart is an *inverse* problem, and in principle it is unsolvable, it is infinitely many source configurations which may result in the measured skin potentials.

We therefore start with the forward problem: from heart models in a conductive medium to surface potentials. Those problems are solvable, but it is difficult to model the heart and it is difficult to model the signal transmission from the heart up to the surface. The model may be an infinite homogeneous volume or a torso filled with saline or with a heterogeneous conductor mimicking the conductivity distribution of a thorax.

The most basic electrical model of the heart is a bound vector with the variable vector moment $m = iL_{cc}$ (cf. eq. 6.10). Plonsey (1966) showed that a model with more than one dipole is of no use because it will not be possible from surface measurements to determine the contribution from each source. The only refinement is to let the single bound dipole be extended to a multipole of higher terms (e.g. with a quadrupole).

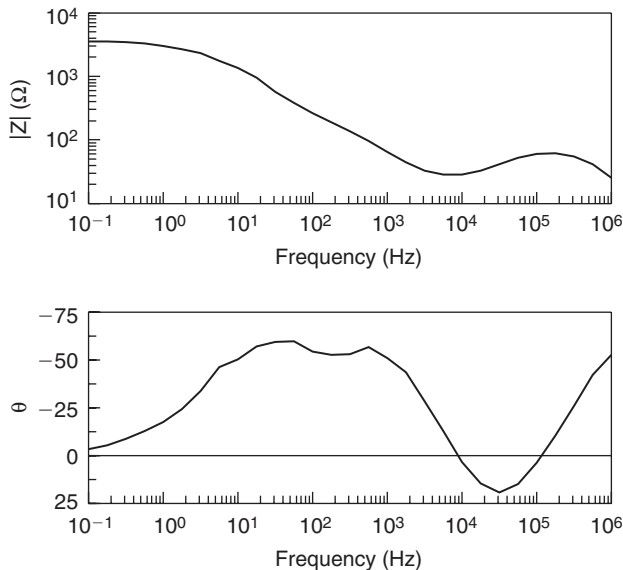


Figure 9.7 Transfer impedance between two chest surface electrodes (apex–sternum) and two electrodes in each of the hands.

The Einthoven triangle was an early solution to the inverse problem: how to characterize the source from surface electrode derived data. It is astonishing how the original Einthoven triangle still is the basis for standard clinical ECG interpretations all over the world even if many improvements have been proposed. Actually the tradition of using a simple theoretical model with an ideal dipole in an infinite, homogeneous volume conductor is uninterrupted. The six limb leads have been heavily attacked for their redundancy. There must be some reason why they have endured all these attacks and reached the overwhelming global spread and acceptance they have today. The large amount of clinical data is one reason; perhaps the value of these data is based on the exceptional reproducibility of their lead vectors. The salt bridge principle assures a well-defined coupling to the shoulders and symphysis, and the position of the electrodes on the limbs is totally uncritical. The chest electrode positions are critical both for the precordial leads and the vector cardiographical leads.

9.1.7 Technology

Signal Amplitude, Limb Lead II

The *R* voltage amplitude is usually around 1 mV. Amplitudes <0.5 mV are characterized as “low voltage” cases, and are pathological. Obesity does not change the ECG waveforms; the *R* amplitude may be somewhat reduced but not into the “low voltage” region.

Frequency Spectrum

Routine bipolar diagnostic ECG is performed with a pass band of, for example, 0.05–60 Hz. The American Heart Association (AHA) recommends 150 Hz as minimum bandwidth and 500 Hz as minimum sampling rate for recording pediatric ECG. DC voltage is thus filtered out because it is related to the electrodes and not to electrophysiology. In monitoring situations the low frequency cut-off frequency may be increased to 0.5 Hz or more because the patient induced motion artefacts are reduced. With skin surface electrodes only the QRS complex has frequency components above 60 Hz, however in the QRS there are components up to and above 1000 Hz (Franke et al., 1962) which are not used clinically. With electrodes in direct connection with the heart the useful frequency spectrum extends to 500 Hz and more. With a pacemaker assisted heart the pacemaker pulses may have a width of <1 ms, and the frequency spectrum extends far above 1 kHz.

Zero Line and Isoelectric Level

Because the ECG amplifier is AC coupled no true zero voltage is recorded. Instead the zero is a line defined by the low-pass filter of the ECG amplifier so that the positive and negative areas of the total ECG waveform are equal. The zero line can be determined by simply shorting the two input wires of a lead (no signal).

Noise

True Physiological Signals

The limb leads presuppose that the patient is lying down so that EMG signals from the limb and body muscles do not intervene. Slow baseline respiration waves are seen if the characteristic frequency of the low-pass filter is 0.05 Hz or lower.

Exogenous Noise

- 50/60 Hz mains noise is electric or magnetic field coupled from power line wires to patient wires or patient body.
- Patient movement generates triboelectricity which may severely disturb the ECG waveform (electrostatic noise).

Solutions are shielding, active op-amp circuit clamping the body to ground (Fig. 7.14), increased distance to the noise source, increased common mode rejection circuitry, averaging over several heart beats, wireless telemetry of electrode pick-up signals.

Indifferent Electrode

With an ideal current dipole in an infinite volume zero potential will exist in all directions if the distance to the dipole is large enough. Unfortunately an indifferent (neutral) ECG electrode does not exist because the human body is not large enough. If we go out in one direction along a limb the limb proper is isoelectric with respect to the heart activity, but not with respect to other sources (e.g. respiration). If we go out along a second limb that too will be isoelectric, however the potential will not be equal to that of the first limb. Therefore none of them represents a true indifferent electrode.

Since this is an unsolvable problem, the ideal unipolar lead does not exist. Non-ideal solutions are to use one electrode at some remote point (e.g. at a limb or an earlobe). Another solution is to add the voltages picked up by more than one electrode, such as two limb electrodes (augmented leads) or three limb electrodes (Wilson central terminal).

Ground, Reference, Indifferent Electrode

In Einthoven's time without amplifiers it was no need for a "ground" electrode, the galvanometer is a floating input device. But mains supplied amplifiers needed a "ground" electrode to reduce noise, and it was the RL which was chosen for that purpose. Later safety philosophy advocated that the patient should be electrically floating with respect to ground (cf. Section 9.17.2). This implied that "ground" was not ground in the meaning the ground wire of the mains. Instead of "ground" this is the *reference* electrode, meaning that the amplifier and the patient are connected together so that they roughly are at the same potential. But then we also

had the ECG tradition that in unipolar leads the reference may not only be one electrode, but for example, a Wilson terminal, used as “zero” or indifferent reference. In our book *ground* means the protective ground electrically connected to the building and the room, supplied by the mains and having the symbol \equiv . The purpose of a *reference* electrode is to obtain potential equalization between the patient and the electronic circuitry, symbol ∇ , $\overline{\text{|||||}}$ or J . The reference electrode is usually an electrode on the RL. A *neutral* or *indifferent* electrode is a part of a unipolar electrode system, and is usually obtained by summing the potentials from more than one electrode (cf. the Wilson terminal).

9.2 IMPEDANCE PLETHYSMOGRAPHY

Plethysmography is the measurement of volume. Dynamic plethysmography is usually associated with volume changes due to the heartbeats, but may also be related to, for example, respiration or peristaltic movements of the alimentary canal. During the heart systole with increased blood flow, the volume, for example, of a limb increases due to the inflow of blood (*swelling*). Impedance may in many cases be regarded as measuring both volume and flow, a volume change must be due to a flow. Measurements may be based on, for example, mechanical dimensional change (strain-gauge plethysmography, light absorption (photo-plethysmography), X-ray absorption or immittance change. Application areas are rather diversified, for example, heart stroke volume (SV), cardiac output (CO), respiration volume, fluid volume in pleural cavities, edema, urine bladder volume, uterine contractions, detection of vein thrombosis.

9.2.1 Ideal Cylinder Models

By ideal we mean that the biomaterial is considered incompressible and homogeneous. The cross sectional area of the cylinder may be circular, elliptic or have any plane form. Estimation of volume from immittance measurement is based on two effects:

1. A geometry-dependent effect illustrated by the cylinder model and the ratio A/L in the equation $G = \sigma A/L$. The resulting effect will be dependent on the constraints on the measured tissue volume: if the volume increase results in a swelling of length L , conductance will fall. If the volume increase results in a swelling of cross sectional area A , the conductance will increase. If the volume increase occurs outside the measured tissue volume, the measured conductance will not change with the geometrical volume increase.
2. A conductivity-dependent component. Of special interest is the flow dependence of the conductivity of blood.

For the further analysis of these effects it is useful to set up some simple cylinder models.

The geometry is shown in Fig. 9.8. For the single cylinder shown at the top of Fig. 9.8 the volume v is easily found from $G = \sigma A/L$ or $R = \rho L/A$:

$$v = G\rho L^2 = R\sigma A^2 = \frac{1}{R} \frac{L^2}{\sigma} \quad (\text{exact}) \quad (9.1)$$

Notice that with the presumption $L = \text{const.}$ the volume v is proportional to G . If the presumption is that $A = \text{const.}$ the volume v is proportional to R . If *swelling is longitudinal* the volume increase Δv is best modeled as a resistance increase in a series model. If *swelling is transverse (as supposed in many cases)*, the volume increase Δv is best modeled as a conductance increase in a parallel model. If it is not known whether the tissue swells in longitudinal or transverse direction, the conductance versions may be preferred because they lead to simpler and more exact expressions.

One-Compartment Model. Cylinder Surrounded by Air (cf. Fig. 9.8 top)

In many applications the absolute volume may remain unknown; the emphasis is instead on the *relative* volume change $\Delta v/v$. Also the relative conductance change $\Delta G/G$ is of special interest, because the ratio is related to the signal-to-noise ratio which should be as high as possible. From eq. 9.1:

$$\frac{\Delta G}{G} = \frac{\Delta v}{v} \quad \text{or} \quad \frac{\Delta G}{\Delta v} = \frac{\sigma}{L^2} \quad \text{or} \quad \Delta v = \Delta G \rho L^2 \quad (\text{exact}) \quad (9.2)$$

From the equation to the left it is clear that relative volume changes can be found without knowing the dimensions of the cylinder. In order to have a high

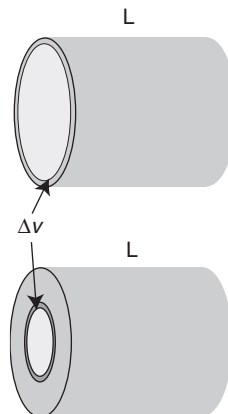


Figure 9.8 Cylinder models of length L and a small parallel volume increment Δv . Upper: one-compartment, lower: two-compartment model.

sensitivity (large ΔG) for a given volume change Δv , the length L should be as short as possible.

Under the presumption that $L = \text{const.}$ the conductance model is preferred. If we still use a resistance model we have from eq. (9.1):

$$\Delta v = \left(\frac{1}{R + \Delta R} - \frac{1}{R} \right) \rho L^2 = -\frac{\Delta R}{R} \frac{1}{R + \Delta R} \rho L^2 \quad (\text{exact}) \quad (9.3)$$

Equation 9.3 becomes linear only if $\Delta R \ll R$:

$$\Delta v \cong -\Delta R \rho \left(\frac{L}{R} \right)^2 \quad (\Delta R \ll R) \quad (9.4)$$

The minus sign in eq. (9.3 and 9.4) is because a resistance *increase* corresponds to a volume *decrease*.

Two-Compartment Model: An Inner Cylinder Surrounded by an Outer Cylinder of Same Resistivity (Fig. 9.8 bottom)

$$\frac{\Delta G}{G} = \frac{\Delta v}{\Delta v + v_A + v_t} \quad (\text{exact}) \quad (9.5)$$

In the two-compartment model the two cylinders are physically in parallel, and the conductance model is preferred with $L = \text{const.}$ $\Delta v + v_A$ is the volume of the inner cylinder, v_t is the volume of the outer cylinder and considered constant (implying that both the inner tube and outer tube swell when $\Delta v > 0$). Equation (9.5) shows that the sensitivity falls with a larger surrounding volume v_t . In plethysmography the measurement should be confined as much as possible to the volume where the volume change occurs. Thus the problem of high sensitivity plethysmography poses the same problem as in electrical impedance tomography (EIT): to selectively measure immittance in a selected volume.

9.2.2 The Effect of Different Conductivities

In the two-compartment, constant length, parallel cylinder model analyzed above the conductivities in the inner and outer cylinders were considered equal. Different conductivities will of course also change G . With a conductivity σ_t of tissue outer cylinder and σ_b of blood in inner cylinder, and with constant geometry, the conductance is found from $G = \sigma A/L$:

$$G = (\sigma_A A_A + \sigma_t A_t) \frac{1}{L} \quad (\text{constant volume}) \quad (9.6)$$

Equation 9.6 is not really a plethysmographic equation when the assumption is that no geometrical change shall occur. However, it relates to flow systems with a varying conductivity of the passing liquid, and flow with time is volume.

9.2.3 Models with Any Geometry and Conductivity Distribution

Figure 9.9 shows a dynamic system in a vessel where, for example, a blood bolus volume on its passage leads to a temporal local volume increase during heart systole. The measured zone in the inner cylinder is filled with blood (inflow phase). Later during the diastole the blood is transported further (outflow phase), but also returned via the venous system. Figure 9.9 shows a tetrapolar electrode system for the measurement of G .

In general a *tetrapolar* system is preferable; it may then be somewhat easier to confine the measured tissue volume to the zone of volume increase. The sensitivity for bolus detection with a tetrapolar electrode system will be dependent on the bolus length with respect to the measured length.

To analyze the situation with a tetrapolar electrode system in contact with, for example, a human body, we must leave our simplified models and turn to lead field theory (Section 6.5). The total measured transfer impedance measured is the ratio of recorded voltage to injected current according to eq. (6.39). The impedance is the sum of the impedance contributions from each small volume dV in the measured volume. In each small volume the resistance contribution is the resistivity multiplied by the vector dot product of the space vectors J'_{reci} (the current density field due to a unit reciprocal current applied to the recording electrodes) and J'_{cc} (the current density field due to a unit current applied to the true current carrying electrodes). With disk-formed surface electrodes the constrictional resistance increase from the proximal zone of the electrodes may reduce sensitivity considerably. A prerequisite for two-electrode methods is therefore large band electrodes with minimal current constriction.

If the system is reciprocal the swapping of the recording and current carrying electrode pairs shall give the same transfer impedance. It is also possible to have the electrode system situated *into the volume* of interest (e.g. as needles or catheters). Such volume calculation (e.g. of CO) is used in some implantable heart pacemaker designs, cf. Section 9.11.

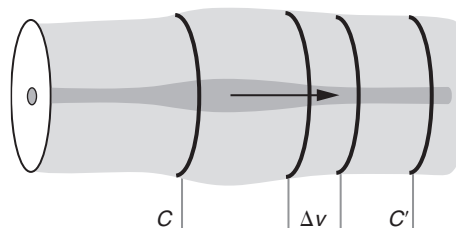


Figure 9.9 Tetrapolar electrode system and the effect of a bolus of blood passing the measured volume.

Changes in Conductivity

Conductivity may change as a function of time (e.g. caused by flow). The special case of a changing conductivity with a general but constant geometry was analyzed by Geselowitz (1971) who developed an expression for ΔZ based on the potential field. Lehr (1972) proposed to use current density instead of potential in the development. Using the nomenclature of our book and putting $\mathbf{E} = -\nabla\Phi$ and as $\mathbf{J} = \sigma\mathbf{E}$ in isotropic media, we have:

$$\Delta Z = \frac{-\Delta\sigma}{\sigma_0^2} \iiint \mathbf{J}'_0 \cdot \mathbf{J}'_{\Delta\sigma} d\nu \quad [\Omega] \quad (9.7)$$

Here the integration is in the volume of conductivity change. The volume is homogeneous but with changing conductance, at a given moment of integration σ is therefore constant and is put outside the integral. \mathbf{J}'_0 is the lead field at $t = 0$ and conductivity σ_0 , $\mathbf{J}'_{\Delta\sigma}$ is the reciprocal lead field dependent on $\Delta\sigma$. The choice of which port is to be current carrying and which is to be potential reading is arbitrary. \mathbf{J}' is current density with unit current excitation [$1/\text{m}^2$]. If $\Delta\sigma$ is positive, ΔZ is negative because of the minus sign in eq. (9.7). If $\Delta\sigma$ is zero, ΔZ is zero, this is not the case for eq. (25.1) in Malmivuo and Plonsey (1995).

Sigman Effect

Sigman et al. (1937) were the first to report that the resistivity of blood is flow dependent. They found that the resistivity fell about 7% when the blood velocity was increased from 10 to 40 cm/s. This is an application area for the Geselowitz (1971) equation, a change in measured conductance not related to volume and therefore not plethysmographic. It is a source of error in volume estimations, but not necessarily in flow estimations.

No Sigman effect is found in plasma or electrolytes (Geddes and Baker, 1989). The Sigman effect is due to the non-spherical bodies in the blood, in particular the erythrocytes. At higher velocities but still linear flow the erythrocytes reorient into the flow direction, and in a tube they also clump together around the central axis. The erythrocyte orientation means less hindrance to electric current flow and lower resistivity if resistance is measured in the axial direction. Kanai et al. (1976) reported that resistivity changes occurred at double the flow pulsation frequency, and that the magnitude became very small $>3\text{Hz}$. This means that the orientation and clumping effects are rather slow.

9.2.4 Rheoencephalography

Rheoencephalography (REG) is a plethysmographic bioimpedance method widely used in countries like Russia and China, but not very well known in the USA and Europe. The ambition is to assess cerebral blood flow, (Geddes and Baker, 1989), however only a little part of the REG signal is caused by changes in brain

conductivity, the rest relates to the pulsating blood flow of the scalp. REGs use has been limited because the reading is so highly contaminated by this scalp component. The anatomical background of REG is not clearly understood, and a multilayer spherical model of the head has been used so that the REG information is split into the extracranial and intracerebral flow signals.

The United States Food and Drug Administration definition states (Anonymous 1, 1997: (a) Identification). A rheoencephalograph is a device used to estimate a patient's cerebral circulation (blood flow in the brain) by electrical impedance methods with direct electrical connections to the scalp or neck area." In other words, the FDA definition includes the word "flow." On the basis of previous data REG is actually a reflection of volume rather than flow (Nyboer, 1960). REG and Cerebral Blood Flow (CBF) correlation have been described earlier (Hadjiev, 1968; Jacquy et al., 1974; Moskalenko, 1980; Jenkner, 1986). However, the correlation of global, local CBF and carotid flow was not investigated. More REG and related references can be found at www.isebi.org/.

REG pulse amplitude change reflects arteriolar, capillary and venular volume changes together rather than absolute brain blood flow. Early CBF-REG studies did not focus on this topic. It was previously described that the involvement of a vessel in CBF autoregulation is size-dependent: larger arteries are less involved than arteriola (Kontos et al., 1978). Consequently, the arteriolar change observed in brain by REG reflects arteriolar function more than it reflects functions in larger arteries (e.g. carotid). The clinical importance of these findings is that REG can be measured more conveniently and continuously in humans than Doppler ultrasound. Therefore, measurement of CBF autoregulation by REG has potential for use as a life sign monitoring modality.

REG is a potential method for cerebrovascular diagnostics as well. In order to reach the potential of widespread application of REG, there is a need for research to clarify the physiological and pathophysiological correlations and adequate data processing.

The physical basis of the REG measurement is based on the fact that blood and cerebrospinal fluid (CSF) are better conductors than the brain or other "dry" tissue. The REG signal reflects the impedance change: during blood inflow into the cranial cavity, electrical conductivity is increased (resistance decreased) represented by increasing REG pulse amplitude. The same electrical impedance change occurs generating pulse wave on peripheral site, as it was first described by Nyboer (1970) in the parallel-column model. In the skull the input is the volume of the arterial pulse, and the output is the venous outflow and the CSF together. The resulting impedance change – REG curve – is the result of the equation – involving all mentioned factors but not detailed individually. The measured electrical impedance value offers the basis of several volume calculations, detailed by Jenkner (1986).

A typical REG change is known to occur as a consequence of arteriosclerosis, expressed as elongation of REG pulse amplitude peak time or decreased slope of anacrotic part (Jenkner, 1986). The possible cause of this alteration is the decreased elasticity of arteriolar wall, which is the most sensitive indicator of disease progression.

Animal studies (Bodo et al., 2004, 2005a,b, 2007) show that REG can be measured more conveniently and continuously in humans than Doppler ultrasound. Therefore, measurement of CBF autoregulation by REG has potential for use as a life sign monitoring modality.

Studies on humans have shown that reproducibility and sensitivity of the bioimpedance measurement – including REG – were comparable to the sensitivities of the pulse oximeter, laser Doppler and Doppler ultrasound. Results demonstrated that bioimpedance offers potential for use as a multifunctional, continuous, non-invasive life sign monitor for both military and civilian purposes (Bodo et al., 2006).

In a comparative population screening study (546 volunteers) REG measurements revealed symptoms of arteriosclerosis in 54% of the subjects; within the identical population the Doppler ultrasound measurements showed 30% with arteriosclerosis (Sipos et al., 1994; Bodo et al., 1995a).

REG may have potential for non-invasive continuous life sign monitoring and detection of early cerebrovascular changes. Since the early days of REG research, advances in the development of electronics, computation and signal processing techniques offer the possibility to reconsider the feasibility of implementing a portable or even wearable version of the REG monitoring technique to evaluate the adequacy of CBF reactivity.

REG is also used in cardiac applications and evaluation of edema in the legs.

In order to fulfill some of the expectations REG must reach a much higher level of standardization of both instrumentation and electrode geometry. The lack of electrode sensitivity analysis of the REG techniques has severely reduced the scientific soundness of the method.

9.3 IMPEDANCE CARDIOGRAPHY

Impedance Cardiography (ICG) is impedance plethysmography based on the measurement of thoracic electrical bioimpedance (TEB). It also includes a component from the resistivity dependence on blood flow (Sigman effect). This is not a plethysmographic but a blood velocity component. Usually a measuring frequency of 50–100 kHz has been used. A TEB picks up both cardiac and respiration signals. The ambition is that the SV (L) and therefore CO (L/min) can be calculated with ICG, as well as the total thoracic fluid volume, for example, according to eq. (9.1)

Nyboer (1950) used two band electrodes around the neck, one band electrode corresponding to the apex of the heart and a fourth further in caudal direction. Nyboer regarded the thorax as a cylinder volume of length L and used the expression:

$$\Delta v = \Delta Z \rho \left(\frac{L}{Z_0} \right)^2 [\text{m}^3] \quad (\text{Nyboer}) \quad (9.8)$$

which is in accordance with eq. (9.4). The ICG tradition has since then been to use impedance Z instead of resistance R , and to use the series model. Equation 9.8 is

surely valid as the condition $\Delta Z \ll Z_0$ is fulfilled in ICG, but the $\Delta Z/Z_0^2$ term is not so directly evident as the simple ΔG term in eq. (9.2). Also an increased volume corresponds to a conductance increase, but to an impedance decrease. Therefore a minus sign is often introduced as in eq. (9.4) (Geddes and Baker, 1989). Typically values for Z_0 is $25\ \Omega$ and ΔZ $0.2\ \Omega$. The Z waveform is similar to the aorta blood pressure curve.

SV as developed by Kubicek et al. (1966) is still compatible with a basic physical model:

$$SV = \left(\frac{dZ}{dt} \right)_{\max} T \rho \left(\frac{L}{Z_0} \right)^2 [\text{m}^2] \quad (\text{Kubicek}) \quad (9.9)$$

The *first time derivative* dZ/dt is called the impedance cardiographic curve (ICG). T is the ventricular ejection time. As the pick-up electrodes are positioned near the heart they also pick-up the ECG signal, and this is used for the time estimation.

In the original Nyboer model the changes in conductance was associated with cylinders of different and changing cross sectional areas. The blood distribution process is of course much more complicated. With chest electrodes we have signals from the filling and emptying of the heart, aorta, lungs, muscles of the chest; as well as the Sigman effect.

Many electrode geometries have been used, in particular the old four-band technique and the newer spot electrode technique with four or eight or more electrodes. Some systems use two current carrying systems with four excitation and four recording electrodes, eight electrodes in total. Then four electrodes are connected around the neck, the others on the lower thorax. With two current sources the sensitivity field is complicated, and many algorithms are possible when weighing the results obtained in the two channels. Kauppinen et al. (1998) compared four different electrode systems using either band or spot electrodes. They used a 3D computer model with data from the US Library of Medicines Visible Human Project. They found that more than 55% of the measured transfer impedance was due to the skeletal muscle mass in the thorax and only about 15% originated from blood, heart and lungs. The sensitivity field for the four tested systems showed only small differences in total sensitivity, but all the same each was a complicated mixture of many factors.

Sramek (1981) and Bernstein (1986) further developed empirical equations also with biometrical data such as patient height, actual weight, ideal weight, body surface area, age and gender. Other transthoracic equations have also appeared (reviewed by Moshkovitz et al., 2004), partly with proprietary modifications making methods more accurate but perhaps less robust in the case of for instance critically ill patients or validity before and after surgery. Bernstein and Osypka (2003), and Bernstein and Lemmens (2005) introduced an index of transthoracic aberrant conduction (e.g. by excess extra-vascular lung water) in their equation. Suttner et al. (2006) tried it on critically ill patients with acceptable results.

Since ICG is a very simple and low cost technique very valuable applications may appear. It must also be remembered that a golden standard method for SV and CO does not exist; the intramethod variability may be larger than the inter-method variability. Reference methods have been thermodilution, dye dilution, oxygen Fick technique, radionuclear radiography and transoesophageal Doppler echocardiography.

9.4 TISSUE CHARACTERIZATION IN UROLOGY

Bioimpedance techniques are interesting candidates for diagnosing disorders in the urinary system. There are many possible applications, ranging from measurements of uterine tone and contractility to assessment of prelabor ripening and detection of cervical cancer. Some examples are as follows.

Mudraya et al. (2007) used different instruments such as a multichannel impedance spectrometer for tetrapolar measurements on an array of nine electrodes, enabling simultaneous recording of six locations along the urinary tract. They found such measurements to be valuable for quantitative assessment of ureteric peristalsis, and they could also locate stricture regions by monitoring the ratio between low and high frequency impedance, Z_{low}/Z_{high} .

Abdul et al. (2005) developed a tetrapolar probe for impedance measurements in the frequency range 2–1200 kHz. They found their system to give similar sensitivity and specificity to currently used screening tests for cervical intraepithelial neoplasia, but with the evident advantage of providing instant results.

Gandhi et al. (2006) measured cervical stromal impedance (CSI) in non-pregnant women and women in different stages of pregnancy. They found the impedance to increase during pregnancy and their results suggest potential utility of CSI measurement for quantifying gestation-dependent changes in cervical stromal tissue.

9.5 EEG, ENG/ERG/EOG

The electrical activity of 10^{11} brain cells are recorded on the skin of the skull with a standardized electrode network of 21 electrodes. The leads may be bipolar or unipolar. The signal amplitude is only of the order of 50 μ V, and the frequency content 1–50 Hz, so DC voltages are filtered out. The low frequency content is a clear sign that the skull has a detrimental effect on the signal transmission. Even so the number of electrodes indicate that the information content is sufficient to roughly localize a source. It is believed that the brain centers are less synchronized the higher the activity, resulting in smaller amplitude and more high frequency content of the EEG. At sleep the waves are with largest amplitude and lowest frequency content. The electrodes used are rather small, often made of tin/lead with collodium as contact/fixation medium.

The brain can be stimulated (e.g. by a sound or by looking at changing patterns). The EEG signal can be time averaged based on synchronization pulses from

the stimulator. Electrical activity and the brain electric response can by this method be extracted from noise. In this way hearing sense of small children and babies can be examined.

Electrocorticography with electrodes placed directly on the cortex during surgery permits direct recording of high amplitude, high frequency EEG.

EOG (electro-oculography) is an electrophysiological method where DC potentials are utilized, and therefore AgCl-electrodes are used. The DC potential is dependent on the position of the eye, and is of particular interest, for example, when the eye lids are closed (REM sleep). As a DC recording method EOG tends to be prone to drift which makes the spatial localization of the point of gaze problematic. It is also sensitive to facial muscle activity and electrical interference. The signals are due to a potential between the cornea and the fundus of an eye with a functioning retina, and are not from the ocular muscles (Geddes and Baker, 1989).

ENG (electro-nystagmography) is also the recording of corneo-retinal potentials, usually used to confirm the presence of nystagmus (special eye movements). The electrodes are placed to the side (lateral), above and below each eye. A reference electrode is attached to the forehead. A special caloric stimulation test is performed, with cold and/or hot water brought into the canal of one ear. The electrodes record the duration and velocity of eye movements that occur when the ear is temperature stimulated.

ERG (electro-retinography) records the AC potentials from the retina. The electrode system is unipolar, with a gold foil or AgCl recording electrode embedded in a special saline filled contact lens in contact with the cornea. The eye may be considered as a fluid-filled sphere in contact with the retina as a thin, sheet-like bioelectric source. The ERG signal caused by a light flash is a very rapid wave with an initial rise time less than 0.1 ms (early receptor potential) and an amplitude around 1 mV, followed by a late receptor potential lasting many milliseconds.

9.6 ELECTROGASTROGRAPHY

The typical electrogastrographical (EGG) signal due to stomach activity is recorded with a bipolar lead using a pair of standard ECG electrodes on the skin (e.g. 4 cm apart). The signal is typically of about 100 μ V amplitude, and periodic with a period of about 20 seconds (0.05 Hz fundamental). Best position for the EGG electrodes is along the projection of the stomach axis on the abdomen.

Internal electrodes are also used, but are in general not considered to provide more information than external EGG signals. Of course the internal electrodes are nearer to the source, implying higher amplitude signals with more high frequency content. Because of the very low frequency spectrum, external noise from, for example, slowly varying skin potentials tends to be greater problem than with internal recordings.

9.7 EMG AND NEUROGRAPHY

EMG

To record signals from muscles (EMG), both skin surface electrodes and invasive needles are used. The distance to the muscle is often short, and the muscle group large, so signals have high amplitude and high frequency content. But the signal is usually coming from many muscle groups, and the signal looks rather chaotic. The muscle activity is related to the rms value of the signal. If the muscle activity is low and controlled, single motor units become discernible with needle electrodes. EMG is often recorded in connection with active neurostimulation, involving both the muscle and the nervous system.

The frequency EMG spectrum covers 50–5000 Hz, and the amplitude may be several millivolt with skin surface electrodes.

ENeG

The sum of activities forming a nerve bundle may be picked up by skin surface electrodes (e.g. on the arm where the distance from the electrodes are not too many millimeters). Action potentials from single nerve fibers must be *measured* with invasive needle electrodes. They may be bipolar or unipolar (Section 7.4.7). To find the right position, the signal is monitored during insertion, often by sounds in a loudspeaker.

Stimulation may be done with the same electrode designs: either transcutaneously right above the bundle of interest, or by needles. Muscles (e.g. in the hand) are stimulated by stimulating efferent nerves in the arm. EMG electrodes can pick-up the result of this stimulation, for instance for nerve velocity determination. It can also be picked up by neurographic electrodes, but the signal is much smaller and must therefore be averaged with multiple stimuli. However, the method is more of interest because there is more information in the response waveform.

9.8 ELECTRICAL IMPEDANCE MYOGRAPHY

Electrical impedance myography (EIM) refers to a group of impedance-based methods for the clinical assessment of muscles. This includes primary disorders of muscle such as myopathic conditions (Rutkove et al., 2002; Tarulli et al., 2005) and the sarcopenia of aging (Aaron et al., 2006) as well as diseases that affect the nerve, such as localized neuropathies or nerve root injuries (Rutkove et al., 2005) and generalized problems, such as amyotrophic lateral sclerosis (Esper et al., 2005). This neuromuscular disease-focused application of bioimpedance is built on the earlier experimental and theoretical work of Shiffman and Aaron (see Aaron et al., 1997; Shiffman et al., 1999; Aaron and Shiffman, 2000). Importantly, the goal of EIM is not to image the muscle, but rather to assess quantitatively changes in its microscopic structure induced by neuromuscular disease states.

All methods utilize a tetrapolar technique and rely on the placement of voltage sensing electrodes along a muscle or muscle group of interest. Depending on the

application, current-injecting electrodes can be placed in close proximity to or at a distance from the voltage electrode array. Both single frequency (50 kHz) and multifrequency (up to 2 MHz) methods have been studied with the former showing very high reproducibility of the major outcome variable, the spatially averaged phase θ_{avg} (Rutkove et al., 2006). The application of EIM in the setting of voluntary or stimulated muscle contraction represents another provocative and potentially important area of investigation that may allow assessment of the contractile apparatus (Shiffman et al., 2003).

Some limited animal work has also been performed. Nie et al. (2006) showed that consistent measurements could be obtained on the hamstring muscles of the rat and that substantial changes occur after experimental sciatic crush, including reductions in the measured phase and loss of the normal frequency dependence. Future animal work will be geared at disease differentiation and determining the relationship between muscle states and their impedance patterns.

The most straightforward application of the technique of EIM for clinical care is for its use as a quantifiable measure of muscle health, such that treatment or rehabilitation programs can be effectively monitored. Indeed, EIM has the potential to serve as a useful new outcome measure in clinical trials work (Tarulli et al., 2005) and studies are ongoing to verify the role of EIM as an outcome measure in amyotrophic lateral sclerosis, spinal muscular atrophy and exercise interventions in aging. It is uncertain whether the technique has the potential of supplanting standard neuromuscular diagnostic methods, most notably needle EMG, and this remains a subject of ongoing research.

9.9 ELECTROTHERAPY

Transcutaneous Stimulation

TENS (transcutaneous electrical nerve stimulation): is electrical stimulation through surface electrodes. The advantage of not using syringe injections is obvious, the electrical pulses stimulate the body's own mechanisms for obtaining pain relief. There are three theories as to how the pain relief is achieved.

Gating Theory

Pain perception is controlled by a gate mechanism in the synapses, particularly in central nervous system (CNS) of the spine. This gate is controlled by separate nerve fibers, and by stimulating with pulses of high frequency (50–200 Hz), these fibers are stimulated and pain relief is obtained.

Endorphines

The body uses natural forms of morphine called endorphines for pain relief. The secretion of endorphines is obtained with low frequency (2–4 Hz) stimulation. These low frequencies correspond to the rhythmic movement of an *acupuncture*

needle (in classical acupuncture it is also necessary to stimulate motor nerve fibers). The effect of endorphines is probably in the higher centers of the CNS.

Vasodilation

This effect is usually linked to pain in cold extremities. Increased blood flow may increase the temperature from the range 22–24°C to 31–34°C, also in the extremities not stimulated. The effect must therefore be elicited in higher centers of the CNS.

The afferent pain nerves have a higher threshold and rheobase than sensory and motor nerves. Thus it is possible to stimulate sensory and motor nerves without eliciting pain. Very short pulses of duration 10–400 μ s are used, with a constant amplitude current up to about 50 mA and a treatment duration of 15 minutes or more. The skin electrodes may be bipolar or monopolar. The position is in the pain region, an electrode pair may, for example, be positioned on the skin on the back of the patient, or implanted with thin leads out through the skin. The electrode pair may also be positioned outside the pain area (e.g. at regions of high afferent nerve fiber densities in the hand).

Electroacupuncture

The secretion of endorphines is obtained with low frequency (2–4 Hz) stimulation, corresponding to the rhythmic movement of an *acupuncture* needle. Instead of, or in addition to the mechanical movement, the needle is used as monopolar electrode, pulsed by a low frequency in the same frequency range (1–4 Hz). This is not a TENS method strictly speaking, as the electrode is invasive and the current not transcutaneous.

9.9.1 Electrotherapy with DC

Applied DC through tissue for *long* duration (e.g. >10 seconds) is a method almost 200-years old, and is traditionally called *galvanization*. Today the DC effect is often ignored, even if it is quite clear that DC through tissue has some very special effects. Generally the physical/chemical effect of a DC through tissue is:

- electrolysis (local depletion or accumulation of ions)
- electrophoresis (e.g. protein and cell migration)
- iontophoresis (ion migration)
- electro-osmosis (volume transport)
- temperature rise.

Some of these effects are special for long duration (>10 seconds) DC or very low frequency AC, in particular electrolysis. Other effects are in common with AC.

Short term effects of DC through the skin is limited to the sweat ducts. The current density is much smaller in the stratum corneum, but long term currents may have an effect. Proximal to the electrode electrolytic effects influences the skin. Possible effects in deeper layers are erythema (skin reddening) and hyperemia (increased blood perfusion) due to the stimulation of vasomotor nerves. If the DC

is applied transcutaneously, there is always a chance of unpleasant pricking, reddening and wound formation in the skin under the electrode.

Iontophoresis

Iontophoresis in the skin (cf. also Section 9.15). If a drug is in ionic form, the migration velocity and direction are determined by the polarity of the DC. It is a very famous experiment whereby strychnine was applied to one of the electrodes attached to a rabbit. With one polarity the rabbit died, with the reverse polarity nothing happened. The ions may be transported from the electrode, and thus have an effect both in the tissue during passage, and when assembled under the other electrode. Anesthetic agents may be introduced in the skin by iontophoresis, for minor surgery or the treatment of chronic pain. Also antibiotics and metallic silver has been introduced iontophoretically, as well as zinc for ischemic ulcers. The mechanism of iontophoresis is of course accompanied by a possible electrophoretic action (see below), but is not necessarily so pH-dependent as the latter. The advantage of iontophoretic instead of local syringe injection is not always obvious.

Electrotonus

Tonus is the natural and continuous slight contraction of a muscle. Electrotonus is the altered electrical state of nerve or muscle cells due to the passage of a DC. Subthreshold DC currents through nerves and muscles may do the tissue more (excitatory effect), or less (inhibitory effect) excitable. Making the outer nerve cell membrane less positive lowers the threshold and has an excitatory effect (at the cathode, *catelectrotonus*), the anode will have a certain inhibitory effect (*anelectrotonus*). This is used in muscle therapy with diadynamic currents, see below.

Wound Healing

Many controlled studies have shown that a small microampere current as a long term treatment leads to accelerated healing. There are two classes of cases: accelerated healing of bone fractures, and of skin surface wounds. Ischemic dermal ulcers are treated with DC, and the healing rate is approximately doubled. It has been found that a monopolar cathodic application during the first days followed by an anodic application, gives the best results. In a skin wound it is believed that positive charge carriers (ions and proteins) are transported to the liquid wound zone by endogenic migration.

An increased rate of bone formation has also been found when small currents are applied to each side of a bone fracture (bipolar electrode system). This is of particular interest in cases of bone fractures that will not grow the natural way: so-called *non-union*). Nordenstrøm (1983) described the use of DC treatment by applied needles into tumors for the treatment of cancer.

DC Ablation

At higher current densities the acid under the anode leads to coagulation, and the alkali under the cathode to liquidification, of the tissue. Warts can thus be treated,

and with a needle cathode in the hair follicle, the local epidermis is destroyed and the hair removed.

DC Shock Pulses

DC shock pulses have also been used for destroying calculi in the urinary tract, *electrolithotripsy*.

Hydrogen Production

The application of a DC current to the inside of the eyeball by a needle electrode is used to produce bubbles of hydrogen in the aqueous humor, *electroparacentesis*.

9.9.2 Electrotherapy of Muscles

Electrotherapy is a broad term, and should for instance include pacing, defibrillation and electroconvulsion. Here we will keep to the traditional meaning, however, which is more limited to methods stimulating *muscles*, either directly or via the nerves. Usually such stimulation also bring data of diagnostic value.

Figure 9.10 shows the minimum stimulus current to an efferent nerve fiber as a function of pulse duration for obtaining a certain muscle response (cf. Section 5.4.8). The coupling (synapses) between the nerve axon end plates and the muscle cells is an important part of this signal transmission line. It is not possible to lower the current under a certain minimum level, the *rheobase* value. The pulse length with current amplitude $2 \times$ rheobase value is called the *chronaxie*.

Pflüger's law relates the muscle effect to the leading or trailing edge of the pulse, and to anodal or cathodal polarity:

Leading edge cathodal	Strongest effect
Leading edge anodal	↓
Trailing edge anodal	↓
Trailing edge cathodal	Weakest effect

If a linear triangular current pulse is used instead of a square wave pulse, an *accommodation* effect will appear, particularly at pulse duration >1 ms. A slowly increasing DC does not excite a nerve to the same extent as a DC step change, and the accommodation implies that the threshold current amplitude will be larger with triangular than with squared waveform. The current-time curves can be recorded for diagnostic purposes, the curves are quite different for degenerated muscles.

The pulses may be of unidirectional current (interrupted DC, *monophasic*), which implies that the current has a DC component. High voltage pulsed galvanic stimulation is also used, with pulse currents up to some amperes, but pulse duration only a few microseconds. If DC effects are to be avoided (e.g. to reduce electrolytic effects or electrode metal corrosion), the current is *biphasic*. *Faradic* currents are biphasic currents of the type generated by an induction coil. If the pulses are slowly increased in amplitude, then reduced, and after a pause again increased, we have a

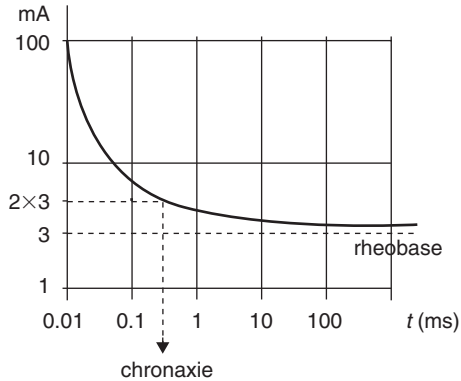


Figure 9.10 Minimum stimulus current to an efferent nerve fiber bundle for obtaining a certain muscle response, as a function of pulse duration.

ramp or *surged* current. As many effects are current controlled, it is often better to use a constant amplitude current mode than a constant amplitude voltage mode of the stimulator output.

Pulse Waveform Treatment of Innervated Muscles (Faradization)

Short (0.5–5 ms) triangular pulses for tetanic muscular contractions, interrupted or with varying amplitude. Interval between pulses 10–25 ms. For muscle pain relief rectangular pulses of length 2 ms and interval 7 ms are used. Transcutaneous nerve stimulation (TENS) for pain relief is different. It is based on stimulating afferent nerve fibers with much shorter pulses (e.g. 0.2 ms).

Pulse Waveform Treatment of Denervated Muscles

As there are no innervation, the stimulation is directly to the muscle. The paralyzed part of the muscle mass can be stimulated selectively, because such muscles has a smaller accommodation at long pulse duration. Very long (1 second) triangular waveforms are used, with even longer intervals between the pulses.

Diadynamic Currents for the Treatment of Pain and Increase of Blood Perfusion.

This is the summation of two currents: a pulse current superimposed on a DC. Each current is separately adjusted. Often the DC level is first increased slowly so that no perception occurs (*electrotonus*), and then with a constant DC flowing the pulse amplitude is increased until a weak vibration is felt. The pulse waveform may be a power line 50 Hz half-rectified (50) or fully rectified (100 Hz) current.

Interferential Currents

Two-electrode pairs are used to set up two different current paths crossing each other in the target tissue volume. Each pair is supplied by a separate oscillator, adjusted to, for example, 5000 and 5100 Hz. The idea is that the target volume is treated with the frequency difference, 100 Hz. The advantage is the possible selective choice of a limited treated volume deep in the tissue, together with lower electrode polarization and skin impedance, plus less sensation in the skin and the tissue outside the treated volume.

If the current level is low enough for linear conditions, the resultant current density in the tissue is the linear summation of the two current densities (cf. Chapter 7.2.2). According to the superposition theorem in network theory and Fourier analysis, the new waveform $f(t)$ does not contain any new frequencies. The linear summation of two currents at two different frequencies remains a current with a frequency spectrum with just the two frequencies, no current at any new frequency is created.

The current density in the treated volume must be high enough to create non-linear effects. The process can then be described mathematically by a multiplication (cf. Chapter 7.2.2). If $\omega_1 \approx \omega_2 \approx \omega$, $f(t)$ is a signal of double frequency and half the amplitude, together with a signal of the low beat frequency $\omega_1 - \omega_2$, also of half the amplitude. The double frequency signal is not of interest, but the low beat frequency $\omega_1 - \omega_2$ is now present in the tissue.

A third electrode pair can be added, with additional flexibility of frequency and amplitude selection. Anyhow it must be taken into account that muscle impedance may be strongly anisotropic, with a possible 1:10 ratio between two directions.

9.10 BODY COMPOSITION ANALYSIS

The parameters of interest in body composition analysis (bioelectric impedance analysis BIA) are total body water (TBW), extracellular/intracellular fluid balance, muscle mass and fat mass. Application areas are as diversified as sports medicine, nutritional assessment and fluid balance in renal dialysis and transplantation.

One of the first to introduce BIA was Thomasset (1965), using a two-electrode method and 1 kHz signal frequency. With just two electrodes it is important to use large area band electrodes in order to reduce the contribution from the current constrictional zones near the electrodes. With a tetrapolar electrode system it is easier to select the preferred volume to be measured. The small circumference of the lower arm, wrist and fingers causes those body segments to dominate measured impedance in a so-called whole body measurement (cf. Fig. 4.26). With measuring electrodes, for example, on one hand and one foot the chest contribution is very small. The impedance of the chest segment is therefore the most difficult one to determine accurately, both because it is much lower than the impedance of the limbs and because it varies with respiration and heartbeats, as exploited in ICG (Section 9.3). Thoracic measurements were compared with whole body measurements by Nescolarde et al. (2006).

By using more than four electrodes it is possible to measure more than one body segment. One method uses eight electrodes, two electrodes at each hand and foot. The body impedance is then modelled in five segments: arms, legs and chest (Fig. 9.11). One segment impedance is determined by letting two limbs be current carrying and use a third limb for zero current potential reading (five electrode lead, pentapolar). The leads are then varied in succession. The system will be highly sensitive for the detection of asymmetrical limb bioimpedance. Standardization of the type of electrodes used and their placement is a major concern (Kyle et al., 2004). Cornish et al. (1999) provided a set of standard electrode sites for bioimpedance measurements.

Calibration is also a major concern in BIA. Calibration can be done with more accurate but cumbersome methods such as using deuterium, underwater weighing or dual energy X-ray absorption. However, dilution methods have their own errors ($>2L$ for TBW) and yield different results (e.g. 4% difference between the deuterium-TBW method and the ^{18}O -TBW method). Although body impedance reflects tissue hydration, soft tissue mass (lean and fat) can also be empirically derived by correlation in healthy subjects because the *compartments of soft tissue are correlated with each other through physiological constants*. However, physiological constants become flawed in patients with fluid disorders, which accounts for most conflicting results in the literature (Kyle et al., 2004).

Body *position* is important because it influences the distribution both of blood and the fluids in the stomach/intestine tissue. Direct body segment to body segment skin contact must be avoided in order to obtain stable readings. The feet should therefore be kept at a distance from each other, and the arms should be held out from the chest. Scharfetter et al. (1998) also analyzed the artefacts produced by stray capacitance during whole body or segmental Bioimpedance Spectroscopy (BIS), and proposed a model for simulating the influence of stray capacitance on the measured data.

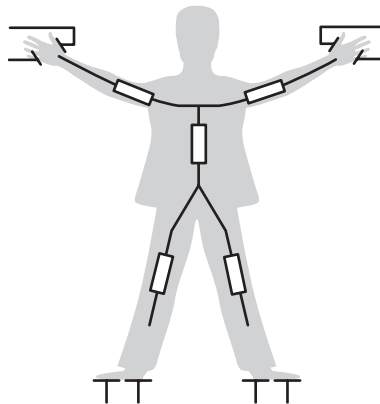


Figure 9.11 Human body divided into five impedance segments, octopolar electrodes.

BIA as a tool for assessment of the hydration of soft tissue may be divided along *three methods of body fluid volume assessment*.

The first and the most validated method is prediction of TBW from whole body impedance measurements at a single frequency, often 50kHz. Either the series impedance electrical model (often with the reactance component X neglected), or the parallel equivalent have been used. Several indexes have been introduced in order to increase the accuracy. Gender, age and anthropometric results such as total body weight and height are parameters used. An often used index is H^2/R_{segm} , where H is the body height and R_{segm} the resistance of a given segment. Because of the $1/R_{\text{segm}}$ term this is therefore actually a *conductance* index. Calibration can be done by determining the k -constants in the following equations:

$$TBW = k_1 \frac{H^2}{R_{\text{segm}}} + k_2 \quad (9.10)$$

$$TBW = k_1 \frac{H^2}{R_{\text{segm}}} + k_2 W + k_3 \quad (9.11)$$

Such equations are not directly derived from biophysical laws, but have been empirically selected because they give the best correlation. The correlation according to eq. (9.10) can be better than 0.95, and it can be slightly improved by also taking into account the body weight W , eq. (9.11). Hundreds of validation studies with isotope dilution have established a solid relation between whole-body impedance at 50 kHz and body fluid volume (Kyle et al., 2004). Complex impedance data can be given also as modulus and phase. Phase has been used as an index of *nutrition*. This is true only in comparison between vectors with the same modulus. For instance, short vectors with a small phase angle are associated with edema whereas long vectors with an increased phase angle indicate dehydration. *Fat free mass* is predicted either from TBW ($TBW/0.73$) or through specific regression equations including the same variables as TBW, with different partial regression coefficients (Sun et al., 2003; Kyle et al., 2004). Fat mass is calculated by difference. The prediction error of best equations while suitable for epidemiological studies is too high for the clinical use (standard error of the estimate in the order of 3–4L for TBW and 3–4kg for the fat free mass) (Sun et al., 2003).

The second method is the use of BIS following the Cole model approach (many groups call it a Cole–Cole model but that is a permittivity model), early used by Cornish et al. (1993). R values are extrapolated at extreme limit frequencies (0 and infinity) for prediction of TBW and extracellular water (ECW) respectively, and by difference intracellular water (ICW). *Body cell mass* is then predicted as a function of the ICW (De Lorenzo et al., 1997). The results of Lozano et al. (1995) showed that there is a sharp disequilibrium between the intracellular and extracellular compartments in the very first dialysis period and they stressed the importance of

continuously monitoring segmental impedance during dialysis. BIS may be accurate with suspended cells, but unfortunately it is impossible to estimate the extracellular electric volume of tissues because of anisotropy and limited low frequency data. It is common practice not to measure below 1 kHz, and low frequency dispersions are therefore neglected. The measuring current is usually around 0.5 mA, higher current levels are difficult to use because the threshold of perception is reached at the lowest frequencies (cf. Section 9.17).

The third method is the prediction of ECW and TBW with low (1–5 kHz) and high (100–500 kHz) frequency impedance data (dual- or multifrequency BIA), with the ICW calculated by difference. Volume calibration is obtained with regression equations as in single-frequency BIA. Like BIS, multifrequency BIA relies on the wrong assumption of tissue isotropy with low frequency current only flowing around cells. If the hydration of the fat free mass is not fixed at 73% (e.g. in hemodialysis, in patients with edema or heart failure) or when body weight is meaningless for body compartments (e.g. in ascites, pregnancy and severe obesity); then BIA, multifrequency BIA and BIS prediction equations should not be used.

A more recent method is to use the complex impedance vector at 50 kHz in a probabilistic Wessel diagram. Such vector BIA (or BIVA) is based upon patterns of the impedance vector relating body impedance to body *hydration* (Piccoli et al., 1994). BIVA is a single frequency BIA that follows a black-box approach considering Z as a random output of a stochastic system (current flow through anisotropic tissues). The method consistently applies to whole body or segmental measurements normalized by the conductor length (height (H) for whole body, body segment length for segmental). BIVA only needs to take care of the measurement error (in the order of 3% at 50 kHz) and of the biological variability of subjects in any clinical condition. The intersubject variability of Z is represented with the bivariate normal distribution (i.e. with elliptical probability regions in the Wessel plane) which are confidence (95%) and tolerance ellipses (50%, 75%, 95%) for mean and individual vectors respectively (cf. Fig. 9.12). The intersubject variability of the impedance vector is represented with the bivariate normal distribution (i.e. with elliptical sex-specific probability regions (50%, 75%, and 95% tolerance ellipses) in the Wessel plane. Vector components are normalized by the subject's height (R/H , and X/H , in Ohm/m). Upper and lower poles of the 75% tolerance ellipses represent bioelectrical thresholds for dehydration and fluid overload, respectively. Vector components can also be transformed into dimensionless z-scores which allow comparisons of vector position between different analyzers (Piccoli et al., 2002). Clinical information on hydration is obtained through patterns of vector distribution with respect to the healthy population of the same race, sex, and class of BMI (body mass index) and age (cf. Fig. 9.12). From clinical validation studies in adults, vectors falling out of the 75% tolerance ellipse indicate abnormal tissue impedance. Vector position is interpreted and ranked following two directions in the Wessel plane, as depicted in Fig. 9.12. The basic pattern has been recently validated with deuterium dilution (Lukaski et al., 2007).

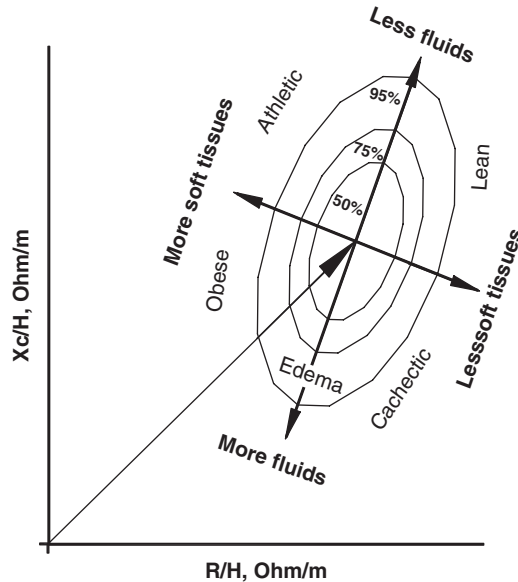


Figure 9.12 Z probability graph. Vector position and migration in the Wessel plane are interpreted and ranked according to directions: (a) Vector displacement parallel to the major axis of an ellipse is associated with a progressive change in soft tissue hydration (short term changes: hours, days). (b) A vector lying on the left or right side of the major axis of an ellipse is associated with more or less cell mass respectively (long term changes: weeks, months).

9.11 IMPLANTED ACTIVE THORACIC DEVICES

Bioimpedance is especially attractive as a potentially useful transducing mechanism in implantable devices such as pacemakers (including pacemakers with cardiac resynchronization therapy (CRT) and internal cardioverter defibrillators (ICD's)) for several reasons: First, the device circuitry and electrode vector configurations to perform such measurements is relatively simple and already exists in many of the current implantable devices and lead configurations. However, sampling resolution is limited in many of these circuits preventing sufficient data for detecting changes in cardiac impedance waveforms. Therefore, low resolution impedance measurements that provide information on fluid status or respiratory impedance trends as a function of time (day(s)/month(s)) are currently employed. Improved circuit designs planned for future generation devices will be ideally suited for implantable impedance applications where high resolution, real-time complex impedance waveform data is required. Second, impedance may be able to provide useful diagnostic information about multiple physiological parameters including heart rate, CO, respiratory rate, minute

ventilation, thoracic fluid accumulation, myocardial contractility and ischemia detection. Third, impedance is a well established sensing means that may provide relevant clinical diagnostic information used independently or in conjunction with other sensors such as pressure transducers or accelerometers.

9.11.1 Physiological Impedance Components

Impedance signals are acquired from selected implantable electrode vector configurations, defined in this context as the electric field generated by the injection current field electrodes and the voltage measured by the sense field electrodes. Signals acquired from each electrode vector configuration can be either bipolar where the injection current electrodes and sense field electrodes are the same, or tetrapolar, where the injection current electrodes and sense field electrodes are isolated from each other. Electrodes in implantable pacing devices consist of unipolar or bipolar electrodes positioned on the distal end of conventional pacing leads. Pacing and ICD leads can be implanted in the right atrium, right ventricle, superior vena cava and left ventricular cardiac vein.

Data acquired from the various possible electrode vectors typically contain three major physiological components that may provide useful information for diagnostics or implantable device control:

- A low frequency respiratory component (fundamental <1 Hz).
- A higher frequency cardiac component; (fundamental = 1–3 Hz).
- A calculated mean impedance (0 Hz).

As shown in Fig.9.13, the higher frequency cardiac component is superimposed on the low frequency respiratory component. The higher frequency cardiac component represents the impedance change during each cardiac cycle that occurs immediately following the QRS deflection on the electrocardiogram. The low frequency respiratory component represents the impedance change during respiration, due to the expansion of the lungs and thorax. Moreover, each component has a different fundamental frequency, typically 1.0–3.0 Hz for cardiac activity and 0.1–1.0 Hz for respiratory activity (Hettrick and Zielinski, 2006). This frequency differentiation allows extraction of each signal by specific filtering techniques. Mean impedance, is represented by a “DC shift” in impedance, changing according to the amount of static conductive fluid in the electrode vector lead field configuration as a function of time (hours/days).

More specifically, change in impedance waveform morphologies may be an indicator of change in blood volume, interstitial volume or tissue integrity. Deviations in the impedance waveform morphologies such as in the positive or negative slope, time duration between minimum and maximum magnitudes, delta between the minimum and maximum magnitudes, changes in the minimum and maximum first derivative, changes in the area under a specific waveform or other deviations in the waveform morphology of complex impedance may be indicative of a vector

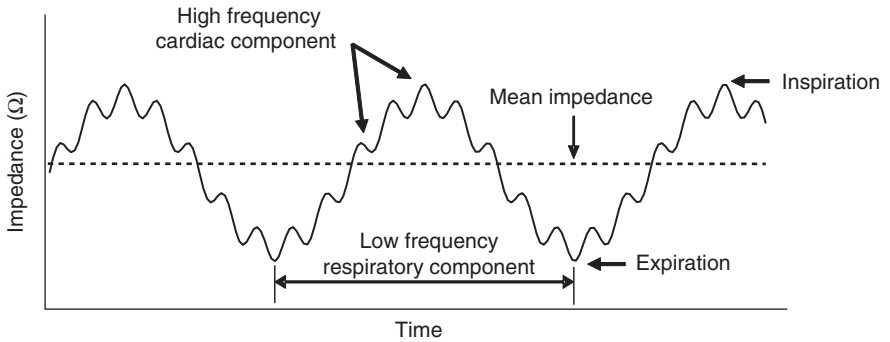


Figure 9.13 Simulated impedance waveform consisting of a higher frequency cardiac component superimposed on a low frequency respiratory component: The dotted line is the calculated mean impedance (measured during two respiratory cycles). An implantable impedance sensor may be able to leverage all three signal components in order to provide useful diagnostic or device control information.

specific change in chamber or vessel blood volume, such as in heart disease, tissue degradation, such as in myocardial ischemia, or interstitial fluid accumulation, such as in peripheral or pulmonary edema, all secondary to cardiac, vascular or renal disease.

9.11.2 Fluid Status Monitoring

Externally measured transthoracic impedance techniques have been shown to reflect alterations in intrathoracic fluid and pulmonary edema in both acute animal and human studies (Fein et al., 1979). The electrical conductivity and the value for transthoracic impedance are determined at any point in time by relative amounts of air and fluid within the thoracic cavity (Gotshall and Davrath, 1999). Additional studies have suggested that transthoracic impedance techniques provide an index of fluid volume in the thorax (Pomerantz et al., 1969; Ebert et al., 1986). Wang et al. (2005) employed a pacing-induced heart failure model to demonstrate that measurement of chronic impedance using an implantable device effectively revealed changes in left ventricular end-diastolic pressure, in dogs with pacing-induced cardiomyopathy. Several factors were identified that may influence intrathoracic impedance with an implantable system. These include: (1) fluid accumulation in the lungs due to pulmonary vascular congestion, pulmonary interstitial congestion and pulmonary edema; (2) as heart failure worsens, heart chamber dilation and venous congestion occur and pleural effusion may develop; (3) after implant, the tissues near the pacemaker pocket swell and surgical trauma can cause fluid buildup (Wang et al., 2005).

Yu et al. (2005) also showed that sudden changes in thoracic impedance predicted imminent hospitalization in 33 patients with severe congestive heart failure

(NYHA Class III–IV). During a mean follow-up of 20.7 ± 8.4 months, 10 patients had a total of 25 hospitalizations for worsening heart failure. Measured impedance gradually decreased before admission by an average of $12.3 \pm 5.3\%$ ($p < 0.001$) over a mean duration of 18.3 ± 10.1 days. The decline in impedance also preceded the symptom onset by a mean lead-time of 15.3 ± 10.6 days ($p < 0.001$). During hospitalization, impedance was inversely correlated with pulmonary wedge pressure (PWP) and volume status with $r = -0.61$ ($p < 0.001$) and $r = -0.70$ ($p < 0.001$), respectively. Automated detection of impedance decreases was 76.9% sensitive in detecting hospitalization for fluid overload with 1.5 false-positive (threshold crossing without hospitalization) detections per patient-year of follow-up. Thus, intrathoracic impedance from the implanted device correlated well with PWP and fluid status, and may predict imminent hospitalization with good sensitivity and low false alarm rate in patients with severe heart failure (Fig. 9.14). Fig. 9.14a shows operation of an algorithm for detecting decreases in impedance over long time. Differences between measured impedance (bottom; circles) and reference impedance (solid line) are accumulated over time to produce fluid index (top). Threshold values are applied to fluid index to detect sustained decreases in impedance which may be indicative of acutely worsening thoracic congestion. Fig. 9.14b shows an example of impedance reduction before heart failure hospitalization (arrow) for fluid overload and impedance increase during intensive diuresis during hospitalization. Label indicates reference baseline (initial reference impedance value when daily impedance value consistently falls below reference impedance line before hospital admission). Magnitude and duration of impedance reduction are also shown. Days in hospital are shaded.

Some commercially available implantable devices for the treatment of CHF and/or ventricular tachyarrhythmias now continually monitor intrathoracic impedance and display fluid status trends. This information is then provided to the clinician via direct device interrogation or by remote telemetry. Recent reports based on actual clinical experience with this feature have attested to critical reliability and utility (Vollmann et al., 2007) and good correlation with other traditional tools (Luthje et al., 2007).

However, besides lung fluid, other physiological parameters might explain device measured changes in intrathoracic impedance. Some of these factors include ventricular dilation, atrial or pulmonary vascular dilation, anemia, hyper or hypovolemia, right and left ventricular preload, hematocrit, electrolyte balance, pocket infection, kidney dialysis, pneumonia, bronchitis; weight change (not related to fluid accumulation), lymphatic fluid changes, etc.

9.11.3 Cardiac Pacemakers

Pacing of the heart may be done transcutaneously, but this is accompanied by pain. The usual method is with two epicardial electrodes and leads out through the chest to an external pacemaker, or with an implanted pacemaker.

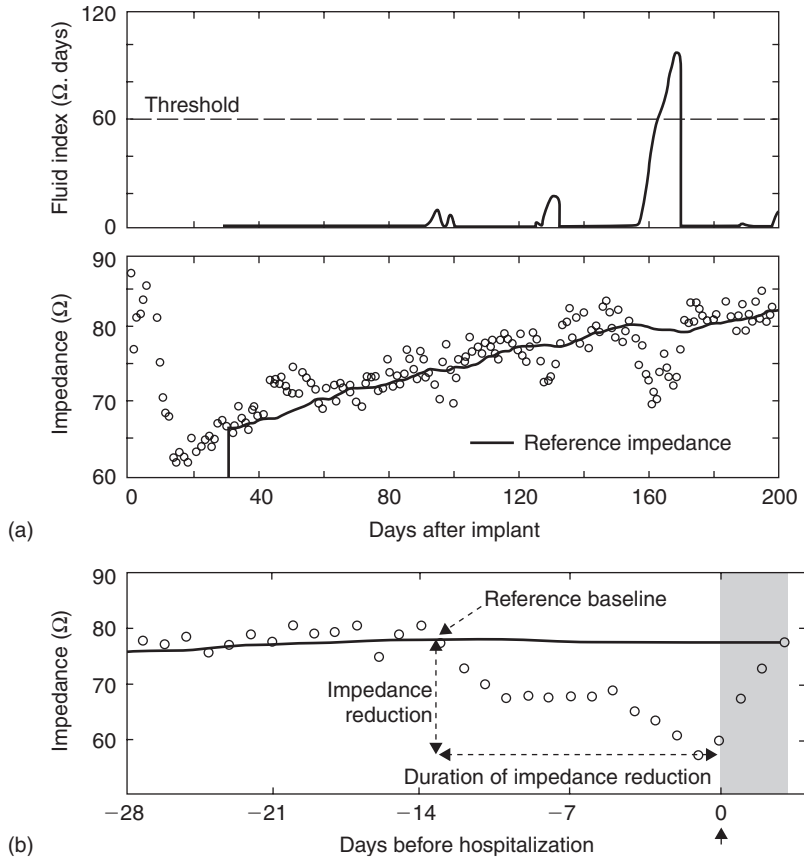


Figure 9.14 (a) Fluid index and impedance over 6 months; (b) example of impedance reduction before heart failure hospitalization (arrow) for fluid overload and impedance increase during intensive diuresis during hospitalization. *Source: Reproduced with permission: Yu et al. (2005).*

The implanted pacemakers are of many models. Let us consider a demand pacemaker, with special recording ring electrodes on the catheter for the demand function. If QRS activity is registered, pacing is inhibited. The pacemaker housing may be of metal (titan) and function as a large neutral electrode. Pacing is done with a small catheter tip electrode, either unipolar with the neutral electrode or bipolar with a catheter ring proximal to the tip electrode.

As can be seen from Fig. 9.15, the chronaxie is less than about $500 \mu\text{s}$, so there is an energy waste choosing the pulse duration much larger than $100 \mu\text{s}$.

A pacemaker may be externally programmed by magnetic pulses. Also because of this a pacemaker is to certain degree vulnerable to external interference. Typical

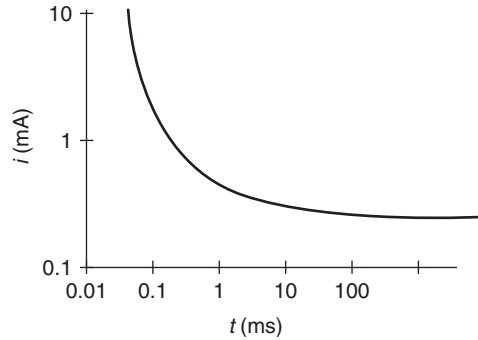


Figure 9.15 Current-time curves for heart pacing with a square wave pulse delivered during diastole with intracardial catheter electrode.

limits are: static magnetic field <1 gauss, 40 kV arcing >30 cm distance (car ignition system), radar 9 GHz E-field <1.2 kV/m. Typical pacemaker data are: pulse amplitude 5 mA, impedance monopolar electrode system $1\text{ k}\Omega$, load voltage 5 V, lithium battery 6.4 V with capacity 1800 mAh. The stimulus electrodes are AC coupled in the pacemaker's output stage, so that no DC can pass and unduly polarize the electrodes. The electrodes are made of noble metals to be biocompatible, and consequently they are highly polarizable (Section 7.4.5). The monopolar electrode system impedance is not very dependent on faradic impedance because the admittance of the double layer capacitance is large at the frequencies used.

Pacemaker implant and the use of electrosurgery are treated in Section 9.13.

9.12 DEFIBRILLATION AND ELECTROSHOCK

9.12.1 Defibrillator

Defibrillator shocks are the largest electric shocks used in clinical medicine, up to 50 A is applied for some milliseconds through the thorax, driven by approximately 5 kV. The electrode system is usually bipolar with two equal electrodes of surface *ca.* 50 cm^2 (adult, defibrillation of children is rare). They are positioned so that as much as possible of the current is passing the heart region. With a more unipolar system with one electrode under the shoulder the current path is more optimal, and this is used if the defibrillation is planned (electro-conversion).

Earlier conductive paste was used on the skin, today contact pads are used because they are quick to apply. They also make it possible to avoid usual contact paste that is easily smeared out on the skin surface and causes stray currents (either short-circuiting the shock energy, or representing a hazard for the personnel involved). The current density is so high that reddening of the skin often occurs, especially at the electrode edge (cf. Section 6.3.4). The large electrode and the large

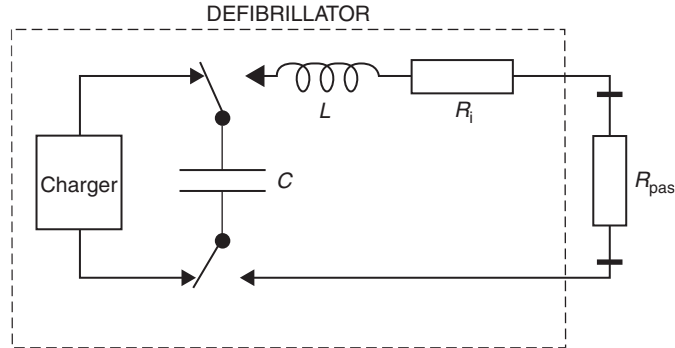


Figure 9.16 Classical defibrillator circuit. Typical values are $C = 20\ \mu\text{F}$, $L = 100\ \text{mH}$, $R_i = 15\ \Omega$, $R_{\text{pas}} = 50\ \Omega$.

current cause an extremely low-ohmic system. Fifty ohm is the standardized resistance of the complete system with two electrodes and the tissue in between. The resistance is falling for each shock given, and this is attributed to tissue damage.

We must assume that it is the local current density in the heart that is the determining parameter for a successful conversion. As this is unknown, it is usual practice to characterize the shock in energy (wattseconds = joules). This refers to the capacitor used to store the energy (Fig. 9.16). Stored energy is $CV^2/2$, so a shock dose is simply chosen by choosing charging voltage. Maximum stored energy is usually 400Ws. Not all the energy will be dissipated in the patient system, a part will be dissipated in the internal resistance R_i of the coil used to shape the waveform of the discharge current pulse. External shock is given transcutaneously, so the voltage must be high enough to break down the skin even at the lowest dose. For internal, direct epicardial application (internal shock), sterile electrode cups are used directly on the heart without any paste or pad. The necessary dose is usually less than 50Ws.

There is a certain range of accepted current duration. Figure 9.17 shows some current discharge current waveforms. Note that some marks use biphasic waveforms, some use truly monophasic.

Defibrillators are also made as implanted types, using intracardial catheter electrodes. In order to reduce energy consumption new waveforms have been taken into use: the exponential truncated waveform. It may be monophasic or biphasic. The idea of the biphasic waveform is that the second pulse shall cancel the net charge caused by the first pulse and thereby reduce the chance of refrillation.

Tissue impedance measurements with the defibrillator electrodes are used both in some external and internal defibrillator models. Measuring current and voltage during a shock gives a high current level, minimum value, non-linear region, peak voltage to peak current ratio. Between shocks the small signal, linear impedance is also monitored. The measured impedance value is used to customize both waveform and energy level for each shock given.

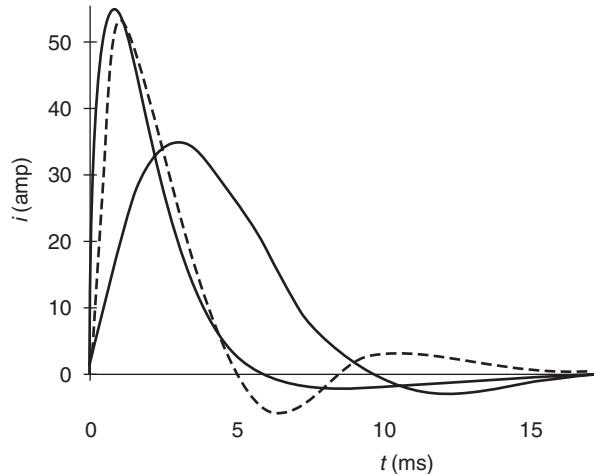


Figure 9.17 Some classical current discharge waveforms.

9.12.2 Electroshock (Brain Electroconvulsion)

Electroshock therapy is a somatic method in psychiatry, for the treatment of depressions. The traditional current waveform is a quarter-period power line 50 Hz sine wave, starting at the waveform maximum. Pulse duration is therefore 5 ms, followed by a pause of 15 ms. Automatic amplitude increase, or pulse grouping, is used. It is now often replaced by another waveform, a train of pulses of 1 ms duration with a total energy around 20 J. It is believed that with this waveform the memory problems are less. The corresponding voltage and current are several hundred volts and milliamps. Large bipolar electrodes are used on the temples. The positioning is usually bilateral, but ipsilateral positioning is also used.

ECT is a much discussed procedure, partly because it has been perceived as a brutal medical treatment. It is performed under anesthesia, and because of the heavy muscle contractions, muscle relaxants are given. The shock elicits a seizure not very different from a grand mal epileptic attack, the seizure is to last longer than 25 seconds. The effect is presumably due to the enormous synchronized activity of the whole CNS. The treatment is usually repeated several times within a few weeks span. The treatment is often followed by a loss of memory for recent events, and the therapeutic effect is not permanent.

9.13 ELECTROSURGERY

High frequency (also called radio frequency, RF) current is used to cut or coagulate tissue. The method must not be confused with *electrocautery*. In *electrosurgery* the current is passing the tissue, with heat development in the tissue and cold electrodes

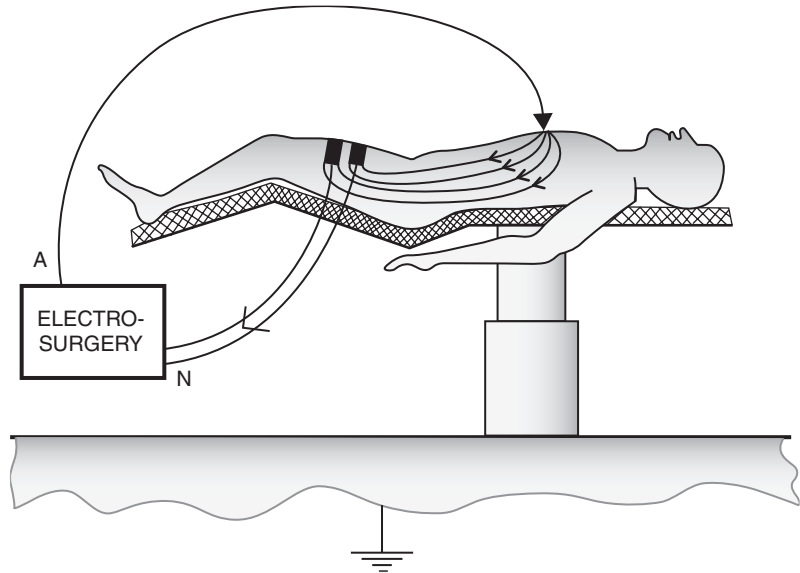


Figure 9.18 Monopolar electrocautery.

(diathermy). With electrocautery the current is passed through a wire and not through tissue, and the wire is accordingly heated. Bipolar forceps are used for microsurgery, they represent a dipole current source in the tissue (cf. Section 6.3.3). A unipolar (in the field of surgery called monopolar) circuit is used in general surgery. The neutral electrode is a large flexible plate covered with sticky hydrogel for direct fixation to the skin. The neutral plate is often split into two, and a small current is passed between the two plates via the skin and tissue. Impedance is measured, and if this impedance is outside pre-set or memory set limits, the apparatus will warn as a sign of poor and dangerous plate contact.

The active electrode may be handhold, or endoscopic: long and thin types either flexible or rigid.

Figure 9.18 illustrates the monopolar circuit. The monopolar coagulation electrode is often in the form of a sphere (cf. Section 6.3).

The waveform used is more or less pure sinusoidal in *cut mode*, to highly pulsed with a crest factor of 10 or more for the *spread coagulation mode*. In spread coagulation tissue contact is not critical, the current is passed to the tissue mostly by *fulguration* (electric arc). The electromagnetic noise generated may be severe over a large frequency spectrum, and this causes trouble for medical instrumentation connected to the same patient.

Electrosurgery is based on the *heat effect* of the current, and this is proportional to the square of the *current density* (and the electric field) and tissue *conductivity*. The power volume density W_v is falling extremely rapidly with distance from the electrode, as shown by the equation for a voltage driven half sphere electrode at

the surface of a half infinite homogeneous medium (eq. 6.7). With constant amplitude current the power volume density is:

$$W_v = \frac{i^2}{4\pi^2\sigma r^4} \quad (\text{half sphere}) \quad (9.12)$$

Tissue destruction therefore occurs only in the very vicinity of the electrode. Power dissipation is linked with conductance, not admittance, because the reactive part just stores the energy and sends it back later in the AC cycle. Heat is also linked with the rms values of voltage and current, ordinary instruments reading average values cannot be used. The temperature rise ΔT is given by (eq. 6.8). Because heat is so current *density* dependent, the effect is larger the smaller the cross sectional area of an electrode, or at a tissue zone constriction. This is an important reason for the many hazard reports with the use of electrosurgery in hospitals. Another reason is that that the whole patient is electroactive in normal mode of electrosurgery use. The RF potentials of many body segments may easily attain some tenths of rms volt in normal mode operation, and insulation of these body segments is critical.

High frequencies have been chosen to avoid nerve and muscle stimulation (cf. the sensitivity curve of Fig. 9.31). The output is neither constant amplitude voltage nor constant amplitude current. The optimal output characteristic is linked with the very variable load resistance. Tissue resistance increases when coagulated, fat has higher resistance than muscles and blood, and the contact geometry is very dependent on the electrode chosen and the way it is held by the surgeon. If a constant amplitude current is chosen, power would be proportional to load resistance, and tissue would quickly be carbonized in high resistance situations. If constant amplitude voltage were chosen, power would be inversely proportional to load resistance, and when tissue layers around the electrode would coagulate, current would stop flowing. Modern instrumentation therefore measures both output voltage and current, and regulates for an isowatt characteristic.

Typical power levels in unipolar electrosurgery is about 80 W (500 Ω , 200 V, 400 mA rms), in bipolar work 15 W (100 Ω , 40 V, 400 mA rms). The frequency content of the sine wave is of course just the repetition frequency, usually around 500 kHz. In pulsed mode the frequency content is very broad, but most of the energy will be in the frequency band 0.5–5 MHz. In pulsed mode the peak voltage can reach 5000 V, so insulation in the very humid surroundings is a problem.

The arc formed particularly in coagulation mode, is a source both of noise and rectification. Rectification is strongly unwanted, because low frequency signal components may be generated which excites nerves and muscles. In order to avoid circulating rectified currents, the output circuit of a monopolar equipment always contain a safety blocking capacitor (Fig. 9.19). Low frequency voltage is generated, but it does not lead to low frequency current flow. Even so, there may be local low frequency current loops in multiple arc situations (Slager et al., 1993). The resulting nerve stimulation is a problem in certain surgical procedures.

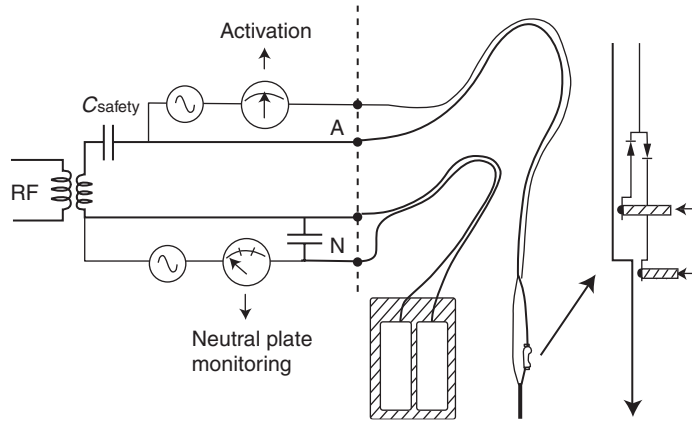


Figure 9.19 Typical electrosurgery output circuit. Notice double plate neutral electrode for monitoring of skin contact. Safety blocking capacitor shall prevent rectified *low frequency* currents in tissue.

Argon gas is sometimes used as an arc guiding medium. The argon gas flows out of the electrode mainly for two purposes: to facilitate and lead the formation of an arc between the electrode and tissue surface, and to impede oxygen in reaching the coagulation zone. In this mode of operation, no physical contact is made between the metal electrode and the tissue, the surgeon points the pen toward the tissue and coagulation is started just as if it was a laser beam (which it is often mixed up with). The gas jet also blows away liquids on the tissue surface, thus facilitating easy surface coagulation.

Implants

The use of electrosurgery on patients with metallic implants or cardiac pacemakers may pose problems. Metallic implants are usually considered not to be a problem if the form is round and not pointed (Etter et al., 1947). The pacemaker electrode tip is a small area electrode, where relative small currents may coagulate endocardial tissue. The pacemaker catheter positioning should therefore not be parallel with the electrosurgery current density lines. This is illustrated in Fig. 9.20 for a heart pacemaker implant.

Ablation

Through catheters it is possible to destroy tissue with RF currents in a minimal-invasive procedure. In cardiology this is called *ablation*. Both DC and RF current has been tried for this purpose. Choice of bipolar or monopolar technique is important (Anfinsen et al., 1998).

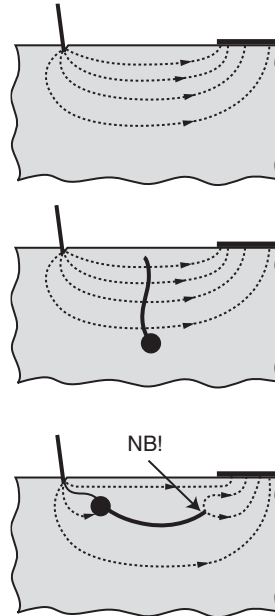


Figure 9.20 Monopolar electrosurgery and an implant, for example a pacemaker with intracardiac catheter electrode. Importance of catheter direction with respect to current density direction.

9.14 CELL SUSPENSIONS

9.14.1 Electroporation and Electrofusion

Electroporation is the phenomenon in which cell membrane permeability to ions and macromolecules is increased by exposing the cell to short (microsecond to millisecond) high voltage electric pulses (Weaver, 2003). While the mechanism for electroporation is not yet completely understood experiments show that the application of electrical pulses can have different effects on the cell membrane, as a function of various pulse parameters; such as amplitude, duration, pulse shape and repetition rate (Mir, 2001). As a function of these parameters, the application of the electrical pulse can have no effect, can have a transient effect known as reversible electroporation or can cause permanent permeation known as irreversible electroporation (IRE) which leads to non-thermal cell death by necrosis (Weaver, 2003; Davalos et al., 2005). It is thought that the induced potential across the cell membrane causes instabilities in the polarized lipid bilayer (Weaver and Barnett, 1992; Weaver and Chizmadzhev, 1996; Edd et al., 2006). The unstable membrane then alters its shape forming aqueous pathways that possibly are nano-scale pores through the cell's plasma membrane (Neumann and Rosenheck, 1972; Neumann et al., 1989; Weaver, 1995). Irreversible behavior is attributed to bilayer rupture by uncontrolled pore growth and the outcome is governed by the local plasma membrane potential, $\Delta\psi_{PM}$, behavior and the relative large membrane tension (Esser et al., 2007).

Irreversible Electroporation for Tissue Ablation

Irreversible Electroporation (IRE) has been studied extensively with *in vitro* cellular systems. IRE has also been studied as method to destroy prokaryotic (Sale and Hamilton, 1967) and eukaryotic cells *in vitro* and has gain momentum recently as a method to kill microorganisms (Vernhes et al., 1999), mammalian normal cells (Vernhes et al., 1999) as well as mammalian cancer cells (Miller et al., 2005) *in vitro* and tumors (Nuccitelli et al., 2006). These studies have demonstrated the ability of IRE, to completely eradicate an entire population of cells *in vitro* without inducing any thermal damage.

Lee et al. hypothesized that electrical injury is often characterized by the preferential death of large mammalian cells (skeletal muscle, nerves) in tissue regions where insignificant temperature rise occurs (Bhatt et al., 1990; Lee et al., 2000; Esser et al., 2007). With the key distinction between shock trauma and temperature change, this research group opened the door to the application of IRE as an alternate tissue ablation technique (Lee and Despa, 2005).

Davalos, Mir and Rubinsky recently postulated that IRE can be used as an independent drug-free tissue ablation modality for particular use in cancer therapy (Davalos et al., 2005). This minimally invasive procedure involves placing electrodes into or around the targeted area to deliver a series of short and intense electric pulses that induce the irreversible structural changes in the cell membrane (Edd and Davalos, 2007). This induced potential is dependent on a variety of conditions such as tissue type and cell size (Edd and Davalos, 2007). Due to the changes in the cell membrane resistance during electroporation the technique can be controlled and monitored with EIT, a real-time imaging method that maps the electrical impedance distribution inside the tissue (Davalos et al., 2004). Ivorra et al. concluded in (Ivorra and Rubinsky, 2007) that impedance measurements can be employed to detect and distinguish reversible and irreversible electroporation *in vivo* and *in situ* liver tissue. IRE produces a well-defined region of tissue ablation, without areas in which the extent of damage changes gradually as during thermal ablation (Rubinsky, 2007). A single cell is either destroyed by IRE or not (Rubinsky, 2007). The IRE pulses do not compromise the blood vessel matrix and appears to be safe and cause no complications as suggested in (Maor et al., 2007). In addition, it has been shown through mathematical modeling that the area ablated by irreversible tissue electroporation prior to the onset of thermal effects is substantial and comparable to that of other tissue ablation techniques, such as cryosurgery (Davalos et al., 2005). Thus, for certain medical applications IRE alone could be used as an effective technique for tissue ablation without the use of cytotoxic drugs like in chemotherapy (Davalos et al., 2005).

Electrical Properties of Tissue During Electroporation

The electrical properties of any material, including biological tissue, can be broadly separated into two categories: conducting and insulating. In a conductor, the electric charges move freely in response to the application of an electric field, whereas in an insulator (dielectric), the charges are fixed and not free to move.

If a conductor is placed in an electric field, charges will move within the conductor until the interior field is zero. In the case of an insulator, no free charges exist, so net migration of charge does not occur. In polar materials, however, the positive and negative charge centers in the molecules do not coincide. An electric dipole moment, p , is said to exist. An applied field, E_0 , tends to orient the dipoles and produces a field inside the dielectric, E_p , which opposes the applied field. This process is called polarization. Most materials contain a combination of orientable dipoles and relatively free charges so that the electric field is reduced in any material relative to its free-space value. The net field inside the material, E , is then

$$E = E_0 - E_p \quad (9.13)$$

The net field is lowered by a significant amount relative to the applied field if the material is an insulator and is essentially zero for a good conductor. This reduction is characterized by a factor ϵ_r , which is called the relative permittivity or dielectric constant, according to

$$E = \frac{E_0}{\epsilon_r} \quad (9.14)$$

Biological systems are electrically heterogeneous (Gift and Weaver, 1995). Application of an electric field pulse results in rapid polarization changes that can deform mechanically unconstrained cell membranes (e.g., suspended vesicles and cells) followed by ionic charge redistribution governed by electrolyte conductivities and distributed capacitance (Weaver, 2000; Ivorra and Rubinsky, 2007). For most cells and tissues the latter charging times are of order $\tau_{\text{CHG}} \approx 10^{-6}$ seconds. Thus, if U_m is to exceed 0.5–1 V, much larger pulses must be used if the pulse is significantly shorter than τ_{CHG} (Weaver, 2000).

Electroporation is hypothesized to involve inhomogeneous nucleation of primary, hydrophilic pores based on transitions from much more numerous hydrophobic pores (Weaver, 2000). The basic idea is that a circular region of membrane is replaced with a pore. As primary pores appear in the membrane, its resistance drops, and the voltages within the system redistribute on a time scale governed by the instantaneous values of the various conductivities and capacitance (Weaver, 2000). Both experiment and theory show that the membrane capacitance change is small (Chernomordik et al., 1982; Freeman et al., 1994), so that the main electrical result is drastically decreased barrier resistance. Overall, bilayer membrane electroporation results in dynamic, non-linear changes as a heterogeneous pore population evolves rapidly in response to the local value of the transmembrane voltage U_{mlocal} along the surface of a cell membrane (Weaver, 2000). At the time of maximum membrane conductance, pores are nevertheless widely separated, occupying only about 0.1% of the electroporated membrane area (Hibino et al., 1991; Freeman et al., 1994). In this sense, electroporation is catalytic (Weaver, 1994). Not only is there the possibility of binding and lateral diffusion to the other side of the membrane as pores form and

then vanish, but there is a tremendous increase in rate (of transport) due to small entities (pores) that occupy a small fraction of the membrane (Weaver, 2000).

Due to the changes in the cell membrane resistance during electroporation the technique can be controlled and monitored with EIT, a real-time imaging method that maps the electrical impedance distribution inside the tissue (Davalos et al., 2004). Ivorra et al. concluded in (Ivorra and Rubinsky, 2007) that impedance measurements can be employed to detect and distinguish reversible and irreversible electroporation in *in vivo* and *in situ* liver tissue.

Single Cell Microelectroporation Technology

There are different techniques to overcome the cell membrane barrier and introduce exogenous impermeable compounds, such as dyes, DNA, proteins and amino acids into the cell. Some of the methods include lipofection, fusion of cationic liposome, electroporation, microinjection, optoporation, electroinjection and biolistics. Electroporation has the advantage of being a non-contact method for transient permeabilization of cells (Olofsson et al., 2003). In contrast to microinjection techniques for single cells and single nuclei (Capecchi, 1980), the electroporation technique can be applied to biological containers of sub-femtoliter volumes, that are less than a few micrometers in diameter. Also, it can be extremely fast and well timed (Hibino et al., 1991; Kinosita et al., 1988), which is of importance in studying fast reaction phenomena (Ryttsen et al., 2000).

In addition to bulk electroporation methods, instrumentation has been developed that can be used for electroporation of a small number of cells in suspension (Kinosita and Tsong, 1979; Chang, 1989; Marszalek et al., 1997), and for a small number of adherent cells grown on a substratum (Zheng and Chang, 1991; Teruel and Meyer, 1997). These electroporation devices create homogeneous electric fields across fixed distances of 0.1–5 mm, several times larger than the size of a single mammalian cell (Ryttsen et al., 2000). Also there are numerous experimental methods for the biochemical and biophysical investigations of single cells. Such methods include (1) patch clamp techniques for measuring transmembrane currents through a single ion channel (Hamill et al., 1981), (2) scanning confocal and multiphoton microscopy for imaging and localizing bioactive components in single cells and single organelles (Maiti et al., 1997), (3) near-field optical probes for measuring pH in the cell interior (Song et al., 1997), (4) ultramicroelectrodes for monitoring the release of single catechol- and indol-amine-containing vesicles (Wightman et al., 1991; Chow et al., 1992), (5) optical trapping and capillary electrophoresis separations for analyzing the chemical composition of individual secretory vesicles (Chiu et al., 1998), (6) electroporation with solid microelectrodes (Lundqvist et al., 1998), (7) electroporation with capillaries and micropipettes (Haas et al., 2001; Nolkranz et al., 2001, Rae and Levis, 2002), (8) microfabricated chips and multiplexed electroporation system (Huang and Rubinsky, 1999; Lin, 2001).

Rubinsky's group presented the first microfluidic device to electroporate a cell (Huang and Rubinsky, 1999; Davalos et al., 2000). Their devices consisted of three silicon chips bonded together to form two chambers, separated by a 1 μm thick

silicon nitride membrane with a 2–10 μm diameter hole. Since silicon nitride is non-conductive, any electrical current flowing from the top chamber to the bottom chamber must pass through this microhole. A cell suspension was introduced into the top chamber, followed by the immobilization of one cell in the hole by lowering the pressure in the bottom chamber. Since the trapped cell impedes the system's electrical path, only low voltage pulses are needed to induce large fields near the trapped cell and only the trapped cell is electroporated. With this chip, they were able to show the natural difference in electroporation behavior between human prostate adenocarcinoma and rat hepatocyte cells by studying the process using current-voltage measurements (Huang and Rubinsky, 1999). Davalos and colleagues advanced this technology by making the chambers and electrodes off-chip, simplifying it to one silicon chip. Such changes enabled ease of use, accessibility of the device and reusability (Lee et al., 2006; Robinson et al., 2007).

In recent years, several microfluidic electroporation designs for the analysis, transfection or pasteurization of biological cells have been reported (Fox et al., 2006a,b). The range of applications for microfluidic electroporation coupled with advances in microfabrication techniques, specifically the use of structural photoresist for soft lithography, has resulted in a variety of designs: microchips in which cells move through a treatment zone (Gao et al., 2004), microchips in which cells are trapped at a specific location (Huang and Rubinsky, 1999) and devices in which the cells are surface-bound (Lin and Huang, 2001; Fox et al., 2006a,b). Of all the types of designs created, only the few designs in which a cell is trapped at a specific location enables us to study the biophysics of electroporation at the single cell level. In addition to the original devices described in the previous paragraph, other designs have been developed in which a cell is trapped at a specific location and electroporated. For example, Huang and Rubinsky advanced their technology using structural photoresist to create microfluidic channels on top of their silicon wafer (Huang and Rubinsky, 2003). Khine et al. fabricated a device using soft lithography which was originally developed as a multiple patch clamp array. Their device contains a main channel with multiple perpendicular small side channels. The individual cells in the main channel are brought into contact with the opening of a side channel using pressure. The cell does pass the constriction because its diameter (12–17 μm) is approximately 4 times larger than the constriction (3.1 μm). The constriction enables potentials of less than 1 V to deliver the high fields needed to induce electroporation, which is applied using an silver–silver chloride-electrode (Khine et al., 2005a,b). Such devices are useful to study the biophysical process of electroporation because the changes in electrical properties of an individual cell as well as the molecular transport into the cell can be tracked (Davalos et al., 2000).

Supraelectroporation

If the applied electric field is very high ($>10\text{ kV/cm}$) and the pulses are very short (nanosecond range), not only the plasma membrane of a cell is rendered permeable but also intracellular structures (Schoenbach et al., 2004; Vasilkoski et al.,

2006). This opens new perspectives for treatment of cells, especially involving intracellular structures.

Electroporation theory works well up to about 2 kV/cm applied electric field. At higher field strength some effects appear which are hardly explainable just by pore formation.

The cell membrane has a capacity on the order of $1 \mu\text{F}/\text{cm}^2$. At 30 MHz its capacitive resistance is small compared to the resistance of the electrolytes (i.e. the membranes are de facto shortened). The conductivity at this frequency is therefore a good guide for the maximum extent of electroporation, which would be when all membranes contain 100% pores. Even if it is practically irrelevant, it gives an idea about the absolute maximum of conductance. As shown in Fig. 9.21, the conductance exceeds this maximum value considerably when the field exceeds about 5 kV/cm. An early explanation involved some kind of Wien effect. The first Wien effect is due to the liberation of ions from the counterion cloud around charged particles like proteins while the second one describes the creation of new charge carriers by field dissociation of weak electrolytes. Both of these effects together can explain a conductivity increase by several percent but not by 140% as seen in Fig. 9.21. Moreover this dramatic conductivity increase is only found in solution containing aggregated amphiphiles like lipids.

The creation of very dense electropores (supra electroporation) is probably the initial step to a complete disintegration of the membrane. If the electric field is sufficiently high, micelles instead of membrane structures become stable. Because of the higher mobility of ions in the vicinity of the membrane, a significant increase in conductivity happens.

Electrofusion is the connection of two separate cell membranes into one by a similar pulse. It is believed that the process is based on the same field-induced restructuring of the bilayer lipid membranes (BLMs), a process which may be reversible or irreversible.

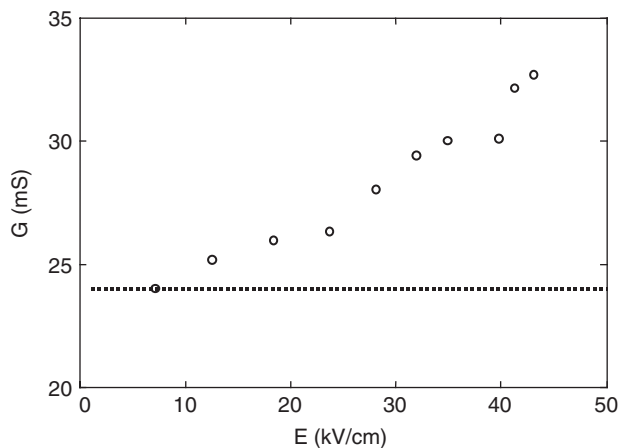


Figure 9.21 Measured conductance versus the field strength for a suspension of Jurkat-cells. The dashed line indicates the conductance at 30 MHz Source: From Pliquett et al. (2007).

It is known that an ordinary cell membrane cannot withstand a prolonged DC potential difference ΔV_m more than about 150–300 mV without irreversible damage. For short pulses in the μs range, it has been found that at a threshold voltage Δv_m of about 1 V, the cell membrane becomes leaky and rather large macromolecules pass in and out of the cell (lysis). The following expression for the electric field in the membrane E_m is valid if the membrane thickness d is much less than cell radius r , and that the conductivity of the membrane material is much less than both the internal and external (σ_0) electrolyte conductivity:

$$E_m = 1.5(r/d) E(1 - e^{-Kt}) \cos \theta \quad (9.15)$$

E is the electric field in the external homogenous medium, $K = \sigma_0/3rC_m$, and θ the angle between the E-field and the cell radius r (cell center is origin).

For electroporation a threshold voltage of about 1 V across the cell membrane has been found. The relationship between the cell membrane potential difference (corresponding to the order of 2–20 kV/cm in the suspension according to cell size, type, etc.), it may still be a reversible electroporation as long as it is caused by a single pulse of a short time duration (e.g. of the order of 20 μs). If a train of such pulses is applied, the cell is killed because of the excessive material exchange. It is believed that a large part of the material exchange (lysis) is an *after-field* effect lasting up to 0.1 seconds or more. If the electroporation is reversible, the pores or cracks then reseal. Electrofusion is certainly an irreversible after-field effect.

The primary field effect shows threshold behavior, about the same value for poration and fusion: The electric field effect in the cell membrane lipid bilayer is a molecular rearrangement with both hydrophobic or hydrophilic pore formation. Hydrophilic pores are considered to be water filled, with pore walls which may comprise embedded lipids. The threshold field strength has been found to be inversely proportional to the cell diameter. At the time of pulse application cell fusion may occur if two cells are in contact with each other, DNA uptake may occur if DNA is adsorbed to the cell surface. Cells may be brought in contact with each other by means of the pearl chain effect (see below). The electroporative cell transformation probability due to DNA entrance is low, typically 10^{-5} . Field values above threshold are believed to increase the pores in number and size, until a critical value is reached where complete membrane rupture occurs (irreversible non-thermal breakdown). The difference between the threshold level and the critical level is not large, so overdoses easily kill the cells. It is interesting to speculate whether electroporation is a mechanism in defibrillator chock treatment. The field strength used is lower (of the order of 500 V/cm), however the pulse duration is longer, of the order of some milliseconds.

The usual source for the electric field pulse is to discharge a charged capacitor (e.g. a 25 μF capacitor charged to 1500 V). The charge voltage and the distance between the capacitor plates determine the E-field strength, and the capacitance together with the system resistance determines the time constant of the discharge current waveform. The circuitry is very similar to the defibrillator circuit shown in Fig. 9.16, except that the inductor extending the time constant into the millisecond range, is not necessarily used. The pulse is accordingly a single exponentially

decaying DC pulse, and the time constant is dependent on the liquid conductivity. With more complicated circuitry it is possible to make a square wave high voltage pulse generator. Because it is DC, it may be an appreciable electrolysis and change in pH near the electrodes. To keep the necessary voltage low, the distance between the electrode plates is small.

It is possible to use a RF pulse instead of DC. The RF causes mechanical vibrations in addition to the electrical effects, and this may increase the poration or fusion yield. As the effect is so dependent on the cell diameter, it may be difficult to fuse or porate cells of different sizes with DC pulses. The threshold level for the smallest cell will kill the largest.

9.14.2 Cell Sorting and Characterization by Electrorotation and Dielectrophoresis

The principles behind electrorotation, dielectrophoresis and other electrokinetic effects are described in Section 2.4.6. The direction and rate of movement of bio-particles and cells due to these mechanisms depend on the dielectric properties of, for example, the cell. These dielectric properties may to some extent reflect the type of cell or the condition of the cell and there is consequently a significant potential in the utilization of these techniques for cell sorting or characterization.

Electrorotation was, for example, used to differentiate between viable and non-viable biofilms of bacteria. Because of their small size, determination of the dielectric properties of bacteria by means of electrorotation is impractical. By forming bacterial biofilms on polystyrene beads, however, Zhou et al. (1995) were able to investigate the effect of biocides on the biofilms.

Masuda et al. (1987) introduced the use of traveling wave configuration for the manipulation of particles. The frequency used was originally relatively low, so that electrophoresis rather than dielectrophoresis was predominant. The technique was later improved by, among others, Fuhr et al. (1991) and Talary et al. (1996), who used higher frequencies where dielectrophoresis dominates. Talary et al. (1996) used traveling wave dielectrophoresis to separate viable from non-viable yeast cells and the same group have used the technique to separate erythrocytes from white blood cells (Burt et al., 1998).

Hydrodynamic forces in combination with stationary electric fields have also been used for the separation of particles. Particles in a fluid flowing over the electrodes will to different extent be trapped to the electrodes by gravitational or dielectrophoretic forces. Separation is achieved by calibration of for example, the conductivity of the suspending medium or the frequency of the applied field. This approach has been used for separation between viable and non-viable yeast cells (Markx et al., 1994), different types of bacteria (Markx et al., 1996), leukemia and breast cancer cells from blood (Becker et al., 1994, 1995). Dielectrophoresis has also been successfully used for other types of bioparticles like DNA (Washizu and Kurosawa, 1990), proteins (Washizu et al., 1994) and viruses (Schnelle et al., 1996).

More recently, dielectrophoretic studies have for instance been reported on T-lymphocytes (Pethig et al., 2002; Pethig and Talary 2007) and on how cell destruction

during dielectrophoresis can be minimized (or utilized) by appropriate choice of AC frequency and amplitude (Menachery and Pethig, 2005). Dielectrophoresis has also been used for measurement of membrane electrical properties such as capacitance and conductance for insulin secreting pancreatic cells (Pethig et al., 2005).

Another interesting approach to particle separation is called field-flow fractionation, and this technique can be used in combination with dielectrophoresis (Davis and Giddings, 1986). Particles are injected into a carrier flow and another force (e.g. by means of dielectrophoresis) is applied perpendicular to the flow. Dielectric and other properties of the particle will then influence the particles distance from the chamber wall and hence its position in the parabolic velocity profile of the flow. Particles with different properties will consequently be released from the chamber at different rates and separation hence achieved. Washizu et al. (1994) used this technique for separating different sizes of plasmid DNA.

9.14.3 Cell-Surface Attachment and Micromotion Detection

Many types of mammalian cells are dependent on attachment to a surface in order to grow and multiply. Exceptions are the different cells of the blood and cancer cells which may spread aggressively (metastases). To study cell attachment a microelectrode is convenient: as shown in Section 6.3.1, the half-cell impedance is more dominated by electrode polarization impedance the smaller the electrode surface is. Figure 9.22 shows the set up used by Giaever's group (Giaever and Keese, 1993).

A monopolar electrode system with two gold electrodes is used. A controlled current of $1\mu\text{A}$, 4kHz is applied to a microelectrode $<0.1\text{mm}^2$, and the

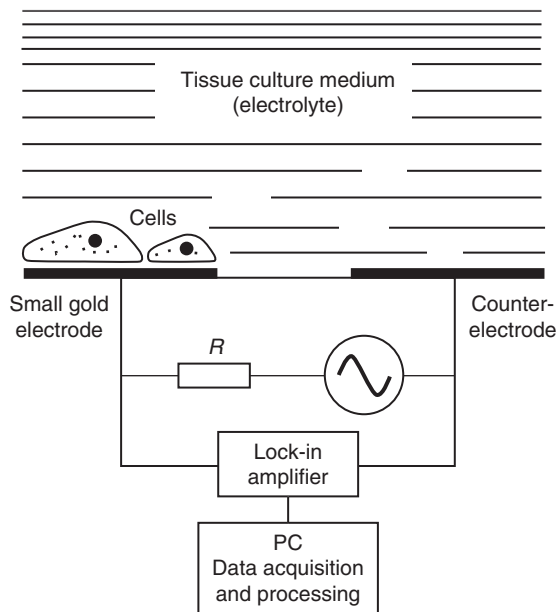


Figure 9.22 Impedance motion sensing with cells on a small gold electrode.

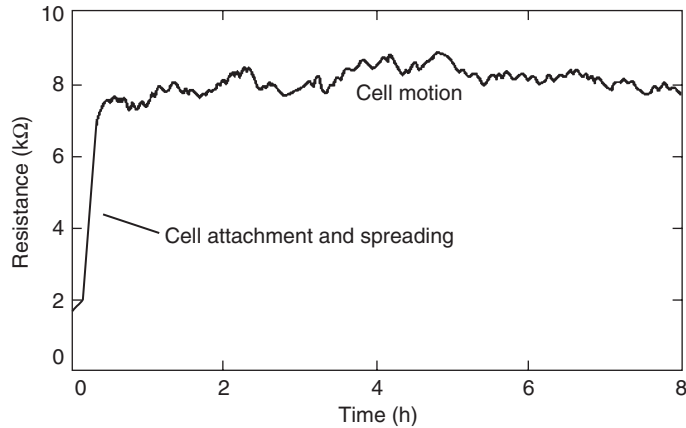


Figure 9.23 Changes in electrical resistance reflecting attachment and motion of cells on a small gold electrode.

corresponding voltage is measured by a lock-in amplifier. With cell attachment and spreading, both the in-phase and quadrature voltage increase as the result of cell-surface coverage. It is possible to follow cell motion on the surface, and the motion sensitivity is in the nm range. The method is very sensitive to subtle changes in the cells (e.g. by the addition of toxins, drugs and other chemical compounds). It is also possible to study the effect of high voltage shocks and electroporation.

Figure 9.23 shows an example of cell attachment and motion as measured with the electric cell-substrate impedance sensing (ECIS) instrument, which is a commercially available version of this system (Applied BioPhysics Inc., Troy, New York, USA).

9.14.4 Coulter Counter

The principle is based on letting cells in suspension pass a narrow orifice. If a cell has different electrical properties than the liquid, the impedance of the pore will change at each cell passage. Cell counting is possible, and it is also possible to have information about each cell's size, form or electrical properties. Figure 9.24 shows the basic

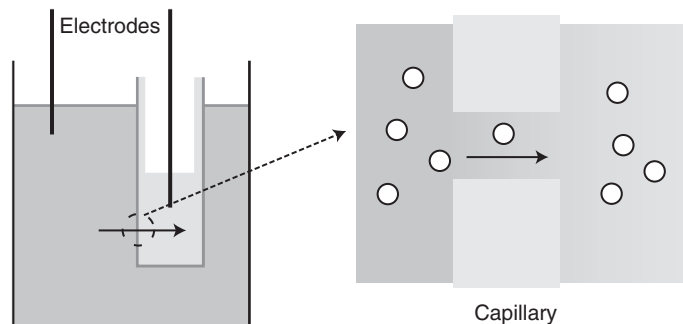


Figure 9.24 The measuring capillary cell of a Coulter counter.

set-up of the two-electrode conductance measuring cell. Typical dimensions (diameter, length) for a capillary is 50 and 60 μm (erythrocytes); 100 and 75 μm (leukocytes).

9.15 SKIN INSTRUMENTATION

9.15.1 Fingerprint Detection

Electronic fingerprint systems will in the near future eliminate the need for keys, pin-codes and access cards in a number of everyday products. While fingerprint recognition traditionally has been used only in high security applications, it is now gaining acceptance in mainstream consumer applications worldwide. One such large-scale application will be the need for secure mobile transactions when paying for the groceries with your mobile phone at the local supermarket. Several bioimpedance based fingerprint sensors have been developed, such as the electrode array based sensor from the company Idex ASA (www.idex.no). An array of electrodes is scanned as the fingertip is swept over the sensor stripe, giving a 500 dpi resolution impedance image of the fingerprint.

The fingerprint sensor market also demands systems for detecting fake fingers on the sensor, and a bioimpedance based solution for spoof detection was described by Martinsen et al. (2007). Their system is based on the simultaneous measurement of skin impedance at different depths, and the use of multivariate models to classify the fingers as living or fake.

9.15.2 Stratum Corneum Hydration

Stratum corneum hydration is essential for proper function and appearance of the skin. The moisture content can be measured in vitro by means of gravimetry or electron microscopy, or by magnetic resonance techniques in vivo. The resolution of the latter technique is, however, currently not sufficiently high to enable isolated measurements on the stratum corneum. Compared to these techniques, assessment of stratum corneum hydration by means of electrical measurements would represent a tremendous reduction in instrumental cost and complexity.

A prerequisite for using electrical measurements in this way is of course a detailed knowledge of how the different parts of the skin influence on the electrical impedance. Furthermore, the current and potential distribution in the skin will also be determined by the electrode geometry, which must be taken into account. As explained in Section 4.2.6, the impedivities of the stratum corneum and the viable skin converge as the measuring frequency is increased. Measurements at high frequencies will hence normally be largely influenced by the deeper layers of the skin. The frequency must therefore be kept low in order to achieve isolated measurements on the stratum corneum. A frequency scan (i.e. impedance spectroscopy) cannot be utilized in stratum corneum hydration measurements, owing to the

problems of interacting dispersion mechanisms explained in Section 8.2.14. Contrary to certain opinions (Salter, 1998), the mere fact that the current distribution in the different skin layers will differ between different measuring frequencies, is enough to discard the multiple frequency approach on stratum corneum *in vivo* (Martinsen et al., 1999). Further complications are introduced by the dispersions of the electrode impedance and deeper skin layers, and also by the Maxwell–Wagner type of dispersion that is due to the interface between the dry stratum corneum and the viable epidermis.

Since the sweat ducts largely contribute to the DC conductance of the skin, the proper choice of electrical parameter for stratum corneum hydration assessment is consequently low frequency AC conductance (where DC conductance is removed) or susceptance.

There are a number of instruments for skin hydration assessment on the market. Most of them measure at rather high frequencies, which mean that they measure deep into the viable skin. Some instruments use closely spaced interdigitated micro-electrodes. This reduces somewhat the contribution from viable skin layers, but the chance of only measuring in redundant moisture on the skin surface is obvious for such systems. Rationales for using a low frequency electrical susceptance method for skin hydration assessment and description of a method for absolute calibration of the measurements can be found in (Martinsen et al., 1998, 2008; Martinsen and Grimnes, 2001).

9.15.3 Skin Irritation and Skin Diseases Including Skin Cancer

Irritant contact dermatitis is a localized, superficial, non-immunological inflammation of the skin resulting from the contact with an external factor. The dermatitis may be acute, for example, if the influence from the external source was strong and of short duration, or of a more chronic kind if the influence is weaker but prolonged. The difference between irritant and allergic contact dermatitis is subtle, and depends mainly on whether the immune system is activated or not. Established signs of irritation are edema, erythema and heat, and any electrical parameter sensitive to these physiological changes could serve as a possible parameter for the assessment of skin irritation. As for other diagnostic bioimpedance measurements, the parameter should be immune to other, irrelevant changes in the skin. To eliminate the large variations in interpersonal electrical impedance baseline, normalization by means of indexes are often used rather than absolute impedance values (cf. Section 8.3.2).

A depth-selective skin electrical impedance spectrometer (formerly called SCIM) developed by S. Ollmar at the Karolinska Institute is an example of a commercial instrument intended for quantification and classification of skin irritation. It measures impedance at 31 logarithmically distributed frequencies from 1 kHz to 1 MHz, and the measurement depth can to some extent be controlled by electronically changing the virtual separation between two concentric surface electrodes (Ollmar, 1998).

Ollmar and Nicander (1995), Nicander et al. (1996), Nicander (1998) used the following indices:

$$\text{Magnitude index (MIX)} = |Z|_{20 \text{ kHz}} / |Z|_{500 \text{ kHz}}$$

$$\text{Phase index (PIX)} = \varphi_{20 \text{ kHz}} - \varphi_{500 \text{ kHz}}$$

$$\text{Real part index (RIX)} = R_{20 \text{ kHz}} / |Z|_{500 \text{ kHz}}$$

$$\text{Imaginary part index (IMIX)} = X_{20 \text{ kHz}} / |Z|_{500 \text{ kHz}}$$

where Z , R , X and φ have their usual meaning. The authors found significant changes in these indexes after treatment with sodium lauryl sulfate, nonanoic acid and benzalkonium chloride, and the measured changes correlated well with the results from subsequent histological examinations. The stratum corneum is soaked with saline before the measurements in order to provide good contact between the electrode system and the skin surface and to focus the measurements on the viable skin, although the barrier function of intact stratum corneum will still give a considerable contribution. The choice of frequencies for the indices hence seems reasonable. The group have also extended their impedance spectroscopy technology to further applications. Examples are the detection of other conditions and diseases in the skin or oral mucosa (Emtestam and Nyrén, 1997; Lindholm-Sethson, et al., 1998; Norlén et al., 1999), the early detection of transplanted organ complications (Ollmar, 1997; Halldorsson and Ollmar, 1998) and assessment of skin cancer (Emtestam et al., 1998).

After publication of a paper by Nicander et al., (1996) where it was demonstrated that skin reactions elicited by three irritants of different polarity created three different histopathological patterns and that each pattern could be correlated to corresponding patterns in the impedance indices, the Ollmar group has taken steps away from the data reduction technique based on the four indices in order to extract more information from the original impedance spectra. However, the indices are still useful for quantification of various aspects of responses to treatment or test substances, an example of which is given by Emtestam et al. (2007).

The finding of correlation between tissue structures (as seen in the microscope) with impedance properties (Nicander et al., 1996) triggered the idea of a potential diagnostic decision support tool intended to assist the doctor in a clinical environment. This idea is not new, for example, Fricke and Morse found a difference in capacity of tumors of the breast compared to normal breast tissue already in 1926. However, this finding is completely unspecific. Almost any tissue alteration can be detected by electrical impedance, but in order to be clinically useful, the method has to be able to differentiate benign alterations from malignant alterations, or be able to distinguish one disease from another in order to select a specific and adequate therapy. In other words: there is a difference between statistical significance and clinical significance. A p -value < 0.001 may sound convincing in a statistical comparison, but may mean nothing in the clinic unless both sensitivity and specificity are good enough in the intended application (cf. Section 8.4.2). Thus, more information had to be extracted from the impedance spectra, and both the electrical

impedance indices, which were sufficient for characterizing elicited skin reactions, and classical Cole-style models, were found inadequate to distinguish various disorders, according to the Ollmar group.

In skin testing, the central area of the volar forearm is very popular, mainly because of ease of access. It is also considered very homogeneous and stable, compared to other areas of the human body, and in extrapolation of this belief there have been studies without randomization of test sites within the volar forearm region. In search of suitable statistical tools to enhance discrimination power, this belief was challenged by Åberg et al. (2002), who used linear projection methods (in this case PARAFAC) to extract clinical information from the impedance spectra. The results showed systematic differences within the test area, which may not be important in comparison of strong reactions to, for example, detergents, but would have devastating impact on the outcome of a comparison of cosmetic preparations, where only small differences would be expected on normal skin, unless randomization of test sites is built into the study protocol.

It is known that diabetics are prone to develop ulcers difficult or impossible to heal, and therefore some difference in the skin properties might be present even when no clinical signs of ulceration, not even slight erythema, are present. Lindholm-Sethson et al. (1998) found such a difference in the skin between diagnosed diabetics without clinical signs in comparison with a healthy control group, but the difference was hidden behind more pronounced factors, such as age and sex, which were identified using PCA (principal component analysis). It seems that multivariate methods, such as PCA, make better use of the information inherent in electrical impedance spectra than simple indices or lumped parameter models, and that the extracted information sometimes reflects clinically interesting physiological or pathological conditions. In certain cases it might be possible to establish a strong correlation between specific principal components and well-defined physiological or pathological conditions.

To date, most skin studies involving electrical impedance are based on pure surface electrodes. Due to the extreme heterogeneity of the skin, such measurements (at least at low frequencies, as demonstrated in a simulation study by Martinsen et al., 1999), reflect mainly the conditions in the *stratum corneum* and the integrity of its inherent skin barrier. However, only living cells get irritated or sick, and if important information about an alteration in the living strata of skin resides in a relatively low frequency range, such information will be overshadowed or diluted by the intact *stratum corneum*. The dilution factor might be 1:100 or even 1:1000, and strongly frequency dependent! In several skin reactions or diseases, the skin barrier will be more or less destroyed by the chemical assault from the outside (fast event), or by sloppy maintenance of the *stratum corneum* provided by the damaged or sick living epidermis from the inside (slow event), and then surface electrodes would be sufficient. If not, something has to be done about the *stratum corneum*, and a number of methods have been tried, such as aggressive electrode gels (which will add to tissue damage), peeling creams or simply grinding or stripping off the outermost layer. The effect of tape stripping to various degrees of damage on skin impedance is illustrated in a book by Ollmar and Nicander (2005), and shows the

dramatic overshadowing power of the intact *stratum corneum* on properties residing in the living strata of skin.

A new approach toward solving the *stratum corneum* dilemma has been presented by Griss et al. (2001), using electrodes furnished with micromachined conductive spikes, thin enough not to leave any damage after removal and short enough to only short circuit the *stratum corneum* without reaching blood vessels and nerve endings in deeper strata. This concept, originally developed as an improvement of ECG and EEG electrodes, has been further developed by the Ollmar group (Åberg et al., 2003a) to an electrode system intended to facilitate skin cancer detection even when the *stratum corneum* happens to be intact on top of any skin tumor.

For a clinical diagnostic decision support tool, it is not enough to detect an alteration; it must also reliably distinguish disease from other alterations. Key concepts in this context is sensitivity and specificity, as well as receiver operating characteristics (ROC) curves (cf. Section 8.4). In the skin context, reasonable clinical requirements on area under ROC curve have been published by Lee and Claridge (2005). A number of classifiers have been tried on data sets prepared by data decomposition techniques using indices as well as PCA, and using impedance data from both surface electrodes and spiked electrodes, by Åberg et al. (2003b, 2004, 2005). It seems that non-melanoma skin cancers (NMSCs), which are slow growing, degrade the skin barrier enough to make it more conductive and in this case there would be no need for demolition or short-circuiting of the *stratum corneum*, while, for example, malignant melanoma at an early stage the *stratum corneum* can be quite normal (electrically insulating) and in this case the spiked electrodes increase diagnostic power.

Figure 9.25 illustrates a PCA plot of NMSC and other lesions (neither normal skin nor malignant melanoma) using two principal components which in this case describe 84% of the variation in the data set that was obtained with non-invasive probes (without spikes). It is obvious that different ways to cut out the data volume including the cancer lesions would include different amounts of non-cancer data points, and that it is generally impossible to avoid classification of at least some harmless lesions as harmful. The choice of classifier and cut-off levels is a matter of risk assessment, common sense and data characteristics. In the case of malignant melanoma, missing a tumor might be assigned an unacceptable risk (life at stake), and therefore an almost 100% sensitivity required, which would entail a reduced specificity at a given area under ROC curve. In other cases it might be more important with high specificity to avoid painful and costly interventions, because a wrong diagnose is not dangerous and the patient simply could come back if the complaint remains.

An update on this group's latest work on validation of their skin cancer detector in multi center clinical studies can be found in Ollmar et al. (2007).

Subcutaneous fibrosis is a common side effect of radiotherapy given, for example, to women with breast cancer. Nuutinen et al. (1998) measured the relative permittivity of the skin at 300 MHz with an open-ended coaxial probe, and found that the permittivity values were higher in fibrotic skin sites than in normal skin. Based

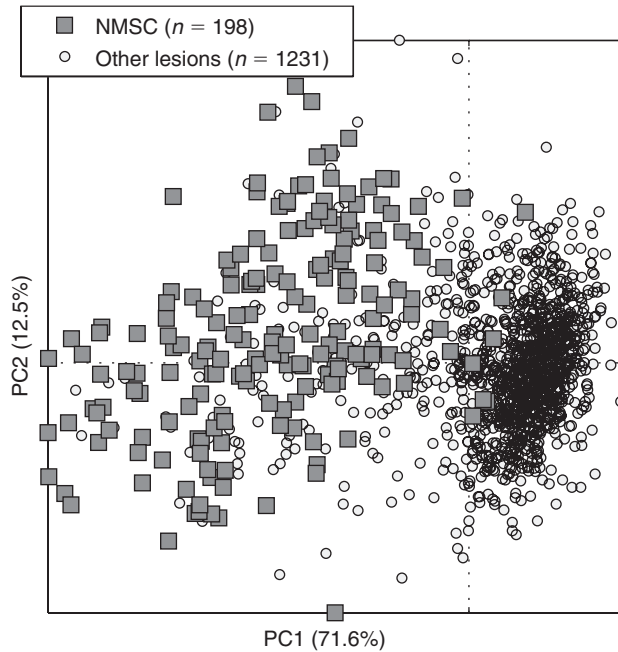


Figure 9.25 PCA plot of NMSC.

on in vitro experiments with protein–water solutions indicating that the slope of the dielectric constant versus the electromagnetic frequency is a measure of the protein concentration, Lahtinen et al. (1999) demonstrated that skin fibrosis can also be measured with the slope technique. Both Nuutinen et al. (1998) and Lahtinen et al. (1999) found a significant correlation between the permittivity parameters and clinical score of subcutaneous fibrosis obtained by palpation. Finally, radiation-induced changes in the dielectric properties were also found in subcutaneous fat by modeling the skin as a three-layer dielectric structure (Alanen et al., 1998).

9.15.4 Electrodermal Response

The sweat activity on palmar and plantar skin sites is very sensitive to psychological stimuli or conditions. One will however usually not be able to perceive these changes in sweat activity as a feeling of changes in skin hydration, except, for example, in stressing situations like speaking to a large audience. The changes are easily detected by means of electrical measurements, however, and since the sweat ducts are predominantly resistive, a low frequency conductance measurement is appropriate (Grimnes, 1982). Electrodermal response (EDR) measurements have during many years been based on DC voltage or current, and accordingly the method has been termed galvanic skin response (GSR).

The measured activity can be characterized as exosomatic or endosomatic. The *exosomatic* measurements are usually conducted as resistance or conductance

measurements at DC or low frequency AC. Resistance and conductance will of course be inverse when using DC excitation, but when AC excitation is used, it is important to remember that resistance generally is part of a series equivalent of a resistor and a capacitor, while conductance is part of a parallel equivalent of these component. In this case it is obvious that resistance and conductance are no longer inverse, as discussed in Section 3.3, and conductance should be preferred to resistance since ionic conduction and polarization basically appear in parallel in biological tissue.

The *endosomatic* measurements are carried out as DC voltage measurements. The mechanisms behind the changes in skin potential during sympathetic activity are not known, but processes like sodium reabsorption across the duct walls and streaming potentials in the sweat ducts should be taken into account. Figure 9.26 shows that the origin of the endosomatic and exosomatic curves is not identical.

The so-called “lie detector” is perhaps the most well-known instrument in which the electrical detection of this activity is utilized. There are, however, several other applications for such measurements, mainly within the two categories; neurological diseases or psycho–physiological measurements. Examples of the first category are neuropathies (from diabetes), nerve lesions, depressions and anxiety. The latter category may include emotional disorders and lie detection. Qiao et al. (1987) developed a method to measure skin potential, skin electrical admittance, skin blood flow and skin temperature simultaneously at the same site of human palmar skin. This was done in order to be able to investigate a broader spectrum of responses to the activity of the efferent sympathetic nerve endings in palmar blood vessels and sweat glands.

Both *evoked* responses (e.g. to light, sound, questions, taking a deep breath) and *spontaneous* activity may be of interest. Measurement of spontaneous EDR is used in areas such as sleep research, the detection of the depth of anesthesia and in sudden infant death syndrome research.

Figure 9.27 shows detection of EDR by means of 88Hz conductance (G) and susceptance (B) measurements (Martinsen et al., 1997a). The measurements were conducted on palmar sites in right and left hand. In Fig. 9.27 both hands show clear conductance waves, but no substantial susceptance waves. No time delay can be seen between the onset of the conductance waves in the two hands, but the almost undetectable susceptance waves appear a few seconds after the changes in conductance. This indicates that these changes have different causes. The rapid conductance change is presumably a sweat duct effect and the slower change in susceptance is most probably due to a resultant increased hydration of the stratum corneum itself. There are no susceptance waves that could indicate any significant capacitance in the sweat ducts.

Venables and Christie (1980) give a detailed suggestion on the analysis of EDR conductance waves based on the calculation of amplitude, latency, rise time and recovery time. They also give extensive statistical data for these parameters in different age groups. As already mentioned several times in this book, the use of absolute values for the electrical properties of tissue is hazardous due to their liability to measurement error and their dependence on, for example, electrode size, gel composition and ambient environment. The use of indexes or other relative parameters

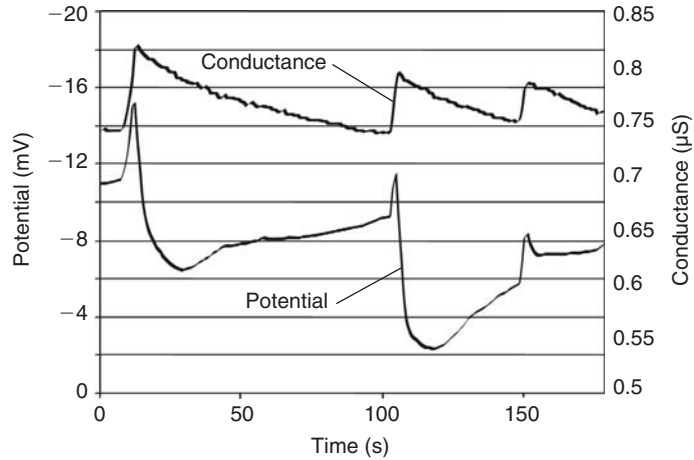


Figure 9.26 Simultaneous registration of exosomatic AC conductance and endosomatic DC voltage. *Source:* Courtesy of Azar Jabbari.

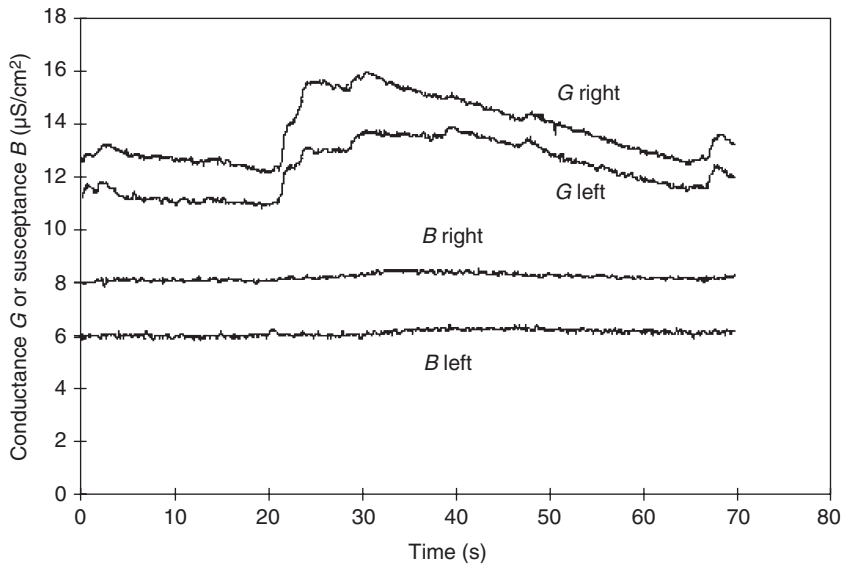


Figure 9.27 Measured 88 Hz admittance GSR activity on palmar skin sites. A deep breath at approximately 20 seconds on the time scale triggered the response.

would presumably prove beneficial also in EDR measurements. Mørkrid and Qiao (1988) analyzed the use of different parameters from the Cole admittance equation in EDR measurements and proposed a method for calculating these parameters from measurements at only two frequencies.

9.15.5 Sweat Measurements

Quantitative assessment of sweat activity is of great importance also for other purposes than the measurement of EDR. Tronstad et al. (2007) have reported on the development of a portable multichannel instrument for long term logging of sweat activity. The instrument is based on conductance measurements and has been developed primarily for the assessment before and after treatment of patients with hyperhidrosis (see Section 9.15.6). Since the instrument is portable it can also be used in sports and during other kinds of physical activities, and with four independent channels it can monitor different body parts simultaneously. Their measurements indicate that the sweat activity of different skin sites behaves differently under physical stress. Hence, such measurements will be valuable for obtaining a better understanding of the physiology controlling thermal sweating.

9.15.6 Iontophoretic Treatment of Hyperhidrosis

Hyperhidrosis is a state of extreme sweat secretion in palmar, plantar or axillary skin sites. The disorder can be treated with drugs (e.g. anticholinergica), tap water iontophoresis or surgical sympathectomy. Tap water iontophoresis has been in use at least since the beginning of this century, and represents a simple, effective, but somewhat painful cure. In its simplest form, the setup used comprises two water filled metal tubs and a DC supply. In case of palmar hyperhidrosis, the hands are placed in the two tubs and a DC current is driven from one hand to the other through the upper body. This treatment has now been stopped in Norway because the current is driven through the heart region. The Drionic is an example of an alternative device for the treatment of palmar hyperhidrosis where this problem is solved. When one hand is placed on the Drionic, half the hand is connected to one electrode through a wet sponge, and the other half to the other electrode through another wet sponge. The current is hence driven locally in the hand, and only one hand is treated at a time.

How tap water iontophoresis can impede excess sweating is still not fully understood. One theory suggests abnormal keratinization in the epidermis as a result of the current being shunted through the sweat ducts, leading to a plugging of the sweat orifices. This plugging cannot be found on micrographies of the skin, however, and a more plausible theory is presumably that the current leads to a reversible destruction of the sweat glands.

9.15.7 Iontophoresis and Transdermal Drug Delivery

The transport of charged substances through the skin was shown early by the famous experiment by Munk (1873). He applied an aqueous solution of strychnine in HCl under two electrodes attached to the skin of a rabbit. Without current flow nothing happened to the rabbit; with application of a DC current for 45 minutes, the rabbit died.

Abramson and Gorin (1939, 1940) found that timothy pollen could be transported into the skin by electrophoresis. They studied the transport of dyes into human skin by electrophoresis. Without the application of electricity, no particular skin marks were seen after the dye had been in contact with the skin for some minutes. With an applied DC current, and after the superfluous dye had been wiped off, small dots were seen corresponding to the pores of the skin. Positively charged methylene blue was transported into the skin under an anode, and negatively charged eosin under a cathode. Some pores were colored with only one of the types.

Iontophoresis of pilocarpine is the classical method for obtaining sweat for the cystic fibrosis test (Gibson and Cooke, 1959). The penetration of pilocarpine in the skin enhances sweat production. The test is usually performed on children with both electrodes placed on the underarm (for safety reasons the current should not pass the thorax). A 0.5% solution of pilocarpine is placed under the positive electrode, and the DC current is slowly increased to a maximum of about 1.5 mA. The iontophoresis time is about 5 minutes.

A skin surface *negative* electrode attracts water from deeper layers, a positive electrode repels water. This is an *electro-osmotic* effect and not iontophoresis (Abramson and Gorin, 1939; Grimnes, 1983b).

The conductivity of human skin is very unevenly distributed. The current pathways have been found to be the pores of the skin, particularly the sweat ducts, only to a small extent through the hair follicles (Abramson and Gorin, 1940; Grimnes, 1984).

Transdermal drug delivery through iontophoresis has received widespread attention. A long term delivery with transdermal DC voltage of <5 V is used (Pliquett and Weaver, 1996). High voltage pulses up to 200 V decaying in about 1 ms have also been used on human skin for enhancement of transport by electroporation (Pliquett and Weaver, 1996). The effect was found to be due to the creation of aqueous pathways in the stratum corneum.

9.16 NON-MEDICAL APPLICATIONS

- Fingerprint detection as described in Section 9.15.1 is a measurement on humans, but not with a medical purpose.
- The monitoring of fermentation processes in beer brewing or pharmaceutical industry is measuring on different sort of cell suspensions.
- Plant tissue is both strongly similar and very different from animal tissue, the cell membranes for instance are quite different.
- Meat quality can be estimated from bioimpedance measurements. See. e.g. Oliver et al., 2001 and Guerro et al., 2004.

In geophysics impedance measurements were used as early as in the 1920s for oil exploration (Schlumberger, 1920). Impedance measurements are also used for monitoring volcanic activity (e.g. on Iceland).

9.17 ELECTRICAL SAFETY

9.17.1 Threshold of Perception

The perception of a current through human skin is dependent on frequency, current density, effective electrode area (EEA) and skin site/condition. Current duration also is a factor, in the case of DC determining the quantity of electricity and thereby the electrolytic effects according to Faraday's law (Section 2.4.1).

DC

If a DC source coupled to two skin surface electrodes is suddenly switched on, a transient sensation may be felt in the skin. The same thing happens when the DC current is switched off. This proves that many nerve endings are only sensitive to *changes* in a stimulus, and not to a *static* stimulus. At the moment a DC is switched on, it is not only a DC, it also contains an AC component. DC must therefore be applied with a slow increase from zero up to the desired level, if the threshold of DC perception is to be examined.

DC causes ion migration (iontophoresis) and cell/charged particle migration (electrophoresis). These charge carriers are depleted or accumulated at the electrodes, or when passing ion-selective membranes in the tissue. In particular, almost every organ in the body are encapsulated in a *macromembrane* of epithelia tissue. There are, for example, three membranes (meninges) around the brain and CNS (pia mater, arachnoidea, dura mater). There are membranes around the abdomen (peritoneum), fetus, heart (pericardium), lungs (pleura), inside the blood vessel (endothelium), around the nerves (myelin, neurolemma in the hand). At some tissue interfaces and at the electrodes the chemical composition will gradually change.

A sensation will start either under one of the electrodes (anode or cathode), or in the tissue between. The chemical reaction at an electrode is dependent on the electrode material and electrolyte, but also on the current level (cf. Sections 2.4 and 8.1). A sensation around threshold current level is slowly developing and may be difficult to discern from other sensations, for example, the mechanical pressure or the cooling effect of the electrode. After the sensation is clear, and the current is slowly reduced to avoid AC excitation, the sensation remains for some time. That proves that the current does not trigger nerve ends directly, but that the sensation is of a chemical, electrolytic nature as described by the law of Faraday. The after current sensation period is dependent on the perfusion of the organ eliciting the sensation.

On palmar skin, with a surface electrode of varying area A , the current I_{th} or current density J_{th} at the threshold of perception follows the following equation for a sensation within 3 minutes after current onset (Martinsen et al., 2004).

$$J_{th} = J_0 A^{-0.83} \quad \text{or} \quad I_{th} = I_0 A^{0.17} \quad (9.16)$$

The perception was only localized under the monopolar electrode, never in the tissue distal to the electrode. Surprisingly, according to eq. (9.16) the threshold as

a function of electrode area A is more dependent on *current* than current density. There may be more than one reason for this:

1. A spatial summation effect in the nervous system. The current *density* is reduced when the same current is spread by a larger electrode, but at the same time a larger number of nerve endings are excited. Consequently the current threshold is not so much altered when electrode area is changed.
2. The DC current is not evenly distributed under a plate electrode (Section 6.3.4), the current density is higher at the edge. The conductance of a surface sphere or plate electrode is proportional to radius or circumference, not to area (eqs 6.1 and 6.9).
3. The DC current is probably concentrated to the sweat ducts and the nerve endings there (Grimnes, 1984).

A practical use of DC perception is the old test of the condition of a battery by placing the poles at the tongue. This test is actually also done clinically: *electrogustometry* is the testing of the sense of taste by applying a DC to the tongue.

Sine Waves

The lowest level ($<1\ \mu\text{A}$) of 50/60 Hz perception is caused by *electrovibration* (Grimnes, 1983d; Fig. 9.28). It is perceived when the current carrying conductor slides on dry skin. Dry skin is a poor conductor, so that potential differences of several tenths of volts may exist across the dielectric which is the stratum corneum of the epidermis. With dry skin only a small microampere current flows. The electric field sets up an electrostatic compression force in the dielectric, pressing the stratum corneum to the metal plate. In the stratum corneum there are no nerve endings, and consequently no perception. However, if the skin is made to slide along the metal, the frictional force will be modulated by the electrostatic force and be felt as a lateral mechanical vibration synchronous with the double frequency of the AC voltage. Even if the voltage across the dielectric is $>20\text{V}$ at threshold, the corresponding (mainly capacitive) current may be $<1\ \mu\text{A}$. If the skin is at rest, or if the skin is wet, no sensation is felt.

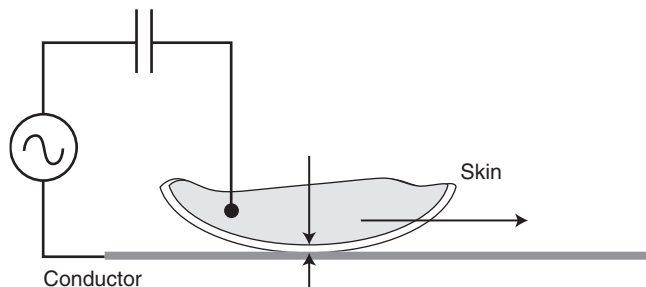


Figure 9.28 Electrovibration perception mechanism.

The second level (1 mA) is due to the *direct electric excitation* of nerve endings, which must be a function of the local current (density). The electric current threshold of perception with firm hand grip contact and contact area several square centimeters, is around 1 mA. Threshold current has a surprisingly small dependence on contact area. The reason for this is mentioned above in the chapter on DC perception. With a small area contact around 1 mm^2 , the threshold of perception is around 0.1 mA, corresponding to 100 A/m^2 .

Interpersonal variations and the dependence on age and sex are small. Skin condition is not important as long as there are no wounds. Skin site may be important. On the fingertips the density of nerve ending is large, but the stratum corneum is thick and the current will be rather uniformly distributed. Other skin sites may have much thinner skin and lower density of nerve endings, but conductive sweat ducts that canalize the current.

Frequency Dependence

For sine waves the maximum sensitivity of our nervous system is roughly in the range 10–1000 Hz (cf. also Fig. 9.31). At lower frequencies each cycle begins to be discernible, and during each cycle it may be charge enough to give electrolytic effects. At frequencies $>1000\text{ Hz}$ the sensitivity is strongly reduced, and at $>100\text{ kHz}$ no perception remains, because the levels are so high that electric stimulation is shadowed by the heat effect of the current. That is the frequency range for electrosurgery.

A single pulse or a repetitive square wave may give both DC and AC effects. In both cases the duration of the pulse or square wave is an important variable (cf. rheobase and chronotaxi).

The exponential decaying discharge waveform is the case of electrostatic discharges (see below).

Electrostatic Discharge Pulse

The perception of an electrostatic discharge is an annoyance, and in some situations a hazard. It is particularly troublesome indoors during the winter with low relative humidity (RH). Low RH reduces the conductivity of most dielectrics (e.g. the stratum corneum, cf. Section 4.2.6) and also the conductivity of clothing, construction materials, tree, concrete, etc. A person may be charged up to more than 30 kV under such circumstances, and with a body capacitance to the room (ground) of about 300 pF, the electrical energy of the person is of the order of 0.1 J. A smaller discharge, near the threshold of perception, is typically with a time constant of a few μs , and the peak current around 100 mA (Fig. 9.29). It is obtained by discharging a capacitor of 100 pF charged to 1.4 kV. The point electrode is approached to the skin until an arc is formed, heard and perceived in the skin.

The maximum current is determined by the voltage drop in the arc (probably less than 100 V) and the resistance in the skin. The arc probably has a very small cross-sectional area, so most of the resistance is in the proximal zone in the stratum corneum. The current density is probably far out in the non-linear breakdown region of

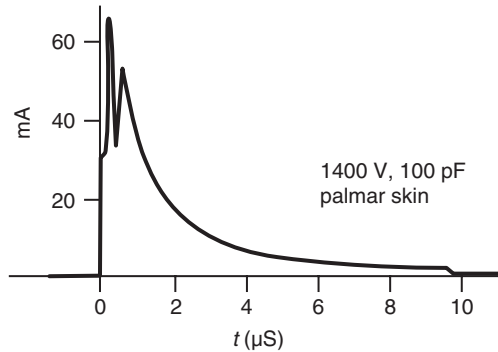


Figure 9.29 Capacitor discharge current flow through palmar skin. Monopolar electrode: 1.3 mm diameter pin of steel, sharpened at the tip. Indifferent electrode on the underarm.

the skin, but because of the short pulse duration the impedance is presumably also determined by the capacitive properties of stratum corneum. A rough calculation based on eqs 5–9 with $\sigma = 0.1 \text{ S/m}$ and calculated resistance from measured current maximum: $20 \text{ k}\Omega$, gives the arc contact diameter with the skin: $2a = 200 \mu\text{m}$.

The charge transferred around threshold level is of the order of 0.2 C . The threshold of perception as a function of stored energy is about $10 \mu\text{J}$. The formation of an arc in the air between the conductor and the skin is possible when the voltage difference is larger than about 400 V . The arc discharge can be heard as a click and felt as a prick in the skin.

9.17.2 Electrical Hazards

Electromagnetic Field Effects

Coupling without galvanic tissue contact is covered in Section 7.4.8. However, electromagnetic hazards are outside the scope of this book. There is a vast amount of experimental data on this subject, and the interested reader is recommended the CRC handbook (Polk and Postow, 1986).

Continuous Current

The risk of sudden death is related to stimulating the cells of three vital organs of the body: the heart, the lungs and the brain stem. Involuntary movements may indirectly lead to sudden deaths (loss of balance, falling). Heat and electrochemical effects may also be fatal by inducing injuries that develop during hours and days after the injury. In electrical injuries the question often arises as to whether the current is evenly distributed in the tissue, or follows certain high-conductance paths. Current marks and tissue destruction often reveal an uneven current distribution (cf. Uglund, 1967).

The current path is important, and organs without current flow are only indirectly affected: to be directly dangerous for the healthy heart, the current must pass the heart region.

Cell, Nerve and Muscle Excitation

Heat effects are certainly related to current density in volume conductors, but this is not necessarily so for nerve and muscle excitation. Excitation under a plate electrode on the skin is more highly correlated to current than current density (cf. Section 9.17.1). The stimulus summation in the nerve system may reduce the current density dependence if the same current is spread out over a larger volume of the same organ. Therefore, and for practical reasons, safe and hazard levels are more often quoted as current, energy or quantity of current in the external circuit, and not current density in the tissue concerned.

Macro/microshock

A *macroshock* situation is when current is applied to tissue far from the organ of interest, usually the heart. The current is then spread out more or less uniformly, and rather large currents are needed in the external circuit (usually quoted $>50\text{ mA @ }50/60\text{ Hz}$) in order to attain dangerous levels (Fig. 9.30).

The heart and the brain stem are particularly sensitive for small areas of high current density. Small area contacts occur, for example, with pacemaker electrodes, catheter electrodes and current carrying fluid-filled cardiac catheters. Small area contact implies a monopolar system with possible high local current densities at *low current levels* in the external circuit. This is called a *microshock* situation. The

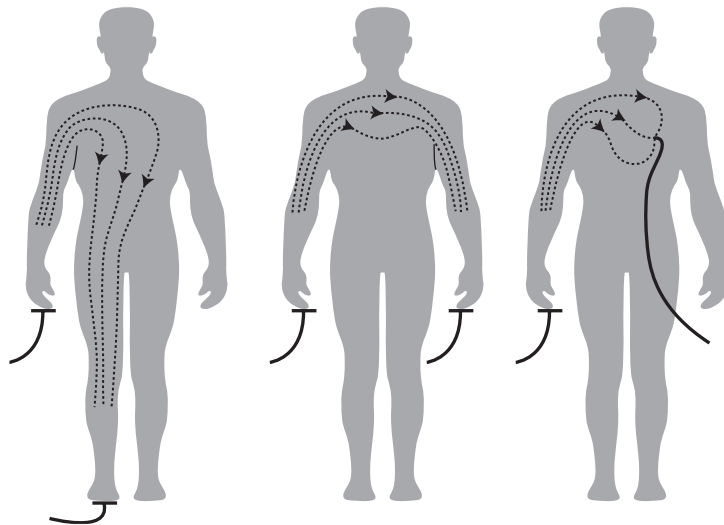


Figure 9.30 Macroshock (left) and microshock (right) situations.

internationally accepted 50/60Hz safety current limit for an applied part to the heart is therefore $10\mu\text{A}$ in normal mode, and $50\mu\text{A}$ under single fault condition (e.g. if the patient by insulation defects is in contact with mains voltage). The difference between macro- and microshock safety current levels is therefore more than three decades.

The heart is most vulnerable for an electric shock in the repolarization interval, that is in the T-wave of the ECG waveform. Therefore the probability of current passage during the approximate 100 ms duration of the T-wave is important. If the current lasts more than one heart cycle, the T-wave is certainly touched. For short current durations <1 seconds, the risk of heart stop is determined by the chance of coincidence with the T-wave.

Let-Go Current

Let-go current threshold ($15\text{ mA @ }50/60\text{ Hz}$) is the current level when the current density in muscles and nerves is so large that the external current controls the muscles. As the grip muscles are stronger than the opening muscles of the hand, a grip around the current carrying conductor cannot be loosened by the person himself. Let-go current levels are therefore the most important data for safety analysis. The result in Fig. 9.31 shows that 1% of the population have a let-go threshold as low as 9 mA at power line frequencies.

Fatal levels are reached at current levels $>50\text{ mA @ }50/60\text{ Hz}$ if the current path is through vital organs: heart, lung or brain stem (cf. the electric chair, Table 9.2).

Heat Effects

Jouleian heat is dependent on the in-phase components of potential difference and current density. The resulting temperature rise is dependent on the power density, the specific heat of the tissue and the cooling effect of the blood perfusion (cf. eq. 6.8).

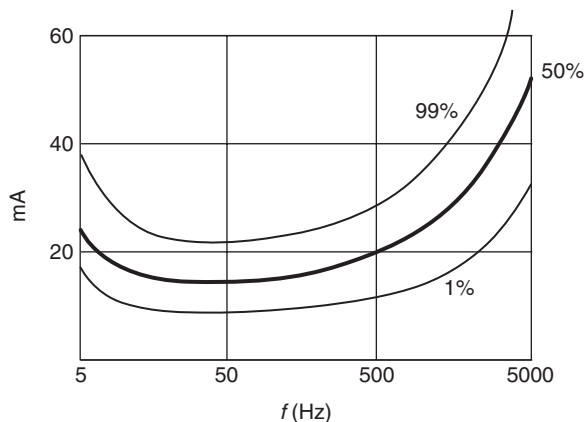


Figure 9.31 Frequency dependence of let-go currents. Statistic for 134 men and 28 women. Source: From Dalziel (1972).

The tissue damage is very dependent on exposure time, cells can tolerate long time exposure of 43°C. Above about 45°C, the time duration becomes more and more critical. In high voltage accidents the heat effect may be very important, and patients are treated as thermal burn patients. In particular, special attention is paid to the fluid balance, because electrical burn patients tend to go into renal failure more readily than thermal burns of equal severity. As electric current disposes thermal energy directly into the tissue, the electric burn is often deeper than a thermal burn caused by thermal energy penetrating from the surface. The general experience is therefore that an electrical burn is more severe than it may look like the first hours after the injury.

Electrolytic Effects

Electrolytic effects are related to DC, applied or rectified by non-linear effects at the electrodes or in the tissue. Also with very low frequency AC (e.g. <10Hz), each half period may last so long as to cause considerable non-reversible electrolytic effects. With large quantities of electricity ($Q = It$) passed, the *electrolytic* effects may be systemic and dangerous (lightning and high voltage accidents). The risk of skin chemical burns is greater under the cathode (alkali formation) than the anode (acid formation), the natural skin pH is on the acidic side (pH < 5.5).

Nerve damage is often reported in high voltage accidents.

Current Limiting Body Resistance

The most important current limiting resistance of the human body is the dry skin. This may be impaired by high-field electrical breakdown, skin moisturizing or a skin wound. Skin breakdown may occur under 10V AC 50/60Hz due to electro-osmotic breakdown (Grimnes, 1983b).

Without the protective action of the skin, the *internal body resistance* may be divided into a *constrictional zone resistance* with increased current density near an electrode, and *segmental resistances* of each body segment with rather uniform current density. With small area electrode contact the constrictional zone resistance will dominate (cf. Section 6.3.2). The segmental resistance may be estimated from the equation $R_{sr} = L/\sigma A$. With constant σ the segmental resistance depends on the ratio L/A , and accordingly varies according to body or limb size.

Table of Threshold Values

From the threshold current levels, the corresponding voltages are found by estimating the minimum current limiting resistance. These worst case minima are found by assuming no protective action from the skin at all, only from the volume resistance of the living parts of the body. The levels are summarized in Table 9.2.

The question of current canalizing effects in tissue is one of the issues of our field. It is well known that the myelin sheet around the nerves serves electrical insulation and current canalization to the Ranvier nodes. But the extent of current canalization in many parts of the body is largely unknown. The blood has a high conductivity, but what are the electrical properties of the endothelium? Does

TABLE 9.2 50/60 Hz Threshold Levels of Perception and Hazard

Current threshold	Voltage threshold (very approximate)	Organs affected	Type	Comments
0.3 μ A	20 V	Skin	Perception threshold	Electrovibration, mechanical
10 μ A	20 mV	Heart	Microshock hazard	Myocard excitation
1 mA	10 V	Skin	Perception threshold	Nerve excitation
15 mA	50 V	Muscles	Let-go	Loss of muscle control
50 mA	250 V	Heart, lung, brain stem	Macroshock hazard	Nerve excitation

TABLE 9.3 Electric Charge Values (Microcoulomb) for Single Monophasic Pulses Through the Chest

	μ C
TENS threshold	3
TENS, max	7
Safe level	20
Hazard threshold	75
Heart pacing	100

electrosurgery current follow the bile duct? The current through skin is canalized through the sweat ducts. The high acid concentration in the stomach must have high electrical conductivity.

Single Pulses

Trigger and safety levels have been examined by Zoll and Linenthal (1964) for external pacing of the heart. For TENS (transcutaneous electrical nerve stimulation) single monophasic pulses of duration <1 ms FDA have set up the following values for the electric charge through the thorax (Table 9.3).

9.17.3 Lightning and Electrocutation

Lightning

An average lightning stroke may have a rise time of 3μ s and duration of 30μ s, energy dissipated 10^5 J/m, length 3 km, peak current 50 000 A, power 10^{13} W. After the main stroke there are continuing currents of typically 100 A and 200 ms duration.

The mechanical hazards are due to the pressure rise in the lightning channel. The energy per meter is equivalent to about 22 g of TNT per meter. A direct hit

from the main stroke is usually lethal, but often the current path is via a tree, the ground (current path from foot to foot, current through tissue determined by the *step voltage*), or from a part of the house or building. The current path is of vital importance, for humans a current from foot to foot does not pass vital organs, for a cow it may do.

It is believed that there are around 500 deaths caused by lightning per year in the USA.

Electrocution

The current path in an electric chair is from a scalp electrode to a calf electrode. The current is therefore passing the brain and the brain stem, the lung and the heart. It is believed that the person gets unconscious immediately after current onset, but it is well known that death is not immediate. The electric chair was used for the first time in 1890, and the first jolt was with 1400 V 60 Hz applied for 17 seconds, which proved insufficient. At present a voltage of about 2000 V applied for 30 seconds is common, followed by a lower voltage, for example, a minute. The initial 60 Hz AC current is about 5 A, and the total circuit resistance is therefore around 400 Ω . The power is around 10 kW and the temperature rise in the body, particularly in the regions of highest current densities in the head, neck and leg region, must be substantial. Because of the cranium the current distribution in the head may be very non-uniform. Temperature rise is proportional to time and the *square* of current density according to eq. 6.8, so there are probably local high temperature zones in the head.

The scalp electrode is a concave metal device with a diameter about 7 cm and an area of about 30 cm². A sponge soaked with saline is used as contact medium.

9.17.4 Electric Fence

The electric fence is used to control animals and livestock. There are two types of controllers: one type delivers a continuous controlled AC current of about 5 mA. The other delivers a capacitive discharge, like the working principle of a defibrillator. The repetitive frequency is around 1 Hz, and the capacitor is charged to a DC voltage up to 10 kV. The large voltage secures that the chock will pass the animals hair-covered skin. The chock is similar to an electrostatic discharge, even if the electric fence shock energy is higher and the duration longer. The capacitor is charged to an energy typically in the range 0.25–10 J.

9.17.5 Electrical Safety of Electromedical Equipment

Special safety precautions are taken for electromedical equipment. Both patient and operator safety is considered (as well as damage of property). *Electromedical equipment* is equipment which is situated in the patient environment and is in physical contact with the patient, or which can deliver energy (electrical, mechanical or

radiation) to the patient from a distance. Equipment for in vitro diagnosis is also important for patient safety with respect to correct diagnostic answers, but as long as it is not in the patient environment the safety aspects are different.

The basis for the national or international standards (IEC, UL, VDE, MDD (the European Medical Device Directive), etc.) is to reduce the risk of hazardous currents reaching the patient under normal conditions. Even under a *single fault condition* patient safety shall be secured.

The part of the equipment in physical contact with the patient is called the *applied part*. It may ground the patient (type B applied part), or keep the patient floating with respect to ground (BF – body floating, or CF – cardiac floating) by *galvanic separation* circuitry (magnetic or optical coupling, battery-operated equipment). In most situations higher safety is obtained by keeping the patient floating. If the patient by accident comes in contact with a live conductor the whole patient will be live, but *little current* will flow.

Figure 9.31 shows the most important parts of an electromedical device. The power line and earth connection are shown to the right. The signal connections to the outside world are shown at the upper part. Important safety aspects are linked with these signal input and output parts: they may be connected to recorders, printers, dataloggers, data networks, coaxial video cables, synchronization devices, etc. These devices may be remotely situated and outside the electrical control of the patient room. With a floating applied part hazardous currents from the outside do not reach the patient, the galvanic separation protects both ways.

The device may be grounded for safety reasons (safety class I, as shown in Fig. 9.32, maximum resistance in the *protective earth* (PE) conductor between power plug and chassis $0.2\ \Omega$), or double insulated (safety class II).

Leakage currents are currents at power line frequency (50 or 60 Hz), they may be due to capacitive currents even with perfect insulation, and are thus difficult to avoid completely. *Patient leakage currents* are the leakage currents flowing to the patient via the applied part. *Patient auxiliary currents* are the functional currents flowing *between* leads of the applied part (e.g. for bioimpedance measurement). They are not leakage currents and therefore usually not at power line frequency. *Earth leakage current* is the current through the ground wire in the power line cord

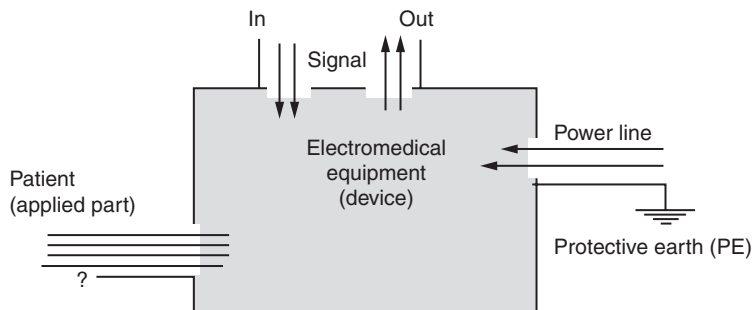


Figure 9.32 Basic parts of a grounded (class I) electromedical device.

TABLE 9.4 Allowable Values of Continuous Leakage and Patient Auxiliary Currents (μA) According to IEC-60601 (N.C. = normal conditions)

Currents	Type B		Type BF		Type CF		
	N.C.	Single fault	N.C.	Single fault	N.C.	Single fault	
Earth leakage	500	1000	500	1000	500	1000	Higher values, for example, stationary equipment
Patient leakage	100	500	100	500	10	50	
Patient leakage				5000		50	Mains on applied part
Patient leakage		5000					Mains on signal part
Patient auxiliary	100	500	100	500	10	50	AC
Patient auxiliary	10	50	10	50	10	50	DC

(not applicable for double insulated devices). According to IEC it shall be $<500\ \mu\text{A}$ during normal conditions for all types B, BF or CF (Table 8.2). *Enclosure leakage current* is a possible current from a conductive accessible part of the device to earth. Grounded small devices have zero enclosure current during normal conditions, but if the ground wire is broken the enclosure leakage current is equal to the earth leakage current found under normal conditions.

The current limits according to IEC-60601-1 (2005) is shown in Table 9.4.

The insulation level is also specified. It is defined both in kV, creepage distances and air clearances in millimeters. Important additional specifications are related to maximum exposed surface temperature, protection against water penetration (drop/splash proof), cleaning–disinfection–sterilization procedures, technical and users documentation.

A non-medical device such as a PC may be situated within a patient environment (instrument B in Fig. 9.33), but in itself it must not have an applied part. An electromedical device (instrument A) must be inserted between the B and the patient. The connection between A and B is via the signal input/output of device A. If the instrument B has higher earth leakage current than $500\ \mu\text{A}$, an insulation power line transformer or extra ground must be provided. The reason for this is that a person can transfer the enclosure leakage current by touching the enclosure of B and the patient simultaneously. During the single fault condition of a broken ground wire to B, the earth leakage current of B may then be transferred to the patient. This would not happen with the interconnected signal ground wires as shown in Fig. 9.33, but could happen if A and B were in the same rack with one common power cord.

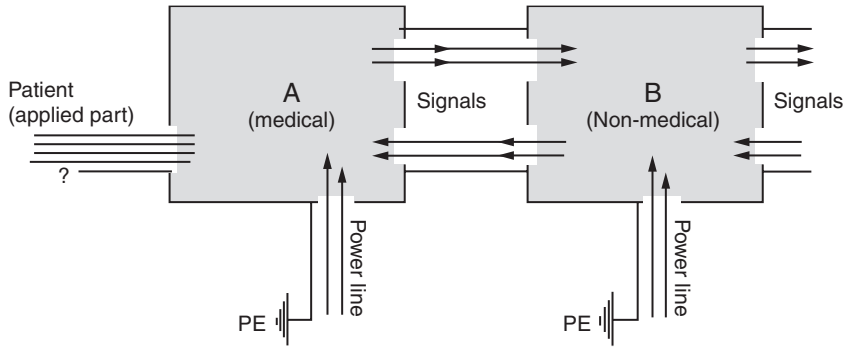


Figure 9.33 A non-electromedical device (B) within the patient environment. *Source:* From IEC-60601-1 (2005).

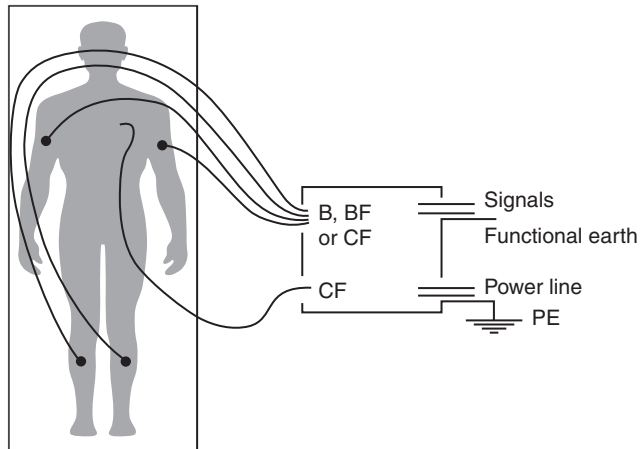


Figure 9.34 Electromedical equipment with two applied parts.

An electromedical device may have more than one applied part (Fig. 9.34). The producer must basically declare the intended use of his equipment. If an applied part is intended to be used in direct connection with the heart, it must be of type CF. The same instrument may have another applied part intended to be used with skin surface electrodes or sensors. That applied part may be of type B, BF or CF. A plug in the instrument may be marked with type B, but a box with a galvanic separation may be inserted in the cable so that the applied part is converted from type B to BF or CF.

This page intentionally left blank

10 HISTORY OF BIOIMPEDANCE AND BIOELECTRICITY

We may imagine that the first sensory experience with electricity was electrostatic discharges by rubbing. Magnetic stones have also been known very early, and the Arabs are believed to have used such a stone floating as a compass around 700. *Leonardo da Vinci* experimented with lodestone and iron, and knew that the forces penetrated a wood wall. *William Gilbert*¹ was the first scientist devoting a whole book exclusively to electromagnetism: “*De Magnete*” in the year 1600, written in Latin. The book is actually considered to be the first real scientific work published in England. Gilbert was the first to use the word “electricity”; to distinguish between static electricity and magnetism and to consider the earth as a giant magnet. Bioelectricity was not mentioned.

A device generating static electricity was first made by *Otto von Guericke* in 1663. He used a rotating sphere of sulfur. A more efficient machine with a rotating glass sphere was invented by *Francis Hauksbee* in 1704. He also experimented with evacuated glass bottles and observed the light generated in high electric fields. By 1740 electrostatic machines with a rotating glass disc had become popular and in widespread use in Europe. In 1745 a new cheap and convenient source of static electricity was invented: the low loss, high voltage capacitor in the form of the Leyden jar. It was a glass bottle with a metal foil on the outside and a conductor at the inside. Not surprisingly, the ability of storing electricity in a jar which can be “filled” and “emptied” made people think of electricity as a fluid. The Leyden jar spread very rapidly in Europe and America.

*Benjamin Franklin*² had an electrostatic machine in Philadelphia, and in the winter of 1746–1747 he began to investigate electrical phenomena. He suggested an experiment

¹William Gilbert (1544–1603), British physician/physicist/natural philosopher at the court of queen Elisabeth I.

²Benjamin Franklin (1706–1790), an American printer and publisher, author, inventor and scientist, diplomat and a religious protestant. Made several stays in London and Paris.

to prove the identity of lightning, but this was first carried out in France. He is believed to have tried the dangerous experiment of flying a kite in a thunderstorm. In 1763 professor Richman in St. Petersburg was killed by such an experiment. He is believed to be the first victim of experimenting with electricity. Franklin and his associates concluded early that the corona discharge “Electrical Fire” or “St. Elmo’s fire” was a discharge that equalized bodies with an excess and deficiency of “electrical fire.” Franklin introduced the concept of positive and negative electricity. He suggested that buildings could be protected from lightning by erecting pointed iron rods. The term *Franklin currents* means currents of electrostatic origin and is named after him. His papers were collected in 1751 in the book “Experiments and Observations on Electricity,” soon translated into French (1752), German (1758) and Italian (1774).

The French abbot *Jean-Antoine Nollet*³ was interested in bioelectric phenomena and made use of electrostatic machines and Leyden jars for electrotherapy. His book “Lettre sur l’électricité” was published in Paris in 1753, and in it he referred to Franklin’s work. It is said that under the French king Louis XV (king from 1715 to 1774) the whole court “se fait electricer.”

All these experiments were carried out with static electricity. The history of continuously flowing electricity started with bioelectricity, and in particular with *Luigi Galvani* (1737–1798) at the university of Bologna. On November 6, 1780 he discovered that while an assistant was touching the sciatic nerve of a frog with a metal scalpel, the frog’s muscle moved when he drew electric arcs on a nearby electrostatic machine (Galvani’s first experiment, performed in his home). Galvani’s frogs were placed on iron gratings, and he used bronze hooks to move them. He then discovered that the muscle twisted at the mere touch of the hook to the spinal cord. This is known as Galvani’s second experiment. His explanation based on “animal electricity” was challenged by Volta, leading to the famous Galvani–Volta controversy. Galvani was a physician (obstetrician) and a natural philosopher, and he also examined the organs of electric fishes. Many expressions reveal this historical origin, we speak of *galvanism*, *galvanic current* (=DC) and galvanic separation, in modern terms galvanic means related to DC current. A *galvanostat* is a DC constant current source, and a *galvanometer* a DC current meter.

It was *Alessandro Volta* (1745–1825), professor in physics at Como (later in Pavia and then Padua), who found the correct explanation of Galvani’s second experiment: Galvani actually experimented with DC created by different metals in contact with the same electrolyte, the animal’s own body fluids. He used the frog muscle both as a part of a battery, and as the first ammeter! The concept of animal electricity was abandoned, but reappeared later under the term animal magnetism, meaning

³L’Abbé Nollet was a member of the l’Académie Royale des Sciences in Paris, the Royal Society in London and the Institute of Bologna, professor at the College of Navarra, and “Maitre de Physique” for the Dauphin. His favorite public experiment was to discharge a Leyden jar through many series-coupled persons. On one occasion he did it in front of King Louis XV with a chain of 180 Royal Guards, on another through a row of Carthusian monks *more than a kilometer long*. At the discharge, the white-robed monks reportedly leapt simultaneously into the air. He also discovered the osmotic pressure across semipermeable membranes.

hypnosis (mesmerism). He invented the new source of continuous electricity, the Volta battery.⁴

The work of *Michael Faraday* was important both in electrochemistry and for the discovery of magnetic induction. He was also interested in bioelectricity. On his European round tour he passed Genoa in 1813, where he studied the electrical discharge from the torpedo fish. In 1820 *Hans Christian Ørsted* published his discovery of the relationship between flowing electricity and magnetism. It was presented in Latin, but within the same year it was translated into French, Italian, German, English and Danish. In 1831 Faraday invented the induction coil, which became very important for bioelectric research and practical use. *Faraday stimulation* means stimulation with high voltage/current pulses, faradic current. The induction coil was further developed by *Nikola Tesla*, who discharged a capacitor through a coil with just a few windings, air coupled to a secondary coil of several hundred windings. Tesla currents were therefore high voltage damped oscillating pulses in the lower MHz range.

Parallel with the discovery of new sources of electricity, the *detection* of small bioelectric currents became possible. Soon after Ørsted's discovery in 1820 the first *galvanometers* appeared. The problem was two-fold: to increase sensitivity and to make them follow the rapid changes of muscle and nerve currents. *Carlo Matteucci* measured muscle current impulses in 1838, and in 1843 *Du Bois-Raymond* measured the current impulse from a frog nerve. He also studied fishes that are capable of generating electrical currents. He created the field of scientific electrophysiology, his book *Untersuchungen über die Tierischer Elektrizität* in 1848 was a very early work.

Richard Caton registered currents from the brain (early form of EEG) in 1875. The problem of registering the activity of the heart was more difficult because the galvanometers of the time were not sufficiently quick. *August Waller* recorded the human ECG in 1887 with the capillary electrometer (a voltage reading device), but the QRS complex was highly distorted because of too slow response. *Willem Einthoven* presented a new sensitive and quick quartz *string galvanometer* in 1903, and with this device he registered more correct ECG curves.

Hermann von Helmholtz measured the conduction velocity of a nerve cell axon around 1850. He formulated the very basic theorems of superposition and reciprocity, and also some very important laws of acoustics. *Hermann Müller* in Königsberg/Zürich during the 1870s found the capacitive properties of tissue and the anisotropy of muscle conductance, based also on AC measurements. Based on Faraday's work, *James Clerk Maxwell* published his famous equations in 1873. He more specifically calculated the resistance of a homogeneous suspension of uniform spheres (also coated, two-phase spheres) as a function of the volume concentration of the spheres. This is the basic mathematical model for cell suspensions and tissues still used today. In 1891, the first electrotherapeutic congress was held in Frankfurt am Main. Around 1900 it was well known that large high frequency currents of more

⁴In 1801 Volta demonstrated his battery in Paris before Napoleon, who made Volta a count and senator of the kingdom of Lombardy.

than 1 A could pass the human body with only heat sensation, *Arsène d'Arsonval* (1893), but that small low frequency currents excited the nerves without heat effects.

The study of bioelectricity before 1900 can be divided into five periods according to the sources of electricity available:

- Continuous static electricity from 1663 – *von Guericke's* electrostatic device (high voltage)
- Static electricity discharge from 1745 – the *Leyden jar* (high voltage)
- Continuous DC current from 1800 – *Volta* electrochemical battery (low voltage, high current)
- High voltage/current pulses from 1831 – *Faraday's* induction coil
- Continuous AC current from 1867 – *Werner von Siemens's* rotating dynamo (high power)

These were the giants of the last centuries. We call them giants also because their influence was of a very general and deep nature, and the whole society was somewhat aware of their achievements. The nineteenth century was important for a broad understanding of some of the chemical and physical processes behind bioelectricity. In the twentieth century the specialization has gradually increased. The achievements are more specialized with a more narrow impact, not so well known to the “public at large.” On the other hand, the *technology*, in the basic sense of the word: the know-how about how to construct devices and have them produced and marketed, they all belong to the twentieth century. These products and their importance for new medical procedures can be seen by everyone. The bringing of medical instrumentation to the marketplace started with the X-ray machine and ECG at the beginning of the twentieth century, electrosurgery and diathermy equipment appeared in the 1930s, the EEG in the 1940s, the pacemaker and the defibrillator in the 1960s.

Rudolf Hoerber discovered the frequency dependence of conductivity of blood, and postulated the existence of cell membranes (1911). *Philippson* in 1921 measured tissue impedance as a function of frequency, and found that the capacitance varied approximately as the inverse square root of the frequency. He called this a polarization capacitance similar to that found for the metal–electrolyte interphase. In the late 1920s *Gildemeister* found the constant phase character of tissue, and *Herman Rein* found electro-osmotic effects.

Kenneth S. Cole (1928a and 1928b papers)

It was the Cole brothers who paved the way for an analytical, mathematical treatment of tissue immittivity and permittivity. K.S. Cole worked for a period in Debye's laboratory. In the theoretical part (1928a) he *calculated* the impedance of a suspension of spheres, where each sphere was coated with a layer having capacitive properties. He found expressions for the impedance at DC and infinite frequency (r_0 and r_∞ , both purely resistive). He introduced a constant phase element (CPE, defined in the paper by the phase angle $\phi_3 = \text{arccotan}(m)$, and $m = r_3/x_3$,

accordingly using m completely differently from Fricke: ideal resistor has $m = \infty$ and $\phi_3 = 0^\circ$), and found as impedance locus for such a system a circular arc with the center below the real axis in the Wessel diagram. A *plot of complex immittance or immittivity in the Wessel diagram with the purpose of searching for circular arcs may according to this paper be called a Cole-plot*.

He discussed the three-component electric equivalent circuit with two resistors (one ideal, lumped, physically realizable electronic component, one frequency dependent not realizable) and a capacitor (frequency dependent) in two different configurations. He discussed his model first as a descriptive model, but later discussed Philippon's explanatory interpretation (extra/intracellular liquids and cell membranes).

In the experimental paper (1928b) he presented the measuring cell and tube oscillator used, and the results obtained with a suspension of small eggs. The results were in accordance with the theory outlined in (1928a).

Peter Debye (1929 book)

In Debye's classical book "Polar Molecules" he regarded molecules as spheres in a continuous medium having a macroscopic viscosity. The model was particularly based on gases and dilute solutions of polar liquids. From the model he deduced the equation:

$$\varepsilon^* - \varepsilon_\infty = \frac{\varepsilon_0 - \varepsilon_\infty}{1 + j\omega\tau_0} \quad \text{The Debye equation} \quad (10.1)$$

where ε^* is the complex permittivity.

Debye's work was not centered on biological materials, it was hardly known at the time that many large organic molecules are strongly polar.

Hugo Fricke (1932 paper)

Hugo Fricke showed that, for example, the electrode polarization capacitance often varies as f^m (in this book written⁵ as f^{m-1}), and that there is a basic empirical relationship between the exponent m and the phase angle of the electrode polarization impedance (Fricke's law): $\varphi = (1 - m)90^\circ$ (in this book $\varphi = m90^\circ$). He found that the frequency exponent m usually is frequency dependent, accordingly Fricke's law does not necessarily imply a CPE. However, for certain electrodes m is frequency independent over an extended frequency range. Such a CPE we may call a Fricke CPE. Fricke did not use circular analysis in the Wessel plane. He laid the basis for the Maxwell-Wagner dispersion model.

The ideal capacitor has (Fricke's symbols) $m = 0$ and $\varphi = 90^\circ$, ideal resistor $m = 1$ and $\varphi = 0^\circ$. His model was a purely descriptive model.

⁵The use of phase angles, loss angles and the parameters m and α has been very confusing since the days of Cole and Fricke. This book is based on the following philosophy: The use of the phase angle coefficient α follows the Cole equations, and the frequency exponent m must then be defined according to $\varphi = m\pi/2$. The frequency dependence of a capacitance is then $C = C_1 f^{m-1}$, $0 \leq m \leq 1$, according to Eq. (8.24).

Kenneth S. Cole (1932 paper)

Kenneth S. Cole repeated the presentation from 1928, but now with a quasi-four-element equivalent circuit with two static resistors, his z_3 is a CPE. *His model implies that the two resistors are not a part of the polarization process.* This is explicitly stated in Cole (1934). He did not discuss a microanatomical, or relaxation theory explanatory model. He pointed out that different equivalent circuits may equally well mimic measured data, all are possible descriptive models. He did point out the similarity between data from tissue/cell suspensions and polarization on metal–electrolyte interphases.

Kenneth S. Cole (1940 paper)

This is an important and original paper. Here the famous Cole equation was presented in this way:

$$z = z_\infty + \frac{r_0 - r_\infty}{1 + (j\omega\tau)^\alpha} \quad (10.2)$$

For the first time there was a mathematical expression for the *impedance* dispersion corresponding to the circular arc found experimentally. The equation introduced a new parameter: the somewhat enigmatic constant α . He interpreted the α as a measure of *molecular interactions*, with no interactions $\alpha = 1$ (ideal capacitor). Comparison was made with the impedance of a semiconductor diode junction (selenium barrier layer photocell). It is logical and has become common practice to replace z_∞ with r_∞ .

In fact the Cole–Cole (1941) permittivity equation (see below) was shortly introduced already in this paper (“in manuscript”).

Kenneth S. Cole and Robert H. Cole (1941 paper)

Here the famous Cole–Cole equation was presented. The emphasis was turned from impedance to permittivity. The two brothers did not link the paper to biological data (with the exception of two references), it is a general paper about dielectrics. It was the first paper by Kenneth S. Cole where the concepts of dielectrics, Debye- and relaxation-theory and dispersion are used. The Cole–Cole equation was presented as:

$$\varepsilon^* - \varepsilon_\infty = \frac{\varepsilon_0 - \varepsilon_\infty}{1 + (j\omega\tau_0)^{1-\alpha}} \quad (10.3)$$

where ε^* is the complex permittivity.

As a permittivity equation they used $1-\alpha$, not α , as exponent. The equation was derived from the Debye equation simply by analogy, based on the overwhelming amount of experimental data for all sorts of dielectrics giving impedance loci of *arcs* of depressed circles (and not complete Debye half circles) in the Wessel diagram.

It is an empirical, purely descriptive equation, with no direct explanatory power. The problem with the Cole–Cole equation has always been its small explanatory

power, and it has led to endless debates about its interpretation. However, already the original paper introduced the concept of a distribution of relaxation times and links this with α . This is then the beginning of an explanatory model.

The paper also presented an equivalent electric circuit for the Cole–Cole equation. The permittivity was modeled as two ideal, lumped capacitors and one frequency-dependent impedance (not physically realizable) modeled as a CPE. They stressed that this impedance was “merely one way of expressing the experimental facts, and that it and its real and imaginary parts have no conventional meaning.” The constant phase impedance was purely a descriptive model.

From this paper a Cole–Cole plot should be defined as a plot of the complex *permittivity* in the Wessel diagram to search for one or more circular arcs.

In the late 1930s *Cole* and *Curtis* extended their investigations to the non-linear effects of excitable membranes. After the war *Hodgkin* and *Huxley* revealed some of the main mechanisms of nerve transmission, for which they won the Nobel prize in 1963.

Herman Paul Schwan (1915–2005)

Herman Paul Schwan was one of the founders of biomedical engineering as a new discipline.⁶ Already before the war at the laboratory of Rajewski at the Frankfurter Institut für Biophysik, he started with some of the most important topics of the field: on the low frequency blood and blood serum conductivity, the counting of blood cells, the selective heating and body tissue properties in the UHF frequency range, electromagnetic hazards and safety standards for microwaves, tissue relaxation, electrode polarization. He also worked with the acoustic and ultrasonic properties of tissue. In 1950 he revealed for the first time the frequency dependence of muscle tissue capacitance, and interpreted it as a relaxation phenomenon. He introduced the concept of dispersion and was first to describe the α -dispersion in muscle tissue (Schwan, 1954). Two of the most cited articles in the field of biomedical engineering are Schwan (1957) and Schwan (1963): “Electrical properties of tissue and cell suspensions” and the more methodology focused article “Determination of biological impedances.” In the 1957 article he introduced the α , β and γ classification (cf. Section 3.8). He pioneered low frequency precision measurements (Schwan et al., 1962), four-electrode techniques and gigahertz measurements. Later he turned also to dielectrophoresis, electrorotation, and non-linear phenomena of interfacial polarization (Schwan’s law of linearity, McAdams and Jossinet, 1994). He is much appreciated for a number of much cited review articles, lately also about the history of our field (Schwan, 1992b, 1993). Some of his students and close collaborators at the University of Pennsylvania are and have been: Edwin Carstensen, Kenneth Foster, David Geselowitz, Dov Jaron, Mariam Moussavi, Banu Onaral and Shiro Takashima.

⁶Working to establish a new discipline. Herman P. Schwan and the roots of biomedical engineering. In: Nebecker F. (Ed.), *Sparks of genius*, IEEE Press, 1993.

The most important papers by Herman Schwan were selected in close cooperation with him and were published in 2001: “Selected papers by Herman P. Schwan,” editors Sverre Grimnes and Ørjan G. Martinsen.

Surface potentials generated by a bioelectric source in a volume conductor

The historic development in this area includes Helmholtz (1853), Einthoven et al. (1913), Burger et al. (1946), McFee and Johnston (1953), Schmitt (1957) and Geselowitz (1971).

It was a long way to go before the genesis of the surface potential differences caused by action potentials deep in the thorax was understood. It was the work of Einthoven and the lead concept that paved the way. It was Burger and van Milaan who introduced the *lead vector* making it possible to find the direction to go. Richard McFee replaced the lead vector by the *lead field* defined as the electric field set up in the body by a unit current applied to the pick-up electrode pair. Otto Schmitt reintroduced the old Helmholtz concept about reciprocity and introduced the concept of *transfer impedance* already known from the use of a four-electrode technique. And it was David Geselowitz who finally put it in the elegant mathematical form. A certain similarity with the Faraday–Maxwell intellectual process runs into our minds.

11 APPENDIX

Chapter Contents

11.1 Vectors and Scalars, Complex Numbers

11.1.1 Vectors and Scalars

11.1.2 Complex Numbers

11.1.3 Sign Conventions

11.1.4 The Phasor, the Sine Wave and the Operator *jot*

11.1.5 Some Algebraic Rules for *Sine Wave* Complex Numbers

11.2 Equivalent Circuit Equations

11.2.1 Equations for Two Resistors + One Capacitor Circuits

11.2.2 Equations for Two Capacitor + One Resistor Circuits

11.2.3 Equations for Four-Component *Series* Circuit (Simple Maxwell–Wagner Model)

11.3 Global Symbols

11.4 Physical Dimensions

11.1 VECTORS AND SCALARS, COMPLEX NUMBERS

Suppose we have a black box with one port = two terminals. Suppose that with sinusoidal excitation all voltage differences and all currents inside are also sinusoidal. Suppose that inside there are only resistors. Then all current maxima and voltage maxima occur simultaneously, there are no delays, no phase shifts.

Suppose that inside the box there is a circuit with resistors and capacitors. Then the voltage across a capacitor is also sinusoidal, but the voltage maximum occurs *after* the current maximum. There is a time lag, a phase shift. The phase shift is measured in degrees, and one complete period is 360° . In such circuits we must keep track not only of the magnitude, but also on the phase. Two voltages cannot just be added, they must be added as *vectors*. Two voltages *added* are actually *subtracted* if they are 180° out of phase, and equal magnitudes then cancel. Each vector quantity must therefore be given with *two* numbers. We must introduce mathematical tools to deal with such double-numbered quantities.

A *vector* or a *complex number* is the answer, both are characterized by two numbers, for example, by magnitude and direction. A vector or complex number symbol is written with **bold** characters in our book, so if a symbol is written in bold it may either be a vector in space or a complex number referring to a plane, the Wessel plane.

11.1.1 Vectors and Scalars

Mathematically, a vector in space is defined as a directed line segment (an arrow), with its initial point undefined. As long as it has the same length and is not rotated, the vector may be translated anywhere in space, it is the same vector. However, in physics we may impose restrictions on the initial point of the vector. A force may for instance be applied anywhere along its line of action to a rigid body, this is a *sliding* vector. The same force applied to an elastic body must be defined at a single initial point, it is a *fixed* or *bound* vector.

A vector is not necessarily referred to a Cartesian coordinate system, but for example, to a neighbor vector with respect to magnitude and direction. Rules about the addition, subtraction and multiplication (dot and cross products) of two vectors are a part of vector algebra.

Temperature for instance has no direction in space, so it is a *scalar*. However, a temperature *gradient* has a direction, so it is a vector.

In addition to vectors in the *space* domain, vectors may also be defined in the *time* domain, in particular rotating vectors with a fixed initial point at the origin of a Cartesian coordinate system. A variable such as the electric field strength may be a vector *both* in time and space. Every space vector may also be a time vector, and often it is not clear what sort of vector an author actually is dealing with. Vectors in the time domain are used for sine waves when the maxima do not occur simultaneously. These 2D (planar) time vectors are more conveniently represented by complex numbers.

11.1.2 Complex Numbers

A complex number is an ordered pair of real numbers, for instance G and B . Introducing the *imaginary unit* $\mathbf{j} = \sqrt{-1}$, the complex number $\mathbf{Y} = G + \mathbf{j}B$. G is the *real* part and can be written Y' , and B the *imaginary* part written Y'' . Y or $|\mathbf{Y}|$ is called the *absolute value*, *magnitude* or *modulus*, and the phase angle is $\varphi = \arctan B/G$.

A real number G can be regarded as a position on a number *line*. A complex number \mathbf{Y} can be regarded as a point in the *plane* of a special Cartesian coordinate system: the complex plane, also called the Argand¹ or Wessel² diagram. G is an

¹Jean Robert Argand (1768–1822), French/Swiss mathematician. Proposed the complex plane presentation in 1806.

²Caspar Wessel (1745–1818), Norwegian surveyor. Proposed the complex plane presentation in 1797, 9 years before Argand. Presentation in the imaginary plane is accordingly called a Wessel diagram in this book.

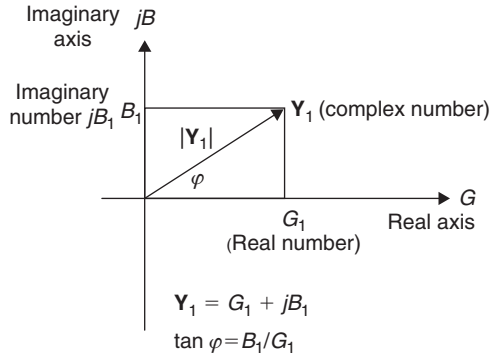


Figure 11.1 The complex plane (Wessel diagram).

ordinary real number situated on the real x -axis. j (actually j) indicates that B is to be situated on the imaginary y -axis. B is a real number, jB is an imaginary number, Y is a complex number.

Complex numbers like Y are written in **bold** in this book. Y is represented by a point in the Wessel diagram determined by G and B , the *locus* of Y , cf. Fig. 11.1. $Y^* = G - jB$ is called the complex *conjugate* to Y . Often the complex conjugate is used in order to obtain positive values for the imaginary component in the Wessel diagram. Impedance loci for instance are usually plotted with the circular arcs up, so instead of $Z = R + jX$, $Z^* = R - jX$ is plotted.

Summing up: What is the difference between a space vector and a complex number in our context?

A space vector represents a quantity having a magnitude and direction in 3D space; reference to a coordinate system is not necessary. A complex number is a time vector in a 2D plane and always referred to a Cartesian coordinate system.

Ohm's law in scalar form is written for alternating current (AC) (small i and u indicate sinusoidal varying quantities): $i = uG$. There is no time lag in the circuit, for example just resistors. i , u and G are scalars, all maxima occur simultaneously. Under the condition that *all waveforms are sinusoidal*, Ohm's law is written:

$$\mathbf{i} = u\mathbf{Y} = uG + uj\omega C \quad (11.1)$$

u is still a scalar, because it is chosen as the reference, the *independent* variable, for example, coming from the signal generator. Phase shift is measured with reference to this sinusoidal voltage. \mathbf{i} and \mathbf{Y} are printed with bold characters, indicating that they are complex quantities. They are given by:

$$\mathbf{i} = i_1 + ji_q \quad (11.2)$$

i_1 is the real part, the *in-phase* current component, meaning that this current is in phase with the imposed sine wave voltage. i_q is the imaginary part, the *quadrature*

current component. The phase shift φ (relative to the voltage u and the in-phase current i_i) is given by:

$$\varphi = \arctan i_q/i_i \quad (11.3)$$

Y is the complex *admittance*, composed of *conductance* G (in phase with the voltage) unit: (siemens), and *susceptance* B (quadrature component) unit: (siemens); in parallel:

$$Y = G + jB = G + j\omega C \quad (11.4)$$

For a capacitor $B = \omega C$, that is proportional to frequency. $f = 0$ gives $B = 0$, this is the direct current (DC) case, with no influence on admittance from the capacitance. If $C = 0$ we have no capacitor, then $i_q = 0$, and $\varphi = 0^\circ$, there is no phase shift, and the expressions reduce to contain only real quantities.

A complex number may also be given in *polar* form based on *Eulers* formula:

$$e^{j\varphi} = \cos \varphi + j \sin \varphi \quad (11.5)$$

Then $Y = Ye^{j\varphi} = Y\cos \varphi + jY\sin \varphi$. Since φ is the argument of sine and cosine functions, it is to be an angle; that is dimensionless.

Another important formula in polar form is that of *De Moivre*: $(\cos \phi + j \sin \phi)^\alpha = \cos \alpha\phi + j \sin \alpha\phi$. With $\phi = \pi/2$ we have the more specialized version used in the Cole equations:

$$j^\alpha = \cos(\alpha\pi/2) + j \sin(\alpha\pi/2) \quad (11.6)$$

11.1.3 Sign Conventions

The convention in the electrical sciences is that in the complex plane (Wessel diagram) the counter-clockwise (CCW) direction corresponds to a positive phase shift between two vectors. From this some sign rules can be deduced:

Admittance

The capacitor model of Fig. 3.1 and the Wessel diagram of Fig. 11.1 is defined with admittance $Y = G + jB$. This corresponds to a parallel GC circuit where both components have the same voltage. The current is the dependent parameter and the current through G is in phase with the voltage. The current through the capacitor leads the voltage, that by convention is defined as a positive phase shift and the current and admittance vector is CCW to the real axis, $B = +\omega C$. With a GL parallel inductive circuit $B = -1/\omega L$.

Impedance

Impedance is the inverse of admittance: $Z = 1/Y = 1/(G + j\omega C) = (G - j\omega C)/|Z|^2 = R + jX$. This corresponds to a series RC circuit where both components pass the same current. The voltage is the dependent parameter and divided between the

R and C components. The voltage in the capacitor lags the current and the voltage across the resistor. By the same convention this is defined as a negative phase shift and the voltage and impedance vector is CW to the real axis, $X = -1/\omega C$ and for inductance $X = +\omega L$.

Material Constant Signs in Capacitive Materials

Complex conductivity $\sigma = \sigma' + j\sigma''$

Complex resistivity: $\rho = \rho' - j\rho''$

Complex permittivity: $\epsilon = \epsilon' - j\epsilon''$. In the parallel GC circuit the current through C corresponds to ϵ' and through G to ϵ'' . The current through G lags the current through C, this corresponds to a negative sign for the current through G and for ϵ'' .

11.1.4 The Phasor, the Sine Wave and the Operator $j\omega t$

A complex number in the time domain is introduced under the assumption that the independent variable is a sinusoidal function of time.

What is so fundamental about the sine wave? It is the only signal containing only one frequency; it is the perfect and simplest form of *periodicity*. The sine wave is closely linked with the *circle*. A point on a circle rotating with constant frequency draws a sine wave if projected on a paper moving with uniform speed. A complex number vector of unity magnitude rotating as a function of time around the origin is called a *phasor*. A phasor is best represented with polar coordinates: $Y = G + jB = Y(\cos \varphi + j \sin \varphi) = Ye^{j\varphi}$. If the angle φ is increasing uniformly with time, $\varphi = \omega t$ (radians). Then the phasor is: $e^{j\omega t} = \cos \omega t + j \sin \omega t$. A clear distinction is made between *frequency* and *angular frequency*. Both terms imply dimension (1/s), but ωt is an angle. In the expression $\cos(ft)$, the product ft is not an angle and the expression is meaningless: in complex signal analysis the operator is $j\omega t$, not jft .

A more general mathematical treatment is possible by introducing the complex frequency $s = \sigma + j\omega$, allowing sine waves of variable amplitude, pulse waveforms, etc. Such Laplace analysis is, however, outside the scope of this book.

Implicit in the complex notation there is an important mathematical simplification. Because $\partial(e^{j\omega t})/\partial t = j\omega e^{j\omega t}$ the necessary differential equations are transformed to algebraic equation: the operator $\partial/\partial t$ becomes the factor $j\omega$.

11.1.5 Some Algebraic Rules for Sine Wave Complex Numbers

1. When a complex number is multiplied by j , the phase angle is increased by 90° ($\pi/2$).
2. When a complex number is divided by j , the phase angle is decreased by 90° ($\pi/2$).
3. $d\mathbf{i}/dt = \mathbf{i}j\omega$ (\mathbf{i} is complex sine wave)
4. $\int \mathbf{i} dt = \mathbf{i}/j\omega$ (\mathbf{i} is complex sine wave)
5. $e^{j\varphi} = \cos \varphi + j \sin \varphi$ (Eulers formula)
6. $YY^* = Y^2 = |Y|^2 = G^2 + B^2$
7. $j^\alpha = \cos(\alpha\pi/2) + j \sin(\alpha\pi/2) = e^{j\alpha\pi/2} \quad |j^\alpha| = 1$

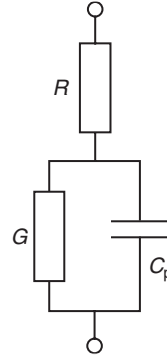


Figure 11.2 2R-1C series model, ideal components.

11.2 EQUIVALENT CIRCUIT EQUATIONS

All the circuits in this chapter are with ideal components, that is frequency independent resistance, conductance and capacitance. Derived parameters, however, are often frequency dependent, cf. for example C_{ext} in eq. (11.14). C_{ext} is the capacitance as seen from the outside at the terminals. Two-component circuits are treated in Section 8.2.3.

11.2.1 Equations for Two Resistors + One Capacitor Circuits

2R-1C Series Circuit (Fig. 11.2)

$$\begin{aligned} Z &= R + (G - j\omega C)/(G^2 + \omega^2 C^2) \\ Z &= R + (1 - j\omega\tau_Z)/G[1 + (\omega\tau_Z)^2] \\ Z &= R + 1/G(1 + j\omega\tau_Z) \end{aligned} \quad (11.7)$$

$$\tau_Z = C/G \quad (11.8)$$

$$\begin{aligned} \varphi &= \arctan[\omega C/(G(1 + RG) + \omega^2 C^2 R)] \\ \varphi &= \arctan[\omega C/G(1 + RG + \omega^2 \tau_Z \tau_2)] \end{aligned} \quad (11.9)$$

$$\begin{aligned} Y &= [G(1 + RG) + \omega^2 C^2 R + j\omega C]/[(1 + RG)^2 + \omega^2 C^2 R^2] \\ Y &= G(1 + RG + \omega^2 \tau_Z \tau_2 + j\omega\tau_Z)/[(1 + RG)^2 + (\omega\tau_Z)^2] \end{aligned} \quad (11.10)$$

$$\tau_2 = CR \quad (11.11)$$

$$C_{\text{ext}} = \varepsilon' = C/[(1 + RG)^2 + (\omega\tau_Z)^2] \quad (\text{unity cell}) \quad (11.12)$$

$$\varepsilon'' = G(1 + RG + \omega^2 \tau_Z \tau_2)/\omega[(1 + RG)^2 + (\omega\tau_Z)^2] \quad (\text{unity cell}) \quad (11.13)$$

Impedance is the preferred parameter characterizing the two resistors, one capacitor series circuit, because it is defined by one unique time constant τ_Z (eq. 11.8). This time constant is independent of R , as if the circuit was current driven. The impedance parameter therefore has the advantage that measured characteristic frequency determining τ_Z is directly related to the capacitance and parallel conductance (e.g. membrane effects in tissue), undisturbed by an access resistance. The same is not true for the admittance: the admittance is dependent both on τ_Z and τ_2 , and therefore on both R and G .

When $\omega \rightarrow 0$:

$$\begin{aligned} Y &\rightarrow G/(1 + RG) \\ B &\rightarrow \omega C/(1 + RG)^2 \\ C_{\text{ext}} &\rightarrow C/(1 + RG)^2 \\ \varphi &\rightarrow 0^\circ \end{aligned}$$

When $\omega \rightarrow \infty$:

$$\begin{aligned} Y &\rightarrow 1/R \\ B &\rightarrow \omega C/\omega^2 C^2 R^2 \rightarrow 0 \\ C_{\text{ext}} &\rightarrow C/\omega^2 C^2 R^2 \rightarrow 0 \\ \varphi &\rightarrow 0^\circ \end{aligned} \tag{11.14}$$

Equation (11.14) is of particular interest. C_{ext} is the capacitance measured on the terminals, for example, with a bridge or a lock-in amplifier. At high frequencies the susceptance part $B = Y''$ is small, and C_{ext} is strongly frequency dependent ($1/\omega^2$). In this frequency range the strong capacitance increase with decreasing frequency is externally true as measured at the network port, but it does not reflect any frequency dependence of the internal capacitor component. It only reflects the simple fact that we do not have direct access to the capacitor, only through the (at high frequencies) dominating series resistance R .

Selectivity

It is important to analyze this circuit with respect to selectivity: let us assume that our black box contains the two resistors – one capacitor series circuit. Under what conditions will measured Y' be proportional to the unknown G and not be disturbed by variations in R and C ? And correspondingly: under what conditions will measured Y'' be proportional to unknown C and not be disturbed by variations in R and G ?

From eq. (11.10) we see that Y' is proportional to G only if the following three conditions are met:

1. $RG \ll 1$
2. $\omega^2 C^2 R^2 \ll 1$
3. $\omega^2 C^2 R \ll G$

Y'' will be proportional to C only if the following two conditions are met:

1. $RG \ll 1$
2. $\omega^2 C^2 R^2 \ll 1$

If the conditions for Y'' are satisfied, then it will be possible to follow, for example, the unknown C directly by single frequency measurement of Y , without calculations based on results from measurements on several frequencies.

2R-1C Parallel Circuit (Fig. 11.3)

$$\begin{aligned} Y &= G + (\omega^2 C^2 R + j\omega C)/(1 + \omega^2 C^2 R^2) \\ Y &= G + (\omega^2 C \tau_Y + j\omega C)/[1 + (\omega \tau_Y)^2] \end{aligned} \quad (11.15)$$

$$\tau_Y = CR \quad (11.16)$$

$$\begin{aligned} \varphi &= \arctan \omega C / [G + \omega^2 C^2 R(1 + RG)] \\ \varphi &= \arctan \omega C / G[1 + \omega^2 \tau_Y \tau_2(1 + RG)] \end{aligned} \quad (11.17)$$

$$\begin{aligned} Z &= [G + \omega^2 C^2 R(1 + RG) - j\omega C]/[G^2 + \omega^2 C^2(1 + RG)^2] \\ Z &= [1 + \omega^2 \tau_Y \tau_2(1 + RG) - j\omega \tau_2]/G[1 + (\omega \tau_2)^2(1 + RG)^2] \end{aligned} \quad (11.18)$$

$$\begin{aligned} \tau_2 &= C/G \\ \varepsilon' &= C_{\text{ext}} = C/(1 + \omega^2 C^2 R^2) \quad (\text{unity cell}) \\ \varepsilon'' &= G/\omega + \omega C^2 R/(1 + \omega^2 C^2 R^2) \quad (\text{unity cell}) \end{aligned} \quad (11.19)$$

The admittance time constant is uniquely defined by τ_Y , independent of G , as if the circuit were voltage driven. The admittance parameter therefore has the advantage that measured characteristic frequency determining τ_Y is directly related to the capacitance (membrane effects) and series resistance in tissue. The same is not true for impedance: the impedance is defined by both τ_Y and τ_2 .

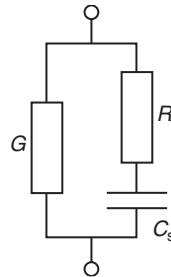


Figure 11.3 2R-1C parallel model, ideal components.

When $\omega \rightarrow 0$:

$$Y \rightarrow G$$

$$B \rightarrow \omega C$$

$$\varphi \rightarrow 0^\circ$$

$$\varepsilon' = C_{\text{ext}} = C \quad (\text{unity cell})$$

$$\varepsilon'' \rightarrow \infty \quad (\text{unity cell}) \quad \text{NB! Loss per cycle diverges!}$$

When $\omega \rightarrow \infty$:

$$Y \rightarrow G + 1/R$$

$$B \rightarrow \omega C / \omega^2 C^2 R^2$$

$$\varphi \rightarrow 0^\circ$$

$$\varepsilon' = C_{\text{ext}} = C / \omega^2 C^2 R^2 \rightarrow 0 \quad (\text{unity cell})$$

$$\varepsilon'' \rightarrow 0 \quad (\text{unity cell})$$

11.2.2 Equations for Two Capacitor + One Resistor Circuits

2C–1R Series Circuit (Fig. 11.4)

$$\varepsilon' = C_{\text{ext}} = C_s [G^2 + \omega^2 C_p (C_p + C_s)] / [G^2 + \omega^2 (C_p + C_s)^2] \quad (\text{unity cell})$$

$$\varepsilon' = C_{\text{ext}} = C_s [1 + \omega^2 \tau_2 (\tau_1 + \tau_2)] / [1 + \omega^2 (\tau_1 + \tau_2)^2] \quad (\text{unity cell})$$

$$\varepsilon'' = \omega C_s^2 G / [G^2 + \omega^2 (C_p + C_s)^2] \quad (\text{unity cell}) \quad (11.20)$$

$$\varepsilon'' = C_s \omega \tau_1 / [1 + \omega^2 (\tau_1 + \tau_2)^2] \quad (\text{unity cell})$$

$$\varepsilon = [C_s (1 + \omega^2 \tau_2 (\tau_1 + \tau_2)) - j \omega \tau_1 C_s] / [1 + \omega^2 (\tau_1 + \tau_2)^2] \quad (\text{unity cell})$$

$$\tau_1 = C_s / G \quad (11.21)$$

$$\tau_2 = C_p / G \quad (11.22)$$

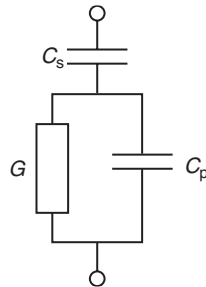


Figure 11.4 2C–1R series model, ideal components.

$$\begin{aligned} Z &= [\omega C_s G - j(\omega^2 C_s C_p + \omega^2 C_p^2 + G^2)] / [\omega C_s (\omega^2 C_p^2 + G^2)] \\ Z &= [\omega \tau_1 - j(\omega^2 \tau_1 \tau_2 + (\omega \tau_2)^2 + 1)] / \omega C_s [(\omega \tau_2)^2 + 1] \end{aligned} \quad (11.23)$$

$$\begin{aligned} \phi &= \arctan[\omega^2 C_p (C_p + C_s) + G^2] / \omega C_s G \\ \phi &= \arctan[\omega^2 \tau_2 (\tau_1 + \tau_2) + 1] / \omega \tau_1 \end{aligned} \quad (11.24)$$

$$\begin{aligned} Y &= [\omega^2 C_s^2 G + j\omega C_s (G^2 + \omega^2 C_p (C_p + C_s))] / [G^2 + \omega^2 (C_p + C_s)^2] \\ Y &= [\omega^2 C_s \tau_1 + j\omega C_s (1 + \omega^2 \tau_2 (\tau_1 + \tau_2))] / [1 + (\omega (\tau_1 + \tau_2))^2] \end{aligned} \quad (11.25)$$

This is not a preferred one resistor, two capacitors circuit because no parameters are uniquely defined with one unique time constant.

When $\omega \rightarrow 0$:

$$\begin{aligned} \varepsilon' &\rightarrow C_s \quad (\text{unity cell}) \\ \varepsilon'' &\rightarrow 0 \\ Y &\rightarrow 0 \\ B &\rightarrow \omega C_s \\ C_{\text{ext}} &\rightarrow C_s \\ \phi &\rightarrow 90^\circ \end{aligned}$$

When $\omega \rightarrow \infty$:

$$\begin{aligned} \varepsilon' &\rightarrow C_s \tau_2 / (\tau_1 + \tau_2) \quad (\text{unity cell}) \\ \varepsilon'' &\rightarrow 0 \\ Y &\rightarrow \infty \\ B &\rightarrow \omega C_p C_s / (C_p + C_s) \\ C_{\text{ext}} &\rightarrow C_p C_s / (C_p + C_s) \\ \phi &\rightarrow 90^\circ \end{aligned}$$

2C-1R Parallel Circuit (Fig. 11.5)

$$\begin{aligned} \varepsilon' &= C_{\text{ext}} = C_p + C_s / [1 + (\omega \tau_Y)^2] \quad (\text{unity cell}) \\ \varepsilon'' &= C_s \omega \tau_Y / [1 + (\omega \tau_Y)^2] \quad (\text{unity cell}) \\ \varepsilon &= C_p + C_s / (1 + j\omega \tau_Y) \quad (\text{unity cell}) \end{aligned} \quad (11.26)$$

$$\begin{aligned} Y &= j\omega C_p + (\omega^2 C_s^2 R + j\omega C_s) / (1 + \omega^2 C_s^2 R^2) \\ Y &= j\omega C_p + j\omega C_s / (1 + j\omega C_s R) \\ Y &= j\omega C_p + j\omega C_s / (1 + j\omega \tau_Y) \end{aligned} \quad (11.27)$$

$$\tau_Y = C_s R \quad (11.28)$$

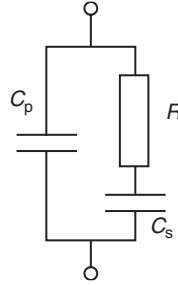


Figure 11.5 2C-1R parallel model, ideal components.

$$\begin{aligned} \varphi &= \arctan[-(C_p + C_s + \omega^2 C_s^2 R^2 C_p) / \omega C_s^2 R] \\ \varphi &= \arctan[-(C_p + C_s + (\omega \tau_Y)^2 C_p) / \omega \tau_Y C_s] \end{aligned} \quad (11.29)$$

$$\begin{aligned} Z &= [\omega C_s^2 R - j(C_p + C_s + \omega^2 C_s^2 R^2 C_p)] / \omega[(\omega C_s C_p R)^2 + (C_p + C_s)^2] \\ Z &= [\omega \tau_Y C_s - j(C_p + C_s + (\omega \tau_Y)^2 C_p)] / \omega[(\omega \tau_Y C_p)^2 + (C_p + C_s)^2] \end{aligned} \quad (11.30)$$

This is a preferred one resistor–two capacitors circuit, because all parameters are uniquely defined with one unique time constant.

When $\omega \rightarrow 0$:

$$\begin{aligned} \varepsilon' &= C_{\text{ext}} \rightarrow C_p + C_s && \text{(unity cell)} \\ \varepsilon'' &\rightarrow 0 && \text{(unity cell)} \\ \mathbf{Y} &\rightarrow 0 \\ B &\rightarrow \omega(C_p + C_s) \\ C_{\text{ext}} &\rightarrow (C_p + C_s) \\ G &\rightarrow \omega^2 C_s^2 R \rightarrow 0 \\ \varphi &\rightarrow 90^\circ \end{aligned}$$

When $\omega \rightarrow \infty$:

$$\begin{aligned} \varepsilon' &= C_{\text{ext}} \rightarrow C_p && \text{(unity cell)} \\ \varepsilon'' &\rightarrow 0 && \text{(unity cell)} \\ \mathbf{Y} &\rightarrow \infty \\ B &\rightarrow \omega C_p \\ G &\rightarrow 1/R \\ \varphi &\rightarrow 90^\circ \end{aligned}$$

11.2.3 Equations for Four-Component *Series* Circuit (Simple Maxwell–Wagner Model) (Fig. 11.6)

$$\begin{aligned} Y' &= [(G_1 + G_2)(G_1 G_2 - \omega^2 C_1 C_2) - \omega^2 (C_1 + C_2)(C_1 G_2 + C_2 G_1)] \\ &\quad \div [(G_1 + G_2)^2 + \omega^2 (C_1 + C_2)^2] \\ Y'' &= \omega[(G_1 + G_2)(C_1 G_2 + C_2 G_1) - (C_1 + C_2)(G_1 G_2 - \omega^2 C_1 C_2)] \\ &\quad \div [(G_1 + G_2)^2 + \omega^2 (C_1 + C_2)^2] \end{aligned} \quad (11.31)$$

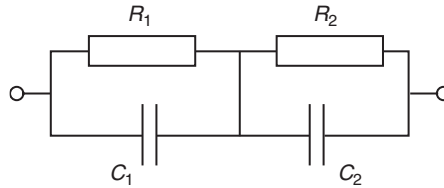


Figure 11.6 2R–2C series circuit, ideal components.

When $\omega \rightarrow 0$:

$$\begin{aligned} Y' &\rightarrow G_1 G_2 / (G_1 + G_2) \\ Y'' &\rightarrow 0 \\ C_{\text{ext}} &\rightarrow (C_1 G_2^2 + C_2 G_1^2) / (G_1 + G_2)^2 \\ \varphi &\rightarrow 0^\circ \end{aligned}$$

When $\omega \rightarrow \infty$:

$$\begin{aligned} Y' &\rightarrow [C_1 C_2 (G_1 + G_2) - (C_1 + C_2)(C_1 G_2 + C_2 G_1)] / (C_1 + C_2)^2 \\ Y'' &\rightarrow \omega C_1 C_2 / (C_1 + C_2) \\ C_{\text{ext}} &\rightarrow C_1 C_2 / (C_1 + C_2) \\ \varphi &\rightarrow 90^\circ \end{aligned}$$

This is the Maxwell–Wagner model of a capacitor with two dielectric layers. Even with only two layers the equations are complicated, with three layers they become much worse. The equations become somewhat simpler by bringing them to the Debye equation form: $Y = Y_0 + \Delta Y / [1 + (\omega\tau_Y)^2]$.

11.3 GLOBAL SYMBOLS (Table 11.1)

A *quantity* is usually defined as the product of a *numerical value* and a *unit*. A current is 4 ampere: current is the quantity, 4 is the numerical value and (ampere) is the unit. In equations we use *symbols* for the quantities (e.g. the symbol for current is I). For the units we also use symbols or abbreviations. The symbol for current is I, the abbreviation for the unit (ampere) is (A). The SI system defines 7 base units. The *dimension* of a derived unit is the product of the powers of the base units. A quantity with dimension [1] is called *dimensionless*. A number, for example of electrons, is dimensionless. A symbol within square brackets is a unit or a dimension.

Global symbols are symbols used in all the chapters, if not otherwise stated. In equations large letters are often used for DC quantities, small letters for AC quantities (e.g.: DC voltage V, AC voltage v). The quantity called *voltage* is used in electric circuits, and *potential* in space. Vectors and complex quantities are printed in **bold**. All space vectors may also be time vectors, and all scalar variables may be time vectors. The subscripts $_0$ and $_\infty$ are used for frequency extremes, except for ϵ_0 where the subscript is for vacuum. The subscript $_s$ sometimes means static in

TABLE 11.1 Global Symbols

Symbol (in equations)		Quantity	(Unit), (dimension) dimensionless = [1]
Scalar	Vector in space		
r	\mathbf{r}	Radius (variable)	[metre], [m], SI system base unit
	$\hat{\mathbf{r}}$	Unity radius vector	[1]
a	\mathbf{a}	Radius (constant)	[m]
L	\mathbf{L}	Length	[m]
v		Volume	[liter], [L], [m ³]
v	\mathbf{v}	Velocity	[m/s]
v		AC voltage	[volt]
D	\mathbf{d}	Diameter, thickness	[m]
A	\mathbf{A}	(Cross sectional) area	[m ²]
f	\mathbf{f}	Force	[newton], [N]
mol		Number of particles, relative mass	[1]. Amount of substance of 6×10^{23} particles. SI system base unit
c		Concentration	[mol/L], %weight or %volume of total [1]
η		Viscosity	[Pa s]
q, F		Charge, quantity of electricity	[coulomb], [C], [As], 1 faraday = 96 500 C
q_v		Volume charge density	[C/m ³]
q_s		Surface charge density	[C/m ²]
e		Elementary charge (one proton or electron)	1.6×10^{-19} C, + or -
z		Number of electrons for transfer (electrovalency)	[1], + or -
n		Number of ions per volume	[1/L], + or -
N		Number of molecules per volume	[1/L]
μ		Ionic mobility	[m ² /Vs] [$\mu = v/E$]
I (DC)		Current	[ampere], [A], SI system base unit.
i (AC)		Current	[ampere], [A]
J	\mathbf{J}	Current density	[A/m ²]
J'	\mathbf{J}'	Unit current density	[1/m ²]
emv ^a		Electromotive voltage	[volt]
Φ		Potential (in space)	[volt]
U, V (DC)		Voltage (in circuit)	[volt]
u, v (AC)		Voltage (in circuit)	[volt]
ϵ		Permittivity = $\epsilon_r \epsilon_0$	[F/m]
ϵ_0		Permittivity of vacuum	8.8×10^{-12} [F/m]
ϵ_s		Static permittivity	[F/m]
ϵ_r		Relative permittivity (dielectric constant)	[1]
M		Modulus function = $1/\epsilon$	[m/F]
E	\mathbf{E}	Electric field	[volt/m]
D	\mathbf{D}	Electric flux density	[C/m ²]
P	\mathbf{P}	Polarization	[Cm/m ³] or [C/m ²]
p	\mathbf{p}	Electric dipole moment	[Cm], debye [D] = 3.3×10^{-30} [qm]
m	\mathbf{m}	Current dipole moment = $i\mathbf{L}$	[Am]
C		Capacitance	farad [F]
C_p		Parallel capacitance	[F]
C_s		Series capacitance	[F]
t		Time	[second], [s]. SI system base unit.

(Continued)

TABLE 11.1 Global Symbols (Continued)

Symbol (in equations)		Quantity	(Unit), (dimension) dimensionless=[1]
Scalar	Vector in space		
τ		Time constant	[s]
f, ν		Frequency	hertz [Hz], periods/s, [1/second]
ω		Angular frequency, $2\pi f$	angle/s, [1/second]
σ		Conductivity	[S/m]
ρ		Resistivity	[Ω m]
G		Conductance	[siemens], [S], [1/ Ω], [mho], [\mathcal{U}]
B		Susceptance	[S]
Y		Admittance	[S]
Y_{sd}		Surface admittance density	[S/m ²]
R		Resistance (in series)	[ohm], [Ω]
X		Reactance	[Ω]
Z		Impedance	[Ω]
Z_{sd}		Surface impedance density	[Ω m ²]
Z_t		Transfer impedance	[$\Omega \geq$]
m		Frequency exponent, f^m	[1], $0 \leq m \leq 1$
ϕ		Phase angle	[1], degrees ($^\circ$)
α		Phase angle coefficient and frequency exponent combined	[1], $\alpha = \phi/90^\circ$, $0 \leq \alpha \leq 1$ For constant phase element (CPE): $\alpha = m$
δ		Loss angle	[1], $\delta = 90^\circ - \phi$
\hat{E}		Energy, work	1J = 1wattsecond [Ws], eV = 1.6×10^{-19} [J]
\hat{E}_v		Energy density	[J/m ³]
W		Power = energy per second	watt = [J/s]
W_v		Power density	[W/m ³]
T		Temperature	[$^\circ$ C], [K]. 0K = $-273,16^\circ$ C. SI system base unit.
j		Imaginary unit	$\sqrt{-1}$
h		Planck's constant	6.6×10^{-34} [Js]
k		Boltzmann's constant	1.38×10^{-23} [J/ $^\circ$ K]
\approx		Approximately equal to	
\sim		Proportional to	

^a Also called electromotance or electromotive force (emf). The term *force* was used by Maxwell because a potential difference exerts a force on a charge. The use of emv in this book is limited to potential differences caused by chemical or thermal energy, or induced in a circuit by a changing magnetic flux. Thus, a potential difference across a resistor or a charged capacitor as ideal components is not termed emv. In the literature before 1940, emf was often used more generally about the voltage difference across any component.

the electrostatic meaning, which is without current flow and must therefore not be confused with DC conditions when current is flowing.

The printing fonts for the Greek letters are not quite standardized: Φ is the large but both ϕ and φ are the small “phi,” Θ and θ are the large and small “theta,” ν and v are a small “ny” and “upsilon,” respectively.

11.4 PHYSICAL DIMENSIONS (Table 11.2)

The physical dimension of a particle is an important parameter: for example the smaller a sphere, the larger the surface to volume ratio ($= 3/r$). The smaller a sphere, the more surface properties dominate. Table 11.2 shows some important

TABLE 11.2 Dimension of Particles

Particle	Dimensions	Remarks
Electron	10^{-15} (= 1 fm)	Gas-like probability
Nuclei, most atoms	10^{-14}	Gas-like probability
Proton	10^{-14} (?)	Nucleus without electrons
Hydrogen	0.037 nm	Radius
Oxygen	0.066 nm	Radius
Nitrogen	0.07 nm	Radius
Ions: Na ⁺ , O ²⁻ , Cl ⁻	0.10; 0.13; 0.18 nm	Solid state
Water molecule, approximately	0.1 nm	
Electric double layer	0.5–30 nm	Strong/diluted solution
Debye length	0.5–30 nm	Space charge region around an ion
Amino acid	0.5 nm	Alanine
Small protein	3.6 nm	Myoglobin
Bilayer membrane, liposome	5 nm	
Membrane, human cell	7 nm	
Molecule (molecular weight) 14 000	1.5 nm	Myoglobin
Molecule (molecular weight) 500 000	50 nm	Myosin, length
Molecule (molecular weight) 4 000 000	120 nm	DNA, double helix length
Ribosome	15 nm	
Liposome sphere	25 nm	
Virus	20–200 nm	
Synaptic cleft	20 nm	
Mitochondria	0.1–5 μ m	
Cell	2 μ m	<i>E. coli</i>
Cell	20 μ m	Liver
Cell	5 μ m; 1 m	Nerve, diameter, length
Colloidal particles	1 nm–1 μ m	3-D unlimited
Erythrocyte (red blood cell)	2; 8 μ m	Thickness; diameter
Bacteria	0.2–2; 1–400 μ m	Diameter; length
Electrode diffusion zone	0.01–0.5 mm	Stirred/unstirred

Note: f(femto) = 10^{-15} , p(pico) = 10^{-12} , n(nano) = 10^{-9} , μ (micro) = 10^{-6} , m(milli) = 10^{-3} .

dimensions of the components we are dealing with. The dimensions of most single atoms are of the same order of 0.1 nm (nm = nanometer = 10^{-9} m), but dependent on measuring conditions and bonds (free, covalent, ionic). Since this is such an important dimension it was given a special unit, the ångström (Å). In the internationally accepted SI system the ångström unit is not used, and $1 \text{ Å} = 0.1 \text{ nm}$.

When the dimension is smaller than the order of 1 nm, the rules of quantum mechanics prevail. The concept of a single, well-defined particle must be abandoned, we know neither the exact dimension nor position nor velocity of each particle. Our picture of a single electron is more like an electron gas or cloud, with a certain probability of finding it at a certain position. So it is also for the atoms of a gas. However, atoms in a solid evidently have more well-defined positions, for example in a crystal. But due to thermal vibrations it is even here a question of a most probable position. Thermal (Brownian) movements are proportional to thermal energy and the Boltzmann factor kT , indicating an increasing uncertainty with temperature.

Our experienced macro-world where the laws of Newtonian physics are valid, is based on so many particles that the law of large numbers dominate. There is a gradual transition from single or a few particles quantum mechanical laws, to the classical laws governed by many particles in sum. *Tunneling* is an example of a quantum mechanical effect violating macro-laws, where single electrons may cross an energy barrier over small distances of some hundred pm, for example from a metal electrode to an ion in the solution.

Defining the dimensions for a molecule may be difficult. Is a whole crystal to be regarded as a macromolecule? The large organic molecules may form a helix or a double helix, with a total string length many times the external helix length. The dimensions may change as a function of, for example, water content, and the whole molecule may be more or less rigid under stretch and torsion. The shape may vary from one moment to the next. Because molecules are continually rotating, their effective (apparent) volume is greater than their real volume. Two parameters are often used to specify dimensions: end-to-end distance and radius of gyration.

Of course *volume* is sometimes a more relevant quantity than a linear dimension. Also weight and therefore density may be of interest. In molecular biology the *dalton* (Da) unit is sometimes used, it is the same as the relative atomic weight (without unit), with carbon-12 defined as 12 dalton.

References

RECOMMENDED BOOKS

General Topics

Attwood SS (1956): *Electric and magnetic fields*, 3rd edn. Dover Publications.

Castellan GW (1971): *Physical chemistry*. Addison-Wesley.

CRC (1998): *Handbook of chemistry and physics*, 79th edn. CRC Press.

Gilbert W (1600): *De Magnete*. Dover.

Kreyszig E (1988): *Advanced engineering mathematics*. John Wiley.

Kuo FF (1962): *Network analysis and synthesis*. Wiley International Edition.

Lorrain P, Corson DP, Lorrain F (1988): *Electromagnetic fields and waves*. WH Freeman and Company.

Maxwell JC (1873): *Treatise on electricity and magnetism*. Oxford University Press.

Specialised Topics

Akay M (1998): *Time frequency and wavelets in biomedical signal processing*. IEEE Press.

Alberts B, Bray D, Lewis J (2007): *Molecular biology of the cell*. Taylor & Francis, London, England.

Bassingthwaighte JB, Liebovitch LS, West BJ (1994): *Fractal physiology*. Oxford University Press.

- Berardesca E, Elsner P, Maibach HI (1995): *Bioengineering of the skin. Cutaneous blood flow and erythema*. CRC Press
- Blaustein MP (1984): *Electrogenic Transport: Fundamental Principles and Physiological Implications*. Raven Print.
- Böttcher CJF (1973): *Theory of electric polarisation, Vol. I. Dielectrics in static fields*, 2nd edn. Elsevier.
- Böttcher CJF, Bordewijk P (1978): *Theory of electric polarisation, Vol. III. Dielectrics in time dependent fields*, 2nd Edn. Elsevier.
- Cole KS (1972): *Membranes, ions and impulses*. University of California Press.
- Cooper R, Osselton JW, Shaw JC (1980): *EEG Technology*. Butterworth.
- Craig DQM (1995): *Dielectric analysis of pharmaceutical systems*. Taylor & Francis.
- Daniel VV (1967): *Dielectric relaxation*. Academic Press.
- Davis M (1965): *Some electrical and optical aspects of molecular behaviour*. Pergamon.
- Debye P (1929/1945): *Polar molecules*. Dover Publications.
- Duck FA (1990): *Physical properties of tissue. A comprehensive reference book*. Academic Press.
- Durney CH, Christensen DA (1999): *Basic introduction to Bioelectromagnetics*. CRC Press
- Elsner P, Berardesca E, Maibach H (1994): *Bioengineering of the skin: water and the stratum corneum*. CRC Press.
- Feder J (1988): *Fractals*. Plenum Press.
- Fluhr J, Elsner P, Berardesca E, Maibach HI (2005): *Bioengineering of the skin. Water and the stratum corneum*. CRC Press.
- Frölich H (1958): *Theory of dielectrics*, 2nd edn. Oxford University Press.
- Gabler R (1978): *Electrical interactions in molecular biophysics: an introduction*. Academic Press.
- Geddes LA (1972): *Electrodes and the measurement of bioelectric events*. Wiley-Interscience.
- Geddes LA, Baker LE (1989): *Applied biomedical instrumentation*. Wiley Interscience.
- Grant EH, Sheppard RJ, South GP (1978): *Dielectric behaviour of biological molecules in solution*. Oxford University Press.
- Hasted JB (1973): *Aqueous dielectrics*. Chapman and Hall.
- Hill N, Vaughan WE, Price AH, Davies M (1969): *Dielectric properties and molecular behaviour*. Van Norstrand.
- Holder DS (2005): *Electrical impedance tomography. Method, history and applications*. Institute of Physics Publishing (IoP).
- Jenkner FL (1986): *Clinical rheoencephalography*. Ertlbruck, Vienna, Austria.
- Jonscher AK (1983): *Dielectric relaxation in solids*. Chelsea Dielectrics Press.
- Koryta J (1991): *Ions, electrodes and membranes*. John Wiley.
- Low J, Reed A (1994): *Electrotherapy explained. Principles and practice*. Butterworth-Heinemann.
- Macdonald JR (1987): *Impedance spectroscopy, emphasizing solid materials and systems*. John Wiley.
- Malmivuo J, Plonsey R (1995): *Bioelectromagnetism*. Oxford University Press.
- Miller HA, Harrison DC (1974): *Biomedical electrode technology. Theory and practice*. Academic Press.
- Morucci J-P, Valentinuzzi ME, Rigaud B, Felice CJ, Chauveau N, Marsili P-M (1996): *Bioelectrical impedance techniques in medicine. Crit Rev Biomed Eng*, 24, 223–681.
- Neumann E, Sowers AE, Jordan CA (1989): *Electroporation and electrofusion in cell biology*. Plenum Press.
- Nordenstrøm B (1983): *Biologically closed electric circuits*. Nordic Medical Publications.

- Nyboer J (1970): *Electrical impedance plethysmography*. Charles Thomas.
- Pethig R (1979): *Dielectric and electronic properties of biological materials*. John Wiley.
- Plonsey R, Barr RC (2000): *Bioelectricity. A quantitative approach*, 2nd edn. Kluwer Academic/Plenum Publishers.
- Plonsey R, Barr RC (1988): *Bioelectricity. A quantitative approach*. Plenum Press.
- Plonsey R, Collin RE (1961): *Principles and applications of electromagnetic fields*. McGraw-Hill.
- Polk C, Postow E (1986): *Handbook of biological effects of electromagnetic fields*. CRC Press.
- Rajewsky B (1938): *Ergebnisse der Biophysikalischen Forschung*. Georg Thieme, Leipzig.
- Reilly JP (1998): *Applied bioelectricity. From electrical stimulation to electropathology*. Springer.
- Riu PJ, Rosell J, Bragos R, Casas O (1999): *Electrical Bioimpedance Methods: Applications to Medicine and Biotechnology*. New York Academy of Sciences.
- Schanne OF, Ruiz P, Ceretti E (1978): *Impedance measurements in biological cells*. John Wiley.
- Schwan HP (2001): Selected papers by Herman P Schwan. Grimnes S, Martinsen ØG (Eds). Medisinsk teknisk avdelings forlag, ogm@fys.uio.no.
- Silveira F and Flandre D (2004). *Low Power Analog CMOS for Cardiac Pacemakers: Design and Optimization in Bulk and SOI Technologies*: Boston, MA (USA), Kluwer Academic Publishers, 2004.
- Smyth CP (1955): *Dielectric behaviour and structure*. McGraw-Hill.
- Takashima S (1989): *Electrical properties of biopolymers and membranes*. Adam Hilger.
- Thomasset A-L (1995): *Impédancemétrie bio-electrique. Principes et applications cliniques*. Meditions.
- Tregear RT (1966): *Physical functions of skin*. Academic Press.
- Webster JG (1998): *Medical instrumentation*. Houghton Mifflin.
- Webster JG (1990): *Electrical impedance tomography*. Adam Hilger.
- Zimmermann U, Neil GA (1996): *Electromanipulation of cells*. CRC Press.

Scientific papers and specialised articles

- Aaron R, Shiffman CA (2000): Using localized impedance measurements to study muscle changes in injury and disease. *Ann NY Acad Sci*, **904**, 171–180.
- Aaron R, Huang M, Shiffman CA (1997): Anisotropy of human muscle via non-invasive impedance measurements. *Phys Med Biol*, **42**, 1245–1262.
- Aaron R, Esper GJ, Shiffman CA, Bradonjic K, Lee KS, Rutkove SB (2006): Effects of age on muscle as measured by electrical impedance myography. *Physiol Meas*, **27**, 953–959.
- Abdul S, Brown BH, Milnes P, Tidy JA (2005): A clinical study of the use of impedance spectroscopy in the detection cervical intraepithelial neoplasia (CIN). *Gynecol Oncol*, **99**, S64–S66.
- Abramson HA, Gorin MH (1939): Skin reactions VII. Relationship of skin permeability to electrophoresis of biologically active materials into the living human skin. *J Phys Chem*, **43**, 335–346.
- Abramson HA, Gorin MH (1940): Skin reactions IX. The electrophoretic demonstration of the patent pores of the living human skin; its relation to the charge of the skin. *J Phys Chem*, **44**, 1094–1102.
- Ackmann JJ, Seitz MA (1984): Methods of complex impedance measurements in biological tissue. *CRC Crit Rev Biomed Eng*, **11**(4), 281–311.

- Akay M (1998): *Time frequency and wavelets in biomedical signal processing*. IEEE Press.
- Alanen E, Lahtinen T, Nuutinen J (1998): Measurement of dielectric properties of subcutaneous fat with open-ended coaxial sensors. *Phys Med Biol*, **43**, 475–485.
- Almasi JJ, Schmitt OH (1970): Systemic and random variations of ECG electrode system impedance. *Ann NY Acad Sci*, **170**, 509–519.
- Amoussou-Guenou KM, Teyssier F, Squitiero B, Voutay M, Rusch Ph, Healy JC (1995): Second generation of cell transit analyzer. *Innov Tech Biol Med*, **16**(5), 609–622.
- Anfinsen O-G, Kongsgaard E, Foerster A, Aass H, Amlie JP (1998): Radio frequency current ablation of porcine right atrium: increased lesion of bipolar two catheter technique compared to unipolar application in vitro and in vivo. *Pacing Clin Electrophys*, **21**, 69–78.
- Anonymous (1997): Rheoencephalograph. (a) Identification. Code of Federal Regulations. Sec. 882.1825. US. Government Printing Office, Washington, DC. Title 21, Vol. 8, Parts 800 to 1299; revised April 1 [CITE: 21CFR882.1825].
- Arnold WM, Zimmerman U (1982): Rotating-field-induced rotation and measurement of the membrane capacitance of single mesophyll cells of *Avena sativa*. *Z Naturforsch*, **C37**, 908–915.
- Åberg P, Geladi P, Nicander I, Ollmar S (2002): Variation of skin properties within human forearms demonstrated by non-invasive detection and multi-way analysis. *Skin Res Technol*, **8**, 194–201.
- Åberg P, Nicander I, Ollmar S (2003a). Minimally invasive electrical impedance spectroscopy of skin exemplified by skin cancer assessment. *Proceedings of the Annual International Conference of the IEEE Engineering in Medicine and Biology*, pp. 3211–3214.
- Åberg P, Nicander I, Holmgren U, Geladi P, Ollmar S (2003b): Assessment of skin lesions and skin cancer using simple electrical impedance indices. *Skin Res Technol*, **9**, 257–261.
- Åberg P, Nicander I, Hansson J, Geladi P, Holmgren U, Ollmar S (2004): Skin cancer identification using multi-frequency electrical impedance – a potential screening tool. *IEEE Trans Biomed Eng*, **51**, 2097–2102.
- Åberg P, Geladi P, Nicander I, Hansson J, Holmgren U, Ollmar S (2005): Non-invasive and microinvasive electrical impedance spectra of skin cancer – a comparison between two techniques. *Skin Res Technol*, **11**, 281–286.
- Baden HP (1970): The physical properties of nail. *J Invest Dermatol*, **55**, 115–122.
- Balleza M, Fornos J, Calaf N et al. (2007) Monitoring of breathing pattern at rest by electrical impedance tomography ARCHIVOS DE BRONCONEUMOLOGIA **43** (6): 300–303
- Barker AT, Jalinous R, Freeston IL (1985): Noninvasive magnetic stimulation of the human motor cortex. *Lancet*, **1**, 1106–1107.
- Barlow DJ, Thornton JM (1983): Ion pairs in proteins. *J Mol Biol*, **168**, 867–885.
- Barnett A (1937): The basic factors involved in proposed electrical methods for measuring thyroid function, III. The phase angle and the impedance of the skin. *West J Surg Obstet Gynecol*, **45**, 540–554.
- Bauer HH (1964): Theory of Faradaic distortion: equation for the 2nd-harmonic current. *Australian J Chem*, **17**, 715.
- Becker FF, Wang X-B, Huang Y, Pethig R, Vykoukal J, Gascoyne PRC (1994): The removal of human leukaemia cells from blood using interdigitated microelectrodes. *J Phys D: Appl Phys*, **27**, 2659–2662.
- Becker FF, Wang X-B, Huang Y, Pethig R, Vykoukal J, Gascoyne PRC (1995): Separation of human breast cancer cells from blood by differential dielectric affinity. *Proc Natl Acad Sci USA*, **92**, 860–864.
- Bernstein DP (1986): A new stroke volume equation for thoracic electrical bioimpedance: theory and rationale. *Crit Care Med*, **14**(10), 904–909.

- Bernstein DP, Lemmens HJM (2005): Stroke volume equation for impedance cardiography. *Med Biol Eng Comput*, 43, 443–450.
- Bernstein DP, Osypka MJ (2003): Apparatus and method for determining an approximation of the stroke volume and cardiac output of the heart. US Patent number 6:511:438 B2.
- Bhatt DL, Gaylor DC, Lee RC (1990): Rhabdomyolysis due to pulses electric fields. *Plast Reconstruct Surg*, 86, 1–11.
- Bickford RG, Fremming BD (1965): Neural stimulation by pulsed magnetic fields in animals and man. *Digest of the 6th International Conference on Medical Electronics and Biological Engineering* (Tokyo), Paper 7–6.
- Blad B (1996): Clinical applications of characteristic frequency measurements: preliminary in vivo study. *Med Biol Eng Comput*, 34(5), 362–365.
- Block H, Hayes EF (1970): Dielectric behavior of stiff polymers in solution when subjected to high voltage gradients. *Trans Farad Soc*, 66, 2512–2525.
- Bodo M et al. (2004): Cerebral blood flow changes: rat studies in rheoencephalography. *Physiol Meas*, 25, 1371–1384.
- Bodo M, Pearce FJ, Baranyi L, Armonda RA (2005a): Changes in the intracranial rheoencephalogram at lower limit of cerebral blood flow autoregulation. *Physiol Meas*, 26, S1–S17.
- Bodo M et al (2005b): Cerebrovascular involvement in liposome – induced cardiopulmonary distress in pigs. *J Liposome Res*, 15, 3–14.
- Bodo M, Pearce FJ, Sowd M (2006): In vitro and in vivo studies for a bio-impedance vital-sign monitor. Technical report. Defense Technical Information Center; DTIC# ADA460555 Fort Belvoir, VA, USA, <http://www.dtic.mil>.
- Bodo M, Pearce F, Van Albert S, Armonda R. (2007): Rheoencephalogram reflects cerebral blood flow autoregulation in pigs. In: Scharfetter H, Merva R (Eds): *ICEBI 2007, IFMBE (International Federation for Biomedical Engineering) Proceedings*, Vol. 17, pp. 695–698. www.springerlink.com. Springer-Verlag Berlin/Heidelberg, 2007.
- Boone K, Barber D, Brown B (1997): Imaging with electricity: report of the European Concerted Action on Impedance Tomography. *J Med Eng Technol*, 21, 201–232.
- Bozler E, Cole KS (1935): Electric impedance and phase angle of muscle in rigor. *J Cell Comp Physiol*, 6, 229–241.
- Bragos R, Rosell J, Riu P (1994): A wide-band AC-coupled current source for electrical impedance tomography. *Physiol Meas*, 15(suppl A), 91–99.
- Brown BH, Barber DC, Wang W, Lu L, Leathard AD, Smallwood RH, Hampshire AR, Mackay R, Hatzigalanis K (1994a): Multi-frequency imaging and modelling of respiratory related electrical impedance changes. *Physiol Meas*, 15(suppl), 1–12.
- Brown BH, Barber DC, Leathard AD, Lu L, Wang W, Smallwood RH, Wilson AJ (1994b): High frequency EIT data collection and parametric imaging. *Innov Tech Biol Med*, 15(1), 1–8.
- Brunner P, Merwa R, Missner A et al. (2006): Reconstruction of the shape of conductivity spectra using differential multi-frequency magnetic induction tomography. *Physiol. Meas*. 27, S237–S248.
- Bull HB, Breese K (1969): Electrical conductance of protein solutions. *J Coll Interface Sci*, 29, 492.
- Burger HC, van Milaan JB (1946): Heart vector and leads. *Br Heart J*, Part I: 8, 157; Part II (1947): 9, 154; Part III (1948): 229.
- Burt JPH, Pethig R, Talary MS (1998): Microelectrode devices for manipulating and analysing bioparticles. *Trans Inst Meas Control* 20, 2, 82–90.
- Capecci MR (1980): High efficiency transformation by direct microinjection of DNA into cultured mammalian cells. *Cell*, 22, 479–488.

- Casas O, Bragos R, Riu P, Rosell J, Tresanchez M, Warren M, Rodriguez-Sinovas A, Carreño A, Cinca J (1999): In-vivo and in situ ischemic tissue characterisation using electrical impedance spectroscopy. *Ann NY Acad Sci*, **873**, 51–59.
- Casañas R, Scharfetter H, Altes A, et al. (2004) Measurement of liver iron overload by magnetic induction using a planar gradiometer: preliminary human results. *Physiological Measurement*, vol 25, n 1, pp. 1095–1103
- Chang DC (1989): Cell poration and cell fusion using an oscillating electric field. *Biophys J*, **56**, 641–652.
- Chernomordik LV, Sabidor IS, Chizmadzhev IGYA (1982): The study of the BLM reversible electrical breakdown mechanism in the presence of UO_2^{2+} . *Bioelectrochem Bioenerg*, **9**, 6.
- Chew WC, Sen PN (1982): Dielectric enhancement due to electrochemical double layer. *J Chem Phys*, **77**, 4683–4693.
- Chilcott TC, Coster HGL (1991): AC impedance measurements on Chara Corallina. 1: Characterization of the static cytoplasm. *Australian J Plant Physiol*, **18**(2), 191–199.
- Chiu DT, Lillard SJ, Scheller RH, Zare RN, Rodriguez-cruz SE, Williams ER, Orwar O, Sandberg M, Lundqvist JA (1998): Probing single secretory vesicles with capillary electrophoresis. *Science*, **279**, 1190–1193.
- Chow RH, Von ruden L, Neher E (1992): Delay in vesicle fusion revealed by electrochemical monitoring of single secretory events in adrenal chromaffin cells. *Nature*, **356**, 60–63.
- Cole R H, Berberian J G, Mashimo S et al. (1989): Time domain reflection methods for dielectric measurements to 10 GHz. *J. Appl. Phys.* **66**, 793–802
- Cole KS (1928a): Electrical impedance of suspension of spheres. *J Gen Physiol*, **12**, 29–36.
- Cole KS (1928b): Electrical impedance of suspension of arbacia cells. *J Gen Physiol*, **12**, 37–54.
- Cole KS (1932): Electrical phase angle of cell membranes. *J Gen Physiol*, **15**, 641–649.
- Cole KS (1934): Alternating current conductance and direct current excitation of nerve. *Science*, **79**, 164–165.
- Cole KS (1940): Permeability and impermeability of cell membranes for ions. *Cold Spring Harbor Sympos Quant Biol*, **8**, 110–122.
- Cole KS (1972): *Membranes, ions and impulses*. University of California Press.
- Cole KS, Cole RH (1941): Dispersion and absorption in dielectrics. I. Alternating current characteristics. *J Chem Pys*, **9**, 341–351.
- Cole KS, Cole RH (1942): Dispersion and absorption in dielectrics. II. Direct current characteristics. *J Chem Pys*, **10**, 98–105.
- Cooper R (1946): The electrical properties of salt-water solutions over the frequency range 1-4000 Mc/s. *J Inst Elect Eng*, **93**, 69–75.
- Cornish BH, Thomas BJ, Ward LC (1993): Improved prediction of extracellular and total body water using impedance loci generated by multiple frequency bioelectrical impedance analysis. *Phys Med Biol*, **38**, 337.
- Cornish BH, Jacobs A, Thomas BJ, Ward LC (1999): Optimising electrode sites for segmental bioimpedance measurements. *Physiol Meas* **20**, 241–250.
- d'Arsonval MA (1893): Production des courants de haute fréquence et de grand intensité; leurs effets physiologiques. *Comptes Rendus Soc de Biol*, **45**, 122–124.
- Dalziel CF (1954): The threshold of perception currents. *AIEE Trans Power App Syst*, **73**, 990–996.
- Dalziel CF (1972): Electric shock hazard. *IEEE Spectrum*, **9**, 41.
- Davalos R, Rubinsky B, Huang Y (2000): Electroporation: bio-electrochemical mass transfer at the nano scale. *Microscale Thermophys Eng*, **4**, 147–159.
- Davalos RV, Otten DM, Mir LM, Rubinsky B (2004): Electrical impedance tomography for imaging tissue electroporation. *IEEE Trans Biomed Eng*, **51**, 761–767.

- Davalos RV, Mir LM, Rubinsky B (2005): Tissue ablation with irreversible electroporation. *Ann Biomed Eng*, **33**, 223–231.
- Davidson DW, Cole RH (1951): Dispersion and absorption in dielectrics. *J Chem Phys*, **9**, 341–351.
- Davis JM, Giddings JC (1986): Feasibility study of dielectric field-flow fractionation. *Sep Sci Technol*, **21**, 969–989.
- De Lorenzo A, Andreoli A, Matthie J, Withers P (1997): Predicting body cell mass with bioimpedance by using theoretical methods: a technology review. *J Appl Physiol*, **82**, 1542–1558.
- de Lema B, Casan P, Riu P (2006) Electrical Impedance Tomography: standardizing the procedure in pneumology. *Archivos de Bronconeumologia*, **42**(6), 299–301.
- Dissado LA, Hill RM (1979): Non-exponential decay in dielectrics and dynamics in correlated systems. *Nature*, **279**, 685–689.
- Ebert T, Smith J, Barney J et al. (1986): The use of thoracic impedance for determining thoracic blood volume changes in man. *Aviat Space Environ Med*, **57**, 49–53.
- Edd J, Horowitz L, Davalos R, Mir L, Rubinsky B (2006): In vivo results of a new focal tissue ablation technique: irreversible electroporation. *IEEE Trans Biomed Eng*, **53**, 1409–1415.
- Edd JF, Davalos RV (2007): Mathematical modeling of irreversible electroporation for treatment planning. *Technol Cancer Res Treat*, **6**, 275–286.
- Einolf CW, Carstensen EL (1973): Passive electrical properties of microorganisms. V. Low frequency dielectric dispersion in bacteria. *Biophys J*, **13**, 8.
- Einthoven W, Fahr G, de Waart A (1913): Über die Richtung und die manifeste Grösse der Potentialschwankungen in menschlichen Herzen und über den Einfluss der Herzlage auf die Form des Elektrokardiogramms. *Pflüger Arch ges Physiol*, **150**, 275–315.
- Elsner P, Berardesca E, Maibach H (1994): *Bioengineering of the skin: water and the stratum corneum*. CRC Press.
- Emtestam L, Nyrén M (1997): Electrical impedance for quantification and classification of experimental skin reactions. *Am J Contact Dermatitis*, **8**(4), 202–206.
- Emtestam L, Nicander I, Stenström M, Ollmar S (1998): Electrical impedance of nodular basal cell carcinoma: a pilot study. *Dermatology*, **197**, 313–316.
- Emtestam L, Kuzmina N, Talme T (2007): Evaluation of the effects of topical clobetasol propionate by visual score, electrical impedance and laser Doppler flowmetry. *Skin Res Technol*, **13**, 73–78.
- Epstein BR, Foster KR (1983): Anisotropy in the dielectric properties of skeletal muscles. *Med Biol Eng Comp*, **21**, 51.
- Esser AT, Smith KC, Gowrishankar TR, Weaver JC (2007): Towards solid tumor treatment by irreversible electroporation: intrinsic redistribution of fields and currents in tissue. *Technol Cancer Res Treat*, **6**, 261–274.
- Esper GJ, Lee KS, Shiffman CA et al. (2005). Electrical impedance myography in the assessment of age-associated muscle change. 52nd Annual scientific meeting for the American Association for Neuromuscular and Electrodiagnostic Medicine, Monterey, CA, USA.
- Etter HS, Pudenz RH, Gersh I (1947): The effects of diathermy on tissues contiguous to implanted surgical materials. *Arch Phys Med Rehab*, **28**, 333–344.
- Falk G, Fatt P (1964): Linear electrical properties of striated muscle fibers observed with intracellular electrodes. *Proc Roy Soc London Ser B*, **160**, 69.
- Fawcett T (2005): An introduction to ROC analysis. *Pattern Recogn Lett*, **27**, 861–874.
- Fein A, Grossman RF, Jones G et al. (1979): Evaluation of transthoracic electrical impedance in the diagnosis of pulmonary edema. *Circulation*, **60**, 1156–1160.
- Feldman, Y. Ermolina, I. Hayashi, Y (2003) Time domain dielectric spectroscopy study of biological systems. *IEEE Trans Dielectr. Elec. Insulation*, **10**, 728–753.

- Fink H-W, Schönenberger C (1999): Electrical conduction through DNA molecules. *Nature*, 398, 407–410.
- Fluhr JW, Gloor M, Lazzerini S, Kleesz P, Grieshaber R, Berardesca E (1999a): Comparative study of five instruments measuring stratum corneum hydration (Corneometer CM 820 and CM 825, Skicon 200, Nova DPM 9003, DermaLab). Part I. In vivo. *Skin Res Technol*, 5, 161–170.
- Fluhr JW, Gloor M, Lazzerini S, Kleesz P, Grieshaber R, Berardesca E (1999b): Comparative study of five instruments measuring stratum corneum hydration (Corneometer CM 820 and CM 825, Skicon 200, Nova DPM 9003, DermaLab). Part II. In vivo. *Skin Res Technol*, 5, 171–178.
- Forslind B (1970): Biophysical studies of the normal nail. *Acta Dermatol Venereol (Stockh)*, 50, 161–168.
- Foster KR, Schwan HP (1986): Dielectric properties of tissue. In: Polk C, Postow E (Eds), *Part I: Dielectric permittivity and electrical conductivity of biological materials. CRC handbook of biological effects of electromagnetic fields*. CRC press, London.
- Foster KR, Schwan HP (1989): Dielectric properties of tissue. *CRC Crit Rev Biomed Eng*, 17, 25–104.
- Foster KR, Epstein BR, Gealt MA (1987): “Resonances” in the dielectric absorption of DNA?. *Biophys J*, 52, 421–425.
- Foster KR, Schepps JL, Stoy RD, Schwan HP (1979): Dielectric properties of brain tissue between 0.01 and 10 GHz. *Phys Med Biol*, 24, 1177.
- Fox MB, Esveld DC, Valero A, Luttgé R, Mastwijk HC, Bartels PV, Van den Berg A, Boom RM (2006a): Single-cell electroporation. *Anal Bioanal Chem*, 385, 474–485.
- Fox MB, Esveld DC, Valero A, Luttgé R, Mastwijk HC, Bartels PV, Van den Berg A, Boom RM (2006b): Electroporation of cells in microfluidic devices: a review. *Anal Bioanal Chem*, 385, 474–485.
- Frantescu CG, Wesner D, Pliquett U, Neumann E (2004): Unsymmetrical non-linearity in cell membranes. *Proceedings of the XII International Conference on Electrical Bio-Impedance*, Gdansk, pp. 41–44.
- Franke EK., Braunstein JR and Zellner DC (1962). Study of high-frequency components in electrocardiogram by power spectrum analysis. *Circ. Res.* 10,870.
- Freeman SA, Wang MA, Weaver JC (1994): Theory of electroporation of planar bilayer membranes: predictions of the aqueous area, change in capacitance, and pore-pore separation. *Biophys J*, 67, 42–56.
- Freiberger H (1933). Der elektrische Widerstand des menschlichen Körpers gegen technischen Gleich- und Wechselstrom. *Elektrizitätswissenschaft*, 32, 373–375, 442–446.
- Fricke H (1924): A mathematical treatment of the electrical conductivity and capacity of disperse systems. I. The electrical conductivity of a suspension of homogeneous spheroids. *Phys Rev*, 24, 575–587.
- Fricke H (1925): A mathematical treatment of the electrical conductivity and capacity of disperse systems. II. The capacity of a suspension of conducting spheroids surrounded by a non-conducting membrane for a current of low frequency. *Phys Rev*, 26, 678–681.
- Fricke H (1932): Theory of electrolytic polarisation. *Phil Mag*, 14, 310–318.
- Fricke H (1953): The Maxwell-Wagner dispersion in a suspension of ellipsoids. *J Phys Chem*, 57, 934–937.
- Fricke H (1955): The complex conductivity of a suspension of stratified particles of spherical cylindrical form. *J Phys Chem*, 59, 168.

- Fricke H, Curtis HJ (1935): The electric impedance of hemolyzed suspensions of mammalian erythrocytes. *J Gen Physiol*, **18**, 821.
- Fricke H, Morse S (1926): The electric capacity of tumors of the breast. *J Cancer Res*, **10**, 340–376.
- Fuhr G, Hagedorn R, Müller T, Benecke W, Wagner B, Gimsa J (1991): Asynchronous travelling-wave induced linear motion of living cells. *Stud Biophys*, **140**, 79–102.
- Fuhr G, Zimmermann U, Shirley SG (1996): Cell motion in time-varying fields: principles and potential. In: Zimmermann U, Neil GA (Eds), *Electromanipulation of cells*. CRC Press, Boca Raton.
- Gabor D (1946): Theory of communication. *JIEE*, **93**, 429–457.
- Gabriel C, Gabriel S, Corthout E (1996a): The dielectric properties of biological tissue: I, literature survey. *Phys Med Biol*, **41**, 2231–2249
- Gabriel S, Lau RW, Gabriel C (1996b): The dielectric properties of biological tissue: II. Measurements in the frequency range 10 Hz to 20 GHz. *Phys Med Biol*, **41**, 2251–2269.
- Gabrielli C (1984): Identification of electrochemical processes by frequency response analysis. Solartron Technical report number 004/83.
- Gandhi SV, Walker D, Milnes P, Mukherjee S, Brown BH, Anumba DOC (2006): Electrical impedance spectroscopy of the cervix in non-pregnant and pregnant women. *Eur J Obster Gynecol Reprod Biol*, **129**, 145–149.
- Gao J, Yin XF, Fang ZL (2004): Integration of single cell injection, cell lysis, separation and detection of intracellular constituents on a microfluidic chip. *Lab Chip*, **4**, 47–52.
- Geddes LA, Baker LE (1966): The relationship between input impedance and electrode area in recording the ECG. *Med Biol Eng*, **4**, 439–450.
- Geddes LA, Baker LE (1967): The specific resistance of biological material – a compendium of data for the biomedical engineer and physiologist. *Med Biol Eng*, **5**, 271–293.
- Geddes LA, Valentinuzzi ME (1973): Temporal changes in electrode impedance while recording the electrocardiogram with “dry” electrodes. *Ann Biomed Eng*, **1**, 356–367.
- Geddes LA, Tacker A, Cabler B, Kidder H, Gothard R (1975a): The impedance of electrodes used for ventricular defibrillation. *Med Instr*, **9**, 177–178.
- Geddes LA, Tacker A, Cabler B, Chapman R, Rivera R, Kidder H (1975b): The decrease in trans-thoracic impedance during successive ventricular defibrillation trials. *Med Instr*, **9**, 179–180.
- Geddes LA, Tacker A, Schoenlein W, Minton M, Grubbs S, Wilcox P (1976): The prediction of the impedance of the thorax to defibrillating current. *Med Instr*, **10**, 159–162.
- Gencer NG, Ider YZ (1994): A comparative study of several exciting magnetic fields for induced current EIT. *Physiol Meas*, **15**(suppl 2A), 51–57.
- Gersing E (1991): Measurement of electrical impedance in organs – measuring equipment for research and clinical applications. *Biomed Tech*, **36**(1–2), 6–11.
- Gersing E (1998): Impedance spectroscopy on living tissue for determination of the state of organs. *Bioelectrochem Bioenerg*, **45**(2), 145–149.
- Gersing E, Krüger W, Osypka M, Vanupel P (1995): Problems involved in temperature measurements using EIT. *Physiol Meas*, **16**(suppl 3A), 153–160.
- Geselowitz DB (1971): An application of electrocardiographic lead theory to impedance plethysmography. *IEEE Trans Biomed Eng*, **18**, 38–41.
- Gheorghiu E (1996): Measuring living cells using dielectric spectroscopy. *Bioelectrochem Bioenerg*, **40**(2), 133–139.
- Gholizadeh G (1998): Human skin perception in open MR and perception related to electrostatic discharge. M.Sc. Thesis, Department of Physics, University of Oslo, Norway.
- Giaever I, Keese CR (1993): A morphological biosensor for mammalian cells. *Nature*, **366**, 591–592, Product Review.

- Gibson LE, Cooke RE (1959): A test for concentration of electrolytes in sweat in cystic fibrosis of the pancreas utilising pilocarpine by iontophoresis. *Pediatrics*, **23**, 545–549.
- Gift EA, Weaver JC (1995): Observation of extremely heterogeneous electroporative molecular uptake by *Saccharomyces cerevisiae* which changes with electric field pulse amplitude. *Biochim Biophys Acta*, **1234**, 52–62.
- Gisser DG, Isaacson D, Newell JC (1987): Current topics in impedance imaging. *Clin Phys Physiol Meas*, **8**(suppl A), 39–46. PMID: 3568569
- Goldman DE (1943): Potential, impedance and rectification in membranes. *J Gen Physiol* **27**: 37–60.
- Gordon DH (1975): Triboelectric interference in the ECG. *IEEE Trans Biomed Eng*, **22**, 252–255.
- Gotshall R, Davrath L (1999): Bioelectric impedance as an index of thoracic fluid. *Aviat Space Environ Med*, **70**(1), 58–61.
- Gougerot L, Foucher M (1972): La membrane de l'hématie est-elle un diélectrique parfait?. *Ann Phys Biol Med*, **6**, 17–42.
- Grahame DC (1952): Mathematical theory of the faradaic admittance. *J Electrochem Soc*, **99**, 370c–385c.
- Grant EH (1965): The structure of water neighbouring proteins, peptides and amino acids as deduced from dielectric measurements. *Ann NY Acad Sci*, **125**, 418–427.
- Greatbatch W (1967): Electrochemical polarization of physiological electrodes. *Med Res Eng*, **6**, 13–17.
- Griffiths H, Ahmed A (1987): Applied potential tomography for non-invasive temperature mapping in hyperthermia. *Clin Phys Physiol Meas*, **8**(suppl A), 147–153.
- Grimnes S (1982): Psychogalvanic reflex and changes in electrical parameters of dry skin. *Med Biol Eng Comput*, **20**, 734–740.
- Grimnes S (1983a): Impedance measurement of individual skin surface electrodes. *Med Biol Eng Comput*, **21**, 750–755.
- Grimnes S (1983b): Skin impedance and electro-osmosis in the human epidermis. *Med Biol Eng Comput*, **21**, 739–749.
- Grimnes S (1983c): Dielectric breakdown of human skin in vivo. *Med Biol Eng Comput*, **21**, 379–381.
- Grimnes S (1983d): Electro-vibration, cutaneous sensation of microampere current. *Acta Physiol Scand*, **118**, 19–25.
- Grimnes S (1984): Pathways of ionic flow through human skin in vivo. *Acta Dermatol Venereol (Stockh)*, **64**, 93–98.
- Grimnes S, Martinsen ØG (2006): Bioimpedance. In: *Wiley encyclopedia of biomedical engineering*.
- Grimnes S, Martinsen ØG (2007a): Comments on “algorithm for tissue ischemia estimation based on electrical impedance spectroscopy”. *IEEE Trans Biomed Eng*, **54**(2), 344.
- Grimnes S, Martinsen ØG (2007b): Sources of error in tetrapolar impedance measurements on biomaterials and other ionic conductors. *J Phys D: Appl Phys*, **40**, 9–14.
- Grimnes S, Martinsen ØG (2005): Cole electrical impedance model – a critique and an alternative. *IEEE Trans. Biomed. Eng.*, **52**(1), 132–135.
- Griss P, Enoksson P, Tolvanen-Laakso HK, Meriläinen P, Ollmar S, Stemme G (2001): Micromachined electrodes for biopotential measurements. *IEEE J Microelectromech Syst*, **10**, 10–16.
- Grosse C, Foster KR (1987): Permittivity of a suspension of charged spherical particles in electrolyte solution. *J Phys Chem*, **91**, 3073.
- Guerrero L, Gobantes I, Oliver MA, et al. (2004) Green Hams Electrical Impedance Spectroscopy (EIS) Measures and Pastiness Prediction of Dry Cured Hams. *Meat Science*, **66**, 289–294

- Guy AW, Davidow S, Yang GY, Chou CK (1982): Determination of electric current distribution in animals and humans exposed to a uniform 60Hz high intensity electric field. *Bioelectromagnetics*, **3**, 47.
- Haas K, Sin WC, Javaherian A, Li Z, Cline HT (2001): Single-cell electroporation for gene transfer in vivo. *Neuron*, **29**, 583–591.
- Hadjiev D (1968): A new method for quantitative evaluation of cerebral blood flow by rheoencephalography. *Brain Res*, **8**(1), 213–215.
- Halldorsson H, Ollmar S (1998): Signal analysis of non-invasive impedance spectra of transplanted kidneys in vivo. *Proceedings of the 10th International Conference on Electrical Bio-Impedance*, Barcelona, April 5–9, pp. 351–354.
- Hamill OP, Marty A, Neher E, Sakmann B, Sigworth FJ (1981): Improved patch-clamp techniques for high-resolution current recording from cells and cell-free membrane patches. *Pflugers Arch*, **391**, 85–100.
- Hanai T (1960): Theory of the dielectric dispersion due to the interfacial polarization and its application to emulsion. *Kolloid Z*, **171**, 23–31.
- Harris ND, Suggett AJ, Barber DC, Brown BH (1987): Applications of applied potential tomography (APT) in respiratory medicine. *Clin Phys Physiol Meas*, **8**(suppl A), 155–165.
- Havriliak S, Negami S (1966): A complex plane analysis of α -dispersions in some polymer systems. *J Polym Sci: Part C*, **14**, 99–117.
- Hayakawa R, Kanda H, Sakamoto M, Wada Y (1975): New apparatus for measuring the complex dielectric constant of a highly conductive material. *Japan J Appl Phys*, **14**, 2039–2052.
- Helmholtz H (1853): Über einige Gesetze der Verteilung elektrischer Ströme in körperlichen Leitern, mit Anwendung auf die thierischelektrischen Versuche. *Ann Physiol Chem*, **3**(29), 222.
- Hettrick DA, Zielinski TM (2006): *Bioimpedance in cardiovascular medicine. Encyclopedia of medical devices and instrumentation*, 2nd edn. John Wiley & Sons, Inc. pp. 197–216.
- Hibino M, Shigemori M, Itoh H, Nagayama K, Kinoshita K (1991): Membrane conductance of an electroporated cell analyzed by submicrosecond imaging of transmembrane potential. *Biophys J*, **59**, 209–220.
- Hodgkin AL, Huxley AF (1952): A quantitative description of membrane current and its application to conductance and excitation in nerve. *J Physiol*, **117**, 500–544.
- Hodgkin AL, Katz B (1949): The effect of sodium ions on the electrical activity of the giant axon of squid. *J physiol*, **108**, 37–77.
- Hoenig SA, Gildenberg PL, Murthy K (1978): Generation of permanent, dry, electric contacts by tattooing carbon into skin tissue. *IEEE Trans Biomed Eng*, **25**, 380–382.
- Holder DS (1992): Detection of cortical spreading depression in anesthetised rat by impedance measurement with scalp electrodes – implications for noninvasive imaging in the brain with electrical impedance tomography. *Clin Phys Physiol Meas*, **13**(1), 77–86.
- Holder DS (1998): Electrical impedance tomography in epilepsy. *Electron Eng*, **70**(859), 69–70.
- Hollaus K, Magele C, Merwa R, Scharfetter H (2004): Numerical simulation of the eddy current problem in magnetic induction tomography for biomedical applications by edge elements. *IEEE Trans Mag*, **40**, 623–626.
- Huang Y, Rubinsky B (1999): Micro-electroporation: improving the efficiency and understanding of electrical permeabilization of cells. *Biomed Microdev*, **2**, 145–150.
- Huang Y, Rubinsky B (2003): Flow-through micro-electroporation chip for high efficiency single-cell genetic manipulation. *Sens Actuators A*, **104**, 205–212.
- IEC 60601-1 (2005): Medical electrical equipment – Part 1: General requirements for basic safety and essential performance. International standard.

- Ivorra A, Rubinsky B (2007): In vivo electrical impedance measurements during and after electroporation of rat liver. *Bioelectrochemistry*, **70**, 287–295.
- Jacquy J et al. (1974): Cerebral blood flow and quantitative rheoencephalography. *Electroencephalogr Clin Neurophysiol*, **37**, 501–511.
- Jaron D, Schwan HP, Geselowitz DB (1968): A mathematical model for the polarisation impedance of cardiac pacemaker electrodes. *Med. Biol. Eng. Comput.*, **6**, 579–594.
- Jaron D, Brillner A, Schwan HP, Geselowitz DB (1969): Nonlinearity of cardiac pacemaker electrodes. *IEEE Trans Biomed Eng*, **16**, 132–138.
- Jentsch TJ (2002): Chloride channels are different. *Nature* **415**, 276–7
- Jones P (1979): High electric field dielectric studies of aqueous myoglobin solutions. *Biophys Chem*, **9**, 91–95.
- Jonscher AK (1974): Hopping losses in polarisable dielectric media. *Nature*, **250**, 191–193.
- Jonscher AK (1977): The “universal” dielectric response. *Nature*, **267**, 673–679.
- Jossinet J (1996): Variability of impedivity in normal and pathological breast tissue. *Med Biol Eng Comput*, **34**(5), 346–350.
- Jossinet J, McAdams ET (1991): The skin/electrode interphase impedance. *Innov Tech Biol Med*, **12**(1), 22–31.
- Jossinet J, Schmitt M (1998): Alternative parameters for the characterisation of breast tissue. *Proceedings of the X International Conference on Electrical Bioimpedance*, pp. 45–48.
- Kanai H, Sakamoto K, Miki M (1976): Impedance of blood; the effects of red cell orientation. *Digest of the 11th International Conference on Medical and Biological Engineering*, pp. 238–239.
- Kao T-J, Boverman G, Kim BS, Isaacson D, Saulnier GJ, Newell JC, Choi MH, Moore RH, Kopans DB (2007): Regional admittivity spectra with tomosynthesis images for breast cancer detection: Preliminary patient study. *IEEE Trans. Medical Imaging*, Submitted, in review.
- Kauppinen PK, Hyttinen JA, Malmivuo JA (1998): Sensitivity distributions of impedance cardiography using band and spot electrodes analyzed by a three-dimensional computer model. *Ann Biomed Eng*, **26**(4), 694–702.
- Khine M, Lau A, Ionescu-Zanetti C, Seo J, Lee LP (2005a): A single cell electroporation chip. *Lab Chip*, **5**, 38–43.
- Khine M, Lau A, Zanetti CI, Seo J, Lee E, Davalos R, Lee LP (2005b): A low-voltage single cell electroporation array for intracellular compound delivery. *The 9th International Conference on Miniaturized Systems for Chemistry and Life Sciences*, Boston, MA, Royal Society of Chemical Special Publications.
- Kinosita K Jr., Tsong TY (1979): Voltage-induced conductance in human erythrocyte membranes. *Biochim Biophys Acta*, **554**, 479–497.
- Kinosita K Jr., Ashikawa I, Saita N, Yoshimura H, Itoh H, Nagayama K, Ikegami A (1988): Electroporation of cell membrane visualized under a pulsed-laser fluorescence microscope. *Biophys J*, **53**, 1015–1019.
- Kirkwood JG (1939): The dielectric polarization of polar liquids. *J Chem Phys*, **7**, 911.
- Knudsen V (1999): Verification and use of a numerical computer program for simulations in bioimpedance. M.Sc. Thesis, Department of Physics, University of Oslo, Norway (in Norwegian).
- Ko WH, Hyneczek J (1974): Dry electrodes and electrode amplifiers. In: Miller HA, Harrison DC (Eds), *Biomedical electrode technology. Theory and practice*. Academic Press.
- Kontos HA et al. (1978): Responses of cerebral arteries and arterioles to acute hypotension and hypertension. *Am J Physiol*, **234**, H371–H383.

- Kontturi K, Murtomäki L, Hirvonen J, Paronen P, Urtti A (1993): Electrochemical characterization of human skin by impedance spectroscopy. The effect of penetration enhancers. *Pharm Res*, **10**(3), 381–385.
- Korjenvsky AV, Cherepenin VA (1998): Measuring system for induction tomography. *Proceedings of the Xth International Conference on Electrical Bio-Impedance*, Barcelona, pp. 365–368.
- Kornhauser SH (1997): Cerebrovascular diagnostic system. *Am J Electromed*, June, 69–71.
- Kramers HA (1926): Theory of dispersion in the X-ray region. *Physik Z*, **30**, 52.
- Kronig RdeL (1929): The theory of dispersion of X-rays. *J Opt Soc Am*, **12**, 547.
- Kubicek WG, Patterson RP, Witsoe DA, Mattson RH (1970): Impedance cardiography as a non-invasive method for monitoring cardiac function and other parameters of the cardiovascular system. *Ann NY Acad Sci*, **170**, 724–732.
- Kubicek WG, Kamegis JN, Patterson RP, Witsoe DA, Mattson RH (1966): Development and evaluation of an impedance cardiac output system. *Aerosp Med* **37**, 1208–1212.
- Kyle UG, Bosaeus I, De Lorenzo AD, Deurenberg P, Elia M, Gomez JM, Heitmann BL, Kent-Smith L, Melchior JC, Pirlich M, Scharfetter H, Schols AMWJ, Pichard C (2004): Bioelectrical impedance analysis – Part I: review of principles and methods. *Clin Nutr*, **23**, 1226–1243.
- Lahtinen T, Nuutinen J, Turunen M, Alanen E, Hopewell JW (1997): Noninvasive assessment of subcutaneous fibrosis at high radiofrequencies. *Proceedings of the XVIII International Conference on Medical and Biological Engineering and XI International Conference on Medical Physics*, Nice, 337.
- Lahtinen T, Nuutinen J, Alanen E, Turunen M, Nuortio L, Usenius T, Hopewell JW (1999): Quantitative assessment of protein content in irradiated human skin. *Int J Radiat Oncol Biol Phys*, **43**, 635–638.
- Lapicque L (1907): Recherches quantitatives sur l'excitation électrique des nerfs traitée comme une polarisation. *J Physiol Paris*, **9**, 620–635
- Lee TK, Claridge E (2005): Predictive power of irregular border shapes for malignant melanomas. *Skin Res Technol*, **11**, 1–8.
- Lee ES, Robinson D, Rognlien JL, Harnett CK, Simmons BA, Ellis CRB, Davalos RV (2006): Robust giant lipid vesicles and micro-electroporation technology for controllable manipulation of picoliter volumes on-chip. *Bioelectrochemistry*, **69**, 117–125..
- Lee RC, Despa F (2005): Distinguishing electroporation from thermal injuries in electrical shock by MR imaging. *Engineering in Medicine and Biology 27th Annual Conference*, Shanghai, China, IEEE.
- Lee RC, Zhang D, Hannig J (2000): Biophysical injury mechanisms in electrical shock trauma. In: Yarmish ML, Diller KR, Toner M (Eds), *Annual review of biomedical engineering*. Annual Review Press, Palo Alto.
- Lehr J (1972): A vector derivation useful in impedance plethysmographic field calculations. *IEEE Trans Biomed Eng*, **19**(2), 156–157.
- Lin Y-C, Huang M-Y (2001): Electroporation microchips for in vitro gene transfection. *J Micromech Microeng*, **11**, 542–547.
- Lindholm-Sethson B, Han S, Ollmar S, Nicander I, Jonsson G, Lithner F, Berthelm U, Geladi P (1998): Multivariate analysis of skin impedance data in long term type 1 diabetic patients. *Chem Intel Lab Syst* **44**(1–2), 381–394.
- Lindsey CP, Patterson GD (1980): Detailed comparison of the William-Watts and Cole-Davidson functions. *J Chem Phys*, **73**, 3348–3357.
- Lionheart WRB (1997): Conformal uniqueness results in anisotropic electrical impedance imaging. *Inverse Prob*, **13**(1), 125–134.

- Lozano A, Rosell J, Pallas-Areny R (1995): A multifrequency multichannel electrical impedance data acquisition system for body fluid monitoring. *Physiol Meas*, **16**, 227–237.
- Lukaski HC, Hall CB, Siders WA (2007): Assessment of change in hydration in women during pregnancy and postpartum with bioelectrical impedance vectors. *Nutrition*, **8**, 543–550.
- Lumry R, Yue RHS (1965): Dielectric dispersion of protein solutions containing small zwitterions. *J Phys Chem*, **69**, 1162–1174.
- Lundqvist JA, Sahlin F, Aberg MA, Stromberg A, Eriksson PS, Orwar O (1998): Altering the biochemical state of individual cultured cells and organelles with ultramicroelectrodes. *Proc Natl Acad Sci USA*, **95**, 10356–10360.
- Luthje L, Vollmann D, Drescher T, Schott P, Zenker D, Hasenfuss G, Unterberg C (2007): Intrathoracic impedance monitoring to detect chronic heart failure deterioration: relationship to changes in NT-proBNP. *Eur J Heart Fail*, **9**(6–7), 716–722.
- Maiti S, Shear JB, Williams RM, Zipfel WR, Webb WW (1997): Measuring serotonin distribution in live cells with three-photon excitation. *Science*, **275**, 530–532.
- Maleev VT, Kashpur VA, Glibitski GM, Krasnitskaya AA, Veretelnik YV (1987): Does DNA absorb microwave energy?. *Biopolymers*, **26**, 1965–1970.
- Mandel M (1977): Dielectric properties of charged linear macromolecules with particular reference to DNA. *Ann NY Acad Sci*, **303**, 74–87.
- Mandel M, Jenard A (1963): Dielectric behavior of aqueous polyelectrolyte solution. *Trans Farad Soc*, **59**, 2158–2177.
- Mandel M, Odijk T (1984): Dielectric properties of polyelectrolyte solutions. *Ann Rev Phys Chem*, **35**, 75–108.
- Mangnall YF, Baxter AJ, Avill R, Bird NC, Brown BH, Barber DC, Seagar AD, Johnson AG, Read NW (1987): Applied potential tomography: a new non-invasive technique for assessing gastric function. *Clin Phys Physiol Meas*, **8**(suppl A), 119–130.
- Maor E, Ivorra A, Leor J, Rubinsky B (2007): The effect of irreversible electroporation on blood vessels. *Technol Cancer Res Treat*, **6**, 307–312.
- Mart M, and Toomas P (2007) Improvement of Lock-in Electrical Bio-Impedance Analyzer for Implantable Medical Devices. *IEEE Transactions on Instrumentation and Measurement*, Vol. 56, No. 3, pp. 968–974.
- Mart M, Paul A, Raul L, et al. (2007a) Bioimpedance Monitoring of Tissue Transplants. *Proc. IEEE Instrumentation and Measurement Technology Conference – IMTC 2007*, Warsaw, Poland, May 1-3, 2007, 4 pp.
- Mart M, Toomas P, Ants R, et al. (2007b) Synchronous Sampling and Demodulation in an Instrument for Multifrequency Bioimpedance Measurement. *IEEE Transactions on Instrumentation and Measurement*, Vol. 56, No. 4, pp. 1365–1372.
- Markx GH, Talary M, Pethig R (1994): Separation of viable and non-viable yeast using dielectrophoresis. *J Biotechnol*, **32**, 29–37.
- Markx GH, Dyda PA, Pethig R (1996): Dielectrophoretic separation of bacteria using a conductivity gradient. *J Biotechnol*, **51**, 175–180.
- Marszalek PE, Farrell B, Verdugo P, Fernandez JM (1997): Kinetics of release of serotonin from isolated secretory granules. II. Ion exchange determines the diffusivity of serotonin. *Biophys J*, **73**, 1169–1183.
- Martinsen ØG, Grimnes S (1998): On using single frequency electrical measurements for skin hydration assessment. *Innov Tech Biol Med*, **19**(5), 395–399.
- Martinsen ØG, Grimnes S (2001): Facts and myths about electrical measurement of stratum corneum hydration state. *Dermatology*, **202**, 87–89.

- Martinsen ØG, Grimnes S, Henriksen I, Karlsen J (1996): Measurement of the effect of topical liposome preparations by low frequency electrical susceptance. *Innov Tech Biol Med*, 17(3), 217–222.
- Martinsen ØG, Grimnes S, Sveen O (1997a): Dielectric properties of some keratinised tissues. Part 1: Stratum corneum and nail in situ. *Med Biol Eng Comput*, 35, 172–176.
- Martinsen ØG, Grimnes S, Kongshaug ES (1997b): Dielectric properties of some keratinised tissues. Part 2: Human hair. *Med Biol Eng Comput*, 35, 177–180.
- Martinsen ØG, Grimnes S, Nilsen S (1997c): Absolute water content and electrical admittance of human nail. *Exp Dermatol*, 6(5), 264.
- Martinsen ØG, Grimnes S, Karlsen J (1998): Low frequency dielectric dispersion of microporous membranes in electrolyte solution. *J Coll Interface Sci*, 199, 107–110.
- Martinsen ØG, Grimnes S, Haug E (1999): Measuring depth depends on frequency in electrical skin impedance measurements. *Skin Res Technol*, 5, 179–181.
- Martinsen ØG, Grimnes S, Mirtaheer P (2000): Non-invasive measurements of postmortem changes in dielectric properties of haddock muscle – a pilot study. *J Food Eng*, 43, 189–192.
- Martinsen ØG, Grimnes S, Nilsen JK, Tronstad C, Jang W, Kim H, Shin K, Naderi M, Thielmann F (2008): Gravimetric method for in vitro calibration of skin hydration measurements. *IEEE Trans Biomed Eng*, 55(2), 728–732.
- Martinsen ØG, Grimnes S, Piltan H (2004): Cutaneous perception of electrical direct current. *Innov. Tech. Biol. Med.*, 25(4), 240–243.
- Martinsen ØG, Clausen S, Nysæther JB, Grimnes S (2007): Utilising characteristic electrical properties of the epidermal skin layers to detect fake fingers in biometric fingerprint systems - A pilot study. *IEEE Trans. Biomed. Eng.*, 54(5), 891–894
- Masuda S, Washizu M, Iwadare M (1987): Separation of small particles suspended in liquid by nonuniform travelling field. *IEEE Trans Ind Appl*, 23, 474–480.
- McAdams ET, Jossinet J (1991a): DC nonlinearity of the solid electrode–electrolyte interface impedance. *Innov Tech Biol Med*, 12, 330–343.
- McAdams ET, Jossinet J (1991b): The impedance of electrode-skin impedance in high resolution electrocardiography. *Automedica*, 13, 187–208.
- McAdams ET, Jossinet J (1994): The detection of the onset of electrode–electrolyte interphase impedance nonlinearity: a theoretical study. *IEEE Trans Biomed Eng*, 41(5), 498–500.
- McFee R, Johnston FD (1953): Electrocardiographic leads. *Circulation*, 8, 554–568.
- Menachery A, Pethig R (2005): Controlling cell destruction using dielectrophoretic forces. *IEE Proc Nanobiotechnol*, 152(4), 145–149.
- Metherall P, Barber DC, Smallwood RH, Brown BH (1996): Three dimensional electrical impedance tomography. *Nature*, 380(6574), 509–512.
- Merwa R, Hollaus K, Brandstätter and Scharfetter H (2003): Numerical solution of the general 3D eddy current problem for magnetic induction tomography (spectroscopy). *Physiol. Meas.* 24, 545–554.
- Miller L, Leor J, Rubinsky B (2005): Cancer cells ablation with irreversible electroporation. *Technol Cancer Res Treat*, 4, 699–705.
- Min M, Parve T (1996): A current mode signal processing in lock-in instruments for bio-impedance measurement. *Med Biol Eng Comput*, 34(suppl 1, part 2), 167–178.
- Min M, Parve T (1997): A current mode signal processing as a challenge for improvement of lock-in measurement instruments. *Proc XIV IMEKO World Congress*, VII, 186–191.
- Mir LM (2001): Therapeutic perspectives of in vivo cell electroporation. *Bioelectrochemistry*, 53, 1–10.

- Mirtaheiri P, Grimnes S, Martinsen ØG (2005): Electrode polarization impedance in weak NaCl aqueous solutions. *IEEE Trans Biomed Eng*, 52(12), 2093–2099.
- Mørkrid L, Qiao ZG (1988): Continuous estimation of parameters in skin electrical admittance from simultaneous measurements at two different frequencies. *Med Biol Eng Comput*, 26, 633–640.
- Morucci JP, Marsili PM, Granie M et al. (1994): A direct sensitivity matrix approach for fast reconstruction in electrical impedance tomography. *Physiol. Meas*, 15 (suppl. 2A), 107–114.
- Mørkrid L, Ohm O-J, Hammer E (1980): Signal source impedance of implanted pacemaker electrodes estimated from spectral ratio between loaded and unloaded electrograms in man. *Med Biol Eng Comput*, 18, 223–232.
- Moshkovitz Y, Kaluski E, Milo O, Vered Z, Cotter G (2004): Recent developments in cardiac output determination by bioimpedance: comparison with invasive cardiac output and potential cardiovascular applications. *Curr Opin Cardiol*, 19, 229–237.
- Moskalenko YE (ed) 1980 *Biophysical Aspects of Cerebral Circulation*. Pergamon, Oxford.
- Moussavi M, Schwan HP, Sun HH (1994): Harmonic distortion caused by electrode polarisation. *Med Biol Eng Comp*, 32, 121–125.
- Mudraya IS, Kirpatovsky VI, Martov AG (2007): Bioimpedance methods in urology functional diagnostics. ICEBI 2007, Graz, *IFMBE Proceedings*, Vol. 17, 707–710.
- Munk H (1873): Über die galvanische Einführung differenter Flüssigkeiten in der unversehrten lebenden Organismus. *Arch Anat Physiol Wissens Med*, 505–516.
- Murphy D, Burton P, Coombs R, Tarassenko L, Rolfe P (1987): Impedance imaging in the newborn. *Clin Phys Physiol Meas*, 8(suppl A), 131–140.
- Neumann E, Katchalsky A (1972): Long lived conformation changes induced by electric impulses in biopolymers. *Proc Nat Acad Sci USA*, 69, 993–997.
- Neumann E, Rosenheck K (1972): Permeability changes induced by electric pulses in vesicular membranes. *J Membrane Biol*, 10, 279–290.
- Neuman RN (1992): Biopotential electrodes. In: Webster JG (Ed.), *Medical instrumentation*. Houghton Mifflin.
- Nescolarde L, Garcález MA, Rossell-Ferrer J (2006) Thoracic vs whole-body bioimpedance measurements: relation to hydration status and hypertension in peritoneal dialysis patients. *Physiol. Meas.*, 27, pp. 961–971
- Newell JC, Peng Y, Edic PM, Blue RS, Jain H, Newell RT (1998): Effect of electrode size on impedance images of two- and three-dimensional objects. *IEEE Trans Biomed Eng*, 45(4), 531–534.
- Nicander I (1998): Electrical impedance related to experimentally induced changes of human skin and oral mucosa. Ph.D. Thesis, Karolinska Institute, Stockholm.
- Nicander I, Ollmar S, Eek A, Lundh Rozell B, Emtestam L (1996): Correlation of impedance response patterns to histological findings in irritant skin reactions induced by various surfactants. *Br J Dermatol*, 134, 221–228.
- Nie R, Chin AB, Lee KS, Sunmonu NA, Rutkove SB (2006): Electrical impedance myography: transitioning from human to animal studies. *Clin Neurophys*, 117, 1844–1849.
- NIH (1994). Bioelectrical impedance analysis in body composition measurements. *National Institute of Health: Technology Assessment Conference Statement*, 1–37.
- Nolkrantz K, Farre C, Brederlau A, Karlsson RID, Brennan C, Eriksson PS, Weber SG, Sandberg M, Orwar O (2001): Electroporation of single cells and tissues with an electrolyte-filled capillary. *Anal Chem*, 73, 4469–4477.

- Norlén L, Nicander I, Lundh RB, Ollmar S, Forslind B (1999): Differences in human stratum corneum lipid content related to physical parameters of skin barrier function in vivo. *J Invest Dermatol*, **112**, 72–77.
- Nuccitelli R, Pliquett U, Chen X, Ford W, Swanson JR, Beebe SJ, Kolb JF, Schoenbach K (2006): Nanosecond pulsed electric fields cause melanomas to self-destruct. *Biochem Biophys Res Comm*, **342**, 351–360.
- Nuutinen J, Lahtinen T, Turunen M, Alanen E, Tenhunen M, Usenius T, Kolle R (1998): A dielectric method for measuring early and late reactions in irradiated human skin. *Radiother Oncol*, **47**, 249–254.
- Nyboer J (1960): Regional pulse volume and perfusion flow measurement. *AMA Arch Int Med*, **105**, 264–276.
- Nyboer J (1970): Electrorheometric properties of tissues and fluids. *Ann NY Acad Sci*, **170**, 410–420.
- Nyboer J (1950): Electrical impedance plethysmography. *Circulation* **2**, 811–887
- Oh SH, Lee BI, Woo EJ et al. (2005): Electrical conductivity images of biological tissue phantoms in MREIT. *Physiol Meas* **26**, S279–S288.
- Oliver MA, Gobantes I, Arnau J et al. (2001) Evaluation of the Electrical Impedance Spectroscopy (EIS) equipment for ham meat quality selection. *Meat Science*, **58**, 305–312
- Ollmar S (1997): Noninvasive monitoring of transplanted kidneys by impedance spectroscopy – a pilot study. *Med Biol Eng Comput*, **35**(suppl part 1), 336.
- Ollmar S (1998): Methods for information extraction from impedance spectra of biological tissue, in particular skin and oral mucosa – a critical review and suggestions for the future. *Bioelectrochem Bioenerg*, **45**, 157–160.
- Ollmar S, Nicander I (1995): Information in multi frequency measurement of intact skin. *Innov Tech Biol Med*, **16**, 745–751.
- Ollmar S, Nicander I (2005): Within and beyond the skin barrier as seen by electrical impedance. In: Fluhr J, Maibach H, Berardesca E, Elsner P (Eds), *Bioengineering of the skin: water and the stratum corneum*, 2nd edn. CRC Press, Boca Raton, pp. 335–350.
- Ollmar S, Eek A, Sundstrøm F, Emtestam L (1995): Electrical impedance for estimation of irritation in oral mucosa and skin. *Med Prog Technol*, **21**, 29–37.
- Ollmar S, Nicander I, Åberg P, Birgersson U (2007): Evolution of a diagnostic decision support tool based on electrical impedance. *Proceedings of the XIII International Conference on Electrical Bioimpedance*. IFMBE Proc, **17**, 4–7.
- Olofsson J, Nolkranz K, Ryttsén F, Lambie BA, Weber SG, Orwar O (2003): Single-cell electroporation. *Curr Opin Biotechnol*, **14**, 29–34.
- Onaral B, Schwan HP (1982): Linear and nonlinear properties of platinum electrode polarisation. Part I: Frequency dependence at very low frequencies. *Med Biol Eng Comp*, **20**, 299–306.
- Onsager L (1934): Deviations from Ohm's law in weak electrolytes. *J Chem Phys*, **2**, 599–615.
- Onsager L (1936): Electrical moments of molecules in liquids. *J Am Chem Soc*, **58**, 1486.
- Oostendorp TF, Delbeke J, Stegeman DF (2000): The conductivity of the human skull: results of in vivo and in vitro measurements. *IEEE Trans Biomed Eng*, **47**, 1487–1492.
- Page CC, Moser CC, Chen X, Dutton L (1999): Natural engineering principles of electron tunnelling in biological oxidation reduction. *Nature*, **402**, 47–52.
- Patterson R (1995): Bioelectric impedance measurement. In: Bronzino JD (Ed.), *The biomedical engineering handbook*. CRC Press, Boca Raton, pp. 1223–1230.
- Pauly H, Schwan HP (1959): Über die Impedanz einer Suspension von Kugelförmigen Teilchen mit einer Schale. *Z Naturfor*, **14b**, 125–131.

- Pauly H, Schwan HP (1966): Dielectric properties and ion mobility in erythrocytes. *Biophys J*, **6**, 621.
- Pearson K (1901): On lines and planes of closest fit to systems of points in space. *Philos Mag*, **2**, 559–572.
- Pere JR and Cristina L (1999) Practical Limits of the Kramers-Kronig Relationships Applied To Experimental Bioimpedance Data. *Annals of the New York Academy of Sciences*, **873**, 374–380
- Pethig R, Kell DB (1987): The passive electrical properties of biological systems: their significance in biology, biophysics and biotechnology. *Phys Med Biol*, **32**, 933–970.
- Pethig R, Talary MS (2007): Dielectrophoretic detection of membrane morphology changes in Jurkat T-cells undergoing etoposide-induced apoptosis. *IET Nanobiotechnol*, **1**, 2–9.
- Pethig R, Bressler V, Carswell-Crumpton C, Chen Y, Foster-Haje L, Garcia-Ojeda ME, Lee RS, Lock GM, Talary MS, Tate KM (2002): Dielectrophoretic studies of the activation of human T lymphocytes using a newly developed cell profiling system. *Electrophoresis*, **23**, 2057–2063.
- Pethig R, Jakubek LM, Sanger RH, Heart E, Corson ED, Smith PJS (2005): Electrokinetic measurements of membrane capacitance and conductance for pancreatic β -cells. *IEE Proc Nanobiotechnol*, **152**(6), 189–193.
- Piccoli A, Rossi B, Pillon L, Buccianto G (1994): A new method for monitoring body fluid variation by bioimpedance analysis: the RXc graph. *Kidney Int*, **46**, 534–539.
- Piccoli A, Pillon L, Dumler F (2002): Impedance vector distribution by sex, race, body mass index, and age in the United States: standard reference intervals as bivariate Z scores. *Nutrition*, **18**, 153–167.
- Piccoli A, Pastori G, Guizzo M, Rebeschini M, Naso A, Cascone C (2005): Equivalence of information from single versus multiple frequency bioimpedance vector analysis in hemodialysis. *Kidney Int*, **67**, 301–313.
- Pliquett U, Weaver JC (1996): Electroporation of human skin: simultaneous measurement of changes in the transport of two fluorescent molecules and in the passive electrical properties. *Bioelectrochem Bioenerg*, **39**, 1–12.
- Pliquett U, Krassen H, Frantescu CG, Wesner D, Neumann E, Schoenbach K (2005): Asymmetric changes in membrane conductance due to hyper- and depolarization: probing with current and voltage clamp. *IFMBE Proc*, **11**, 1923.
- Pliquett U, Joshi RP, Sridhara V, Schoenbach K (2007): High electrical field effects on cell membranes. *Bioelectrochemistry*, **70**, 275–282.
- Plonsey R, Barr R (1982): The four-electrode resistivity technique as applied to cardiac muscle. *IEEE Trans Biomed Eng*, **29**(7), 541–546.
- Pohl HA (1958): Some effects of nonuniform fields on dielectrics. *J Appl Phys*, **29**, 1182–1188.
- Pomerantz M, Baumgartner R, Lauridson J et al. (1969): Transthoracic electrical impedance for the early detection of pulmonary edema. **66**, 260–268.
- Qiao ZG, Mørkrid L, Grimnes S (1987): Three-electrode method to study event-related responses in skin electrical potential, admittance and blood flow. *Med Biol Eng Comput*, **25**, 567–572.
- Qu M, Zhang Y, Webster JG, Tompkins WJ (1986): Motion artefact from spot and band electrodes during impedance cardiography. *IEEE Trans Biomed Eng*, **33**(11), 1029–1036.
- Rae JL, Levis RA (2002): Single-cell electroporation. *Pflugers Arch*, **443**, 664–670.

- Riu P, Rosell J, Lozano A, Pallas-Areny R (1992): A broadband system for static imaging in electrical impedance tomography. *Clin Phys Physiol Meas*, 13(suppl A), 61–66.
- Riu P, Rosell J, Lozano A, Pallas-Areny R (1995): Multifrequency static imaging in electrical impedance tomography. Part 1: instrumentation requirements. *Med Biol Eng Comput*, 33, 784–792.
- Riu PJ, Rosell J, Bragos R, Casas O (1999): Electrical bioimpedance methods: Applications to medicine and biotechnology. *Ann N.Y Acad of Sci*. Vol 873.
- Robbins CR (1979): *Chemical and physical behaviour of human hair*. Van Norstrand Reinhold, New York.
- Robinson D, Lee ES, Iqbal Z, Rognlien JL, Davalos RV (2007): Reinforced vesicles withstand rigors of microfluidic electroporation. *Sens Actuat: B Chem*, 125, 337–342.
- Roberto E, Serrano, Bruno de Lema, Oscar Casas et al. (2002) Use of Electrical Impedance Tomography (EIT) for the Assessment of Unilateral Pulmonary Function. *Physiological Measurement*, 23:1, 211–220
- Rosell J, Riu P (1992): Common-mode feedback in electrical impedance tomography. *Clin Phys Physiol Meas*, 13(suppl A), 11–14.
- Rosell J, Colominas J, Riu P, Pallas-Areny R, Webster JG (1988a): Skin impedance from 1 Hz to 1 MHz. *IEEE Trans Biomed Eng*, 35(8), 649–651.
- Rosell J, Murphy D, Pallas-Areny R, Rolfe P (1988b): Analysis and assessment of errors in a parallel data acquisition system for electrical impedance tomography. *Clin Phys Physiol Meas*, 9(suppl A), 93–100.
- Rosell J, Casañas R, Scharfetter H (2001): Sensitivity maps and system requirements for magnetic induction tomography using a planar gradiometer. *Physiol Meas*, 22, 121–130.
- Rosen D (1963): Dielectric properties of protein powders with adsorbed water. *Trans Farad Soc*, 59, 2178–2191.
- Rosendal T (1940): The conducting properties of the human organism to alternating currents. Thesis, Munksgaard, Copenhagen.
- Ruiz GA, Felice CJ, Valentinuzzi ME (2005). Non-linear response of electrode–electrolyte interface at high current density. *Chaos, Solitons and Fractals* 25, 649–654.
- Rubinsky B (2007): Irreversible electroporation in medicine. *Technol Cancer Res Treat*, 6, 255–260.
- Rutkove SB, Aaron R, Shiffman CA (2002): Localized bioimpedance analysis in the evaluation of neuromuscular disease. *Muscle Nerve*, 25, 390–397.
- Rutkove SB, Esper GJ, Lee KS, Aaron R, Shiffman CA (2005): Electrical impedance myography in the detection of radiculopathy. *Muscle Nerve*, 32, 335–341.
- Rutkove SB, Lee KS, Shiffman CA, Aaron R (2006): Test-retest reproducibility of 50 kHz linear-electrical impedance myography. *Clin Neurophys*, 117, 1244–1248.
- Ryttsen F, Farre C, Brennan C, Weber SG, Nolkranz K, Jardemark K, Chiu DT, Orwar O (2000): Characterization of single-cell electroporation by using patch-clamp and fluorescence microscopy. *Biophys J*, 79, 1993–2001.
- Sachs J, Peyerl P, Woeckel S, Kmec M, Herrmann R, Zetik R (2007). Liquid and moisture sensing by ultra wideband pseudo noise sequence signals, *Meas. Sci. Technol*, 18:1074–1087
- Sakamoto K, Kanai H (1979): Electrical characteristics of flowing blood. *IEEE Trans Biomed Eng*, BME-20, 687–695.
- Sale AJ, Hamilton WA (1967): Effects of high electric fields on micro-organisms. 1. Killing of bacteria and yeasts. *Biochim Biophys Acta*, 148, 781–788.

- Salter DC (1979): Quantifying skin disease and healing in vivo using electrical impedance measurements. In: Rolfe P (Ed.), *Non-invasive physiological measurements*, Vol. 1. Academic Press.
- Salter DC (1981). Studies in measurement, form and interpretation of some electrical properties of normal and pathological skin in vivo. Ph.D. Thesis, University of Oxford, UK.
- Salter DC (1998): Examination of stratum corneum hydration state by electrical methods. In: Elsner P et al. (Eds) *Skin Bioengineering. Techniques and applications in dermatology and cosmetology*. Karger.
- Saulnier G, Liu JN, Tamma C, Xia H, Kao T-J, Newell JC, Isaacson D (2007). An Electrical Impedance Spectroscopy System for Breast Cancer Detection. *Proc IEEE-EMBS Conf.* 1, 4154–4157.
- Scaife JM, Tozer RC, Freestone IL (1994): Conductivity and permittivity images from an induced current electrical impedance tomography system. *IEE Proc-Sci Meas Technol*, 141(5), 356–362.
- Schäfer M, Schlegel C, Kirlum H-J, Gersing E, Gebhard MM (1998): Monitoring of damage to skeletal muscle tissue caused by ischemia. *Bioelectrochem Bioenerg*, 45, 151–155.
- Scharfetter H, Hartinger P, Hinghofer SH, Hutten H (1998): A model of artefacts produced by stray capacitance during whole body or segmental bioimpedance spectroscopy. *Physiol Meas*, 19(2), 247–261.
- Scharfetter H, Casañas R, Rosell J (2003): Biological tissue characterization by magnetic induction spectroscopy (MIS): requirements and limitations. *IEEE Trans Biomed Eng*, 50, 870–880.
- Scharfetter H, Brunner P, Merwa R (2006a): Magnetic induction tomography single-step solution of the 3-D inverse problem for differential image reconstruction. *Int J Informat Syst Sci*, 2(4), 585–606.
- Scharfetter H, Hollaus K, Rosell-Ferrer J, Merwa R. (2006b) Single-step 3-D image reconstruction in magnetic induction tomography: Theoretical limits of spatial resolution and contrast to noise ratio. *Annals of Biomedical Engineering* 34: 1786–1798.
- Schlumberger C (1920): *Etude sur la Prospection Electrique du Sous-sol*. Gauthier-Villars, Paris.
- Schmitt OH (1957): Lead vectors and transfer impedance. *Ann NY Acad Sci*, 65, 1092–1109.
- Schnelle T, Mueller T, Fiedler S, Shirley SG, Ludwig K, Herrmann A, Fuhr G, Wagner B, Zimmermann U (1996): Trapping of viruses in high-frequency electric field cages. *Naturwissenschaften*, 83, 172–176.
- Schoenbach K, Joshi RP, Kolb J, Chen N, Stacey M, Blackmore PF, Buescher ES, Beebe SJ (2004): Ultrashort electrical pulses open a new gateway into biological cells. *Proc IEEE*, 92, 1122.
- Schwan HP (1954): Die elektrischen Eigenschaften von Muskelgewebe bei Niederfrequenz. *Z Naturfor*, 9b, 245.
- Schwan HP (1957): Electrical properties of tissue and cell suspensions. In: Lawrence JH, Tobias CA (Eds), *Advances in biological and medical physics*, Vol. V. Academic Press, pp. 147–209.
- Schwan HP (1963): Determination of biological impedances. In: Nastuk WL (Ed.), *Physical techniques in biological research*, Vol. 6. Academic Press, pp. 323–406.
- Schwan HP (1968): Electrode polarization impedance and measurements in biological materials. *Ann NY Acad Sci*, 148, 191–208.
- Schwan HP (1982): Nonthermal cellular effects of electromagnetic fields: ac-field induced ponderomotive forces. *Br J Cancer*, 43(suppl 5), 220–224.

- Schwan HP (1985): Dielectric properties of the cell surface and biological systems. *Stud Biophys*, **110**, 13–18.
- Schwan HP (1988): Biological effects of non-ionizing radiations: cellular properties and interactions. *Ann Biomed Eng*, **16**, 245–263
- Schwan HP (1992a): Linear and non-linear electrode polarisation and biological materials. *Ann Biomed Eng*, **20**, 269–288.
- Schwan HP (1992b): Early history of bioelectromagnetics. *Bioelectromagnetics*, **13**, 453–467.
- Schwan HP (1993): Early organizations of biomedical engineering in the US. *IEEE Eng Med Biol Mag*, Sept., 25–29.
- Schwan HP (2001): Selected papers by Herman P Schwan. Grimnes S, Martinsen ØG (Eds), *Medisinsk-teknisk avdelings forlag*, ISBN 82-7642-008-7, ogm@fys.uio.no.
- Schwan HP, Ferris CD (1968): Four-electrode techniques for impedance measurement with high resolution. *Rev Sci Instr*, **39**(4), 481–485.
- Schwan HP, Foster KR (1980): RF-field interactions with biological systems: electrical properties and biophysical mechanism.
- Schwan HP, Kay CF (1957): The conductivity of living tissue. *Ann NY Acad Sci*, **65**, 1007.
- Schwan HP, Morowitz HJ (1962): Electrical properties of the membranes of the pleuro-pneumonia-like organism A5969. *Biophys J*, **2**, 295.
- Schwan HP, Sher LD (1969): Electrostatic fields induced forces and their biological implications. In: Pohl HA, Pickard WF (Eds), *Dielectrophoretic and electrophoretic deposition*. The Electrochemical Society, Inc, New York, pp. 107–126.
- Schwan HP, Schwartz G, Maczuk J, Pauly H (1962): On the low frequency dielectric dispersion of colloidal particles in electrolyte solution. *J Phys Chem*, **66**, pp. 2626–2636.
- Schwan HP, Takashima S, Miyamoto VK, Stoeckenius W (1970): Electrical properties of phospholipid vesicles. *Biophys J*, **10**, 1102.
- Schwartz G (1962): A theory of the low frequency dispersion of colloidal particles in electrolyte solution. *J Phys Chem*, **66**, 2636.
- Schwartz G (1967): On dielectric relaxation due to chemical rate processes. *J Phys Chem*, **71**, 4021–4030.
- Schwartz G (1972): Dielectric relaxation of biopolymers in solution. *Adv Mol Relax Process*, **3**, 281.
- Serrano RE, Riu PJ, De Lema B, Casan P (2004): Assessment of the Unilateral Pulmonary function by means of Electrical Impedance Tomography using a Reduced Electrode Set. *Physiological Measurement*, **25**:4, 803–813
- Shankar TMR, Webster JG, Shao S-Y (1985): The contribution of vessel volume change and blood resistivity change to the electrical impedance pulse. *IEEE Trans Biomed Eng*, **32**(3), 192–198.
- Shiffman CA, Aaron R, Amoss V, Therrien J, Coomler K (1999): Resistivity and phase in localized BIA. *Phys Med Biol*, **44**, 2409–2429.
- Shiffman CA, Aaron R, Rutkove SB (2003): Electrical impedance of muscle during isometric contraction. *Physiol Meas*, **24**, 213–234.
- Sigman E, Kolin A, Katz LN, Jochim K (1937): Effect of motion on the electrical conductivity of the blood. *Am J Physiol*, **118**, 708–719.
- Sipos K, Bodo M, Veer A, Hagtvet KA, Banyasz A (1994): Neurosis, depression, anxiety and stroke risk factors in a Hungarian village. *Kalokagathia* (Review of the Hung. Univ. of Physical Education) XXXII, 94–114, Budapest.

- Slager CJ, Schuurbiens JCH, Oomen JAF, Bom N (1993): Electrical nerve and muscle stimulation by radio frequency surgery: role of direct current loops around the active electrode. *IEEE Trans Biomed Eng*, **40**, 182–187.
- Smallwood RH, Mangnallm YF, Leathard AD (1994): Transport of gastric contents. *Physiol Meas*, **15**(suppl 2A), 175–188.
- Smith SR, Foster KR (1985): Dielectric properties of low water content tissues. *Phys Med Biol*, **30**, 965.
- Song A, Parus S, Kopelman R (1997): High-performance fiber-optic pH microsensors for practical physiological measurements using a dual-emission sensitive dye. *Anal Chem*, **69**, 863–867.
- Song CG, Kim SC, Nam KC and Kim DW (2005). Optimum electrode configuration for detection of leg movement using bio-impedance. *Physiol. Meas.* **26**, S59–S68.
- South GP, Grant EH (1972): Dielectric dispersion and dipole moment of myoglobin in water. *Proc Roy Soc London*, **A(328)**, 371–387.
- South GP, Grant EH (1973): The contribution of proton fluctuation to dielectric relaxation in protein solutions. *Biopolymers*, **12**, 1937–1944.
- Sramek BB (1981): Noninvasive technique for measurement of cardiac output by means of electrical impedance. *Proceedings of the Vth ICEBI*, Tokyo, pp. 39–42.
- Sun SS, Chumlea WC, Heymsfield SB, et al. (2003): Development of bioelectrical impedance analysis prediction equations for body composition with the use of a multicomponent model for use in epidemiological surveys. *Am J Clin Nutr* **77**, 331–340
- Stoy RD, Foster KR, Schwan HP (1982): Dielectric properties of mammalian tissues from 0.1 to 100 MHz. A summary of recent data. *Phys Medical Biol*, **27**, 501–513.
- Suttner S, Schollhorn T, Boldt J et al. (2006): Noninvasive assessment of cardiac output using thoracic electrical bioimpedance in hemodynamically stable and unstable patients after cardiac surgery: a comparison with pulmonary artery thermodilution. *Intensive Care Med*, **32**, 2053–2058.
- Suttner S, Schollhorn T, Boldt J, Mayer J, Rohm KD, Lang K, Piper SN (2006): Noninvasive assessment of cardiac output using thoracic electrical bioimpedance in hemodynamically stable and unstable patients after cardiac surgery: a comparison with pulmonary artery thermodilution. *Intensive care med*, **32**, 2053-2058
- Stuchly MA, Stuchly SS (1990): Electrical properties of biological substances. In: Gandhi OP (Ed.), *Biological effects and medical applications of electromagnetic energy*. Prentice Hall.
- Surowiec A, Stuchly SS, Swap A (1986): Postmortem changes of the dielectric properties of bovine brain tissue at low radiofrequencies. *Bioelectromagnetics*, **7**, 31.
- Swanson DK, Webster JG (1983): Errors in four-electrode impedance plethysmography. *Med Biol Eng Comput*, **21**, 674–680.
- Takashima S (1962): Dielectric dispersion of protein solutions in viscous solvents. *J Polymer Sci*, **56**, 257–265.
- Takashima S (1967): Effect of ions on the dielectric relaxation of DNA. *Biopolymers*, **5**, 899–913.
- Takashima S, Schwan HP (1965): Dielectric dispersion of crystalline powders of amino acids, peptides and proteins. *J Phys Chem*, **69**, 4176–4182.
- Takashima S, Schwan HP (1974): Passive electrical properties of the squid axon membrane. *J Membr Biol*, **17**, 51–68.
- Takashima S, Yantorno RE (1977): Investigation of the voltage dependent membrane capacity of squid axon. *Ann NY Acad Sci*, **303**, 306–321.

- Talary MS, Burt JPH, Tame JA, Pethig R (1996): Electromanipulation and separation of cells using travelling electric fields. *J Phys D: Appl Phys*, **29**, 2198–2203.
- Tarulli A, Esper GJ, Lee KS, Aaron R, Shiffman CA, Rutkove SB (2005): Electrical impedance myography in the bedside assessment of inflammatory myopathy. *Neurology*, **65**, 451–452.
- Teruel MN, Meyer T (1997): Electroporation-induced formation of individual calcium entry sites in the cell body and processes of adherent cells. *Biophys J*, **73**, 1785–1796.
- Therkildsen P, Hædersdal M, Lock-Andersen J, Olivarius FdF, Poulsen T, Wulf HC (1998): Epidermal thickness measured by light microscopy: a methodological study. *Skin Res Technol*, **4**, 174–179.
- Thomasset AL (1965): Mesure du volume des liquides extra-cellulaires par la methode electro-chimique signification biophysique de l'impedance a 1 kilocycle du corps humain. *Lyon Med*, **214**, 131–143.
- Tian-Hua Yu, Jing Liu, Yi-Xin Zhou (2004) Using electrical impedance detection to evaluate the viability of biomaterials subject to freezing or thermal injury. *Anal Bioanal Chem* **378**: 1793–1800
- Tozer JC, Ireland EH, Barber B (1998): Magnetic impedance tomography. *Proceedings of the X International Conference on Electrical Bio-Impedance*, Barcelona, pp. 369–372.
- Tregear RT (1965): Interpretation of skin impedance measurements. *Nature*, **205**, 600–601.
- Tronstad C, Grimnes S, Martinsen ØG, Fosse E (2007): Development of a medical device for long-term sweat activity measurements. H. Scharfetter, R. Merva (Eds.): ICEBI 2007, IFMBE Proceedings 17, pp. 236–239.
- Ugland OM (1967): Electrical burns. *Scand J Plast Reconstr Surg*, suppl. 2, 1–74.
- Vasilkoski Z, Esser AT, Gowrishankar TR, Weaver JC (2006): Membrane electroporation: the absolute rate equation and nanosecond time scale pore creation. *Phys Stat Sol*, **74**, 021904.
- Venables PH, Christie MJ (1980): Electrodermal activity. In: Martin I, Venables PH (Eds), *Techniques in psychophysiology*. John Wiley & Sons.
- Vernhes MC, Cabanes PA, Teissie J (1999): Chinese hamster ovary cells sensitivity to localized electrical stresses. *Bioelectrochem Bioenerg*, **48**, 17–25.
- Vistnes AI, Wormald DI, Isachsen S, Schmalbein D (1984): An efficient digital phase-sensitive detector for use in electron-spin-resonance spectroscopy. *Rev Sci Instr*, **55**, 527–532.
- Vollmann D, Nagele H, Schauerte P et al. (2007): Clinical utility of intrathoracic impedance monitoring to alert patients with an implanted device of deteriorating chronic heart failure. *Eur Heart J*, **28**(15), 1835–1840.
- Wada A, Nakamura H (1981): Nature of charge distribution in proteins. *Nature*, **293**, 757–758.
- Wagner KW (1914): Explanation of the dielectric fatigue phenomena on the basis of Maxwell's concept. *Arch Elektrotech (Berlin)*, **2**, 271.
- Wang L, Lahtinen S, Lentz L et al. (2005): Feasibility of using and implantable system to measure thoracic congestion in an ambulatory chronic heart failure canine model. *PACE*, **28**, 404–411.
- Wang X-B, Huang Y, Hölzel R, Burt JPM, Pethig R (1993): Theoretical and experimental investigations of the interdependence of the dielectric dielectrophoretic and electro-rotational behaviour of colloidal particles. *J Phys D: Appl Phys*, **26**, 312–322.
- Warburg E (1899): Über das Verhalten sogenannte unpolarisierbare Elektroden gegen Wechselstrom. *Ann Phys Chem*, **67**, 493–499.
- Washizu M, Kurosawa O (1990): Electrostatic manipulation of DNA in microfabricated structures. *IEEE Trans Ind Appl*, **26**, 1165–1172.

- Washizu M, Suzuki S, Kurosawa O, Nishizaka T, Shinohara T (1994): Molecular dielectrophoresis of biopolymers. *IEEE Trans Ind Appl*, 30, 835–843.
- Weaver JC (1994): Theory of electroporation. *Biomembrane electrochemistry*, pp. 447–470.
- Weaver JC (1995). Electroporation theory: concepts and mechanisms. *Methods in molecular biology*. Humana Press, Inc, Totowa, NJ.
- Weaver JC (2000): Electroporation of cells and tissues. *IEEE Trans Plasma Sci*, 28, 24–33.
- Weaver JC (2003): Electroporation of biological membranes from multicellular to nano scales. *IEEE Trans Dielect Elect Ins*, 10, 754–768.
- Weaver JC, Barnett A (1992): Progress toward a theoretical model of electroporation mechanism: membrane electrical behavior and molecular transport. In: *Guide to electroporation and electrofusion 26*.
- Weaver JC, Chizmadzhev YA (1996): Theory of electroporation: a review. *Bioelectrochem Bioenerg*, 41, 135–160.
- Weiss G (1901): Sur la possibilite de rendre comparables entre eux les appareils servant a l'excitation électrique. *Arch Ital Biol*, 35, 413–446.
- Wien M (1928): Über die Abweichungen der Elektrolyte vom Ohmischen Gesetz. *Phys Z*, 29, 751–755.
- Wien M (1931): Über Leitfähigkeit und Dielektrizität Konstante von Elektrolyten bei Hochfrequenz. *Phys Z*, 32, 545–547.
- Wightman RM, Jankowski JA, Kennedy RT, Kawagoe KT, Schroeder TJ, Leszczyszyn DJ, Near JA, Diliberto EJ Jr., Viveros OH (1991): Temporally resolved catecholamine spikes correspond to single vesicle release from individual chromaffin cells. *Proc Natl Acad Sci USA*, 88, 10754–10758.
- Williams G, Watts DC (1970): Non-symmetrical dielectric relaxation behavior arising from a simple empirical decay function. *Trans Farad Soc*, 66, 80–85.
- Wilson FN (1953): Foreword to “Electrocardiographic Leads”, cf. McFee and Johnston (1953).
- Yamamoto T, Yamamoto Y (1976): Electrical properties of the epidermal stratum corneum. *Med Biol Eng*, 14, 592–594.
- Yamamoto T, Yamamoto Y (1978): Dispersion and correlation of the parameters for skin impedance. *Med Biol Eng*, 14, 151–158.
- Yamamoto T, Yamamoto Y (1981): Non-linear electrical properties of the skin in the low frequency range. *Med Biol Eng Comp*, 19, 302–310.
- Yamamoto Y, Yamamoto T (1977): Analysis for the change of skin impedance. *Med Biol Eng*, 16, 219–227.
- Yamamoto Y, Yamamoto T, Ozawa T (1986): Characteristics of skin admittance for dry electrodes and the measurement of skin moisturisation. *Med Biol Eng Comput*, 24, 71–77.
- Yelamos D, Casas O, Bragos R, Rosell J (1999): Improvement of a front end for bioimpedance spectroscopy. *Ann NY Acad Sci*, 873, 306–312.
- Yolocauhtli Salazar, Ramon Bragos, Oscar Casas et al. (2004) Transmural Versus Non-transmural In Situ Electrical Impedance Spectrum for Healthy, Ischemic, and Healed Myocardium. *IEEE Transactions on Biomedical Engineering*, vol. 51, no. 8, pp. 1421–1427
- Yu C, Wang L, Chau E, Chan RHW, Kong SL, Tang MO, Christensen J, Stadler RW, Lau CP, (2005): Intrathoracic impedance monitoring in patients with heart failure. Correlation with fluid status and feasibility of early warning preceding hospitalization. *Circulation*, 112, 841–848.

- Zhang MIN, Repo T, Willison JHM, Sutinen S (1995): Electrical impedance analysis in plant tissues: on the biological meaning of Cole-Cole α in Scots pine needles. *Eur Biophys J*, **24**, 99–106.
- Zheng QA, Chang DC (1991): High-efficiency gene transfection by in situ electroporation of cultured cells. *Biochim Biophys Acta*, **1088**, 104–110.
- Zhou X-F, Markx GH, Pethig R, Eastwood IM (1995): Differentiation of viable and non-viable bacterial biofilms using electrorotation. *Biochim Biophys Acta*, **1245**, 85–93.
- Zoll PM, Linenthal AJ (1964): External electrical stimulation of the heart. *Ann NY Acad Sci*, **III**, 932–937.

This page intentionally left blank

INDEX

- α parameter, 311
- Ablation, 377
- Accommodation effect, 361
- Action potential, 140, 143–147
- Activation energy, 49
- Acupuncture, 358–359
- Adipose tissue, 106
- Admittance, 2, 69, 206–207, 238, 290–292, 422
 - faradaic, 51
- Adsorption, 33
 - specific, 35
- After-field effect, 384
- Aggregates, 88
- Aliasing errors, 227
- Amino acids, 95–99
- Amplitude magnitude frequency spectrum, 221
- Amplitude, 215
- Analog lock-in amplifier, 240–241
- Anelectrotonus, 360
- Anisotropy, 124–126
- Anode, 14, 42
- Aperiodic waveforms, 222–224
- Applied part, 233, 407
- Arachnoid, 149
- Argand diagram, xi
- Argand, Jean Robert, 420
- Arrhenius, Svante August, 15
- Arsonval, Arsène d', 414
- Atrioventricular (AV) node, 342
- Autocorrelation, 227
- Auxiliary currents, 407
- Axon, 151–157
- Baby wavelet, 330
- Band electrode, 270
- Basic capacitor experiment, 64–65
- Basic electrolytic experiment, 12–15
- Basic measuring circuit, 229–230
- Basic membrane experiment, 85–87
- Basic suspension experiment, 87–89
- Bidomain model, 198, 290, 342
- Bilayer lipid membrane, 100
- Bioelectric dipole, 169–173
- Bioelectric impedance analysis (BIA), 363–367
- Bioelectric signals, 139–159

- Bioelectricity, 1, 3
- Bioimmittance, 2
- Bioimpedance, 1–2
- Biomaterial, 2, 93–102
- Biometry, 388
- Biopermittivity, 2
- Biosensor, 253
- Biot, Jean-Baptiste, 201
- Bipolar, 165
 - lead, 164
 - recording, 181
- Bispectral analysis (BIS), 228
- Black box theory, 206
- Blood, 106–109
 - coagulation, 36
- Bode diagram, 294–296
- Body composition analysis, 363–367
- Body fluid volume assessment, 365
- Body forces, 37
- Body liquids, 94–95
- Body mass index (BMI), 366
- Body measurements, 119–122
- Body segment resistance, 121
- Bois-Raymond, 413
- Boltzmann equation, 32
- Bone fracture growth, 130
- Bone tissue, 106
- Bootstrapping, 231
- Bound water, 94
- Boundary value problem, 163
- Brain, 149–151
- Breakdown, 130–135
- Bridges, 237–238
- Buffer, 231
- Butler-Volmer equation, 52

- Cabrera sequence, 336
- Carbohydrates, 99–100
- Carbon tattooing, 261
- Cardiac electrophysiology, 342–343
- Cardiac pacemakers, 370–372
- Cardiac resynchronization therapy (CRT), 367
- Catelectrotonus, 360
- Cathode, 14, 42
- Caton, Richard, 413
- Causal network, 208
- CBF, 352
- CC, 164
- Cell membrane, 100–102, 133–135
- Cell polarization, 140–143
- Cell potential, 145–147
- Cell sorting/characterization, 385–386
- Cell suspension, 82, 378–388
- Cell oscillator, 147
- Cell-surface attachment, 386–387
- Cellular spin resonance, 39
- Cerebral blood flow (CBF), 352
- Cerebral circulation, 352
- Cerebrospinal fluid (CSF), 149
- Channel gating, 143–145
- Channels, 140
- Chaos theory, 327–328
- Characteristic frequency, 294
- Characteristic relaxation frequency, 73, 294
- Chemical bonds, 10–11
- Chênes, Parseval des, 225
- Chronaxie, 156, 361
- Circuit problems, 1
- Classifier, 324
- Clausius-Mosotti equation, 62
- Clinical applications, 333–409
- Clinical applications, 4
- Clinical performance, 324–326
- Clotting, 36
- Cole equations, 304–309, 416
- Cole plot, 306, 415
- Cole, Kenneth S., 414–417
- Cole, Robert H., 416–417
- Cole-Cole equations, 309–310, 416
- Cole-Cole plot, 309, 417
- Cole-compatible CPE, 301–302
- Colloidal electrolyte, 22
- Colloids, 88
- Common mode rejection ratio (CMRR), 233
- Common mode voltage, 223, 233–236
- Common-mode feedback, 201
- Complex numbers, 419–423
- Concentration wave, 53
- Conductance, 238
 - equivalent, 18
 - specific, 68
- Conductivity
 - complex, 67–68
 - ionic, 17
 - molar, 18
 - temperature dependence, 22
 - tissue, 103

- Conductor, 1, 203
 - electronic, 254–258
 - mixed, 23
- Conformal mapping, 60
- Constant phase element (CPE), 296–302
- Constricting zone, 169
- Constructional resistance, 121–122
- Contact electrolytes, 258
- Continuous frequency spectrum, 222, 225
- Convolution, 227
- Correlation, 227
- Cortex, 149
- Coulomb's law, 59–60
- Coulter counter, 387
- Counterion polarization, 34
- Counterions, 31, 83–85, 90, 98
 - in pores, 84–85
- Covalent bonds, 10–11, 95
- Current carrying (CC) electrodes, 164
- Current
 - clamp, 229
 - density field lines, 127
 - density, 17, 27
 - step, 211, 222
 - auxiliary, 407
 - electronic/ionic, 7
 - Franklin, 412
 - galvanic, 412
 - leakage, 407
 - diadynamic, 362
 - interferential, 363
- Cyclic voltammetry, 47
- Da Vinci, Leonardo, 411
- Data analysis, 322–331
- Data presentation, 321–322
- DC (direct current), 213
 - ablation, 360
 - conductance, 15–26
 - conduction, 7–11
 - conductivity, 26, 130
 - potential/current, endogenic, 129
 - properties, 129–130
 - resistance, incremental, 46–47
 - shock pulses, 361
- Death process, 122–123
- Debye equation, 62, 415
- Debye length, 16, 32
- Debye relaxation model, 71–77
 - Debye single dispersion, 71
 - Debye unit, 60
 - Debye, Peter Joseph, 16, 415
 - Debye-Falkenhagen effect, 22
 - Debye-Hückel approximation, 32
- Defibrillator, 131, 269, 361, 372–373
- Denaturation, 98
- Dendrites, 147
- Dental galvanism, 129
- Depth of measurement, 190
- Descriptive models, 284–286
- Diadynamic currents, 362
- Dialysis, 36
- Dielectric constant, 61, 66
- Dielectric decrement, 66
- Dielectric increment, 96
- Dielectric spectroscopy, 89–91
- Dielectric, 1
 - Dielectrics, 57–92, 203
- Dielectrophoresis, 38–39, 385–386
- Diffuse electric double layer, 31
- Diffusion, 28–30
- Digital lock-in amplifier, 238–240
- Dipolar ions, 96
- Dipolar, 165
- Dipole, 90
 - moment, 16, 60–63
 - bioelectric, 169–173
 - electrostatic, 203
 - heart vector, 185
 - moving current, 152
 - permanent, 77
 - technically ideal, 170–186
- Dipole-dipole interaction, 63
- Direct current (DC), *see* DC
- Disc electrode, 173–175
- Discharge, 132, 137
- Dispersing zone, 169
- Dispersion magnitudes, 103
- Dispersion model in accordance with relaxation theory, 312–313
- Dispersion, 70–71, 89–91
- Displacement current, 79, 288
- Dissipation factor, 68
- Dissociation, 15
- Distribution of relaxation times (DRT), 89, 311–315
- DNA molecule, 98–100
- Donnan effect, 142

- Donnan potentials, 44
- Double insulation, 233
- Double layer, electric, 30–35
- Driving point immittance, 207
- Dura mater, 149

- Earth, 346, 407
- ECG, 335–347
- Eddy currents, 276
- EEG, 355
- Effective electrode area (EEA), 270
- EGG, 356
- Einthoven triangle, 185, 337–340
- Einthoven, Willem, 335, 413
- Electrets, 62
- Electric arc, 261
- Electric dipole moment, 16
- Electric double layer, 30–35
- Electric fence, 406
- Electric field coupling to tissue, 278–281
- Electric field, 60
- Electrical axis of the heart, 338
- Electrical Fire, 412
- Electrical hazards, 401–405
- Electrical impedance myography (EIM), 357–358
- Electrical impedance tomography (EIT), 198–202
- Electrical model, 285
- Electrical safety, 398–409
- Electricity, quantity of, 27
- Electroacupuncture, 359
- Electrocardiography (ECG), 335–347
- Electrocautery, 374
- Electroconvulsion, 361, 374
- Electrocution, 406
- Electrode design, 270–276
- Electrode materials, 13
- Electrode polarization, 252–253
 - immittance, 53
- Electrode process, 54–55
 - equivalent circuit, 49–53
- Electrode reactions, 14–15
- Electrode systems
 - four-electrode/tetrapolar, 193–195
 - three-electrode, 191–193
 - two-electrode, 163–165
- Electrode, 8, 13, 253–281
 - (non-) polarizable, 48–49
 - band, 270
 - current carrying (CC), 164
 - cylinder/stripe, 178–179
 - disc, 173–175
 - ellipsoidal needle, 175–177
 - indifferent, 45, 346
 - invasive, 341–342
 - micro, 273–275
 - needle, 104, 175–177, 271–273
 - neutral, 45
 - pick-up (PU), 164
 - reference, 263, 346
 - spherical, 166–169
 - working, 45
- Electrodermal response (EDR), 129, 393–395
- Electrodialysis, 36
- Electrodiffusion, 28
- Electroencephalography (EEG), 355
- Electrofusion, 378–385
- Electrogastrography (EGG), 356
- Electrogenic transport, 28
- Electrogram, 165
- Electrogustometry, 399
- Electrokinesis, 36–40
- Electrokinetic effect, 385
- Electrolithotripsy, 361
- Electrolyte classification, 23
- Electrolytes, 7, 54
 - colloidal, 22
 - contact, 258
 - fused, 23
 - solid gel (hydrogel), 261, 267–268
 - solid, 23
 - wet gel, 258–260, 265
 - concentration in body liquids, 24
- Electrolytic cell, 12
- Electrolytic concentrations, 18
- Electrolytics, 7–55
- Electromagnetic field effects, 401
- Electromagnetic wave coupling, 280–281
- Electromedical equipment, 406–409
- Electromyography (EMG), 357
- Electron affinity, 10
- Electron shell configuration, 9
- Electron transfer process, 49
- Electron, valence, 9
 - velocity, 8
- Electronegativity, 9
- Electroneurography (ENeG), 357
- Electroneutrality, 17

- Electronic
 - conductor, 254–258
 - currents, 7
 - polarization, 63
- Electronystagmography (ENG), 356
- Electro-oculography (EOG), 356
- Electro-osmosis, 37, 130, 397
- Electroparacentesis, 361
- Electrophoresis, 37, 398
- Electrophoretic mobility, 37
- Electrophysiology, 3
- Electroporation, 378–385
- Electroretinography (ERG), 356
- Electrorotation, 39, 385–386
- Electroshock, 374
- Electrostatic
 - dipole, 203
 - discharge, 132, 137, 400
- Electrostriction, 135
- Electrosurgery, 132, 374–377
- Electrotherapy, 358–363
- Electrotonus, 157, 360–362
- Electrovibration, 399
- Ellipsoidal needle electrode, 175–177
- EMG, 357
- Endogenic electricity, 1
- Endogenic signal source, 230
- Endoneurium, 154
- Endorphins, 358
- Endosomatic measurements, 393
- ENeG, 357
- Energy, 78
- ENG, 356
- EOG, 356
- Epineurium, 154
- Equivalent circuits, 286–321
- Equivalent conductance, 18
- ERG, 356
- Event-related signal, 228
- Evoked potential, 228
- Evoked responses, 394
- Excitable tissue, 139–159
- Excitation, 155–156
 - cell/nerve/muscle, 402
- Exogenic electricity, 1
- Exosomatic measurements, 393
- Explanatory models, 284–286

- Faradaic admittance, 51
- Faradaic current, 27
- Faraday constant, 42
- Faraday stimulation, 413
- Faraday, Michael, 27, 413
- Faraday's law, 27
- Faradizations, 362
- Fascicle, 153
- Fast Fourier transform, 224
- Fat free mass, 365
- Fick's laws, 28
- Field problems, 1
- Field-flow fractionation, 386
- Filters, 231–233
- Fingerprint detection, 388
- Finite element method, 196–198
- Fluid status monitoring,
 - 369–370
- Flux density, 17, 61
- Flux, 27
- Forward problem, 163, 343–345
- Four-electrode system, 193–195
- Fourier analyzers, 245
- Fourier series, 214, 219, 224
- Fourier transforms, 223–228, 328
- Fourier, Joseph, 224
- Fractal curve, 223
- Fractals, 327–328
- Franklin currents, 412
- Franklin, Benjamin, 411
- Frequency domain, 224
- Frequency response, 89–91
- Fricke compatibility, 310–311
- Fricke CPE, 300–301
- Fricke, Hugo, 415
- Fricke's law, 299–301, 415
- Fulguration, 375
- Functional grounding, 233
- Funiculus, 154
- Fused electrolyte, 23

- Galvani, Luigi, 412
- Galvanic current, 213, 412
- Galvanic separation, 233–234, 407
- Galvanic skin response (GSR), 129
- Galvanism, 412
- Galvani-Volta controversy, 412
- Galvanization, 359
- Galvanometer, 412
- Galvanostat, 412
- Gap junctions, 110, 122, 155
- Gating theory, 358

- Geometrical analysis, 161–203
 Gilbert, William, 411
 Global symbols, 430–432
 Glycocalyx, 101
 Gouy-Chapman's model, 31
 Greek/Latin, 165
 Grey matter, 149
 Ground, 233–236
 Guericke, Otto von, 411
 Guldberg, Cato Maximilian, 21
 Guldberg-Waage law, 21
- Hair, 116–119
 Half-cell, 41, 254
 Hanai's equation, 82
 Harmonics, 214
 Hauksbee, Francis, 411
 Heart dipole vector, 185
 Heaviside, Oliver, 287
 Helmholtz, Hermann von, 413
 Helmholtz layer, 31
 Helmholtz' model, 31
 Henderson equation, 44
 Heterodyning, 245
 High-pass filter, 232
 Hillock, 147–148
 His Jr., Wilhelm, 342
 His-bundle, 342
 History of bioimpedance and bioelectricity, 411–418
 Hoeber, Rudolf, 414
 Hurst exponent, 327
 Hurst's rescaled range analysis (R/S analysis), 327
 Hydration number, 18
 Hydration, 16, 35
 Hydrogel, 261, 267–268
 Hydrogen
 ion, 20
 production, 361
 Hydronium, 20
 Hydroxonium, 20
 Hyperhidrosis, 396
- Ice, 95
 ICG, 353–355
 IEC, -60601–1, 408
 Immittance, 2, 69, 165, 206–207
 driving point, 207
 polarization, 264–269
- Immittivity, 69
 Impedance analyzer, 244–245
 Impedance cardiography (ICG), 353–355
 Impedance plethysmography, 347–353
 Impedance, 69, 206–207, 239, 292, 422
 electrode polarization, 53
 incremental, 132
 polarization, 166, 253, 264–269
 transfer, 187, 418
 Warburg, 52
 Implanted active thoracic devices, 367–372
 Implants, 377
 Impurities (semiconductors), 25
 In vitro data, 105
 In vivo data, 105
 Incremental DC resistance, 46–47
 Incremental impedance, 132
 Indexes, 321–322
 Indifferent electrode, 45, 346
 Inductive coil coupling, 280
 Injury potentials, 130
 Instrumentation, 205–281
 Instrumentational amplifier, 231, 234
 Insulation, 233
 Insulators, 25
 Interfaces, 28, 126–128
 Interfacial polarization, 79–85
 Interferential currents, 363
 Internal cardioverter defibrillator (ICD), 367
 International system of units (SI), xi
 Interphase phenomena, 26–40
 Interphase, 28
 Intracellular voltage clamp, 193
 Invasive electrodes, 341–342
 Inverse Fourier transform, 225
 Inverse problem, 163, 343–345
- Ion
 channels, 143
 exchanger, 36
 pumps, 140
 velocity, 8
- Ionic
 atmosphere, 16
 bonds, 10–11
 conductivity, 17
 currents, 7
 liquid, 23
 pairs, 19
 polarization, 63

- Ionization, 8–10
- Iontophoresis, 132, 269, 360, 396–398
- Irreversible electrode reactions, 43
- Irreversible electroporation (IRE), 378
- Ischemia, 123
- Isoelectric point/range, 36, 96
- Isoelectric, 165

- Joule effect, 78–79

- Keratin, 24
- Keratinized tissue, 110–119
- Kohlrausch, Friedrich Wilhelm Georg, 17
- Kramers-Kronig transform, 74, 211–212

- Laboratory applications, 5
- Langmuir adsorption isotherm, 33
- Laplace equation, 288
- Laplace, Pierre Simon de, 210
- Laplace transform, 210
- Lateral diffusion, 83–85
- Latin/Greek, 165
- LCR-meters, 244–245
- Lead, 164
- Lead field, reciprocal, 186
- Lead vector, 183–186, 337–340
- Leakage currents, 407
- Let-go current, 403
- Levitation, 39
- Leyden jar, 414
- Lie-detector, 394
- Ligands, 154
- Lightning, 405–406
- Linear behavior, 54
- Linear network, 208
- Linear projection methods, 391
- Lipids, 100–102
- Liposome, 102
- Liquid junction potential, 44, 262
- Loadings plot, 324
- Lock-in amplifier
 - analog, 240–241
 - digital, 238–240
 - microelectronic mode, 241–244
- Lock-in technique, 215–219
- Loss factor/angle/tangent, 68
- Low-pass filter, 232

- Macroshock, 402–403
- Magnetic induction tomography (MIT), 200–201
- Magnetic nerve stimulation, 276–277
- Magnetic resonance electrical impedance tomography (MREIT), 105
- Magnetic resonance imaging (MRI), 277
- Mains noise reduction, 235
- Mass action law, 21
- Material constants, 69
- Mateucci, Carlo, 413
- Maxwell, James Clark, 287, 413
- Maxwell's equations, 286–290
- Maxwell's spherical particles mixture equation, 82
- Maxwell-Fricke equation, 82
- Maxwell-Wagner effect, 80–83, 90
- Measurements, 205–281
- Measuring depth, 110, 190
- Meat quality, 397
- Medical sensor, 253
- Metallic bonds, 10–11
- Metal-liquid overvoltage, 269
- Microelectrode, 273–275
- Microelectroporation, 381–382
- Micromotion detection, 386–387
- Micropipette, 273–274
- Microshock, 402–403
- Migration, 28–30
- Minimum phase shift network, 211
- Mixed conductors, 23
- Models, 4, 283–332
 - bidomain, 198, 290
 - two-component, 290–297
- Modulus function, 68
- Molar conductivity, 18
- Molecular
 - bonds, 10–11
 - interactions, 416
- Monopolar basic experiment with DC current flow, 45–49
- Monopolar system, 45
- Monopolar, 165
- Mother wavelet, 330
- Moving current dipole, 152
- Multiple Cole systems, 315–321
- Multivariate analysis, 322–324, 391
- Muscle tissue, 105–106
- Müller, Hermann, 413

- Nail, 116–119
- Needle electrode, 104, 175–177, 271–273
- Neocortex, 149
- Nernst equation, 42, 141
- Nerve propagation velocity, 153
- Nerve tissue, 106
- Nerve, 153–156
- Network analyzers, 245
- Network theory, 206–212
- Neural networks, 326
- Neurilemma, 153
- Neuron excitation, 155–156
- Neuron, 147–151
- Neurostimulation, 269
- Neurotransmitter, 154
- Neutral electrode, 45, 164
- Node of Ranvier, 153
- Noise, 264
- Nollet, Jean-Antoine, 412
- Non-biological applications, 5
- Non-galvanic coupling, 276–281
- Non-linear black box, 210
- Non-linear parameters, 130–135
- Non-medical applications, 5
- Non-polarizable electrode, 49
- Nyquist criterion, 227

- Onsager, Lars, 20
- Operational amplifier (opamp), 231–233
- Organs, 102–124
- Orientational polarization, 63
- Osmotic pressure, 116
- Overvoltage, 47, 52
 - metal-liquid, 269
- Oxonium, 20

- Pacemaker, 269, 370–372
- Pacing, 361
- Pacinian corpuscles, 157
- Pain, 157
- Partial least squares (PLS) regression, 324
- Particle charge, 36
- Passage effect, 182–183
- Passive electrical properties, 93–137
- Passive network, 208
- Patch clamp, 158–159, 275
- Pauling, Linus, 9
- Pauly-Schwan equations, 83
- Pearl chain formation, 40

- Peptides, 97
- Perineurium, 154
- Permanent dipoles, 77
- Permittivity, 59
 - complex, 67
 - relative, 61, 66
 - static, 66
- pH electrode, 23
- Phase angle, 68, 215
- Phase shift, 65
- Phase spectrum, 221
- Phasor, 215, 423
- Phospholipids, 100
- Physical dimensions, 432–434
- Pia mater, 149
- Pick-up (PU) electrodes, 164
- Piezoelectric effect, 135–137
- Pilocarpine, 397
- Plant tissue, 124
- Platinum black, 257, 265
- Platinum, 257
- Poisson equation, 32, 288
- Poisson's law, 43
- Polar substances, 22
- Polarizability, 62
- Polarizable electrode, 48–49, 253
- Polarization, 58–64, 70–79
 - cell, 140–143
 - electronic, 63
 - immittance, 264–269
 - impedance, 166, 253
 - interfacial, 79–85
 - ionic, 63
 - orientational, 63
- Polarography, 45
- Polyelectrolyte, 98
- Polymers, 97
- Ponderomotive forces, 37–40
- Post mortem, 122–123
- Potential
 - action, 140
 - cell, 145–147
 - Donnan, 44
 - electrode, 41–44
 - flow generated, 38
 - injury, 130
 - liquid junction, 44, 262
 - redox equilibrium, 42
 - sedimentation, 36

- streaming, 33, 36
 - zeta, 33
- Potentiometry, 41
- Potentiostat, 192
- Power density spectrum, 226
- Power, 78
- Precipitation, 36
- Presynaptic terminals, 147
- Principal component analysis (PCA), 323, 391
- Probability density function, 228
- Product of two sine waves, 215–219
- Protective earth, 407
- Proteins, 23, 95–99
- Proton hopping, 20
- Protons, 97
- PU, 164

- QRS complex, 338
- Quadropolar, 165
- Quantity of electricity, 27
- Quasi-circular arcs, 314–315

- Rayleigh scattering, 280
- Reactance, 239
- Reactive power, 78
- Receiver operating characteristics (ROC) graph, 324–325
- Receptors, 157–159
- Reciprocal lead field, 186
- Reciprocity theorem, 188, 207, 209
- Redox systems, 42
- Reference electrode, 263, 346
- Reference voltage, 233–236
- Refractory period, 144
- REG, 351–353
- Relative permittivity, 61, 66
- Relaxation time, 16, 311–315
 - distribution of, 89
- Relaxation, 70–79
 - Debye model, 71–77
- Resistance, 239
 - series, 50–53
 - specific, 68
- Resistivity, complex, 68
- Resonance, 99
- Reversible electrode reaction, 42
- Rheobase, 156, 361
- Rheoencephalography (REG), 351–353
- Root-mean-square (rms), 79

- Saccharides, 99–100
- Safety grounding, 233
- Salt bridge, 44, 262
- Savart, Félix, 201
- Schwan, Herman P., 417–418
- Schwarz theory, 34, 84
- Score plot, 323
- Seawater, 19
- Sebum, 117
- Sedimentation potential, 36–38
- Self-affine curves, 327
- Self-similar curves, 327
- Self-similarity, 327
- Semiconductors, energy levels, 25
- Sensitivity field, 188–191
- Sensitivity, 324
- Sensor, 253
- Series resistance, 50–53
- Short time Fourier transform (STFT), 223, 329
- SI units, xi
- Siemens, Werner von, 414
- Sigman effect, 351
- Signal averaging, 228
- Signal generators, 228–229
- Signal transfer, 180
- Signal-to-noise ratio (SNR), 228
- Silver-silver chloride, 256
- Sine waves, sum and product, 215–219
- Single fault condition, 407
- Sinoatrial (SA) node, 342
- Sinusoidal excitation, 211
- Skin abrasion, 261
 - cancer, 389–393
 - depth, 277
 - diseases, 389–393
 - instrumentation, 388–397
 - irritations, 389–393
 - tissue, 110–119
- Sodium reabsorption, 394
- Soft independent modeling of class analogies (SIMCA), 324
- Solid electrolyte, 23
- Solid gel, 261, 267–268
- Solute, 12
- Solvent, 12
- Spatial summation, 155, 399
- Specific adsorption, 35
- Specific resistance/conductance, 68
- Specificity, 324

- Spectrum analyzers, 245
 Spectrum analysis, 224–228
 Spherical electrode, 166–169
 Spontaneous activity, 394
 Sport medicine, 5
 St. Elmo's fire, 412
 Static permittivity, 66
 Step waveform excitation, 211, 222
 Stern theory, 32–33
 Stoke's law, 18, 77
 Strange attractor, 327
 Stratum corneum hydration, 388–389
 Stratum corneum, 110
 Streaming potential, 33–38, 394
 Sum of two sine waves, 215–219
 Summation, spatial/temporal, 155
 Superposition, 130, 203
 Supraelectroporation, 382–385
 Surface impedance density, 70
 Surface lateral immitivity, 69–70
 Surface perpendicular imittance, 70
 Susceptance, 238
 Susceptibility, 61
 Susceptivity, 61
 Suspension of spherical particles, 81–83
 Sweat measurements, 396
 Sweat, 19
 Symmetry paradox, 189
 Sympathectomy, 396
 Synapses, 154–155
 Synchronous rectifier, 240

 Tabulated data, 103–105
 Technically ideal dipole, 170–186
 Technology, 414
 Temperature coefficient, 102
 Temperature rise, 78–79
 Temporal summation, 155
 TENS, 358
 Tesla, Nikola, 413
 Tetrapolar electrode system, 193–195
 Tetrapolar, 165
 Three-electrode system, 191–193
 Threshold levels (perception/hazards), 405
 Threshold of perception, 398–405
 Tight junctions, 110
 Time constant, 211
 Time domain reflectometry, 249–253
 Time domain spectroscopy, 245–246

 Time domain transmissometry, 246–249
 Time domain, 224
 Tissue ablation, 379
 Tissue conductivity, 103
 Tissue damage, 122
 Tissue, 102–124
 Titanium alloys, 257
 Tomography (EIT/MIT), 198–202
 Total body water (TBW), 363
 Transconductance, 209
 Transcutaneous electrical nerve stimulation (TENS), 358
 Transdermal drug delivery, 396–397
 Transfer impedance, 187, 418
 Transfer signal equation, 186
 Transference number, 17
 Transmembrane voltage, 133
 Transmittance, 165, 207
 Transporters, 140
 Transresistance amplifier, 208, 231
 Traveling wave dielectrophoresis, 40
 Triboelectric effect, 135–137
 Tripolar, 165
 Two-component model, 290–297
 Two-electrode system, 163–165

 Unipolar, 165
 augmented leads, 336
 lead, 164
 recording, 181
 Unit impulse, 222
 Urine, 19
 Urology, 355

 Valence electrons, 9
 Van der Waals bonds, 10–11
 Vasodilation, 359
 Vector cardiography, 343
 Vectors, 419–423
 Velocity of electrons/ions, 8
 Visual human project, 354
 Volcanic activity, 5
 Volta, Alessandro, 412
 Voltage
 clamp, 228
 follower, 231
 transmembrane, 133
 Voltammetry, 45–47
 Volume conductors, 162–163

- Von Guericke, Otto, 411
Von Helmholtz, Hermann, 413
Von Siemens, Werner, 414
- Waage, Peter, 21
Waller, August, 413
Warburg diffusion, 311
Warburg immittance, 52
Water, 20
 bound, 94
Wavelet analysis, 328–331
Weak acids, 21
Wessel diagram, xi, 294–296
Wessel, Caspar, 420
- Wet gel electrolytes, 258–260, 265
White matter, 149
White noise, 223
Whole body measurements, 119–122
Wien effect, 54, 383
Wien, Max Karl Werner, 54
Working electrode, 45
Wound healing, 360
- Zeta potential, 33
Zwitterions, 96
- Ørsted, Hans Christian, 413